Publication Series of the John von Neumann Institute for Computing (NIC)
NIC Series Volume 15

John von Neumann Institute for Computing (NIC)

Numerical Methods for Limit and Shakedown Analysis

Deterministic and Probabilistic Problems

edited by
Manfred Staat
Michael Heitzer

Report of the European project:
FEM-Based Limit and Shakedown Analysis for Design and Integrity Assessment in European Industry – LISA

Project funded by the European Commission under the Industrial & Materials Technologies Programme (Brite-EuRam III)
Contract n°: BRPR-CT97-0595
Project n°: BE 97-4547
Period: January 1, 1998 to May 31, 2002

NIC Series Volume 15 ISBN 3-00-010001-6

Central Institute for Applied Mathematics

Die Deutsche Bibliothek – CIP-Cataloguing-in-Publication-Data
A catalogue record for this publication is available from Die Deutsche Bibliothek

Publisher: NIC-Directors
Distributor: NIC-Secretariat
Research Centre Jülich
52425 Jülich
Germany
Internet: www.fz-juelich.de/nic
Printer: Graphische Betriebe, Forschungszentrum Jülich

NIC Series Volume 15 ISBN 3-00-010001-6

Foreword

The Commission of the European Communities has supported the LISA project on **Li**mit and **S**hakedown **A**nalysis for industrial use, which connects direct methods of plasticity with stochastic methods of structural reliability in a general purpose Finite Element package. There was no commercial Finite Element Code that could perform either of this kind of analysis at the time when Professor P.D. Panagiotopoulos and I began the first planning of the LISA project ten years ago. Therefore, we had to answer ourselves three questions: Who may benefit?, Why now?, and Is the idea challenging, can it be realized and will it be successful?

The first question was easily answered from observing recent trends in engineering design codes and standards. Instead of the traditional reinterpretation of Finite Element Analyses by stress assessment, modern design codes address structural failure modes directly with the objective to use inelastic deformations of ductile materials for the extension the load carrying capacity. More economic steel structures, pressure vessels and piping can be designed with checks against plastic collapse (gross plastic deformation) and ratchetting (progressive plastic deformation) by Limit and Shakedown Analysis. Optionally, Low Cycle Fatigue (alternating plasticity) may be excluded. Parallel to the LISA project, the new European pressure vessel standard EN 13445-3 has been established with a direct route for design by limit and shakedown analysis. It is a second trend in modern design codes to base partial safety factors on the stochastic concepts of structural reliability analysis. Limit analysis also forms the basis of a number of simplified two-criteria assessment methods in ductile fracture mechanics. Limit and shakedown analysis found applications in a wide range, spanning from soil mechanics to wear in rolling and sliding contact. This answers the second question 'a posteriori'.

Although being based on exact theorems of classical plasticity, limit and shakedown analysis are considered as simplified methods. Simplification is achieved without any additional approximation, by restricting analysis to only the failure states of the structure. From an engineering design standpoint, the merit of more elaborate analyses has to be judged in the light of the uncertainty of material data and the difficulties in obtaining suitable constitutive equations. One of the most important results of the simplification is that limit and shakedown analysis makes robust assessments of structural safety. Robustness of a method is its ability to provide acceptable results on the basis of a less than ideal input data.

Limit and shakedown analysis states the design problem as a nonlinear optimization problem for the maximum of a safe load or for its dual, the minimum of a failure load. This is a challenging concept, because the number of constraints defining a safe load and a failure load in lower and upper bound analysis, respectively, is huge with Finite Element discretization. Realistic industrial problems are modelled with several 100 thousands of unknowns and constraints today. Different methods for large-scale optimization have been developed by the research groups contributing to the LISA project. The present report includes: basis reduction by plastic analyses and search for the maximum in a sequence of

low dimensional subspace by Sequential Quadratic Programming (SQP); dual upper and lower bound analysis of the full size problem by large-scale nonlinear programming methods based on a sequence of linear elastic analyses; reformulation of the problem in the form of a Second Order Cone Programming problem (SOCP). Zarka's method has been contributed as an additional direct plasticity method, which estimates the plastic deformation prior to failure. Methods which try to go around the difficulties of optimisation are not considered in the LISA project: deviatoric map and methods based on elastic moduli modification such as the Generalized Local Stress Strain (GLOSS) analysis, the elastic compensation method or the linear matching method.

The LISA project extends the perfect plasticity models that are used in design code applications. More realistic structural behaviour is modelled by a two-surface plasticity model for bounded kinematic hardening, by the inclusion of moderately large deformations and displacements, and by continuum damage models. Two contributions treat the structural reliability problem for uncertain material data and loading by First and Second Order Reliability Methods (FORM/SORM). These methods become particularly effective with limit and shakedown analysis yielding linear limit state functions. Moreover, the solution of the optimization problem in limit and shakedown analysis generates already the sensitivities needed for the reliability analysis. The extension to chance constraint stochastic programming is indicated.

The contributions from the different research groups to this report have been written self-contained such that they can be read independently. Some effort has been made to use similar notations for the convenience of the reader. Few test problems have been chosen to demonstrate that limit and shakedown analysis combine conceptual insight with the economy of computational effort for a wide range of component geometry and loading conditions.

I thank all LISA project partners and the authors for their contribution to this book. I also thank Mr. D. Koschmieder, Prof. Dr. E.F. Hicken, and Dr. M. Heitzer for assisting me during the coordination of the LISA project.

It was sad that Prof. Panagiotopoulos unexpectedly passed away seven months after project start. The project would not have come into existence without his personal commitment to our plans and his encouraging promotion. I will always be grateful for the experience of his authentic warmth, brightness and reliability.

Manfred Staat

Contents

List of Figures

List of Tables

Part I

Basis reduction technique for limit and shakedown problems

Michael Heitzer

Central Institute for Applied Mathematics (ZAM)
Forschungszentrum Jülich, D-52425 Jülich, Germany

E-mail: m.heitzer@fz-juelich.de

Manfred Staat

Department of Physical Engineering
Fachhochschule Aachen Div. Jülich
Ginsterweg 1, D-52428 Jülich, Germany

E-mail: m.staat@fh-aachen.de

Nomenclature

$\mathbf{e}$	total strain
$\dot{\mathbf{e}}^p$	plastic strain vector
$\mathbf{f}, \mathbf{f}_0$	body force
$\mathbf{p}, \mathbf{p}_0$	surface traction
$\mathbf{n}$	outer normal vector
$\mathbf{s}$	stress vector
$\mathbf{r}$	strength vector
t	time
$\mathbf{u}$	actual displacement
$\dot{\mathbf{u}}, \dot{\mathbf{u}}^0$	velocity, given velocity
$\mathbf{x}$	coordinate vector
$\mathbf{C}$	system dependent matrix
E	Young's modulus
$\mathbf{E}$	tensor of elasticity, matrix
$D(\dot{\boldsymbol{\varepsilon}}^p)$	plastic dissipation
F	yield function ($F \leq \sigma_y^2$ or σ_u^2)
$\mathbf{P}$	loads
T	absolute temperature
T_0	reference temperature
NE	number of elements
NF	number of DOF's
NG	number of Gaussian points
NSK	number of stress components
NV	number of load vertices
V	structure
∂V	boundary ($\partial V = \partial V_p \cup \partial V_u$)
$\dot{W}_{ex}$	external power of loading
$\dot{W}_{in}$	internally dissipated power
$\boldsymbol{\varepsilon}, \dot{\boldsymbol{\varepsilon}}$	total strain and rate
$\boldsymbol{\varepsilon}^E, \dot{\boldsymbol{\varepsilon}}^E$	elastic strain and rate
$\boldsymbol{\varepsilon}^p, \dot{\boldsymbol{\varepsilon}}^p$	plastic strain and rate
$\boldsymbol{\varepsilon}^{th}, \dot{\boldsymbol{\varepsilon}}^{th}$	thermal strain and rate
$\dot{\varepsilon}_{eq}^P$	effective plastic strain rate
$\boldsymbol{\pi}$	back-stress
$\bar{\boldsymbol{\pi}}$	time-independent back-stress
$\boldsymbol{\rho}, \dot{\boldsymbol{\rho}}$	residual stress and rate
$\bar{\boldsymbol{\rho}}$	time-independent residual stress
$\boldsymbol{\sigma}$	actual stress
$\boldsymbol{\sigma}^E$	fictitious elastic stress
$\boldsymbol{\sigma}^D$	deviatoric stress
Ψ	thermodynamic potential
∇	gradient-operator
$\mathcal{B}, \mathcal{B}_d$	residual stress spaces
$\mathcal{L}$	load domain
$\mathcal{I}, \mathcal{J}, \mathcal{A}$	index sets
α_t	coefficient of thermal expansion
α	load factor
α_{SD}	shakedown factor
α_s	lower bound shakedown factor
α_k	upper bound shakedown factor
θ	Temperature difference $T - T_0$
ν	Poisson's ratio
σ_u	uniaxial limit strength
σ_y	yield stress

Code_Aster	FEM software by EDF, France
DOFs	Degrees of Freedoms
FEM	Finite Element Method
FZJ	Forschungszentrum Jülich GmbH
INTES	Ingenieurgesellschaft für technische Software mbH, Stuttgart
LCF	Low Cycle Fatigue
LISA	Limit and Shakedown Analysis
PDE	Partial Differential Equation
PERMAS	FEM software by INTES
SQP	Sequential Quadratic Programming
ULg	University of Liege
V4, V7	PERMAS Version 4, Version 7

1 Formulation of the problem

1.1 Introduction to limit and shakedown analysis

Static theorems are formulated in terms of stress and define safe structural states giving an optimization problem for safe loads. The elasto-plastic behaviour of a structure subjected to variable loads, is characterized by one of the following possibilities:

- purely elastic behaviour,
- purely elastic behaviour after initial plastic flow (shakedown),
- Low Cycle Fatigue (LCF) by alternating plasticity,
- Incremental collapse by accumulation of plastic deformations over subsequent load cycles (ratchetting),
- Instantaneous collapse by unrestricted plastic flow at limit load.

The maximum safe load is defined as the limit load avoiding collapse and the shakedown load avoiding LCF and ratchetting. Alternatively, kinematic theorems are formulated in terms of kinematic quantities and define unsafe structural states yielding a dual optimization problem for the minimum of unsafe loads. Any admissible solution to the static or kinematic theorem is a true lower or upper bound to the safe load, respectively. Both can be made as close as desired to the exact solution. Let us define a load factor $\alpha = \mathbf{P}_l/\mathbf{P}_0$, where $\mathbf{P}_l = (\mathbf{f}_l, \mathbf{p}_l)$ and $\mathbf{P}_0 = (\mathbf{f}_0, \mathbf{p}_0)$ are the plastic limit load and the chosen reference load, respectively. We will first suppose that all loads (**f** body forces and **p** surface loads) are applied in a monotonic and proportional way. Then we may first state the limit load theorems.

1. *Static limit load theorem (lower bound):* An elastic–plastic structure will not collapse under monotone loads if it is in static equilibrium and if the yield function is nowhere violated.
2. *Kinematic limit load theorem (upper bound):* The structure fails by plastic collapse if there is an (kinematically admissible) velocity field such that the power of the external loads is higher than the power which can be dissipated within the structure.

If the loads vary in the load domain $\mathcal{L}$ one may ask by which load factor $\alpha \geq 1$ it may safely be enlarged to $\alpha\mathcal{L}$. This question is answered by the shakedown theorems.

1. *Static shakedown theorem (lower bound):* An elastic–plastic structure will not fail with macroscopic plasticity under time variant loads if it is in static equilibrium, if the yield function is nowhere and at no instance violated, and if all plastic deformations decay.

2. *Kinematic shakedown theorem (upper bound):* The structure fails with macroscopic plasticity under time variant loads if there is an (kinematically admissible) velocity field such that the power of the external loads is higher than the power which can be dissipated within the structure.

1.2 Lower bound approach

1.2.1 Limit analysis

The objective of the lower bound approach of limit analysis is to find the maximum load factor α_L for which the structure is safe. A maximum problem can be formulated:

$$\begin{aligned} \max \quad & \alpha \\ \text{s. t.} \quad & F(\boldsymbol{\sigma}) \leq \sigma_y^2 \ \text{ in } V \\ & \operatorname{div}\boldsymbol{\sigma} = -\alpha \mathbf{f}_0 \ \text{ in } V \\ & \boldsymbol{\sigma}\,\mathbf{n} = \alpha \mathbf{p}_0 \ \text{ on } \partial V_p \end{aligned} \tag{1.1}$$

for the structure V, traction boundary ∂V_p (with outer normal $\mathbf{n}$), yield function F, yield stress σ_y, body forces $\alpha\mathbf{f}_0$ and surface loads $\alpha\mathbf{p}_0$. From now on F is chosen as the square of the von Mises yield function (1.14).

1.2.2 Shakedown analysis

The concepts for time-variant loading are more involved. Time is denoted by t. The stresses $\boldsymbol{\sigma}$ can be decomposed into fictitious elastic stresses $\boldsymbol{\sigma}^E$ and residual stresses $\boldsymbol{\rho}$ by

$$\boldsymbol{\sigma} = \boldsymbol{\sigma}^E + \boldsymbol{\rho}. \tag{1.2}$$

$\boldsymbol{\sigma}^E = \mathbf{E} : \boldsymbol{\varepsilon}$ are stresses which would appear in an infinitely elastic material for the same loading, so that the $\boldsymbol{\rho}$ result from plastic deformations. The residual stresses (eigen stresses) $\boldsymbol{\rho}$ satisfy the homogeneous static equilibrium and boundary conditions

$$\operatorname{div}\boldsymbol{\rho} = \mathbf{0} \ \text{ in } V \tag{1.3}$$

$$\boldsymbol{\rho}\,\mathbf{n} = \mathbf{0} \ \text{ on } \partial V_p. \tag{1.4}$$

One criterion for an elastic, perfectly plastic material to *shake down elastically* is that the plastic strains $\boldsymbol{\varepsilon}^P$ and therefore the residual stresses $\boldsymbol{\rho}$ become stationary for given loads $\mathbf{P}(t) = (\mathbf{f}, \mathbf{p})$ in a load domain $\mathcal{L}$:

$$\begin{aligned} &\lim_{t\to\infty} \dot{\boldsymbol{\varepsilon}}^P(\mathbf{x}, t) = \mathbf{0}, \\ &\lim_{t\to\infty} \dot{\boldsymbol{\rho}}(\mathbf{x}, t) = \mathbf{0}, \ \ \forall\, \mathrm{x} \in V. \end{aligned} \tag{1.5}$$

In every considered failure mode there is at least one point **x** of the structure where condition (1.5) is violated. Thus there exists at least one point **x** for which the density of the plastic energy dissipation w_p per unit volume

$$w_p(\mathbf{x},t) = \int_0^t \boldsymbol{\sigma}(\mathbf{x},\tau) : \dot{\boldsymbol{\varepsilon}}^P(\mathbf{x},\tau)\, d\tau \tag{1.6}$$

increases infinitely in time. To avoid the possibility of plastic failure the maximum possible plastic energy dissipation

$$W_p(\mathbf{x}) = \lim_{t\to\infty} w_p(\mathbf{x},t) \le c(\mathbf{x}) \tag{1.7}$$

must be bounded above for all points $\mathbf{x} \in V$. We restrict ourselves to the shakedown criterion (1.5). This means, that independent of the loading history the system has to approach asymptotically an elastic limit state. For details of the extended theorem see [27]. The following static shakedown theorem holds [33].

Theorem (Melan):

If there exists a factor $\alpha > 1$ and a time-independent residual stress field $\bar{\boldsymbol{\rho}}(\mathbf{x})$ with $\int_V \bar{\boldsymbol{\rho}} : \mathbf{E} : \bar{\boldsymbol{\rho}}\, dV < \infty$, such that for all loads $\mathbf{P}(t) \in \mathcal{L}$ it is satisfied,

$$F[\alpha\boldsymbol{\sigma}^E(\mathbf{x},t) + \bar{\boldsymbol{\rho}}(\mathbf{x})] \le \sigma_y^2 \qquad \forall\, \mathbf{x} \in V \tag{1.8}$$

then the structure will shake down elastically under the given load domain $\mathcal{L}$.

The greatest value α_{SD} which satisfies the theorem is called *shakedown*-factor. The static shakedown theorem is formulated in terms of stresses and gives a lower bound to α_{SD}. This leads to the mathematical optimization problem

$$\max \quad \alpha \tag{1.9}$$

$$\text{s. t.} \quad F[\alpha\boldsymbol{\sigma}^E(\mathbf{x},t) + \bar{\boldsymbol{\rho}}(\mathbf{x})] \le \sigma_y^2 \qquad \forall \mathbf{x} \in V \tag{1.10}$$

$$\operatorname{div} \bar{\boldsymbol{\rho}}(\mathbf{x}) = \mathbf{0} \qquad \forall \mathbf{x} \in V \tag{1.11}$$

$$\bar{\boldsymbol{\rho}}(\mathbf{x})\, \mathbf{n} = \mathbf{0} \qquad \forall \mathbf{x} \in \partial V_p \tag{1.12}$$

with infinitely many restrictions, which has to be reduced to a finite optimization problem by FEM discretization (see the following sections). Shakedown analysis gives the largest range in which the loads may safely vary with arbitrary load history. If the load domain $\alpha\mathcal{L}$ shrinks to the point of a single monotone load, limit analysis is obtained as special case.

Remark

In special cases the load domain $\mathcal{L}$ can be divided in a load domain $\mathcal{L}_t$ of the time-variant load P_t and a time-independent (dead) load P_0, such that $\mathcal{L} = \mathcal{L}_t \oplus P_0 := \{P \mid P = P_t + P_0, P_t \in \mathcal{L}_t\}$. With $\boldsymbol{\sigma}_0^E(\mathbf{x})$ corresponding to the

dead load P_0 the condition (1.10) in the shakedown analysis is transformed into:

$$F[\alpha\boldsymbol{\sigma}_t^E(\mathbf{x},t)+\boldsymbol{\sigma}_0^E(\mathbf{x})+\bar{\boldsymbol{\rho}}(\mathbf{x})]\leq\sigma_y^2 \tag{1.13}$$

where $\boldsymbol{\sigma}_t^E(\mathbf{x},t)$ corresponds to the load $P_t\in\mathcal{L}_t$ and $\boldsymbol{\sigma}_0^E(\mathbf{x})$ is constant in time.

1.3 Upper bound approach

Koiter has formulated an upper bound theorem in kinematic quantities [26]. It may be obtained from Markov's theorem for rigid perfectly plastic material [56], [62]. We will derive it as the formal dual of the static or lower bound theorem.

The simplest smooth J_2-yield function was proposed by von Mises

$$F(\boldsymbol{\sigma})=\frac{3}{2}\boldsymbol{\sigma}^D:\boldsymbol{\sigma}^D=3J_2,\quad J_2=\frac{1}{2}\boldsymbol{\sigma}^D:\boldsymbol{\sigma}^D \tag{1.14}$$

$$\boldsymbol{\sigma}^D=\mathrm{dev}\boldsymbol{\sigma}=\boldsymbol{\sigma}-\frac{1}{3}(\mathrm{tr}\boldsymbol{\sigma})\mathbf{I}.$$

In associated plastic flow the plastic deformation rate is normal to the yield surface $F=\sigma_y^2$

$$\dot{\boldsymbol{\varepsilon}}^P=\lambda\frac{\partial\sqrt{F}}{\partial\boldsymbol{\sigma}} \tag{1.15}$$

with the nonnegative consistency parameter $\lambda\geq 0$. The irreversible response to loading and unloading obeys the following Karush-Kuhn-Tucker *complementarity conditions*

$$\lambda[F(\boldsymbol{\sigma})-\sigma_y^2]=0,\qquad\lambda\geq 0,\qquad F(\boldsymbol{\sigma})-\sigma_y^2\leq 0. \tag{1.16}$$

additionally $\lambda\geq 0$ satisfies the *consistency condition*

$$\lambda\frac{\partial\sqrt{F}}{\partial\boldsymbol{\sigma}}:\dot{\boldsymbol{\sigma}}=0. \tag{1.17}$$

These flow rules are non-smooth. For the von Mises yield function (1.14) one obtains

$$\frac{\partial\sqrt{F}}{\partial\boldsymbol{\sigma}}=\sqrt{\frac{3}{2}}\frac{\boldsymbol{\sigma}^D}{\sqrt{\boldsymbol{\sigma}^D:\boldsymbol{\sigma}^D}}=\frac{3}{2}\frac{\boldsymbol{\sigma}^D}{\sqrt{F(\boldsymbol{\sigma})}}. \tag{1.18}$$

Inserted into (1.15) it holds

$$\dot{\boldsymbol{\varepsilon}}^P=\lambda\frac{3}{2}\frac{\boldsymbol{\sigma}^D}{\sqrt{F(\boldsymbol{\sigma})}}. \tag{1.19}$$

which satisfies the incompressibility requirement

$$\mathrm{tr}\dot{\boldsymbol{\varepsilon}}^P=0,$$

so that $\dot{\boldsymbol{\varepsilon}}^P$ is equivalent with its deviator. Now the effective plastic strain rate $\dot{\boldsymbol{\varepsilon}}^P_{eq}$ may be computed

$$\dot{\varepsilon}^P_{eq} = \sqrt{\frac{2}{3}\dot{\boldsymbol{\varepsilon}}^P : \dot{\boldsymbol{\varepsilon}}^P} = \lambda\sqrt{\frac{2}{3}\frac{\partial\sqrt{F}}{\partial\boldsymbol{\sigma}} : \frac{\partial\sqrt{F}}{\partial\boldsymbol{\sigma}}} = \lambda\sqrt{\frac{2}{3}\frac{3}{2}\frac{\sqrt{\boldsymbol{\sigma}^D : \boldsymbol{\sigma}^D}}{\sqrt{F(\boldsymbol{\sigma})}}} = \lambda \geq 0, \tag{1.20}$$

which equals the consistency parameter λ. The internally dissipated power $\dot{W}_{in}$ is obtained from the plastic dissipation density $D(\dot{\varepsilon}^P_{eq})$

$$D(\dot{\varepsilon}^P_{eq}) = \dot{\boldsymbol{\varepsilon}}^P : \boldsymbol{\sigma} = \dot{\varepsilon}^P_{eq}\sigma_y = \lambda\sigma_y. \tag{1.21}$$

We could then formulate a minimum principle

$$\begin{aligned}
\text{min} \quad & \alpha_k \\
\text{with} \quad & \alpha_k = \dot{W}_{in} = \int\limits_V \dot{\boldsymbol{\varepsilon}}^P_{eq}\sigma_y dV \\
\text{s. t.} \quad & 1 = \dot{W}_{ex} = \int\limits_V \mathbf{f}_0^T\dot{\mathbf{u}}dV + \int\limits_{\partial V_p} \mathbf{p}_0^T\dot{\mathbf{u}}dS \geq 0, \\
& \dot{\boldsymbol{\varepsilon}}(t) = \frac{1}{2}(\nabla\dot{\mathbf{u}} + (\nabla\dot{\mathbf{u}})^T) \quad \text{in } V\ , \\
& \dot{\mathbf{u}}(t) = \dot{\mathbf{u}}^0(t) \qquad \text{on} \quad \partial V_u,
\end{aligned} \tag{1.22}$$

for the structure V, boundary $\partial V = \partial V_p \cup \partial V_u$, displacement boundary ∂V_u, given velocity $\dot{\mathbf{u}}^0$.

The objective function α_k is non-smooth on the boundary of the plastic region. Then the optimization problem resulting from a FEM discretization is also non-smooth. It may be solved with a bundle method [65]. As a practical alternative, different regularization methods are used as smoothing tools in [56] and in [24], [25], [63]. The regularized minimization problem is solved by a reduced-gradient algorithm in conjunction with a quasi-Newton algorithm [35].

1.4 Discretization with FEM

While using the FEM for the limit and shakedown analysis, the boundary conditions of the lower and upper bound approach eventually vanish because of the approximative calculation of the stresses and displacements. To handle a wide range of complex structures it was decided to use the commercial FEM-Code PERMAS (INTES, Stuttgart, [36]) for the lower bound approach. The program calculates the fictitious elastic stresses $\boldsymbol{\sigma}^E$, the optimization procedure is a decoupled process (see [14]).

For the FEM the structure V is decomposed in NE finite elements with the Gaussian points $\mathbf{x}_i,\ i = 1, \ldots, NG$. The restrictions of the optimization problems are checked only in the Gaussian points.

The structure V is subjected to the load $P(t)$ and the discretized fictitious elastic stresses $\boldsymbol{\sigma}_i^E(t) = \boldsymbol{\sigma}^E(\mathbf{x}_i, t)$ are calculated with the displacement FEM (see [36]). With the discretized residual stresses $\bar{\boldsymbol{\rho}}_i = \bar{\boldsymbol{\rho}}(\mathbf{x}_i)$ the discretized necessary limit and shakedown conditions are derived with the yield stress $\sigma_{y,i}$ in every Gaussian point i:

$$F(\boldsymbol{\sigma}_i^E(t) + \bar{\boldsymbol{\rho}}_i) \leq \sigma_{y,i}^2. \tag{1.23}$$

With the element matrices $\mathbf{c}_i$, the element incidence matrix and the global matrix $\mathbf{C}$ the discretized equilibrium equations of the residual stresses are derived ([1], [14], [36], [64]):

$$\sum_{i=1}^{NG} \mathbf{c}_i \bar{\boldsymbol{\rho}}_i = \mathbf{0}. \tag{1.24}$$

We use the abbreviations[1]

NE	number of elements of the structure
NF	number of DOF's
NG	number of Gaussian points of the structure
NSK	number of stress components of each Gaussian point
NV	number of load vertices

The element matrices $\mathbf{c}_i$ are calculated by the nodal point displacements and the boundary conditions of the structure such that $\mathbf{c}_i \in I\!R^{NF \times NSK}$ and $\bar{\boldsymbol{\rho}}_i \in I\!R^{NSK}$ holds. With the abbreviations $\mathbf{C} = (\mathbf{c}_1, \ldots, \mathbf{c}_{NG})$ and $\bar{\boldsymbol{\varrho}}^T = \left(\bar{\boldsymbol{\rho}}_1^T, \ldots, \bar{\boldsymbol{\rho}}_{NG}^T\right)$, eq. (1.24) yields

$$\mathbf{C}\bar{\boldsymbol{\varrho}} = \mathbf{0}. \tag{1.25}$$

The matrix $\mathbf{C} \in I\!R^{NF \times (NSK \cdot NG)}$ has maximum rank because rigid body movements are excluded. The rank is defined by the number NF of DOF's of the structure V. All vectors $\bar{\boldsymbol{\varrho}}$ which fulfill eq. (1.25) are the kernel of the linear mapping defined by the matrix $\mathbf{C}$ and define with the addition and scalar multiplication a vector space $\mathcal{B}$, the so called *residual stress space*. The dimension of $\mathcal{B}$ is given by $\dim(\mathcal{B}) = NSK \cdot NG - NF$. This dimension is dominated by product of the number of Gaussian points NG and the number of stress components NSK. The discretized problem of the lower bound approach is defined by

$$\begin{aligned} \max \quad & \alpha \\ \text{s. t.} \quad & F[\alpha \boldsymbol{\sigma}_i^E(t) + \bar{\boldsymbol{\rho}}_i] \ \leq \sigma_{y,i}^2 \qquad i = 1, \ldots, NG, \quad P(t) \in \mathcal{L}, \quad \bar{\boldsymbol{\varrho}} \in \mathcal{B}. \end{aligned} \tag{1.26}$$

This problem has $NSK \cdot NG + 1$ unknowns: $\bar{\boldsymbol{\rho}}_i$ and the load factor α. Because of the time dependence of the fictitious elastic stresses $\boldsymbol{\sigma}_i^E$ we have still infinite restrictions. So we have to discretize also the load domain to obtain an effective algorithm for the limit and shakedown analysis.

[1] For simplicity of notation we assume here that all elements have the same number of Gaussian points.

1.5 Discretization of the load domains

Let $\mathcal{L}$ be a load domain containing any possible load which acts on the structure V. Any load $P(t) \in \mathcal{L}$ could be specified by a variable t. For a variable cyclic loading the load domain contains infinitely many loads (for a monotonic load in limit analysis it is presented by one single load.) In shakedown analysis the sufficient conditions must be verified for all the non-countable loads $P(t)$.

Usually the cyclic loading could be described by a finite number of load cases $P(k),\ k = 1,\ldots,NV$. These load cases $P(k)$ vary between given load limits $P(k)^-$ and $P(k)^+$, e.g. for a cyclic pressure load the pressure is bounded by minimum and maximum pressure (see [28]). We restrict ourselves to problems where the traction boundary ∂V_p remains constant (see e.g. [27], [43] for moving loads on plates and [23] structures with contact). By defining the load cases $P(1),\ldots,P(NV)$ via the load limits in each case, any load $P(t) \in \mathcal{L}$ is given by an unique convex combination of the $P(j)$, s.t.

$$P(t) = \sum_{j=1}^{NV} \lambda_j P(j), \qquad \sum_{j=1}^{NV} \lambda_j = 1, \quad \text{and} \quad \lambda_j \geq 0,\ j = 1,\ldots,NV. \tag{1.27}$$

This yields, that the load domain $\mathcal{L}$ is a convex polyhedron and the load cases form the vertices of the polyhedron, so they are called *load vertices*.

Let $\boldsymbol{\sigma}_i^E(j)$ be the fictitious elastic stress in the Gaussian point $\mathbf{x}_i$ corresponding to the j-th load vertices. From the principle of superposition for the elastic stresses we derive the convex combination of the stresses $\boldsymbol{\sigma}_i^E(t)$ by

$$\boldsymbol{\sigma}_i^E(t) = \sum_{j=1}^{NV} \lambda_j \boldsymbol{\sigma}_i^E(j). \tag{1.28}$$

For the verification of inequality (1.26) in the point $\mathbf{x}_i$ the reduced verification for the stresses $\boldsymbol{\sigma}_i^E(j)$ is sufficient [47]

$$F(\alpha \boldsymbol{\sigma}_i^E(j) + \bar{\boldsymbol{\rho}}_i) \leq \sigma_{y,i}^2. \tag{1.29}$$

Because of the convexity of F in all $\mathbf{x}_i$ we derive from (1.27)-(1.29) for all $P(j)$

$$\begin{aligned} F[\alpha \boldsymbol{\sigma}_i^E(t) + \bar{\boldsymbol{\rho}}_i] &= F[\alpha \sum_{j=1}^{NV} \lambda_j \boldsymbol{\sigma}_i^E(j) + \bar{\boldsymbol{\rho}}_i] = F[\sum_{j=1}^{NV} \lambda_j (\alpha \boldsymbol{\sigma}_i^E(j) + \bar{\boldsymbol{\rho}}_i)] \\ &\leq \sum_{j=1}^{NV} \lambda_j F[\alpha \boldsymbol{\sigma}_i^E(j) + \bar{\boldsymbol{\rho}}_i] \leq \sum_{j=1}^{NV} \lambda_j \sigma_{y,i}^2 = \sigma_{y,i}^2. \end{aligned} \tag{1.30}$$

The sufficient shakedown conditions (1.26) must be verified only in the load vertices, such that we deduce the discretized minimum problem for the loads for perfectly plastic material

$$\begin{aligned} \max \quad & \alpha \\ \text{s.t.} \quad & F[\alpha \boldsymbol{\sigma}_i^E(j) + \bar{\boldsymbol{\rho}}_i] \ \leq \sigma_{y,i}^2 \quad i = 1, \ldots, NG, \ \ j = 1, \ldots, NV, \ \ \bar{\boldsymbol{\varrho}} \in \mathcal{B}. \end{aligned} \tag{1.31}$$

The unknowns are the time independent residual stresses $\bar{\boldsymbol{\rho}}_i$ and the load factor α. This means a reduction to $NV \cdot NG$ inequality and NF equality constraints, resulting from the yield condition and the equilibrium condition, respectively.

The number of restrictions is finite and for structures with NG Gaussian points we have to handle $O(NG)$ unknowns and $O(NG)$ restrictions. For realistic FEM models of industrial structures no effective solution algorithms for nonlinear optimization problems of such a size are available.

Remark

In the special case of a load domain $\mathcal{L}$ with one dead load P_0 and a variable load $0 \leq P(t) \leq P_{max}$ the conditions (1.31) and (1.13), have the form:

$$\begin{aligned} F[\boldsymbol{\sigma}_{0,i}^E + \bar{\boldsymbol{\rho}}_i] \ &\leq \ \sigma_{y,i}^2 \\ F[\alpha \boldsymbol{\sigma}_i^E(j) + \boldsymbol{\sigma}_{0,i}^E + \bar{\boldsymbol{\rho}}_i] \ &\leq \ \sigma_{y,i}^2. \end{aligned}$$

On the other hand, the convex combination of the load vertices $P_1 = P_0$ and $P_2 = P_0 + P$ gives with $0 \leq \lambda \leq 1$:

$$\lambda P_1 + (1-\lambda) P_2 = \lambda P_0 + (1-\lambda)(P_0 + P) = P_0 + (1-\lambda) P, \tag{1.32}$$

such that the load domain $\mathcal{L}$ is spanned by the load vertices P_1 and P_2. Therefore, by choosing different ratios of P_0 / P_{max} a whole shakedown interaction diagram can be generated with the shakedown analysis (1.31) instead of (1.13).

1.6 Duality

The minimum and maximum problems resulting from the static and kinematic theorems for the discretized structures are dual. In case of limit analysis we give a prove of this statement ([2]).

Let the lower bound problem be the primal problem

$$\begin{aligned} \text{Maximize} \quad & \alpha_s \\ \text{s. t.} \quad & \boldsymbol{f}(\boldsymbol{s}) - \boldsymbol{r} \leq \boldsymbol{0}, \\ & \boldsymbol{C}\boldsymbol{s} - \alpha_s \boldsymbol{p} = \boldsymbol{0}. \end{aligned} \tag{1.33}$$

The quantities in the NG Gaussian points were collected to the vectors $\boldsymbol{f}, \boldsymbol{s}, \boldsymbol{r}$, and $\boldsymbol{p}$ to formulate the matrix notation of the constraints. The unknowns are the limit load factor α_s and the stresses $\boldsymbol{s}$. The minimum problem with restrictions is transformed into an unrestricted problem by the Lagrangian $L(\alpha_s, \boldsymbol{s}, \dot{\boldsymbol{u}}, \boldsymbol{\lambda})$, such that the optimality conditions for unrestricted problems hold (see [2], [7], [30]). With the Lagrange factors $\boldsymbol{\lambda} \geq \boldsymbol{0}$ and $\dot{\boldsymbol{u}}$ it holds

$$L(\alpha_s, \boldsymbol{s}, \dot{\boldsymbol{u}}, \boldsymbol{\lambda}) \;=\; \alpha_s + \dot{\boldsymbol{u}}^T(\boldsymbol{C}\boldsymbol{s} - \alpha_s \boldsymbol{p}) - \boldsymbol{\lambda}^T(\boldsymbol{f}(\boldsymbol{s}) - \boldsymbol{r}). \tag{1.34}$$

In the minimum the Lagrangian $L(\alpha_s, \boldsymbol{s}, \dot{\boldsymbol{u}}, \boldsymbol{\lambda})$ has a saddle point, so that the optimal value is the solution of

$$\min_{\dot{\boldsymbol{u}}, \boldsymbol{\lambda}} \max_{\alpha_s,\, \boldsymbol{s}} L(\alpha_s, \boldsymbol{s}, \dot{\boldsymbol{u}}, \boldsymbol{\lambda}). \tag{1.35}$$

The necessary optimality conditions of the maximum are

$$\frac{\partial L}{\partial \alpha_s} \;=\; 1 - \dot{\boldsymbol{u}}^T \boldsymbol{p} = 0, \tag{1.36}$$

$$\frac{\partial L}{\partial \boldsymbol{s}} \;=\; \dot{\boldsymbol{u}}^T \boldsymbol{C} - \boldsymbol{\lambda}^T \frac{\partial \boldsymbol{f}}{\partial \boldsymbol{s}} = \boldsymbol{0}. \tag{1.37}$$

Equation (1.36) means a normalization of the external power of loading $\dot{W}_{ex} = \dot{\boldsymbol{u}}^T \boldsymbol{p} = 1$ of the discretized structure. By substituting (1.36), (1.37) in the dual objective function $l(\dot{\boldsymbol{u}}, \boldsymbol{\lambda}) = \max\limits_{\alpha_s,\, \boldsymbol{s}} L(\alpha_s, \boldsymbol{s}, \dot{\boldsymbol{u}}, \boldsymbol{\lambda})$, with the Euler PDE for the homogeneous function $\boldsymbol{f}(\boldsymbol{s})$,

$$\boldsymbol{s}^T \frac{\partial \boldsymbol{f}(\boldsymbol{s})}{\partial \boldsymbol{s}} \;=\; \boldsymbol{f}(\boldsymbol{s}), \tag{1.38}$$

and with $\boldsymbol{\lambda} \geq \boldsymbol{0}$ it follows

$$l(\boldsymbol{\lambda}) \;=\; \max_{\alpha_s,\, \boldsymbol{s}} L(\alpha_s, \boldsymbol{s}, \dot{\boldsymbol{u}}, \boldsymbol{\lambda}) = \boldsymbol{\lambda}^T \boldsymbol{r} = \dot{W}_{in}(\dot{e}). \tag{1.39}$$

Equation (1.35) is derived by eq. (1.36), (1.37) and (1.39), such that the dual problem is defined by the non-smooth mathematical program

$$\begin{aligned} \text{Minimize} \quad & \boldsymbol{\lambda}^T \boldsymbol{r} \quad (= \quad \alpha_k) \\ \text{s. t.} \quad & \boldsymbol{\lambda} \geq \boldsymbol{0}, \\ & \dot{\boldsymbol{u}}^T \boldsymbol{p} = 1, \\ & \boldsymbol{C}^T \dot{\boldsymbol{u}} - \boldsymbol{\lambda}^T \frac{\partial \boldsymbol{f}}{\partial \boldsymbol{s}} = \boldsymbol{0}. \end{aligned} \tag{1.40}$$

Because of the normalization $\dot{W}_{ex} = \dot{\boldsymbol{u}}^T \boldsymbol{p} = 1$ it holds $\alpha_k = l(\boldsymbol{\lambda}) = \dot{W}_{in}(\dot{\boldsymbol{e}})$.

The Lagrange factors of the primal problem are the unknowns of the dual problem. The dual problem is formulated in the kinematic terms $\dot{\boldsymbol{u}}$ and $\boldsymbol{\lambda}$. With

$$\dot{\boldsymbol{e}}^p \;=\; \boldsymbol{\lambda}^T \frac{\partial \boldsymbol{f}(\boldsymbol{s})}{\partial \boldsymbol{s}} \tag{1.41}$$

(1.37) could be formulated for the associated flow rule and $\dot{\boldsymbol{e}}^p = \dot{\boldsymbol{e}}$ in the collapse state

$$\boldsymbol{C}^T \dot{\boldsymbol{u}} - \dot{\boldsymbol{e}} = \boldsymbol{0}, \tag{1.42}$$

which is automatically satisfied in a displacement FEM discretization. Equation (1.21) shows that $\boldsymbol{\lambda}$ may be replaced by the collection of effective strain rates $\dot{\boldsymbol{e}}_{eq}$ and always $\boldsymbol{\lambda} = \dot{\boldsymbol{e}}_{eq} \geq \boldsymbol{0}$ by inequality (1.20). Then the dual problem reduces to

$$\begin{aligned} \text{Minimize} \quad & \dot{\boldsymbol{e}}_{eq}^T \boldsymbol{r} \quad (= \quad \alpha_k) \\ \text{s. t.} \quad & \dot{\boldsymbol{u}}^T \boldsymbol{p} = 1. \end{aligned} \tag{1.43}$$

The saddle point properties of the Lagrangian show, that the maximum problem is concave and the minimum problem in convex such that both problem have the same optimal value

$$\max \alpha_s = \alpha = \min \alpha_k. \tag{1.44}$$

Because of the convexity of the problem the obtained local optimum is a global one (see [2], [7]) such that the limit load factor is unique.

2 The basis reduction technique

For a Finite Element (FE) discretization a finite but generally large number of constraints is achieved. The basis reduction method keeps only a small number of unknowns. It was developed for linear optimization in [43] making use of the special structure of the shakedown problem for perfectly plastic material. In the same constitutive setting the method has been extended to nonlinear optimization in [10], [14], [46], [64].

Instead of searching the whole vector space $\mathcal{B}$ for a solution of the maximum problem, a d–dimensional subspace $\mathcal{B}_d$ is searched. In the k-th step of the algorithm different subspaces $\mathcal{B}_d^k$ are chosen iteratively to improve the obtained load factor α^k. The dimension of the chosen subspace is rather small compared to the dimension of $\mathcal{B}$, we use typically $\dim \mathcal{B}_d^k \leq 6$. The subspaces $\mathcal{B}_d^k \subset \mathcal{B}$ could be generated by d linear independent base vectors $\mathbf{b}_i^k$, such that for all $\boldsymbol{\rho}^k \in \mathcal{B}_d^k$ there exists $\mu_1, \ldots, \mu_d \in I\!R$ with

$$\boldsymbol{\rho}^k = \mu_1 \mathbf{b}_1^k + \mu_2 \mathbf{b}_2^k + \ldots + \mu_d \mathbf{b}_d^k. \tag{2.1}$$

Instead of the unknown residual stresses $\boldsymbol{\rho} \in \mathcal{B}^d$ the unknowns $\mu_1, \ldots, \mu_d$ are chosen. If we collect the base vectors $\mathbf{b}_i^k,\ i = 1, \ldots, d$ of $\mathcal{B}_d^k \subset \mathcal{B}$ to a matrix $\mathbf{B}^{d,k}$ it holds

$$\mathbf{B}^{d,k} = \left(\mathbf{b}_1^k, \ldots, \mathbf{b}_d^k\right),$$

such that for all $\boldsymbol{\rho}^k \in \mathcal{B}_d^k$ exists a vector $\boldsymbol{\mu}^k = (\mu_1^k, \ldots, \mu_d^k)^T \in I\!R^d$ with

$$\boldsymbol{\rho}^k = \mu_1 \mathbf{b}_1^k + \ldots + \mu_d \mathbf{b}_d^k = \mathbf{B}^{d,k} \boldsymbol{\mu}^k.$$

With the load factor α^{k-1} and the stresses $\boldsymbol{\rho}^{k-1}$ ($\boldsymbol{\rho}^0 = \mathbf{0}$) resulting from the step $k-1$ of the algorithm the new problem in $\mathcal{B}_d^k$ is given by

$$\begin{aligned} &\max \quad \alpha^k \\ &\text{s.t.} \quad F[\alpha^k \boldsymbol{\sigma}_i^E(j) + \boldsymbol{\rho}_i^{k-1} + \mathbf{B}_i^{d,k} \bar{\boldsymbol{\mu}}^k] \ \leq \sigma_{y,i}^2 \qquad i = 1, \ldots, NG, j = 1, \ldots, NV, \bar{\boldsymbol{\mu}}^k \in I\!R^d. \end{aligned} \tag{2.2}$$

This problem has $d+1$ unknowns (α^k and $\boldsymbol{\mu}^k$) and $NG \cdot NV$ restrictions. This basis reduction technique is well known in the field of optimization. Instead of searching the whole feasible region for the optimum a search direction (one– or small dimensional) is chosen to find the best value in this direction (see ([2], [7]). A sketch of this method for a two dimensional feasible region is shown in Fig. 2.1. The subspaces are chosen as one dimensional search directions such that each search step is one step k in the subspace technique.

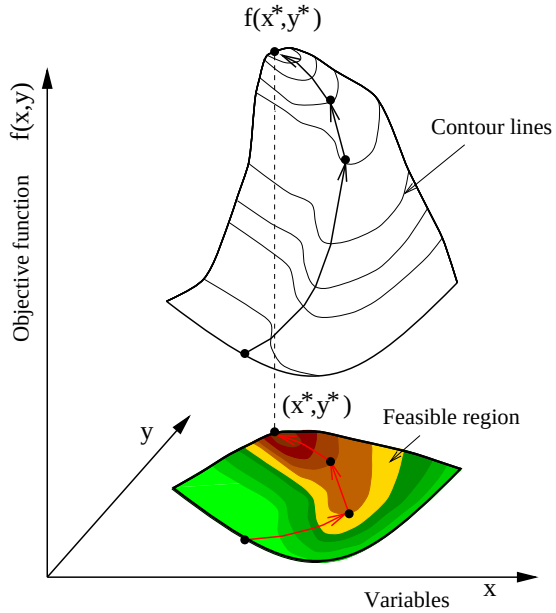

Figure 2.1: Sketch of the subspace technique for optimization problems

It has to be clarified how the base vectors of the residual subspace $\mathcal{B}_d^k$ have to be chosen, such that the optimum in the residual stress space $\mathcal{B}$ will be reached. Further it has to be pointed out if it is possible to guarantee that every step yields an improvement of the load factor α^k.

2.1 Generation of residual stress space $\mathcal{B}_d$

Some authors offer different methods for the generation of the residual stress space. Shen suggests in [43] a method for generating the residual stress space with FEM. The base vectors are calculated by an equilibrium iteration. Gross–Weege and Weichert suggest in [10] a modified method. Buckthorpe and White calculate the base vectors by thermal loading ([4], [5]), because all thermal stresses are residual stresses. We will follow the method of Shen, because of its easy implementation into a commercial FEM-Code.

The base vectors of $\mathcal{B}_d$ are generated by an equilibrium iteration with the FEM-Code PERMAS V4 (see [36]). By using a general purpose FE-Code it is possible to treat all loading cases, element types and structures. The basis reduction technique could be implemented in all FE-Codes which could generate plastic stresses and residual stress bases.

In the plastic part of the equilibrium iteration in PERMAS V4 additional load increments were applied iteratively. The following algorithm is implemented in PERMAS V4. For the special nomenclature see also [1], [36], [43].

Starting from the actual nodal stress and strain $\boldsymbol{\sigma}_0$ and $\boldsymbol{\varepsilon}_0$, respectively, resulting from the preceeding load step, the following steps are performed

1. The plastic strain increment $\boldsymbol{\varepsilon}^P_\Delta$ is derived from the estimated equivalent plastic strain increment $\varepsilon^P_{eq\Delta}$ and a nodal stress $\boldsymbol{\sigma^d}$ proportional to the deviator of $\boldsymbol{\sigma}$:

$$\boldsymbol{\varepsilon}^P_\Delta = \varepsilon^P_{eq\Delta}\, \boldsymbol{\sigma^d}.$$

2. With the elastic material stiffness matrix $\mathbf{E}$ the initial elemental nodal load increment $\mathbf{J}_{p\Delta}$ is calculated

$$\mathbf{J}_{p\Delta} = -h\mathbf{E}\, \boldsymbol{\varepsilon}^P_\Delta.$$

3. The total nodal load increment $\mathbf{p}_{t\Delta}$ of the assembled structure is generated by the total initial load increment $\mathbf{p}_{\Delta 1}$, the $\mathbf{J}_{p\Delta}$ and the element matrix $\mathbf{a}$ by

$$\mathbf{p}_{t\Delta} = \mathbf{p}_{\Delta 1} - \mathbf{a}^T\, \mathbf{J}_{p\Delta}.$$

4. The nodal displacement increment $\mathbf{u}_\Delta$ is calculated with the structural stiffness matrix $\mathbf{K}$ from

$$\mathbf{u}_\Delta = \mathbf{K}^{-1}\, \mathbf{p}_{t\Delta}.$$

5. The element nodal displacement increments $\mathbf{u}^e_\Delta$ are

$$\mathbf{u}^e_\Delta = \mathbf{a}\, \mathbf{u}_\Delta.$$

6. By the strain-displacement matrix $\mathcal{D}$, the elastic material stiffness $\mathbf{E}$ the fictitious stress increments $\boldsymbol{\sigma}_{t\Delta}$ are calculated:

$$\boldsymbol{\sigma}_{t\Delta} = \mathbf{E}\, \mathcal{D}\, \mathbf{u}^e_\Delta.$$

7. The actual nodal stress increment $\boldsymbol{\sigma}_\Delta$ is derived from $\boldsymbol{\sigma}_{t\Delta}$ and $\boldsymbol{\varepsilon}^P_\Delta$

$$\boldsymbol{\sigma}_\Delta = \boldsymbol{\sigma}_{t\Delta} - \mathbf{E}\,\boldsymbol{\varepsilon}^P_\Delta.$$

8. Now the actual nodal stresses are the sum of the initial nodal stresses $\boldsymbol{\sigma}_0$ and the nodal stress increment $\boldsymbol{\sigma}_\Delta$

$$\boldsymbol{\sigma} = \boldsymbol{\sigma}_0 + \boldsymbol{\sigma}_\Delta.$$

9. From the actual nodal stresses the equivalent plastic strain increment $\varepsilon^P_{eq\Delta}$ is generated and the convergence is analyzed.

If the given convergence criterion is fulfilled the new initial nodal stresses $\boldsymbol{\sigma}_0 = \boldsymbol{\sigma}$ and a new load increment $\mathbf{p}_{\Delta 1}$ are defined. Otherwise, all steps are repeated with the new equivalent plastic strain increment $\varepsilon^P_{eq\Delta}$ and the old load increment $\mathbf{p}_{\Delta 1}$. The stiffness matrix is not updated during the iteration, because this would be ineffective for large structures (see [44] and [11] for an updating schema of the stiffness matrix). In the conventional algorithm the iteration is repeated until convergence is reached.

In the basis reduction technique we define a residual nodal stress by $\boldsymbol{\rho} = \boldsymbol{\sigma}_m - \boldsymbol{\sigma}_n$ following a suggestion in [43]. The nodal stresses $\boldsymbol{\sigma}_m,\ \boldsymbol{\sigma}_n$ are calculated during one iteration corresponding to the same load increment $\mathbf{p}_{\Delta 1}$ for different iteration steps m, n. The static equilibrium conditions of the discretized structure to the load increment $\mathbf{p}$ are:

$$\mathbf{p} = \mathbf{K}\mathbf{u} + \mathbf{a}^T\mathbf{J}_{p\Delta}.$$

For the nodal stresses $\boldsymbol{\rho} = \boldsymbol{\sigma}_m - \boldsymbol{\sigma}_n$ it yields

$$\begin{aligned} \mathbf{p} &= \mathbf{p}_m - \mathbf{p}_n = \mathbf{K}(\mathbf{u}_m - \mathbf{u}_n) + \mathbf{a}^T(\mathbf{J}_{p\Delta m} - \mathbf{J}_{p\Delta n}) \\ &= [\mathbf{p}_{\Delta 1} - \mathbf{a}^T\,\mathbf{J}_{p\Delta m} - \mathbf{p}_{\Delta 1} + \mathbf{a}^T\,\mathbf{J}_{p\Delta n}] + \mathbf{a}^T(\mathbf{J}_{p\Delta m} - \mathbf{J}_{p\Delta n}) = 0, \end{aligned} \qquad (2.3)$$

such that $\boldsymbol{\rho}$ is in fact a residual nodal stress. For the generation of a d–dimensional residual subspace $\mathcal{B}_d$ we iterate $d+1$ times to get the nodal stresses $\boldsymbol{\sigma}^1, \ldots, \boldsymbol{\sigma}^{d+1}$ and the differences $\boldsymbol{\rho}_1 = \boldsymbol{\sigma}^2 - \boldsymbol{\sigma}^1,\ \ldots,\ \boldsymbol{\rho}_d = \boldsymbol{\sigma}^{d+1} - \boldsymbol{\sigma}^1$. All $\boldsymbol{\rho}_1, \ldots, \boldsymbol{\rho}_d$ are residual nodal stresses if the iteration converges or not.

In shakedown analyses NV load vertices have to be considered in every step k. In order to obtain an effective algorithm, a new load increment $\mathbf{p}_j$ is defined only in the active load vertices of the preceding load step $k-1$ to generate j^0_d new base vectors. The number of base vectors is restricted to 3,. . .,6, such that eventually not all active load vertices generate the same number of base vectors. Nevertheless, usually all active load vertices are taken into consideration. By iterating this base vector generation, a d–dimensional subspace $\mathcal{B}^k_d$ of the residual stress space $\mathcal{B}$ is obtained in every step k. In the subspace $\mathcal{B}^k_d$ the problem (2.2) is solved and one gets the improved solutions α_k and $\boldsymbol{\rho}_k$. These values are the new starting values for the next iteration step $k+1$.

2.2 A convergence criterion

The main objective of this section is a criterion which guarantees, that in every new subspace $\mathcal{B}_d^k$ of the residual stress space $\mathcal{B}$ an improvement of the load factor α^k is obtained (i.e. $\alpha^k - \alpha^{k-1} > 0$). For 2–dimensional problems a similar criterion is achieved in [64]. The criterion below is an extension of this criterion to 3–dimensional problems. Let $\mathbf{b}_i^{1,k}$ a base vector of an one-dimensional subspace $\boldsymbol{\mathcal{B}}^{1,k}$ of $\boldsymbol{\mathcal{B}}^d$. In step $k-1$ the load factor α^{k-1} and the residual stresses $\boldsymbol{\rho}^{k-1}$ are known, such that

$$\boldsymbol{\sigma}_i^{k-1} = \alpha^{k-1}\boldsymbol{\sigma}_i^E + \boldsymbol{\rho}_i^{k-1}. \tag{2.4}$$

We search a base vector $\mathbf{b}^{1,k}$ such that the increase $\Delta\alpha = \alpha^k - \alpha^{k-1}$ is maximal. This means a solution $(\Delta\alpha^k,\ u^k)$ is searched of

$$\begin{aligned} &\Delta\alpha^k \rightarrow \max \\ &F(\alpha^k\boldsymbol{\sigma}_i^E + \boldsymbol{\rho}_i^{k-1} + \mathbf{b}_i^{1,k}u^k) = F(\boldsymbol{\sigma}_i^{k-1} + \Delta\alpha^k\boldsymbol{\sigma}_i^E + \mathbf{b}_i^{1,k}u^k) \leq \sigma_y^2 \ \ \forall\, i \in I \end{aligned} \tag{2.5}$$

with $\Delta\alpha > 0$. In step $k-1$ not the whole structure reaches the yield stress in all Gaussian points. We split the set of indices I in the set of active indices $\mathcal{A}^{k-1}$ and the set of inactive indices $\mathcal{C}^{k-1}$, such that $I = \mathcal{A}^{k-1} \cup \mathcal{C}^{k-1}$ and $\mathcal{A}^{k-1} \cap \mathcal{C}^{k-1} = \emptyset$. It follows

$$F(\boldsymbol{\sigma}_i^{k-1}) = \sigma_y^2 \ \ \forall\, i \in \mathcal{A}^{k-1}. \tag{2.6}$$

Gaussian points corresponding to inactive indices $i \in I \setminus \mathcal{A}^{k-1}$ admit a small additional load increment, such that they are not taken into consideration further. We consider only such indices $i \in \tilde{\mathcal{A}}^{k-1} \subseteq \mathcal{A}^{k-1}$ such that the stresses in the corresponding Gaussian points further reach the yield limit due to an increase of the load increment. The Gaussian points corresponding to the indices $i \in \mathcal{A}^{k-1} \setminus \tilde{\mathcal{A}}^{k-1}$ are relieved from stress, such that we study the following optimization problem

$$\begin{aligned} &\Delta\alpha \rightarrow \max \\ &F(\boldsymbol{\sigma}_i^{k-1} + \Delta\alpha\boldsymbol{\sigma}_i^E + u^k\mathbf{b}_i^{1,k}) \leq \sigma_y^2 \ \ \forall\, i \in \tilde{\mathcal{A}}^{k-1} \end{aligned} \tag{2.7}$$

The next lemma is an extension of the 2-dimensional one (see [64]) to the 3-dimensional case. The proof is given in [14]

Lemma

The problem (2.7) has a solution $(\Delta\alpha^k,\ u^k)$ with $\Delta\alpha^k > 0$, if and only if either

$$\left.\frac{\partial F}{\partial \boldsymbol{\sigma}}\right|_{\boldsymbol{\sigma}_i^{k-1}} \cdot \mathbf{b}_i^{1,k} < 0 \ \ \forall\, i \in \tilde{\mathcal{A}}^{k-1}$$

or

$$\left.\frac{\partial F}{\partial \boldsymbol{\sigma}}\right|_{\boldsymbol{\sigma}_i^{k-1}} \cdot \mathbf{b}_i^{1,k} > 0 \ \ \forall\, i \in \tilde{\mathcal{A}}^{k-1} \text{ holds.}$$

The residual stresses bases are generated by the equilibrium iteration by PERMAS in the given way. If the equilibrium iteration converges, then the residual stresses fulfill the assumptions of the lemma. This is derived from the vanishing of the $\dot{\varepsilon}^p$ during the convergence and the convexity of the yield surface. Thus we have to guarantee, that the applied load increment is lower than the limit or shakedown load. In general the limit or shakedown load is unknown, such that we have to apply a strategy for the decrease of the load increments. Additionally the load increments have to be chosen such that the *constraint qualifications* (see [2], [7]) of the optimization problem are fulfilled. This means that the generated residual base vectors are linearly independent. In all limit load models a bisection of the load increments after 2 or 3 load steps yields good convergences. For all models with known analytic solution of the limit loads the solution is achieved within 10 iteration steps with an error of 5 %. After 20 iteration steps the error is typically less than 1–2 %, so we limit the number of steps to 20. Shakedown analysis is typically much faster.

If the applied load increment exceeds the limit or shakedown load, we could not guarantee that we get an improved load factor, but the base vectors are still residual stresses. Nevertheless, after the next bisection of the applied load increment we get an improved load factor.

3 Mathematical optimization techniques

In this section the mathematical basis for the solution of the limit and shakedown analysis is given (see [37], [38], [39], [40], [41] and [42]). The constrained optimization problems were analyzed and a strategy based on a Sequential Quadratic Programming (SQP) algorithm is derived. Because of the special structure of the optimization problem and the close connection to the FEM-code PERMAS a self-implemented version of the SQP-algorithm is used instead of a commercial mathematical software like LANCELOT or MINOS (see [6], [35]). The complete algorithm is summarized in the flowchart in fig. 3.1

The mathematical formulation of the shakedown analysis in step k of the SQP-algorithm is given. The limit analysis can be derived by modifying the structure for one load vertex.

(OP')	Maximize	α^k
	s.t.	$F(\alpha^k \boldsymbol{\sigma}_i^E(j) + \boldsymbol{\rho}_i^{k-1} + \mathbf{B}_i^{d,k}\mathbf{x}) \leq \sigma_y^2 \quad \forall\, i \in \mathcal{I},\ j \in \mathcal{J}$

with the fictitious elastic stresses $\boldsymbol{\sigma}_i^E(j)$ corresponding to the Gaussian point i and to the load j. All stresses were handled as vectors. The $\mathbf{B}_i^{d,k}$ are generated by the basis vectors of the subspace $\mathcal{B}^d$ ($d = \dim \mathcal{B}^d$) of point i in the k–th step of the iteration. $\mathbf{x}$ is the vector of the coefficients of the basis vectors (see eq. (2.2)).

The indices k and d from α^k and $\mathbf{B}_i^{d,k}$ are omitted in this section for abbreviation. Let $\boldsymbol{\rho}_i^{k-1}$ be the optimal residual stress of iteration step $k-1$ of point i to the load j (with $\boldsymbol{\rho}^0 = \mathbf{0}$). Let $|\mathcal{I}| = NG$ and $|\mathcal{J}| = NV$ be the number of Gaussian points and the number of load

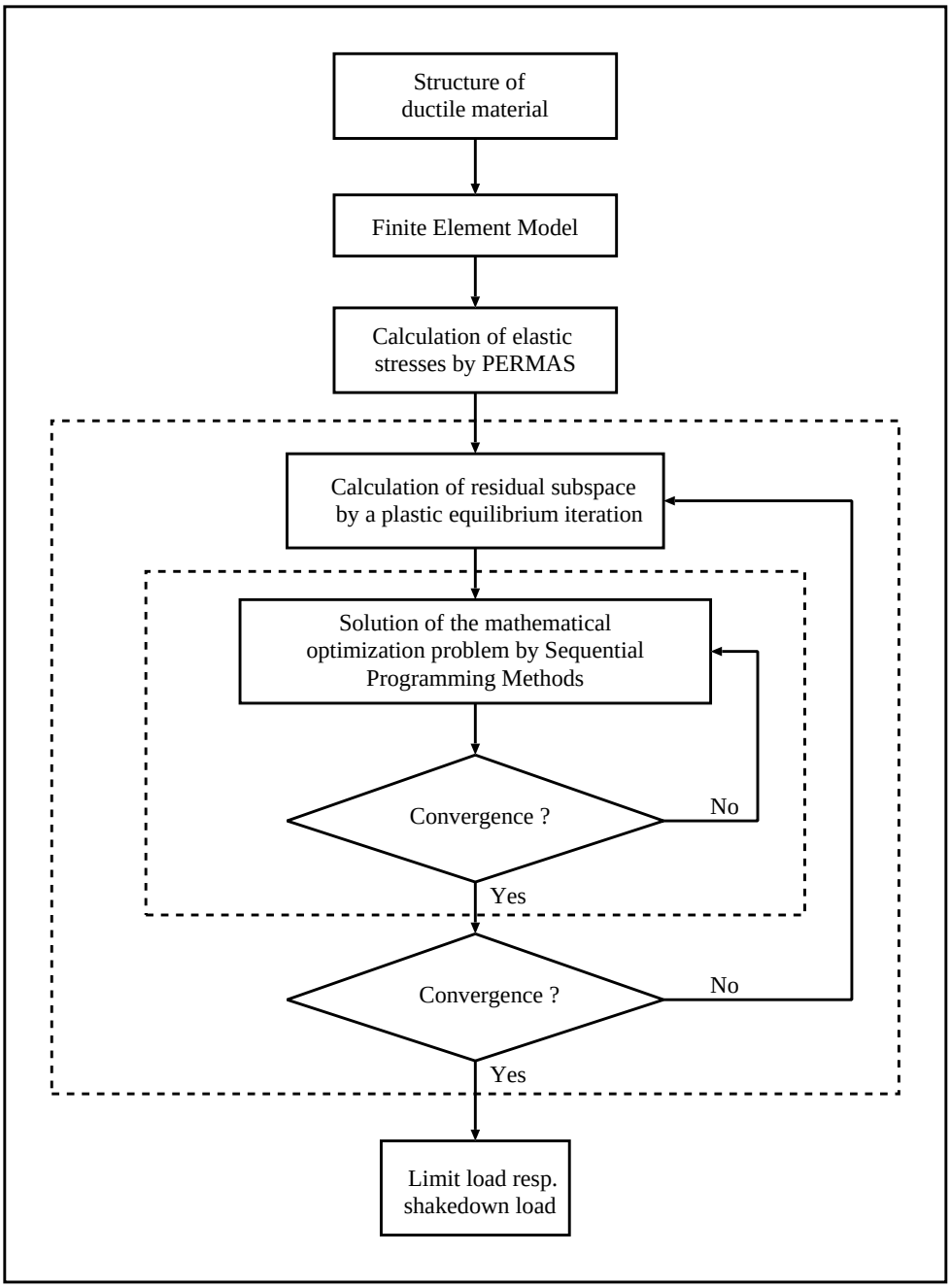

Figure 3.1: Flowchart of lower bound limit and shakedown analyses

vertices, respectively. With the definition $F(\boldsymbol{\sigma}) = \boldsymbol{\sigma}^T \mathbf{Q} \boldsymbol{\sigma}$ it holds for the constraints holds:

$$\begin{aligned} & F(\alpha \boldsymbol{\sigma}_i^E(j) + \boldsymbol{\rho}_i^{k-1} + \mathbf{B}_i \mathbf{x}) && (3.1) \\ = \;& \alpha^2 F(\boldsymbol{\sigma}_i^E(j)) + 2\alpha (\boldsymbol{\sigma}_i^E(j))^T \mathbf{Q} (\mathbf{B}_i \mathbf{x}) + F(\mathbf{B}_i \mathbf{x}) \\ + \;& 2\alpha (\boldsymbol{\sigma}_i^E(j))^T \mathbf{Q} \boldsymbol{\rho}_i^{k-1} + 2(\boldsymbol{\rho}_i^{k-1})^T \mathbf{Q} (\mathbf{B}_i \mathbf{x}) + F(\boldsymbol{\rho}_i^{k-1}) \\ = \;& \alpha^2 a_i(j) + 2\alpha \mathbf{b}_i^T(j) \mathbf{x} + \mathbf{x}^T \mathbf{C}_i(j) \mathbf{x} + 2\alpha d_i(j) + 2\mathbf{e}_i^T(j) \mathbf{x} + f_i && (3.2) \end{aligned}$$

$$\begin{aligned} \text{with} \qquad a_i(j) &= F(\boldsymbol{\sigma}_i^E(j)) \in I\!R & d_i(j) &= (\boldsymbol{\sigma}_i^E(j))^T \mathbf{Q} \boldsymbol{\rho}_i^{k-1} \in I\!R \\ \mathbf{b}_i(j) &= \mathbf{B}_i^T(j) \mathbf{Q} \boldsymbol{\sigma}_i^E(j) \in I\!R^{\,d} & \mathbf{e}_i(j) &= \mathbf{B}_i^T(j) \mathbf{Q} \boldsymbol{\rho}_i^{k-1} \in I\!R^d \\ \mathbf{C}_i(j) &= \mathbf{B}_i^T(j) \mathbf{Q} \mathbf{B}_i \in I\!R^{\,d \times d} & f_i &= F(\boldsymbol{\rho}_i^{k-1}) \in I\!R \end{aligned} \qquad (3.3)$$

and for 3-dimensional problems it holds

$$\mathbf{Q}_3 = \left(\begin{array}{ccc|ccc} 1 & -0.5 & -0.5 & 0 & 0 & 0 \\ -0.5 & 1 & -0.5 & 0 & 0 & 0 \\ -0.5 & -0.5 & 1 & 0 & 0 & 0 \\ \hline 0 & 0 & 0 & 3 & 0 & 0 \\ 0 & 0 & 0 & 0 & 3 & 0 \\ 0 & 0 & 0 & 0 & 0 & 3 \end{array} \right). \qquad (3.4)$$

In point i to the load j (and with the abbreviation $\cdot\,|_{i,j}$) it holds with $\mathbf{B}_i = (b_{kl})_{k,l}\,|_{i,j}$ and $\mathbf{Q} = (q_{kl})_{k,l}$:

$$\mathbf{C}_i(j) = \left(\begin{array}{ccc} b_{11} & \dots & b_{m1} \\ \vdots & & \vdots \\ b_{1d} & \dots & b_{md} \end{array} \right) \left(\begin{array}{ccc} q_{11} & \dots & q_{1m} \\ \vdots & & \vdots \\ q_{m1} & \dots & q_{mm} \end{array} \right) \left(\begin{array}{ccc} b_{11} & \dots & b_{1d} \\ \vdots & & \vdots \\ b_{m1} & \dots & b_{md} \end{array} \right) \Bigg|_{i,j} \qquad (3.5)$$

$$= \left(\begin{array}{ccc} \sum_{k=1}^m \sum_{l=1}^m b_{k1} q_{kl} b_{l1} & \dots & \sum_{k=1}^m \sum_{l=1}^m b_{k1} q_{kl} b_{ld} \\ \vdots & & \vdots \\ \sum_{k=1}^m \sum_{l=1}^m b_{kd} q_{kl} b_{l1} & \dots & \sum_{k=1}^m \sum_{l=1}^m b_{kd} q_{kl} b_{ld} \end{array} \right) \Bigg|_{i,j} \qquad (3.6)$$

$\mathbf{C}_i(j)$ is symmetric by definition and therefore it holds

$$\mathbf{D}_i(j) = \left(\begin{array}{c|c} a_i(j) & \mathbf{b}_i^T(j) \\ \hline \mathbf{b}_i(j) & \mathbf{C}_i(j) \end{array} \right) \in I\!R^{(d+1)\times(d+1)}.$$

With $\mathbf{y} = (\alpha, \mathbf{x})^T \in I\!R^{d+1}$ and $\mathbf{F}_i(j) = (d_i(j), \mathbf{e}_i(j))$ it follows for the constraints of the problem (OP') with equation (3.1)

$$F(\alpha \boldsymbol{\sigma}_i^E(j) + \boldsymbol{\rho}_i^{k-1}(j) + \mathbf{B}_i \mathbf{x}) = \mathbf{y}^T \mathbf{D}_i(j) \mathbf{y} + 2\mathbf{F}_i(j) \mathbf{y} + f_i \quad \forall\, i \in \mathcal{I},\ j \in \mathcal{J}.$$

$\mathbf{Q}$ is positive definite in the deviatoric stress space and the same holds for $\boldsymbol{D}_i(j)$. From now on, we analyze the following optimization problem with linear objective function and quadratic constraints

$$\begin{array}{lll} \text{(OP)} & \text{Minimize} & -y_1 \\ & \text{s.t.} & -\mathbf{y}^T\mathbf{D}_i(j)\mathbf{y} - 2\mathbf{F}_i(j)\mathbf{y} - f_i + \sigma_y^2 \geq 0 \quad \forall\, i \in \mathcal{I},\ j \in \mathcal{J}. \end{array}$$

Remark

By scaling the constraints of (OP) with a constant factor t^2, i.e. by considering the problem

$$-t^2\mathbf{y}^T\mathbf{D}_i(j)\mathbf{y} - 2t^2\mathbf{F}_i(j)\mathbf{y} - t^2 f_i + t^2\sigma_y^2 \geq 0 \quad \forall\, i \in \mathcal{I},\ j \in \mathcal{J},$$

the solution of the optimization problem is not changed. The scaled constraints of problem (OP') are

$$F(\alpha t\boldsymbol{\sigma}_i^E(j) + t\boldsymbol{\rho}_i^{k-1} + t\mathbf{B}_i\mathbf{x}) \leq (t\sigma_y)^2 \quad \forall\, i \in \mathcal{I},\ j \in \mathcal{J}.$$

If we consider the stresses $\boldsymbol{\sigma}^E$, $\boldsymbol{\rho}^{k-1}$ and the matrix $\mathbf{B}$ of point i and load j the optimal value is not changed. In the case of numerical instabilities based on nearly singular matrices it is of benefit to use scaled stresses.

The idea of the SQP-algorithm is to replace a nonlinear problem by a sequence of quadratic subproblems. The sequence of solutions of the subproblems converges to the solution of the original problem. Therefore, we define the following general nonlinear problem by

$$\begin{array}{lll} \text{(GNP)} & \text{Minimize} & f(\mathbf{x}) \\ & \text{s.t.} & g_i(\mathbf{x}) \geq 0 \qquad\qquad \forall\, i \in \mathcal{I}, \end{array}$$

with $\mathbf{x} \in I\!R^n$ and $f, g_i : I\!R^n \rightarrow I\!R\ \forall\, i \in \mathcal{I}$. Let $\mathcal{R}$ (*feasible region*) be the set of admissible points for (GNP), i. e. $\mathcal{R} = \{\mathbf{x} \in I\!R^n | g_i(\mathbf{x}) \geq 0, i \in \mathcal{I}\}$. In general not every constraint g is active ($g_i(\mathbf{x}) = 0$) in a point **x** of the feasible region. So we define the active mapping by

$$\mathcal{I}_0(\mathbf{x}) = \{i \in \mathcal{I} | g_i(\mathbf{x}) = 0\}.$$

Let $\mathcal{T}_{\mathbf{x}}(\mathcal{R})$ be the tangential space of $\mathcal{R}$ in point **x**

$$\mathcal{T}_{\mathbf{x}}(\mathcal{R}) = \{\boldsymbol{\xi} \in I\!R^n | \boldsymbol{\xi}^T\nabla g_i(\mathbf{x}) = 0,\ i \in \mathcal{I}\}.$$

We define the Lagrangian function L of the problem (GNP) by

$$\mathrm{L}(\mathbf{x}, \boldsymbol{\mu}) = f(\mathbf{x}) - \sum_{i \in \mathcal{I}} \mu_i g_i(\mathbf{x}).$$

Let $\mathbf{x}^* \in \mathcal{R}$ be a local minimum of the problem (GNP) and the *constraint qualifications* are fulfilled in $\mathbf{x}^*$ (e.g. if the vectors $\nabla g_i(\mathbf{x}^*)$ are linear independent for $i \in \mathcal{I}_0(\mathbf{x}^*)$) then there exists Lagrangian multipliers μ_i^* such that with $\nabla(\cdot) = \left(\frac{\partial(\cdot)}{\partial x_1}, \ldots, \frac{\partial(\cdot)}{\partial x_n}\right)^T$ holds

1)
$$\begin{aligned} \mu_i^* &\geq 0\,, \quad \forall\, i \in \mathcal{I} \\ \mu_i^* g_i(\mathbf{x}^*) &= 0\,, \quad \forall\, i \in \mathcal{I} \\ \nabla \mathrm{L}(\mathbf{x}^*, \boldsymbol{\mu}^*) &= \mathbf{0}\,, \end{aligned}$$
2)
$$\boldsymbol{\xi}^T \nabla^2 \mathrm{L}(\mathbf{x}^*, \boldsymbol{\mu}^*) \boldsymbol{\xi} \geq 0 \quad \forall\, \boldsymbol{\xi} \in \mathcal{T}_{\mathbf{X}^*}(\mathcal{R}).$$

The first necessary condition is called Kuhn-Tucker–condition. It means that in a local minimum the gradient of the objective function is a positive linear combination of the gradients of the constraints. The second necessary condition means, that $\nabla^2 \mathbf{L}(\mathbf{x}^*, \boldsymbol{\mu}^*)$ is positive semi-definite on the tangential space $\mathcal{T}_{\mathbf{X}^*}(\mathcal{R})$.

The condition $\mu_i^* g_i(\mathbf{x}^*) = 0 \;\forall\; i \in \mathcal{I}$ is the *complementary conditions*, because it holds $\mu_i = 0$ for $i \in \mathcal{I} \setminus \mathcal{I}_0(\mathbf{x}^*)$, such that the Lagrangian multipliers vanish in the inactive constraints. With the complementary condition and the Lagrangian multipliers μ_i^* we write the first necessary condition of a minimum $\mathbf{x}^*$ only in the active constraints:

1')
$$\begin{aligned} \mu_i^* &\geq 0\,, \qquad \forall\, i \in \mathcal{I}_0(\mathbf{x}^*) \\ \sum_{i \in \mathcal{I}_0(\mathbf{X}^*)} \mu_i^* \nabla g_i(\mathbf{x}^*) &= \nabla f(\mathbf{x}^*). \end{aligned}$$

If a point $\mathbf{x}^* \in \mathcal{R}$ with the Lagrangian multipliers μ_i^* fulfills additionally to the Kuhn-Tucker-conditions the conditions

1. $\mu_i^* > 0 \;\forall\; i \in \mathcal{I}_0(\mathbf{x}^*)$
2. $\nabla^2 \mathrm{L}(\mathbf{x}^*, \boldsymbol{\mu}^*)$ is positive definite on $\mathcal{T}_{\mathbf{X}^*}(\mathcal{R})$

then $\mathbf{x}^*$ is a local minimum of the problem (GNP). Instead of solving the problem (GNP) the SQP-algorithm analyzes linearized constraints and a quadratic approximation of the objective function. If we expand the objective function f in the kth step of the SQP-algorithm in a Taylor series in points $\mathbf{x}_k$ of (GNP) it holds

$$\begin{aligned} f(\mathbf{x}) &= f(\mathbf{x}_k) + \nabla f(\mathbf{x}_k)(\mathbf{x} - \mathbf{x}_k) + \frac{1}{2}(\mathbf{x} - \mathbf{x}_k)^T \nabla^2 f(\mathbf{x}_k)(\mathbf{x} - \mathbf{x}_k) + \ldots \\ g(\mathbf{x}) &= g(\mathbf{x}_k) + \nabla g(\mathbf{x}_k)(\mathbf{x} - \mathbf{x}_k) + \ldots \end{aligned} \tag{3.7}$$

If we use only the first order expansion we derive the algorithm of the Sequential Linear Programming (SLP) (see [32]). The SQP-algorithm yields a better approximation, because the structure of the problem could be modeled more precisely.

We define $\mathbf{d} = \mathbf{x} - \mathbf{x}_k$ as search direction in (3.7), such that we derive the transformation

$$\begin{array}{lll} \text{Minimize} & \frac{1}{2}\mathbf{d}^T \nabla^2 f(\mathbf{x}_k)\mathbf{d} + \nabla f(\mathbf{x}_k)\mathbf{d} + f(\mathbf{x}_k) & \\ \text{s.t.} & \nabla g_i^T(\mathbf{x}_k)\mathbf{d} + g_i(\mathbf{x}_k) \geq 0 & \forall\, i \in \mathcal{I}. \end{array}$$

The optimal value of a problem with a translated objective function by a scalar is the same as the original optimal value. With the approximation $\mathbf{A}_k \approx \nabla^2 f(\mathbf{x}_k)$ we derive the problem

$$\begin{array}{lll} \text{(QP)} \quad \text{Minimize} & \frac{1}{2}\mathbf{d}^T \mathbf{A}_k \mathbf{d} + \nabla f(\mathbf{x}_k)\mathbf{d} & \\ \text{s.t.} & \nabla g_i^T(\mathbf{x}_k)\mathbf{d} + g_i(\mathbf{x}_k) \geq 0 & \forall\, i \in \mathcal{I}. \end{array}$$

This problem has the unknowns $\mathbf{d} \in I\!R^n$ and the feasible region

$$\mathcal{R}' = \{\mathbf{d} \in I\!R^n | \nabla g_j^T(\mathbf{x}_k)\mathbf{d} + g_i(\mathbf{x}_k) \geq 0, i \in \mathcal{I}\}.$$

The Lagrangian function L is given by

$$\begin{aligned} \mathrm{L}(\mathbf{d}, \boldsymbol{\mu}) &= \frac{1}{2}\mathbf{d}^T\mathbf{A}_k\mathbf{d} + \nabla f(\mathbf{x}_k)\mathbf{d} - \sum_{i\in\mathcal{I}} \mu_i(\nabla g_i(\mathbf{x}_k)\mathbf{d} + g_i(\mathbf{x}_k)), \\ \nabla\mathrm{L}(\mathbf{d}, \boldsymbol{\mu}) &= \mathbf{A}_k\mathbf{d} + \nabla f(\mathbf{x}_k) - \sum_{i\in\mathcal{I}} \mu_i \nabla g_i(\mathbf{x}_k) \text{ and} \\ \nabla^2\mathrm{L}(\mathbf{d}, \boldsymbol{\mu}) &= \mathbf{A}_k. \end{aligned} \tag{3.8}$$

The matrix $\mathbf{A}_k$ is positive definite and is an approximation of the Hessian of the Lagrangian function of (GNP) in the minimum with $\mathbf{A}_0 = \mathbf{I}$. Therefore, the second necessary condition of a minimum is fulfilled, because with $\mathbf{A}_k$ also $\nabla^2\mathrm{L}(\mathbf{d}^*, \mu^*)$ is positive definite on $\mathcal{T}_{\mathbf{d}^*}(\mathcal{R}')$.

For the active constraints we must solve the following linear system

$$\begin{aligned} \nabla\mathrm{L}(\mathbf{d}, \boldsymbol{\mu}) &= 0 \\ \nabla g_i^T(\mathbf{x}_k)\mathbf{d} + g_i(\mathbf{x}_k) &= 0 \quad \forall\, i \in \mathcal{I}_0(\mathbf{d}). \end{aligned} \tag{3.9}$$

If for a solution $(\mathbf{d}^*, \boldsymbol{\mu}^*)$ of this system it holds $\mu_i^* > 0 \; \forall \; i \in \mathcal{I}_0(\mathbf{d}^*)$, then $\mathbf{d}^*$ is a local minimum of (QP) because of the positive definiteness of $\nabla^2\mathrm{L}(\mathbf{d}^*, \boldsymbol{\mu}^*) = \mathbf{A}_k$. We write the linear system in the form $\mathbf{Hz} = \mathbf{h}$ with $m = |\mathcal{I}_0(\mathbf{d}^*)|$ and

$$\underbrace{\left(\begin{array}{c|ccc} \mathbf{A}_k & -\nabla g_1(\mathbf{x}_k) & \dots & -\nabla g_m(\mathbf{x}_k) \\ \hline -\nabla g_1^T(\mathbf{x}_k) & 0 & \dots & 0 \\ \vdots & \vdots & \ddots & \vdots \\ -\nabla g_m^T(\mathbf{x}_k) & 0 & \dots & 0 \end{array}\right)}_{\mathbf{H}} \underbrace{\begin{pmatrix} \mathbf{d} \\ \mu_1 \\ \vdots \\ \mu_m \end{pmatrix}}_{\mathbf{z}} = \underbrace{\begin{pmatrix} -\nabla f(\mathbf{y}_k)) \\ g_1(\mathbf{x_k}) \\ \vdots \\ g_m(\mathbf{x_k}) \end{pmatrix}}_{\mathbf{h}}.$$

$\mathbf{H}$ is symmetric but not positive definite, because with $\mathbf{S} = (\nabla g_1(\mathbf{x}_k), \dots, \nabla g_m(\mathbf{x}_k)) \in I\!R^{n\times m}$ it holds

$$\mathbf{H} = \left(\begin{array}{c|c} \mathbf{A}_k & -\mathbf{S} \\ \hline -\mathbf{S}^T & \mathbf{0} \end{array}\right).$$

After one step of a Gauss' elimination method we have two quadratical blocks and it holds $\det(\mathbf{H}) = \det(\mathbf{A}_k)$ det$(-\mathbf{S}^T\mathbf{A}_k^{-1}\mathbf{S})$. In the point $\mathbf{x}_k$ the constraint qualifications are fulfilled (i.e. $\mathbf{S}$ has maximum rank) and $\mathbf{A}_k$ (and $\mathbf{A}_k^{-1}$) is positive definite, such that we derive det$(\mathbf{H}) < 0$. For the problem (OP) the sequential subproblem (SOP) in the kth step with $d_1 = \nabla f(\mathbf{x}_k)\mathbf{d} = (-1, 0, \dots, 0)\mathbf{d}$ is given by:

$$\begin{array}{lll} \text{(SOP)} & \text{Minimize} & \frac{1}{2}\mathbf{d}^T\mathbf{A}_k\mathbf{d} - d_1 \\ & \text{s.t.} & -2(\mathbf{y}_k^T\mathbf{D}_i+\mathbf{F}_i)\mathbf{d}-(\mathbf{y}_k^T\mathbf{D}_i+2\mathbf{F}_i)\mathbf{y}_k-f_i+\sigma_y^2 \geq 0 \quad \forall\, i \in \mathcal{I}, \end{array}$$

The Lagrangian function L and $\nabla_d \mathrm{L}$ are given by

$$\begin{aligned} \mathrm{L}(\mathbf{d},\boldsymbol{\mu}) &= \frac{1}{2}\mathbf{d}^T\mathbf{A}_k\mathbf{d} - d_1 + \sum_{i\in\mathcal{I}} \mu_i(2(\mathbf{y}_k^T\mathbf{D}_i+\mathbf{F}_i)\mathbf{d} + (\mathbf{y}_k^T\mathbf{D}_i+2\mathbf{F}_i)\mathbf{y}_k + f_i - \sigma_y^2) \\ \nabla_d \mathrm{L}(\mathbf{d},\boldsymbol{\mu}) &= \mathbf{A}_k\mathbf{d} + \mathbf{d}_1 + 2\sum_{i\in\mathcal{I}} \mu_i(\mathbf{D}_i\mathbf{y}_k + \mathbf{F}_i), \end{aligned} \tag{3.10}$$

with $\mathbf{d}_1 = (-1, 0, \ldots, 0)^T$. If we use only the active constraints the necessary conditions of problem (SOP) for every load case are given by (with (3.9) and (3.10))

$$\begin{aligned} \mathbf{A}_k\mathbf{d} + \mathbf{d}_1 + 2\sum_{i\in\mathcal{I}} \mu_i(\mathbf{D}_i\mathbf{y}_k + \mathbf{F}_i) &= 0 \\ -2(\mathbf{y}_k^T\mathbf{D}_i+\mathbf{F}_i)\mathbf{d} - (\mathbf{y}_k^T\mathbf{D}_i+2\mathbf{F}_i)\mathbf{y}_k - f_i + \sigma_y^2 &= 0 \quad \forall\, i \in \mathcal{I}_0(\mathbf{d}), \end{aligned} \tag{3.11}$$

such that in every load vertex we solve the linear system $\mathbf{Hz} = \mathbf{h}$ with $m = |\mathcal{I}_0(\mathbf{d}^*)|$,

$$\begin{aligned} \mathbf{H} &= \left(\begin{array}{c|ccc} \mathbf{A}_k & 2(\mathbf{D}_1\mathbf{y}_k+\mathbf{F}_1) & \ldots & 2(\mathbf{D}_m\mathbf{y}_k+\mathbf{F}_m) \\ \hline 2(\mathbf{y}_k^T\mathbf{D}_1+\mathbf{F}_1) & 0 & \ldots & 0 \\ \vdots & \vdots & \ddots & \vdots \\ 2(\mathbf{y}_k^T\mathbf{D}_m+\mathbf{F}_m) & 0 & \ldots & 0 \end{array}\right) \\ \mathbf{h} &= (1, \ldots, 0, \sigma_y^2 - (\mathbf{y}_k^T\mathbf{D}_1+2\mathbf{F}_1)\mathbf{y}_k - f_1, \ldots, \sigma_y^2 - (\mathbf{y}_k^T\mathbf{D}_m+2\mathbf{F}_m)\mathbf{y}_k - f_m)^T \\ \mathbf{z} &= (d_1, \ldots, d_{d+1}, \mu_1, \ldots, \mu_m)^T, \end{aligned} \tag{3.12}$$

with $\mathbf{H} \in I\!R^{(d+1+m)\times(d+1+m)}$, $\mathbf{h} \in I\!R^{d+1+m}$ and $\mathbf{z} \in I\!R^{d+1+m}$. For the solution of this problem we use an active set strategy (see [7], [30]). The solution of (SOP) is based on an iterative solution of finite linear systems.

Let $\mathbf{d}_k$ be an admissible approximation of (SOP) and let $\mathcal{I}_0(\mathbf{d}_k)$ be the set of active indices in the point $\mathbf{d}_k$. With the introduction of the slack variables $\boldsymbol{\delta}$ and $\mathbf{d} = \mathbf{d}_k + \boldsymbol{\delta}$ the problem (SOP) of active constraints is equivalent with the problem

$$\begin{array}{lll} \text{(GSOP)} & \text{Minimize} & \frac{1}{2}\boldsymbol{\delta}^T\mathbf{A}_k\boldsymbol{\delta} + (\mathbf{d}_1^T + \mathbf{d}_k^T\mathbf{A}_k)\boldsymbol{\delta} \\ & \text{s.t.} & (-2\mathbf{y}_k^T\mathbf{D}_i - 2\mathbf{F}_i)\boldsymbol{\delta} = 0 \qquad\qquad \forall\, i \in \mathcal{I}_0(\mathbf{d}_k). \end{array}$$

This is equivalent for every load vertex with the linear system $\bar{\mathbf{H}}\bar{\mathbf{z}} = \bar{\mathbf{h}}$ with

$$\underbrace{\left(\begin{array}{c|c} \mathbf{A}_k & 2(\mathbf{D}_i\mathbf{y}_k+\mathbf{F}_i),\, i \in \mathcal{I}_0(\mathbf{d}_k) \\ \hline 2(\mathbf{y}_k^T\mathbf{D}_i+\mathbf{F}_i)q,\, i \in \mathcal{I}_0(\mathbf{d}_k) & 0 \end{array}\right)}_{\bar{\mathbf{H}}} \underbrace{\left(\begin{array}{c} \boldsymbol{\delta} \\ \boldsymbol{\nu} \end{array}\right)}_{\bar{\mathbf{z}}} = \underbrace{\left(\begin{array}{c} -\mathbf{d}_1 - \mathbf{A}_k\mathbf{d}_k \\ 0 \end{array}\right)}_{\bar{\mathbf{h}}}.$$

Let $\boldsymbol{\delta}^*$ be a solution of $\bar{\mathbf{H}}\bar{\mathbf{z}} = \bar{\mathbf{h}}$. If it holds $\boldsymbol{\delta}^* \neq \mathbf{0}$ maybe the feasible region of (SOP) is deserted. If not, we define the new approximation $\mathbf{d}_{k+1} = \mathbf{d}_k + \boldsymbol{\delta}^*$. If the feasible region

is deserted we search on a semi ray (in direction of $\boldsymbol{\delta}^*$) starting from $\mathbf{d}_k$ for the first point $\mathbf{d}_{k+1}$ which violates one inequality constraint of (SOP). This means we search along the ray $\mathbf{s}^*(\equiv \boldsymbol{\delta}^*)$ starting from $\mathbf{d}_k$ for a maximal γ_k, such that the approximation $\mathbf{d}_{k+1} = \mathbf{d}_k + \gamma_k \mathbf{s}^*$ is admissible. γ_k is the minimum for all $i \notin \mathcal{I}_0(\mathbf{d}_k)$ with $-2(\mathbf{y}_k^T\mathbf{D}_i + \mathbf{F}_i)\mathbf{s}^* < 0$ of

$$\gamma_k = \min \left\{ 1, \frac{2(\mathbf{y}_k^T\mathbf{D}_i + \mathbf{F}_i)\mathbf{d}_k + (\mathbf{y}_k^T\mathbf{D}_i + 2\mathbf{F}_i)\mathbf{y}_k + f_i - \sigma_y^2}{-2(\mathbf{y}_k^T\mathbf{D}_i + \mathbf{F}_i)\mathbf{s}^*} \right\}.$$

For $\gamma_k = 1$, i.e. $\forall\, i \notin \mathcal{I}_0(\mathbf{d}_k)$ it holds

$$\begin{aligned}
& \frac{2(\mathbf{y}_k^T\mathbf{D}_i+\mathbf{F}_i)\mathbf{d}_k+(\mathbf{y}_k^T\mathbf{D}_i+2\mathbf{F}_i)\mathbf{y}_k+f_i-\sigma_y^2}{-2(\mathbf{y}_k^T\mathbf{D}_i+\mathbf{F}_i)\mathbf{s}^*} && \geq 1 \\
\iff \quad & 2(\mathbf{y}_k^T\mathbf{D}_i + \mathbf{F}_i)\mathbf{d}_k + (\mathbf{y}_k^T\mathbf{D}_i + 2\mathbf{F}_i)\mathbf{y}_k + f_i - \sigma_y^2 && \leq -2(\mathbf{y}_k^T\mathbf{D}_i + \mathbf{F}_i)\mathbf{s}^* \\
\iff \quad & 2(\mathbf{y}_k^T\mathbf{D}_i + \mathbf{F}_i)\mathbf{d}_k + (\mathbf{y}_k^T\mathbf{D}_i + 2\mathbf{F}_i)\mathbf{y}_k + f_i - \sigma_y^2 && \leq -2(\mathbf{y}_k^T\mathbf{D}_i + \mathbf{F}_i)(\mathbf{d}_{k+1} - \mathbf{d}_k) \\
\iff \quad & -2(\mathbf{y}_k^T\mathbf{D}_i + \mathbf{F}_i)\mathbf{d}_{k+1} - (\mathbf{y}_k^T\mathbf{D}_i + 2\mathbf{F}_i)\mathbf{y}_k - f_i + \sigma_y^2 && \geq 0, \qquad (3.13)
\end{aligned}$$

such that $\mathbf{d}_{k+1}$ is admissible for (SOP) and we replace $\mathbf{d}_k$ by $\mathbf{d}_{k+1}$.

If it holds $\gamma_k < 1$ we define $\mathbf{d}_{k+1} = \mathbf{d}_k + \gamma_k \mathbf{s}^*$ and $\mathcal{I}_0(\mathbf{d}_{k+1}) = \mathcal{I}_0(\mathbf{d}_k) \cup \{i^*\}$, were i^* is the index yielding to the minimal γ_k. The feasible region is enlarged and we solve (GSOP) with the new input data. This procedure could be repeated only finite times, such that we arrive after k steps $\boldsymbol{\delta}^* = \mathbf{0}$, i.e. $\mathbf{d}_k$ is the optimum for (GSOP). If the Lagrangian multipliers ν_i of $\mathbf{d}_k$ are non-negative $\mathbf{d}_k$ is the optimum of (SOP). If at least one multiplier is negative we define i^{**} as the index of the lowest Lagrangian multiplier $\nu_{i^{**}}$. This constraint is deleted, i.e. we replace the feasible region of (GSOP) by $\mathcal{I}_0(\mathbf{d}_k) \setminus \{i^{**}\}$ and then we solve (GSOP) again.

If we use all constraints instead of an active-set strategy we derive with the complementary conditions the nonlinear system:

$$\begin{aligned}
\nabla \mathrm{L}(\mathbf{d}, \boldsymbol{\mu}) &= \mathbf{0} \\
\mu_i(\nabla g_i^T(\mathbf{x}_k)\mathbf{d} + g_i(\mathbf{x}_k)) &= 0 \quad \forall\, i \in \mathcal{I}. \qquad (3.14)
\end{aligned}$$

For problem (SOP) it holds for all $j \in \mathcal{J}$:

$$\begin{aligned}
\mathbf{A}_k\mathbf{d} + \mathbf{d}_1 + 2\sum_{i\in\mathcal{I}} \mu_i(\mathbf{D}_i + \mathbf{F}_i)\mathbf{y}_k &= 0 \\
-2\mu_i(\mathbf{y}_k^T\mathbf{D}_i + 2\mathbf{F}_i)\mathbf{d} - \mu_i[(\mathbf{y}_k^T\mathbf{D}_i + 2\mathbf{F}_i)\mathbf{y}_k + f_i - \sigma_y^2] &= 0 \quad \forall\, i \in \mathcal{I}. \qquad (3.15)
\end{aligned}$$

For every load vertex the system $\hat{\mathbf{H}}\hat{\mathbf{z}} = \hat{\mathbf{h}}$ must be solved with $\hat{m} = |\mathcal{I}|$,

$$\hat{\mathbf{H}} = \left(\begin{array}{c|ccccc}
\mathbf{A}_k & 2(\mathbf{D}_1\mathbf{y}_k + \mathbf{F}_1) & \dots & & 2(\mathbf{D}_{\hat{m}}\mathbf{y}_k + \mathbf{F}_{\hat{m}}) \\
\hline
2\mu_1(\mathbf{y}_k^T\mathbf{D}_1 + \mathbf{F}_i) & (\mathbf{y}_k^T\mathbf{D}_1 + 2\mathbf{F}_1)\mathbf{y}_k + f_1 - \sigma_y^2 & 0 & \dots & 0 \\
\vdots & \vdots & \ddots & \ddots & \ddots & \vdots \\
2\mu_{\hat{m}}(\mathbf{y}_k^T\mathbf{D}_{\hat{m}} + \mathbf{F}_{\hat{m}}) & 0 & \dots & 0 & (\mathbf{y}_k^T\mathbf{D}_{\hat{m}} + 2\mathbf{F}_{\hat{m}})\mathbf{y}_k + f_{\hat{m}} - \sigma_y^2
\end{array}\right),$$

$\hat{\mathbf{z}} = (d_1, d_2, \ldots, d_{d+1}, \mu_1, \ldots, \mu_{\hat{m}})^T$ and $\hat{\mathbf{h}} = (1, 0, \ldots, 0)^T$. If the Lagrangian multipliers of a solution $\mathbf{d}^*$ of the active constraints are positive the solution $\mathbf{d}^*$ is a local minimum of (SOP) and from convex optimization theory therefore the global optimum. A set $M \in I\!R^n$ is called convex, if with $\mathbf{x}, \mathbf{y} \in M$ also $\lambda\mathbf{x} + (1-\lambda)\mathbf{y} \in M$ holds $\forall\ \lambda \in (0,1)$.

Let $\mathbf{d}_1$ and $\mathbf{d}_2$ be points of the feasible region of (SOP) then it holds for $\lambda\mathbf{d}_1 + (1-\lambda)\mathbf{d}_2$:

$$\begin{aligned} & -2(\mathbf{y}_k^T\mathbf{D}_i + \mathbf{F}_i)(\lambda\mathbf{d}_1 + (1-\lambda)\mathbf{d}_2) - (\mathbf{y}_k^T\mathbf{D}_i + 2\mathbf{F}_i)\mathbf{y}_k - f_i + \sigma_y^2 \\ = \ & \lambda(\underbrace{-2(\mathbf{y}_k^T\mathbf{D}_i + \mathbf{F}_i)\mathbf{d}_1 - (\mathbf{y}_k^T\mathbf{D}_i + 2\mathbf{F}_i)\mathbf{y}_k - f_i + \sigma_y^2}_{\geq 0}) \\ + \ & (1-\lambda)(\underbrace{-2(\mathbf{y}_k^T\mathbf{D}_i + \mathbf{F}_i)\mathbf{d}_2 - (\mathbf{y}_k^T\mathbf{D}_i + 2\mathbf{F}_i)\mathbf{y}_k - f_i + \sigma_y^2}_{\geq 0}) \\ \geq \ & 0 \qquad \forall\ \lambda \in (0,1). \end{aligned} \tag{3.16}$$

This means that the feasible region of (SOP) is a convex set. A function $f : M \to I\!R$ (M convex) is called convex if $f(\lambda\mathbf{x} + (1-\lambda)\mathbf{y}) \leq \lambda f(\mathbf{x}) + (1-\lambda)f(\mathbf{y})$ holds $\forall\ \mathbf{x}, \mathbf{y} \in M, \forall\ \lambda \in (0,1)$ (f is called concave if $-f$ is convex). If the strict inequality holds the function is called strictly convex. Let $f : I\!R^n \to I\!R$ be twice continuous differentiable then the following statements are equivalent ([30]):

1. f is convex
2. $f(\mathbf{y}) - f(\mathbf{x}) \geq \nabla^T f(\mathbf{x})(\mathbf{y} - \mathbf{x})$
3. $\nabla^2 f(\mathbf{x})$ is positive semi-definite $\forall\ \mathbf{x} \in I\!R^n$.

$\mathbf{A}_k$ is positive definite and thus the objective function $\frac{1}{2}\mathbf{d}^T\mathbf{A}_k\mathbf{d} - d_1$ of (SOP) is convex. The following equivalence holds for convex functions $f : I\!R^n \to I\!R$ and convex feasible regions $\mathcal{R}$:

1. $\mathbf{x}^*$ is a local minimum for f with respect to $\mathcal{R}$
2. $\mathbf{x}^*$ is a global minimum for f with respect to $\mathcal{R}$
3. $\mathbf{x}^*$ is a critical point of f, i.e. $\nabla f(\mathbf{x}^*) = 0$.

We derive the following connection between the feasible regions $\mathcal{R}$ and $\mathcal{R}'$ of the problems (GNP) and (QP), respectively (see [8]). Let $\mathbf{x}_k$ be an approximation of the solution of (GNP) and $\mathbf{d}_k = \mathbf{x} - \mathbf{x}_k$ (search direction with constant step length) then

$$\mathcal{R}_k = \{\mathbf{x} \mid g_i(\mathbf{x}_k) + \nabla g_i(\mathbf{x}_k)(\mathbf{x} - \mathbf{x}_k) \geq 0, \forall\ i \in \mathcal{I}\}$$

is the shifted feasible region of (QP). If $\mathcal{R}$ is non empty and all g_i are concave then $\mathcal{R} \subset \mathcal{R}_k$ holds. Therefore, we assume that all g_i are concave. For $\mathbf{x} \in \mathcal{R}$ and the approximation $\mathbf{x}_k$ holds

$$-g_i(\mathbf{x}) + g_i(\mathbf{x}_k) \geq -\nabla g_i(\mathbf{x}_k)(\mathbf{x} - \mathbf{x}_k q), \ \text{ bzw. } \ g_i(\mathbf{x}) \leq g_i(\mathbf{x}_k) + \nabla g_i(\mathbf{x}_k)(\mathbf{x} - \mathbf{x}_k).$$

Thus we derive for $\mathbf{x} \in \mathcal{R}$

$$0 \leq g_i(\mathbf{x}) \leq g_i(\mathbf{x}_k) + \nabla g_i(\mathbf{x}_k)(\mathbf{x} - \mathbf{x}_k) \quad \forall i \in \mathcal{I},$$

this means $\mathbf{x} \in \mathcal{R}_k$ and $\mathcal{R} \subset \mathcal{R}_k$. Because of the convexity of the von Mises–function this also holds for the feasible regions of (OP) and (SOP).

Let $\mathbf{y}_k$ be an approximation of the minimum and $\boldsymbol{\lambda}_k$ be an approximation of the Lagrangian multipliers of (OP) in step k. If we solve (SOP) in step k we have the solution $\mathbf{d}_k$ with the Lagrange multipliers $\boldsymbol{\mu}_k$. A new approximation of the solution of (OP) we derive with $\gamma_k \in I\!R$ by

$$\begin{pmatrix} \mathbf{y}_{k+1} \\ \boldsymbol{\lambda}_{k+1} \end{pmatrix} = \begin{pmatrix} \mathbf{y}_k \\ \boldsymbol{\lambda}_k \end{pmatrix} + \gamma_k \begin{pmatrix} \mathbf{d}_k \\ \boldsymbol{\mu}_k - \boldsymbol{\lambda}_k \end{pmatrix}.$$

Therefore, the solution $\mathbf{d}_k$ is a new search direction of the problem (OP). The following theorem describes the relation between the solution of (OP) and (SOP) (see [7]).

Theorem:

Let $\mathbf{d}_k^*$ be the solution of the quadratic problem (SOP) in the kth step and $\boldsymbol{\mu}^*$ the corresponding Lagrangian multipliers and $\mathbf{y}_k$ be an approximation of the minimum of (OP). If $\mathbf{d}_k^* = \mathbf{0}$ holds, then the necessary conditions of a local minimum of (OP) are fulfilled for $\mathbf{y}_k$ and $\boldsymbol{\mu}^*$.

Proof:

$\mathbf{d}_k$ is a solution of (SOP) and therefore the first necessary condition of (SOP) are fulfilled because of

$$\begin{aligned} \mu_i^* &\geq 0 \quad ,\forall\, i \in \mathcal{I} \\ \mu_i^*[-2(\mathbf{y}_k^T\mathbf{D}_i + \mathbf{F}_i)\mathbf{d}_k^* - (\mathbf{y}_k^T\mathbf{D}_i + 2\mathbf{F}_i)\mathbf{y}_k - f_i + \sigma_y^2] &= 0 \quad ,\forall\, i \in \mathcal{I}, \\ \mathbf{A}_k\mathbf{d}_k^* + \mathbf{d}_1 + 2\sum_{i\in\mathcal{I}} \mu_i^*(\mathbf{D}_i\mathbf{y}_k + \mathbf{F}_i) &= 0 \quad . \end{aligned} \tag{3.17}$$

With $\mathbf{d}_k^* = 0$ it holds

$$\begin{aligned} \mu_i^* &\geq 0 \quad ,\forall\, i \in \mathcal{I} \\ \mu_i^*[-(\mathbf{y}_k^T\mathbf{D}_i + 2\mathbf{F}_i)\mathbf{y}_k - f_i + \sigma_y^2] &= 0 \quad ,\forall\, i \in \mathcal{I}, \\ \mathbf{d}_1 + 2\sum_{i\in\mathcal{I}} \mu_i^*(\mathbf{D}_i\mathbf{y}_k + \mathbf{F}_i) &= 0 \quad . \end{aligned} \tag{3.18}$$

The problem (SOP) and (OP) have the same Hessian of the Lagrangian function and thus the second necessary condition is fulfilled. □

(SOP) is a convex problem and thus a local minimum is also a global. We must show that (OP) is a convex problem. The objective function $-\mathbf{y}_1$ is convex as linear function. Let $\mathcal{S} = \{\mathbf{y}| - (\mathbf{y}^T\mathbf{D}_i + 2\mathbf{F}_i)\mathbf{y} - f_i + \sigma_y^2 \geq 0\}$ be the feasible region for each load vertex of (OP). If we choose two points $\mathbf{y}_1 = (\alpha_1, \mathbf{x}_1)^T$ and $\mathbf{y}_2 = (\alpha_2, \mathbf{x}_2)^T \in \mathcal{S}$ with

$\boldsymbol{\sigma}_1 = \alpha_1 \boldsymbol{\sigma}_i^E + \boldsymbol{\rho}_i^{k-1} + \mathbf{B}_i \mathbf{x}_1$ and $\boldsymbol{\sigma}_2 = \alpha_2 \boldsymbol{\sigma}_i^E + \boldsymbol{\rho}_i^{k-1} + \mathbf{B}_i \mathbf{x}_2$ it holds $\forall\ \lambda \in (0,1)$ and $\lambda \mathbf{y}_1 + (1-\lambda)\mathbf{y}_2$:

$$\begin{aligned} & -[(\lambda \mathbf{y}_1 + (1-\lambda)\mathbf{y}_2)^T \mathbf{D}_i + 2\mathbf{F}_i][\lambda \mathbf{y}_1 + (1-\lambda)\mathbf{y}_2] - f_i + \sigma_y^2 \\ = \ & -F[(\lambda\alpha_1 + (1-\lambda)\alpha_2)\boldsymbol{\sigma}_i^E + \boldsymbol{\rho}_i^{k-1} + \mathbf{B}_i(\lambda \mathbf{x}_1 + (1-\lambda)\mathbf{x}_2)] + \sigma_y^2 \\ = \ & -F[\lambda(\alpha_1 \boldsymbol{\sigma}_i^E + \boldsymbol{\rho}_i^{k-1} + \mathbf{B}_i \mathbf{x}_1) + (1-\lambda)(\alpha_2 \boldsymbol{\sigma}_i^E + \boldsymbol{\rho}_i^{k-1} + \mathbf{B}_i \mathbf{x}_2)] + \sigma_y^2 \\ = \ & -F(\lambda \boldsymbol{\sigma}_1 + (1-\lambda)\boldsymbol{\sigma}_2) + \sigma_y^2 \geq 0, \end{aligned} \tag{3.19}$$

because $F(\boldsymbol{\sigma})$ is convex. The convexity of the von Mises–function F in the variables $\boldsymbol{\sigma}$ is transformed into the convexity of F in the variables $\mathbf{y}$, such that a local minimum of (OP) is also a global one.

We derive the following characteristic of the SQP methods for convex problems (GNP):

Lemma:

Let $\mathbf{x}_k$ be an admissible point of (GNP), $\mathbf{d}_k$ be a solution of the kth sub-problem with the Lagrangian multipliers $\boldsymbol{\mu}_k$, $\mu_{ki} \geq 0\ \forall\ i \in \mathcal{I}$ and $\gamma \in [0,1]$ a step length, then it holds

$$\begin{aligned} g_i(\mathbf{x}_k + \gamma \mathbf{d}_k) &\leq g_i(\mathbf{x}_k) \quad \text{und} \\ \nabla^T g_i(\mathbf{x}_k + \gamma \mathbf{d}_k)\mathbf{d}_k &\leq \nabla^T g_i(\mathbf{x}_k)\mathbf{d}_k \leq 0 \quad \forall\ i \in \mathcal{I}. \end{aligned}$$

Proof:

$\mathbf{d}_k$ as solution of the sub-problem fulfills the complementary conditions such that it holds

$$\mu_{ki}(g_i(\mathbf{x}_k) + \nabla^T g_i(\mathbf{x}_k)\mathbf{d}_k) = 0 \quad \forall\ i \in \mathcal{I}.$$

From the admissibility of $\mathbf{x}_k$ follows, that $\nabla^T g_i(\mathbf{x}_k)\mathbf{d}_k$ is negative. All g_i are concave such that

$$g_i(\mathbf{x}_k + \gamma \mathbf{d}_k) - g_i(\mathbf{x}_k) \leq \gamma \nabla^T g_i(\mathbf{x}_k)\mathbf{d}_k \leq 0 \quad \forall\ i \in \mathcal{I}$$

holds, this is the first assumption of the lemma. Further follows on one hand

$$g_i(\mathbf{x}_k) - g_i(\mathbf{x}_k + \gamma \mathbf{d}_k) \leq -\gamma \nabla^T g_i(\mathbf{x}_k + \gamma \mathbf{d}_k)\mathbf{d}_k \quad \forall\ i \in \mathcal{I}$$

and on the other hand follows

$$g_i(\mathbf{x}_k + \gamma \mathbf{d}_k) - g_i(\mathbf{x}_k) \leq \gamma \nabla^T g_i(\mathbf{x}_k)\mathbf{d}_k \quad \forall\ i \in \mathcal{I}.$$

Adding the two inequalities it follows

$$0 \leq \gamma[\nabla^T g_i(\mathbf{x}_k)\mathbf{d}_k - \nabla^T g_i(\mathbf{x}_k + \gamma \mathbf{d}_k)\mathbf{d}_k] \quad \forall\ i \in \mathcal{I}.$$

With $\gamma \in [0,1]$, the admissibility of $\mathbf{x}_k$ and the complementary condition of the sub-problem follows the second assumption of the lemma. □

The second assumption follows independently of the solution $\mathbf{d}_k$. We derive from the concave g_i for two step lengths γ_1 and γ_2 with $0 \leq \gamma_1 \leq \gamma_2 \leq 1$

$$\nabla^T g_i(\mathbf{x}_k + \gamma_2 \mathbf{d}_k)\mathbf{d}_k \leq \nabla^T g_i(\mathbf{x}_k + \gamma_1 \mathbf{d}_k)\mathbf{d}_k \quad \forall\, i \in \mathcal{I}.$$

The first assumption is extended for γ_1 and γ_2 with $0 \leq \gamma_1 \leq \gamma_2 \leq 1$ by

$$\begin{aligned} g_i(\mathbf{x}_k + \gamma_2 \mathbf{d}_k) - g_i(\mathbf{x}_k + \gamma_1 \mathbf{d}_k) &\leq (\gamma_2 - \gamma_1)\nabla^T g_i(\mathbf{x}_k + \gamma_1 \mathbf{d}_k)\mathbf{d}_k \\ &\leq (\gamma_2 - \gamma_1)\nabla^T g_i(\mathbf{x}_k)\mathbf{d}_k \leq 0. \end{aligned} \tag{3.20}$$

All functions $\bar{g}_i(\gamma) = g_i(\mathbf{x}_k + \gamma \mathbf{d}_k)$ are monotone decreasing on $[0, 1]$. For convex problems the solution converges to the boundary of the feasible region.

We must guarantee that with the choose of the step length γ_k the new value $\mathbf{y}_{k+1}$ is in the feasible region of (OP). We define in step k the one dimensional penalty function

$$\Gamma(\gamma_k) = \Psi_r(\mathbf{z}_k - \gamma_k \mathbf{p}_k) \text{ with } \mathbf{z}_k := \begin{pmatrix} \mathbf{y}_k \\ \boldsymbol{\lambda}_k \end{pmatrix} \text{ and } \mathbf{p}_k := -\begin{pmatrix} \mathbf{d}_k \\ \boldsymbol{\mu}_k - \boldsymbol{\lambda}_k \end{pmatrix}.$$

The function Ψ_r is defined with a penalty parameter r (see [30], [31] and [39]). We define the augmented Lagrangian function with $\mathbf{z} := (\mathbf{y}^T, \boldsymbol{\lambda}^T)^T$ (see [39])

$$\Psi_r(\mathbf{z}) = f(\mathbf{y}) - \sum_{i \in \mathcal{I}} \begin{cases} \lambda_i g_i(\mathbf{y}) - \frac{1}{2} r g_i(\mathbf{y})^2 & \text{, if } g_i(\mathbf{y}) \leq \frac{\lambda_i}{r} \\ \frac{1}{2}\frac{\lambda_i^2}{r} & \text{, else} \end{cases}$$

with the derivative

$$\nabla^* \Psi_r(\mathbf{z}) = \begin{pmatrix} \nabla_{\mathbf{y}} f(\mathbf{y}) & -\sum\limits_{i \in \mathcal{I}} \begin{cases} \nabla_{\mathbf{y}} g_i(\mathbf{y})(\lambda_i - r g_i(\mathbf{y})) & \text{, if } g_i(\mathbf{y}) \leq \frac{\lambda_i}{r} \\ 0 & \text{, else} \end{cases} \\ -\bar{\boldsymbol{g}}(\mathbf{y}) & \end{pmatrix}$$

with

$$\begin{aligned} \nabla^*(\cdot) &= \left(\frac{\partial(\cdot)}{\partial y_1}, \ldots, \frac{\partial(\cdot)}{\partial y_{r+1}}, \frac{\partial(\cdot)}{\partial \lambda_1}, \ldots, \frac{\partial(\cdot)}{\partial \lambda_{|\mathcal{I}|}} \right)^T, \\ \bar{\boldsymbol{g}}^T &= (\bar{g}_1, \ldots, \bar{g}_{|\mathcal{I}|})^T \\ \bar{g}_i(\mathbf{y}) &= \begin{cases} g_i(\mathbf{y}) & \text{, if } g_i(\mathbf{y}) \leq \frac{\lambda_i}{r} \\ \frac{\lambda_i}{r} & \text{, else} \end{cases} \quad \text{, } \forall i \in \mathcal{I}. \end{aligned}$$

The augmented Lagrangian function gives a penalty if the feasible region $\mathcal{R}$ is deserted. In Schittkowski's SQP - algorithm we choose for a solution $\mathbf{d}_k$ of (SOP) the positive constants $\bar{r} > 1, \bar{\varepsilon} < 1$ and define the parameter δ_k, ε_k with $\delta_{-1} := 1$ by

$$\delta_k = \min \left\{ \frac{\mathbf{d}_k^T \mathbf{A}_k \mathbf{d}_k}{\|\mathbf{d}_k\|^2}, \delta_{k-1} \right\} \text{ and } \varepsilon_k = \begin{cases} \frac{\|\mathbf{d}_k\|^2}{\|\boldsymbol{\mu}_k - \boldsymbol{\lambda}_k\|^2} & \text{, if } \boldsymbol{\mu}_k \neq \boldsymbol{\lambda}_k \\ \bar{\varepsilon} & \text{, else.} \end{cases} \tag{3.21}$$

With this parameters we calculate the smallest j_k with

$$\frac{1}{\bar{r}^j} < \frac{1}{4}\varepsilon_k\delta_k\left(1-\frac{1}{4}\delta_k\right) \text{ holds, i.e. } \quad j_k = \min\left\{j \in I\!N, j > \frac{\ln \frac{16}{\varepsilon_k\delta_k(4-\delta_k)}}{\ln \bar{r}}\right\}.$$

The penalty parameter r_k is given by $r_k = \max\{r_{k-1}, \bar{r}^{j_k}\}$ with $r_{-1} := \bar{r}$. We choose the start values $\gamma < 1$ and $\xi < \frac{1}{2}$ and calculate the smallest non negative i_k with

$$i_k = \min\{i \in I\!N, \Psi_{r_k}(\mathbf{z}_k - \gamma^i\mathbf{p}_k) \leq \Psi_{r_k}(\mathbf{z}_k) - \xi\gamma^i\nabla^*\Psi_{r_k}^T(\mathbf{z}_k)\mathbf{p}_k\},$$

such that we derive the step length γ_k by $\gamma_k = \gamma^{i_k}$. It holds

$$\begin{aligned}\nabla^*\Psi_{r_k}^T(\mathbf{z}_k)\mathbf{p}_k &= -\nabla_{\mathbf{y}}^T f(\mathbf{y}_k)\mathbf{d}_k \\ &+ \sum_{i\in\mathcal{I}}\begin{cases}(\lambda_{ki} - r g_i(\mathbf{y}_k))\nabla_{\mathbf{y}}^T g_i(\mathbf{y}_k)\mathbf{d}_k & \\ +g_i(\mathbf{y}_k)(\mu_{ki}-\lambda_{ki}) & , \text{if } g_i(\mathbf{y}_k) \leq \frac{\lambda_{ki}}{r} \\ \frac{\lambda_{ki}}{r}(\mu_{ki}-\lambda_{ki}) & , \text{else}\end{cases} \end{aligned} \tag{3.22}$$

This guarantees that the step length is small enough to stay in the feasible region but large enough to achieve an improved solution. The algorithm begins with positive step length and decreases the step length iteratively (Armijo-rule). The update of the matrix $\mathbf{A}_k$ is given by the modified BFGS-update of Powell (see [39]). Starting with a positive definite matrix $\mathbf{A}_0$ we calculate $\mathbf{A}_{k+1}$ by

$$\mathbf{A}_{k+1} = \mathbf{A}_k - \frac{\mathbf{A}_k\mathbf{s}_k\mathbf{s}_k^T\mathbf{A}_k}{\mathbf{s}_k^T\mathbf{A}_k\mathbf{s}_k} + \frac{\mathbf{q}_k\mathbf{q}_k^T}{\mathbf{q}_k^T\mathbf{s}_k}. \tag{3.23}$$

$\mathbf{s}_k = \mathbf{y}_{k+1} - \mathbf{y}_k$ is the increment of the solutions and it holds for $\mathbf{q}_k$

$$\mathbf{q}_k = \theta_k\mathbf{t}_k + (1-\theta_k)\mathbf{A}_k\mathbf{s}_k \quad \text{with} \quad \mathbf{t}_k = \nabla \mathrm{L}(\mathbf{y}_{k+1}, \boldsymbol{\mu}^*) - \nabla \mathrm{L}(\mathbf{y}_k, \boldsymbol{\mu}^*).$$

$\boldsymbol{\mu}^* := \boldsymbol{\lambda}_{k+1}$ are the Lagrangian multipliers of the solution $\mathbf{y}_{k+1}$. θ_k is defined by

$$\theta_k = \begin{cases} 1 & , \text{if } \mathbf{s}_k^T\mathbf{t}_k \geq 0.2\mathbf{s}_k^T\mathbf{A}_k\mathbf{s}_k \\ \frac{0.8\mathbf{s}_k^T\mathbf{A}_k\mathbf{s}_k}{\mathbf{s}_k^T\mathbf{A}_k\mathbf{s}_k - \mathbf{s}_k^T\mathbf{t}_k} & , \text{else.}\end{cases}$$

$\mathbf{y}_{k+1}$ is calculated with the augmented Lagrangian function such that $\mathbf{s}_k = \gamma_k\mathbf{d}_k$ holds with the step length γ_k obtained by the Armijo-rule. We derive with equation (3.10) for $\mathbf{t}_k$ in every load vertex

$$\mathbf{t}_k = \sum_{i\in\mathcal{I}} 2\mu_i^*\mathbf{D}_i(\mathbf{y}_{k+1} - \mathbf{y}_k) = \sum_{i\in\mathcal{I}} 2\mu_i^*\mathbf{D}_i\mathbf{s}_k. \tag{3.24}$$

If it holds $\mathbf{s}_k^T\mathbf{t}_k \geq 0.2\mathbf{s}_k^T\mathbf{A}_k\mathbf{s}_k$ then we derive $\theta = 1$ and $\mathbf{q}_k^T\mathbf{s}_k = \mathbf{s}_k^T\mathbf{t}_k$. If $\mathbf{s}_k^T\mathbf{t}_k < 0.2\mathbf{s}_k^T\mathbf{A}_k\mathbf{s}_k$ holds it follows

$$\mathbf{q}_k = \frac{0.8\mathbf{s}_k^T\mathbf{A}_k\mathbf{s}_k}{\mathbf{s}_k^T\mathbf{A}_k\mathbf{s}_k - \mathbf{s}_k^T\mathbf{t}_k}\mathbf{t}_k + \left(\frac{0.2\mathbf{s}_k^T\mathbf{A}_k\mathbf{s}_k - \mathbf{s}_k^T\mathbf{t}_k}{\mathbf{s}_k^T\mathbf{A}_k\mathbf{s}_k - \mathbf{s}_k^T\mathbf{t}_k}\right)\mathbf{A}_k\mathbf{s}_k.$$

Finally it holds

$$\mathbf{q}_k^T \mathbf{s}_k = \frac{0.8(\mathbf{s}_k^T \mathbf{A}_k \mathbf{s}_k)\mathbf{s}_k^T \mathbf{t}_k + 0.2(\mathbf{s}_k^T \mathbf{A}_k \mathbf{s}_k)^2 - (\mathbf{s}_k^T \mathbf{A}_k \mathbf{s}_k)\mathbf{s}_k^T \mathbf{t}_k}{\mathbf{s}_k^T \mathbf{A}_k \mathbf{s}_k - \mathbf{s}_k^T \mathbf{t}_k} = 0.2\mathbf{s}_k^T \mathbf{A}_k \mathbf{s}_k \qquad (3.25)$$

and therefore $\mathbf{q}_k^T \mathbf{s}_k = \max\{\mathbf{s}_k^T \mathbf{t}_k, 0.2\mathbf{s}_k^T \mathbf{A}_k \mathbf{s}_k\} > 0$, because of $\mathbf{s}_k \neq \mathbf{0}$ and the positive definiteness of $\mathbf{A}_k$. With this definition follows that $\mathbf{A}_{k+1}$ is positive definite (see [14]).

4 Validation

4.1 Benchmarks

The meshes for the following limit load tests [57] have been provided by EDF, FZJ and ULg and are shared between the partners (FZJ, ULg, EDF and INTES):

- A thick plate (plane strain) under tension with a centered hole. The main geometrical parameter are the ratio of square length L and hole diameter D.
- A vessel-head under pressure. Two different geometries with longer and shorter cylindrical part of the vessel are given.

The computing times were made independent on the computing environment by normalizing to the time for an elastic step. For examples with defects see the report [50].

EDF: The upper bound solutions of EDF were calculated with Code_Aster® which is also used for incremental plastic analyses (see [56]). Lower bounds are estimated by a post-processor from the computed upper bounds.

FZJ: The lower bound solution of FZJ were calculated with a deterministic LISA software which was developed and implemented into PERMAS V4 (Version 4) (see [14], [45], [46]). Fully integrated finite elements are used.

ULg: The benchmark calculations of ULg are carried out by a direct upper bound programming method via the FEM code ELSA.

INTES: INTES has contributed some additional incremental analyses of the benchmark tests with PERMAS V7 (Version 7).

The calculations are performed on rectangular meshes. The numerical tests achieved some quite close results. Others exhibited differences which may be perhaps attributed to the used finite elements rather than to the different LISA software. The required computing time as multiples of the time for an elastic calculation has been used as fairly machine independent performance measure. Initial differences between the different algorithms could be reduced during the project. At project end all direct methods achieved convergent limit analyses in a time needed for 20 equivalent elastic calculations typically. A much more rapid convergence is observed in shakedown analyses, which typically need the time of only 2-4 elastic analyses.

4.1.1 Thick plate with a centered hole under uniaxial tension

There is a well known exact plane stress solution for $D/L = 0.2$ (see [9]). Estimating the corresponding plane strain solution yields the value 0.924, which shows that the numerical errors are small. However, the lower bounds estimated by EDF from its upper bound solution appears to be too low i.e. too conservative. Fig. 4.1.1 shows a FE–mesh of the plate with $D/L = 0.2$. Further, a plate with $D/L = 0.5$ is investigated. The results of the different partners are shown in Tab. 4.1

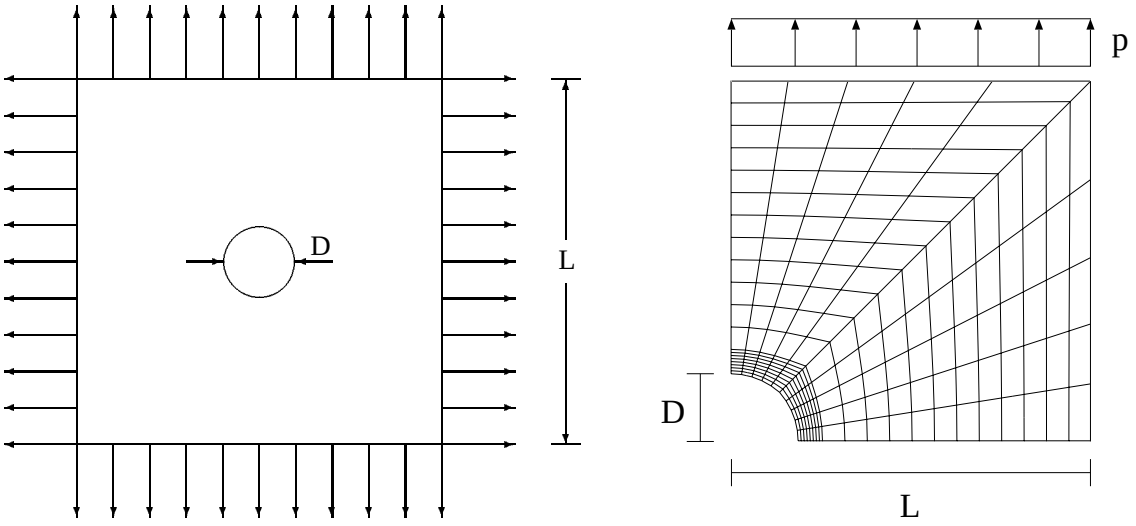

Figure 4.1: Finite element mesh of the plate with a hole

Plate with a centered hole under biaxial tension			
D/L		0.2	0.5
inf. EDF	T_{lim}/σ_0	0.710	0.367
sup EDF	T_{lim}/σ_0	0.947	0.527
inf. FZJ	T_{lim}/σ_0	0.913	0.486
sup. ULg	T_{lim}/σ_0	0.926	0.513
incr. INTES	T_{lim}/σ_0	0.904	0.494

Table 4.1: Comparison of the limit load results

4.1.2 Torispherical vessel head under internal pressure

Both geometries were modeled by a coarser and a finer mesh. The limit loads have been found by the partners close to the collapse load of the spherical part. Here, INTES observed a high influence of the accuracy of the solution on the limit pressure values. This needs some discussion on the failure criterion and the meshing.

Torispherical vessel head under internal pressure					
		short/coarse	short/fine	long/coarse	long/fine
analytical sphere solution	P_{lim}	4.0	4.0	4.0	4.0
inf. EDF	P_{lim}	3.837	-	-	-
sup EDF	P_{lim}	3.940	-	-	-
inf FZJ	P_{lim}	3.997	3.982	3.940	3.937
sup. ULg	P_{lim}	3.931	3.929	3.942	3.905
incr. INTES	P_{lim}	3.918	3.891	3.890	3.832

Table 4.2: Comparison of the limit load results

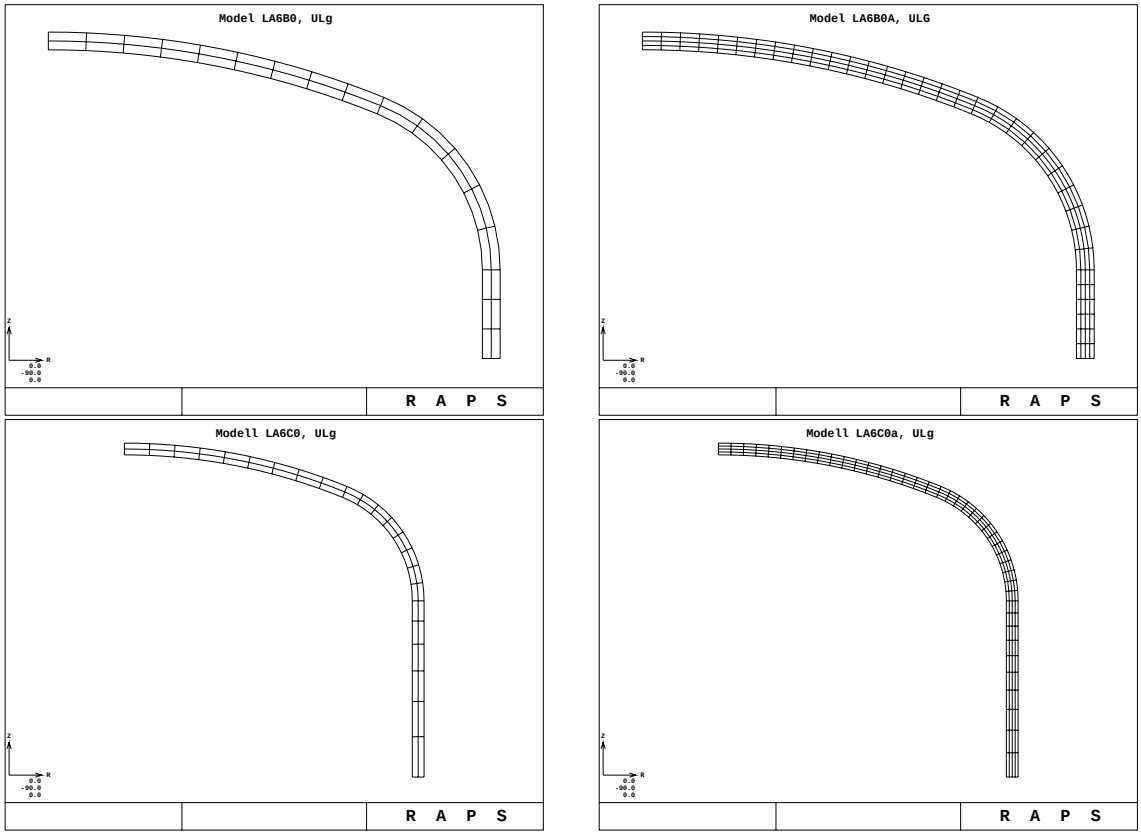

Figure 4.2: Finite element meshes

4.2 Mixing device

A mixing device is considered as a complex industrial practice problem with high thermal transient loading, internal pressure and external piping loads. Framatome/Siemens performed some FE-calculations on the mixing device and finished the thermal analyses. The modeling details (ANSYS-FEM files) are transformed into a PERMAS V4 mesh with 30,480 eight nodes volume elements (HEXE8) and 38,196 nodes. For the shakedown analysis seven load vertices are chosen from the dataset of given temperature distributions. These temperature loads T_j are chosen at seven time steps t_j: $t_1 = 0s$, $t_2 = 14.5s$, $t_3 = 18.7s$, $t_4 = 33.2s$, $t_5 = 614.5s$, $t_6 = 618.7s$ and $t_7 = 633.2s$. They are applied as temperature differences $\theta_j = T_j - 50°C$. In addition a constant inner pressure of $P = 3.3$MPa is applied. The load domain $\mathcal{L}$ is spanned by seven independent load vertices which makes an illustration impossible.

Different to the model of Framatome/Siemens, the model is fixed at the coolant pipe in x, y and z direction, because it is not possible to introduce multi-point constraints (MPC) in the plasticity part of PERMAS V4[1]. At the end of the hot-water pipe precalculated stress resultants are applied. Due to the symmetry of the model the shakedown analysis is performed only for one half of the model. The shakedown constraints are checked in only two of eight Gaussian points of every element, because of the memory restrictions. Different choices of the two nodes in the element give no significant difference in the shakedown analysis. The corresponding shakedown optimization problems with reduced basis have up to 5 unknowns and some 213,360 nonlinear constraints. Nevertheless, the FEM-computation of the model is performed with PERMAS for the whole structure. The material data are temperature dependent (see the following table) corresponding to KTA 3201.1:

T	50	100	200	300	400	$[°C]$
σ_y	191	177	157	136	125	[MPa]
E	200	194	186	179	172	[GPa]
ν	0.3	0.3	0.3	0.3	0.3	-
α_t	1.6	1.6	1.7	1.7	1.8	$\cdot 10^{-5}$ [K^{-1}]

Due to the loading the material data are chosen at $400°C$ in the first step, such that $\nu = 0.3$, $E = 172$ GPa, $\sigma_y = 125$ MPa, $\alpha_t = 1.8\ 10^{-5}K^{-1}$. A good fit for the yield stress in the given temperature range is the function

$$\sigma_y(T) = 197.2\text{MPa} - 0.19\text{MPa}/°\text{C} \cdot T.$$

After the first shakedown analysis the maximal temperature is estimated and the temperature dependent material data are updated. Under constant pressure loading without

[1]MPC are available with plasticity from PERMAS Version 6 onwards

cold water injection ($t_1 = 0s$) the highest von Mises stresses in the mixing device are $\sigma_{max} = 53$ MPa, such that no yielding occurs.

The highest fictitious elastic equivalent stresses occur at $t_4 = 33.2s$ such that the corresponding load vertex is decisive for the behaviour of the structure. The model starts to yield at the maximal highest temperature difference $\theta_{elast} = 57°C$ for a fixed cold water temperature of $50°C$.

The obtained shakedown load factor α corresponding to the initial load domain $\mathcal{L}$ induced by the seven temperature differences θ_j is $\alpha = 1.3$, such that the maximum allowed temperature T_{max} for a fixed cold water temperature of $T_0 = 50°C$ is $T_{max} = \alpha\theta_{elast} + 50°C = 124°C$, instead of the applied maximum temperature of $T_{max} = 237°C$. The corresponding yield stress is $\sigma_y(T = 124°C) = 173.6$MPa.

Therefore no shakedown is achieved for perfectly plastic material. However, it may be expected that the kinematic hardening effect leads to elastic shakedown.

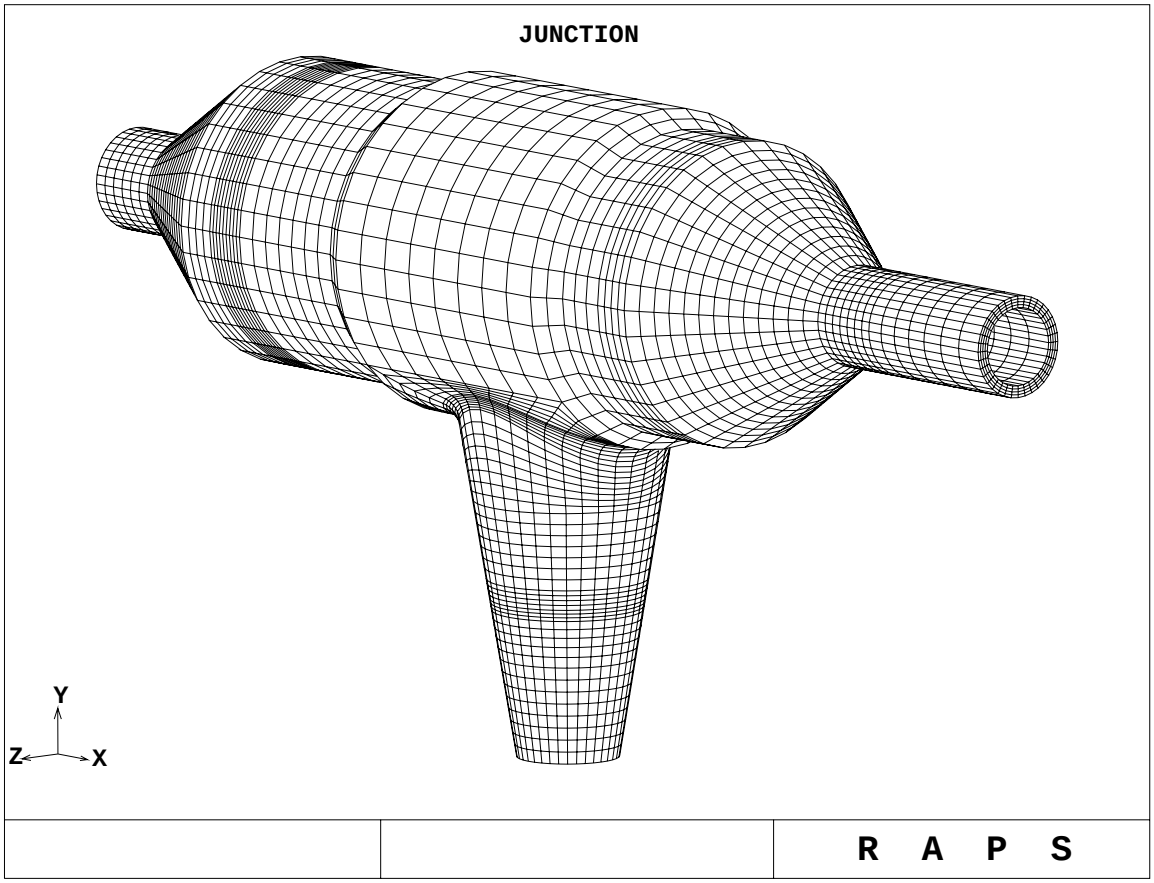

Figure 4.3: Mixing device with high thermal transient loading, internal pressure and external piping loads

4.3 Experimental validation

In the LISA project shakedown experiments were carried out for Framatome/Siemens using a 4-bar model comprising a water-cooled internal tube and three insulated heatable outer test bars. The system was subjected to alternating axial forces, superimposed with alternating temperatures at the outer bars. The test parameters were partly selected on the basis of previous shakedown analyses. PERMAS shakedown analyses and detailed ANSYS FEM ratchetting analyses are compared with the experiments in [29]. A tension–torsion shakedown experiment and shakedown analyses are presented in [18], [49].

Limit analyses have been compared to of fracture mechanics tests in [50] and to 281 burst tests of pressure vessels and piping in [51]. It is found that limit analysis makes close predictions of collapse loads for structures with crack like defects if the material is not brittle.

5 Kinematic hardening material model

The static limit and shakedown theorem has been formulated by Melan for perfectly plastic and for unbounded kinematic hardening material [34]. Using a two–surface plasticity model, a generalization to bounded kinematic hardening has been proposed in [58]. The bounded hardening is the key to realistic shakedown analyses and the simple two–surface plasticity model compares well with the Armstrong and Frederick hardening model [49].

Originally, the basis reduction method has been formulated for a perfectly plastic material model. Its extension to the more realistic bounded kinematic hardening material has been achieved in [64], [53] by use of the overlay model (also called fraction or multiple subvolume model) which preserves the characteristic structure of the perfectly plastic formulation. However, before this approach can be used with a commercial FE code it would be necessary to implement the overlay model for different types of finite elements.

It is the purpose of this section to propose a modified basis reduction method for the structure of a two-surface plasticity formulation of bounded kinematic hardening [17]. It can be used for any type of finite elements with no need to make any changes in the plasticity section of the FE code. The new method is implemented in the general FE–code PERMAS [36]. An increase of the load carrying capacity due to hardening is shown in some numerical examples.

5.1 Bounded kinematic hardening

The Generalized Standard Material Model is used to describe the theoretical frame [13]. An elastic–plastic body of finite volume V with a sufficiently smooth surface ∂V, subjected to the quasi–statical thermo–mechanical loads $\mathbf{P}(t)$ varying in the load domain $\mathcal{L}$

is considered. The hypothesis of small displacements and small strains is made and the strains are decomposed in:

$$\boldsymbol{\varepsilon} = \boldsymbol{\varepsilon}^E + \boldsymbol{\varepsilon}^p + \boldsymbol{\varepsilon}^{th} \text{ with } \boldsymbol{\varepsilon}^{th} = \alpha_t \, \theta \, \mathbf{I}. \tag{5.1}$$

Here α_t is the coefficient of isotropic thermal expansion and $\theta = T - T_0$, where T_0 is a reference temperature. The observable variables are the total strain $\boldsymbol{\varepsilon}$ and the temperature T. The internal variables $\boldsymbol{\varepsilon}^p$ and κ will describe the influence of the past history. The thermodynamic potential ψ has the form

$$\psi = \psi(\boldsymbol{\varepsilon}^E, \kappa \, , T) = \psi_e(\boldsymbol{\varepsilon}^E, T) + \psi_p(\kappa). \tag{5.2}$$

It is assumed that $\rho\psi_p$ is a quadratic form in the variable κ and

$$\rho\psi_e = \frac{1}{2}(\boldsymbol{\varepsilon}^E - \alpha_t\theta\mathbf{I}) : \mathbf{E} : (\boldsymbol{\varepsilon}^E - \alpha_t\theta\mathbf{I}) + C_\varepsilon\theta^2, \tag{5.3}$$

where ρ is the mass density, $\mathbf{E}$ is the elasticity tensor, C_ε is the specific heat at constant strain.

The associated variables, i.e. the observable stresses $\boldsymbol{\sigma}$ and the internal back–stresses $\boldsymbol{\pi}$, are derived from the potential ψ as follows:

$$\boldsymbol{\sigma} = \rho\frac{\partial\psi}{\partial\boldsymbol{\varepsilon}^E} \, ; \qquad \boldsymbol{\pi} = \rho\frac{\partial\psi}{\partial\kappa}. \tag{5.4}$$

The internal variable κ is a kinematic hardening variable and its associated variable $\boldsymbol{\pi}$ is associated with the center of the elastic domain.

Assuming the decoupling between intrinsic (mechanical) dissipation and thermal dissipation, the Clausius–Duhem inequality gives:

$$\boldsymbol{\sigma} : \dot{\boldsymbol{\varepsilon}}^p - \boldsymbol{\pi} : \dot{\kappa} \geq 0. \tag{5.5}$$

The linear kinematic hardening corresponds to the translation of the loading surface:

$$F[\boldsymbol{\sigma} - \boldsymbol{\pi}] = \sigma_y^2. \tag{5.6}$$

The interior of the loading surface $\left\{\boldsymbol{\sigma} \mid F[\boldsymbol{\sigma} - \boldsymbol{\pi}] < \sigma_y^2\right\}$ is the elastic domain which is described by the yield function F and the yield stress σ_y. The stress $\boldsymbol{\sigma}$ is bounded by the uniaxial limit strength σ_u (somewhat below the ultimate stress) and the limit surface is described with the same von Mises function:

$$F[\boldsymbol{\sigma}] \leq \sigma_u^2. \tag{5.7}$$

The elastic domain remains always in the limit surface and any stress point in it may be reached if and only if

$$F[\boldsymbol{\pi}] \leq \left(\sigma_u - \sigma_y\right)^2. \tag{5.8}$$

The associated normality hypothesis is made for the plastic flow:

$$\dot{\kappa} = \dot{\boldsymbol{\varepsilon}}^p = \dot{\lambda}\frac{\partial\sqrt{F}}{\partial\boldsymbol{\sigma}}[\boldsymbol{\sigma}-\boldsymbol{\pi}], \text{ with } \begin{cases} \dot{\lambda}=0, & \text{if } F[\boldsymbol{\sigma}-\boldsymbol{\pi}] < \sigma_y^2 \\ \dot{\lambda}=0, & \text{if } F[\boldsymbol{\sigma}-\boldsymbol{\pi}] = \sigma_y^2 \text{ and} \\ & (\dot{\boldsymbol{\sigma}}-\dot{\boldsymbol{\pi}}) : \dfrac{\partial\sqrt{F}}{\partial\boldsymbol{\sigma}}[\boldsymbol{\sigma}-\boldsymbol{\pi}] < 0 \\ \dot{\lambda}>0, & \text{else.} \end{cases} \tag{5.9}$$

5.2 Lower bound approach

The extended static shakedown theorem can be formulated for a bounded kinematic hardening material as follows [53]:

> If there exist a time–independent back–stresses field $\bar{\boldsymbol{\pi}}(\mathbf{x})$ satisfying
>
> $$F[\bar{\boldsymbol{\pi}}(\mathbf{x})] \le \left(\sigma_u(\mathbf{x}) - \sigma_y(\mathbf{x})\right)^2, \tag{5.10}$$
>
> a factor $\alpha > 1$ and a time–independent residual stress field $\bar{\boldsymbol{\rho}}(\mathbf{x})$ such that
>
> $$F[\alpha\boldsymbol{\sigma}^E(\mathbf{x},t) + \bar{\boldsymbol{\rho}}(\mathbf{x}) - \bar{\boldsymbol{\pi}}(\mathbf{x})] \le \sigma_y^2(\mathbf{x}) \tag{5.11}$$
>
> holds for all possible loads $\mathbf{P}(t) \in \mathcal{L}$ and for all material points $\mathbf{x}$, then the structure will shake down elastically under the given load domain $\mathcal{L}$.

The greatest value α_{sd} for which the theorem holds is called shakedown-factor. This lower bound approach leads to the convex optimization problem

$$\begin{aligned} \max \quad & \alpha \\ \text{s.t.} \quad & F[\alpha\boldsymbol{\sigma}^E(\mathbf{x},t) + \bar{\boldsymbol{\rho}}(\mathbf{x}) - \bar{\boldsymbol{\pi}}(\mathbf{x})] \le \sigma_y^2(\mathbf{x}) \qquad \forall \mathbf{x} \in V \\ & F[\boldsymbol{\pi}(\mathbf{x})] \le \left(\sigma_u(\mathbf{x}) - \sigma_y(\mathbf{x})\right)^2 \qquad \forall \mathbf{x} \in V \\ & \operatorname{div} \bar{\boldsymbol{\rho}}(\mathbf{x}) = \mathbf{0} \qquad \forall \mathbf{x} \in V \\ & \bar{\boldsymbol{\rho}}(\mathbf{x})\,\mathbf{n} = \mathbf{0} \qquad \forall \mathbf{x} \in \partial V_p \end{aligned} \tag{5.12}$$

with infinitely many constraints, which can be reduced to a finite problem by FEM discretization (see the preceeding sections). For the perfectly plastic behavior ($\sigma_u = \sigma_y$), the back–stresses $\bar{\boldsymbol{\pi}}$ are identical zero due to the second inequality. Melan's original theorem for unbounded kinematic hardening can be also deduced from the previous formulation if $\sigma_u \to \infty$. Then the second inequality is not relevant anymore and the back–stresses $\bar{\boldsymbol{\pi}}$ are free variables.

The 3–dimensional overlay (microelement) model, known also as Besseling's fraction model [3], was used in [53] for solving numerically the problem (5.12). In the overlay

model an infinite number of microelements denoted by the scalar $\xi \in [0,1]$ are associated with each material point of the given structure $\mathbf{x} \in V$. In a simple model each layer (characterized by a constant ξ) behaves elastic, perfectly plastic. All layers have the same elasticity tensor, but they have different yield stresses denoted by $k(\xi)$. It is assumed that the internal strength $k(\xi)$ is a monotonously increasing function of ξ and for each $\mathbf{x}$ holds,

$$k(\mathbf{x},0) = \sigma_y(\mathbf{x}), \quad \int_0^1 k(\mathbf{x},\xi)d\xi = \sigma_u(\mathbf{x}). \tag{5.13}$$

It has been proven in [64] that the solution of the problem (5.12) depends only on the values $\sigma_u(\mathbf{x})$ and $\sigma_y(\mathbf{x})$, i.e. it does not depend on the function $k(\xi)$.

5.3 Discretization of the problem

The discretization is similar to the perfectly plastic case, such that with the fictitious elastic stresses $\boldsymbol{\sigma}_i^E(j)$, the residual stresses $\bar{\boldsymbol{\rho}}_i$, the back-stresses $\bar{\boldsymbol{\pi}}_i$, the yield stresses $\sigma_{y,i}$ and the uniaxial limit strength $\sigma_{u,i}$ in the Gaussian points i for the load vertices j the discretized shakedown problem of the lower bound approach for bounded kinematic hardening becomes:

$$\begin{aligned} \max \quad & \alpha \\ \text{s.t.} \quad & F[\alpha\boldsymbol{\sigma}_i^E(j) + \bar{\boldsymbol{\rho}}_i - \bar{\boldsymbol{\pi}}_i] \le \sigma_{y,i}^2 \\ & F[\bar{\boldsymbol{\pi}}_i] \le (\sigma_{u,i} - \sigma_{y,i})^2 \\ & \text{for} i = 1,\ldots,NG,\ j = 1,\ldots,NV,\ \bar{\boldsymbol{\rho}}_i \in \mathcal{B} \text{ and} \boldsymbol{\pi}_i \in I\!R^{NSK\cdot NG}. \end{aligned} \tag{5.14}$$

The number of constraints is finite and for structures with NG Gaussian points we have to handle $O(NG)$ unknowns and $O(NG)$ constraints. Compared to the perfectly plastic and the unbounded kinematic hardening models, the problem (5.14) has almost a double number of unknowns. The number of inequality constraints increases by NG because of the limiting conditions $F[\bar{\boldsymbol{\pi}}_i] \le (\sigma_{u,i} - \sigma_{y,i})^2$.

5.4 Proposed method for bounded kinematic hardening

The basis reduction and the subspace iteration technique described in the preceeding section cannot be directly applied to the shakedown problem for bounded kinematic hardening model. A method using the overlay model and the basis reduction was developed in [64], [53]. The overlay model imposes that all the layers are discretized in the same way, i.e. the elements which lay on top of each other have the same nodes. Therefore, the implementation described in these papers can be applied only for two–dimensional finite elements

or for particular three–dimensional finite elements. The method proposed in this section is applicable with arbitrary three–dimensional finite elements.

Under the condition

$$\sigma_u < 2\sigma_y \tag{5.15}$$

we propose a new method for estimating the shakedown load factor corresponding to a bounded kinematic hardening behavior described through the constitutive equations of the preceeding section (see also the following Remark 3).

Let α_{pp} be the solution of the optimization problem corresponding to the perfectly plastic case (1.31). The basis reduction technique for perfectly plastic material can be used for this problem. Let $\bar{\boldsymbol{\rho}}_{pp}$ be a residual stress such that $(\alpha_{pp}\ , \bar{\boldsymbol{\rho}}_{pp})$ is a feasible point for problem (1.31) and at least for one Gaussian point i^* and one load vertex j^*, the equality is achieved (i.e. the vertex j^* is active). Corresponding to this load vertex the back–stress $\boldsymbol{\pi}^*$ is chosen:

$$\boldsymbol{\pi}_i^* = \frac{\sigma_{u,i} - \sigma_{y,i}}{\sigma_{y,i}} \left(\alpha_{pp}\boldsymbol{\sigma}_i^E(j^*) + \bar{\boldsymbol{\rho}}_{pp,i}\right) \quad \text{with } i = 1, \ldots, NG. \tag{5.16}$$

The following optimization problem gives an estimation of the bounded kinematic hardening load factor α_{BSD} regarding the back-stresses $\boldsymbol{\pi}_i^*$ as the elastic response to a fictitious dead load:

$$\begin{aligned} \max \quad & \alpha \\ \text{s.t.} \quad & F[\alpha\boldsymbol{\sigma}_i^E(j) + \bar{\boldsymbol{\rho}}_i - \boldsymbol{\pi}_i^*] \le \sigma_{y,i}^2 \\ & \text{for } i = 1, \ldots, NG,\ \ j = 1, \ldots, NV,\ \ \bar{\boldsymbol{\rho}}_i \in \mathcal{B}. \end{aligned} \tag{5.17}$$

The basis reduction technique for perfectly plastic problems with dead loads (1.13) applies to the problem (5.17), this time with the stresses $\boldsymbol{\sigma}_0^E = -\boldsymbol{\pi}^*$. The condition (5.15) assures that $(0, \mathbf{0})$ is a feasible point for this problem, therefore its admissible set is non-empty.

The solution α^* of the problem (5.17) is an estimation of the load factor α_{BSD}.

If $(\alpha, \bar{\boldsymbol{\rho}})$ is a feasible point for the problem (5.17), then $(\alpha, \bar{\boldsymbol{\rho}}, \boldsymbol{\pi}^*)$ is a feasible point for the optimization problem which gives the shakedown load factor α_{SD} for problem (5.14), such that it follows $\alpha^* \le \alpha_{BSD}$.

Also, we must notice that if $(\alpha, \bar{\boldsymbol{\rho}})$ is a feasible point for the problem (1.31), then $\sigma_y/\sigma_u\,(\alpha, \bar{\boldsymbol{\rho}})$ is a feasible point for the problem (5.14). Consequently, the greatest possible value of α_{BSD} is $\sigma_u/\sigma_y\alpha_{pp}$. The constants σ_y and σ_u denote the minimum, respectively the maximum, over all the Gaussian points $\mathbf{x}_i$ of $\sigma_{y,i}$ and $\sigma_{u,i}$, respectively.

Remark 1

Let us consider the particular load domain $\mathcal{L} = [\mathbf{0}, \mathbf{P}]$, i.e. $\mathcal{L}$ is the convex set generated by the load vertices $\mathbf{0}$ and $\mathbf{P}$. For homogeneous material the yield and the uniaxial limit strength do not vary with the Gaussian points. In this case, if $(\alpha, \bar{\boldsymbol{\rho}})$ is a feasible point for the problem (1.31), then $F[\bar{\boldsymbol{\rho}}_i] \le \sigma_y^2$ for each i and it follows easily that $(\alpha, (2 - \sigma_u/\sigma_y)\,\bar{\boldsymbol{\rho}})$ is a feasible point for the problem (5.17). Consequently, in this particular case $\alpha_{pp} \le \alpha^*$.

Remark 2

In limit analysis, i.e. for the load domain $\mathcal{L} = \{\mathbf{P}\}$, if the yield stress and the uniaxial limit strength are constant then a well–known result proves that $\alpha_{BSD} = \sigma_u/\sigma_y\alpha_{pp}$. Moreover, it follows easily that in this hypotheses also $\alpha^* = \alpha_{BSD}$. For a general load domain this assertion is not true anymore, α_{BSD} could take any value in the closed interval $[\alpha_{pp}, \sigma_u/\sigma_y\alpha_{pp}]$.

Remark 3

Let us consider the particular load domain $\mathcal{L}$ which contains the zero load (e.g. as load vertex). We will prove that in the case $\sigma_u \geq 2\sigma_y$ the load factor α_{BSD} for the bounded kinematic hardening shakedown problem (5.14) is equal to the load factor α_{USD} for the unbounded kinematic hardening shakedown problem.

The unbounded kinematic hardening shakedown problem is:

$$\begin{aligned} \max \quad & \alpha \\ \text{s.t.} \quad & F[\alpha\boldsymbol{\sigma}_i^E(j) + \bar{\boldsymbol{\rho}}_i - \bar{\boldsymbol{\pi}}_i] \leq \sigma_{y,i}^2 \\ & \text{for } i = 1,\ldots,NG,\ j = 1,\ldots,NV,\ \bar{\boldsymbol{\rho}}_i \in \mathcal{B} \text{ and} \bar{\boldsymbol{\pi}}_i \in I\!R^{NSK\cdot NG}. \end{aligned} \tag{5.18}$$

As the feasible set of the maximum problem (5.14) is obviously in the feasible set of the maximum problem (5.18), it follows immediately that $\alpha_{BSD} \leq \alpha_{USD}$. On the other hand, α_{USD} is the solution of the problem (5.18), therefore there exist $\boldsymbol{\rho}^*$, $\boldsymbol{\pi}^*$ such that $(\alpha_{USD}, \boldsymbol{\rho}^*, \boldsymbol{\pi}^*)$ is a feasible point for this problem. The first inequality of (5.18) gives for the zero load:

$$F[\boldsymbol{\rho}_i^* - \boldsymbol{\pi}_i^*] \leq \sigma_{y,i}^2 \text{ for } i = 1,\ldots,NG. \tag{5.19}$$

From the hypothesis $\sigma_u \geq 2\sigma_y$ it follows that

$$F[\boldsymbol{\rho}_i^* - \boldsymbol{\pi}_i^*] \leq (\sigma_{u,i} - \sigma_{y,i})^2 \text{ for } i = 1,\ldots,NG. \tag{5.20}$$

On the other hand,

$$F[\alpha_{USD}\boldsymbol{\sigma}_i^E(j) + \boldsymbol{\rho}_i^* - \boldsymbol{\pi}_i^*] \leq \sigma_{y,i}^2 \text{ for} i = 1,\ldots,NG,\ j = 1,\ldots,NV. \tag{5.21}$$

Therefore, $(\alpha_{USD}, 0, \boldsymbol{\pi}^* - \boldsymbol{\rho}^*)$ is a feasible point for the problem (5.14) of bounded kinematic hardening and it follows $\alpha_{BSD} \geq \alpha_{USD}$. We have proved that $\alpha_{BSD} = \alpha_{USD}$ in the case $\sigma_u \geq 2\sigma_y$.

Remark 4

Let us consider the particular load domain $\mathcal{L}$ which contains the zero load (e.g. as load vertex). Let α_{BSD} be the load factor for the bounded kinematic hardening shakedown problem (5.14) and let $(\alpha_{BSD}, \bar{\boldsymbol{\rho}}, \bar{\boldsymbol{\pi}})$ be a feasible point for this problem. As the zero load is part of the load domain $\mathcal{L}$, from the first inequality of (5.14) it follows that

$$F[\bar{\boldsymbol{\rho}}_i - \bar{\boldsymbol{\pi}}_i] \leq \sigma_{y,i}^2 \text{ for} i = 1,\ldots,NG. \tag{5.22}$$

By using now the first inequality for arbitrary load vertices, one obtains

$$\sqrt{F[\alpha_{BSD}\boldsymbol{\sigma}_i^E(j)]} \leq \sqrt{F[\alpha_{BSD}\boldsymbol{\sigma}_i^E(j) + \bar{\boldsymbol{\rho}}_i - \bar{\boldsymbol{\pi}}_i]} + \sqrt{F[\bar{\boldsymbol{\rho}}_i - \bar{\boldsymbol{\pi}}_i]} \leq 2\sigma_{y,i} \tag{5.23}$$

Therefore

$$F\left[\frac{\alpha_{BSD}}{2}\boldsymbol{\sigma}_i^E(j)\right] \leq \sigma_{y,i}^2 \text{ for} i = 1,\ldots,NG, j = 1,\ldots,NV. \tag{5.24}$$

We proved that $\alpha_{BSD}/2$ is a feasible point for the problem

$$\begin{aligned} \max \quad & \alpha \\ \text{s.t.} \quad & F[\alpha\boldsymbol{\sigma}_i^E(j)] \leq \sigma_{y,i}^2 \text{ for} i = 1,\ldots,NG,\ j = 1,\ldots,NV. \end{aligned}$$

The solution of the previous problem is the *elastic load factor* α_{el}, because it allows the enlargement of the load domain until the yielding starts in a point of the structure. Consequently, $\alpha_{BSD} \leq 2\alpha_{el}$. With similar arguments, it can be proved that the same upper limit is valid for the unbounded kinematic hardening case, i.e. $\alpha_{USD} \leq 2\alpha_{el}$. This means, that the enlargement of the load domain is limited up to $2\alpha_{el}$ if the load domain $\mathcal{L}$ contains the zero load in the case of bounded or unbounded kinematic hardening material law.

5.5 Local Failure

The shakedown factor for perfectly plastic material α_{pp} could not be greater than the shakedown factor α_{BSD} for bounded kinematic hardening material. Furthermore the relation $\alpha_{BSD} \leq \alpha_{USD}$ holds for the shakedown factor α_{USD} for unbounded kinematic hardening material. The local failure in one point of a structure of unbounded kinematic hardening material corresponds to the weakest failure mode and leads to the greatest shakedown factor α_{local} such that the following chain holds:

$$\alpha_{pp} \leq \alpha_{BSD} \leq \alpha_{USD} \leq \alpha_{local}. \tag{5.25}$$

If α_{pp} equals the value α_{local} all other shakedown factors are the same independent of the specific hardening mode. For structures made of unbounded kinematic hardening material the shakedown behaviour is dominated by some points of the structure, where the maximum expansion of the elastic domain is the minimum over all points $\mathbf{x} \in V$:

$$\alpha_{USD} = \min_{\mathbf{x}\in V}(\max_{\bar{\boldsymbol{\rho}}} \alpha). \tag{5.26}$$

If only one point dominates the behaviour it is possible to solve the optimization problem analytically. In this case the shakedown load for perfectly plastic and unbounded kinematic

hardening material correspond (see [64]). The shakedown optimization problem is solved analytically for unbounded kinematic hardening material in the case of local failure in proportional loading. The backstresses $\bar{\boldsymbol{\pi}}$ have no restrictions in the case of unbounded kinematic hardening material, so that $\mathbf{y} = \bar{\boldsymbol{\rho}} - \bar{\boldsymbol{\pi}}$ are free variables. Assuming that the maximum effective stress would appear at one point of the system, then the optimization problem with the backstresses $\bar{\boldsymbol{\pi}}$ has to be solved

$$\begin{array}{ll} \max & \alpha \\ \text{s.t.} & F(\alpha\boldsymbol{\sigma}_j^E + \mathbf{y}) \leq \sigma_y^2 \quad j = 1, \ldots, NV \end{array} \tag{5.27}$$

only in this point (see [52]). The corresponding Lagrange function is defined as [7]

$$\mathrm{L}(\alpha, \mathbf{y}) = -\alpha - \sum_{j=1}^{NV} \lambda_j [\sigma_y^2 - F(\alpha\boldsymbol{\sigma}_j^E + \mathbf{y})]. \tag{5.28}$$

With the abbreviation $\boldsymbol{\sigma}_j := \boldsymbol{\sigma}_j^E$ it holds

$$F(\alpha\boldsymbol{\sigma}_j + \mathbf{y}) = \alpha^2 \boldsymbol{\sigma}_j^T \mathbf{Q} \boldsymbol{\sigma}_j + 2\alpha \boldsymbol{\sigma}_j^T \mathbf{Q}\mathbf{y} + \mathbf{y}^T \mathbf{Q}\mathbf{y} = (\alpha, \mathbf{y}) \underbrace{\left(\begin{array}{c|c} \boldsymbol{\sigma}_j^T \mathbf{Q} \boldsymbol{\sigma}_j & \boldsymbol{\sigma}_j^T \mathbf{Q} \\ \hline \mathbf{Q}\boldsymbol{\sigma}_j & \mathbf{Q} \end{array} \right)}_{=:\mathbf{A}_j} \left(\begin{array}{c} \alpha \\ \mathbf{y} \end{array} \right). \tag{5.29}$$

The matrix $\mathbf{Q} \in I\!R^{6\times 6}$ is defined for a 3-dimensional problem by the von Mises function. With $\mathbf{z} := (\alpha, \mathbf{y})^T$ and $\mathbf{y} \in I\!R^6$ the short form of (5.28) is

$$\mathrm{L}(\mathbf{z}) = (-1, 0, \ldots, 0)\mathbf{z} - \sum_{j=1}^{NV} \lambda_j [\sigma_y^2 - \mathbf{z}^T \mathbf{A}_j \mathbf{z}] \tag{5.30}$$

$$\text{and} \quad \nabla_{\mathbf{z}} \mathrm{L}(\mathbf{z}) = (-1, 0, \ldots, 0)^T + 2 \sum_{j=1}^{NV} \lambda_j \mathbf{A}_j \mathbf{z} \tag{5.31}$$

with the differential operator $\nabla_{\mathbf{z}} \mathrm{L}(\cdot) = \left(\frac{\partial(\cdot)}{\partial\alpha}, \frac{\partial(\cdot)}{\partial y_1}, \ldots, \frac{\partial(\cdot)}{\partial y_6} \right)$. From the Kuhn–Tucker–conditions $\nabla_{\mathbf{z}} \mathrm{L}(\mathbf{z}^*) = \mathbf{0}$ of a local maximum $\mathbf{z}^* = (\alpha^*, \mathbf{y}^*)^T$ [7] it follows with the optimal Lagrange multipliers λ_j^*

$$\left(\begin{array}{c} 1 \\ 0 \\ \vdots \\ 0 \end{array} \right) = 2 \sum_{j=1}^{NV} \lambda_j^* \left(\begin{array}{c|c} \boldsymbol{\sigma}_j^T \mathbf{Q} \boldsymbol{\sigma}_j & \boldsymbol{\sigma}_j^T \mathbf{Q} \\ \hline \mathbf{Q}\boldsymbol{\sigma}_j & \mathbf{Q} \end{array} \right) \mathbf{z}^* = 2 \left(\begin{array}{c|c} \displaystyle\sum_{j=1}^{NV} \lambda_j^* \boldsymbol{\sigma}_j^T \mathbf{Q} \boldsymbol{\sigma}_j & \left(\displaystyle\sum_{j=1}^{NV} \lambda_j^* \boldsymbol{\sigma}_j \right)^T \mathbf{Q} \\ \hline \mathbf{Q} \left(\displaystyle\sum_{j=1}^{NV} \lambda_j^* \boldsymbol{\sigma}_j \right) & \left(\displaystyle\sum_{j=1}^{NV} \lambda_j^* \right) \mathbf{Q} \end{array} \right) \mathbf{z}^*. \tag{5.32}$$

In the local maximum $\mathbf{z}^*$ the complementary condition of every restriction reads:

$$\lambda_j^*(\sigma_y^2 - \mathbf{z}^{*T}\mathbf{A}_j\mathbf{z}^*) = 0 \quad j = 1, \ldots, NV. \tag{5.33}$$

After summation of all complementary conditions, it is deduced with (5.32)

$$\sigma_y^2 \sum_{j=1}^{NV} \lambda_j^* = \sum_{j=1}^{NV} \lambda_j^* \mathbf{z}^{*T}\mathbf{A}_j\mathbf{z}^* = \mathbf{z}^{*T} \sum_{j=1}^{NV} \lambda_j^* \mathbf{A}_j \mathbf{z}^* = \frac{1}{2}(1, 0, \ldots, 0)\mathbf{z}^* = \frac{1}{2}\alpha^*. \tag{5.34}$$

There is a unique representation of α^* by the Lagrange multipliers λ_j^*:

$$\alpha^* = 2\sigma_y^2 \sum_{j=1}^{NV} \lambda_j^*. \tag{5.35}$$

With Eq. (5.35) it follows from (5.32)

$$\mathbf{0} = \left(\mathbf{Q} \sum_{j=1}^{NV} \lambda_j^* \boldsymbol{\sigma}_j \, , \, \sum_{j=1}^{NV} \lambda_j^* \mathbf{Q} \right) \mathbf{z}^* = \alpha^* \sum_{j=1}^{NV} \lambda_j^* \mathbf{Q}\boldsymbol{\sigma}_j + \left(\sum_{j=1}^{NV} \lambda_j^* \right) \mathbf{Q}\mathbf{y}^* \tag{5.36}$$

$$= \alpha^* \sum_{j=1}^{NV} \lambda_j^* \mathbf{Q}\boldsymbol{\sigma}_j + \frac{\alpha^*}{2\sigma_y^2} \mathbf{Q}\mathbf{y}^*, \tag{5.37}$$

and with $\alpha^* > 0$

$$\mathbf{Q}\mathbf{y}^* = -2\sigma_y^2 \sum_{j=1}^{NV} \lambda_j^* \mathbf{Q}\boldsymbol{\sigma}_j. \tag{5.38}$$

Now with Eq. (5.32) it follows

$$\frac{1}{2} = \left(\sum_{j=1}^{NV} \lambda_j^* \boldsymbol{\sigma}_j^T \mathbf{Q}\boldsymbol{\sigma}_j \, , \, \sum_{j=1}^{NV} \lambda_j^* \boldsymbol{\sigma}_j^T \mathbf{Q} \right) \mathbf{z}^* = \alpha^* \sum_{j=1}^{NV} \lambda_j^* \boldsymbol{\sigma}_j^T \mathbf{Q}\boldsymbol{\sigma}_j + \sum_{j=1}^{NV} \lambda_j^* \boldsymbol{\sigma}_j^T \mathbf{Q}\mathbf{y}^* \tag{5.39}$$

and with Eq. (5.38) it is

$$\frac{2\alpha^* \sum_{j=1}^{NV} \lambda_j^* \boldsymbol{\sigma}_j^T \mathbf{Q}\boldsymbol{\sigma}_j - 1}{4\sigma_y^2} = \left(\sum_{j=1}^{NV} \lambda_j^* \boldsymbol{\sigma}_j \right)^T \left(\sum_{j=1}^{NV} \lambda_j^* \mathbf{Q}\boldsymbol{\sigma}_j \right) = \left(\sum_{j=1}^{NV} \lambda_j^* \boldsymbol{\sigma}_j \right) \mathbf{Q}^T \left(\sum_{j=1}^{NV} \lambda_j^* \boldsymbol{\sigma}_j \right) \tag{5.40}$$

In the case of proportional loading the load domain $\mathcal{L}$ has two vertices in shakedown analysis. The corresponding fictitious elastic stresses $\boldsymbol{\sigma}_1$ and $\boldsymbol{\sigma}_2$ with $F(\boldsymbol{\sigma}_1) = 0$ and $F(\boldsymbol{\sigma}_2) = \sigma_y^2$ to the two load vertices read

$$\boldsymbol{\sigma}_1 = (0, 0, 0, 0, 0, 0) \text{ and } \boldsymbol{\sigma}_2 = (s_1, s_2, s_3, s_4, s_5, s_6) \tag{5.41}$$

From Eq. (5.35) follows

$$\alpha^* = 2\sigma_y^2(\lambda_1^* + \lambda_2^*) \tag{5.42}$$

such that with Eq. (5.35) and Eq. (5.40) it is

$$(\lambda_1^* + \lambda_2^*)\lambda_2^* - \frac{1}{4\sigma_y^2} = \lambda_2^*\sigma_y^2 \quad \text{or} \quad \lambda_1^*\lambda_2^* = \frac{1}{4\sigma_y^4}. \tag{5.43}$$

This means, that both restrictions must be active in the local maximum. From the Kuhn–Tucker–conditions and equations (5.35) and (5.43) follows

$$\lambda_1^* = \lambda_2^* = \frac{1}{2\sigma_y^2} \qquad \text{and} \qquad \alpha^* = 2. \tag{5.44}$$

In proportional loading the shakedown load is twice the elastic load for unbounded kinematic hardening material if the failure is local, such that it holds $\alpha_{local}^{prop} = 2$. This result holds independently of the hardening exponent and also for perfectly plastic material due to the local failure.

For elastic-plastic structures subjected to thermal loading the elastic stresses are residual stresses $\bar{\boldsymbol{\rho}} = \boldsymbol{\sigma}^E$, such that a lower bound for the shakedown load is $\alpha = 2$ independent of the hardening type. Therefore, for structures subjected to thermal loading the shakedown load factor is twice the elastic load independent of the hardening type, i.e. for perfectly plastic, bounded and unbounded kinematic hardening materials.

5.6 Implementation

The method proposed in the previous paragraph for obtaining an estimation of the shakedown factor has the advantage that instead of solving the optimization problem (5.14) with $1 + \dim \mathcal{B} + NSK \cdot NG$ unknowns, two optimization problems are solved which can be treated with the basis reduction method for perfectly plastic material with dead loads. Consequently, even for large–scale optimization problems we have to solve a sequence of optimization problems with a small number of unknowns (maximum 7 unknowns).

The numerical tests performed for the mechanical problems described in the next paragraph give values of α^* which are superior to α_{pp}. For particular load domains the new method gives a value of α^* equal to the limit value $\sigma_u/\sigma_y\alpha_{pp}$.

For the considered examples, a reiteration of the method proposed in section 5.4 does not give an improvement of the load factor α^*. We expect that if the residual stress $\boldsymbol{\rho}^*$ is chosen such that $(\alpha^*, \boldsymbol{\rho}^*)$ is a feasible point for the problem (5.17) and if the fictitious elastic stress $\widetilde{\boldsymbol{\sigma}}^E$ corresponds to an active load vertex, then α^* is an approximation for the numerical solution of the problem

$$\begin{aligned} \max \quad & \alpha \\ \text{s.t.} \quad & F[\alpha\boldsymbol{\sigma}_i^E(j) + \bar{\boldsymbol{\rho}}_i - \widetilde{\boldsymbol{\pi}}_i] \le \sigma_{y,i}^2 \\ & \text{for } i = 1, \ldots, NG, \;\; j = 1, \ldots, NV, \;\; \bar{\boldsymbol{\rho}}_i \in \mathcal{B} \end{aligned}$$

with the back–stress $\widetilde{\boldsymbol{\pi}}$ given by

$$\widetilde{\boldsymbol{\pi}}_i = \frac{\sigma_{u,i} - \sigma_{y,i}}{\sigma_{y,i}} \left(\alpha^* \widetilde{\boldsymbol{\sigma}}_i^E + \boldsymbol{\rho}_i^* \right) \qquad i = 1, \ldots, NG. \tag{5.45}$$

Therefore, we consider that a better estimation of the shakedown load factor α_{SD} cannot be obtained in this way. The numerical tests have shown that the particular choice of an active load vertex j^* has no influence on the value obtained for α^*.

5.7 Numerical results

5.7.1 Problem 1

A thin rectangular plate supported in the vertical direction is considered. The tension p is applied on the lateral sides and the temperature T is equally distributed on the plate (see Figure 5.1). The numerical results for the bounded kinematic hardening material correspond to the choice $\sigma_u = 1.5\,\sigma_y$. Due to the symmetry of the problem, only a quarter of the plate is considered. The nodes on the symmetry plane $x = 0$ can move only in the horizontal direction and the nodes on the symmetry plane $y = 0$ only in the vertical direction. Because of the homogeneity of the problem we have used only one 9-noded quadrilateral plane membrane element QUAM9 [36]. The load factors corresponding to the elastic, the perfectly plastic and the bounded kinematic hardening material were computed for different ratios of p and T. The load domain $\mathcal{L}$ represented in the tension–temperature space has

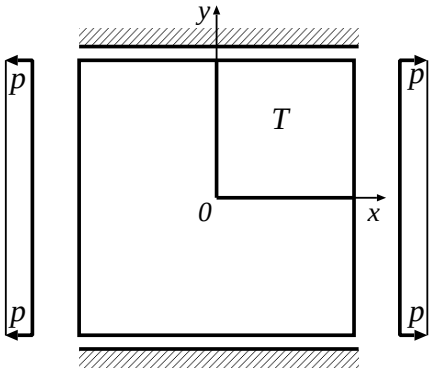

Figure 5.1: Thin plate

four load vertices:

$$\mathbf{P}(1) = (p, 0),\ \mathbf{P}(2) = (0, T),\ \mathbf{P}(3) = (p, T),\ \mathbf{P}(4) = (0, 0). \tag{5.46}$$

The enlarged domain $\alpha\mathcal{L}$ is completely determined by the load vertex $(\alpha p, \alpha T)$. The points $(\alpha p, \alpha T)$, where α is the computed load factor, are represented for different ratios of p and

T. The obtained numerical results are shown in the Figure 5.2. The analytical elastic solution for purely mechanical and purely thermal load,

$$p_0 = \frac{1}{\sqrt{1-\nu+\nu^2}}\sigma_y \quad \text{and} \quad T_0 = \frac{1}{E\alpha_t}\sigma_y, \tag{5.47}$$

respectively, are used for scaling. Here, ν is the Poisson's ratio, E is the Young's modulus for the considered material and α_t is the coefficient of thermal expansion.

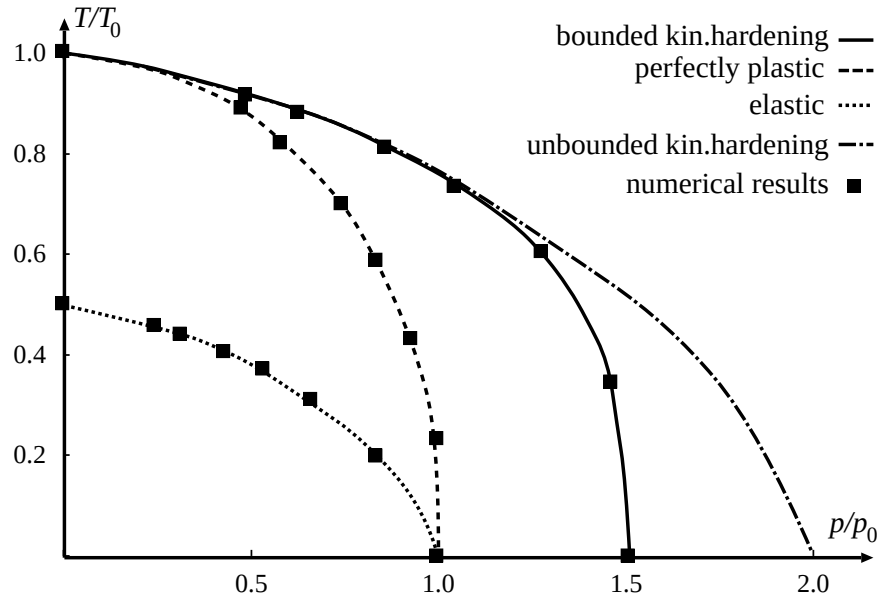

Figure 5.2: Shakedown diagram for thin plate

We have observed only a small influence of the bounded hardening for predominant thermal loadings. A significant increase of the load factor due to the bounded hardening is noticed if the pressure is dominant. The maximal possible shakedown load factor of $1.5\,\alpha_{pp}$ (i.e. σ_u/σ_y–times the perfectly plastic α_{pp}) is achieved when there is no temperature load. The curve obtained from the elastic curve through a homothety by factor 2 gives an analytical lower bound of the shakedown load factors for unbounded kinematic hardening behavior. In the purely mechanical loading case the plate yields homogeneously, thus the elastic and perfectly plastic factors coincide. Due to this behavior it is impossible to generate nontrivial residual stresses and therefore numerical problems occur in the optimization algorithm.

5.7.2 Problem 2

A thin pipe with the radius R and the thickness $d = 0.1\,R$ is fixed in the axial direction. The pressure p and the temperature diffference $\theta \geq 0$ are applied on the interior side (see

Figure 5.3). The numerical results for the bounded kinematic hardening behavior correspond to the choice $\sigma_u = 1.35\,\sigma_y$. Eight axisymmetric ring elements with quadrilateral cross section QUAX9 [36] are used for the discretization. A linear temperature distribution is chosen for the thin pipe. The load factors corresponding to the elastic, the perfectly plastic and the bounded kinematic hardening material were computed for different ratios of p and T.

The load domain $\mathcal{L}$ represented in the pressure–temperature space has four load vertices:

$$\mathbf{P}(1) = (p, 0),\ \mathbf{P}(2) = (0, T),\ \mathbf{P}(3) = (p, T),\ \mathbf{P}(4) = (0, 0). \tag{5.48}$$

The enlarged domain $\alpha\mathcal{L}$ is completely determined by the load vertex $(\alpha p, \alpha T)$. The maximal pressure p_0 computed for purely mechanical loads and the maximal temperature T_0 for purely thermal loads are used for scaling,

$$p_0 \ = \tfrac{2\sigma_y}{\sqrt{3}} \ln\left(1 + \tfrac{e}{R}\right) \quad \text{and} \quad T_0 \ = \frac{2(1-\nu)\sigma_y}{E\alpha_t}. \tag{5.49}$$

The points $(\alpha p, \alpha T)$ are represented for different ratios of p and T in Figure 5.4. No influence of the bounded hardening for predominant thermal loadings is observed. An increase of the load factor due to the bounded hardening is observed for predominant pressure loading. The increase of the load factor due to the considered hardening has been observed for those ratios of p and T for which the influence of the mechanical load on the initial yielding is significant.

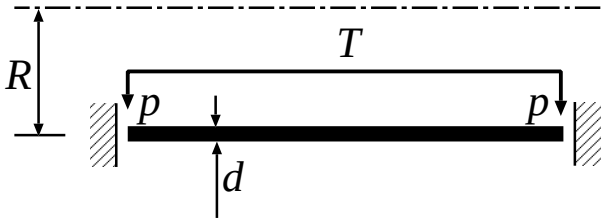

Figure 5.3: Thin pipe

5.7.3 Problem 3

A turbine with uniform thickness rotating around its axis at an angular velocity ω. A radial temperature distribution $T(r) = \frac{r^2}{R^2} T^R$ with outer radius R is applied (see Fig. 5.5). Twenty axisymmetric ring elements with quadrilateral cross section QUAX9 [36] are used for the discretization. Due to the symmetry of the problem only the upper half of the turbine is considered. The load factors corresponding to the elastic, the perfectly plastic and the bounded kinematic hardening material were computed for different ratios of ω and T^R.

The load domain $\mathcal{L}$ has four load vertices:

$$\mathbf{P}(1) = (\omega^2, 0),\ \mathbf{P}(2) = (0, T^R),\ \mathbf{P}(3) = (\omega^2, T^R),\ \mathbf{P}(4) = (0, 0). \tag{5.50}$$

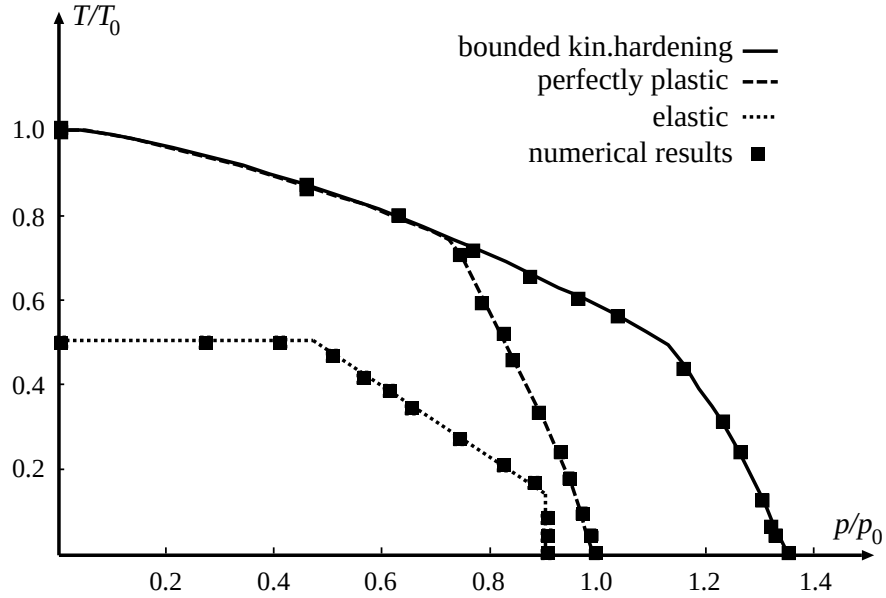

Figure 5.4: Shakedown diagram for thin pipe

The enlarged domain $\alpha\mathcal{L}$ is completely determined by the load vertex $\left(\alpha\omega^2, \alpha T^R\right)$. The points $\left(\alpha\omega^2, \alpha T^R\right)$ where α is the corresponding computed load factor, are represented for different ratios of ω^2 and T^R. The obtained numerical results are shown in Fig. 5.5.

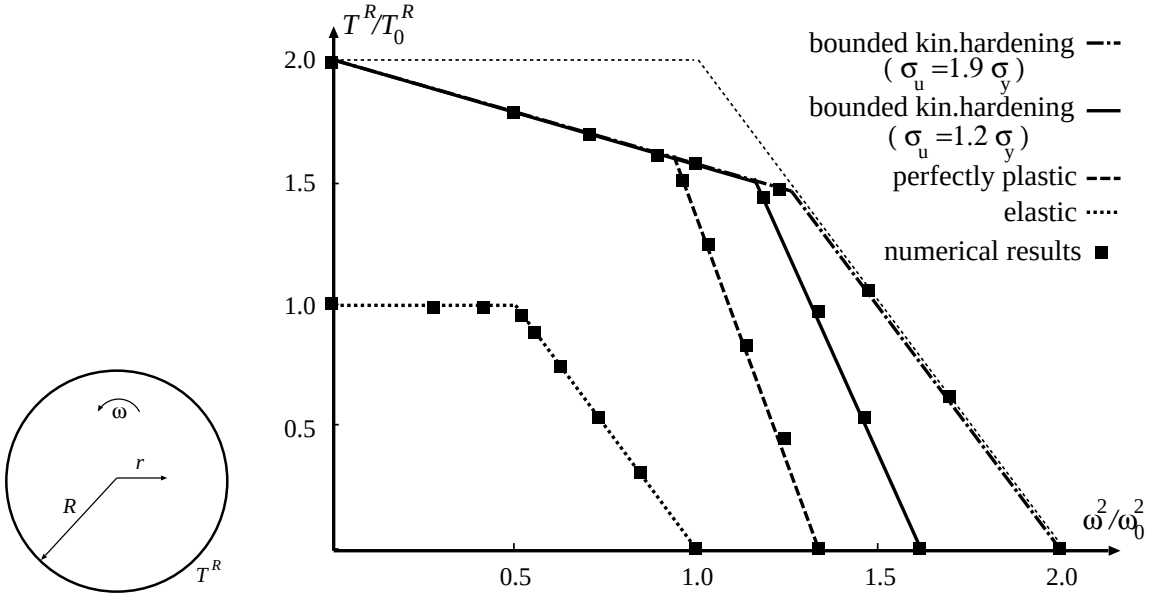

Figure 5.5: Turbine model and shakedown diagram for turbine

The elastic limits for purely mechanical and for purely thermal load

$$\omega_0^2 = \frac{8\sigma_y}{(3+\nu)\rho R^2} \text{ and } T_0^R = \frac{2\sigma_y}{E\alpha_t}, \tag{5.51}$$

respectively, are used for scaling with the the mass density ρ (see the following remark).

Remark

It is assumed that the stresses on planes parallel to the plane of the turbine are zero, the solution corresponding to an elastic behaviour of the turbine is given in [55] by

$$\begin{aligned}\boldsymbol{\sigma}_r(r) &= \frac{3+\nu}{8}\rho\omega^2R^2\left(1-\frac{r^2}{R^2}\right)+\frac{E\alpha_t}{4}T^R\left(1-\frac{r^2}{R^2}\right)\\ \boldsymbol{\sigma}_\varphi(r) &= \frac{3+\nu}{8}\rho\omega^2R^2\left(1-\frac{1+3\nu}{3+\nu}\frac{r^2}{R^2}\right)+\frac{E\alpha_t}{4}T^R\left(1-\frac{3r^2}{R^2}\right)\end{aligned}$$

The polar coordinates are denoted by r and φ. In this case the von Mises yield function becomes

$$F[\boldsymbol{\sigma}(r)] = \boldsymbol{\sigma}_r^2(r)+\boldsymbol{\sigma}_\varphi^2(r)-\boldsymbol{\sigma}_r(r)\boldsymbol{\sigma}_\varphi(r).$$

Its maximum

$$\max\left\{\left(\frac{3+\nu}{8}\rho\omega^2R^2+\frac{E\alpha_t}{4}T^R\right)^2,\left(\frac{1-\nu}{4}\rho\omega^2R^2-\frac{E\alpha_t}{2}T^R\right)^2\right\}$$

is achieved for $r=0$ or for $r=R$. For the considered load domain the elastic load factor is given by the solution of the following problem

$$\begin{aligned}\max\quad & \alpha\\ \text{s.t.}\quad & \max\left\{\alpha\left(\frac{3+\nu}{8}\rho\omega^2R^2+\frac{E\alpha_t}{4}T^R\right),\alpha\left|\frac{1-\nu}{4}\rho\omega^2R^2-\frac{E\alpha_t}{2}T^R\right|\right\}\le\sigma_y\\ & 0\le\alpha\frac{E\alpha_t}{2}T^R\le\sigma_y \text{ and } 0\le\alpha\frac{3+\nu}{8}\rho\omega^2R^2\le\sigma_y\end{aligned}$$

1. If $T^R=0$, the elastic load factor is

   $$\alpha=\frac{8\sigma_y}{(3+\nu)\rho\omega^2R^2},$$

   such that the elastic limit for purely mechanical load is $\omega_0^2=\alpha\omega^2$, which is used for scaling.

2. If $\frac{3+\nu}{8}\rho\omega^2R^2\ge\frac{E\alpha_t}{4}T^R>0$ then the elastic load factor is

   $$\alpha=\sigma_y\left(\frac{3+\nu}{8}\rho\omega^2R^2+\frac{E\alpha_t}{4}T^R\right)^{-1}.$$

   The obtained points $(\alpha\omega^2,\alpha T^R)$ are situated on the line

   $$\frac{3+\nu}{8}\rho\omega^2R^2+\frac{E\alpha_t}{4}T^R=\sigma_y$$

3. If $\frac{3+\nu}{8}\rho\omega^2 R^2 < \frac{E\alpha_t}{4}T^R$ then the elastic load factor is

$$\alpha = \frac{2\sigma_y}{E\alpha_t T^R}.$$

The obtained points $(\alpha\omega^2, \alpha T^R)$ are situated on the line

$$T^R = \frac{2\sigma_y}{E\alpha_t}.$$

The elastic limit of T^R for purely thermal load is T_0^R.

6 Conclusions

Limit and shakedown analyses are simplified but exact methods of classical plasticity, which do not contain any restrictive prerequisites apart from sufficient ductility. The simplifications are obtained by restricting the analysis to the failure state of the structure. Different to the classical handling of nonlinear problems in structural mechanics, the methods lead to optimization problems. A procedure for the direct calculation of the load-carrying capacity of ductile structures is developed on the basis of the industrial FEM program PERMAS using the basis-reduction technique. With this implementation it is possible to perform shakedown analysis for industrial applications with above 100,000 degrees of freedom.

The operation range of a structure can be extended to the plastic regime, without increasing the efforts in relation to elastic analyses substantially. The computing time permits parameter studies and the calculation of interaction diagrams, which give a fast overview on the possible operation ranges. No details of material behaviour and of the load history are needed. This is an important advantage if such data is expensive, uncertain or unavailable in principle.

The basis-reduction technique could be extended for the shakedown analysis of a two-surface plasticity model of bounded linear kinematic hardening. An analytical proof is given, that the shakedown load of structures of unbounded kinematic hardening material subjected to proportional loading and local failure, is twice the elastic load for any hardening exponent. Therefore, shakedown bounds obtained for this failure mode do not increase with kinematic hardening. For structures made of perfectly plastic or of unbounded kinematic hardening material subjected to only thermal proportional loading the shakedown load factor is twice the elastic load independent of the failure mode.

Acknowledgement
The research has been funded by the European Commission as part of the Brite–EuRam III project LISA: FEM–Based Limit and Shakedown Analysis for Design and Integrity Assessment in European Industry (Project N°: BE 97–4547, Contract N°: BRPR–CT97–0595).

Bibliography

[1] J. Argyris, H.-P. Mlejnik: *Die Methode der Finiten Elemente: Band I – II*. Vieweg Braunschweig (1986–1987).

[2] M. S. Bazaraa, H. D. Sherali, C. M. Shetty: *Nonlinear Programming. Theory and Algorithms*. John Wiley New York (1993).

[3] J. F. Besseling: Models of metal plasticity: theory and experiment, in A. Sawczuk, and G. Bianchi (eds.): *Plasticity Today*, London, New York, Elsevier Applied Science Publishers (1985), 97–113.

[4] D. E. Buckthorpe, P. S. White: Incorporation of alternating plasticity in the shakedown method. *Transactions of SMiRT* **12** (1993) E 119–124.

[5] D. E. Buckthorpe, P. S. White: Shakedown: a design tool for high temperature. *The GEC Journal of Research: Incorporation of the Marconi Review and the Plessey Research Review* **11** (1993) 24–38.

[6] A. Conn, N. Gould, P. Toint: *LANCELOT: A fortran package for large-scale nonlinear optimization (Release A)*. Springer-Verlag Berlin (1992).

[7] R. Fletcher: *Practical Methods of Optimization*. John Wiley & Sons New York (1987).

[8] U. M. Garcia Palomares, O. L. Mangasarian: Superlinearly convergent quasi–newton algorithms for nonlinearly constrained optimization problems. *Mathematical Programming* **11** (1976) 1–13.

[9] F. A. Gaydon, A. W. McCrum: On the yield–point loading of a square plate with concentric circular hole. *Journal of the Mechanics and Physics of Solids* **2** (1954) 170–176.

[10] J. Gross-Weege: On the numerical assessment of the safety factor of elastic–plastic structures under variable loading. *International Journal of Mechanical Sciences* **39** (1996) 417–433.

[11] F. Gruttmann, E. Stein: Tangentiale Steifigkeitsmatrizen bei Anwendung von Projektionsverfahren in der Elastoplastizitätstheorie. *Ingenieur–Archiv* **58** (1988) 15–24.

[12] A. Hachemi and D. Weichert: Numerical shakedown analysis of damaged structures. Computer Methods in Applied Mechanics and Engineering **160** (1998) 57–70.

[13] B. Halphen, Q.S. Nguyen: Sur les matériaux standards généralisés, *J. Mécanique* **14** (1975) 39–63.

[14] M. Heitzer: Traglast– und Einspielanalyse zur Bewertung der Sicherheit passiver Komponenten. *Berichte des Forschungszentrums Jülich* **Jül–3704** (1999).

[15] M. Heitzer: Plastic limit loads of defective pipes under combined internal pressure and axial tension, *International Journal of Mechanical Sciences* **44** (2002) 1219-1224.

[16] M. Heitzer: Structural Optimization with FEM-based Shakedown Analyses, *Journal of Global Optimization* **24** (2002) 371–384.

[17] M. Heitzer, G. Pop, M. Staat: Basis reduction for the shakedown problem for bounded kinematic hardening material, *Journal of Global Optimization* **17** (2000) 185–200.

[18] M. Heitzer, H. Reiners, F. Schubert, M. Staat: Einspielen und Ratchetting bei Zug- und Torsionsbelastung: Analyse und Experimente. 27. MPA-Seminar, Stuttgart, October 4-5, 2001, pp. 24.1.-24.16.

[19] M. Heitzer, M. Staat: FEM–computation of load carrying capacity of highly loaded passive components by direct methods. *Nuclear Engineering and Design* **193** (1999) 349–358.

[20] M. Heitzer, M. Staat: Direct FEM-approach to design-by-analysis of pressurized components. ACHEMA (2000) 79–81.

[21] M. Heitzer, M. Staat: Direct static FEM approach to limit and shakedown analysis, in M. Papadrakakis, A. Samartin, E. Onate: CD-ROM Proceedings of the Fourth International Colloquium on Computation of Shell & Spatial Structures, Chania-Crete, Greece (2000) paper 058, 14 pages.

[22] M. Heitzer, M. Staat: Reliability Analysis of Elasto-Plastic Structures under Variable Loads, in D. Weichert, G. Maier: Inelastic Analysis of Structures under Variable Loads: Theory and Engineering Applications, Kluwer Academic Publisher, Dordrecht (2000) 269-288.

[23] A. Kapoor, K. L. Johnson: Plastic ratchetting as a mechanism of metallic wear. *Proceedings of the Royal Society of London Series A* **445** (1994) 367–381.

[24] V. D. Khoi: *Dual Limit and Shakedown Analysis of Structures*, PhD Thesis, Université de Liège, Belgium, 2001.

[25] V. D. Khoi, A. M. Yan and D. H. Nguyen: A new dual shakedown analysis of structures. *ECCM-2001 European conference on computational mechanics*. June 26-29, 2001, Cracow, Poland

[26] W. T. Koiter: General theorems for elastic–plastic solids in *Progress in Solid Mechanics* Vol. 1. North–Holland Publishing Company, Amsterdam (1960).

[27] J. A. König: *Shakedown of Elastic–Plastic Structures*. Elsevier and PWN Amsterdam and Warschau (1987).

[28] J. A. König, M. Kleiber: On a new method of shakedown analysis. *Bulletin de l'Academie Polonaise des Sciences, Serie des sciences techniques* **26** (1978) 165–171.

[29] H. Lang, K. Wirtz, M. Heitzer, M. Staat, R. Oettel: Cyclic Plastic Deformation Tests to Verify FEM-Based Shakedown Analyses. *Nuclear Engineering and Design* **206** (2001) 227–239.

[30] D. G. Luenberger: *Linear and Nonlinear Programming*. Addison–Wesley Publishing Company, Reading (1984).

[31] R. Mahnken: Duale Methoden zur nichtlinearen Optimierung in der Strukturmechanik. Thesis Institut für Baumechanik und Numerische Mechanik, Universität Hannover (1991).

[32] G. P. McCormick: *Nonlinear Programming*. John Wiley & Sons, New York (1983).

[33] E. Melan: Theorie statisch unbestimmter Systeme aus ideal–plastischem Baustoff. *Sitzungsbericht der Österreichischen Akademie der Wissenschaften der Mathematisch–Naturwissenschaftlichen Klasse IIa* **145** (1936) 195–218.

[34] E. Melan: Zur Plastizität des räumlichen Kontinuums, *Ingenieur–Archiv* **8** (1938), 116–126.

[35] B. A. Murtagh, M. A. Saunders:. *MINOS 5.1 - User's Guide.* Stanford University 1987. Technical Report SOL 83-20R.

[36] PERMAS: *User's Reference Manuals*. INTES Publications No. 202, 207, 208, 302, UM 404, UM 405 Stuttgart (1988).

[37] M. J. D. Powell: Some convergence properties of the conjugate gradient method. *Mathematical Programming* **11** (1976) 42–49.

[38] M. J. D. Powell: A fast algorithm for nonlinearly constrained optimization calculations. *Lecture Notes in Mathematics* **630** (1978) 144–157.

[39] K. Schittkowski: The nonlinear programming method of Wilson, Han and Powell with augmented Lagrangian type line search function. *Numerische Mathematik* **38** (1981) 83–114.

[40] K. Schittkowski: NLPQL: a fortran subroutine solving constrained nonlinear programming problems. *Annals of Operation Research* **5** (1985/86) 485–500.

[41] K. Schittkowski: Solving nonlinear programming problems with very many constraints. *Optimization* **25** (1992) 179–196.

[42] K. Schittkowski, C. Zillober, R. Zotemantel: Numerical comparison of nonlinear programming algorithms for structural optimization. *Structural Optimization* **7** (1994) 1–19.

[43] W. Shen: *Traglast– und Anpassungsanalyse von Konstruktionen aus elastisch, ideal plastischem Material*. Thesis Universität Stuttgart (1986).

[44] J. C. Simo, R. L. Taylor: Consistent tangent operatos for rate–independent elastoplasticity. *Computer Methods in Applied Mechanics and Engineering* **48** (1985) 101–118.

[45] M. Staat, M. Heitzer: Limit and shakedown analysis for design. *Proceedings of* 7^{th} *German–Japanese Joint Seminar on Research in Structural Strength and NDE-Problems in Nuclear Engineering, Stuttgart* (1997) 4.3.1–4.3.19.

[46] M. Staat, M. Heitzer: Limit and shakedown analysis for plastic safety of complex structures. *Transactions of SMiRT* **14** (1997) B02/2.

[47] M. Staat, M. Heitzer: Limit and shakedown analysis using a general purpose finite element code in *Proceedings of the NAFEMS World Congress '97*. NAFEM Stuttgart (1997) 522–533.

[48] M. Staat, M. Heitzer: LISA a European Project for FEM-based Limit and Shakedown Analysis, *Nuclear Engineering and Design* **206** (2001) 151–166.

[49] M. Staat, M. Heitzer: The Restricted Influence of Kinematic Hardening on Shakedown Loads, Proceedings of the Fifth World Congress on Computational Mechanics (WCCM V), July 7-12, 2002, Vienna, Austria, Editors: H. A. Mang, F. G. Rammerstorfer, J. Eberhardsteiner, Publisher: Vienna University of Technology, Austria, ISBN 3-9501554-0-6.

[50] M. Staat, M. Heitzer, A. Yan, V. Khoi, D. Nguyen, F. Voldoire, A. Lahousse: Limit Analysis of Defects. *Berichte des Forschungszentrums Jülich* **Jül-3746** (2000).

[51] M. Staat, E. Szelinski, M. Heitzer: Kollapsanalyse von längsfehlerbehafteten Rohren und Behältern. 27. MPA-Seminar, Stuttgart, October 4-5, 2001, pp. 4.1-4.20.

[52] E. Stein, Y. Huang: Shakedown investigations of systems with ductile materials, in *Beiträge zur Mechanik*. TU Berlin 1993: 325–340.

[53] E. Stein, G. Zhang, R. Mahnken: Shakedown analysis for perfectly plastic and kinematic hardening materials, in E. Stein (ed.): *Progress in computational analysis of inelastic structures*, Wien, Springer, (1993), 175–244.

[54] I. Szabo: *Höhere Technische Mechanik*. Springer, Berlin (1972).

[55] W. Traupel: *Thermische Turbomaschinen: 2.Band* Springer–Verlag, Berlin Heidelberg New York, 1982.

[56] F. Voldoire: Regularised limit analysis and applications to the load carrying capacities of mechanical components. CD-ROM Proceedings of the European Congress on Computational Methods in Applied Sciences and Engineering, ECCOMAS 2000, Barcelona, Spain (2000), paper 643, 20 pages.

[57] F. Voldoire: LISA Minutes of the Brite-EuRam Meeting (3.04.98): Validation and industrial applications (task 5.2). CR EDF/MMN 98-083 1998.

[58] D. Weichert, J. Gross-Weege: The numerical assessment of elastic–plastic sheets under variable mechanical and thermal loads using a simplified two–surface yield condition, *International Journal of Mechanical Science* **30** (1988) 757–767.

[59] D. Weichert and A. Hachemi: Influence of geometrical nonlinearities on the shakedown of damaged structures. International Journal of Plasticity **14** (1998) 891–907.

[60] D. Weichert, A. Hachemi and F. Schwabe: Shakedown analysis of composites, Mechanics Research Communications **26** (1999) 309–318.

[61] S. Yamamoto, S. Asada, A. Okamoto: Round robin calculations of collapse loads – a torisperical pressure vessel head with a conical transition. *Transactions of the ASME, Journal of Pressure Vessel Technology* **119** (1997) 503–509.

[62] A.-M. Yan: Contribution to the direct limit state analysis of plastified and cracked structures, PhD thesis (1997), Collection des Publications de la Faculté des Sciences Appliquées n ˚ 190, (1999).

[63] Yan A.M., Nguyen-Dang H.: Direct finite element kinematical approaches in limit and shakedown analysis of shells and elbows, in D. Weichert, G. Maier (eds): *Inelastic analysis of structures under variable loads*, Kluwer Academic Publishers, Dordrecht (2000), 233-254

[64] G. Zhang: *Einspielen und dessen numerische Behandlung von Flächentragwerken aus ideal plastischem bzw. kinematisch verfestigendem Material*. Thesis Universität Hannover (1991).

[65] J. Zowe: Nondifferentiable optimization in K. Schittkowski (ed.): *Computational Mathematical Programming*. Springer, Berlin (1985) 323–356.

Part II

Some nonclassical formulations of shakedown problems

Abdelkader Hachemi, Mohand Ameziane Hamadouche,

Dieter Weichert

Institute of General Mechanics
RWTH Aachen, Templergraben 64, D-52062 Aachen, Germany

E-mail: {hachemi,weichert}@rwth-aachen.de

Nomenclature

$\mathbf{P}$	loads
$\mathbf{f}_0$	body force
$\mathbf{p}_0$	surface traction
$\mathbf{u}^0$	given displacement
ϑ_0	prescribed temperature
$\mathbf{n}$	outer normal vector
$\mathbf{u}$	actual displacement
$\mathbf{u}^E$	fictitious elastic displacement
$\Delta\mathbf{u}$	increment of residual displacement
$\mathbf{s}$	generalized stress
$\mathbf{s}^S$	safe state of generalized stress
$\mathbf{e}$	generalized total strain
$\mathbf{e}^e$	generalized elastic strain
$\mathbf{e}^t$	generalized thermal strain
$\mathbf{e}^p$	generalized plastic strain
$\boldsymbol{\varepsilon}$	total strain
$\dot{\boldsymbol{\varepsilon}}$	total strain rate
$\boldsymbol{\varepsilon}^e$	elastic strain
$\dot{\boldsymbol{\varepsilon}}^e$	elastic strain rate
$\boldsymbol{\varepsilon}^p$	plastic strain
$\dot{\boldsymbol{\varepsilon}}^p$	plastic strain rate
$\boldsymbol{\varepsilon}^t$	thermal strain
$\Delta\boldsymbol{\varepsilon}^p$	plastic strain increment
$\boldsymbol{\omega}$	vector of internal elastic parameters
$\boldsymbol{\kappa}$	vector of internal plastic parameters
$\boldsymbol{\sigma}$	actual stress
$\boldsymbol{\sigma}^E$	fictitious elastic stress
$\boldsymbol{\sigma}^S$	safe state of stress
$\boldsymbol{\sigma}^D$	deviatoric stress
$\mathbf{E}$	tensor of elasticity
$\mathbf{Z}$	tensor of internal el. parameters
$\boldsymbol{\rho}$	residual stress
$\dot{\boldsymbol{\rho}}$	residual stress rate
$\bar{\boldsymbol{\rho}}$	time-independent residual stress
$\boldsymbol{\pi}$	back-stress
$\bar{\boldsymbol{\pi}}$	time-independent back-stress
$\mathbf{F}$	deformation gradient
Ψ	thermodynamic potential
D	damage parameter
G	energy release rate
$\mathbf{x}$	coordinate vector
$\mathbf{I}$	identity tensor
$[\mathbf{C}]$	system dependent matrix
$[\mathbf{B}]$	compatibility matrix
$\{\Delta\mathbf{U}\}$	vector of nodal displacements
$[\mathbf{N}]$	shape function matrix
$\{\mathbf{X}\}$	vector of optimization variables
$\lvert\mathbf{J}\rvert$	determinant of the Jacobian matrix
$\mathcal{L}$	load domain
$\mathcal{C}$	convex elastic domain
$\mathcal{B}$	body or structure
$\mathcal{B}^E$	elastic reference body
ρ	mass density
α_t	coefficient of thermal expansion
V	volume (structure)
∂V	boundary ($\partial V = \partial V_p \cup \partial V_u$)
σ_H	hydrostatic stress
σ_U	uniaxial limit strength
σ_Y	yield stress
F	yield function ($F \leq \sigma_Y$ or σ_U)
t	time
T	absolute temperature
T_0	reference temperature
D^p	plastic dissipation
α	load factor
α_{SD}	shakedown factor
α_{SD}^L	lower bound of shakedown factor
α_{SD}^U	upper bound of shakedown factor
Ω_i	initial configuration
Ω_R	reference configuration
Ω_t	actual configuration
m	viscosity parameter
w_i	weighting factors
μ	scalar multiplier
μ^+	upper bounds of scalar multiplier
μ^-	lower bounds of scalar multiplier
NG	number of Gaussian points
NV	number of load vertices
Φ	augmented Lagrangian function
$\varepsilon_l, \varepsilon_c$	tolerances
:	double contraction
∇	gradient-operator
$\delta(.)$	symbol for virtual quantities
$\tilde{}$	symbol for effective quantities

1 Introduction

The development of numerical methods for the assessment of the long-time behaviour, the usability and safety against failure of structures subjected to variable repeated loading is of great importance in mechanical and civil engineering. A particular kind of failure is caused by an excessive plastic deformations during the loading process, leading to either incremental collapse or alternating plasticity. If, on the contrary, after some time plastic strains cease to develop further and the accumulated dissipated energy in the whole structure remains bounded such that the structure responds purely elastically to the applied variable loads, one says that the structure "shakes down".

The foundations of these theories have been given by [1] and [2], who derived sufficient criteria for shakedown and non-shakedown, respectively, of elastic-perfectly plastic structures. Both criteria presume the existence of a convex yield surface and the validity of the normality rule for the plastic strain rates. Moreover, the influences of material hardening, geometrical effects and material damage are neglected. Consequently, extensions of the classical shakedown theorems have attracted much interest in the last years. Reviews of former investigations can be found for example in [3]-[18].

In contrast to the theoretical extensions of shakedown theorems, there has been comparatively little effort in the development of numerical techniques able to compute the safety factor against failure of structures. It appears that the existing packages have been developed with the aim of performing academic research or specific applications. Nowadays, shakedown packages including a complete library of finite elements able to model various structures and loading occurring in industrial applications do not exist yet.

In this report, a discrete formulation of static and kinematic shakedown theorems for large-scale problems is presented. This formulation is a direct method to compute the safety factor against failure, which leads to a problem of mathematical programming.

Section 2 of this report is devoted to the formulation of the statical and kinematical shakedown problem in the framework of continuum mechanics. The adopted constitutive equations and general assumptions will be reviewed by considering a quasi-static evolution of a three-dimensional elastic-plastic body taken into account kinematical hardening, material damage and geometrical changes.

In section 3, a discrete formulation of statical shakedown theorem is presented for large-scale problems using a mathematical programming method for the complete space of residual stresses and, alternatively, the reduced subspace of residual stresses. The discrete formulation is restricted to elastic-perfectly plastic body.

In section 4, a discrete formulation of kinematical shakedown theorem will be developed for large-scale problems using a mathematical programming method for the complete space. The discrete formulation is restricted to elastic-perfectly plastic body.

2 Formulation of the problem

2.1 Basic relations

We consider the behaviour of an elastic-plastic body $\mathcal{B}$ of finite volume V with a sufficiently smooth surface ∂V consisting of the disjoint parts ∂V_p and ∂V_u, where statical and kinematical boundary conditions, respectively, are prescribed ($\partial V = \partial V_p \cup \partial V_u$, $\partial V_p \cap \partial V_u = \emptyset$). The body $\mathcal{B}$ (Fig. 2.1) is subjected to the quasi-statically varying external agencies $\mathbf{P}(\mathbf{x}, t) \in \mathcal{L}$ at time t consisting of body forces $\mathbf{f}_0$ in V, surface tractions $\mathbf{p}_0$ on ∂V_p, given displacements $\mathbf{u}^0$ on ∂V_u and prescribed temperature ϑ_0 in V and on ∂V.

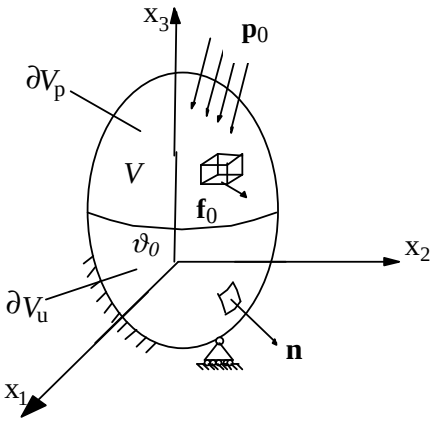

Figure 2.1: Structure or body $\mathcal{B}$

For the theoretical formulation, linear kinematical hardening is taken into account by using internal parameters according to the concept of Generalized Standard Material Model "GSMM" [19]. For this, generalized total, elastic, plastic and thermal strains and generalized stresses are introduced defined by the sets

$$\mathbf{e} = [\boldsymbol{\varepsilon}, \mathbf{0}]^T, \mathbf{e}^e = [\boldsymbol{\varepsilon}^e, \boldsymbol{\omega}]^T, \mathbf{e}^p = [\boldsymbol{\varepsilon}^p, \boldsymbol{\kappa}]^T, \mathbf{e}^t = [\boldsymbol{\varepsilon}^t, \mathbf{0}], \mathbf{s} = [\boldsymbol{\sigma}, \boldsymbol{\pi}]^T. \tag{2.1}$$

Here, $\boldsymbol{\varepsilon}^e$, $\boldsymbol{\varepsilon}^p$ and $\boldsymbol{\varepsilon}^t$ are respectively the observed elastic, plastic and thermally induced parts of the total strain tensor $\boldsymbol{\varepsilon}$. The observable stresses are represented by the stress tensor $\boldsymbol{\sigma}$ and the quantities $\boldsymbol{\omega}$, $\boldsymbol{\kappa}$ and $\boldsymbol{\pi}$ are the r-dimensional vectors of internal elastic and plastic parameters and "back-stresses", respectively. The dimension r depends upon the particular choice of hardening model.

The elastic-plastic damage behaviour of materials is introduced through the concept of effective stress [20]. Using this concept, the behaviour of damaged material can be represented by the constitutive equations of the virgin material where the usual generalized stresses on the micro-level are replaced by the effective generalized stresses defined by

$$\tilde{\mathbf{s}} = \frac{\mathbf{s}}{1 - D} \tag{2.2}$$

Here, the value D = 0 corresponds to the undamaged state, $D \in (0, D_c)$ corresponds to a partly damaged state and $D = D_c$ defines the complete local rupture ($D_c \in [0, 1]$). In the sequel superposed tilde indicates quantities related to the damaged state of the material.

According to the restriction to geometrically linear theory, the total generalized strains **e** can be split into purely elastic, purely plastic and temperature induced parts $\mathbf{e}^e$, $\mathbf{e}^p$ and $\mathbf{e}^t$, respectively

$$\mathbf{e} = \mathbf{e}^e + \mathbf{e}^p + \mathbf{e}^t \tag{2.3}$$

with

$$\boldsymbol{\varepsilon} = \boldsymbol{\varepsilon}^e + \boldsymbol{\varepsilon}^p + \boldsymbol{\varepsilon}^t \tag{2.4}$$

$$\mathbf{0} = \boldsymbol{\omega} + \boldsymbol{\kappa}. \tag{2.5}$$

In order to introduce the constitutive equations in the formulation of shakedown theorem, we consider the thermodynamic potential Ψ, assumed to be a convex function of all observable and internal variables (cf. [21]-[22])

$$\Psi(\boldsymbol{\varepsilon}^e, \boldsymbol{\kappa}, D, T) = \Psi_e(\boldsymbol{\varepsilon}^e, D, T) + \Psi_p(\boldsymbol{\kappa}, D) \tag{2.6}$$

with

$$\rho\Psi_e = \frac{1}{2}(1 - D)(\boldsymbol{\varepsilon}^e - \alpha_t\theta\mathbf{I}) : \mathbf{E} : (\boldsymbol{\varepsilon}^e - \alpha_t\theta\mathbf{I}) + C_\varepsilon\theta^2 \tag{2.7}$$

$$\rho\Psi_p = \frac{1}{2}(1 - D)\boldsymbol{\kappa} \cdot \mathbf{Z} \cdot \boldsymbol{\kappa} \tag{2.8}$$

where ρ is the mass density, C_ε is the specific heat at constant strain, α_t the coefficient of isotropic temperature expansion, θ the difference between the absolute temperature (T) and the reference temperature (T_0). **E** and **Z** are the tensors of elasticity of observable elastic strains and internal elastic parameters and **I** is the identity tensor of second rank. The operators $(\cdot)$ and (:) stand for simple and double tensor contraction, respectively. Then, the material constitutive equations read as

$$\boldsymbol{\sigma} = \rho\frac{\partial\Psi}{\partial\boldsymbol{\varepsilon}^e} = (1 - D)\mathbf{E} : (\boldsymbol{\varepsilon}^e - \alpha_t\theta\mathbf{I}) \tag{2.9}$$

$$\boldsymbol{\pi} = -\rho\frac{\partial\Psi}{\partial\boldsymbol{\kappa}} = -(1 - D)\mathbf{Z} \cdot \boldsymbol{\kappa} \tag{2.10}$$

$$G = -\frac{\partial\Psi}{\partial D} = \frac{1}{2}(\boldsymbol{\varepsilon}^e - \alpha_t\theta\mathbf{I}) : \mathbf{E} : (\boldsymbol{\varepsilon}^e - \alpha_t\theta\mathbf{I}) + \frac{1}{2}\boldsymbol{\kappa} \cdot \mathbf{Z} \cdot \boldsymbol{\kappa}. \tag{2.11}$$

Hence, the thermodynamic force G conjugate to the damage variable D is the energy function of the undamaged material [22].

We assume the validity of the normality rule for plastic flow, such that

$$\dot{\mathbf{e}}^p \in \delta\varphi(\mathbf{s}) \tag{2.12}$$

where $\delta\varphi(\mathbf{s})$ denotes the sub-gradients of the plastic potential $\varphi(\mathbf{s})$ [19] which is the indicator function of a convex generalized elastic domain C of all plastically admissible stress states

$$\boldsymbol{s} \in \mathcal{C} \tag{2.13}$$

$\mathcal{C}$ is defined by means of a yield function $F(\tilde{\mathbf{s}})$

$$\mathcal{C} = \{\mathbf{s} | F(\tilde{\mathbf{s}}) \leq \sigma_Y\}. \tag{2.14}$$

Here, it is assumed that the yield function $F(\tilde{\mathbf{s}})$ is of von Mises type

$$F(\tilde{\mathbf{s}}) = \sqrt{\frac{3}{2}\left(\frac{\boldsymbol{\sigma}^D}{1-D} - \frac{\boldsymbol{\pi}}{1-D}\right) : \left(\frac{\boldsymbol{\sigma}^D}{1-D} - \frac{\boldsymbol{\pi}}{1-D}\right)} \tag{2.15}$$

$\boldsymbol{\sigma}^D$ denotes the deviatoric part of stress tensor $\boldsymbol{\sigma}$ defined by

$$\boldsymbol{\sigma}^D = \boldsymbol{\sigma} - \sigma_H \mathbf{I} \tag{2.16}$$

where $\sigma_H = 1/3\sigma_{ii}$ denotes the hydrostatic stress (i = 1, 2, 3).

The convexity of $F(\tilde{\mathbf{s}})$ and the validity of the normality rule can be expressed by the generalized maximum plastic work inequality

$$(\mathbf{s} - \mathbf{s}^s) : \dot{\mathbf{e}}^p \geq 0 \tag{2.17}$$

where $\mathbf{s}^s = [\boldsymbol{\sigma}^s, \boldsymbol{\pi}^s]^T$ is any safe state of generalized stresses such that $F(\tilde{\mathbf{s}}^s) \leq \sigma_Y$.

We remark that the conditions of convexity and validity of normality rule can be relaxed by use of the concept of "Sanctuary of Elasticity", introduced by Nayroles and Weichert [23].

2.2 Structural behaviour

The behaviour of the body $\mathcal{B}$ subjected to variable loads $\mathbf{P}(t)$ (Fig. 2.1), can be classified by one of the following way [7] (Fig. 2.2):

(1) If the load intensities remain sufficiently low, the response of the body is purely elastic (with the exception of stress singularities).

(2) If the load intensities become sufficiently high, the instantaneous load-carrying capacity of the structure becomes exhausted and unconstrained plastic flow $\dot{\mathbf{e}}^p = [\dot{\boldsymbol{\varepsilon}}^p, \dot{\boldsymbol{\kappa}}]$ and damage $\dot{D}$ occur. The structure collapses in this case.

(3) If the plastic strain increments in each load cycle are of the same sign then, after a sufficient number of cycles, the total strains (and therefore displacements) become so large that the structure departs from its original form and becomes unserviceable. This phenomenon is called "incremental collapse" or "ratchetting".

(4) If the strain increments change sign in every cycle, they tend to cancel each other and total deformations remain small leading to “alternating plasticity”. In this case, however, the material at the most stressed points may fail due to low-cycle fatigue.

(5) If, after some time plastic flow and damage evolution cease to develop further and the accumulated dissipated energy in the whole structure remains bounded such that the structure responds purely elastically to the applied variable loads, one says that the structure “shakes down“.

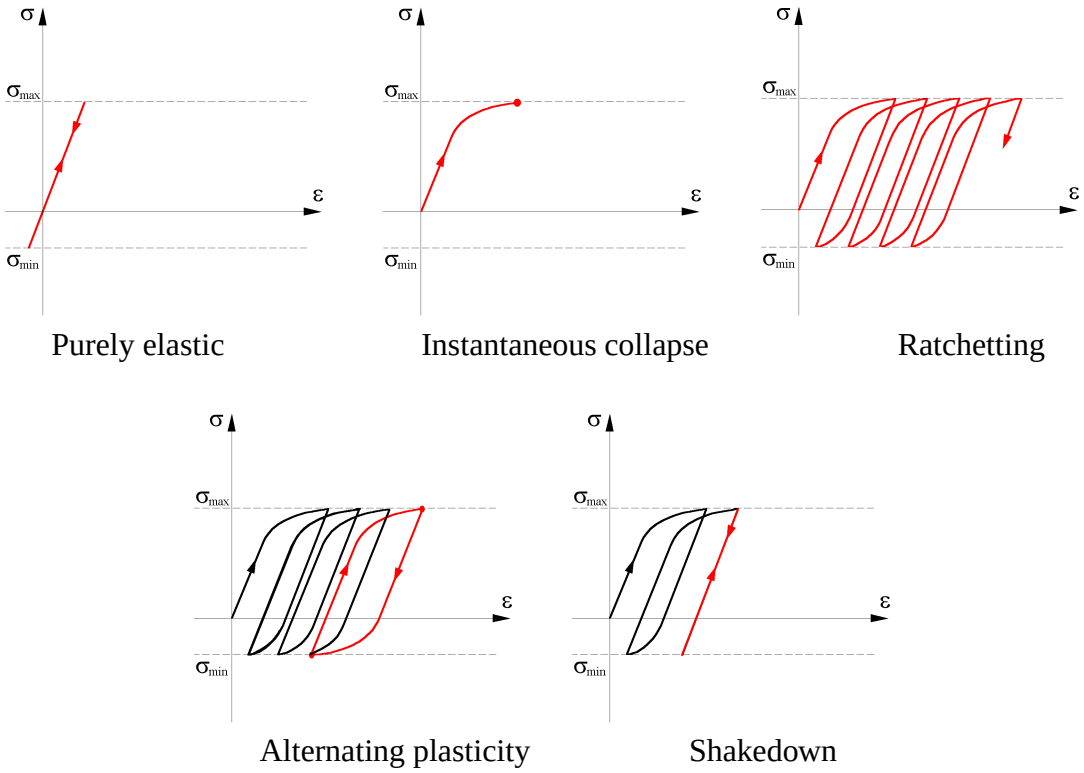

Figure 2.2: Possibilities of local response to cyclic loading

The behaviour of the body according to the first point does not influence its integrity, since plastic deformation and damage do not occur at all. However, the load carrying potential of the body is not fully exploited.

The failure of types (2)-(4) are characterized by the fact, that plastic flow and damage evolution do not cease and that related quantities such as plastic deformation and accumulated damage do not become stationary. Thus, there exist parts of the volume for which the following holds

$$\lim_{t\to\infty} \dot{\mathbf{e}}^p(\mathbf{x},t) \neq 0, \lim_{t\to\infty} \dot{D}(\mathbf{x},t) \neq 0, \tag{2.18}$$

If the case (5) occurs, the body shakes down for the given history of loading $\mathbf{P}(t) \in \mathcal{L}$. It follows that

$$\lim_{t\to\infty} \dot{\mathbf{e}}^p(\mathbf{x},t) = 0, \lim_{t\to\infty} \dot{D}(\mathbf{x},t) = 0. \tag{2.19}$$

If one accounts for plastic deformation and damage in structural design, it seems natural to require that, for any possible loading history, the plastic deformation and damage in the considered body will stabilize, i.e. the structure will shake down (see [24]-[28]). It is worthwhile mentioning that the phenomena of incremental collapse and alternating plasticity (low-cycle fatigue) may appear simultaneously, e.g. if one component of the plastic strain tensor increases with each load cycle whereas another oscillates.

The question of shakedown could be answered by examining the structural behaviour by means step-by-step procedure (see e.g. [25]). However, such a procedure is in general very cumbersome and, in many cases, inapplicable. Therefore, direct methods, namely the static method expressed in stress variables and kinematic method expressed in velocity variables, respectively have been developed allowing to find out whether a given body will shake down, without recurring on the evaluation of stresses and strains. Both methods can be related to a mixed formulation and lead to bounds of the shakedown or limit load: a lower bound by the static method and upper bound by the kinematic method.

2.3 Formulation of the lower bound method

2.3.1 Assumptions

In the following, we introduce the notion of a "**purely elastic reference body** $\mathcal{B}^E$" (Fig. 2.3), differing from the real body $\mathcal{B}$ only by the fact that its material reacts purely elastically with the same elastic moduli as for the elastic part of the material law in the real body.

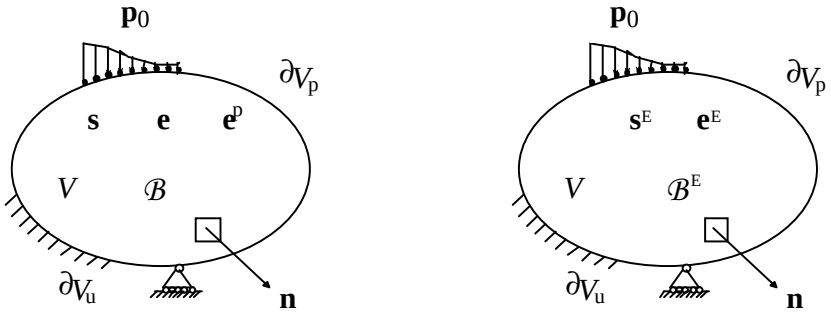

Elastic-plastic body Purely-elastic body

Figure 2.3: Purely elastic and elastic-plastic body

All quantities related to this reference body are indicated by superscript $(^E)$. The internal parameters to describe the state of hardening and damage in the material vanish naturally for the reference body $\mathcal{B}^E$, so that the generalized strains and stresses are given by

$$\mathbf{e}^E = (\mathbf{e}^e)^E = [\boldsymbol{\varepsilon}^E, \mathbf{0}]^T, (\mathbf{e}^p)^E = [\mathbf{0}, \mathbf{0}]^T, (\mathbf{e}^t)^E = [\boldsymbol{\varepsilon}^t, \mathbf{0}]^T, \mathbf{s}^E = [\boldsymbol{\sigma}^E, \mathbf{0}]^T. \tag{2.20}$$

2.3.2 Static shakedown theorem

The extended static (Melan's) theorem of shakedown can be expressed as follows:

> If there exists a safety factor $\alpha > 1$, a time-independent field of effective residual stresses $\tilde{\bar{\boldsymbol{\rho}}}(\mathbf{x})$ and time-independent limited back-stresses $\tilde{\bar{\boldsymbol{\pi}}}(\mathbf{x})$ such that the time-independent field of effective generalized stresses $\tilde{\bar{\mathbf{s}}} = [\tilde{\bar{\boldsymbol{\rho}}}, \tilde{\bar{\boldsymbol{\pi}}}]^T$ superimposed on effective generalized purely elastic stresses $\tilde{\mathbf{s}}^E = [\tilde{\boldsymbol{\sigma}}^E, \mathbf{0}]^T$ does not exceed the yield condition for any time $t > 0$
>
> $$F(\alpha\tilde{\mathbf{s}}^E(\mathbf{x}, t) + \tilde{\bar{\mathbf{s}}}(\mathbf{x})) \leq \sigma_Y, \forall \mathbf{x} \in V \tag{2.21}$$
>
> then the body $\mathcal{B}$ will shake down with respect to the given loading $\mathbf{P}(t) \in \mathcal{L}$.

The field of purely elastic stresses satisfies the following system of equations

$$\begin{aligned} \text{div}\, \boldsymbol{\sigma}^E &= -\mathbf{f}_0 && \text{in } V && (2.22)\\ \mathbf{n} \cdot \boldsymbol{\sigma}^E &= \mathbf{p}_0 && \text{on } \partial V_p && (2.23)\\ \mathbf{u}^E &= \mathbf{u}^0 && \text{on } \partial V_u && (2.24) \end{aligned}$$

with

$$\begin{aligned} \boldsymbol{\varepsilon}^E &= \frac{1}{2}\left(\nabla(\mathbf{u}^E) + \nabla(\mathbf{u}^E)^T\right) && (2.25)\\ \boldsymbol{\varepsilon}^E &= \mathbf{E}^{-1} : \boldsymbol{\sigma}^E + \alpha_t \theta \mathbf{I} && (2.26) \end{aligned}$$

and the field of residual stress satisfies

$$\begin{aligned} \text{div}\, \bar{\boldsymbol{\rho}} &= \mathbf{0} && \text{in } V && (2.27)\\ \mathbf{n} \cdot \bar{\boldsymbol{\rho}} &= \mathbf{0} && \text{on } \partial V_p && (2.28) \end{aligned}$$

where $\mathbf{n}$ is the outward normal vector to ∂V_p.

Then, the static shakedown theorem for the determination of the safety factor against failure due to inadmissible damage or unlimited accumulation of plastic deformations can then be expressed by the following optimization problem [29]

$$\alpha_{SD}^L = \max_{\bar{\rho}, \bar{\pi}, D} \alpha \tag{2.29}$$

with the subsidiary conditions (2.27), (2.28) and

$$D < D_c \qquad \text{in } V \tag{2.30}$$

$$F_I\left[\alpha\frac{\boldsymbol{\sigma}^E}{1-D}+\frac{\bar{\boldsymbol{\rho}}}{1-D}-\frac{\bar{\boldsymbol{\pi}}}{1-D}\right]\leq\boldsymbol{\sigma}_Y \qquad \text{in } V \tag{2.31}$$

$$F_L\left[\alpha\frac{\boldsymbol{\sigma}^E}{1-D}+\frac{\bar{\boldsymbol{\rho}}}{1-D}\right]\leq\boldsymbol{\sigma}_U \qquad \text{in } V \tag{2.32}$$

This is a problem of mathematical programming, with α as objective function to be optimized with respect to $\bar{\boldsymbol{\rho}}, \bar{\boldsymbol{\pi}}$ and D and with the inequalities (2.30)-(2.32) as nonlinear constraints. Here, F_I and F_L denote the initial yield condition and the limit yield condition, respectively, with uniaxial yield stress σ_Y and uniaxial limit strength σ_U. The condition (2.30) assures structural safety against failure due to material damage and (2.31) assures that safe states of stresses $\mathbf{s}^s = \alpha\mathbf{s}^E + \bar{\mathbf{s}}$ are never outside the limit surface F_L and so guarantees implicitly the boundedness of the back-stresses. Condition (2.32) controls the shakedown requirement of existence of a time-independent back-stress vector $\bar{\boldsymbol{\pi}}$ describing a fixed translation of the initial yield surface F_I inside the limit surface F_L and so assures that safe states of observable stresses $\boldsymbol{\sigma}^s$ are related to a fixed time independent position of the initial yield surface F_I inside the limit surface F_L [30].

2.3.3 Geometrical effects

The formulation of statical shakedown theorem presented above can be extended to broader classes of problems in order to include the influence of geometrical changes. For that we assume that the external variable loads $\mathbf{P}(\mathbf{x}, t)$ are of a special type: Up to an instant t^R the body $\mathcal{B}$ undergoes finite and given displacement $\mathbf{u}^R$ with respect to the initial configuration Ω_i at time $t = 0$ in such a way that $\mathcal{B}$ is in the known configuration Ω_R in equilibrium under time-independent loads $\mathbf{P}^R$. For times $t > t^R$ the body $\mathcal{B}$ is submitted to additional variable loads $\mathbf{P}^r$ such that:

$$\mathbf{P}(\mathbf{x}, t) = \mathbf{P}^R(\mathbf{x}) + \mathbf{P}^r(\mathbf{x}, t) \tag{2.33}$$

and occupies the actual configuration Ω_t (see [6], [9]-[10]). Since the actual configuration should also be an equilibrium configuration and the following equations hold:

(i) *Statical equations*

$$\operatorname{div}(\boldsymbol{\tau}^R + \boldsymbol{\tau}^r) = -\mathbf{f}_0^R - \mathbf{f}_0^r \qquad \text{in } V \tag{2.34}$$

$$\mathbf{n}\cdot(\boldsymbol{\tau}^R + \boldsymbol{\tau}^r) = \mathbf{p}_0^R + \mathbf{p}_0^r \qquad \text{on } \partial V_p \tag{2.35}$$

with

$$\boldsymbol{\tau}^R + \boldsymbol{\tau}^r = (\mathbf{F}^r\mathbf{F}^R)(\boldsymbol{\sigma}^R + \boldsymbol{\sigma}^r) \tag{2.36}$$

(ii) *Kinematical equations*

$$\mathbf{u} = \mathbf{u}^R + \mathbf{u}^r \qquad \text{in } V \tag{2.37}$$
$$\mathbf{F} = \mathbf{F}^r\mathbf{F}^R = \mathbf{I} + \nabla\mathbf{u}^R + \nabla\mathbf{u}^r \qquad \text{in } V \tag{2.38}$$
$$\boldsymbol{\varepsilon} = \boldsymbol{\varepsilon}^R + \boldsymbol{\varepsilon}^r = \frac{1}{2}(\mathbf{C} - \mathbf{I}) \qquad \text{in } V \tag{2.39}$$
$$\mathbf{u} = \mathbf{u}_0^R + \mathbf{u}_0^r \qquad \text{on } \partial V_u \tag{2.40}$$

with

$$\mathbf{C} = (\mathbf{F}^r\mathbf{F}^R)^T(\mathbf{F}^r\mathbf{F}^R) \tag{2.41}$$

where all quantities caused by the time-independent loads $\mathbf{P}^R$ are marked by a superscript $(^R)$, whereas the additional field quantities caused by the time-dependent loads $\mathbf{P}^r$ are marked by superscript $(^r)$. The additional field quantities caused by $\mathbf{P}^r$ have to satisfy the following equations:

(i) *Statical equations*

$$\text{div}(\boldsymbol{\tau}^r) = -\mathbf{f}_0^r \qquad \text{in } V \tag{2.42}$$
$$\mathbf{n}\cdot\boldsymbol{\tau}^r = \mathbf{p}_0^r \qquad \text{on } \partial V_p \tag{2.43}$$

with

$$\boldsymbol{\tau}^r = \mathbf{H}^r\mathbf{F}^R\boldsymbol{\sigma}^R + \mathbf{F}^R\boldsymbol{\sigma}^r + \mathbf{H}^r\mathbf{F}^R\boldsymbol{\sigma}^r \tag{2.44}$$

(ii) *Kinematical equations*

$$\mathbf{F}^r = \mathbf{I} + \mathbf{H}^r \qquad \text{in } V \tag{2.45}$$
$$\boldsymbol{\varepsilon}^r = \frac{1}{2}(\mathbf{F}^R)^T[(\mathbf{H}^r)^T + \mathbf{H}^r + (\mathbf{H}^r)^T\mathbf{H}^r](\mathbf{F}^R) \qquad \text{in } V \tag{2.46}$$
$$\mathbf{u}^r = \mathbf{u}_0^r \qquad \text{on } \partial V_u \tag{2.47}$$

with

$$\mathbf{H}^r = \nabla_R\mathbf{u}^r \tag{2.48}$$

In the sequel, we restrict our considerations to loading histories characterized by the motion of a fictitious comparison body $\mathcal{B}^E$, having at time t^R the same field quantities as $\mathcal{B}$ but reacting, in contrast to $\mathcal{B}$, purely elastically to the additional time-dependent loads $\mathbf{P}^r$, superimposed on $\mathbf{P}^R$ for $t > t^R$ (Fig. 2.4 (cf. [6],[9]). The differences between the states in $\mathcal{B}$ and $\mathcal{B}^E$ are then described by the difference fields:

$$\Delta\mathbf{u} = \mathbf{u}^r - \mathbf{u}^{rE}; \Delta\mathbf{F} = \mathbf{F}^r - \mathbf{F}^{rE}; \Delta\boldsymbol{\varepsilon} = \boldsymbol{\varepsilon}^r - \boldsymbol{\varepsilon}^{rE} \tag{2.49}$$
$$\Delta\boldsymbol{\tau} = \boldsymbol{\tau}^r - \boldsymbol{\tau}^{rE}; \Delta\boldsymbol{\sigma} = \boldsymbol{\sigma}^r - \boldsymbol{\sigma}^{rE} \tag{2.50}$$

and have to fulfill the following equations:

$$\operatorname{div}(\Delta\boldsymbol{\tau}) = \mathbf{0} \qquad \text{in } V \tag{2.51}$$

$$\mathbf{n}\cdot\Delta\boldsymbol{\tau} = \mathbf{0} \qquad \text{on } \partial V_p \tag{2.52}$$

and

$$\Delta\mathbf{F} = \mathbf{H}^r - \mathbf{H}^{rE} \qquad \text{in } V \tag{2.53}$$

$$\begin{aligned}\Delta\boldsymbol{\varepsilon} = {} & \frac{1}{2}(\mathbf{F}^R)^T[(\Delta\mathbf{F})^T + (\Delta\mathbf{F})](\mathbf{F}^R) \\ + {} & \frac{1}{2}(\mathbf{F}^R)^T[(\mathbf{H}^r)^T(\mathbf{H}^r) - (\mathbf{H}^{rE})^T(\mathbf{H}^{rE})](\mathbf{F}^R) \qquad \text{in } V\end{aligned} \tag{2.54}$$

$$\Delta\mathbf{u} = \mathbf{0} \qquad \text{on } \partial V_p \tag{2.55}$$

with

$$\Delta\boldsymbol{\tau} = (\Delta\mathbf{F})\mathbf{F}^R\boldsymbol{\sigma}^R + \mathbf{F}^R(\Delta\boldsymbol{\sigma}) + \mathbf{H}^r\mathbf{F}^R\boldsymbol{\sigma}^r - \mathbf{H}^{rE)}\mathbf{F}^R\boldsymbol{\sigma}^{rE} \tag{2.56}$$

In the following, we restrict our considerations to situations where the state of deforma-

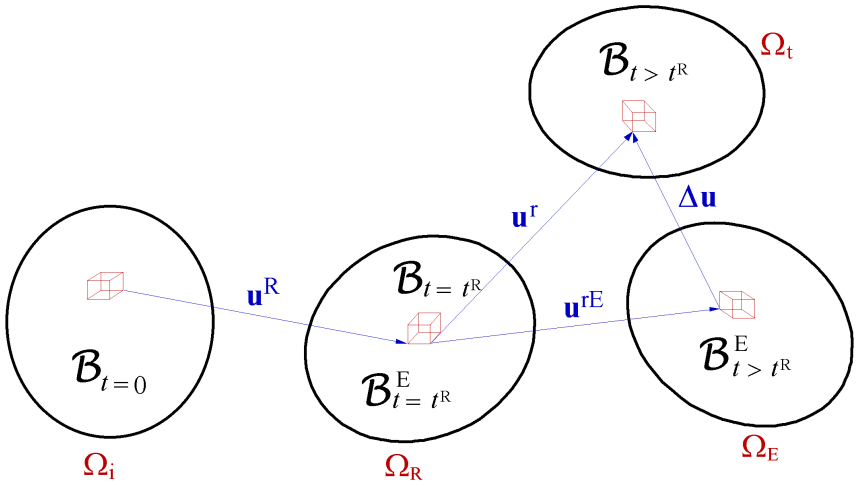

Figure 2.4: Evolution of real body $\mathcal{B}$ and comparison body $\mathcal{B}^E$

tion and the state of stress in $\mathcal{B}$ are subjected to small variations in time [6]. Consequently, we neglect in the governing eqns. (2.49-2.56) all terms, which are nonlinear in the time-dependent additional field quantities marked by a superscript $(^r)$. This excludes to study buckling effects induced by the additional time-dependent loads. Then the following extension of Melan's theorem holds:

If there exists a time-independent field of effective residual stresses $\Delta\tilde{\bar{\boldsymbol{\sigma}}}$ such that the following relations hold:

$$
\begin{aligned}
&\text{(i)} && \operatorname{div}(\mathbf{F}^R\boldsymbol{\sigma}^R) = -\mathbf{f}_0^R && \text{in } V && (2.57)\\
&&& \mathbf{n}\cdot(\mathbf{F}^R\boldsymbol{\sigma}^R) = \mathbf{p}_0^R && \text{on } \partial V_p && (2.58)\\
&&& \mathbf{u} = \mathbf{u}_0^R && \text{on } \partial V_u && (2.59)\\
&\text{(ii)} && \operatorname{div}(\Delta\bar{\boldsymbol{\tau}}) = \mathbf{0} && \text{in } V && (2.60)\\
&&& \mathbf{n}\cdot(\Delta\bar{\boldsymbol{\tau}}) = \mathbf{0} && \text{on } \partial V_p && (2.61)\\
&&& \Delta\bar{\mathbf{u}} = \mathbf{0} && \text{on } \partial V_u && (2.62)\\
&\text{with} && \Delta\bar{\boldsymbol{\tau}} = (\Delta\bar{\mathbf{F}})\mathbf{F}^R\boldsymbol{\sigma}^R + \mathbf{F}^R(\Delta\bar{\boldsymbol{\sigma}}) && && (2.63)\\
&\text{(iii)} && F(\alpha\tilde{\mathbf{s}}^{rE} + \tilde{\mathbf{s}}^R + \Delta\tilde{\bar{\mathbf{s}}}) \le \sigma_Y && \text{in } V && (2.64)
\end{aligned}
$$

with $\tilde{\mathbf{s}}^R = [\tilde{\boldsymbol{\sigma}}^R, \tilde{\boldsymbol{\pi}}^R]^T$ for all time $t > t^R$, then the original body $\mathcal{B}$ will shakedown under given program of loading $\mathbf{P}$.

Then the safety factor against failure due to non-shakedown or inadmissible damage is defined by [18]

$$\alpha_{SD}^L = \max_{\Delta\bar{\tau}, D} \alpha \tag{2.65}$$

with the subsidiary conditions

$$
\begin{aligned}
&\operatorname{div}(\Delta\bar{\boldsymbol{\tau}}) = \mathbf{0} && \text{in } V && (2.66)\\
&\mathbf{n}\cdot(\Delta\bar{\boldsymbol{\tau}}) = \mathbf{0} && \text{on } \partial V_p && (2.67)\\
&D - D_c < 0 && \text{in } V && (2.68)\\
&F_I\left(\alpha\frac{\boldsymbol{\sigma}^{rE}}{1-D} + \frac{\boldsymbol{\sigma}^R}{1-D} - \frac{\boldsymbol{\pi}^R}{1-D} + \frac{\Delta\bar{\boldsymbol{\sigma}}}{1-D} - \frac{\Delta\bar{\boldsymbol{\pi}}}{1-D}\right) \le \sigma_Y && \text{in } V && (2.69)\\
&F_L\left(\alpha\frac{\boldsymbol{\sigma}^{rE}}{1-D} + \frac{\boldsymbol{\sigma}^R}{1-D} + \frac{\Delta\bar{\boldsymbol{\sigma}}}{1-D}\right) \le \sigma_U && \text{in } V && (2.70)
\end{aligned}
$$

This is again a problem of mathematical programming, with α as objective function to be optimized with respect to $\Delta\bar{\boldsymbol{\tau}}$ and D ($D = D^R + D^r$) and with inequalities (2.68-2.70) as nonlinear constraints. The condition (2.68) assures structural safety against failure due to material damage and the condition (2.70) assures that safe states of stresses are never outside the limit surface.

It should be mentioned, that if we neglect the influence of material damage ($D = 0$) and geometrical effects ($\boldsymbol{\sigma}^R = \mathbf{0}$), we get the extended theorem given by [30], [40] and in addition if we put and $\bar{\boldsymbol{\pi}}$ equals to zero, we get the original Melan's theorem [1].

2.4 Formulation of upper bound method

2.4.1 Kinematic shakedown theorem

To formulate the upper bound theorem, we restrict ourselves to perfectly plastic material with the assumption of small geometrical transformations. Using the associated flow rule (eqn. (2.12)) and the von Mises yield criterion (eqn. (2.15)), the plastic dissipation can be expressed by

$$D^p(\dot{\boldsymbol{\varepsilon}}^p) = \boldsymbol{\sigma} : \dot{\boldsymbol{\varepsilon}}^p = (1-D)\sigma_Y \sqrt{\frac{2}{3}\dot{\boldsymbol{\varepsilon}}^p : \dot{\boldsymbol{\varepsilon}}^p} \tag{2.71}$$

which is a non-negative scalar convex function. The admissible set of stresses in the static formulation is unbounded: the addition of a scalar function in the diagonal of $\boldsymbol{\sigma}$, corresponding to adding hydrostatic pressure, does not affect the yield condition. This is why one need in this case so called "incompressible finite elements" to perform the calculation of the shakedown loading factor. Then, the shakedown loading factor α_{SD} is the minimum of the following optimization problem:

$$\alpha_{SD}^U = \min_{\dot{\varepsilon}^p, \Delta u} \sqrt{\frac{2}{3}}\sigma_Y (1-D) \int_0^T \int_V (\dot{\boldsymbol{\varepsilon}}^p : \dot{\boldsymbol{\varepsilon}}^p) dV dt \tag{2.72}$$

with the subsidiary conditions

$$D < D_c \qquad \text{in } V \tag{2.73}$$

$$\int_0^T \int_V \boldsymbol{\sigma}^E : \dot{\boldsymbol{\varepsilon}}^p dV dt \qquad \text{in } V \tag{2.74}$$

$$\text{tr}\, \dot{\boldsymbol{\varepsilon}}^p = 0 \qquad \text{in } V \tag{2.75}$$

$$\Delta\boldsymbol{\varepsilon}^p = \int_0^T \dot{\boldsymbol{\varepsilon}}^p dt = \frac{1}{2}(\nabla(\Delta\mathbf{u}) + \nabla(\Delta\mathbf{u})^T) \qquad \text{in } V \tag{2.76}$$

$$\Delta\mathbf{u} = \mathbf{0} \qquad \text{on } \partial V_u \tag{2.77}$$

where $\dot{\boldsymbol{\varepsilon}}^p$ and $\Delta\boldsymbol{\varepsilon}^p$ denote plastic strain rate and plastic strain increment, respectively, $\Delta\mathbf{u}$ is the increment of residual displacement and $\boldsymbol{\sigma}^E$ is the fictitious elastic stresses caused by external loads. The period of cyclic loading programs is denoted by T.

2.4.2 Regularization by the Norton-Hoff-Friaâ method

The objective function (eqn. (2.71)) is not differentiable at 0. To overcome this difficulty Friaâ proposed a regularized method [31]-[32] which consists of replacing the plastic dissipation $D^p(\dot{\boldsymbol{\varepsilon}}^p)$ of perfectly plastic material by the regularized and differentiable support

function $[D^p(\dot{\boldsymbol{\varepsilon}}^p)]^{NH}$ of Norton-Hoff viscoplastic material:

$$[D^p(\dot{\boldsymbol{\varepsilon}}^p)]^{NH} = \frac{k^{1-m}}{m}[D^p(\dot{\boldsymbol{\varepsilon}}^p)]^m = \frac{\sigma_Y^{2-m}}{m}[3\mu]^{m-1}(1-D)^m\sqrt{\left(\frac{2}{3}\dot{\boldsymbol{\varepsilon}}^p : \dot{\boldsymbol{\varepsilon}}^p\right)^m} \tag{2.78}$$

where μ is Lamé's coefficient and m is the viscosity parameter ($1 \leq m \leq 2$). The viscoplastic dissipation tends to the plastic dissipation when the viscosity parameter tends to one (see, e.g. [33]-[34].

For load factors greater than α_{SD}, two types of collapse can occur

- incremental collapse, corresponding to an unlimited growth of plastic strains,
- low-cycle fatigue, corresponding to alternating plastic strains.

3 Discrete formulation of lower bound method

In the discrete formulation of shakedown problem, we restrict ourselves to the original Melan's theorem. Any discrete version of the statical formulation of the shakedown theorem presented above preserves the relevant bounding properties [2] if the following conditions are satisfied simultaneously:

(i) the solution of the fictitious elastic stresses (eqns. (2.22)–(2.24)) is exact;

(ii) the residual stress field satisfies point-wise the homogeneous equilibrium equations (eqns. (2.27)-(2.28))

(iii) the yield condition (eqn. (2.21)) is satisfied everywhere in V.

In the numerical analysis of shakedown problems based on the classical Melan's theorem, the existence of the bounding properties was the reasons why many authors (see e.g. [30], [35]-[38]) used the finite element stress method with a discretization of the stress field. Moreover, since the extended Melan's theorem is formulated in static quantities, it is meaningful to discretize the stress field rather than the displacement field. Obviously, with the same degree of discretization the stress method gives better results for the stresses than the displacement formulation.

However, in statical formulations the discretized stress field a priori has to satisfy the equilibrium equations and the statical boundary conditions. Since these conditions are more difficult to fulfill than the respective conditions for the displacement field in the kinematical formulations, the FE-stress based method is not widely used. The majority of commercially available FE systems are based on displacement formulations.

On the other hand, it is very difficult to preserve the bounding properties (i)-(iii). Especially the first conditions can hardly be satisfied, if other than one-dimensional structures are studied. Thus, in order to make the numerical approach as general as possible, we use

the displacement method. In this case the well-known displacement element formulations involving e.g. isoparametric elements can be applied. For that purpose it is necessary to transform the statical equations from their local form into the equivalent global form.

3.1 Discretization of the purely elastic stresses

To calculate the elastic stresses $\boldsymbol{\sigma}^E$ in the reference body $\mathcal{B}^E$, we use the virtual work principle combined with the finite element discretization with test functions for the displacement fields. Then, the elastic stresses $\boldsymbol{\sigma}^E$ are in equilibrium with body forces $\mathbf{f}_0$ and surface tractions $\mathbf{p}_0$ if the following equality holds

$$\delta U_{int} = \delta U_{ext} \tag{3.1}$$

or

$$\int_V \{\boldsymbol{\sigma}^E\}\{\delta\boldsymbol{\varepsilon}^E\}dV = \int_{\partial V_p} \{\mathbf{p}_0\}\{\delta\mathbf{u}^E\}dS + \int_V \{\mathbf{f}_0\}\{\delta\mathbf{u}^E\}dV \tag{3.2}$$

for any virtual displacement $\delta\mathbf{u}^E$ and any virtual strains $\delta\boldsymbol{\varepsilon}^E$ satisfying the compatibility condition (eqn. (2.25)). The virtual displacement field $\delta\mathbf{u}^E$ of each element e is approximated according to

$$\{\delta\mathbf{u}^E\} = \sum_{k=1}^{NK} \mathbf{N}_k \delta\mathbf{u}_k^e \tag{3.3}$$

where $\mathbf{N}_k$ and $\delta\mathbf{u}_k^e$ denote the k-th shape function matrix and the vector of virtual displacements of the k-th node of the element e, respectively. *NK* denotes the total number of nodes of each element. The virtual strain field $\delta\boldsymbol{\varepsilon}^E(\mathbf{x})$ is derived by substitution of eqn. (3.3) into eqn. (2.25), such that

$$\{\delta\boldsymbol{\varepsilon}^E(\mathbf{x})\} = \sum_{k=1}^{NK} \mathbf{B}_k(\mathbf{x})\delta\mathbf{u}_k^e \tag{3.4}$$

where [**B**] is the compatibility matrix depending on the coordinates. The integration of eqn. (3.3) has to be carried out over all Gaussian points NG with their weighting factors w_i in the considered element e, where the index i refers to the i-th Gaussian point. The corresponding coordinate vector shall be denoted by $\mathbf{x}_i$, i.e.

$$\begin{aligned}
\int_V \{\delta\boldsymbol{\varepsilon}^E(\mathbf{x})\}^T\{\boldsymbol{\sigma}^E(\mathbf{x})\}dV &= \{\delta\mathbf{u}^e\}^T \left\{ \sum_{k=1}^{NGE} w_i |\mathbf{J}|_i [\mathbf{B}(\mathbf{x}_i)]^T [\mathbf{E}][\mathbf{B}(\mathbf{x}_i)] \right\} \{\mathbf{u}^e\} \\
&= \{\delta\mathbf{u}^e\}^T[\mathbf{K}]\{\mathbf{u}^e\} \\
&= \{\delta\mathbf{u}^e\}^T\{\mathbf{F}\}
\end{aligned} \tag{3.5}$$

where $\{\mathbf{F}\}$ denotes the vector of nodal forces, w_i the weighting factors, $|\mathbf{J}|_i$ the determinant of the Jacobian matrix and [**K**] the stiffness matrix.

This integral leads for the i-th Gaussian point to

$$\{\boldsymbol{\sigma}^E(\mathbf{x}_i)\} = [\mathbf{E}][\mathbf{B}(\mathbf{x}_i)]\{\mathbf{u}^e\}. \tag{3.6}$$

3.2 Discretization of the residual stress field

Analogously, the field of residual stress can be determined by

$$\int_V \{\bar{\boldsymbol{\rho}}\}\{\delta\boldsymbol{\varepsilon}\}dV = 0. \tag{3.7}$$

By introducing a vector form for the strain tensor $\boldsymbol{\varepsilon}$, the corresponding virtual strains $\delta\boldsymbol{\varepsilon}$ are given in each element e by

$$\{\delta\boldsymbol{\varepsilon}^e\} = \sum_{k=1}^{NK} \mathbf{B}_k \delta\mathbf{u}_k^e \tag{3.8}$$

The shape functions of the considered element are the same as for the determination of the purely elastic stresses. Using this relation and introducing the unknown residual stress vector $\{\bar{\boldsymbol{\rho}}_i\}$ at each Gaussian point i, the equilibrium condition (3.7) is integrated numerically by using the well-known Gauss-Legendre technique. The integration has to be carried out over all Gaussian points NG

$$\int_{V^e} \{\bar{\boldsymbol{\rho}}\}\{\delta\boldsymbol{\varepsilon}^e\}dV = \sum_{i=1}^{NG} w_i |\mathbf{J}|_i \left[\sum_{k=1}^{NK} \mathbf{B}_k \delta\mathbf{u}_k^e]\right] \bar{\boldsymbol{\rho}}_i. \tag{3.9}$$

By summation of the contributions of all elements and by variation of the virtual node-displacements with regard to the boundary conditions, one finally gets the linear system of equations (see [39]-[42])

$$\sum_{i=1}^{NG} \mathbf{C}_i \bar{\boldsymbol{\rho}}_i = [\mathbf{C}]\{\bar{\boldsymbol{\rho}}\} = \{\mathbf{0}\} \tag{3.10}$$

where NG denotes the total number of Gaussian points of the reference body $\mathcal{B}^E$, $[\mathbf{C}]$ is a constant matrix, uniquely defined by the discretized system and the boundary conditions and $\{\bar{\boldsymbol{\rho}}\}$ is the global residual stress vector of the discretized reference body $\mathcal{B}^E$.

3.3 Discretization of the time variable

Up to now, no restrictions have been made to the load domain $\mathcal{L}$. Thus $\mathcal{L}$ can be of arbitrary form. However in many practical cases the number of independent loads is restricted, each

varying between some given bounds. If the number of such independent loads is n, then the load domain is defined by an n-dimensional polyhedron

$$\mathcal{L} = \left\{ P | P(\mathbf{x}, t) = \sum_{j=1}^{n} \mu_j(t) P_j(\mathbf{x}), \mu_j \in [\mu_j^-, \mu_j^+] \right\} \tag{3.11}$$

where P is the vector of generalized loads, μ_j are scalar multipliers with upper and lower bounds μ_j^+ and μ_j^-, respectively. P_j represents n fixed and independent generalized loads (e.g. body forces, surface tractions, prescribed boundary displacements, temperature changes or combinations of them). For subsequent considerations the corners of the polyhedron (load domain $\mathcal{L}$) are numbered by the index j, such that $j = 1, \ldots, NV$, where NV denotes the total number of corners. The loads, which correspond to each corner of $\mathcal{L}$ are characterized symbolically by P_j. In view of the convexity of the yield function F (eqn. (2.21)), where D = 0 and $\bar{\boldsymbol{\pi}} = \mathbf{0}$, and due to the above assumption on the load domain $\mathcal{L}$ it can be shown that [43]

$$F(\alpha \boldsymbol{\sigma}^E(\mathbf{x}, t) + \bar{\boldsymbol{\rho}}(\mathbf{x})) \leq \sigma_Y \tag{3.12}$$

is fulfilled at any time t, if

$$F(\alpha \boldsymbol{\sigma}_i^E(P_j) + \bar{\boldsymbol{\rho}}_i) \leq \sigma_Y \tag{3.13}$$

holds for all $j \in [1, NV]$ and for all $i \in [1, NG]$. Then the discretized formulation of the static shakedown theorem for the determination of the shakedown loading factor is given by

$$\alpha_{SD}^L = \max_{\bar{\rho}} \alpha \tag{3.14}$$

with the subsidiary conditions

$$[\mathbf{C}]\{\bar{\boldsymbol{\rho}}\} = \{\mathbf{0}\} \tag{3.15}$$

$$F(\alpha \boldsymbol{\sigma}_i^E(P_j) + \bar{\boldsymbol{\rho}}_i) \leq \sigma_Y \quad \forall i \in [1, NG] \text{ and } \forall j \in [1, NV]. \tag{3.16}$$

The yield criterion has to be fulfilled at Gaussian points $i \in [1, NG]$ and in each load corner $j \in [1, NV]$, where $NV = 2^n$. The number of unknowns of the optimization problem (3.14)-(3.16) is $N = 1 + NG \times NSK$ corresponding to α and $\{\bar{\boldsymbol{\rho}}\}$. The number of constraints is $NV \times NG + NF$, where NSK is the dimension of the stress vector at each Gaussian point and NF denotes the degrees of freedom of displacements of the discretized body. This problem can be solved by classical algorithms of optimization because for practical problems the number of unknowns is in general very high. The direct approach presented above of shakedown analysis leads to a problem of mathematical programming, which requires a large amount of computer memory if other than one or two-dimensional structures are studied. Furthermore, for nonlinear yield conditions (e.g. von Mises criteria), the solution of the respective nonlinear optimization problem often requires highly iterative procedures and is therefore very time-consuming. This results from the fact, that the nonlinear programming approaches imply adopting solution schemes based more on purely

mathematical considerations disregarding simplifying physical or technological features. A Method to overcome the time-consumption is to use a software package for solving large-scale nonlinear optimization problems (see e.g. [44]-[46]) or to apply the so-called reduced basis technique (see e.g. [39]-[41], [47]-[50]).

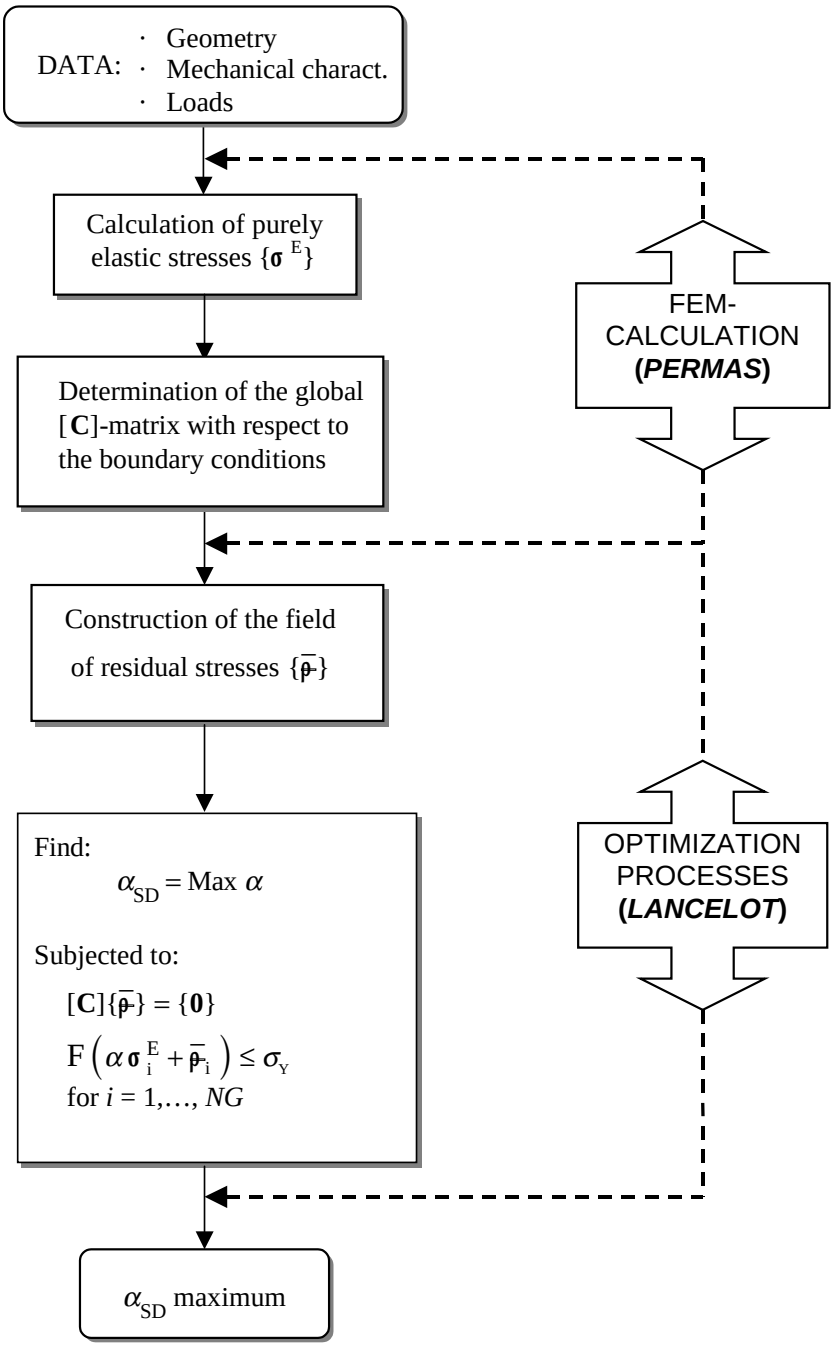

Figure 3.1: Flowchart of the implemented algorithm

3.4 Large-scale nonlinear optimization problem

The resolution of large-scale non-linear optimization problems can been carried out by using the advanced code LANCELOT [51] which is based on an augmented Lagrangian method. LANCELOT automatically transforms inequality constraints (3.16) into equations. This technique is extensively used in simplex-like methods for large-scale linear and nonlinear programs [52]. The constrained maximization problem (3.14)-(3.16) is solved by finding approximate maximizers of the augmented Lagrangian function Φ, for a carefully constructed sequence of Lagrange multiplier estimates η_i, constraint scaling factors s_{ii} and penalty parameter β

$$\Phi(X, \eta, s, \beta) = f(X) + \sum_{i=1}^{m} \eta_i b_i(X) + \frac{1}{2\beta} \sum_{i=1}^{m} s_{ii} b_i(X)^2 \tag{3.17}$$

with

$$\begin{aligned} f(X) &= \alpha & (3.18)\\ b_p(X) &= C_{pq}\bar{\boldsymbol{\rho}}_q \quad p = 1, \ldots, NF; q = 1, \ldots, NG \times NSK & (3.19)\\ b_r(X) &= F(\alpha \boldsymbol{\sigma}_r^E + \bar{\boldsymbol{\rho}}_r) \leq \sigma_Y \quad r = NF+1, \ldots, NG \times NV & (3.20) \end{aligned}$$

The number of optimization variables X which corresponds to α and $\{\bar{\boldsymbol{\rho}}\}$ is equal to N. The first-order necessary conditions for a feasible point $X^{(k)} = (\alpha^{(k)}, \{\bar{\boldsymbol{\rho}}\}^{(k)})$ of the iteration k to solve the problem (3.17), require that there are Lagrangian multipliers, $\eta^{(k)}$, for which the projected gradient of the Lagrangian function at $X^{(k)}$ and $\eta^{(k)}$ and the general constraints (3.18)-(3.20) at $X^{(k)}$ vanish. For $k = 0$ we set $\alpha^{(k)} = \alpha_E$ and $\{\bar{\boldsymbol{\rho}}\}^{(k)} = \{\mathbf{0}\}$ where α_E denotes the elastic limit factor of the reference body $\mathcal{B}^E$. One can then assess the convergence of the augmented Lagrangian method by the size of the projected gradient and constraints at $X^{(k)}$ and $\eta^{(k)}$. The optimization will be terminated if the conditions

$$||X^{(k)} - P(X^{(k)} - \nabla_x \Phi(X^{(k)}, \eta^{(k)}, s^{(k)}, \beta^{(k)}))|| \leq \varepsilon_l \tag{3.21}$$

and

$$||b(X^{(k)})|| \leq \varepsilon_c \tag{3.22}$$

hold for some appropriate small convergence tolerances ε_l and ε_c, where P denotes the projection operator.

It turns out that the elements of $\{\bar{\boldsymbol{\rho}}\}$ are not independent of each other and so a Gauss-Jordan elimination procedure [53] can be applied to the matrix [**C**] to eliminate the equality constraints (3.19) and to reduce the size of the problem. Then, we obtain the matrix [**b**] with the following property

$$[\mathbf{C}][\mathbf{b}] = \mathbf{0} \tag{3.23}$$

By this means, an arbitrary vector **X** with $NX = NG \times NSK - NF$ components yields with the relation

$$\{\bar{\boldsymbol{\rho}}\} = [\mathbf{b}]\{\mathbf{X}\} \tag{3.24}$$

a residual stress vector $\{\bar{\boldsymbol{\rho}}\}$, satisfying eqn. (3.19) for any vector $\{\mathbf{X}\}$. The column vectors of [**b**] represent linearly independent residual stress states of the discretized body. Then, we get the following reduced optimization problem

$$\alpha_{SD}^{L} = \max_{X} \alpha \tag{3.25}$$

with the subsidiary conditions

$$F(\alpha \boldsymbol{\sigma}_i^E(P_j) + [\mathbf{b}_i]\{\mathbf{X}\}) \leq \sigma_Y \qquad \forall i \in [1, NG], \forall j \in [1, NV]. \tag{3.26}$$

3.5 Reduced basis technique

Instead of solving the optimization problem (3.14) - (3.16) in the complete space of residual stresses, it can be solved iteratively in a sequence of subspaces with very low dimensions [39]-[41], [47]-[50]. At the beginning of the iteration k, we have a known feasible point of the optimization problem represented by a load factor $\alpha^{(k-1)}$ and a residual stress distribution $\{\bar{\boldsymbol{\rho}}\}^{(k-1)} = [\mathbf{b}_i]^{(k-1)}\{\mathbf{X}\}^{(k-1)}$. Thus, the total stresses in the Gaussian point i for the load P_j, corresponding to the j-th corner of the load domain, are given by

$$\{\boldsymbol{\sigma}_i(P_j)\}^{(k-1)} = \alpha^{(k-1)}\{\boldsymbol{\sigma}_i^E(P_j)\} + \{\bar{\boldsymbol{\rho}}_i\}^{(k-1)} \tag{3.27}$$

and satisfy the inequality

$$F\left(\{\boldsymbol{\sigma}_i(P_j)\}^{(k-1)}\right) \leq \sigma_Y \qquad \forall i \in [1, NG], \forall j \in [1, NV]. \tag{3.28}$$

If we add a load increment, defined by $\Delta\alpha^{(k)} > 0$ to the known load factor $\alpha^{(k-1)}$, additional plastic strains will develop. These plastic strains cause a redistribution of the stress state due to additional residual stresses. This residual stress state is a meaningful base vector for the shakedown problem, because it takes care of the corresponding load domain $\mathcal{L}$. The residual stress state can be determined by a simple linear elastic analysis accounting for initial plastic strains, provided that the plastic strain distribution is known. For the determination of the plastic strain distribution at the k-th iteration, we use the normality rule (eqn. (2.12))

$$\boldsymbol{\varepsilon}_j^p = \lambda \frac{\partial F(\boldsymbol{\sigma}_j)}{\partial \boldsymbol{\sigma}_j} \tag{3.29}$$

with

$$\lambda = 1 - \frac{F(\boldsymbol{\sigma}_j)}{F(\mathbf{0})} - \gamma \qquad \text{for } 1 - \frac{F(\boldsymbol{\sigma}_j)}{F(\mathbf{0})} > \gamma \tag{3.30}$$

$$\lambda = 0 \qquad \text{for } 1 - \frac{F(\boldsymbol{\sigma}_j)}{F(\mathbf{0})} \leq \gamma \tag{3.31}$$

and

$$0 \leq \gamma \leq 1 \tag{3.32}$$

where

$$\boldsymbol{\varepsilon}_j^p = \{\boldsymbol{\varepsilon}^p(P_j)\}^{(k)} \text{ and } \boldsymbol{\sigma}_j = \{\boldsymbol{\sigma}(P_j)\}^{(k)} \tag{3.33}$$

A linear elastic analysis accounting for initial plastic strains according to eqn. (3.29) then yields the respective residual stress distribution. This way, one gets for each load P_j one residual stress state, i.e. one reduced base vector. Thus, the number of base vectors NXR is equal to the number of corners of the load domain NV. The factor γ in eqn. (3.32) is a control parameter for the iteration process and plays the role of weighting factor. If there is no advance in α, γ will be increased until it reaches the value 1. The k-th improved state is determined by solving the reduced optimization problem

$$\alpha_{SD}^{L(k)} = \max_X \alpha^{(k)} \tag{3.34}$$

and satisfy the inequality

$$F\left(\alpha^{(k)}\{\boldsymbol{\sigma}_i^E(P_j)\} + \{\bar{\boldsymbol{\rho}}_i\}^{(k-1)} + [\mathbf{b}_i^R]^{(k)}\{\mathbf{X}^{(R)}\}^{(k)}\right) \leq \sigma_Y, \quad \forall i \in [1, NG], \forall j \in [1, NV]. \tag{3.35}$$

The NXR column vectors of the matrix $[\mathbf{b}^R]^{(k)}$ represent the selected base vectors. The upper index "R" indicates, that $[\mathbf{b}^R]$ is a reduced subspace. Here, $\alpha^{(k)}$ and $\{\mathbf{X}^{(R)}\}^{(k)}$ are the primary unknowns of the actual sub-problem (3.34) - (3.35). After solving this problem, we obtain the improved state by the updates

$$\{\bar{\boldsymbol{\rho}}\}^{(k)} = \{\bar{\boldsymbol{\rho}}\}^{(k-1)} + [\mathbf{b}^R]^{(k)}\{\mathbf{X}^{(R)}\}^{(k)} \tag{3.36}$$

The iteration process is repeated with the selection of new base vectors until the convergence criterion

$$|\Delta\alpha^{(k)}| = \alpha^{(k)} - \alpha^{(k-1)} \leq \varepsilon_l \tag{3.37}$$

is fulfilled for some appropriate small convergence tolerances ε_l.

It must be mentioned, that this criterion is not sufficient for the convergence of the original problem (3.14) - (3.16), because the value of $\Delta\alpha^{(k)}$ at each iteration strongly depends on the choice of the reduced base vectors. It may happen, that $\Delta\alpha^{(k)}$ is very small at the beginning of the iteration process, while the true load factor is much higher than $\alpha^{(k)}$. The check of the Kuhn-Tucker conditions of the original problem [54] is the only way to assess the quality of the approximation.

4 Discrete formulation of upper bound method

4.1 Discretization of the time variable and space

We restrict ourselves to the original Koiter's theorem. The presence of time integrals involves in principle difficulties in the application. For that, we consider the stress and strain rate field only at every vertex j instead the integration over the time cycle. The plastic strain rate $\dot{\boldsymbol{\varepsilon}}^p$ can differ from zero at a point of the body only if the stress state $\boldsymbol{\sigma}_j$ corresponding to the loading corner j attains the yield surface. Let us denote, respectively, the fictitious elastic stress and the plastic strain sub-increments during loading at corner j of domain $\mathcal{L}$ by $\boldsymbol{\sigma}_j^E$ and $\boldsymbol{\varepsilon}_j^p$. At each load vertex, the kinematical condition may not be satisfied. However, the accumulated strain in a load cycle

$$\Delta\boldsymbol{\varepsilon}^p = \sum_{j=1}^{NV} \boldsymbol{\varepsilon}_j^p \tag{4.1}$$

is a compatible strain field in the sense of Koiter. The discretization in space of the problem (2.72) - (2.77) can be carried out by standard finite element procedures. Then, the vectors of increments of residual displacement $\{\Delta\mathbf{u}\}$ and plastic strain $\{\Delta\boldsymbol{\varepsilon}^p\}$ for an element e are approximated by

$$\{\Delta\mathbf{u}\} = [\mathbf{N}]\{\Delta\mathbf{U}\}, \{\Delta\boldsymbol{\varepsilon}^p\} = [\mathbf{B}]\{\Delta\mathbf{U}\} \tag{4.2}$$

where $\{\Delta\mathbf{U}\}$ is the vector of nodal displacements, [**N**] is the shape function matrix and [**B**] the resulting compatibility matrix. Then the discretized formulation of the kinematic shakedown theorem for the determination of the shakedown loading factor is given by

$$\alpha_{SD}^U = \min_{\varepsilon_{ij}^p, \Delta u} \sum_{j=1}^{NV}\sum_{i=1}^{NG} \frac{\sigma_Y^{2-m}}{m}[3\mu]^{m-1} w_i |\mathbf{J}|_i \sqrt{\left(\frac{2}{3}\{\boldsymbol{\varepsilon}_{ji}^p\}^T[\mathbf{X}]\{\boldsymbol{\varepsilon}_{ji}^p\}\right)^m} \tag{4.3}$$

with the subsidiary conditions

$$\sum_{j=1}^{NV}\sum_{i=1}^{NG} w_i |\mathbf{J}|_i \{\boldsymbol{\sigma}_{ji}^E\}^T\{\boldsymbol{\varepsilon}_{ji}^p\} = 1 \tag{4.4}$$

$$\{\mathbf{Y}\}^T\{\boldsymbol{\varepsilon}_{ji}^p\} = 0 \tag{4.5}$$

$$\{\Delta\boldsymbol{\varepsilon}^p\} = \sum_{j=1}^{NV}\{\boldsymbol{\varepsilon}_{ji}^p\} = [\mathbf{B}_i]\{\Delta\mathbf{U}\} \tag{4.6}$$

Here, $\mathbf{Y}^T = \{1,1,1,0,0,0\}$ and $\mathbf{X}$ = diag [**I**, ½ **I**], where **I** denotes the identity matrix of order 3. The vector $\{\Delta\mathbf{U}\}$ contains all unconstrained nodal displacements of the finite element model and $[\mathbf{B}_i]$ is the assembled compatibility matrix for strains at Gauss points $i \in$

$[1, NG]$. It is worth noting that the plastic incompressibility is enforced at each load vertex j for the relevant plastic strain sub-increment (eqn. (4.5)), while geometric compatibility is imposed on the cumulative plastic strains of the admissible cycle (eqn. (4.6)) [55]-[58].

4.2 Large-scale nonlinear optimization problem

The above outlined discretization with respect to time and space reduces the optimization problem (2.72)-(2.77) to a mathematical programming problem in a finite-dimensional space. The constrained minimization for the kinematic shakedown problem (2.72)-(2.77) is solved by finding approximate minimizers of the augmented Lagrangian function Φ

$$\Phi(\boldsymbol{\varepsilon}_{ji}^p, \Delta\mathbf{U}, \eta, \mathbf{L}_i) = f(x) + \eta b_1(x) + b_2(x) + \frac{1}{2}\beta b_3(x) \tag{4.7}$$

with

$$f(x) = \sum_{j=1}^{NV}\sum_{i=1}^{NG} \frac{\sigma_Y^{2-m}}{m}[3\mu]^{m-1} w_i |\mathbf{J}|_i \sqrt{\left(\frac{2}{3}\{\boldsymbol{\varepsilon}_{ji}^p\}^T[\mathbf{X}]\{\boldsymbol{\varepsilon}_{ji}^p\}\right)^m} \tag{4.8}$$

$$b_1(x) = 1 - \sum_{j=1}^{NV}\sum_{i=1}^{NG} w_i |\mathbf{J}|_i \{\boldsymbol{\sigma}_{ji}^E\}^T\{\boldsymbol{\varepsilon}_{ji}^p\} \tag{4.9}$$

$$b_2(x) = \sum_{i=1}^{NG}\{\mathbf{L}_i\}^T \sum_{j=1}^{NV}\left(\{\boldsymbol{\varepsilon}_{ji}^p\} - [\mathbf{B}_i]\{\Delta\mathbf{U}\}\right) \tag{4.10}$$

$$b_3(x) = \sum_{j=1}^{NV}\sum_{i=1}^{NG} w_i |\mathbf{J}|_i \{\boldsymbol{\varepsilon}_{ji}^p\}^T\{\mathbf{Y}\}^T\{\mathbf{Y}\}\{\boldsymbol{\varepsilon}_{ji}^p\}. \tag{4.11}$$

The resolution of the augmented Lagrangian problem above consists to find a feasible point $(\boldsymbol{\varepsilon}_{ji}^p, \Delta\mathbf{U}, \eta, \mathbf{L}_i)$ so that $(\boldsymbol{\varepsilon}_{ji}^p, \Delta\mathbf{U})$ is the solution of the constrained problem. The limit load factor α_{SD}^U is the limit of $\alpha_{SD}^U(m)$ when m tends to 1. It may be proven that the duality theory of mathematical programming provides a meaningful link between the lower and the upper bound of limit load (see e.g. [43]). The unique exact shakedown load factor occurs when the lower and upper bounds coincide so that $\alpha_{SD}^L = \alpha_{SD}^U = \alpha_{SD}$.

Acknowledgement
The research has been funded by the European Commission as part of the Brite–EuRam III project LISA: FEM–Based Limit and Shakedown Analysis for Design and Integrity Assessment in European Industry (Project N°: BE 97–4547, Contract N°: BRPR–CT97–0595).

Bibliography

[1] Melan, E.: Theorie statisch unbestimmter Systeme aus ideal-plastischem Baustoff. *Sitzber. Akad. Wiss., Wien, Abt. IIA* 145, 195-218 (1936).

[2] Koiter, W.T.: General theorems for elastic-plastic solids. In Sneddon, I.N., Hill; R., eds., *Progress in solid mechanics,* pp. 165-221. North-Holland, Amsterdam (1960).

[3] Maier, G.: Shakedown theory in perfect elastoplasticity with associated and nonassociated flow-laws: A finite element, linear programming approach. *Meccanica* 4, 250-260 (1969).

[4] Maier, G.: A shakedown matrix theory allowing for workhardening and second-order geometric effects. In Sawczuk, A., ed., *Foundations in plasticity*, pp. 417-433, Noordoff, Leyden (1973).

[5] Gokhfeld, D.A.; Cherniavsky, O.F.: *Limit analysis of structures at thermal cycling*. Sijthoff and Noordhoff, Leyden (1980).

[6] Weichert, D.: On the influence of geometrical nonlinearities on the shakedown of elastic-plastic structures. *Int. J. Plasticity* 2, 135-148. (1986).

[7] König, J.A.: *Shakedown of elastic-plastic structures*. Elsevier, Amsterdam (1987).

[8] Kleiber, M.; König, J.A.: Inelastic solids and structures. A. Sawczuk memorial volume, Pineridge Press, Swansea, U.K. (1990).

[9] Gross-Weege, J.: A unified formulation of statical shakedown criteria for geometrically nonlinear problems. *Int. J. Plasticity* 6, 433-447 (1990).

[10] Saczuk, J.; Stumpf, H.: On Statical Shakedown Theorems for Non-Linear Problems. IfM-Report, No 74, Ruhr-Universität, Bochum (1990).

[11] Polizzotto, C.; Borino, G.; Caddemi, S.; Fuschi, P.: Shakedown problems for material models with internal variables. *Eur. J. Mech. A/Solids* 10, 621-639 (1991).

[12] Stumpf, H.: Theoretical and computational aspects in the shakedown analysis of finite elastoplasticity. *Int. J. Plasticity* 9, 583-602 (1993).

[13] Mróz, Z.; Weichert, D.; Dorosz, S., eds.: *Inelastic behaviour of structures under variable loads*. Kluwer Academic Publishers, Dordrecht (1995).

[14] Corigliano, A.; Maier, G.; Pycko, S.: Dynamic shakedown analysis and bounds for elastoplastic structures with nonassociative internal variable constitutive laws. *Int. J. Solids Struct.* 32, 3145-3166 (1995).

[15] Polizzotto, C.; Borino, G.: Shakedown and steady-state responses of elastic-plastic solids in large displacements. *Int. J. Solids Struct.* 33, 3415-3437 (1996).

[16] Saczuk, J.: The influence of deformation path on adaptation process of a solid. *Arch. Mech.* 49, 525 (1997).

[17] Weichert, D.; Hachemi, A.: Influence of geometrical nonlinearities on the shakedown analysis of damaged structures. *Int. J. Plasticity* 14, 891-907 (1998).

[18] Weichert, D.; Maier, G., eds.: *Inelastic Analysis of Structures under Variable Loads: Theory and Engineering Applications*, Kluwer Academic Publishers, Dordrecht, The Netherlands (2000)

[19] Halphen, B.; Nguyen, Q.S.: Sur les matériaux standards généralisés. *J. Méc.* 14, 39-63 (1975).

[20] Kachanov, L.M.: Time of the rupture process under creep conditions. *Izv. Akad. Nauk, S.S.R., Otd. Tech. Nauk* 8, 26. (1958).

[21] Lemaitre, J.; Chaboche, J.L.: *Mécanique des matériaux solides*. Dunod, Paris (1985).

[22] Ju, J.W.: On energy-based coupled elastoplastic damage theories: Constitutive modeling and computational aspects. *Int. J. Solids Struct.* 25, 803-833 (1989).

[23] Nayroles, B.; Weichert, D.: La notion de sanctuaire d'élasticité et l'adaptation des structures. *C.R. Acad. Sci.* 316, 1493-1498 (1993).

[24] Hachemi, A.; Weichert, D.: An extension of the static shakedown theorem to a certain class of inelastic materials with damage. *Arch. Mech.* 44, 491-498 (1992).

[25] Siemaszko, A.: Inadaptation analysis with hardening and damage. *Eur. J. Mech. A/Solids* 12, 237-248 (1993).

[26] Feng, X.Q.; Yu, S.W.: Damage and shakedown analysis of structures with strain-hardening. *Int. J. Plasticity* 11, 237-249 (1995).

[27] Polizzotto, C.; Borino, G.; Fuschi, P.: An extended shakedown theory for elastic-plastic-damage material models. *Eur. J. Mech. A/Solids* 15, 825-858 (1996).

[28] Druyanov, B.; Roman, I.: On adaptation (shakedown) of a class of damaged elastic plastic bodies to cyclic loading. *Eur. J. Mech. A/Solids* 17, 71. (1998).

[29] Hachemi, A.; Weichert, D.: Application of shakedown theory to damaging inelastic material under mechanical and thermal loads. *Int. J. Mech. Sci.* 39, 1067-1076 (1997).

[30] Weichert, D.; Gross-Weege, J.: The numerical assessment of elastic-plastic sheets under variable mechanical and thermal loads using a simplified two-surface yield condition. *Int. J. Mech. Sci.* 30, 757-767 (1988).

[31] Friaâ, A.: *Loi de Norton-Hoff généralisée en plasticité et viscoplasticité*. Ph.D. Thesis, Université Pierre et Marie Curie, Paris (1979)

[32] Frémond, M.; Friaâ, A.: Les méthodes statique et cinématique en calcul à la rupture et en analyse limite. *J. Méc. Théo. Appl.* 1, 881-905 (1982).

[33] Guennouni, A. T.; Le Tallec, P.: Calcul à la rupture, régularisation de Norton-Hoff et Lagrangien augmenté. *J. Méc. Théo. Appl.* 2, 75-99 (1982).

[34] Voldoire, F.: Regularised limit analysis and applications to the load carrying capacities of mechanical components. CD-ROM Proceedings of the European Congress on Computational Methods in Applied Sciences and Engineering, ECCOMAS 2000, Barcelona, Spain (2000), paper 643, 20 pages.

[35] Belytschko, T.: Plane stress shakedown analysis by finite elements. *Int. J. Mech. Sci.* 14, 619-625 (1972).

[36] Nguyen Dang Hung; König, J.A: A finite element formulation for shakedown problems using a yield criterion of the mean. *Comput. Methods Appl. Mech. Engng.* 8, 179-192 (1976).

[37] Morelle, P.; Nguyen Dang Hung: Etude numérique de l'adaptation plastique des plaques et coques de révolution par les éléments finis d'équilibre. *J. Méc. Théo. Appl.* 2, 567-599 (1983).

[38] Hachemi, A.; Weichert, D.: Numerical shakedown analysis of damaged structures. *Comput. Methods Appl. Mech. Engng.* 160, 57. (1998)

[39] Zhang, G.: *Einspielen und dessen numerische Behandlung von Flächentragwerken aus ideal plastischem bzw. kinematisch verfestigendem Material*. Ph.D. Thesis, Universität Hannover (1991).

[40] Stein, E.; Zhang, G.; Huang, Y.: Modeling and computation of shakedown problems for nonlinear hardening materials. *Comput. Methods Appl. Mech. Engng.* 103, 247-272 (1993).

[41] Groß-Weege, J.: On the numerical assessment of the safety factor of elastic-plastic structures under variable loading. *Int. J. Mech. Sci.* 39, 417-433 (1997).

[42] Weichert, D.; Hachemi, A.; Schwabe, F.: Shakedown analysis of composites. *Mech. Res. Comm.* 26, 309-318 (1999).

[43] König, J.A.; Kleiber, M.: On a new method of shakedown analysis. *Bull. Acad. Polon. Sci., Sér. Sci.* 26, 165-171 (1978).

[44] Christiansen, E.: Limit analysis of collapse states. In: Ciarlet, P.G.; Lions, J.L., eds., *Handbook of numerical analysis* Vol. 4, pp. 193-312, North-Holland: Amsterdam (1996).

[45] Andersen, K.D.; Christiansen, E.; Overton, L.: Computing limit loads by minimizing a sum of norms. *SIAM J. Sci. Comput.* 19, 1046-1062 (1998).

[46] Weichert, D.; Hachemi, A.; Schwabe, F.: Application of shakedown analysis to the plastic design of composites. *Arch. Appl. Mech* 69, 623-633 (1999).

[47] Shen, W.P.: Traglast- und Anpassungsanalyse von Konstruktionen aus ideal plastischem Material. Dissertation, Universität Stuttgart (1986).

[48] Stein, E.; Zhang, G.; Mahnken, R.: Shakedown analysis for perfectly plastic and kinematic hardening materials. In: Stein, E., ed., *Progress in computational analysis of inelastic structures*, CISM No. 321, pp. 175-244, Springer–Verlag, Wien (1993).

[49] Staat, M.; Heitzer, M.: Limit and shakedown analysis for plastic safety of complex structures. *Trans. 14th Int. Conf. SMiRT 14*, pp. B33-B40, Lyon (1997).

[50] Staat, M.; Heitzer, M.: Limit and shakedown analysis using a general purpose finite element code. *Proc. NAFEMS World Congress'97, NAFEM*, pp. 522-533 Stuttgart (1997).

[51] Conn, A.R.; Gould, N.I.M.; Toint, Ph.L.: LANCELOT: *A fortran package for large-scale nonlinear optimization (Release A)*. Springer -Verlag: Berlin (1992).

[52] Gill, P.E.; Murray, W.; Wright, M.H.: *Practical optimization*. Academic press: London and New York (1981).

[53] Stiefel, E.: Note on Jordan elimination, linear programming and Tchebycheff approximation. *Numer. Math.* 2, 1. (1960).

[54] Kuhn, H. W.; Tucker, A. W.: Nonlinear Programming. In: Neyman, J., ed., Proc. Second Berkeley Symp. Math. Statistics and Probability, pp. 481-493, University of California Press, Berkeley (1951).

[55] Zhang Y. G., Zhang P., Lu M. W.: Computational limit analysis of rigid-plastic bodies in plane strain. *Acta Mech. Sol. Sinica* 6, 341-348 (1993).

[56] Liu Y. H., Cen Z. Z., Xu B. Y.: A numerical method for plastic limit analysis of 3-D structures. *Int. J. Solids Struct.* 32, 1645-1658 (1995).

[57] Zhang Y. G.: An iterative algorithm for kinematic shakedown analysis. *Comput. Methods Appl. Mech. Engrg.* 127, 217-226 (1995).

[58] Carvelli, V.; Cen, Z. Z.; Liu, Y.; Maier, G.: Shakedown analysis of defective pressure vessels by a kinematic approach. *Arch. Appl. Mech.* 69, 751-764 (1999).

Part III

Kinematical formulation of limit and shakedown analysis

Yan Ai-Min, Khoi Vu Duc, Nguyen Dang Hung

LTAS- Institut de Mécanique et Génie Civil (B52)
Université de Liège, Chemin des Chevreuils 1, Sart Tilman, B-4000 Liège, Belgique

E-mail: H.NguyenDang@ulg.ac.be

Summary

In this report, we deal with a general non-linear kinematical approach for limit and shakedown analysis of structures. The developed methods may be implemented with any displacement-based finite element code. Plastic regularization methods are presented to overcome the non-differentiability of the objective function. The temperature-dependence of the yield limit is taken into account in shakedown analysis and the strain hardening effect of the material is discussed. By the developed methodologies, two inadaptation factors may be separately determined or a combined shakedown solution is presented. Several effective numerical methods are developed. The non-linear programming problem is transformed into a series of linear-elastic-like calculations. At every iteration, upper bound and lower bound of limit and shakedown solutions may be dually obtained. With a rapid convergence, the numerical solutions obtained tend to the accurate ones with low calculating costs.

In Section 1, the modified kinematical limit and shakedown theorems are described The calculating methods are implemented in displacement-based finite element formulations.

In Section 2, the non-differentiability problem of the objective function is dealt with. Three regularization procedures are presented

Section 3 concerns the numerical approach for the incremental plasticity analysis. Two Newton-type algorithms are developed. Upper and lower bounds of limit solution are dually given. The convergence of the solutions is proved.

Section 4 describes a kinematic shakedown algorithm, which may be considered as a simplified form of the dual method presented in section 5 without static conditions considered.

In section 5, we present a new dual shakedown analysis. Starting from kinematic theorem, but we introduce also static variables and optimization conditions to lead to a rapid convergence and accurate dual solutions (lower and upper bounds of shakedown limits).

In section 6, several numerical examples are illustrated to show the efficiency and the convergence of the methods. The numerical results are compared to those appeared in the literature.

Section 7 gives some general remarks and conclusions.

We note that some other developments at University of Liège (ULg) on LISA project, such as pipe finite elements and limit-shakedown analysis by equilibrium backstress field (Zarka's analysis) are not presented in this report, which are referred, respectively, to [31] and [34].

1 General kinematical theorems and methods

1.1 Loading domains, plastic collapse and shakedown limits

Let us suppose a general loading case: a body occupying the bounded domain V, is subjected to n time-dependent loads $P_k(t), k = 1, \ldots, n$ and a time-independent (dead) load P_0. Generally loads consist of body force **f** and surface traction **p**. Thermal loading due to the temperature field will be included when it concerns shakedown analysis. We classify n active loading into three cases:

1) Every load *varies independently* within a given range of itself:

$$\bar{P}_k^0 \in I_k^0 = \left[\bar{P}_k^-; \bar{P}_k^+\right] = \left[\mu_k^-; \mu_k^+\right] P_k^0 \qquad k = 1, \ldots, n \tag{1.1a}$$

The loading function may be represented as

$$P(t) = \sum_{k=1}^{n} \mu_k(t) P_k^0 \quad \mu_k^- \leq \mu_k(t) \leq \mu_k^+ \tag{1.1b}$$

This forms a $n-$dimensional loading domain $\mathcal{L}$: a convex hyperpolyhedron in load space. Fig. 1.1(a) shows such a loading domain (rectangle) taking two variable loads as example.

2) If n loads, instead of varying independently, can be described by a set (m) of linear inequalities such that

$$\sum_{i=}^{n} A_{ij} \mu_i^- \bar{P}_j^0 \leq 0 \qquad j = 1, \quad m \tag{1.2}$$

The loading domain becomes a polyhedron enveloped inside the domain $\mathcal{L}$ of (1.1a), see Fig. 1.1(b).

3) A straight line in Fig. 1.1(c), represents a proportional and monotonic loading.

Now let us multiply the nominal loading domains by a load multiplier α. The objective of shakedown analysis is to find the largest value α_{SD} such that $\alpha_{SD} P(t) + P_0$, which still guarantees *elastic shakedown*. This situation means that after certain time t^* or some cycles of loading, the plastic strain may cease to develop and the structure returns to the elastic behaviour.

$$\dot{\varepsilon}_{ij}^p(\mathbf{x}, t) = 0 \qquad \text{when } t > t^* \tag{1.3}$$

Therefore, the total amount of plastic energy dissipated anywhere must be finite. Generally the structure may be thought safe if above shakedown condition is satisfied.

When $\alpha > \alpha_{SD}$, we can distinguish the following cases:

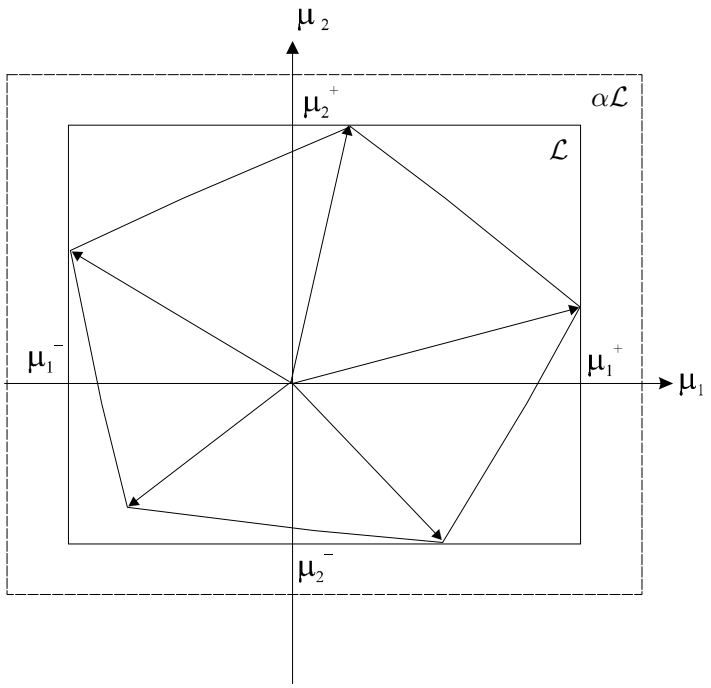

Figure 1.1: Three types of loading domain: (a) Independently varying (b) dependently varying (c) proportional and monotonic loading

1) *Alternating plasticity* (*plastic shakedown or low-cycle fatigue*). Local break occurs after a small number of cycles, as the result of local (or sometimes global) plastic deformations alternating in sign (for example, plastic compression succeeds plastic extension, and so on). In this case we have the following local relation

$$\Delta\varepsilon_{ij}^{p} = \int_{\tau} \dot{\varepsilon}_{ij}^{p} dt = 0, \qquad \text{but } \dot{\varepsilon}_{ij}^{p} \neq 0 \tag{1.4}$$

where τ is the cycle time period. If alternating plasticity occurs, the structure may be unsafe. However in some practical cases, very local alternating plasticity is permitted in engineering design. By consequence a small plastic cell is surrounded by a large elastic body. This is called overall shakedown. For example through a local thickness of a shell, the alternating plasticity should be restricted to less than 20% of the section for safety assessment.

2) *Incremental plasticity* (*ratchetting*). Plastic deformation does not change in sign, but grows with cycles. This leads to the unlimited accumulation of plastic deformation a mechanism is formed

$$\Delta\varepsilon_{ij}^{p} = \int_{\tau} \dot{\varepsilon}_{ij}^{p} dt \neq 0 \quad \dot{\varepsilon}_{ij}^{p} \neq 0 \tag{1.5a}$$

$$\dot{\varepsilon}_{ij}^{p} = \dot{\Lambda}(t)\Delta\varepsilon_{ij}^{p} \quad \dot{\Lambda}(t) \text{ is monotonic} \tag{1.5b}$$

This phenomenon is never allowed in engineering design. So we see that it is sometimes significant to distinguish the above two inadaptation modes. On the other hand in engineering practice the prevention against these two failure modes may be quite different.

Obviously situation 1) and 2) may happen simultaneously. However, this does not pose the difficulty in determining separately two inadaptation factors, because the two inadaptation limits are independent from each other.

3) If one load vertex $\hat{P}_i$ of load the domain attains the plastic collapse limit, the structure may fail instantaneously during this loading process. In this case the shakedown limit does really coincide with the plastic collapse limit. So we know that limit analysis is a special case of shakedown analysis when only one loading vertex is concerned. The plastic collapse load is represented as $\alpha_L P + P_0$. There exist some situations where, even if dead load P_0 cannot be carried alone, the combination $\alpha P + P_0$, with $\alpha_{L1} < \alpha < \alpha_{L2}$, can be carried. This happens when there is a compensation effect between force P and P_0.

By defining the limit multiplier α_L and shakedown limit α_{SD}, as well as α_D (shakedown limit of dependent loading), it is clear that:

$$\alpha_{SD} \leq \alpha_D \tag{1.6}$$

$$\alpha_{SD} \leq \alpha_L \tag{1.7}$$

However, we do not have a general relation between α_D and α_L except that the proportional load be enveloped within the dependent load domain. In this case we have also

$$\alpha_D \leq \alpha_L. \tag{1.8}$$

1.2 Limit analysis

It is assumed that a body is subjected to a monotonic and proportional load $P(\mathbf{f,p})$ besides dead a load $P_0(\mathbf{f}_0, \mathbf{p}_0)$. Limit analysis concerns a direct estimation of the plastic collapse load such that $\alpha_L P + P_0$, beyond which plastic collapse happens. Classical upper bound analysis is based on Markov's variational principle applicable to a rigid-perfectly plastic and incompressible material. It may be stated:

Among all kinematically admissible and incompressible velocity fields **v**, *the actual velocity field corresponding to the limit state renders the following functional an absolute minimum:*

$$\Pi(\mathbf{v}) = \int_V D^p(\dot{\boldsymbol{\varepsilon}}) dV - L \tag{1.9a}$$

$$L = \alpha \left(\int_V \mathbf{f}^T \mathbf{v} dV + \int_{\partial V_p} \mathbf{p}^T \mathbf{v} dS \right) + \int_V \mathbf{f}_0^T \mathbf{v} dV + \int_{\partial V_p} \mathbf{p}_0^T \mathbf{v} dS \tag{1.9b}$$

By adopting von Mises criterion, we have the following plastic dissipation function.

$$D^p(\dot{\varepsilon}_{ij}) = \sigma_{ij}^D \dot{\varepsilon}_{ij} = 2k_v \sqrt{J_2(\dot{\varepsilon}_{ij})}, J_2 = \frac{1}{2}\dot{\varepsilon}_{ij}\dot{\varepsilon}_{ij} - \frac{1}{6}\dot{\varepsilon}_{ii}\dot{\varepsilon}_{ii} \tag{1.10}$$

where $k_v = \sigma_y/\sqrt{3}$, σ_y is the yield limit of the material, σ_{ij}^D is the stress deviator, and J_2 is the second strain rate invariant.

It is noticed that the incompressibility condition, although it is true for plastic deformations of metals, introduces some numerical difficulty. By using plane stress or shell-type elements, this condition can be naturally achieved by adopting the Kirchhoff hypothesis. However it could not be automatically satisfied by using general finite elements (plane strain, 3D…) formulae. To overcome this difficulty, various methods have been used, which may be classified as follows:

1) Incompressible or mixed finite element formulations were used by some authors. Jiang [13] introduced the complementary strain variables satisfying the incompressibility condition. A similar method has been adopted by EDF [28] by using mixed finite element formulation. Both velocity and a hydrostatic pressure field are discretized. The incompressibility is ensured by dualization in a weak form and it is inserted in the equations of the tangent matrix corresponding to velocity variables.

2) A method using a modification of Markov variational principle was proposed [29], [30]. The fictitious volume strain power is introduced in internal dissipation calculation. By this a modification, the variational functional (1.9a) becomes

$$\Pi(\dot{\mathbf{u}}) = \int_V (D^p(\dot{\varepsilon}_{ij}) + \frac{1}{2}\bar{k}\dot{\varepsilon}_{ii}^2) dV - L \tag{1.11a}$$

where

$$D^p(\dot{\varepsilon}_{ij}) = \sigma_{ij}^D \dot{\varepsilon}_{ij} = 2k_v \sqrt{J_2(\dot{\varepsilon}_{ij})}, J_2 = \frac{1}{2}\dot{\varepsilon}_{ij}\dot{\varepsilon}_{ij} - \frac{1}{6}\dot{\varepsilon}_{ii}\dot{\varepsilon}_{ii} \tag{1.11b}$$

$$\bar{k} = \frac{\bar{E}}{3(1-2\nu)}. \tag{1.11c}$$

$\bar{E}$ is the fictitious linear-viscous Young's modulus; $\bar{k}$ the corresponding bulk modulus; ν Poisson's ratio.

3) Penalty function method was used by Liu *et al.* [22]. The incompressibility as a constraint condition is enforced in the optimization process. In fact, the second method of using the modified Markov's functional is equivalent numerically to the penalty method when one takes $\bar{k}$ as a penalty function coefficient (large enough) and cancels the volume term in the calculation of J_2.

We used methods 2 and 3 in limit and shakedown analysis to obtain equivalent calculating efficiency. The methods permit us to use any usual displacement-based finite elements without any modification. As methods 2 and 3 are similar, we will use mainly penalty-method description in the following development. From the kinematical theorem, it may be stated that:

The actual limit load multiplier α_L is the smallest of multiplier set α^+ corresponding to the sets of kinematically admissible velocity field **v**:

$$\alpha_L = \min_{\mathrm{v}} \alpha^+, \tag{1.12a}$$

$$\alpha^+ = \int_V \sqrt{2} k_v \sqrt{\dot{\varepsilon}_{ij}\dot{\varepsilon}_{ij}} + \frac{1}{2}\bar{k}\dot{\varepsilon}_{ii}^2 dV - \left(\int_V \mathbf{f}_0^T \mathbf{v} dV + \int_{\partial V_p} \mathbf{p}_0^T \mathbf{v} dS \right) \tag{1.12b}$$

$$\text{s.t.} \quad \int_V \mathbf{f}_0^T \mathbf{v} dV + \int_{\partial V_p} \mathbf{p}_0^T \mathbf{v} dS = 1 \tag{1.12c}$$

$$\dot{\varepsilon}_{ij} = \frac{1}{2}(\dot{u}_{i,j} + \dot{u}_{j,i}) \ \text{ in } V \tag{1.12d}$$

$$\dot{u}_i^0 = 0 \quad \text{on } \partial V_u \tag{1.12e}$$

The penalty function coefficient $\bar{k}$ should be chosen large enough to assure the incompressibility condition during the optimization process. Equation (1.12c) represents a normalization to the original problem. It is well known that the dissipation function is convex and homogeneous of order one. So the unique minimization of (1.12a) exists, however the corresponding optimal field **v** is not unique. In fact there are infinitely many such field. Here we use (1.12e) to fix the velocity field in a certain convex hull that contains the exact solution of the problem. Consequently, the number of optimal field becomes finite but the limit of functional (1.12b) remains unchanged. It should be pointed out that thermal loading, by its self-equilibrating property, has no influence on the limit load if the geometric effect of thermal load is ignored. However if we consider the yield limit of the material as temperature dependent, the temperature field will have certain influence on the limit load calculation through the variation of k_v or σ_y. On the other hand, we may use the flow stress instead of the yield stress to consider the effect of strain hardening of the material.

The above formulation may be discretized by any displacement-based finite element. We define the following discretized terms:

- Displacement rate vector:

$$\mathbf{v} = \mathbf{N}\dot{\mathbf{q}}_e \tag{1.13}$$

- Strain rate vector:

$$\dot{\boldsymbol{\varepsilon}} = \mathbf{B}\dot{\mathbf{q}}_e \tag{1.14}$$

- Dissipation density function

$$D^p = 2k_v\sqrt{(\mathbf{B}\dot{\mathbf{q}}_e)^T\bar{\mathbf{D}}\mathbf{B}\dot{\mathbf{q}}_e} = \sqrt{(\dot{\mathbf{q}}_e\mathbf{B})^T\mathbf{D}\mathbf{B}\dot{\mathbf{q}}_e} \tag{1.15}$$

- Penalty function density

$$\frac{1}{2}\bar{k}(\mathbf{B}\dot{\mathbf{q}}_e)^T\mathbf{D}_v\mathbf{B}\dot{\mathbf{q}}_e \tag{1.16}$$

- External power due to dead load $P_0(\mathbf{f}_0, \mathbf{p}_0)$

$$\sum_e \int_{V_e} (\mathbf{N}\dot{\mathbf{q}}_e)^T\mathbf{f}_0 dV + \int_{\partial V_e} (\mathbf{N}\dot{\mathbf{q}}_e)^T\mathbf{p}_0 dS = \mathbf{g}_0^T\dot{\mathbf{q}} \tag{1.17}$$

- External power due to nominal load $P(\mathbf{f}, \mathbf{p})$

$$\sum_e \int_{V_e} (\mathbf{N}\dot{\mathbf{q}}_e)^T\mathbf{f} dV + \int_{\partial V_e} (\mathbf{N}\dot{\mathbf{q}}_e)^T\mathbf{p} dS = \mathbf{g}^T\dot{\mathbf{q}} \tag{1.18}$$

Where **N** is the interpolation matrix; **B** the strain matrix; $\dot{\mathbf{q}}_e$ and $\dot{\mathbf{q}}$ are, respectively, elemental and global node velocity vector. **g** and $\mathbf{g}_0$ are global load vector due to respectively nominal and dead loads. **D** and $\mathbf{D}_v$ are the coefficient matrices. The transformation between elemental and global node velocity vector is realized by means of localization matrix $\mathbf{L}_e$ such that $\dot{\mathbf{q}}_e = \mathbf{L}_e\dot{\mathbf{q}}$. For the sake of simplicity, we will only use $\dot{\mathbf{q}}$ instead of $\dot{\mathbf{q}}_e$ in the following description. The calculation of limit load multiplier may be represented in the following discretized form:

$$\alpha_L = \min_{\dot{q}} \sum_i^{NG} w_i \left(\sqrt{\dot{\mathbf{q}}^T\mathbf{B}^T\mathbf{D}\mathbf{B}\dot{\mathbf{q}}} + \frac{1}{2}\bar{k}\dot{\mathbf{q}}^T\mathbf{B}^T\mathbf{D}_v\mathbf{B}\dot{\mathbf{q}}\right) - \mathbf{g}_0^T\dot{\mathbf{q}} \tag{1.19a}$$

$$\text{s.t.} \quad \mathbf{g}^T\dot{\mathbf{q}} = 1 \tag{1.19b}$$

where w_i is the integral weight.

1.3 Shakedown analysis

Shakedown analysis needs to be performed when structures are subjected to variable mechanical and thermal loading. These loads may be repeated (cyclic) or varying arbitrarily in certain range. Such variable loads less than the plastic collapse limit may cause failure of structures either due to excessive deformation or due to a local fatigue break after a

finite number of loading cycles (time). As we have pointed out in 1.1, shakedown analysis may be an extension of limit analysis by taking an integration of the functional over a time cycle. So the principal discussion in limit analysis above is still valid for the present shakedown analysis. Here we give only a simple description.

We introduce, according to Koiter [17], an admissible cycle of plastic strain field $\Delta\varepsilon_{ij}^p$ corresponding to a cycle of displacement field Δu_i. At each instant t during the time cycle τ, the plastic strain rate $\dot{\varepsilon}_{ij}^p$ may not be compatible, but the plastic strain accumulated over the cycle is required to be compatible. Hence we have the following relations:

$$\Delta\varepsilon_{ij} = \int_\tau \dot{\varepsilon}_{ij}^p dt \tag{1.20}$$

such that:

$$\Delta\varepsilon_{ij}^p = \frac{1}{2}\left(\frac{\partial\Delta u_i}{\partial x_j} + \frac{\partial\Delta u_j}{\partial x_i}\right) \quad \text{in V} \tag{1.21}$$

$$\Delta u_i = 0 \quad \text{on } \partial V_u \tag{1.22}$$

On the other hand, in order to overcome the numerical difficulty concerning the incompressibility as in limit analysis, we introduced a modification of Koiter's theorem. So we have the following general kinematical shakedown criterion:

1) *Shakedown happens if the following inequality is satisfied:*

$$\int_\tau \int_V \sigma_{ij}^E \dot{\varepsilon}_{ij}^p dV\ dt \le \int_\tau \int_V \left(D^p(\dot{\varepsilon}_{ij}) + \frac{1}{2}\bar{k}\dot{\varepsilon}_{ii}^2\right) dV\ dt \tag{1.23a}$$

2) *Shakedown cannot happen when the following inequality holds:*

$$\int_\tau \int_V \sigma_{ij}^E \dot{\varepsilon}_{ij}^p dV\ dt > \int_\tau \int_V \left(D^p(\dot{\varepsilon}_{ij}) + \frac{1}{2}\bar{k}\dot{\varepsilon}_{ii}^2\right) dV\ dt \tag{1.23b}$$

where σ_{ij}^E is the fictitious elastic stress corresponding to a combination of external loads (a set of variable load $P(t)$ and dead load P_0):

$$\sigma_{ij}^E \propto \alpha P(t) + P_0 \tag{1.24}$$

where α is a load multiplier. Correspondingly, we can decompose σ_{ij}^E into two parts

$$\sigma_{ij}^E = \alpha\sigma_{ij}^{E*}(t) + \sigma_{ij}^{E0}. \tag{1.25}$$

The term $1/2\int_\tau\int_v \bar{k}\dot{\varepsilon}_{ii}^2 dV dt$ is a penalty function. We would point out that shakedown is a limit evolution of the body after a history of repeated loading but not a state fixed in the time. As it is shown by Koiter's theorem, such situation will appear if the applied loading does not give more work than the dissipated energy in the body during the loading cycle.

Starting from the above general shakedown criterion, we can establish a kinematical upper bound formula to determine the shakedown limit:

The actual shakedown load multiplier α_{SD} is the smallest of multiplier set α^+ corresponding to the sets of kinematically admissible velocity field **v**:

$$\alpha_{SD} = \min \alpha^+ \tag{1.26a}$$

$$\alpha^+ = \int_\tau \int_V \left(\sqrt{2} k_v \sqrt{\dot{\varepsilon}_{ij} \dot{\varepsilon}_{ij}} + \frac{1}{2} \bar{k} \dot{\varepsilon}_{ii}^2 \right) dV \; dt - \int_\tau \int_V \sigma_{ij}^{E0} \dot{\varepsilon}_{ij} dV \; dt \tag{1.26b}$$

$$\text{s.t.} \int_\tau \int_V \sigma_{ij}^{E*} \dot{\varepsilon}_{ij} dV \; dt = 1 \tag{1.26c}$$

$$\Delta \varepsilon_{ij} = \frac{1}{2} \left(\frac{\partial \Delta u_i}{\partial x_j} + \frac{\partial \Delta u_j}{\partial x_i} \right) \quad \text{in V} \tag{1.26d}$$

$$\Delta u_i = 0 \;\; \text{on} \; \partial V_u \tag{1.26e}$$

1.4 Temperature-dependent yield stress

As long as thermal load exists, represented here as thermal stress, the octahedral shearing limit k_v, in fact, changes during the loading cycle. When considering the yield stress of material temperature (T) -dependent, the upper bound property of shakedown solution by (1.26a) will not be able to be assured unless the dissipation function D remain convex. To achieve this convexity, we assume a convex yield function f in the $\boldsymbol{\sigma} - T$ space:

$$f = F(\sigma_{ij}) - k_v(T). \tag{1.27}$$

When using von Mises criterion, $F(\sigma_{ij}) = \frac{1}{2} \sigma_{ij}^D \sigma_{ij}^D$, σ_{ij}^D is the stress deviator, $k_v(T) = \sigma_y(T)/\sqrt{3}$, and $\sigma_y(T)$ is the yield stress of the material depending on the actual temperature. Since $F(\sigma_{ij})$ is convex, $\sigma_y(T)$ is required to be concave or linearized for an appropriate upper bound statement [6], [20]. This condition may be satisfied by many metal and alloys for a rather wide range of T [21]. However, there exists some situation where $\sigma_y(T)$ is convex. In this case, the solution obtained by the present method is an approximation instead of a strict upper bound. The error due to this approximation is generally small, because a linear $\sigma_y(T)$ function is a good approximation in the interesting range of T. Therefore, we use the following dissipation function:

$$D(\dot{\varepsilon}_{ij}^p, \sigma_y^t) = \sqrt{\frac{2}{3} \dot{\varepsilon}_{ij}^p \dot{\varepsilon}_{ij}^p} \tag{1.28}$$

with $\sigma_y^t = \sigma_y(T)$. As an approximation, the temperature-dependence of Young's modulus E and thermal extension coefficient α_t may also be considered in the calculation of elastic response σ_{ij}^e, although a theoretic proof is expected. In this case, the elastic property of material will have somewhat influence on shakedown behaviour. This effect is not considered in this work for simplicity. However, Borino *et al.* [6] pointed out that the method represented by (1.26a) does not give a "proper upper bound" when considering temperature-dependent yield stress by the fact that shakedown factor α^+ is inside the dissipation function. Denoting T as a nominal temperature field $D(\dot{\varepsilon}_{ij}^p, \sigma_y^t)$ is defined by (1.28) but with $\sigma_y^t = \sigma_y(\alpha^+ T)$. Due to this difficulty, they have developed a so-called consistent kinematic theorem [6], in which an additional "plastic entropy rate" field conjugated with T was introduced. This method opens a new numerical way although the finite element implementation with this method has not yet be realized. However, it suffers an increment of variables due to "plastic entropy rate" field. Alternatively in the present paper, we use a simple strategy. Since the resolving of optimization (1.26a) may be realized by an iterative procedure, $\sigma_y(\alpha^+ T)$ may be updated with the actual shakedown factor at every iteration until final convergence. Therefore the difficulty mentioned in [6] can be overcome in the range of the classical theorem. In comparison with the theoretic method proposed by Borino *et al.* [6], the present approach does not require to handle additional variables and it is easy to be implemented in numerical calculations. For more details of the method, we refer to [36].

1.5 Numerical methods of shakedown analysis

The time integral over the above shakedown formulae need special numerical techniques to work with a discretized time history. Two numerical methods were developed in our work, which are briefly presented as follows. We refer to [30], [35], [15] for the details of the methods.

1.5.1 Separate Shakedown Limit method (SSL)

This approach finds separately two inadaptation factors concerning the incremental plasticity (ratchetting) and the alternating plasticity (plastic shakedown), respectively. It is very interesting to distinguish these two failure modes because in many practical engineering problems only the incremental plasticity (ratchetting) limit is used as a design parameter and it is often not possible to design the structure in the strict elastic shakedown domain.

1.5.1.1 Incremental plasticity limit

To identify the ratchetting limit, a special numerical way was developed to transform the incremental plasticity analysis into an equivalent limit analysis by the following formulae

[37]

$$\alpha_{IP} = \min_{q} \sum_{i=1}^{NG} w_i \left(k_v^i \sqrt{\dot{\mathbf{q}}^T \mathbf{B}^T \bar{\mathbf{D}} \mathbf{B} \dot{\mathbf{q}}} + \frac{\bar{k}}{2} \dot{\mathbf{q}}^T \mathbf{B}^T \mathbf{D}_v \mathbf{B} \dot{\mathbf{q}} \right) - \mathbf{g}_0^T \dot{\mathbf{q}} \tag{1.29a}$$

$$\text{s.t. } \mathbf{g}^T \dot{\mathbf{q}} = 1 \tag{1.29b}$$

with

$$\mathbf{g}_0 = \sum_{i=1}^{NG} w_i \mathbf{B}^T \boldsymbol{\sigma}^{E0} \tag{1.29c}$$

$$\mathbf{g} = \sum_{i=1}^{NG} \sum_{k=1}^{NL} w_i (\bar{\mu}_k \mathbf{B}^T \boldsymbol{\sigma}_k^E)_i \tag{1.29d}$$

$$\bar{\mu}_k^{=} \begin{cases} \mu_k^+ & \text{if } \boldsymbol{\sigma}_k^E(\mathbf{x}) \Delta\bar{\boldsymbol{\varepsilon}}(\mathbf{x}) \geq 0 \\ \mu_k^- & \text{if } \boldsymbol{\sigma}_k^E(\mathbf{x}) \Delta\bar{\boldsymbol{\varepsilon}}(\mathbf{x}) < 0 \end{cases} \tag{1.29e}$$

where we define $\Delta\bar{\boldsymbol{\varepsilon}} = \mathbf{B}^T \dot{\mathbf{q}}$. This formula is completely similar to (1.12a) except that the variable loading vector (1.29e) should be updated during the optimization process. So we have succeeded to transform the shakedown analysis into an equivalent limit analysis. The method shows an advantage of having fewer variables to optimize (independent of the number of varying loads). When using a standard optimization code to solve this problem, it may concern a minimization with a non-linear (or non-stable) constraint.

Remark 1

When we consider strain-hardening effect of the material by the above formulae, k_v (or σ_y) may be replaced by the hardening strength of the material. Consequently the incremental load factor is proportional to the chosen ultimate stress σ_u. However the obtained load limit may be unsafe due to the possible geometrical effect. As engineering application, it is maybe simple and approximate to use flow stress σ_F of the material such that $\sigma_y \leq \sigma_F < \sigma_u$. So a special consideration for strain hardening effect is generally not necessary in the incremental limit calculation unless the geometrical effect is also considered.

Remark 2

When we consider the yield limit temperature-dependent, k_v^i (or σ_y^i) should be also updated according to (1.29e) for the thermal stress (corresponding to the temperature field) and to the current load factor. Denoting T_1 andT_2, respectively, the lower bound and upper bound of nominal temperature field T, there are two possible values of k_v^i such that $k_v^i(\alpha_{IP}^+ T_1)$ or $k_v^i(\alpha_{IP}^+ T_2)$ to be chosen at each Gauss point.

1.5.1.2 Alternating plasticity limit

To identify the alternating plastic limit, one needs to perform only several elastic calculations on all vertices of loading domain. We define a general stress response

$$\sigma_{ij}^{E} = \sum_{k=1}^{n} (\bar{\mu}_k + \mu_k)\sigma_{ij}^{Ek} \tag{1.30}$$

where σ_{ij}^{Ek} is the elastic stress solution of k-th nominal load P_k (including thermal loading) and

$$\bar{\mu}_k = \frac{\mu_k^+ + \mu_k^-}{2} \quad , \quad |\mu_k| = \frac{\mu_k^+ - \mu_k^-}{2} \tag{1.31}$$

The sign of μ_k should be decided to render maximum the value of von Mises function F. The alternating plasticity limit can be represented as

$$\alpha_{AP} = \min_x \frac{1}{F\left(\sum\limits_{k=1}^{n} \mu_k \sigma_{ij}^{Ek}(\mathbf{x})\right)}. \tag{1.32}$$

Remark 1

Eq. (1.32) states that the plastic fatigue limit is determined by the fact that anywhere in the structure, the maximum varying magnitude of equivalent fictitious elastic stress $\Delta\boldsymbol{\sigma}_{eq}$ can not exceed two times the yield limit of the material.

Remark 2

The constant (or monotonic) loads have no influence on the plastic fatigue limit if these constant loads do not change the geometry and the material property

Remark 3

Kinematical strain hardening has no influence on the alternating plasticity limit because it does not change the allowed stress variation. On the other hand, the alternating plasticity limit is proportional to the current material strength for an isotopic strain hardening material.

Remark 4

If the yield limit of material is considered temperature-dependent, (1.32) may be represented in another simple form

$$\alpha_f = \frac{\sigma_y^{t_1} + \sigma_y^{t_2}}{\max\limits_x(\Delta\boldsymbol{\sigma}_{eq})} \tag{1.33a}$$

or

$$\alpha_f = \frac{2\bar{\sigma}_y}{\max\limits_x(\Delta\boldsymbol{\sigma}_{eq})} \quad , \quad \bar{\sigma}_y = \frac{\sigma_y^{t_1} + \sigma_y^{t_2}}{2} \tag{1.33b}$$

where $\sigma_y^{t_1}$ and $\sigma_y^{t_2}$ are the yield points corresponding to the actual temperature at the beginning and at the end of the half-cycle.

Remark 5

By the presence of the singularity at crack tips, the cracked structures under varying loads are always unsafe according to the strict alternating plasticity criterion. In this case, we should consider, by means of fracture mechanics, the fatigue propagation of cracks and their lifetime in service condition. However, owing to the blunting phenomena at crack tips, the singularity of cracks may reduce or vanish during the loading cycle. So in certain situations, crack growth may cease and the structure may still be safe in point of view of shakedown.

1.5.2 United Shakedown Limit method (USL)

This method finds directly the elastic shakedown limit (that is the smallest one of the incremental plasticity limit and the alternating plasticity limit). We consider a special loading path consisting of all load vertices of the loading domain. The kinematical condition is satisfied by the accumulated strain in a load cycle. Assuming n variable loads with $m = 2^n$ load vertices. The (elastic) shakedown limit may be found by the following minimization:

$$\alpha_{SD} = \min_{\dot{\mathbf{q}}_e^k} \sum_{k=1}^{NV} \sum_{i=1}^{NG} w_i \left(\frac{2\sigma_y^{i,k}}{\sqrt{3}} \sqrt{\left(\dot{\mathbf{q}}_e^k\right)^T \mathbf{B}^T \bar{\mathbf{D}} \mathbf{B} \dot{\mathbf{q}}_e^k} + \frac{\bar{k}}{2} \left(\dot{\mathbf{q}}_e^k\right)^T \mathbf{B}^T \mathbf{D}_v \mathbf{B} \dot{\mathbf{q}}_e^k - \mathbf{g}_0^T \dot{\mathbf{q}}_e^k \right) \quad (1.34a)$$

$$\text{s.t.} \quad \sum_k^{NV} \sum_e^{NE} (\mathbf{g}_e^k)^T \dot{\mathbf{q}}_e^k = 1 \quad (1.34b)$$

$$\sum_{k=1}^{NV} \dot{\mathbf{q}}_e^k = \mathbf{L}_e \dot{\mathbf{q}} \quad (1.34c)$$

where

$$\mathbf{g}_e^k = \int_{V_e} \mathbf{B}^T \boldsymbol{\sigma}_k^E dV \quad (1.34d)$$

where $\dot{\mathbf{q}}_e^k$ and $\mathbf{g}_e^k$ are the nodal displacement rate and load vector of element relative to $\hat{P}_k$ load vertex, respectively. This formula is similar to the former one for limit analysis but with increased number of variables. However, the optimization size of (1.34a) may be reduced with appreciate numerical technique, which will be presented in section 4 and 5. We note also that yield stress $\sigma_y^{i,k}$ depend on the temperature field (with respect to Gauss point i) and its variation (with respect to load domain vertex k).

2 Regularization of plastic dissipation

Almost all algorithms of limit and shakedown analysis require knowledge of the gradient of the objective function. However, the objective function is non-differential in the non-

plastic region of structures where the plastic strain rate vanishes: $\dot{\boldsymbol{\varepsilon}} = \mathbf{B}\dot{\mathbf{q}} = \mathbf{0}$. This major numerical problem has been noted by many authors. In this section we will present some approaches to overcome this difficulty.

2.1 Norton-Hoff-Friaâ method

This method is developed by EDF [28] on the basis of the previous work of Casciaro in 1971, Hutula in 1976 [12] and Friaâ in 1979. The method is also applied in [13]. It involves using a viscous plastic material obeying Norton-Hoff constitutive relation, instead of the original perfectly plastic one and replacing the dissipation function D^p by the regularized and differentiable function D^v_m:

$$D^v_m = \frac{k_v^{1-m}}{m}(\dot{\varepsilon}_{ij}\dot{\varepsilon}_{ij})^{\frac{m}{2}}, \text{ with } 1 \leq m \leq 2 \tag{2.1}$$

In practical calculation with *Code_Aster* developed by EDF, one uses the regularizing parameter $n$instead of m

$$n = \frac{1}{m-1}, \text{ or } m = \frac{n+1}{n} \text{ with } 1 \leq n \leq \infty \tag{2.2}$$

when $m \to 1$, $n \to \infty$, it gives the original plastic dissipation function. So with a finite parameter n (or m) the regularization function D^v_m is differentiable everywhere. By this regularization method, the limit load solution is obtained by an iterative calculation with a sequence of increasing parameter n to find the limit corresponding to $n \to \infty$. Specially, the calculation can be stop at any iterative step and restart from the previous solution even with an updated calculating parameter n (or m). This may speed up the convergence.

2.2 Viscous-plastic regularization method

This method was developed at ULg [25], [30]. It involves the use of a fictitious linear viscous-perfectly-plastic material instead of original one. It gives the perfectly plastic condition when the fictitious Young's modulus tends towards infinity.

The strain rate tensor is decomposed into two parts: linear viscous components $\dot{\varepsilon}^v_{ij}$ and perfectly plastic ones $\dot{\varepsilon}^p_{ij}$.

$$\dot{\varepsilon}_{ij} = \bar{H}_{ijkl}\sigma_{kl} + \beta\dot{\lambda}\frac{\partial f}{\partial \sigma_{ij}} \tag{2.3a}$$

where $\bar{H}_{ijkl}$ is fictitious Hooke's tensor, and

$$\beta = 1 \text{ if } f = 0 \text{ and } \frac{\partial f}{\partial \sigma_{ij}}\dot{\sigma}_{ij} = 0 \tag{2.3b}$$

$$\beta = 0 \quad \begin{cases} \text{if } \ f < 0 \\ \text{if } \ f = 0 \ \text{ and } \ \dfrac{\partial f}{\partial \sigma_{ij}} \dot{\sigma}_{ij} < 0 \end{cases} \tag{2.3c}$$

$f = 0$ represents yield surface of the von Mises criterion.

For one-dimensional problem, the density of linear viscous–perfectly plastic dissipation may be represented as

$$D^{vp}(\boldsymbol{\varepsilon}) = \frac{1}{2}(\boldsymbol{\sigma}^* \dot{\boldsymbol{\varepsilon}} - \beta \boldsymbol{\sigma}^* \dot{\boldsymbol{\varepsilon}}^p) = \frac{\bar{E}}{2}\left[\dot{\boldsymbol{\varepsilon}}^2 - \beta(\dot{\boldsymbol{\varepsilon}}^p)^2\right] \tag{2.4a}$$

with

$$\beta = 0 \quad \text{if } \ |\boldsymbol{\sigma}| < \sigma_y \tag{2.4b}$$

$$\beta = 1 \quad \text{if } \ |\boldsymbol{\sigma}| = \sigma_y \tag{2.4c}$$

where $\bar{E}$ is the fictitious Young modulus representing a linear relation between stress and viscous strain rate. Introducing a dual yield limit in strain rate space,

$$\dot{\varepsilon}_y = \frac{\sigma_y}{\bar{E}} \tag{2.5}$$

(2.4a) can be transformed into

$$D^{vp} = \frac{\bar{E}}{2}\left[\dot{\boldsymbol{\varepsilon}}^2 - \beta(|\dot{\boldsymbol{\varepsilon}}| - \dot{\varepsilon}_y)^2\right] \tag{2.6a}$$

with

$$\beta = 0 \quad \text{if } \ |\dot{\boldsymbol{\varepsilon}}| < \dot{\varepsilon}_y \tag{2.6b}$$

$$\beta = 1 \quad \text{if } \ |\dot{\boldsymbol{\varepsilon}}| \geq \dot{\varepsilon}_y \tag{2.6c}$$

Considering a general multiaxial stress state, the density of the fictitious linearly viscous-perfectly plastic dissipation may be formulated in the following form:

$$D^{vp}(\dot{\varepsilon}_{ij}) = \frac{1}{2}(\dot{\varepsilon}_{ij} \bar{D}_{ijkl} \dot{\varepsilon}_{kl} - \beta \dot{\varepsilon}^p_{ij} \bar{D}_{ijkl} \dot{\varepsilon}^p_{kl}) \tag{2.7}$$

where $\bar{D}_{ijkl}$ is the inverse of the fictitious viscous Hooke tensor. The stress deviator σ^D_{ij} and strain rate deviator $\dot{e}_{ij}$ are defined as:

$$\sigma^D_{ij} = \sigma_{ij} - s_m \delta_{ij} \quad , \quad s_m = \frac{1}{3}\sigma_{ii}, \quad \dot{e}_{ij} = \dot{\varepsilon}_{ij} - \frac{1}{3}\dot{e}_m \delta_{ij} \quad , \quad \dot{e}_m = \dot{\varepsilon}_{ii}$$

where s_m is hydrostatic pressure and $\dot{e}_m$ volume strain rate. The decomposition of the strain rate deviator gives:

$$\dot{e}_{ij} = \dot{e}^v_{ij} + \dot{e}^p_{ij}, \quad \dot{e}_m = \dot{e}^v_m + \dot{e}^p_m. \tag{2.8}$$

Since the plastic deformation does not involve the change of volume one has

$$\dot{e}^p_m = 0, \quad \dot{e}_m = e^v_m = \frac{s_m}{\bar{k}} \tag{2.9}$$

$$\sigma^D_{ij} = 2\bar{G}\dot{e}^v_{ij}, \quad \dot{e}_{ij} = \frac{\sigma^D_{ij}}{2\bar{G}} + \dot{e}^p_{ij} \tag{2.10}$$

where $\bar{k}$ presents physically the fictitious volume modulus. Using (2.7) the density of viscous-plastic dissipation becomes

$$D^{vp} = \bar{G}(\dot{e}_{ij}\dot{e}_{ij} - \beta\dot{e}^p_{ij}\dot{e}^p_{ij}) + \frac{1}{2}\bar{k}\dot{e}^2_m \tag{2.11}$$

or

$$D^{vp} = \bar{G}\dot{e}^v_{ij}\dot{e}^v_{ij} + D^p + \frac{1}{2}\bar{k}\dot{e}^2_m. \tag{2.12}$$

Three terms in (2.12) represent viscous deviatoric, perfectly plastic and viscous volume strain dissipation, respectively. The von Mises criterion is written as the following function of the stress deviator:

$$f(\sigma^D_{ij}) = F(\sigma^D_{ij}) - 1 \leq 0 \tag{2.13a}$$

where

$$F(\sigma^D_{ij}) = \frac{1}{k_v}\sqrt{J_2(\sigma^D_{ij})}, \quad J_2(\sigma^D_{ij}) = \frac{1}{2}\sigma^D_{ij}\sigma^D_{ij} \tag{2.13b}$$

It is possible to write yield the criterion in terms of the strain deviator:

$$g(\dot{e}_{ij}) = G(\dot{e}_{ij}) - 1 \tag{2.14a}$$

with

$$G(\dot{\mathbf{e}}) = \frac{1}{\dot{e}_y}\sqrt{J_2(\dot{e}_{ij})}, \quad J_2(\dot{e}_{ij}) = \frac{1}{2}\dot{e}_{ij}\dot{e}_{ij} \tag{2.14b}$$

$$\text{and} \quad \dot{e}_y = \frac{k_v}{2\bar{G}} \tag{2.14c}$$

$\dot{e}_y$ is dual to plastic yield limit σ_y or k_v. Then we can define the internal dissipation density depending on the strain state at any point of the structure:

- If $\sqrt{J_2(\dot{e}_{ij})} < e_p$, it is in fictitious linearly-viscous state

$$D^{vp}(\dot{e}_{ij}) = 2\bar{G}J_2(\dot{e}_{ij}) + \frac{1}{2}\bar{k}\dot{e}^2_m. \tag{2.15}$$

- If $\sqrt{J_2(\dot{e}_{ij})} \geq e_p$, the plastic deformation occurs. By the normality law, one has:

$$\dot{e}^p_{ij} = \dot{\lambda}\frac{\partial f}{\partial \sigma^D_{ij}} = \dot{\lambda}\frac{\sigma^D_{ij}}{2k^2_v} \tag{2.16}$$

$$\sigma_{ij}^{D} = 2\bar{G}(\dot{e}_{ij} - \dot{e}_{ij}^{p}) = 2\bar{G}\dot{e}_{ij} - \bar{G}\frac{\dot{\lambda}\sigma_{ij}^{D}}{k_v^2} \tag{2.17}$$

$$\sigma_{ij}^{D} = \frac{2\bar{G}}{1 + \frac{\dot{\lambda}\bar{G}}{k_v^2}}\dot{e}_{ij} \tag{2.18}$$

Substituting (2.18) into (2.14a), we express the yielding state in term of total strain rate deviator:

$$f(\dot{e}_{ij}) = \frac{1}{k_v}\frac{2\bar{G}}{1 + \frac{\dot{\lambda}\bar{G}}{k_v^2}}\sqrt{J_2(\dot{e}_{ij})} - 1. \tag{2.19}$$

This gives the plastic intensity:

$$\dot{\lambda} = 2k_v\left[\sqrt{J_2(\dot{e}_{ij})} - \frac{k_v}{2\bar{G}}\right] \geq 0. \tag{2.20}$$

It is really equal to the plastic dissipation related to the incompressible plastic strain rate. In fact, according to the definition of plastic dissipation, we have (2.14a)

$$D^{p} = \sigma_{ij}\dot{\varepsilon}_{ij}^{p} = \dot{\lambda}\sigma_{ij}^{D}\frac{\partial F}{\partial \sigma_{ij}^{D}} = \dot{\lambda}F = \dot{\lambda}. \tag{2.21}$$

Therefore by adding the linear viscous and fictitious volume strain energy as (2.12), we may write the total internal dissipation density as follows:

$$D^{vp}(\dot{e}_{ij}, \dot{e}_m) = \dot{\lambda} + \frac{k_v^2}{2\bar{G}} + \frac{1}{2}\bar{k}\dot{e}_m^2 = 2k_v\left\{\sqrt{J_2(\dot{e}_{ij})} - \frac{k_v}{4\bar{G}}\right\} + \frac{1}{2}\bar{k}\dot{e}_m^2 \tag{2.22}$$

when $\bar{E} \to \infty$, $\bar{G} \to \infty$ but we assume $\bar{k}$ remain finite, (2.22) reaches the following limit:

$$\lim_{\bar{E},\bar{G}\to\infty} D^{vp}(\dot{e}_{ij}, \dot{e}_m) = 2k_v\sqrt{J_2(\dot{e}_{ij})} + \frac{1}{2}\bar{k}\dot{e}_m^2 \tag{2.23}$$

This procedure leads to the modified Markov functional in functional in Section 1.2 The total internal dissipation is established by assembling over all finite elements.

$$W_p = \sum_i w_i D^{vp}. \tag{2.24}$$

It is obvious that the gradient of the regularized objective function may always be obtained in both the plastic and the fictitious viscous regions.

2.3 Smooth regularization method

This simple method has been applied by many authors, for example [1]-[3], [8],[38]-[39] etc., also adopted in our work. It concerns using the hyperbolic approximation procedure: a small real positive number δ as a smoothing parameter is introduced in the dissipation function. It leads to a perturbed objective function:

$$D^p = \sqrt{\dot{\mathbf{q}}^T \mathbf{B}^T \mathbf{D} \mathbf{B} \dot{\mathbf{q}} + \delta} \tag{2.25}$$

It is differential everywhere for $\varepsilon \neq 0$ and remains convex. This method is simple and easy to be implemented. However, a suitable choice of ε is sometimes important to have real optimization solution of the original problem and have a good convergence, especially for a Newton type algorithm. Andersen [1] used a Newton barrier method to consider ε as a variable of the optimization procedure. As a simple strategy, we use a decreasing ε sequence depending on the reduction of limit multiplier α. Defining i as the current iteration, the following relation may be used:

$$\gamma = \frac{\alpha^i - \alpha^{i-1}}{\alpha^{i-1} - \alpha^{i-2}} \tag{2.26a}$$

$$\delta^i = \gamma^m \delta^{i-1} \text{ if } \gamma < 1 \tag{2.26b}$$

$$\delta^i = \delta^{i-1} \text{ if } \gamma > 1 \tag{2.26c}$$

where m is a calculating parameter. Generally we use: $1 \leq m \leq 2$. When using the direct iteration method (see section 3.1), the regularization is performed only in the rigid region.

3 Optimization algorithm of limit and incremental plasticity analyses

It is shown in section 1 that limit and shakedown load finding concerns a standard minimization with non-linear objective function and linear constraints. To solve this optimization problem, several methods are developed and applied in our work such that 1) a reduced-gradient algorithm (due to Wolfe, 1962) in conjunction with a quasi-Newton algorithm (due to Davidon, 1959); 2) direct iteration method (Newton-Raphson type algorithm) to transform the optimization into a series of linear-elastic-like calculations, 3) Newton-penalty method consisting of Newton's reducing direction and a linear research; 4) Dual optimization method considering the duality of static and kinematic formulation. The first method involves applying of a standard optimization code MINOS [23]; Methods

2-4 were developed specially for the present applications; All methods concern finding a reducing direction and performing an iterative calculation.

In this chapter, we discuss mainly method 2 (direct Newton-Raphson algorithm) and method 3 (Newton-penalty algorithm). These two methods may be conveniently used limit or incremental shakedown (ratchetting) analyses. As shown in section 1.5.1 the latter has been transformed into an equivalent limit analysis. Method 4 (dual algorithm) will be presented in section 5. More details were given in [16], [37].

3.1 Newton-Raphson iteration method

3.1.1 Upper bound estimation

Starting from (1.19a), we transform it into a non-constraint optimization problem by using Lagrange multiplier λ

$$L = \sum_{i}^{NG} w_i \left(\sqrt{\dot{\mathbf{q}}^T \mathbf{B}^T \mathbf{D} \mathbf{B} \dot{\mathbf{q}}} + \frac{1}{2} \bar{k} \dot{\mathbf{q}}^T \mathbf{B}^T \mathbf{D}_v \mathbf{B} \dot{\mathbf{q}} \right) - \mathbf{g}_0^T \dot{\mathbf{q}} - \lambda (\mathbf{g}^T \dot{\mathbf{q}} - 1) \tag{3.1}$$

Its optimization condition is

$$\sum_{i} w_i \left(\frac{\mathbf{B}^T \mathbf{D} \mathbf{B} \dot{\mathbf{q}}}{\sqrt{\dot{\mathbf{q}}^T \mathbf{B}^T \mathbf{D} \mathbf{B} \dot{\mathbf{q}}}} + \bar{k} \mathbf{B}^T \mathbf{D}_v \mathbf{B} \dot{\mathbf{q}} \right) = \lambda \mathbf{g} + \mathbf{g}_0 \tag{3.2}$$

$$\mathbf{g}^T \dot{\mathbf{q}} = 1 \tag{3.3}$$

Where the regularization described in section 2 should be applied to avoid the singularity in rigid region of the structure. Since the functional (3.1) is quadratic, we, according to the suggestion of Yang [38] and Zhang *et al* [39], use the standard finite element iterative method to change (3.2) into the following iteration (from n to$n+1$):

$$\left(\sum_{i} w_i \frac{\mathbf{B}^T \mathbf{D} \mathbf{B}}{\sqrt{\dot{\mathbf{q}}_n^T \mathbf{B}^T \mathbf{D} \mathbf{B} \dot{\mathbf{q}}_n}} + w_i \bar{k} \mathbf{B}^T \mathbf{D}_v \mathbf{B} \right) \dot{\mathbf{q}}_{n+1} = \lambda_{n+1} \mathbf{g} + \mathbf{g}_0 \tag{3.4}$$

It may be written in a simple form

$$\mathbf{K}_n \dot{\mathbf{q}}_{n+1} = \lambda_{n+1} \mathbf{g} + \mathbf{g}_0 \tag{3.5}$$

This is a classical linear system where $\mathbf{K}_n = \mathbf{K}_n(\dot{\mathbf{q}}_n)$ is supposed constant for current $n+1$ iteration. To resolve (3.5), we decompose the nodal velocity solution into two parts:

$$\dot{\mathbf{q}}_{n+1} = \lambda_{n+1} \dot{\mathbf{q}}_I + \dot{\mathbf{q}}_{II} \tag{3.6}$$

with

$$\dot{\mathbf{q}}_I = \mathbf{K}_n^{-1}\mathbf{g} \tag{3.7}$$

$$\dot{\mathbf{q}}_{II} = \mathbf{K}_n^{-1}\mathbf{g}_0 \tag{3.8}$$

By normalization condition (3.3): $\mathbf{g}^T\dot{\mathbf{q}}_{n+1} = 1$, we can determine the current Lagrange multiplier as:

$$\lambda_{n+1} = \frac{1}{\mathbf{g}^T\dot{\mathbf{q}}_I}\left(1 - \mathbf{g}^T\dot{\mathbf{q}}_{II}\right). \tag{3.9}$$

So an upper bound estimation of limit load multiplier is

$$\alpha_{n+1}^{+} = \sum_i w_i\sqrt{\dot{\mathbf{q}}_{n+1}^T\mathbf{B}^T\mathbf{D}\mathbf{B}\dot{\mathbf{q}}_{n+1}} - \mathbf{g}_0^T\dot{\mathbf{q}}_{n+1} \tag{3.10}$$

Then we update the matrix $\mathbf{K}_n$ with the new velocity solution to carry out next step calculation. Such an iterative process described as above produces a sequence of load multiplier $\{\alpha_n^+\}$, a sequence of Lagrangian multiplier $\{\lambda_n\}$ and a sequence of nodal velocity arrays $\left\{\dot{\mathbf{q}}_{n+1}\right\}$. It can be proved that all of these sequences converge to their limit. In fact, by the convexity of objective function (1.19a), the optimization solution of (3.1) or (3.2) exists and the minimization of limit load multipliers is unique, i.e.

$$\lim_{n\to\infty}\alpha_n^+ = \alpha^+ \geq \alpha_L \tag{3.11}$$

and

$$\lim_{n\to\infty}\dot{\mathbf{q}}_n = \dot{\mathbf{q}} \tag{3.12}$$

Moreover in order to prove the convergence of $\{\lambda_n\}$, we do a point multiplication by $\dot{\mathbf{q}}_{n+1}$ for the two sides of (3.4). By normalization condition (3.3), we have:

$$\lambda_{n+1} = \sum_i\left(w_i\frac{\dot{\mathbf{q}}_{n+1}^T\mathbf{B}^T\mathbf{D}\mathbf{B}\dot{\mathbf{q}}_{n+1}}{\sqrt{\dot{\mathbf{q}}_n^T\mathbf{B}^T\mathbf{D}\mathbf{B}\dot{\mathbf{q}}_n}} + w_i\bar{k}\dot{\mathbf{q}}_{n+1}^T\mathbf{B}^T\mathbf{D}_v\mathbf{B}\dot{\mathbf{q}}_{n+1}\right) - \mathbf{g}_0^T\dot{\mathbf{q}}_{n+1} \tag{3.13}$$

Now we need to prove that the second term is small enough to be ignored in comparison with the other terms. Let us consider the following minimization concerning the volume strain rate:

$$\min_{\dot{q}}\sum_i w_i\dot{\mathbf{q}}^T\mathbf{B}^T\mathbf{D}_v\mathbf{B}\dot{\mathbf{q}} \tag{3.14a}$$

$$\text{s.t.}\quad \mathbf{g}^T\dot{\mathbf{q}} = 1 \tag{3.14b}$$

By taking the same procedure as above, this problem can be transformed into a linear system:

$$\sum_i w_i\mathbf{B}^T\mathbf{D}_v\mathbf{B}\dot{\mathbf{q}} = \bar{\lambda}\mathbf{g} \tag{3.15a}$$

or

$$\mathbf{K}_v\dot{\mathbf{q}} = \bar{\lambda}\mathbf{g} \tag{3.15b}$$

Since matrix $\mathbf{D}_v^{-1}$ is singular so $\mathbf{K}_v^{-1}$ is also. To overcome this difficulty, we add a small projection:

$$(\mathbf{K}_v + \mathbf{K}/\bar{k})\dot{\mathbf{q}} = \bar{\lambda}\mathbf{g} \tag{3.16}$$

where $\bar{k}$ is large penalty function coefficient. From the property of problem (3.14a), the solution of (3.16) is approximately incompressible. Moreover by the similarity between (3.16) and (3.4), we know that the solution of (3.4) in every iterative calculation is also approximately incompressible. That is, we have $\dot{\varepsilon}_{ii} \approx 0$ at every iteration step. On the other hand we can prove that the second term in (3.4) represents approximately a hyperstatic pressure:

$$\bar{k}\dot{\varepsilon}_{ii} = \bar{k}\mathbf{B}^T\mathbf{D}_v\mathbf{B}\dot{\mathbf{q}}_{n+1} \approx \frac{1}{3}\sigma_{ii} \tag{3.17}$$

So we have

$$\bar{k}\dot{\varepsilon}_{ii}^2 = \bar{k}\dot{\mathbf{q}}_{n+1}^T\mathbf{B}^T\mathbf{D}_v\mathbf{B}\dot{\mathbf{q}}_{n+1} \approx 0 \tag{3.18}$$

By neglecting the second term in (3.13) and considering (3.12) and comparing with (3.10), we have

$$\lim_{n\to\infty}\lambda_n = \lambda = \alpha^+. \tag{3.19}$$

Our calculating practice shows that at least in the case without dead load P_0, λ_n is also an upper bound of the limit load multiplier and it has a convergence a little better than α_n^+.

3.1.2 Lower bound estimation

The method was proposed by Zhang and Lu [39] for shell-type structures where the incompressibility condition can be satisfied by usual finite element discretization. We have extended this method for a general case as follows. According to the lower bound theorem of Hill, a lower bound estimation of the limit load can be found by any static stress field that does not violate anywhere the plastic admissible condition (yield criterion). Now we examine (3.4) that represents in fact a static equilibrium between internal stress term and external load because we can rewrite (3.4) into the following form:

$$\sum_i w_i\mathbf{B}^T\boldsymbol{\sigma}_{n+1} = \lambda_{n+1}\mathbf{g} + \mathbf{g}_0 \tag{3.20}$$

$$\boldsymbol{\sigma}_{n+1} = \mathbf{s}_{n+1} + \mathbf{s}_{m,n+1} \tag{3.21}$$

where $\mathbf{s}_{n+1}, \mathbf{s}_{m,n+1}$ are the equivalent stress deviator and hyperstatic pressure at $n+1$ iteration defined by (3.4), respectively. For the convenience of calculation, we write the following equilibrium relations

$$\sum_{i=1}^{NG} w_i\mathbf{B}^T(\mathbf{s}_I + \mathbf{s}_{mI}) = \mathbf{g} \tag{3.22}$$

$$\sum_{i=1}^{NG} w_i \mathbf{B}^T(\mathbf{s}_{II} + \mathbf{s}_{mII}) = \mathbf{g}_0 \tag{3.23}$$

where

$$\mathbf{s}_I = \frac{\mathbf{DB}\dot{\mathbf{q}}_I}{\sqrt{\dot{\mathbf{q}}_n^T \mathbf{B}^T \mathbf{DB}\dot{\mathbf{q}}_n}}, \qquad \mathbf{s}_{II} = \frac{\mathbf{DB}\dot{\mathbf{q}}_{II}}{\sqrt{\dot{\mathbf{q}}_n^T \mathbf{B}^T \mathbf{DB}\dot{\mathbf{q}}_n}}, \tag{3.24}$$

$$\mathbf{s}_{mI} = \bar{k}\mathbf{D}_v \mathbf{B}\dot{\mathbf{q}}_I, \quad \mathbf{s}_{mII} = \bar{k}\mathbf{D}_v \mathbf{B}\dot{\mathbf{q}}_{II} \tag{3.25}$$

They correspond to solutions (3.6-3.8). It is well known that the hyperstatic pressure does not contribute the plasticity criterion, it is not necessary to calculate (3.25) for the present lower bound estimation. According to the static theorem, we have a lower bound at every iteration step:

$$\alpha_{n+1}^- = \lim_{i \in NG} \alpha_{i,n+1}^- \tag{3.26}$$

$$\text{s.t.} \quad f(\alpha_{i,n+1}^- \mathbf{s}_I + \mathbf{s}_{II}) \leq 0 \tag{3.27}$$

where f represents the von Mises criterion which can be written as $\mathbf{s}^T\mathbf{D}^{-1}\mathbf{s} - 1 = 0$. So for the present application we have

$$(\alpha_{i,n+1}^- \dot{\mathbf{q}}_I + \dot{\mathbf{q}}_{II})^T (\mathbf{B}^T\mathbf{DB})_i (\alpha_{i,n+1}^- \dot{\mathbf{q}}_I + \dot{\mathbf{q}}_{II}) = h_{i,n} \tag{3.28}$$

Defining:

$$h_{i,n} = \dot{\mathbf{q}}_n^T (\mathbf{B}^T\mathbf{DB})_i \dot{\mathbf{q}}_n \tag{3.29}$$

$$x = \dot{\mathbf{q}}_I^T (\mathbf{B}^T\mathbf{DB})_i \dot{\mathbf{q}}_I \tag{3.30}$$

$$y = \dot{\mathbf{q}}_I^T (\mathbf{B}^T\mathbf{DB})_i \dot{\mathbf{q}}_{II} \tag{3.31}$$

$$z = \dot{\mathbf{q}}_{II}^T (\mathbf{B}^T\mathbf{DB})_i \dot{\mathbf{q}}_{II} \tag{3.32}$$

The solution of (3.28) at any integral point is

$$\alpha_{i,n+1}^- = \frac{\sqrt{y^2 + x(h_{i,n} - z)} - y}{x} \tag{3.33}$$

The lower bound of the structure is found by using (3.26). This procedure produces a sequence of load multiplier $\{\alpha_n^-\}$. Since we generally check the yield criterion only at integration points so the obtained solution is only a quasi lower bound. Now we prove the convergence of $\{\alpha_n^-\}$. Considering at iteration step $n+1$, from (3.6) and (3.29)-(3.32), one has

$$h_{i,n+1} = \dot{\mathbf{q}}_{n+1}^T (\mathbf{B}^T\mathbf{DB}) \dot{\mathbf{q}}_{n+1} = \lambda_{n+1}^2 x + 2\lambda_{n+1} y + z \tag{3.34}$$

Solving this equation, one gets

$$\lambda_{i,n+1} = \frac{\sqrt{y^2 + x(h_{i,n+1} - z)} - y}{x} \tag{3.35}$$

Since the velocity field converges according to (3.12), one has

$$\lim_{n\to\infty}(\lambda_{i,n}-\lambda_{i,n+1})=0 \tag{3.36}$$

Eqs. (3.19), (3.33) and (3.35)-(3.36) lead to

$$\lim_{n\to\infty}\alpha_n^+=\lim_{n\to\infty}\lambda_n=\lim_{n\to\infty}\alpha_n^-=\alpha_L. \tag{3.37}$$

This shows that upper bound and lower bounds, as well as the Lagrange multiplier have identical limiting value. Therefore, the obtained solutions in limit are all theoretically exact. Note that the above lower bound analysis needs to be carried out only in the plastic region of the structure. If we examine the plastic admissible condition passing over all possible dangerous points of the structure (for example on the surface, corners and other stress singular points), the calculating error of the lower bound can be reduced.

3.2 Newton-penalty method

3.2.1 Newton's decent direction

It is well known that when the gradient and Hessian matrix of the objective function can be given, Newton's optimization procedure can be used to lead to generally a rapid convergence rate. For this sake, we use the penalty method to transform the constrained problem (1.19a) into an unconstrained one:

$$\min_{\dot{q}} W(\dot{\mathbf{q}}) \tag{3.38a}$$

with

$$W(\dot{\mathbf{q}})=\sum_i^{NG} w_i\left(\sqrt{\dot{\mathbf{q}}^T\mathbf{B}^T\mathbf{D}\mathbf{B}\dot{\mathbf{q}}}+\frac{\bar{k}}{2}\dot{\mathbf{q}}\mathbf{B}^T\mathbf{D}_v\mathbf{B}\dot{\mathbf{q}}\right)+\frac{\bar{\mu}}{2}(\mathbf{g}^T\dot{\mathbf{q}}-1)^2-\mathbf{g}_0^T\dot{\mathbf{q}} \tag{3.38b}$$

where $\bar{k},\bar{\mu}$ are penalty parameters. The Newton method consists of the iteration

$$\dot{\mathbf{q}}_{n+1}=\dot{\mathbf{q}}_n+\Phi_n\mathbf{d}_n \tag{3.39}$$

where Φ_n is iteration step size that will be discussed later; $\mathbf{d}_n$ is the Newton's decent direction for $n+1$ iteration:

$$\mathbf{d}_n=-\mathbf{H}_n^{-1}\mathbf{G}_n \tag{3.40}$$

with gradient vector $\mathbf{G}_n$

$$\mathbf{G}_n=\sum_i w_i\left(\frac{\mathbf{B}^T\mathbf{D}\mathbf{B}\dot{\mathbf{q}}_n}{\sqrt{\dot{\mathbf{q}}_n^T\mathbf{B}^T\mathbf{D}\mathbf{B}\dot{\mathbf{q}}_n}}+\bar{k}\mathbf{B}^T\mathbf{D}_v\mathbf{B}\dot{\mathbf{q}}_n\right)+\bar{\mu}\mathbf{g}(\mathbf{g}^T\dot{\mathbf{q}}_n-1)-\mathbf{g}_0 \tag{3.41}$$

with Hessian matrix $\mathbf{H}_n$

$$\mathbf{H}_n = \sum_i w_i \left(\frac{\mathbf{B}^T\mathbf{D}\mathbf{B}}{\sqrt{\dot{\mathbf{q}}_n^T\mathbf{B}^T\mathbf{D}\mathbf{B}\dot{\mathbf{q}}_n}} - \frac{\dot{\mathbf{q}}_n^T\mathbf{B}^T\mathbf{D}\mathbf{B}\dot{\mathbf{q}}_n}{\sqrt{\left(\dot{\mathbf{q}}_n^T\mathbf{B}^T\mathbf{D}\mathbf{B}\dot{\mathbf{q}}_n\right)^3}} + \bar{k}\mathbf{B}^T\mathbf{D}_v\mathbf{B} \right) + \bar{\mu}\mathbf{g}^T\mathbf{g} \tag{3.42}$$

Using the definition of $\mathbf{K}_n$ by (3.5), the gradient vector and Hessian matrix of W can be written as

$$\mathbf{G}_n = \mathbf{K}_n\dot{\mathbf{q}}_n + \mu\mathbf{g} - \mathbf{g}_0 \tag{3.43}$$

$$\mathbf{H}_n = \bar{\mathbf{K}}_n + \bar{\mu}\mathbf{g}^T\mathbf{g} \tag{3.44}$$

with

$$\mu = \bar{\mu}(\mathbf{g}^T\dot{\mathbf{q}}_n - 1) \tag{3.45}$$

$$\bar{\mathbf{K}}_n = \mathbf{K}_n + \mathbf{K}'_n \tag{3.46}$$

$$\mathbf{K}'_n = -\sum_i W_i \frac{\dot{\mathbf{q}}_n^T\mathbf{B}^T\mathbf{D}\mathbf{B}\dot{\mathbf{q}}_n}{\sqrt{\left(\dot{\mathbf{q}}_n^T\mathbf{B}^T\mathbf{D}\mathbf{B}\dot{\mathbf{q}}_n\right)^3}} \tag{3.47}$$

As in direct iteration method, the gradient and Hessian exist only when the objective function at the Gauss point is strictly positive, this means that plastic flow occurs at this point. So the smooth regularization method presented in section 2.2 is used to overcome this obstacle. From the point of view of numeric calculation, the calculation involving in (3.40) is also similar as a linear elastic calculation. However, a difficulty is encountered: although the $\bar{\mathbf{K}}_n$, as $\mathbf{K}_n$, has same form as elastic stiffening matrix, Hessian matrix $\mathbf{H}_n$ does not, due to the last term in (3.44). In some loading cases, $\mathbf{H}_n$ may be a almost-full symmetric matrix. The solving the inverse of $\mathbf{H}_n$ in a usual way may lead to high calculating cost. To overcome this difficulty, we apply a Sherman-Morrison-Woodbury formula [4] to transform (3.40) into

$$\mathbf{d}_n = -\bar{\mathbf{K}}_n^{-1}\mathbf{G}_n + \frac{\bar{\mathbf{K}}_n^{-1}\mathbf{g}(\bar{\mathbf{K}}_n^{-1}\mathbf{g})^T}{1 + \bar{\mu}\mathbf{g}^T\bar{\mathbf{K}}_n^{-1}\mathbf{g}} \tag{3.48}$$

So only one inverse of matrix $\bar{\mathbf{K}}_n$ and some simple additional calculations (such that $\bar{\mathbf{K}}_n^{-1}\mathbf{g}$ and $\bar{\mathbf{K}}_n^{-1}\mathbf{G}$ are needed. This is still approximately equivalent to a linear-elastic-like analysis. Specially when Hessian matrix $\mathbf{H}_n$ or $\bar{\mathbf{K}}_n$ appears singular, we may simply replace the Newton's decent direction $\mathbf{d}_n$ by Cauchy's one for this iteration, that is to take $\mathbf{d}_n = -\mathbf{G}_n$.

When the iteration step-size Φ_n is taken as 1 (this generally happens when the optimal point will be found in this iteration). The method is referred to as the pure form of Newton's method. This means that the objective function near optimal point may be approximated well by a quadratic function. However, this is not a general case. It should be pointed out that the present objective function is strongly non-linear and has complex form (see after the discussion in line search method). So we need to take a line search to increase the calculating efficiency.

3.2.2 Line search

The line search plays a important role in reducing the computation time. A line search procedure should be suitable to the special characteristics of the function to be minimized, and if possible an exact line search procedure should be carried out. For the present problem, the line search takes the following form of:

$$\min_{s\geq 0} f\left(\dot{\mathbf{q}}_{n+1} = \dot{\mathbf{q}}_n + \Phi \mathbf{d}_n\right) \tag{3.49}$$

with

$$\begin{aligned} f &= \sum_i w_i \left[\sqrt{(\dot{\mathbf{q}}_n + \Phi\mathbf{d}_n)^T \mathbf{B}^T \mathbf{D}\mathbf{B}(\dot{\mathbf{q}}_n + \Phi\mathbf{d}_n) + \delta}\right. \\ &+ \left.\frac{\bar{k}}{2}(\dot{\mathbf{q}}_n + \Phi\mathbf{d}_n)^T \mathbf{B}^T \mathbf{D}_v \mathbf{B}(\dot{\mathbf{q}}_n + \Phi\mathbf{d}_n)\right] \\ &+ \frac{\bar{\mu}}{2}\left(\mathbf{g}^T(\dot{\mathbf{q}}_n + \Phi\mathbf{d}_n) - 1\right)^2 - \mathbf{g}_0^T(\dot{\mathbf{q}}_n + \Phi\mathbf{d}_n). \end{aligned} \tag{3.50}$$

where a small positive real value δ is used to avoid the singularity, see section 2.2. Fig. 3.1 gives an example of line search function f. Since the first and second derivatives of the regularized function can be found, an ordinal Newton's method may be used in this one-dimensional problem. However, if considering the special property of the function, we could find a more effective way. Particularly for the present problem, we find that the following function may be used to well approximate the original function, especially when the dead load is absent.

$$\varphi = \sqrt{a\phi^2 + b\phi + c} \tag{3.51}$$

where a, b, c are constant coefficients to be determined. This is different from Newton's method that uses a quadratic one. However, it has the same optimal point and similar property as Newton's method when the current solution is near to the optimal point. Now we derive the iterative formula of Φ. Starting from k-th iteration with current solution Φ_k, the first and second derivatives of function (3.51) are as follows:

$$\varphi' = \frac{2a\Phi_k + b}{2\sqrt{a\Phi_k^2 + b\Phi_k^2 + c}} \tag{3.52}$$

$$\varphi'' = \frac{a}{\sqrt{a\Phi_k^2 + b\Phi_k^2 + c}} - \frac{(2a\Phi_k + b)^2}{4\sqrt{(a\Phi_k^2 + b\phi_k^2 + c)^3}} \tag{3.53}$$

Suppose that the original function (3.50), and its first and second derivatives have current values as f_k, g_k, h_k. By defining $\dot{\mathbf{q}}_k = \dot{\mathbf{q}}_n + \Phi_k \mathbf{d}_n$, we have

$$f_k = \sum_i w_i \left[\sqrt{\dot{\mathbf{q}}_k^T(\mathbf{B}^T\mathbf{D}\mathbf{B})\dot{\mathbf{q}}_k + \delta} + \frac{\bar{k}}{2}\dot{\mathbf{q}}_k^T(\mathbf{B}^T\mathbf{D}_v\mathbf{B})\dot{\mathbf{q}}_k\right] + \frac{\bar{\mu}}{2}\left(\mathbf{g}^T\dot{\mathbf{q}}_k - 1\right)^2 - \mathbf{g}_0^T\dot{\mathbf{q}}_k \tag{3.54}$$

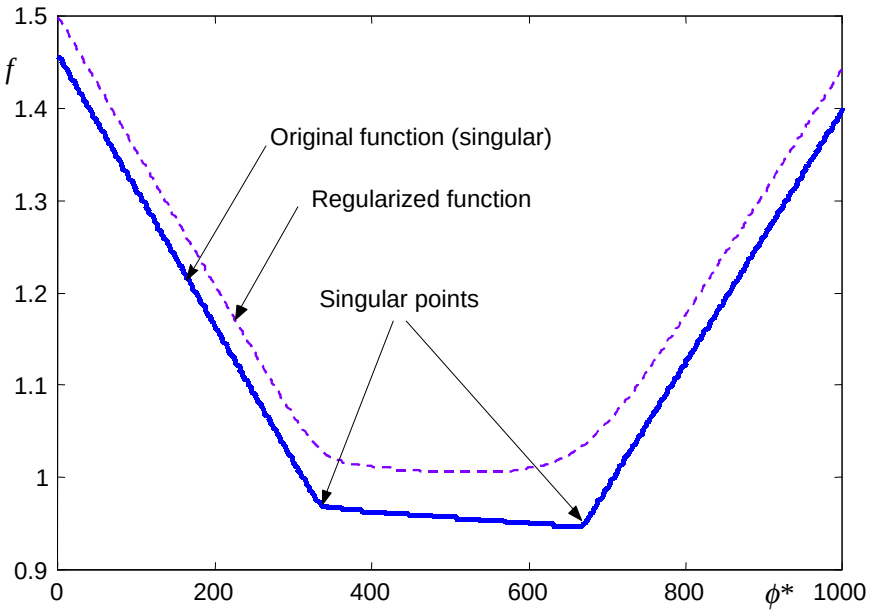

Figure 3.1: The original function with $\delta = 0$ and the regularized function with $\delta \neq 0$

$$g_k = \sum_i w_i \left[\frac{\dot{\mathbf{q}}_k^T (\mathbf{B}^T \mathbf{D} \mathbf{B}) \mathbf{d}_n}{\sqrt{\dot{\mathbf{q}}_k^T (\mathbf{B}^T \mathbf{D} \mathbf{B}) \dot{\mathbf{q}}_k + \delta}} + \bar{k} \dot{\mathbf{q}}_k^T (\mathbf{B}^T \mathbf{D}_v \mathbf{B}) \mathbf{d}_n \right] + \bar{\mu} (\mathbf{g}^T \dot{\mathbf{q}}_k - 1) \mathbf{g}^T \mathbf{d}_n - \mathbf{g}_0^T \mathbf{d}_n \tag{3.55}$$

$$\begin{aligned} h_k &= \sum_i w_i \left[\frac{\mathbf{d}_n^T (\mathbf{B}^T \mathbf{D} \mathbf{B}) \mathbf{d}_n}{\sqrt{\dot{\mathbf{q}}_k^T (\mathbf{B}^T \mathbf{D} \mathbf{B}) \dot{\mathbf{q}}_k + \delta}} - \frac{\left(\dot{\mathbf{q}}_k^T (\mathbf{B}^T \mathbf{D} \mathbf{B}) \mathbf{d}_n \right)^2}{\sqrt{\left(\dot{\mathbf{q}}_k^T (\mathbf{B}^T \mathbf{D} \mathbf{B}) \dot{\mathbf{q}}_k + \delta \right)^3}} + \bar{k} \mathbf{d}_n^T \mathbf{B}^T \mathbf{D}_v \mathbf{B}) \mathbf{d}_n \right] \\ &+ \bar{\mu} (\mathbf{g}^T \mathbf{d}_n)^2 \end{aligned} \tag{3.56}$$

The equality between replacing function (f_k, g_k, h_k) and original function (3.54)-(3.56) leads to:

$$a = f_k h_k + g_k^2 \tag{3.57}$$

$$b = 2 f_k g_k - 2 a \Phi_k \tag{3.58}$$

The optimal point of the replacing function is determined by the condition $\varphi' \big|_{\Phi_{k+1} = \Phi_k + \Delta\Phi_k} = 0$, we obtain:

$$\Phi_{k+1} = \Phi_k - \frac{f_k g_k}{f_k h_k + g_k^2} \tag{3.59}$$

This is the deduced iterative formula of step-size. Specially, when the current point is very closing to the optimal point, $g_k \to 0$, so g_k^2 may be neglected in comparison with term $f_k h_k$, (3.59) becomes:

$$\Phi_{k+1} = \Phi_k - \frac{g_k}{h_k}. \tag{3.60}$$

Therefore, we recover the original Newton's iterative formula in the neighbourhood of the optimal point. It is shown by numerical tests that (3.59) leads to generally a better convergence than (3.60) for the present problem.

However, we sometimes encounter another difficulty: the function to be minimized behaves nearly piece-wise linearity (cf. Fig. 3.1), which sometimes could not be well simulated even by the proposed the replacing function (3.51). Fig 3.2 shows a numerical example to illustrate this situation. Starting from point A2 that is closer to the optimal point P than another point A1, however, its iterative solution P2 is less better than P1 from A1. That means that sometimes there may not be a converge solution. In order to avoid this situation, we use an alternative method to speed the convergence. Seeing Fig 3.3, starting from the k iteration $A_k\Phi_k, f_k, g_k)$, we obtain the $k+1$ solution $A_{k+1}(\Phi_{k+1}, f_{k+1}, g_{k+1})$ by (3.59). If a gradient condition defined by $g_k g_{k+1} < 0$ is satisfied, we perform a linear intersection as (3.61) to obtain point P'1 $(\Phi'_{k+1}, f'_{k+1}, g'_{k+1})$ that is better than A_k and A_{k+1}.

$$\Phi'_{k+1} = \frac{f_{k+1} - f_k + \Phi_k g_k - \Phi_{k+1} g_{k+1}}{g_k - g_{k+1}} \tag{3.61}$$

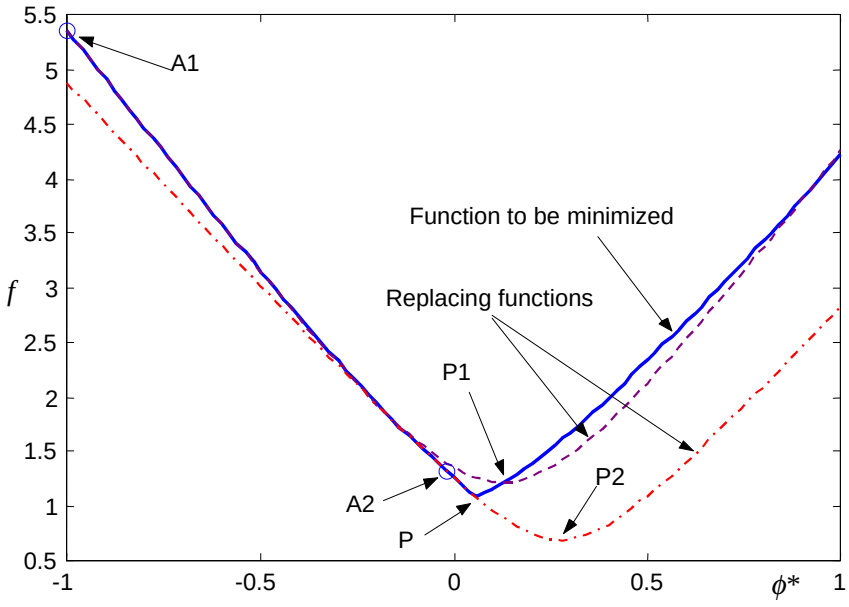

Figure 3.2: Approximation by the replacing functions

Therefore, after each iteration, we could guarantee to obtain an improved solution. Generally only one such linear intersection is enough because an additional liner intersection to get P'2 may not be better than P'1. The calculating practice shows that with this complementary line-intersection, the line search becomes more effective. On the other hand, line search speeds the optimization procedure. The calculation in line search represents less than 10% of total calculation. So approximately, a global iteration is equivalent to about 1.1 times a linear-elastic like calculation.

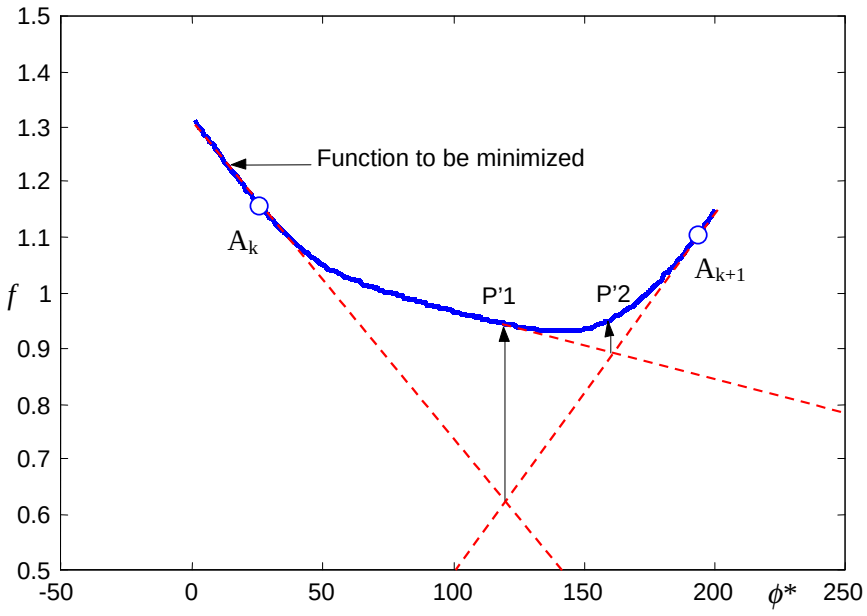

Figure 3.3: Linear intersection in line search

3.3 Direct iteration and Newton method

In Sections 3.1 and 3.2 above, we give a complete description of two optimization methods developed specially for the present kinematical limit and shakedown analysis. Although two methods are independently developed, we hope to find their essential relation in order to understand well the convergence property of solutions. For this sake, we use a Lagrange's function as (3.1) used for the direct iteration method instead of the penalty form (3.14a). In this case, by using the previous definition (3.5), (3.23), we have the first and second derivatives of the function

$$\mathbf{G}_n = \mathbf{K}_n \dot{\mathbf{q}}_n - \lambda \mathbf{g} - \mathbf{g}_0 \tag{3.62}$$

$$\mathbf{H}_n = \mathbf{K}_n + \mathbf{K}'_n \tag{3.63}$$

By neglecting $\mathbf{K}'_n$ (since it is less important than $\mathbf{K}_n$) and taking a constant step size $\Phi \equiv 1$, we have the following classical Newton's iteration formula:

$$\dot{\mathbf{q}}_{n+1} = \dot{\mathbf{q}}_n + \mathbf{d}_n \tag{3.64}$$

where

$$\mathbf{d}_n = \mathbf{K}_n^{-1}\mathbf{G}_n = -\dot{\mathbf{q}}_n + \mathbf{K}_n^{-1}(\lambda \mathbf{g} + \mathbf{g}_0) \tag{3.65}$$

Substituting (3.65) into (3.64), we get:

$$\dot{\mathbf{q}}_{n+1} = \mathbf{K}_n^{-1}(\lambda \mathbf{g} + \mathbf{g}_0) \tag{3.66}$$

where Lagrange multiplier $\lambda = \lambda_{n+1}$, determined by condition (3.3), so equation (3.66) is just the iterative formula of the direct iteration method. Therefore, we have demonstrated that the direct iteration method may be explained as a simplified and modified form of Newton-penalty method in two ways 1) a simplified Newton decent direction and a constant step-size are adopted; 2) Lagrange method, instead of the penalty method, is used and Lagrange multiplier λ is accurately determined by the normalization condition at each iteration. Generally speaking, the Newton-penalty method leads to faster converge solution while the direct iteration method is simpler and also a good converge rate (although it is a little slower than the Newton-penalty method). Specially, the direct iteration method may provide at every iteration, besides a upper bound, a lower estimation of the limit load, which is very interesting and sometimes important. In comparison with Newton's penalty method, the direct iteration method is numerically more stable.

4 A kinematic shakedown algorithm

Specially for the united shakedown limit method (USL), we develop a numerical technique, already proposed by Zhang [40] for shell type problems and recently by Carvelli et al. [7] for general structures. We in this chapter give an independent demonstration. A lower bound shakedown limit is also formulated as a by-product of upper bound analysis.

4.1 Optimization condition of shakedown

Considering the modified Koiter's theorem that the kinematic condition is satisfied after a loading cycle (representing here by the vertices of loading domain), we can rewrite (1.34) into the following form by taking the strain rate at each loading vertex as the principal variables.

$$\alpha_{SD} = \min \sum_{i=1}^{NG} \sum_{k=1}^{NV} w_i \left(\frac{2\sigma_y^{ki}}{\sqrt{3}} \sqrt{\dot{\mathbf{e}}_{ki}^T \bar{\mathbf{D}} \dot{\mathbf{e}}_{ki}} + \frac{\bar{k}}{2} \dot{\mathbf{e}}_{ki}^T \mathbf{D}_v \dot{\mathbf{e}}_{ki} - \dot{\mathbf{e}}_{ki}^T \boldsymbol{\sigma}_0^E \right) \tag{4.1a}$$

$$\text{s.t.} \quad \sum_{k=1}^{NV} \dot{\mathbf{e}}_{ki} = \mathbf{B}_i \dot{\mathbf{q}} \qquad \forall i = 1, NG \tag{4.1b}$$

$$\sum_{i=1}^{NG} \sum_{k=1}^{NV} w_i \dot{\mathbf{e}}_{ki}^T \boldsymbol{\sigma}_{ki}^E = 1 \tag{4.1c}$$

where $\dot{\mathbf{e}}_{ki}$ is the strain rate vector at the ith Gauss point, related to the kth loading vertex. $\dot{\mathbf{q}}$ is the nodal velocity vector after a cycle of loading. $\boldsymbol{\sigma}_0^E, \boldsymbol{\sigma}_{ki}^E$ are the linear elastic stress vectors at ith Gauss point due to, respectively, the dead load and the kth loading vertex.

Using Lagrange multiplier λ and $\boldsymbol{\rho}_i, i = 1, \ldots NG$, the non-constrained Lagrange function is written as

$$\begin{aligned} L(\dot{\mathbf{e}}_{ki}, \dot{\mathbf{q}}, \lambda, \boldsymbol{\rho}_i) &= \sum_{i=1}^{NG}\sum_{k=1}^{NV} w_i \left(\frac{2\sigma_y^{ki}}{\sqrt{3}} \sqrt{\dot{\mathbf{e}}_{ki}^T \bar{\mathbf{D}} \dot{\mathbf{e}}_{ki}} + \frac{\bar{k}}{2} \dot{\mathbf{e}}_{ki}^T \mathbf{D}_v \dot{\mathbf{e}}_{ki} - \dot{\mathbf{e}}_{ki}^T \boldsymbol{\sigma}_0^E \right) \\ &- \lambda \left(\sum_{i=1}^{NG}\sum_{k=1}^{NV} w_i \dot{\mathbf{e}}_{ki}^T \boldsymbol{\sigma}_{ki}^E - 1 \right) - \sum_{i=1}^{NG} w_i \boldsymbol{\rho}_i^T \left(\sum_{k=1}^{NV} \dot{\mathbf{e}}_{ki} - \mathbf{B}_i \dot{\mathbf{q}} \right) \end{aligned} \quad (4.2)$$

where $\boldsymbol{\rho}_i$ is, in physical, the Gauss-point related residual stress vector. The KKT conditions for (4.2) are written as follows:

(with respect to $\dot{\mathbf{e}}_{ki}$)

$$\sum_{i=1}^{NG}\sum_{k=1}^{NV} w_i \left(\frac{2\sigma_y^{ki}}{\sqrt{3}} \frac{\bar{\mathbf{D}}\dot{\mathbf{e}}_{ki}}{\sqrt{\dot{\mathbf{e}}_{ki}^T \bar{\mathbf{D}} \dot{\mathbf{e}}_{ki}}} + \bar{k}\mathbf{D}_v \dot{\mathbf{e}}_{ki} - \boldsymbol{\sigma}_0^E \right) - \lambda \sum_{i=1}^{NG}\sum_{k=1}^{NV} w_i \boldsymbol{\sigma}_{ki}^E - NV \sum_{i=1}^{NG} w_i \boldsymbol{\rho}_i = \mathbf{0} \quad (4.3)$$

(with respect to $\dot{\mathbf{q}}$)

$$\sum_{i=1}^{NG} w_i \mathbf{B}_i^T \boldsymbol{\rho}_i = \mathbf{0}. \quad (4.4)$$

The derivation to $\boldsymbol{\rho}_i$ and λ recoveries (4.1b) and (4.1c), respectively. Eq.(4.4) shows a self-equilibrium relation of residual stress. It can be proven that (4.4) represents also a static equilibrium at each loading vertex. In fact, if we write (4.3) in any Gauss point and any loading vertex, we get

$$\boldsymbol{\rho}_i = \left(\frac{2\sigma_y^{ki}}{\sqrt{3}} \frac{\bar{\mathbf{D}}\dot{\mathbf{e}}_{ki}}{\sqrt{\dot{\mathbf{e}}_{ki}^T \bar{\mathbf{D}} \dot{\mathbf{e}}_{ki}}} + \bar{k}\mathbf{D}_v \dot{\mathbf{e}}_{ki} \right) - \left(\lambda \boldsymbol{\sigma}_{ki}^E + \boldsymbol{\sigma}_0^E \right). \quad (4.5)$$

Substituting (4.5) into (4.4), we obtain

$$\sum_{i=1}^{NG} w_i \left(\frac{2\sigma_y^{ki}}{\sqrt{3}} \frac{\mathbf{B}_i^T \bar{\mathbf{D}}\dot{\mathbf{e}}_{ki}}{\sqrt{\dot{\mathbf{e}}_{ki}^T \bar{\mathbf{D}} \dot{\mathbf{e}}_{ki}}} + \bar{k}\mathbf{B}_i^T \mathbf{D}_v \dot{\mathbf{e}}_{ki} \right) = \sum_{i=1}^{NG} w_i \mathbf{B}_i \left(\lambda \boldsymbol{\sigma}_{ki}^E + \boldsymbol{\sigma}_0^E \right) \quad (4.6)$$

The left-hand terms of (4.6) represent the internal stress deviator and hydrostatic stress, which are in equilibrium with the right-hand terms representing the applied force at k loading vertex and the dead loads. It is known from the definition of (4.2)-(4.4) that the residual stress $\boldsymbol{\rho}_i$ should be independent of the loading vertex (cycle time). However this can be attained only when the optimal field is found. So by static relations (4.6) or (4.5) as well as the plastic admissible condition, we can give later a lower bound estimation of shakedown limit. For the simplicity, we temporarily do not consider the second term of

the right hand side of (4.5) since the incompressibility condition is enforced by the penalty method. From (4.5) we have

$$\dot{\mathbf{e}}_{ki} = \frac{\sqrt{3}}{2\sigma_y^{ki}}\bar{\mathbf{D}}^{-1}\sqrt{\dot{\mathbf{e}}_{ki}^T\bar{\mathbf{D}}\dot{\mathbf{e}}_{ki}}\left(\boldsymbol{\rho}_i + \boldsymbol{\sigma}_0^E\right) + \frac{\sqrt{3}}{2\sigma_y^{ki}}\left(\lambda\boldsymbol{\sigma}_{ki}^E\right) \tag{4.7}$$

By using the compatibility condition (4.1b) we can write

$$\boldsymbol{\rho}_i = \frac{\bar{\mathbf{D}}}{\sum_{k=1}^{NV}\frac{\sqrt{3\dot{\mathbf{e}}_{ki}^T\bar{\mathbf{D}}\dot{\mathbf{e}}_{ki}}}{2\sigma_y^{ki}}}\left[\mathbf{B}_i\dot{\mathbf{q}}_i - \lambda\sum_{k=1}^{NV}\frac{\bar{\mathbf{D}}^{-1}\sqrt{3\dot{\mathbf{e}}_{ki}^T\bar{\mathbf{D}}\dot{\mathbf{e}}_{ki}}\boldsymbol{\sigma}_{ki}^E}{2\sigma_y^{ki}}\right] - \boldsymbol{\sigma}_0^E \tag{4.8}$$

This shows that residual stress $\boldsymbol{\rho}_i$ is independent of loading vertex (time). Inserting (4.8) in (4.7) we get back a recursive formula for strain rate deviator:

$$\dot{\mathbf{e}}_{ki} = \frac{\frac{\sqrt{\dot{\mathbf{e}}_{ki}^T\bar{\mathbf{D}}\dot{\mathbf{e}}_{ki}}}{\sigma_y^{ki}}}{\sum_{h=1}^{NV}\frac{\sqrt{\dot{\mathbf{e}}_{hi}^T\bar{\mathbf{D}}\dot{\mathbf{e}}_{hi}}}{\sigma_y^{ki}}}\left[\mathbf{B}_i\dot{\mathbf{q}}_i + \lambda\sum_{h=1}^{NV}\frac{\bar{\mathbf{D}}^{-1}\sqrt{3\dot{\mathbf{e}}_{hi}^T\bar{\mathbf{D}}\dot{\mathbf{e}}_{hi}}(\boldsymbol{\sigma}_{ki}^E - \boldsymbol{\sigma}_{hi}^E)}{2\sigma_y^{ki}}\right] \tag{4.9}$$

In the case of without thermal loading or the yield limit is temperature-independent, (4.9) may be simplified into:

$$\dot{\mathbf{e}}_{ki} = \frac{\sqrt{\dot{\mathbf{e}}_{ki}^T\bar{\mathbf{D}}\dot{\mathbf{e}}_{ki}}}{\sum_{h=1}^{NV}\sqrt{\dot{\mathbf{e}}_{hi}^T\bar{\mathbf{D}}\dot{\mathbf{e}}_{hi}}}\left[\mathbf{B}_i\dot{\mathbf{q}}_i + \lambda\sum_{h=1}^{NV}\frac{\bar{\mathbf{D}}^{-1}\sqrt{3\dot{\mathbf{e}}_{hi}^T\bar{\mathbf{D}}\dot{\mathbf{e}}_{hi}}(\boldsymbol{\sigma}_{ki}^E - \boldsymbol{\sigma}_{hi}^E)}{2\sigma_y^{ki}}\right] \tag{4.10}$$

This is similar to a formula proposed by Zhang [40]. Here, $\dot{\mathbf{e}}_i = \sum_{k=1}^{NV}\dot{\mathbf{e}}_{ki} = \mathbf{B}_i\dot{\mathbf{q}}_i$ and $\dot{\mathbf{e}}_{ki}$, are the cycle strain rate (deviator) corresponding to nodal velocity (after a cycle of loading) and the strain rate (deviator) at k loading vertex, respectively. Now we substitute (4.8) into (4.4) to obtain a new optimal condition

$$\frac{\sum_{i=1}^{NG}w_i\mathbf{B}_i^T\bar{\mathbf{D}}\mathbf{B}_i\dot{\mathbf{q}}}{\sum_{k=1}^{NV}\frac{\sqrt{3\dot{\mathbf{e}}_{ki}^T\bar{\mathbf{D}}\dot{\mathbf{e}}_{ki}}}{2\sigma_y^{ki}}} = \lambda\frac{\sum_{i=1}^{NG}w_i\sum_{k=1}^{NV}\frac{\sqrt{3\dot{\mathbf{e}}_{ki}^T\bar{\mathbf{D}}\dot{\mathbf{e}}_{ki}}}{2\sigma_y^{ki}}\mathbf{B}_i^T\boldsymbol{\sigma}_{ki}^E}{\sum_{k=1}^{NV}\frac{\sqrt{3\dot{\mathbf{e}}_{ki}^T\bar{\mathbf{D}}\dot{\mathbf{e}}_{ki}}}{2\sigma_y^{ki}}} - \sum_{i=1}^{NG}w_i\mathbf{B}_i^T\boldsymbol{\sigma}_0^E \tag{4.11}$$

If the yield limit of material is independent of loading vertex (or temperature) we define $\mathbf{D}_i = (2\sigma_y^i/\sqrt{3})^2\bar{\mathbf{D}}$, (4.11) is simplified into

$$\frac{\sum_{i=1}^{NG} w_i \mathbf{B}_i^T \mathbf{D} \mathbf{B}_i \dot{\mathbf{q}}}{\sum_{k=1}^{NV} \sqrt{\dot{\mathbf{e}}_{ki}^T \mathbf{D} \dot{\mathbf{e}}_{ki}}} = \lambda \frac{\sum_{i=1}^{NG} w_i \sum_{k=1}^{NV} \sqrt{\dot{\mathbf{e}}_{ki}^T \bar{\mathbf{D}} \dot{\mathbf{e}}_{ki}} \mathbf{B}_i^T \boldsymbol{\sigma}_{ki}^E}{\sum_{k=1}^{NV} \sqrt{\dot{\mathbf{e}}_{ki}^T \bar{\mathbf{D}} \dot{\mathbf{e}}_{ki}}} - \sum_{i=1}^{NG} w_i \mathbf{B}_i^T \boldsymbol{\sigma}_0^E \tag{4.12}$$

Based on the above analysis, we can establish an iteration algorithm for dual shakedown limits (upper bound and lower bound).

4.2 Upper bound estimation

Starting from n iteration with $\dot{\mathbf{e}}_{ki}^n$ known, we look for the solution by $n+1$ iteration

$$\left(\sum_{i=1}^{NG} w_i \frac{\mathbf{B}_i^T \mathbf{D}_i \mathbf{B}_i}{\sum_{k=1}^{NV} \sqrt{(\dot{\mathbf{e}}_{ki}^n)^T \mathbf{D} (\dot{\mathbf{e}}_{ki}^n)}} + \sum_{i=1}^{NG} w_i \bar{k} \mathbf{B}_i^T \mathbf{D}_v \mathbf{B}_i \right) \dot{\mathbf{q}}_{n+1} = \lambda_{n+1} \mathbf{g}_n + \mathbf{g}_0 \tag{4.13}$$

where

$$\mathbf{g}_n = \sum_{i=1}^{NG} \frac{w_i \mathbf{B}_i}{\sum_{k=1}^{NV} \sqrt{(\dot{\mathbf{e}}_{ki}^n)^T \mathbf{D}_i (\dot{\mathbf{e}}_{ki}^n)}} \sum_{k=1}^{NV} \sqrt{(\dot{\mathbf{e}}_{ki}^n)^T \mathbf{D}_i (\dot{\mathbf{e}}_{ki}^n)} \boldsymbol{\sigma}_{ki}^E \tag{4.14}$$

$$\mathbf{g}_0 = \sum_{i=1}^{NG} w_i \mathbf{B}_i \boldsymbol{\sigma}_{0i}^E \tag{4.15}$$

This iteration algorithm is similar as a method proposed by Zhang [40]. Eq. (4.13) represents an equilibrium relation between equivalent external load and equivalent internal stress field. Since it is completely similar to (3.2), we can perform a calculating procedure similar to the direct iteration method in limit analysis (c.f. section 2.1):

$$\mathbf{K}_n \dot{\mathbf{q}}_{n+1} = \lambda_{n+1} \mathbf{g}_n + \mathbf{g}_0 \tag{4.16}$$

with

$$\mathbf{K}_n = \sum_{i=1}^{NG} w_i \frac{\mathbf{B}_i^T \mathbf{D}_i \mathbf{B}_i}{\sum_{k=1}^{NV} \sqrt{(\dot{\mathbf{e}}_{ki}^n)^T \mathbf{D} (\dot{\mathbf{e}}_{ki}^n)}} + \sum_{i=1}^{NG} w_i \bar{k} \mathbf{B}_i^T \mathbf{D}_v \mathbf{B}_i \tag{4.17}$$

For solving it, we decompose the nodal velocity solution into two parts:

$$\dot{\mathbf{q}}_{n+1} = \lambda_{n+1}\dot{\mathbf{q}}_I + \dot{\mathbf{q}}_{II} \tag{4.18}$$

with

$$\dot{\mathbf{q}}_I = \mathbf{K}_n^{-1}\mathbf{g} \tag{4.19}$$

$$\dot{\mathbf{q}}_{II} = \mathbf{K}_n^{-1}\mathbf{g}_0 \tag{4.20}$$

The corresponding strain vectors at k loading vertex

$$\dot{\mathbf{e}}_{ki}^{n+1} = \lambda_{n+1}\left(\dot{\mathbf{e}}_{ki}^{n+1}\right)_I + \left(\dot{\mathbf{e}}_{ki}^{n+1}\right)_{II} \tag{4.21}$$

with $k = 1, NV$

$$\left(\dot{\mathbf{e}}_{ki}^{n+1}\right)_I = \frac{\sqrt{(\dot{\mathbf{e}}_{ki}^n)^T\mathbf{D}_i(\dot{\mathbf{e}}_{ki}^n)}}{\sum_{h=1}^{NV}\sqrt{(\dot{\mathbf{e}}_{hi}^n)^T\mathbf{D}(\dot{\mathbf{e}}_{hi}^n)}}\left[\mathbf{B}_i\dot{\mathbf{q}}_I + \sum_{h=1}^{NV}\mathbf{D}_i^{-1}\sqrt{(\dot{\mathbf{e}}_{hi}^n)^T\mathbf{D}_i(\dot{\mathbf{e}}_{hi}^n)}(\boldsymbol{\sigma}_{ki}^E - \boldsymbol{\sigma}_{hi}^E)\right] \tag{4.22}$$

$$\left(\dot{\mathbf{e}}_{ki}^{n+1}\right)_{II} = \frac{\sqrt{(\dot{\mathbf{e}}_{ki}^n)^T\mathbf{D}_i(\dot{\mathbf{e}}_{ki}^n)}}{\sum_{h=1}^{NV}\sqrt{(\dot{\mathbf{e}}_{hi}^n)^T\mathbf{D}(\dot{\mathbf{e}}_{hi}^n)}}\mathbf{B}_i\dot{\mathbf{q}}_{II}, \quad k = 1, NV \tag{4.23}$$

By normalization condition (4.12): we can determine the current Lagrangian multiplier as:

$$\lambda_{n+1} = \frac{1 - \sum_{i=1}^{NG}\sum_{k=1}^{NV} w_i\left(\dot{\mathbf{e}}_{ki}^{n+1}\right)_{II}^T\boldsymbol{\sigma}_{ki}^E}{\sum_{i=1}^{NG} w_i\sum_{k=1}^{NV}\left(\dot{\mathbf{e}}_{ki}^{n+1}\right)_I^T\boldsymbol{\sigma}_{ki}^E} \tag{4.24}$$

So an upper bound estimation of the shakedown limit at the current iteration:

$$\alpha_{n+1}^+ = \sum_{i=1}^{NG}\sum_{k=1}^{NV} w_i\sqrt{(\dot{\mathbf{e}}_{ki}^n)^T\mathbf{D}_i(\dot{\mathbf{e}}_{ki}^n)} - \dot{\mathbf{q}}_{n+1}^T\mathbf{g}_0 \tag{4.25}$$

Then we update the matrix $\mathbf{K}_n$ and $\mathbf{g}_n$ with the new velocity solution to carry out next step calculation. As described in section 3.1 in the case of limit analysis, such an iterative process described as above produces a sequence of load multiplier $\{\alpha_n^+\}$, a sequence of Lagrangian multiplier $\{\lambda_n\}$, a sequence of nodal velocity arrays $\{\dot{\mathbf{q}}_n\}$ and a sequence of Gauss point-Loading vertex strain rate arrays $\{\dot{\mathbf{e}}_{ki}^n\}$. All of these sequences converge to their limits.

$$\lim_{n\to\infty}\alpha_n^+ = \alpha_{SD}^+ \geq \alpha_{SD} \tag{4.26}$$

and

$$\lim_{n\to\infty} \dot{\mathbf{q}}_n = \dot{\mathbf{q}} \tag{4.27}$$

$$\lim_{n\to\infty} \dot{\mathbf{e}}_{ki}^n = \dot{\mathbf{e}}_{ki} \tag{4.28}$$

$$\lim_{n\to\infty} \lambda_n = \lambda = \alpha_{SD}^+ \tag{4.29}$$

Generally, λ_n is also an upper bound of the limit load multiplier and it has a convergence a little better than α_n^+.

4.3 Lower bound estimation

As stated above, (4.8) give a time-independent residual stress field and (4.13) represents the equilibrium relation for an equivalent load that characteristic the loading domain. According to Melan's static shakedown theorem, cf. [24], [26], a lower bound estimation of the shakedown load can be found by any residual stress field independent of time adding to elastic stress and leading to the plastic admissible stress field that does not violate anywhere plastic yield criterion. So we can give a lower bound estimation of shakedown limit by following analysis. We rewrite (4.8) in iterative form as

$$\begin{aligned} \bar{\boldsymbol{\rho}}_i^{n+1} &= \boldsymbol{\rho}_i^{n+1} - \boldsymbol{\sigma}_0^E \\ &= \frac{\mathbf{D}_i}{\sum_{k=1}^{NV} \sqrt{(\dot{\mathbf{e}}_{ki}^n)^T \mathbf{D}_i (\dot{\mathbf{e}}_{ki}^n)}} \left[\mathbf{B}_i \dot{\mathbf{q}}_i^{n+1} - \lambda^{n+1} \sum_{k=1}^{NV} \mathbf{D}_i^{-1} \sqrt{(\dot{\mathbf{e}}_{ki}^n)^T \mathbf{D}_i (\dot{\mathbf{e}}_{ki}^n)} \boldsymbol{\sigma}_{ki}^E \right] \end{aligned} \tag{4.30}$$

Therefore, we can obtain a lower bound estimation of shakedown limit by the following calculation

$$\alpha_{n+1}^- = \lim_{i,k} \alpha_{ki}^{n+1} \qquad i = 1, NG, k = 1, NV \tag{4.31}$$

$$\text{s.t.} \quad f(\alpha_{ki}^{n+1} \boldsymbol{\sigma}_{ki}^E + \bar{\boldsymbol{\rho}}_i^{n+1}) \le 0 \tag{4.32}$$

where f represents the von Mises criterion which can be written as $\boldsymbol{\sigma}^T \mathbf{D} \boldsymbol{\sigma} - 1 = 0$.

Alternatively we can perform another procedure for the lower bound estimation by considering the equilibrium relation represented by (4.13) for an equivalent load that characteristic the loading domain. We rewrite (4.13) into

$$\sum_{i=1}^{NG} w_i \mathbf{B}_i^T \boldsymbol{\sigma}_{ki}^{n+1} = \lambda_{n+1} \mathbf{g}_n + \mathbf{g}_0 \tag{4.33}$$

$$\boldsymbol{\sigma}_{ki}^{n+1} = \mathbf{s}_{ki}^{n+1} + \mathbf{s}_{m,ki}^{n+1} \tag{4.34}$$

where $\mathbf{s}_{ki}^{n+1}, \mathbf{s}_{m,ki}^{n+1}$ are the current $(n+1)$ equivalent stress deviator and hyperstatic pressure-like vector related to k loading vertex, respectively. For the convenience of calculation, we write the following equilibrium relations

$$\sum_{i=1}^{NG} w_i \mathbf{B}_i^T (\mathbf{s}_I + \mathbf{s}_{mI}) = \mathbf{g}_n \tag{4.35}$$

$$\sum_{i=1}^{NG} w_i \mathbf{B}_i^T (\mathbf{s}_{II} + \mathbf{s}_{mII}) = \mathbf{g}_0 \tag{4.36}$$

where

$$\mathbf{s}_I = \frac{\mathbf{D}_i \mathbf{B}_i \dot{\mathbf{q}}_I}{\sqrt{(\dot{\mathbf{q}}_{ki}^n)^T \mathbf{D}_i (\dot{\mathbf{q}}_{ki}^n)}}, \qquad \mathbf{s}_{II} = \frac{\mathbf{D}_i \mathbf{B}_i \dot{\mathbf{q}}_{II}}{\sqrt{(\dot{\mathbf{q}}_{ki}^n)^T \mathbf{D}_i (\dot{\mathbf{q}}_{ki}^n)}}, \tag{4.37}$$

$$\mathbf{s}_{mI} = \bar{k} \mathbf{D}_v \mathbf{B}_i \dot{\mathbf{q}}_I, \quad \mathbf{s}_{mII} = \bar{k} \mathbf{D}_v \mathbf{B}_i \dot{\mathbf{q}}_{II} \tag{4.38}$$

It is well known that only stress deviator related to incompressible strain rate is concerned in the plasticity criterion, so only (3.24) is performed for the present lower bound estimation. According to the static theorem, we have a lower bound at every iteration step:

$$\alpha_{n+1}^- = \lim_{i \in NG} \alpha_{i,n+1}^- \tag{4.39}$$

$$\text{s.t.} \quad f(\alpha_{i,n+1}^- \mathbf{s}_I + \mathbf{s}_{II}) \leq 0 \tag{4.40}$$

Since von Mises criterion can be written as $\mathbf{s}^T \mathbf{D}_i \mathbf{s} - 1 = 0$, for the present application we have

$$(\alpha_{i,n+1}^- \dot{\mathbf{q}}_I + \dot{\mathbf{q}}_{II})^T (\mathbf{B}^T \mathbf{D} \mathbf{B})_i (\alpha_{i,n+1}^- \dot{\mathbf{q}}_I + \dot{\mathbf{q}}_{II}) = h_{i,n}^2 \tag{4.41}$$

Defining:

$$h_{i,n} = \sum_{k=1}^{NV} \sqrt{(\dot{\mathbf{e}}_{ki}^n)^T \mathbf{D}_i (\dot{\mathbf{e}}_{ki}^n)} \tag{4.42}$$

$$x = \dot{\mathbf{q}}_I^T (\mathbf{B}^T \mathbf{D} \mathbf{B})_i \dot{\mathbf{q}}_I \tag{4.43}$$

$$y = \dot{\mathbf{q}}_I^T (\mathbf{B}^T \mathbf{D} \mathbf{B})_i \dot{\mathbf{q}}_{II} \tag{4.44}$$

$$z = \dot{\mathbf{q}}_{II}^T (\mathbf{B}^T \mathbf{D} \mathbf{B})_i \dot{\mathbf{q}}_{II} \tag{4.45}$$

The solution of (4.38) at any integral point is

$$\alpha_{i,n+1}^- = \frac{\sqrt{y^2 + x(h_{i,n}^2 - z)} - y}{x} \tag{4.46}$$

The lower bound of the structure is found by using (4.39). This procedure also produces a sequence of load multiplier $\{\alpha_n^-\}$. We do not yet find a proof for the convergence for the present lower bound solution. However, according to Melan's theorem and by duality

between Melan's theorem and Koiter's theorem, (4.39) should give correct lower bound. On the other hand, (4.46) may give an approximate estimate of lower bound, by which we need not carry out an examination passing over all loading vertices.

5 A new dual shakedown analysis

In the above development, we used kinematical method on basis of Koiter's kinematic theorem. The shakedown solution is found in principal along a decreasing direction (of upper bounds) although the lower bounds may be also given by the obtained static fields during the process of optimization. On the other hand, the static shakedown analysis is developed by other partners basing on Melan's static shakedown theorem. In this case, the shakedown solution is found along an increasing direction (of lower bounds)

However, up to now by all these existing shakedown analyses, the duality of the static lower bound and the kinematic upper bound have not been practically used in numerical calculations. The optimization variables are either purely static or purely kinematic. This fact explains the difficulty in further improvement of the calculating efficiency. On the other hand, although Newton's method has shown its high efficiency in limit analysis, it was not applied effectively in shakedown analysis. The application of the duality was explored in limit analysis by Zouain *et al.* (1993) [41] in the case where the plastic incompressibility condition could be automatically satisfied with the used finite elements. Recently, Anderson *et al.* (2000) [3] developed an excellent analysis for minimizing a sum of Euclidean norms by a primal-dual interior-point method. They have shown that the application of the duality combining with Newton's method may lead to very accurate results in limit analysis with high efficiency. The present work constitutes a new development along this direction in shakedown analysis with variable loading. It may be thought an improvement and development of the methods presented in the previous chapters.

5.1 Normalized kinematic shakedown formulae

In this new dual analysis, we rewrite the upper bound of shakedown theorem in the following normalized form, which is in fact equivalent to that in section 1.2:

$$
\begin{aligned}
&\alpha^{+} = \min \sum_{k\in I_D} \int_V D^p(\dot{\varepsilon}_{ij}^k) dV && (a)\\
&\text{s.t. :} \begin{cases}
\Delta\varepsilon_{ij} = \sum\limits_{k\in I_D} \dot{\varepsilon}_{ij}^k & (b)\\
\Delta\varepsilon_{ij} = \frac{1}{2}\left(\frac{\partial \Delta u_i}{\partial x_j} + \frac{\partial \Delta u_j}{\partial x_i}\right) \quad \text{in } V & (c)\\
\Delta u_i = 0 \quad \text{on } \partial V_u & (d)\\
\sum\limits_{k\in I_D} \int_V \sigma_{ij}^E\left(x, P_k^0\right) \dot{\varepsilon}_{ij}^k dV = 1 & (e)
\end{cases}
\end{aligned}
\tag{5.1}
$$

where α^+ denotes the shakedown load factor; u is the displacement at point $\mathbf{x}$ of V, $\dot{\varepsilon}_{ij}^k$ is the corresponding strain rate at load vertex k; $\Delta\varepsilon_{ij}$ is the plastic strain increment after a loading cycle; I_D is the set of all load vertices and $D^p\left(\dot{\varepsilon}_{ij}^k\right)$ denotes the plastic dissipation rate. By using von Mises' yield criterion, the discretized form of (5.1) by means of the finite element method can be expressed as following:

$$\begin{aligned} \alpha^+ &= \min \sum_{k=1}^{m}\sum_{i=1}^{NG} \sqrt{2} w_i k_v \sqrt{\dot{\boldsymbol{\varepsilon}}_{ik}^T \mathbf{D} \dot{\boldsymbol{\varepsilon}}_{ik} + \varepsilon_0^2} \\ \text{s.t. :} & \begin{cases} \sum_{k=1}^{m} \dot{\boldsymbol{\varepsilon}}_{ik} = \mathbf{B}_i \mathbf{q} & \forall i = 1, NG \\ \mathbf{D}_v \dot{\boldsymbol{\varepsilon}}_{ik} = \mathbf{0} & \forall i = 1, NG \\ \sum_{k=1}^{m}\sum_{i=1}^{NG} w_i \dot{\boldsymbol{\varepsilon}}_{ik}^T \boldsymbol{\sigma}_{ik}^E = 1 \end{cases} \end{aligned} \tag{5.2}$$

where $\dot{\boldsymbol{\varepsilon}}_{ik}$, $\boldsymbol{\sigma}_{ik}^E$ denote the vector of deformation rate and vector of the fictitious elastic stress at Gauss point i and load vertex k; $\mathbf{q}$ is the nodal displacement vector, $\mathbf{B}_i$ is the strain matrix; $m = 2^n$, n is the number of varying loads; NG denotes the total number of Gauss points of the whole structure with integration weight w_i at Gauss point i, ε_0 is a small parameter of regularization.

5.2 Duality

By restricting ourselves to a polyhedral form of load domain, we show in this section that the static lower bound based on Melan's theorem is exactly the dual form of the kinematic upper bound (5.2). For the sake of simplicity, let us rewrite the upper bound limit (5.2) in a simpler form by setting:

- The new strain rate vector $\mathbf{e}_{ik}$ (the dot mark denoting time derivative has been omitted for simplicity):
$$\mathbf{e}_{ik} = w_i \mathbf{D}^{1/2} \dot{\boldsymbol{\varepsilon}}_{ik} \tag{5.3}$$
- The new fictitious elastic stress field $\mathbf{t}_{ik}$:
$$\mathbf{t}_{ik} = \mathbf{D}^{-1/2} \boldsymbol{\sigma}_{ik}^E \tag{5.4}$$
- The new deformation matrix $\mathbf{B}_i$:
$$\hat{\mathbf{B}}_i = w_i \mathbf{D}^{1/2} \mathbf{B}_i \tag{5.5}$$

In the above definition $\mathbf{D}^{1/2}$ and $\mathbf{D}^{-1/2}$ are symmetric matrices (of the size 6×6 in the three dimensional case) such that:

$$\begin{aligned} \mathbf{D}^{-1/2} &= \left(\mathbf{D}^{1/2}\right)^{-1} \\ \mathbf{D} &= \mathbf{D}^{1/2}\mathbf{D}^{1/2} \end{aligned} \tag{5.6}$$

With these definitions, the objective function in (5.2) becomes:

$$\sum_{k=1}^{m}\sum_{i=1}^{NG}\sqrt{2}w_i k_v\sqrt{\dot{\boldsymbol{\varepsilon}}_{ik}^T\mathbf{D}\dot{\boldsymbol{\varepsilon}}_{ik}+\varepsilon_0^2}=\sqrt{2}k_v\sum_{k=1}^{m}\sum_{i=1}^{NG}\sqrt{\boldsymbol{\varepsilon}_{ik}^T\boldsymbol{\varepsilon}_{ik}+\varepsilon^2} \tag{5.7}$$

In the formulation (5.7), ε^2 is a small positive number suitably chosen to avoid the singularity of the objective function. By substituting (5.3)-(5.7) into (5.2) one obtains a simplified version for upper bound of shakedown limit:

$$\begin{aligned}
&\alpha^+ = \min \sqrt{2}k_v \sum_{k=1}^{m}\sum_{i=1}^{NG}\sqrt{\boldsymbol{\varepsilon}_{ik}^T\boldsymbol{\varepsilon}_{ik}+\varepsilon^2} && (a)\\
\text{s.t:}\ &\begin{cases}
\sum\limits_{k=1}^{m}\mathbf{e}_{ik}-\hat{\mathbf{B}}_i\mathbf{q}=\mathbf{0} \qquad \forall i=1,NG & (b)\\
\frac{1}{3}\mathbf{D}_v\mathbf{e}_{ik}=\mathbf{0} \qquad \forall i=1,NG,\forall k=1,m & (c)\\
\sum\limits_{i=1}^{NG}\sum\limits_{k=1}^{m}\mathbf{e}_{ik}^T\mathbf{t}_{ik}-1=0 & (d)
\end{cases}
\end{aligned} \tag{5.8}$$

where factor 1/3 is added in (5.8c) for a technical reason. This kinematic formulation is called henceforth the modified kinematic formulation.

Andersen *et al.* [3] have found that in case of limit analysis there exists a dual form for (5.8), while considering a problem of minimizing a sum of Euclidean norms. A generalization for shakedown analysis is presented hereafter through the following propositions:

Proposition 1:

If there exists a finite solution α^+ for the kinematic shakedown load multiplier (5.8) and if $\varepsilon^2=0$ then α^+ has its dual form as:

$$\begin{aligned}
&\alpha^- = \max_{\gamma_{ik},\boldsymbol{\beta}_i,\alpha}\ \alpha\\
\text{s.t:}\ &\begin{cases}
||\gamma_{ik}+\boldsymbol{\beta}_i+\mathbf{t}_{ik}\alpha|| \le \sqrt{2}k_v & (a)\\
\sum\limits_{i=1}^{NG}\mathbf{B}_i^T\boldsymbol{\beta}_{ik}=0 & (b)
\end{cases}
\end{aligned} \tag{5.9}$$

having no gap to α^+ where: $||\cdot||$ denotes Euclidean vector norm.

Proof:

By setting $\varepsilon^2=0$, let us write the Lagrange dual function of (5.8) as:

$$\begin{aligned}
F_L \;=\; &\sum_{i=1}^{NG}\left\{\sum_{k=1}^{m}\sqrt{2}k_v\sqrt{\mathbf{e}_{ik}^T\mathbf{e}_{ik}}-\sum_{k=1}^{m}\frac{1}{3}\left(\gamma_{ik}^T\mathbf{D}_v\mathbf{e}_{ik}\right)-\boldsymbol{\beta}_i^T\left(\sum_{k=1}^{m}\mathbf{e}_{ik}-\hat{\mathbf{B}}_i\mathbf{q}\right)\right\}\\
-\;&\alpha\left(\sum_{i=1}^{NG}\sum_{k=1}^{m}\mathbf{e}_{ik}^T\mathbf{t}_{ik}-1\right)
\end{aligned} \tag{5.10}$$

where $\gamma_{ik}, \boldsymbol{\beta}_i, \alpha$ are Lagrange multipliers. Note that $\gamma_{ik}, \boldsymbol{\beta}_i$ are vectors at Gauss point i for each load vertex k while α is merely a scalar.

The dual problem of (5.8) is now:

$$\max_{\gamma_{ik},\beta_i,\alpha} \left(\min_{e_{ik},q} F_L \right) \tag{5.11}$$

Because a finite solution for (5.8) exists, the constraint system (5.8b)-(5.8d) is affine and the objective function is convex, then the duality theorem states that there exists no dual gap between primal and dual solutions:

$$\min_{h(e_{ik},q)=0} \sum_{i=1}^{NG} \sum_{k=1}^{m} \sqrt{2} k_v \sqrt{\mathbf{e}_{ik}^T \mathbf{e}_{ik}} = \max_{\gamma_{ik},\beta_i,\alpha} \left(\min_{e_{ik},q} F_L \right) \tag{5.12}$$

where $\mathbf{h}(\mathbf{e}_{ik}, \mathbf{q}) = 0$ stands for linear constraint system (5.8b)-(5.8d).

The Lagrange dual function (5.10) may be written in another form:

$$F_L = \sum_{i=1}^{NG} \sum_{k=1}^{m} \left(\frac{\sqrt{2} k_v \mathbf{e}_{ik}}{\sqrt{\mathbf{e}_{ik}^T \mathbf{e}_{ik}}} - \gamma_{ik} - \boldsymbol{\beta}_i - \mathbf{t}_{ik} \alpha \right)^T \mathbf{e}_{ik} + \sum_{i=1}^{NG} \boldsymbol{\beta}_i^T \hat{\mathbf{B}}_i \mathbf{q} + \alpha \tag{5.13}$$

In writing (5.10) in the form (5.13) we adopt here the convention that if the vector norm of strain rate $||\mathbf{e}_{ik}||$ is equal to zero then: $\dfrac{\sqrt{2} k_v \mathbf{e}_{ik}}{\sqrt{\mathbf{e}_{ik}^T \mathbf{e}_{ik}}} \mathbf{e}_{ik} = 0$.

Due to the existence of a dual solution α^- having no gap to the primal α^+, it is required that for any solution set of Lagrange multipliers $(\gamma_{ik}, \boldsymbol{\beta}_i, \alpha)$ the function $\left(\min_{e_{ik},q} F_L \right)$ must have a finite value. To this end, the following system must be satisfied:

$$\begin{cases} \left(\dfrac{\sqrt{2} k_v \mathbf{e}_{ik}}{\sqrt{\mathbf{e}_{ik}^T \mathbf{e}_{ik}}} - \gamma_{ik} - \boldsymbol{\beta}_i - \mathbf{t}_{ik} \alpha \right)^T \mathbf{e}_{ik} \geq 0 \quad \forall \mathbf{e}_{ik} \quad (a) \\ \sum\limits_{i=1}^{NG} \boldsymbol{\beta}_i^T \hat{\mathbf{B}}_i \mathbf{q} = 0 \quad \forall \mathbf{q} \qquad (b) \end{cases} \tag{5.14}$$

otherwise we always have:

$$\min_{e_{ik},q} F_L \to -\infty \tag{5.15}$$

According to (5.14), the function of $\left(\min_{e_{ik},q} F_L \right)$ is bounded from below:

$$\min_{e_{ik},q} F_L \geq \alpha \tag{5.16}$$

It reaches α when, for example, all strain rates and displacement are equal to zero. This fact leads to the conclusion:

$$\min_{e_{ik},q} F_L = \alpha \tag{5.17}$$

The condition (5.14b) is equivalent to:

$$\sum_{i=1}^{NG} \mathbf{B}_i^T \boldsymbol{\beta}_i = \mathbf{0} \tag{5.18}$$

Further more, it is possible to point out that the condition (5.14a) is equivalent to restriction on only multipliers $\gamma_{ik}, \boldsymbol{\beta}_i, \alpha$:

$$||\gamma_{ik} + \boldsymbol{\beta}_i + \mathbf{t}_{ik}\alpha|| \leq \sqrt{2}k_v \ \ \forall i,k \tag{5.19}$$

Equalities (5.17), (5.18) and inequality (5.19) conclude our proof. We explain in physical meaning $\gamma_{ik}, \boldsymbol{\beta}_i, \mathbf{t}_{ik}$ as the hydrostatic, residual and elastic stress of structures, respectively.

Admitting that kinematic formulation (5.8) has its finite solution and its dual form (5.9), it is also amenable to present the primal-dual forms as a set of stationary conditions or Karush-Kuhn-Tucker (KKT) conditions as following:

$$\begin{aligned}
&\frac{\sqrt{2}k_v \mathbf{e}_{ik}}{\sqrt{\mathbf{e}_{ik}^T \mathbf{e}_{ik}}} - (\gamma_{ik} + \boldsymbol{\beta}_i + \alpha \mathbf{t}_{ik}) &&= \mathbf{0} \quad (a)\\
&\mathbf{D}_v \mathbf{e}_{ik} &&= \mathbf{0} \quad (b)\\
&\sum_{k=1}^{m} \mathbf{e}_{ik} - \hat{\mathbf{B}}_i \mathbf{q} &&= \mathbf{0} \quad (c)\\
&\sum_{i=1}^{NG} \left(\hat{\mathbf{B}}_i^T \boldsymbol{\beta}_i \right) &&= \mathbf{0} \quad (d)\\
&\sum_{i=1}^{NG} \sum_{k=1}^{m} \mathbf{e}_{ik}^T \mathbf{t}_{ik} - 1 &&= \mathbf{0} \quad (e)
\end{aligned} \tag{5.20}$$

Despite the fact that the dual form of (5.8) exists, equation (5.9) does not appear as the discretized Melan's theorem. In order to have von Mises' condition in the dual form, the Lagrange multiplier γ_{ik} in the above system must be eliminated and the following proposition can be proved without any difficulty:

Proposition 2:

If there exists a finite solution α^+ for the kinematic shakedown load multiplier (5.8) and if $\varepsilon^2 = 0$ then the kinematic formulation has its dual form as the static one resulted from Melan's theorem, if the incompressibility condition may be automatically satisfied with the used elements:

$$\min_{h(e_{ik},q)=0} \sum_{i=1}^{NG} \sum_{k=1}^{m} \sqrt{2}k_v \sqrt{\mathbf{e}_{ik}^T \mathbf{e}_{ik}} = \max_{\substack{B^T \bar{\rho} = 0 \\ f(\alpha \bar{\sigma}_{ik}^E + \bar{\rho}_{ik}) \leq 0}} \alpha \tag{5.21}$$

A demonstration of the proof is given in [16].

5.3 A dual algorithm

The developed dual algorithm aims at obtaining simultaneously both primal and dual values (the upper bound from velocity and strain rate field, and the lower bound from stress field) by solving the system of stationary conditions (5.20). Unfortunately, solving directly this system is not a good idea because it results in a system of equations much bigger than that in the case of purely elastic computation. The resulted system thus requires large amount of computer memory as well as computational effort to solve. Trying to keep our problem size as small as possible, we use here the penalty method to handle equality conditions (5.20b)-(5.20c) with Lagrange multipliers (stresses) playing intermediate roles. A similar technique, which showed great efficiency in large scale problems, has been successfully applied to limit analysis by Andersen et al. [3]. Numerically speaking, the stationary conditions (5.20) are very difficult to satisfy due to the singular property of the problem in consideration and therefore we lack an appropriate criterion to stop optimization procedure or to assess the exactness of the solution (the shakedown load multiplier α). However, if a strictly lower bound is found at the same time with a strictly upper bound, we will possess a very useful tool to control the obtained results. Although those strict bounds are hard to find, in the following algorithm we will try to build some of their approximations while using Newton method to solve (5.20):

Algorithm:

1) Initialize displacement and strain rate vectors $\mathbf{q}^0$ and $\mathbf{e}^0$ such that the normalized condition is satisfied:

$$\sum_{i=1}^{NG}\sum_{k=1}^{m}\mathbf{t}_{ik}^T\mathbf{e}_{ik}^0 = 1$$

Set all stress vectors to nulls:

$$\begin{cases} \gamma_{ik}^0 = \mathbf{0} \\ \boldsymbol{\beta}_i^0 = \mathbf{0} \end{cases} \quad \forall i = 1, NG,\ k = 1, 2n$$

Set up initial values for penalty parameter c and for ε. Set up convergence criteria.

2) Calculate incremental vectors $d\mathbf{q}, d\mathbf{e}_{ik}$ of displacement, deformations and $(d\alpha + \alpha)$ at the current values of $\mathbf{q}, \mathbf{e}$ by solving the following system:

$$\begin{cases} d\mathbf{e}_{ik} = \sqrt{\mathbf{e}_{ik}^T\mathbf{e}_{ik} + \varepsilon^2}\hat{\mathbf{M}}_{ik}^{-1}\left(-\mathbf{g}_{ik} + d\boldsymbol{\beta}_i + \mathbf{t}_{ik}d\alpha\right) - \hat{\mathbf{M}}_{ik}^{-1}\mathbf{f}_{ik} \\ \sum\limits_{i=1}^{NG}\sum\limits_{k=1}^{m}\mathbf{t}_{ik}^T\left(\mathbf{e}_{ik} + d\mathbf{e}_{ik}\right) = 1 \\ d\mathbf{q} = -\mathbf{q} + \hat{\mathbf{S}}^{-1}\hat{\mathbf{f}}_1 + (\alpha + d\alpha)\hat{\mathbf{S}}^{-1}\hat{\mathbf{f}}_2 \end{cases}$$

where:

$$
\begin{aligned}
\hat{\mathbf{S}} &= \sum_{i=1}^{NG} \hat{\mathbf{B}}_i^T \hat{\mathbf{K}}_i^{-1} \hat{\mathbf{B}}_i^T \\
\hat{\mathbf{f}}_1 &= \sum_{i=1}^{NG} \hat{\mathbf{B}}_i^T \hat{\mathbf{K}}_i^{-1} \left(\sum_{k=1}^{m} \mathbf{e}_{ik} - \sum_{k=1}^{m} \hat{\mathbf{M}}_{ik}^{-1} \mathbf{e}_{ik} - c \sum_{k=1}^{m} \sqrt{\mathbf{e}_{ik}^T \mathbf{e}_{ik} \varepsilon^2} \hat{\mathbf{M}}_{ik}^{-1} \mathbf{D}_v \mathbf{e}_{ik} \right) \\
\hat{\mathbf{f}}_2 &= \sum_{i=1}^{NG} \hat{\mathbf{B}}_i^T \hat{\mathbf{K}}_i^{-1} \sum_{k=1}^{m} \sqrt{\mathbf{e}_{ik}^T \mathbf{e}_{ik} + \varepsilon^2} \hat{\mathbf{M}}_{ik}^{-1} \mathbf{t}_{ik} \\
\hat{\mathbf{K}}_i &= \left[\mathbf{I} + c \sum_{k=1}^{m} \sqrt{\mathbf{e}_{ik}^T \mathbf{e}_{ik} + \varepsilon^2} \hat{\mathbf{M}}_{ik}^{-1} \right] \\
\hat{\mathbf{M}}_{ik} &= \left[\mathbf{I} - \frac{(\gamma_{ik} + \boldsymbol{\beta}_i + \alpha \mathbf{t}_{ik}) \mathbf{e}_{ik}^T}{\sqrt{\mathbf{e}_{ik}^T \mathbf{e}_{ik} + \varepsilon^2}} \right] + \sqrt{\mathbf{e}_{ik}^T \mathbf{e}_{ik} + \varepsilon^2} c \mathbf{D}_v \\
\mathbf{f}_{ik} &= \mathbf{e}_{ik} - \sqrt{\mathbf{e}_{ik}^T \mathbf{e}_{ik} + \varepsilon^2} (\gamma_{ik} + \boldsymbol{\beta}_i + \alpha \mathbf{t}_{ik})
\end{aligned}
$$

$$
\begin{aligned}
\mathbf{g}_{ik} &= \gamma_{ik} + c \mathbf{D}_v \mathbf{e}_{ik} \\
\mathbf{h}_i &= \boldsymbol{\beta}_i + c \left(\sum_{k=1}^{m} \mathbf{e}_{ik} - \hat{\mathbf{B}} \mathbf{q} \right)
\end{aligned}
$$

3) Perform a line-search to find $\hat{\lambda}_q$ such that:

$$
\hat{\lambda}_q = \min F_P \left(\mathbf{q} + \lambda d\mathbf{q}, \mathbf{e} + \lambda d\mathbf{e} \right)
$$

where F_P is the penalty function:

$$
\begin{aligned}
F_P &= \sum_{i=1}^{NG} \left\{ \sqrt{2} k_v \sum_{k=1}^{m} \sqrt{\mathbf{e}_{ik}^T \mathbf{e}_{ik} + \varepsilon^2} + \frac{c}{2} \sum_{k=1}^{m} \mathbf{e}_{ik}^T \mathbf{D}_v \mathbf{e}_{ik} \right. \\
&+ \left. \frac{c}{2} \left(\sum_{k=1}^{m} \mathbf{e}_{ik} - \mathbf{B}_i \mathbf{q} \right)^T \left(\sum_{k=1}^{m} \mathbf{e}_{ik} - \mathbf{B}_i \mathbf{q} \right) \right\}
\end{aligned}
$$

4) Update the displacement and strain rate vectors as:

$$
\begin{aligned}
\mathbf{q} &= \mathbf{q} + \hat{\lambda}_q d\mathbf{q} \\
\mathbf{e}_{ik} &= \mathbf{e}_{ik} + \hat{\lambda}_q d\mathbf{e}_{ik}
\end{aligned}
$$

5) Calculate the incremental vectors of stress vectors $\gamma_{ik}, \boldsymbol{\beta}_i$:

$$\begin{cases} d\gamma_{ik} = -c\mathbf{D}_v d\mathbf{e}_{ik} - \mathbf{g}_{ik} \\ d\boldsymbol{\beta}_i = -c\left(\sum_{k=1}^{m} d\mathbf{e}_{ik} - \hat{\mathbf{B}}_i d\mathbf{q}\right) - \mathbf{h}_i \end{cases}$$

Perform a line-search to find $\hat{\lambda}_s$ such that:

$$\begin{aligned} & \hat{\lambda}_s = \max \lambda \\ \text{s.t:} \quad & ||(\gamma_{ik} + \boldsymbol{\beta}_i + \mathbf{t}_{ik}\alpha) + \lambda(d\gamma_{ik} + d\boldsymbol{\beta}_i + \mathbf{t}_{ik}d\alpha)|| \leq 1 \end{aligned}$$

Update stress vectors $\boldsymbol{\gamma}_{ik}, \boldsymbol{\beta}_i$ and shakedown limit α (with a chosen parameter τ: $0 < \tau \leq 1$):

$$\begin{cases} \boldsymbol{\gamma}_{ik} = \boldsymbol{\gamma}_{ik} + \tau\hat{\lambda}_s d\boldsymbol{\gamma}_{ik} \\ \boldsymbol{\beta}_i = \boldsymbol{\beta}_i + \tau\hat{\lambda}_s d\boldsymbol{\beta}_i \\ \alpha = \alpha + \tau\hat{\lambda}_s d\alpha \end{cases}$$

6) Check the convergence criteria: if they are all satisfied then stop, otherwise repeat steps 2-5.

Theoretically, the algorithm may fail due to some reasons such that unappreciated initialization step, or failure in computing the matrix inversion $\hat{\mathbf{S}}^{-1}$. Regardless of these possible numerical obstacles, we can show that the algorithm converges to a solution set $(\bar{\mathbf{q}}, \bar{\mathbf{e}}\bar{\alpha})$. The proof will not be presented here due to the limited space. Indeed to our calculating experiences, a very satisfying convergence is always obtained.

As noted before, limit analysis is a special case of shakedown when the structure is loaded with only one monotonic load, i.e. $[\mu_0, \mu_0]P_0$, thus the above algorithm is also expected to give accurate solution in limit analysis. Numerical examples hereafter shows that such requirement is fairly satisfied.

6 Numerical applications

Some applications to extensive structures are reported elsewhere, see for instant [30],[27]. Special applications to cracked structures and to pipe structures are referred to [27], [32] and [31], [33], [35]. In the present report, we present some problems in the LISA project. Shakedown analysis with temperature dependent yield stress concerns some pipes and pressure vessels. These premier results are discussed to give a general guidance for designers

6.1 Plate with a centered hole under traction

Due to the symmetry (see Fig 6.1), only one quarter of the structure is discretized with quadratic finite elements. Both plane stress and plane strain states are considered. The limit load is represented by limit multiplier defined by (6.1) :

$$\alpha_L = \frac{\sigma_L}{\sigma_y} \tag{6.1}$$

Where σ_L is the limit traction; σ_y is the yield limit of the material.

It is seen in Table 6.1 that accurate solutions may be obtained by using very coarse element meshes. For example in comparison with exact solution, the error is of 3.6% by using only 2 elements. The error is already reduced to 0.6% with only 16 elements. This show high efficiency of the present method

Table 6.1: Limit load multiplier in the case of D/L=0.2, von Mises criterion

Number of elements	2	16	56	100	Reference
Plane stress	0.829	0.805	0.8025	0.8022	0.8 *[1]
Plane strain	0.935	0.9309	0.9256	0.9277	0.924 *[2]

*1) The exact analytic solution of [9]

*2) Simple lower bound estimation as: $0.8 \times (2/\sqrt{3})$

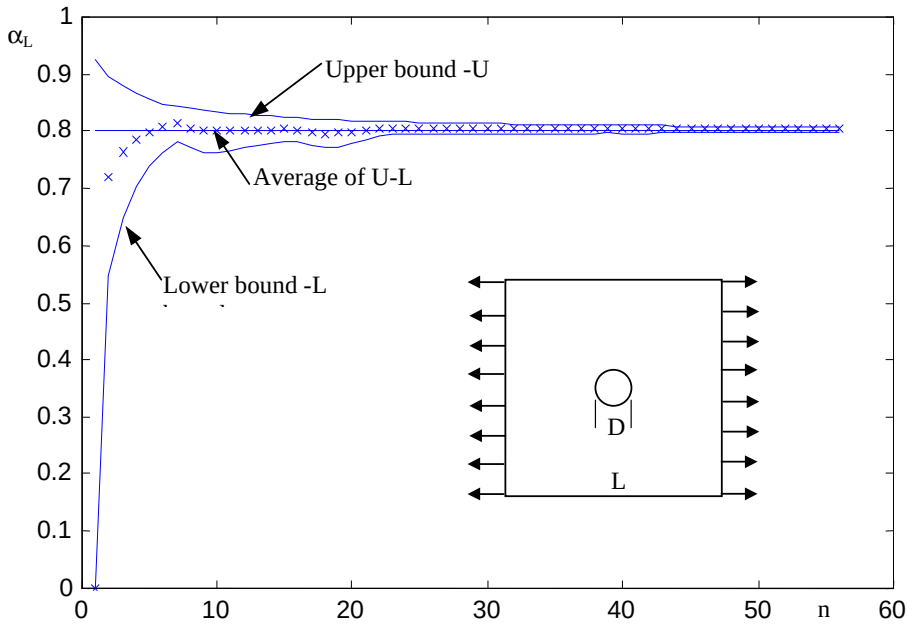

Figure 6.1: The convergence of upper and lower bound limit load solution; D/L=0.2; plane stress (Newton-Raphson method)

In order to show the convergence of the solutions for both upper bound and lower bound by the presented direct iteration method, we show evolution of the results (56 elements) with

iteration in Fig. 6.1, where the average values of the upper bound and lower bound and the exact solution (0.8) are presented. It is clear that the upper bound decreases monotonically with iteration n. On the other hand, the lower bound increases, although it is not strictly monotonic, with iteration n. The convergence is obtained with a finite iteration depending on the chosen calculating precision (generally 20-50 iterations for a precision of 1%). If we take the average value of the upper bound and lower bound as approximation of the solution, we can obtain a good precision with less iteration. For example, the average solution has precision of 1% after only 4 iterations. Note that by this method, each iteration is equivalent to a linear-elastic-like calculation. In order to estimate the convergence of the methods when using a refined element mesh, we have tested this problem with 3000 quadratic elements (9221 nodes, 18240 d.o.f) by the direct iteration method (section 3.1) and Newton-penalty optimization method (section 3.2).

6.2 Limit pressure of a grooved cylinder

A complete description of the problem was reported in [27]: a pressurized tube with a circumferential defect. Axisymetrical quadratic elements are used for discretization. We present the results by both direct iteration method and Newton-penalty method in Fig. 6.2.

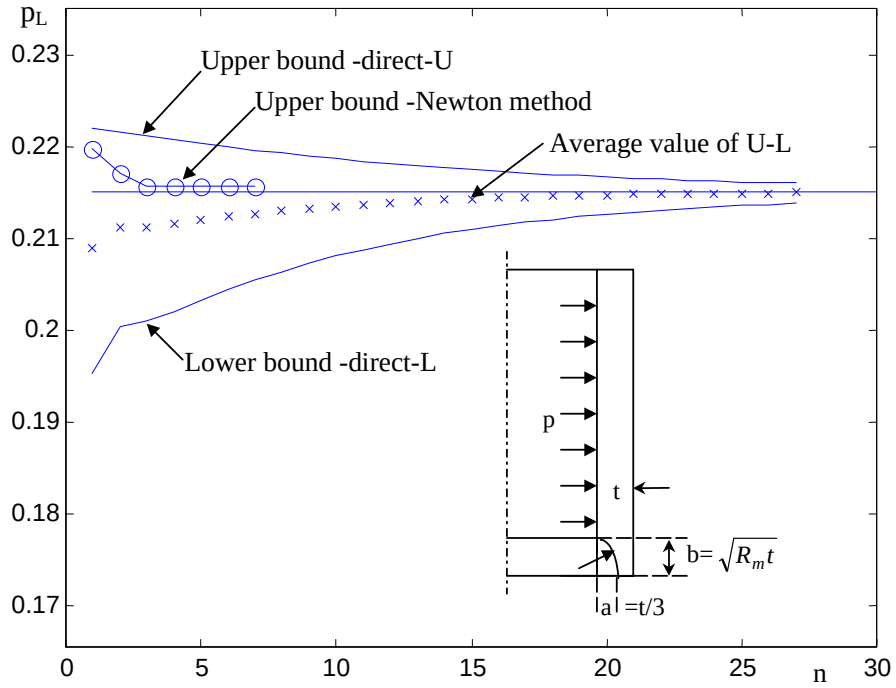

Figure 6.2: Limit bending moment of a pipe under dead pressure and axial force ($R_m = 5t$)

It appears that Newton-penalty method shows high efficiency. Only 3 iterations is needed to give a converge solution. By the direct iteration method, both upper bound and lower bound solution converge to an almost same value. If we take the average value of lower bound and upper bound as solution, we have a good precision of 1% after 7 iterations.

6.3 Torispherical vessel head under internal pressure

Fig 6.3 gives geometry and elastic stress field with a simple finite element mesh. In the present limit analysis, two different lengths of cylinder are calculated in order to investigate their influence of the limit pressure. Four finite element meshes are used for the numerical comparison. The limit analysis results are summarized in Table 6.2.

Table 6.2: Limit pressure of the vessel head (σ_y=100 MPa).

Length of cylinder L	0.1 R		0.3 R		Approx. by sphere solution
No. of elements	34	136	46	168	
Limit pressure [MPa]	3.931	3.929	3.942	3.905	4.0

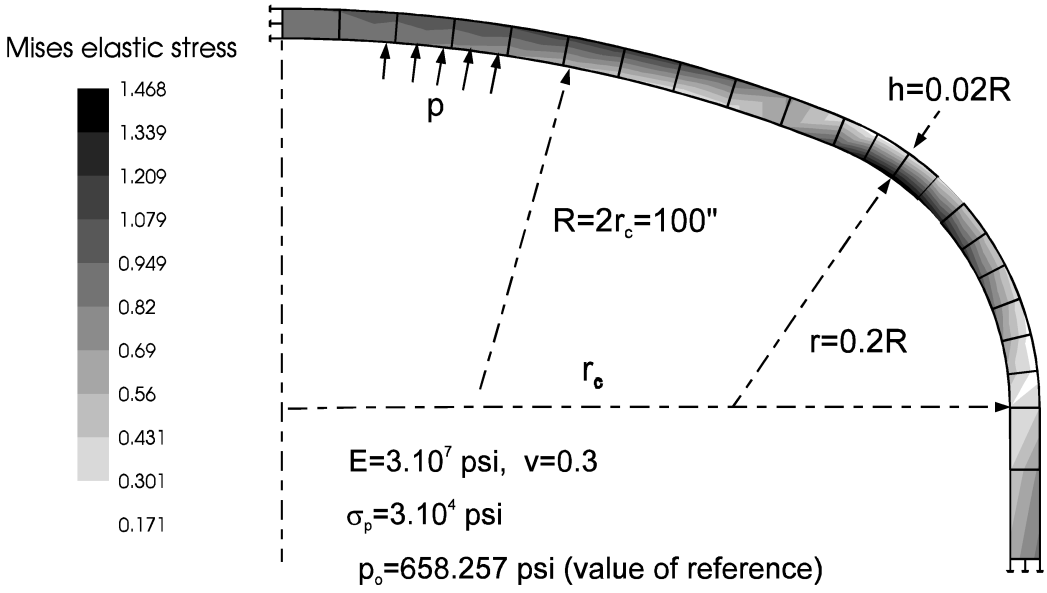

Figure 6.3: Torispherical vessel head under internal pressure, finite element meshing and fictitious elastic stress field (note: R and r are mean radius)

Remarks

1) We have not got the exact analytic solution for this problem. However, we could give an estimation. As the structure is constructed of three part (cylindrical shell, one part of sphere and one par of spherical ring), limit pressure of the whole structure should

approach to the minimum of the limit pressure of the three one separately. In the present case, it is the sphere that has the smallest limit pressure as $P_l = 4$ MPa. However, from the numerical results, it seems that the deformation of spherical ring causes a bending effect in the part of sphere and consequently it causes a non-uniform stress distribution. So the limit pressure of the sphere is reduced a little (about 2%).

2) The length of cylinder don't have obvious effect on the limit pressure of the structure, because the cylinder is far from the initial collapse region.

3) The choice of Gauss points is proved to have certain effect on the limit load calculation. For example, using Gauss points as 4×4 will increase a little the limit pressure solution. However in our upper bound method, using Gauss points as 2×2 is proved to have a stable and better precision in most situations.

4) For 1% precision, the calculation by the direct iteration method takes about 8-15 iterations for the upper bound solution (but it needs about 40 iteration for the lower bound). It takes a fewer iterations (about 5-10 iterations) by using the Newton-penalty method.

6.4 Shakedown limit of straight pipe under internal pressure and axial thermal load

Now we consider shakedown of structures involving thermal loads. Particularly we will take into account the effect of temperature-dependence of the yield stress on shakedown solution. As illustrative examples, the data of a kind of 316L(N) steel will be used in the following calculations. For the numerical convenience, we write the yield stress in the following explicit form by fitting the material data (see Fig. 6.4):

$$\sigma_y^t = 230.65 - 0.5599T + 0.00096T^2 - 6 \times 10^{-7}T^3(\text{MPa}) \tag{6.2}$$

where T denotes temperature. It should be pointed out that due to the convexity of curve $\sigma_y^t(T)$, the present method gives only an approximate estimation instead of strict upper bound solutions (see discussion in section 1.3).

As shown in Fig 6.5, a cylindrical pipe with thickness h and mean radius R is subjected to a constant (or variable) internal pressure p and a uniformly distributed temperature T which varies within $[T_0, T_0 + \Delta T]$. Its two ends are fixed but the radial extension is allowed. Without considering the possible buckling failure, the shakedown limit can be presented as follows [40].

$$3\left(\frac{p}{p_l}\right)^2 + \left(\frac{T}{T_l}\right)^2 = 4 \tag{6.3a}$$

where

$$p_l = \frac{\sigma_y h}{R}, \quad T_l = \frac{\sigma_y}{\alpha_t E} \tag{6.3b}$$

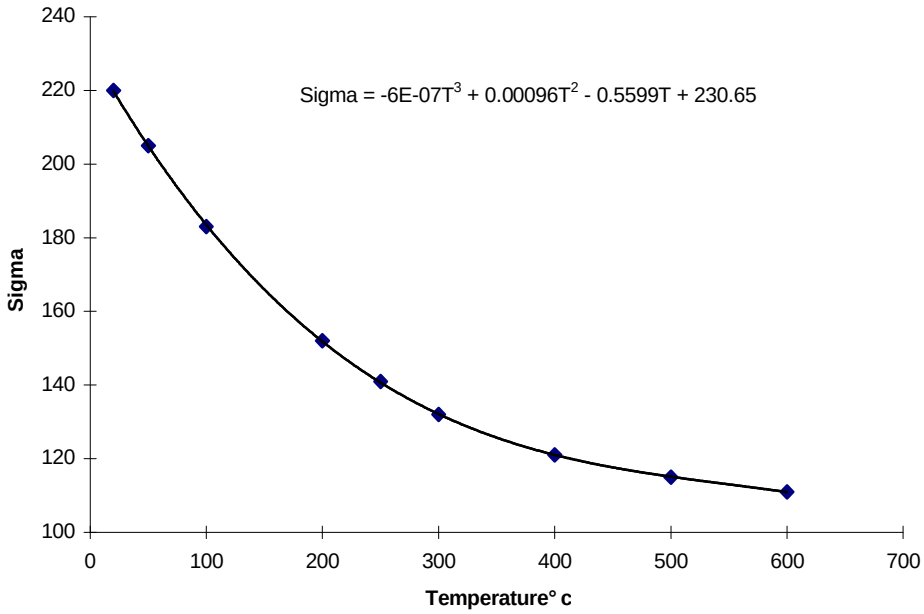

Figure 6.4: Yield limit of the material depending on temperature

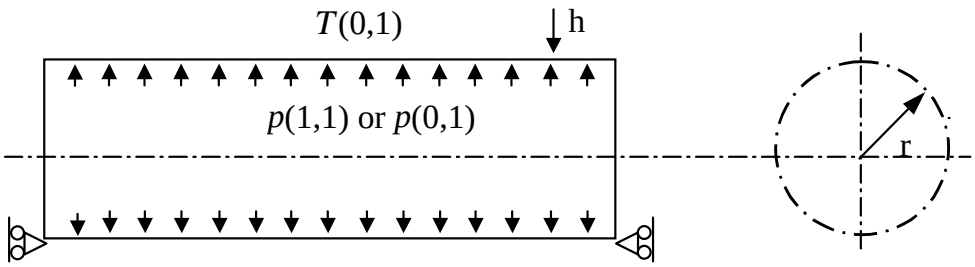

Figure 6.5: Cylindrical shell under internal pressure and temperature variation

Two kinds of finite elements (axisymmetric solid elements and pipe elements, Fig. 6.6), are applied to take a comparison. Three elements are placed along axial direction.

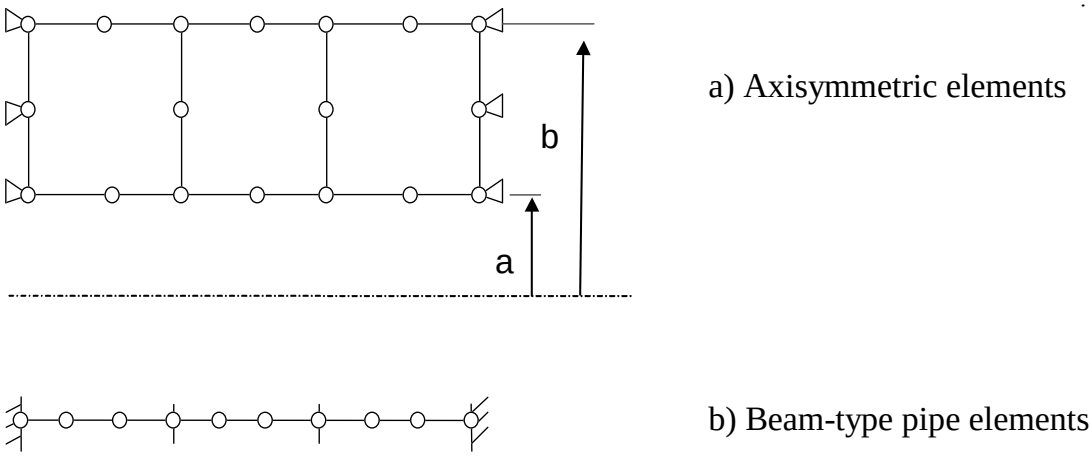

Figure 6.6: Finite element meshes for a cylindrical pipe

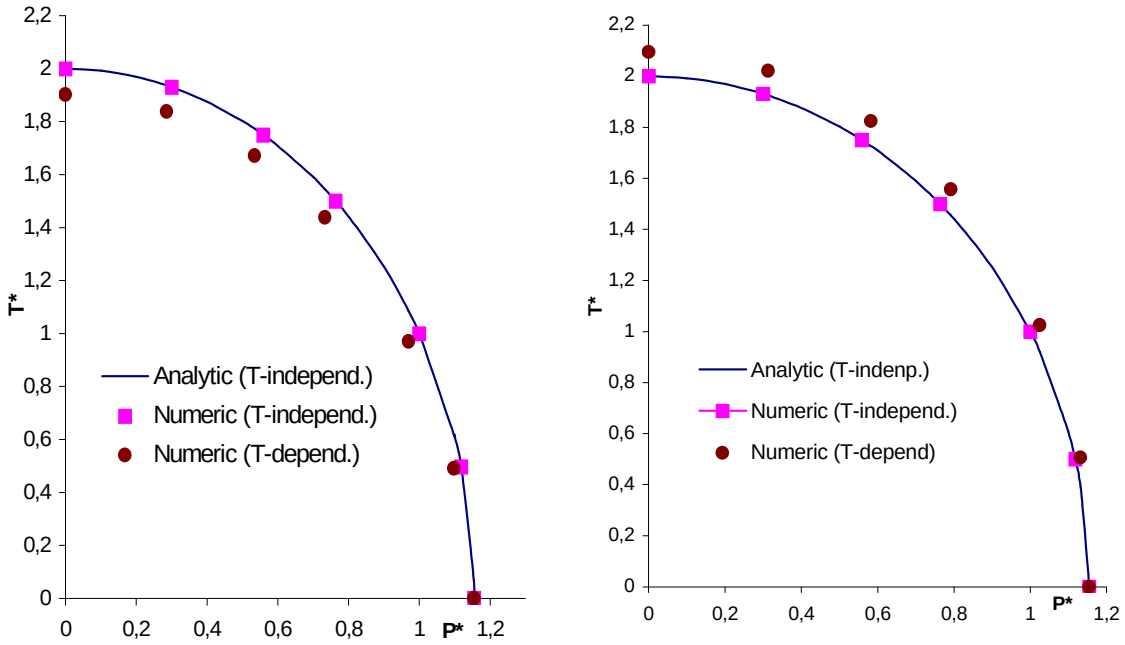

Figure 6.7: Shakedown limit curve ($P^* = p/p_l$; $T^* = T/T_l$)

Note: when considering $\sigma_y^t(T)$ as temperature-dependent: The analytic calculations use (a) σ_y corresponding to the lowest T; (b) σ_y corresponding to the highest T

First we consider the yield limit T-independent. Numerical tests using both USL and

SSL methods give almost same results that are in excellent agreement with analytic one (6.3a), as shown in Fig. 6.7. Same results are obtained when the internal pressure varies between p(0,1). It is clear that incremental plasticity happens only when $p$attains its maximum value. When considering the yield limit T-dependent, the results by USL method is shown in Fig 6.7(a) and 6.7(b), which show the difference due to the different choice of the constant yield stress of the material in the analytic calculation. It seems that when using average yield stress corresponding to the mean temperature, a better agreement between analytical and numerical solutions could be obtained. However for safe consideration, the lowest yield limit of material corresponding to the highest temperature is recommended to be used in engineering practice.

6.5 A thick-walled sphere under radial thermal loading and internal pressure

A thick-walled sphere subjected to radial thermal loading T and internal pressure p, varying independently. The distribution of T is described by (6.4). Owing to the central symmetry, only one-fourth of the sphere is modelled by axisymmetric quadratic finite elements.

$$T = T_0 \frac{b/r - 1}{k - 1} \tag{6.4}$$

where $k = b/a = 2.5(a, b$ are respectively the internal and external radii of the sphere. The load domain may be described by $T \subset (0, T_{max})$ and $p \subset (0, 1)p_{max}$ or $p \subset (1, 1)p_{max}$.

The analytic solution of shakedown limit was reported in [10]. The comparisons between analytic and numerical results of shakedown are represented in Bree diagram, Fig. 6.8-6.9.

- Incremental limit

$$\frac{p_0}{p_l} + \frac{T_0}{T_l} = 1 \tag{6.5a}$$

where

$$p_l = 2\sigma_y \ln k \tag{6.5b}$$

$$T_l = \frac{6(1-\nu)\sigma_y}{\alpha_t E} \frac{(k-1)(k^2+k+1)\ln k}{\frac{2}{\sqrt{3}}(k^2+k+1)^{3/2} - 3(k^2+k)} \tag{6.5c}$$

- Alternating plasticity limit

$$\frac{p_0}{p_f} + \frac{T_0}{T_f} = 1 \tag{6.6a}$$

where

$$p_f = \frac{4\sigma_y}{3}(1 - \frac{1}{k^3}) \tag{6.6b}$$

$$T_f = \frac{4(1-\nu)\sigma_y}{\alpha_t E}\frac{k^2+k+1}{k+2k^2} \tag{6.6c}$$

We begin shakedown analysis by considering the yield limit of material temperature-independent, and taking its minimum value at the highest temperature. The numerical results are in excellent agreement with analytic solutions despite of a very coarse FE mesh used. Bree diagram of Fig. 6.8 is subdivided into some sub-regions that correspond to the different modes of deformation:

1) Completely elastic behaviour in regions A;
2) Shakedown happens in region B if internal pressure varies arbitrarily or in (B+C) if the pressure is constant. In this region, the structure plastified in initial loading cycles will retune to elasticity. So the structure may be considered safe;
3) Alternating plasticity in region D (or D+C if p varies); Possibly the structure will fail by fatigue crack in internal skin of sphere after finite time or loading cycles;
4) Incremental plasticity in region E. The structure fails finally due to excess radial plastic deformation.
5) Beyond these regions, the structure will fail in a possibly mixed mode .

Now we consider the yield limit of material temperature-dependent. The results are represented by the solid points and the dashed line in Fig. 6.8. As shown, the present results are higher than the previous ones obtained with constant yield stress. This means that if we take the lowest yield stress at the highest temperature, the obtained shakedown limits are generally on the side of safety.

In order to give a better analytic prediction, we suggest using the mean yield stress of material at a mean temperature. By this approximation, the comparison between analytic and numerical results is presented in Fig. 6.9. We see that the numerical results (with temperature dependent yield limit) agree well with the modified analytic solution. The difference in incremental limit calculation may be due to the fact that the temperature distribution is really non-linear along the thickness while it is taken simply as linear average in the modification of analytic solution.

For practical application, we need still to discuss another problem: which mean temperature should be taken in theoretical prediction? Let us consider the following example of temperature cycle: (denote T_i and T_o as internal wall and external wall temperature of the sphere, respectively).

Time 1: $T_i = 20°C, T_o = 20°C, \Delta T_1 = 0°C$

Time 2: $T_i = 500°C, T_o = 300°C, \Delta T_1 = 200°C$

Consider separately the incremental plasticity and alternating plasticity. For first one, the failure behaves as uniform radial expansion resulting from the interaction of pressure and

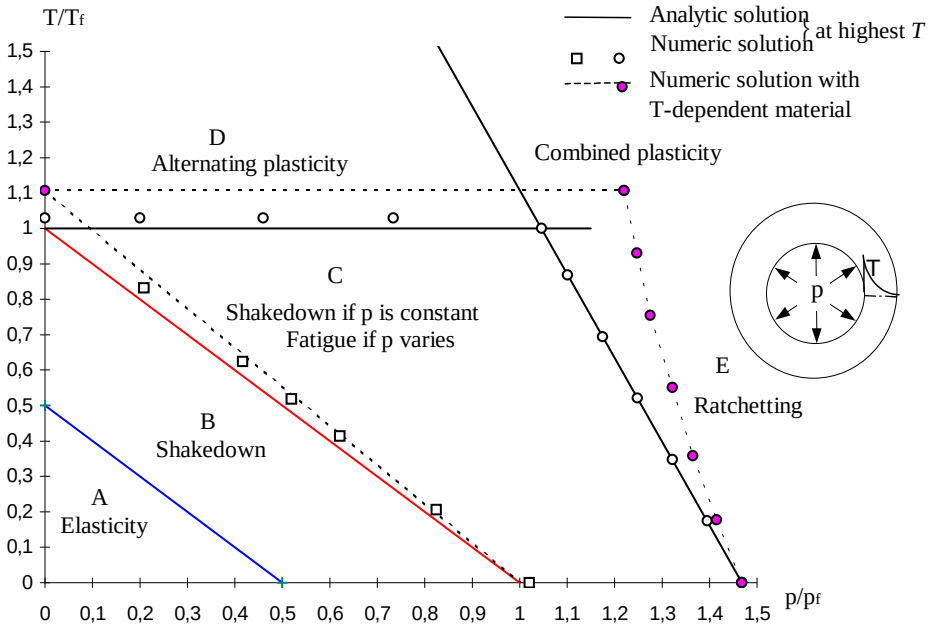

Figure 6.8: Bree diagram of sphere with temperature-independent or -dependent yield limit p_f : (6.6b), T_f : (6.6c), using the smallest yield limit (at highest temperature) in the prediction

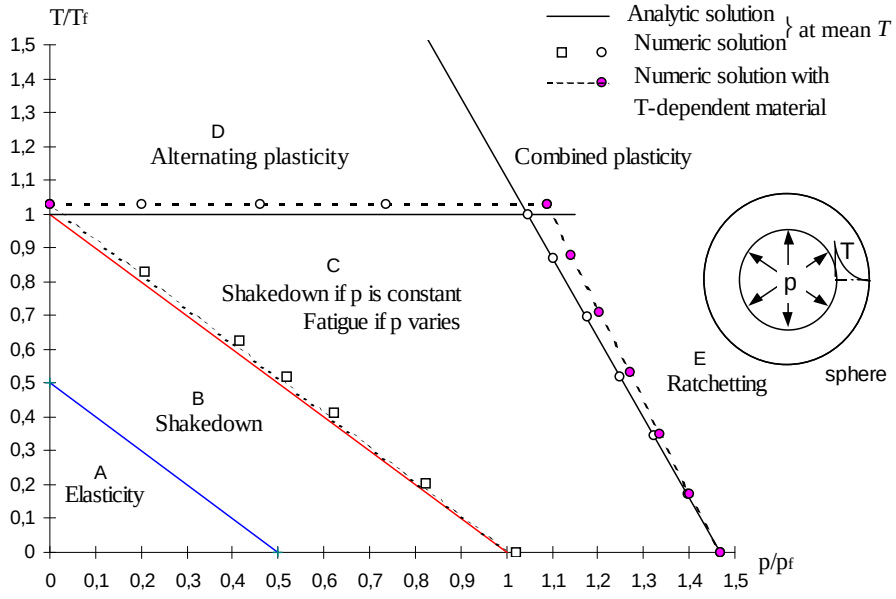

Figure 6.9: Bree diagram of sphere with temperature-independent or -dependent yield limit p_f : (6.6b), T_f : (6.6c), using the mean yield limit of material in the prediction

temperature along the thickness. So generally we should take the mean temperature along the thickness as $400°C$. By contrary, the plastic fatigue failure happens locally at internal wall. Its load limit is determined uniquely by the stress change at internal wall. So we could theoretically take the mean temperature as $260°C$. However, the practical situation may be quite complex. There is also the effect of elastic property ($E\alpha_t$) that needs to be considered. It may be appreciate to take a conservative choice of $400°C$. It appears that we might always take the lowest yield limit at highest temperature to give a safe prediction in most cases.

6.6 Limit and shakedown analysis by new dual method

In this section, we present some new applications to show high efficiency of the recently developed dual method presented in section 5. Firstly we reconsider the example with which limit analysis has been presented in section 6.1. Then we present a 3D shakedown analysis: a structure to compare with the results of other partners.

6.6.1 Plate with a centered hole under traction

A square plate with central circular hole is subjected to two loads $p_1$and p_2 varying independently. In the present analysis, the plate is modelled by 800 plane quadrilateral 8-node elements as shown in Fig. 6.10. The analytical solution of limit load is known to be exact for $p_1 \neq 0,\ p_2 = 0$ with $0 < R/L \leq 0.204$ since in this range the lower bound and upper bound coincide: $p_{\lim} = (1 - R/L)\sigma_y$. As example, the exact limit load in the case of $R/L = 0.2$ is $p_{lim} = 0.8\sigma_y$ (σ_y is the yield stress). Our corresponding numerical values obtained in this case are $0.79924\sigma_y$ for lower bound and $0.80038\sigma_y$ for upper bound. Based on an elastic calculation, the alternative shakedown limit can be estimated as indicated section 1.4 while numerical results obtained by the dual algorithm in section 5 represent the minimum between alternative limit and incremental limit. For $R/L = 0.2$, $p_1 \neq 0,\ p_2 = 0$ alternative limit based on elastic analysis is $0.59947\sigma_y$ while present method gives $0.59947\sigma_y$ as lower bound and $0.59949\sigma_y$ as upper bound (Fig. 6.11)

Exact values of limit load are also known for $p_1 = p, p_2 = p, p \neq 0$ in the range $0.483 < R/L \leq 1$ where analytical lower bound coincides with upper one:

$$p_{lim} = \frac{2}{\sqrt{3}} \sin\left(\alpha - \frac{\pi}{6}\right) \sigma_y, \frac{1}{(R/L)^2} = \frac{\sqrt{3}}{2\cos(\alpha)} e^{\sqrt{3}(\alpha - \frac{\pi}{6})}$$

Numerical results for limit analysis and shakedown show an excellent precision and very rapid convergence. In limit analysis, both numerical lower and upper bound tend to analytical lower bound. This fact suggests that analytical lower bound is a better approximation.

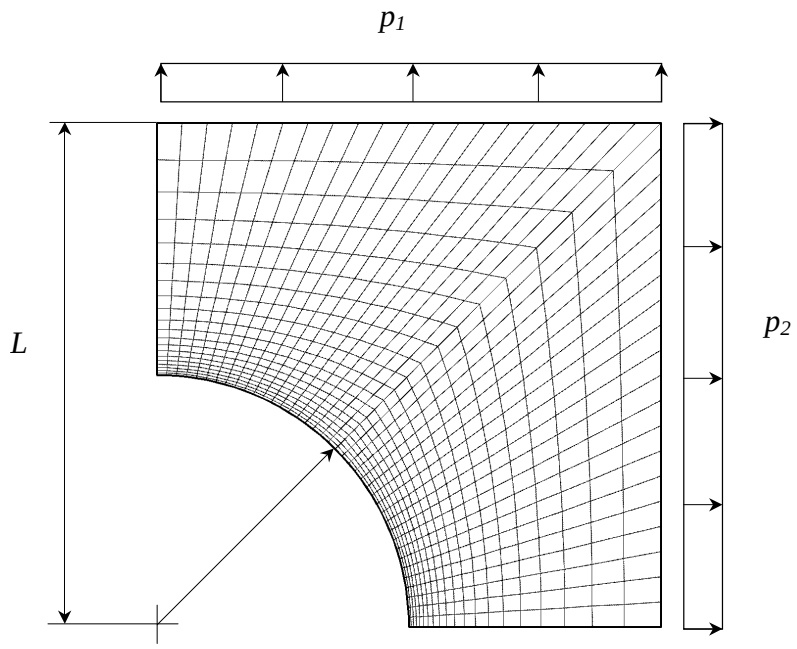

Figure 6.10: FE model

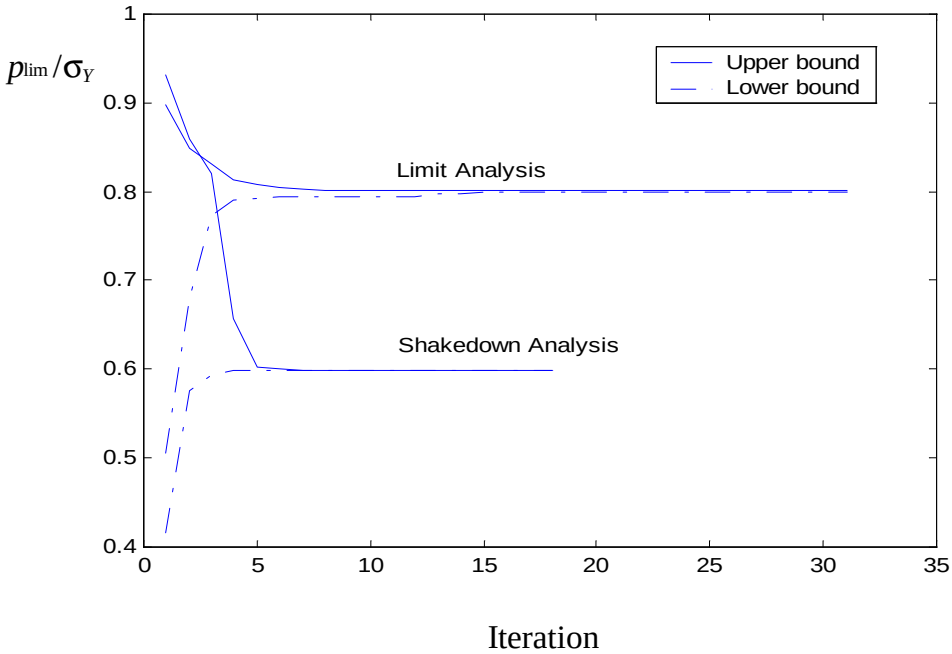

Figure 6.11: Limit and shakedown analyses ($R/L = 0.2, p_1 \neq 0, p_2 = 0$)

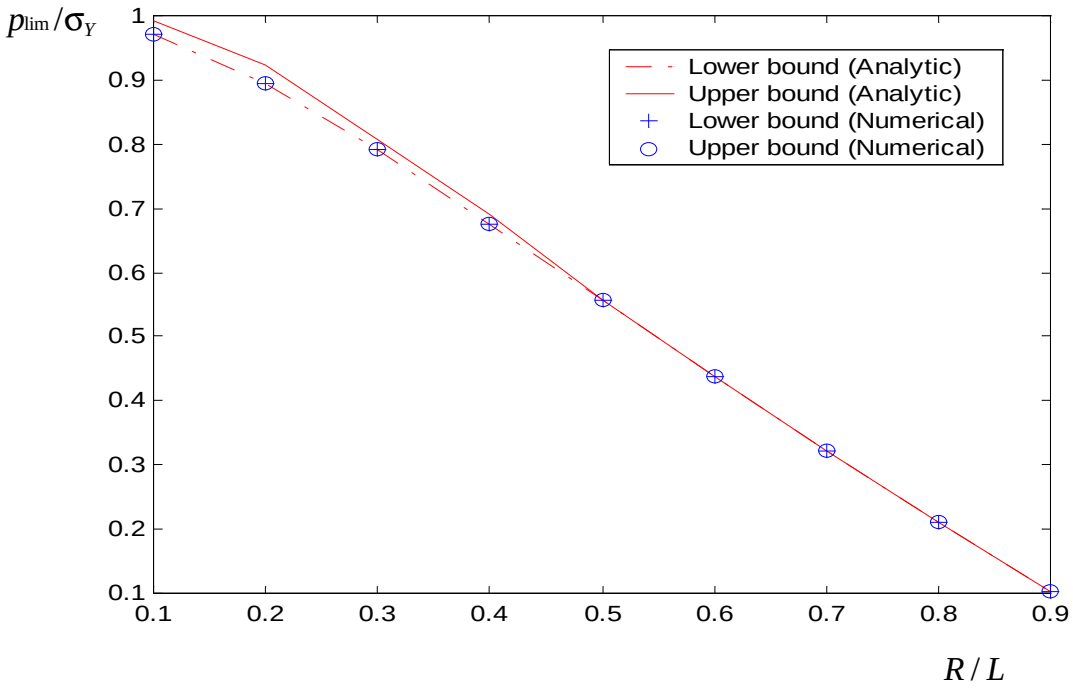

Figure 6.12: Limit analysis ($p_1 = p_2$)

Table 6.3: Shakedown analysis ($||p_1|| = ||p_2||$, varying independently)

R/L	Alternative limit (From Elastic Analysis)	Lower bound (Numerical)	Upper bound (Numerical)
0.1	0.49082	0.49082	0.49086
0.2	0.43384	0.43384	0.43390
0.3	0.36128	0.36128	0.36131
0.4	0.27635	0.27635	0.27638
0.5	0.19442	0.19442	0.19445
0.6	0.12360	0.12360	0.12364
0.7	0.06763	0.06763	0.06765
0.8	0.02903	0.02903	0.02905
0.9	0.00709	0.00709	0.00710

In shakedown analysis, the results are really two time the elastic limits. This means here the dominance of alternative plasticity mechanism: the structure may fail due to a plastic fatigue phenomenon. All tests are carried out with 2×2 Gauss points. The penalty and other parameters are $c = 10^8$, $\tau = 0.9$, $\varepsilon = 10^{-10}$.

6.6.2 Pipe-junction under internal pressure

The problem has been examined by Staat & Heitzer (1997) [26] who used 125 hexahedron elements (27 nodes/element) for this pipe junction. One quarter of the structure is modelled because of its symmetries. In our analysis, the FEM mesh is presented in Fig. 6.13a: it contains 720 solid 20-node hexahedron elements. The structure is subjected to internal pressure p varying within $[0, p_0]$. Numerical integrations are realized with $2 \times 2 \times 2$ Gauss points. The penalty and other parameters are $c = 10^8$, $\tau = 0.9$, $\varepsilon = 10^{-10}$.

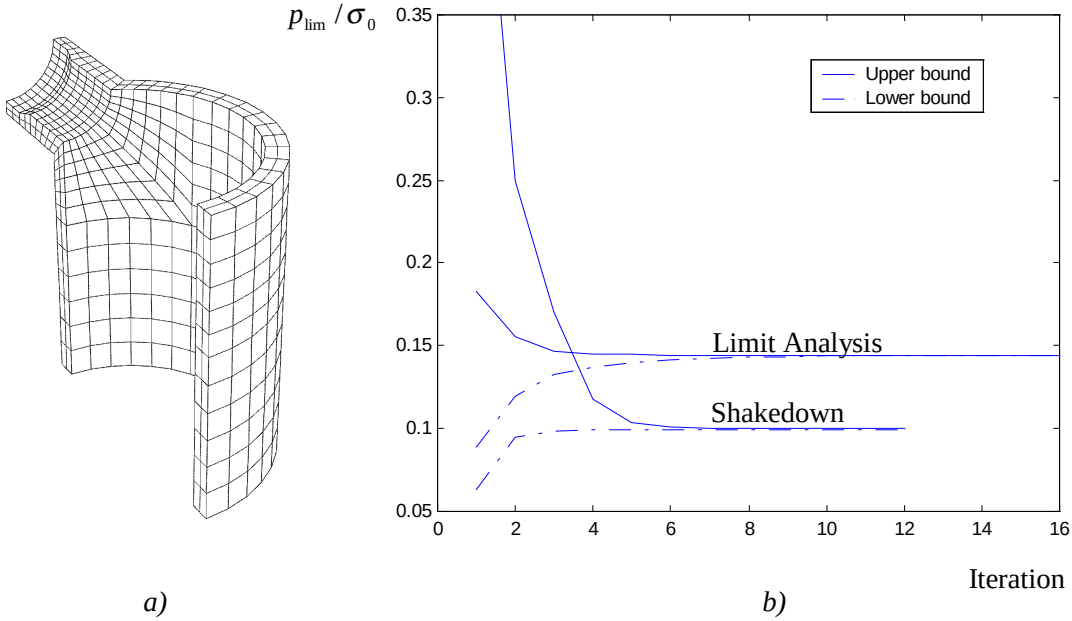

Figure 6.13: FE mesh and numerical results

Numerical analysis leads to a collapse pressure of $0.14433\sigma_y$ (upper bound) and $0.14429\sigma_y$ (lower bound) compared with lower bound of $0.134\sigma_y$ obtained by Staat & Heitzer [26]. Shakedown analysis gives $0.11044\sigma_y$ (upper bound) and $0.10983\sigma_y$ (lower bound) compared with lower bound of $0.0952\sigma_y$ by Staat & Heitzer. The alternative shakedown calculated based on elastic solution gives $0.10983\sigma_y$ by the present FE mesh. Note that in this test, the structure fails due to alternative shakedown, therefore shakedown load factor can be evaluated more precisely if we use a set of $3 \times 3 \times 3$ Gauss points in numerical integration: shakedown analysis in this case gives $0.10031\sigma_y$ (upper bound) and

$0.099388\sigma_y$ (lower bound) while alternative shakedown calculated based on elastic solution leads to $0.099388\sigma_y$. The results depicted in Fig. 6.13b are obtained for shakedown with $3 \times 3 \times 3$ Gauss points and for limit analysis with $2 \times 2 \times 2$ Gauss points. The convergence by the present dual method is rapidly attained in few iterations (note that each iteration is approximately equivalent to a linear-elastic-like calculation)

7 General remarks and conclusions

In this report, a general kinematical limit and shakedown formulation is presented. The advantages of the developed methods may be summarized as follows

The methods allow us to use any displacement-based finite elements. In fact, only some principal data from finite element solution such that the strain matrix, elemental information ... are needed for the present limit and shakedown formulation. So any existing finite element code may be used to implement the present methods.

The non-linear programming procedure is transformed into a series of linear-elastic-like calculations. So there is not a practical calculating-size limitation if a commercial finite element code is used for the implementation.

Several different limit and shakedown computational methods are available in calculating code ELSA developed at ULg. This provides alternative calculating means. A numerical comparison is easy to be performed.

In most situations, upper bound and lower bound solutions are given in pair at every iteration step of calculation and they converge to same limit. Specially the lower bound is obtained as a by-product of the upper bound calculation with little calculating effort. The numerical tests show a satisfactory precision, and the calculating efficiency is much higher than the usual elastic plastic calculation.

Two inadaptation factors may be separately identified, which is very meaningful in engineering practice. Specially, the incremental plasticity analysis has been transformed into an equivalent limit analysis.

The temperature dependence of the yield limit of the material is included numerically in shakedown formulation. Its influence is evaluated for some simple numerical examples.

The developed dual shakedown analysis shows specially its efficiency. This method is very promoting for further development.

The developed methods are implemented principally in an independent finite element code ELSA at ULg. Although the methods are already well verified by benchmark tests, it is strongly expected to implement them into a commercial FE code to improve the applying efficiency.

We note also that some other developments at ULg concerning the LISA project, such that a special pipe finite element, limit and shakedown analysis by equilibrium analysis of

backstress field (also known as Zarka's method) are not presented in the present report. They are referred, respectively, to [31] and [34].

Acknowledgement
The research has been funded by the European Commission as part of the Brite–EuRam III project LISA: FEM–Based Limit and Shakedown Analysis for Design and Integrity Assessment in European Industry (Project N°: BE 97–4547, Contract N°: BRPR–CT97–0595).

Bibliography

[1] Andersen K.D.: An efficient Newton barrier method for minimizing a sum of Euclidean norms. *SIAM J. Optimization,* **6** (1996), 74-95.

[2] Andersen K.D., Christiansen E., Overton A.: Computing limit loads by minimizing a sum of norms. *SIAM J. SIAM J. Sci. Comput.,* **19** (1998), 1046-1062.

[3] Andersen K.D., Christiansen E., Conn A.R., Overton A.: An efficient primal-dual interior-point method for minimizing a sum of Euclidean norms. *SIAM J. Sci. Comput.,* **22** (2000), 243-262.

[4] Bazaraa M.S, Sherali H.D., Shetty C.M.: Nonlinear Programming, Theory and Algorithms, (second edition), John Wiley & Sons, Inc., New York, 1993.

[5] Borkowski A., Kleiber M.: On a numerical approach to shakedown analysis of structures. *Computer methods in applied mechanics and engineering,* **22**(1980), 110-119.

[6] Borino G & Polizzotto C: Shakedown theorems for a class of materials with temperature-dependent yield stress, in Owen DRJ, Oñate E & Hinton E (ed.) *Computational Plasticity,* CIMNE, Barcelona, Part 1, 1997, 475-480.

[7] Carvelli V., Cen Z.Z., Liu Y., Maier G.: Shakedown analysis of defective pressure vessels by a kinematic approach. *Archive of Applied Mechanics*, **69** (1999) 751-764.

[8] Gaudrat V.F.: A Newton type algorithm for plastic limit analysis, *Comput. Methods Appl. Mech. Engrg.*, **88** (1991), 207-224.

[9] Gaydon F.A., McCrum A.W.: A theoretical investigation on the yield point loading of a square plate with a central circular hole, *Int. J. Solids Structures,* **2** (1954), 156-169.

[10] Gokhfeld D.A., Cherniavsky O.F.: *Limit analysis of structures at thermal cycling*, Sijthoff & Noordhoff, The Netherlands, 1980.

[11] Huh H., W.H. Yang: A general algorithm for limit solutions of plane stress problems, *Int. J. Solids Structures*, **28** (1991), 727-738.

[12] Hutula D.N.: Finite element limit analysis of two-dimensional plane structure, *Proc. Meeting of ASME- Limit analysis using finite elements,* New York, 1976, 35-51.

[13] Jiang G.L.: Non linear finite element formulation of kinematic limit analysis, *Int. J. Num. Meth. Engng.* **38** (1995), 2775-2807.

[14] Karadeniz S., Ponter A.R.S.: A linear programming upper bound approach to the shakedown limit of thin shells subjected to variable thermal loading, *Journal of strain analysis* **19** (1984), 221-230.

[15] V.D. Khoi: *Dual Limit and Shakedown Analysis of Structures*, PhD Thesis, Université de Liège, Belgium, 2001.

[16] Khoi V.D., Yan A.M., Nguyen D.H.: A new dual shakedown analysis of structures. *ECCM-2001 European conference on computational mechanics*. June 26-29, 2001, Cracow, Poland.

[17] Koiter W.T.: General theorems for elastic plastic solids, in Sneddon I. N. & Hill R.(eds.): *Progress in Solid Mechanics,* Nord-Holland, Amsterdam, 1960, 165-221.

[18] König J.A., Kleiber M.: On a new method of shakedown analysis, *Bull. Acad. Pol. Sci., Sér. Sci. Techn.* **4** (1978), 165-171.

[19] König J.A.: On the incremental collapse criterion accounting for temperature dependence of yield point stress. *Archives of Mechanics,***31**(1979), 317-325.

[20] König J.A.: Shakedown analysis in the case of loading and temperature variation. *Journal de Méchanique Théoretique et Appliquee*, **34** (1982); No. Spécial, 99-108.

[21] König J.A.: *Shakedown of elastic-plastic structure,* Elsevier & PWN-Polish Scientific Publishers, 1987.

[22] Liu Y.H., Cen Z.Z., Xu B.Y.: A numerical method for plastic limit analysis of 3-D structures, *Int. J. Solids Structures* **32** (1995), 1645-1658.

[23] Murtagh B. A., Saunders M. A. (1987): "MINOS 5.1 - User's Guide," *Technical Report SOL 83-20R,* Stanford University.

[24] Nguyen-Dang H., Morelle P.: Plastic shakedown analysis, in Smith D.L. (ed.), *Mathematical programming methods in structural plasticity,* Springer-Verlag Wien-New York, 1990,183-205.

[25] Save M., Jospin R. J. & Nguyen D. H.: Limit loads of pipe elbows. *Final report, Contract RA1-0134-B.* See also *Nuclear science and technology,* Report EUR 15696 EN, European Commission, 1995.

[26] Staat M., Heitzer M.: Limit and shakedown analysis for plastic safety of complex structures. *Transactions of the 14th International Conference on Structural Mechanics in Reactor Technology (SMiRT 14*), Vol. B, Lyon, France, August 17-22, 1997, B02/2.

[27] Staat M., Heitzer M., Yan A.M., Khoi V.D., Nguyen-Dang H., Voldoire F., Labousse A.: Limit analysis of defects. Berichte des Forschungszentrums Jülich, **Jül-3746** (2000).

[28] F. Voldoire: Regularised limit analysis and applications to the load carrying capacities of mechanical components. CD-ROM Proceedings of the European Congress on Computational Methods in Applied Sciences and Engineering, ECCOMAS 2000, Barcelona, Spain (2000), paper 643, 20 pages.

[29] Yan A.M., Nguyen-Dang H: Shakedown of structures by improved Koiter's theorem, *Proceeding of 4th National Congress on Theoretical & Applied Mechanics*, Leuven, 22-23 May, 1997, 449-452.

[30] Yan A.M.: Contribution to the direct limit state analysis of plastified and cracked structures, PhD thesis (1997), Collection des Publications de la Faculté des Scinces Appliquées n ° 190, 1999.

[31] Yan A.M., Jospin R.J., Nguyen-Dang H.: An enhanced pipe elbow element-Application in plastic limit analysis of pipe structures, *Int. J. Num. Meth. Engng.* **46** (1999), 409-431.

[32] Yan A.M., Nguyen-Dang H.: Limit analysis of cracked structures by mathematical programming and finite element technique. *Comput. Mechanics*, **24** (1999), 319-333.

[33] Yan A.M., Nguyen D.H., Gilles Ph.: Practical estimation of the plastic collapse limit of curved pipe subjected to complex loading. *Structural Engineering and Mechanics*, N ° 4, Vol.8, (1999), pp421-438.

[34] Yan A.M., Khoi V.D., Nguyen D. H., Jospin R.J.: Limit load and deformation estimates by equilibrium back stress field analysis. *Proceeding of International colloquium in mechanics of solids, fluids, structures and interactions*, (ed. Nguyen-Dang H. et al.), Nha Trang 2000, Aug. 14-18, pp520-530.

[35] Yan A.M., Nguyen-Dang H.: Direct finite element kinematical approaches in limit and shakedown analysis of shells and elbows, in Weichert D, Maier G. (eds): *Inelastic analysis of structures under variable loads*, Kluwer Academic Publishers (2000), 233-254.

[36] Yan A.M., Nguyen-Dang H.: Kinematical shakedown analysis with temperature-dependent yield stress. *Int. J. Num. Meth. Engng.* **50** (2001), 1145-1168.

[37] Yan A.M., Khoi V.D., Nguyen-Dang H.: Incremental Plasticity limit of structures subjected to variable loading. *EPMESC'VIII - the 8^{th} international conference of enhancement and Promotion of computing methods for engineering and science*, Shanghai. July 25-28, 2001.

[38] Yang W.H.: A variational principle and an algorithm for limit analysis of beams and plates, *Comput. Methods Appl. Mech. Engrg.***33** (1982), 575-582.

[39] Zhang Y.G., Lu M.W.: An algorithm for plastic limit analysis, *Comput. Methods Appl. Mech. Engrg.***126** (1995), 333-341.

[40] Zhang Y.G.: An iteration algorithm for kinematic shakedown analysis, *Comput. Methods Appl. Mech. Engrg.***127** (1995), 217-226.

[41] Zouain N., Herskovits J., Borges L.A., Feijoo R.A.: An iterative algorithm for limit analysis with nonlinear yield functions. *Int. J. Solids Structures,* **30** (10) (1993), 1397-1417.

[42] Zouain N., Silveira J.L.: Bounds to shakedown loads. *Int. J. Solids Structures,* **38** (2001), 2249-2266.

Part IV

Limit analysis by the Norton-Hoff-Friaâ regularizing method

Francois Voldoire

Deptartment of Acoustics and Mechanical Analyses
Direction des Etudes et Recherches, Electricité de France
1 Avenue du Général de Gaulle, F-92141 Clamart Cedex, France

E-mail: Francois.Voldoire@edfgdf.fr

1 Introduction

The aim of the limit analysis is the determination of the admissible loading of a mechanical structure, the geometry of which being fixed, constituted by materials satisfying a strength criterion, for instance a yield stress. We consider the case of combinations of any dead (constant) load and another parametrized by the loading factor, the maximum value of which we are seeking. The objectives of this study are to provide a F.E.M. tool to assess the safety of mechanical components with respect to the risk of plastic collapse, and to get some parameter needed in simplified fracture mechanics methods, like R6. Moreover, the limit analysis is an useful tool for the geomechanical structures design.

After a review of the theoretical formulation and a brief summary of the proposed numerical methods in the literature, we present the kinematical regularized approach (upper bound method) we have chosen, applied to von Mises yield criterion, by the Norton-Hoff-Frémond-Friaâ method, and implemented in the *Code_Aster*® software. It leads to mixed finite continuous elements. The advantage of this regularized formulation is to provide convergence theorems, leading to safe upper bounds associated to an estimated lower bound. This formulation has been implemented into the general purpose finite element software Code_Aster, by introducing a specific constitutive relation and post-processing of the solution. We present the calculation of the numerical solutions of this non linear problem and the post-processing giving estimations of the limit loading factor.

We give some numerical applications on 2D and 3D structures, making some comments on the advantages and drawbacks. We observed that in 2D plane strain situation, this algorithm is not very efficient without adaptive meshing, because the collapse mode present shear bands, hard to represent with continuous velocities fields. Nevertheless, the same method seems to be very efficient in 2D-axisymmetric and 3D situations. Finally, we have made a comparison with a direct analysis of an industrial component (2D-axisymmetric), using an elastoplastic finite strain simulation, to assess if another kind of failure mode (plastic snap-through) can occur. Indeed, the results are corroborated, and it appears that the efficiency of both simulations are quite similar.

2 Theoretical formulation of the limit analysis

2.1 Definition of the limit load

We consider a body occupying the bounded domain V, submitted to surface loads $\alpha\mathbf{p}+\mathbf{p}_0$ on the boundary Γ_f, and body forces $\alpha\mathbf{f}+\mathbf{f}_0$ on V. A distinction is made between the loading $(\mathbf{p},\mathbf{f})$, parametrized by the positive scalar α, and the dead or constant loading $(\mathbf{p}_0,\mathbf{f}_0)$. The homogeneous Dirichlet boundary conditions or perfect connections are applied on the complementary boundary Γ_u of ∂V. Any non zero prescribed displacement nor inelastic initial strain – thermal, plastic…– have no effect on the admissible loading domain. We can refer to [23] for several other useful properties.

The constitutive material is characterized by a strength criterion, expressed by a scalar function of the stresses, negative for any admissible stress. For perfectly plastic material, with von Mises threshold, the criterion reads:

$$\begin{aligned} g(\boldsymbol{\sigma}) &= J(\boldsymbol{\sigma})-\sigma_y=\sqrt{\frac{3}{2}\boldsymbol{\sigma}^D:\boldsymbol{\sigma}^D}-\sigma_y \\ &= \frac{\sqrt{2}}{2}.\sqrt{(\sigma_1-\sigma_2)^2+(\sigma_2-\sigma_3)^2+(\sigma_1-\sigma_3)^2}-\sigma_y \end{aligned} \tag{2.1}$$

$\boldsymbol{\sigma}^D$	is the deviatoric stress tensor,
σ_y	is the strength for uniaxial tensile condition (as a yield stress), eventually depending on the localization in the considered solid,
σ_i	being the principal stresses of the tensor $\boldsymbol{\sigma}$.

This strength criterion being chosen, we are seeking to calculate the limit value of α, called the limit load factor or yield-point load α_{lim}, such as the solid can carry the surface tractions $\alpha_{lim}\mathbf{p}+\mathbf{p}_0$ and the body force $\alpha_{lim}\mathbf{f}+\mathbf{f}_0$.

Strictly speaking, the α_{lim} value is the limit of the potentially supportable loading, but for materials satisfying the Maximal Plastic Work Principle, this value is the true value of the supported loading.

Two approaches are at our disposition for the yield design and limit analysis: the static approach (expressed in stress variables) and the kinematical approach (expressed in velocities variables). Both can be related to a mixed formulation, and lead, after numerical discretization, to bounds of the limit load: a lower bound by the statical approach, an upper bound by the kinematical approach. When both values are the same, the obtained limit load is exact.

2.2 Mixed approach of the limit load

For the given load $(\mathbf{p}, \mathbf{f})$, we define the kinematically admissible and normalized velocities space:

$$\mathcal{V}_a^1 = \left\{ \mathbf{v} \text{ admissible, } \mathbf{v}=\mathbf{0} \text{ on} \partial V_u, \mathcal{L}(\mathbf{v}) = \int_V \mathbf{f} \cdot \mathbf{v} dV + \int_{\partial V_p} \mathbf{p} \cdot \mathbf{v} ds = 1 \right\} \tag{2.2}$$

This normalization corresponds to a unit work rate value of the load $(\mathbf{p}, \mathbf{f})$. The dead load $(\mathbf{p}_0, \mathbf{f}_0)$ work rate is denoted by: $\mathcal{L}_0(\mathbf{v})$. From the strength criterion $g(\boldsymbol{\sigma})$, we define:

- the set of admissible stress tensors: $G_{(\mathrm{x})} = \{\boldsymbol{\sigma}(\mathbf{x}), g(\boldsymbol{\sigma}(\mathbf{x})) \leq 0\}$ ($G_{(\mathrm{x})}$ is convex, as well as g)
- the indicator function: $\Psi_G(\boldsymbol{\sigma}(\mathbf{x})) = \left\{ \begin{array}{cc} 0 & \text{if } \boldsymbol{\sigma}(\mathbf{x}) \in G_{(\mathrm{x})} \\ +\infty & \text{if } \boldsymbol{\sigma}(\mathbf{x}) \notin G_{(\mathrm{x})} \end{array} \right.$
- the support function: $\pi(\dot{\boldsymbol{\varepsilon}}) = \sup_{\sigma \in I\!R^6} [\boldsymbol{\sigma} : \dot{\boldsymbol{\varepsilon}} - \Psi_G(\boldsymbol{\sigma})]$

We call Σ the space of the stress fields $\boldsymbol{\tau}$ on V – whose regularity is such as we can define the internal work rate for any field from $\mathcal{V}_a$. For the sake of simplicity, we do not treat in the following the internal discontinuities surfaces of velocities, lying in the body V. Assume the Lagrangian $\mathcal{S}_m(\mathbf{v}, \boldsymbol{\tau})$ ($\dot{\boldsymbol{\varepsilon}}(\mathbf{v})$ is the velocity strain tensor associated to $\mathbf{v}$), expressing the equilibrium equations and the belonging to the criterion G *via* the indicator function $\Psi_G(\boldsymbol{\tau})$, playing the role of a potential:

$$\mathcal{S}_m(\mathbf{v}, \tau) = \int_V (\boldsymbol{\tau} : \dot{\boldsymbol{\varepsilon}}(\mathbf{v})) - \Psi_G(\boldsymbol{\tau}) \, dV - \mathcal{L}_0(\mathbf{v}) \tag{2.3}$$

The extreme load corresponds to the saddle-point of this Lagrangian (because the maximization in α is included):

$$\alpha_{lim} = \inf_{\mathrm{v} \in \mathcal{V}_a^1} \sup_{\tau \in \Sigma} \mathcal{S}_m(\mathbf{v}, \boldsymbol{\tau}) = \sup_{\tau \in \Sigma} \inf_{\mathrm{v} \in \mathcal{V}_a^1} \mathcal{S}_m(\mathbf{v}, \boldsymbol{\tau}) \tag{2.4}$$

2.3 Statical approach of the limit load (lower bound)

The lower bound approach uses the stress fields defined in the space:

$$\Sigma_a^\alpha = \left\{ \boldsymbol{\tau} \in \Sigma, \mathcal{W}(\mathbf{v}, \boldsymbol{\tau}) = \int_V \boldsymbol{\tau} : \dot{\boldsymbol{\varepsilon}}(\mathbf{v}) \, dV = \alpha \mathcal{L}(\mathbf{v}) = \alpha, \forall \mathbf{v} \in \mathcal{V}_a^1 \right\}. \tag{2.5}$$

The extreme load factor is given by:

$$\alpha_{lim} \sup_{\tau \in \Sigma_a^\alpha \cap G} \mathcal{S}_i(\boldsymbol{\tau}), \text{where } \mathcal{S}_i(\boldsymbol{\tau}) = \inf_{\mathrm{v} \in \mathcal{V}_a^1} \mathcal{S}_m(\mathbf{v}, \boldsymbol{\tau}) = \alpha - \int_V \Psi_G(\boldsymbol{\tau}^D) \, dV \tag{2.6}$$

2.4 Kinematical limit load approach (upper bound)

The $\sup$ in the support function $\pi(\dot{\boldsymbol{\varepsilon}})$ can be reached only if $\boldsymbol{\sigma}$ is chosen in $G_{(\mathrm{x})}$, such that: $\boldsymbol{\sigma} = \lambda \dot{\boldsymbol{\varepsilon}}^D + \mu \mathbf{I}$ (this ensures that $\boldsymbol{\sigma} || \dot{\boldsymbol{\varepsilon}}^D$). The optimum corresponds to $g(\bar{\boldsymbol{\sigma}}) = 0 \Rightarrow \bar{\lambda} = \sigma_y \sqrt{2/3} \left(\dot{\boldsymbol{\varepsilon}}^D \cdot \dot{\boldsymbol{\varepsilon}}^D \right)^{-1/2}$. Then the support function is given by

$$\pi(\dot{\boldsymbol{\varepsilon}}(\mathbf{v})) = \sigma_y \sqrt{\frac{2}{3}} \sqrt{\dot{\boldsymbol{\varepsilon}}(\mathbf{v}) : \dot{\boldsymbol{\varepsilon}}(\mathbf{v})} + \sup_{\mu \in I\!R} (\mu \mathrm{div}\ \mathbf{v}).$$

It is interpreted as the density of dissipation work rate through the $\dot{\boldsymbol{\varepsilon}}(\mathbf{v})$ at the material point. We can observe that the $\pi(\dot{\boldsymbol{\varepsilon}})$ function is not differentiable at $\mathbf{0}$. We do not treat in the *Code_Aster* the support function associated to the internal discontinuities surfaces, lying in the V body [22]: the interfaces are disregarded.

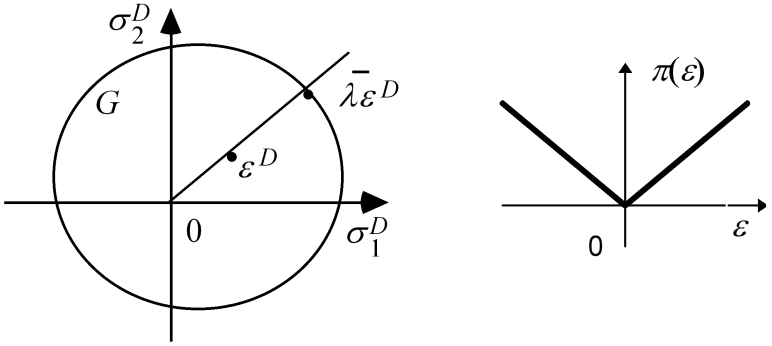

Figure 2.1: Optimum $\bar{\boldsymbol{\sigma}}$ and graph of the support function $\pi(\dot{\boldsymbol{\varepsilon}})$ in 1D situations

The kinematical approach is defined by the convex functional $\mathcal{S}_e(\mathbf{v})$, which is positively homogeneous of degree one, for any $\mathbf{v} \in \mathcal{V}_a^1$, in the whole domain:

$$\mathcal{S}_e(\mathbf{v}) = \sup_{\tau \in \Sigma} \mathcal{S}_m(\mathbf{v}, \boldsymbol{\tau}) = \int_V \pi(\dot{\boldsymbol{\varepsilon}}(\mathbf{v})) dV - \mathcal{L}_0(\mathbf{v}) \tag{2.7}$$

This functional is the integral on the body of the support function π of the convex $G_{(\mathrm{x})}$, calculated for the $\dot{\boldsymbol{\varepsilon}}(\mathbf{v})$ strain rate, and can be interpreted as the maximal dissipation work rate in the velocities field $\mathbf{v}$ (the contribution of the interface strength vanishing). The support function π being positively homogeneous of degree one, consequently the functional $\mathcal{S}_e(\mathbf{v})$ is too. With the von Mises criterion, the dissipation work rate functional $\mathcal{S}_e(\mathbf{v})$ reads:

$$\mathcal{S}_e(\mathbf{v}) = \int_V \left[\sigma_y \sqrt{\frac{2}{3}} \sqrt{\dot{\boldsymbol{\varepsilon}}(\mathbf{v}) : \dot{\boldsymbol{\varepsilon}}(\mathbf{v})} + \sup_{q \in I\!R} (q \mathrm{div}\ \mathbf{v}) \right] dV - \mathcal{L}_0(\mathbf{v}) \tag{2.8}$$

We can observe that only the $\mathbf{v}$ fields belonging to the subspace

$$C = \left\{ \mathbf{v} \in \mathcal{V}_a^1, \mathrm{div}\ \mathbf{v} = 0 \text{ in } V \right\}$$

give finite values of $\mathcal{S}_e(\mathbf{v})$. The $\mathbf{v}$ fields have to satisfy the isochoric condition:

$$\text{div } \mathbf{v} = \text{tr } \dot{\boldsymbol{\varepsilon}}(\mathbf{v}) = 0.$$

It is why we need incompressible finite elements to perform the calculation of limit load factor with the von Mises criterion. The (quite general) method used to deal with the incompressibility consists in mixed finite elements (velocities, mean pressure), ensuring by dualization the isochoric condition in a weak form. These elements have to verify the so-called LBB condition, to avoid spurious solutions. For instance, see [27] for the formulation adopted by *Code_Aster*.

The limit load factor α_{lim} given by the kinematical approach is the solution of this optimization problem:

$$\alpha_{lim} = \inf_{\mathrm{v} \in \mathcal{V}_a^1} \mathcal{S}_e(\mathbf{v}) = \inf_{\substack{\mathrm{v} \in \mathcal{V}_a \\ L(\mathrm{v}) > 0}} \frac{\mathcal{S}_e(\mathbf{v})}{\mathcal{L}(\mathbf{v})} = \sup_{\alpha > 0} \inf_{\mathrm{v} \in \mathcal{V}_a^1} \left(\mathcal{S}_e(\mathbf{v}) - \alpha(\mathcal{L}(\mathbf{v}) - 1) \right).$$

When the optimum is reached, we get a solution $\mathbf{u}$ and the limit load factor α_{lim} there is no uniqueness of the field $\mathbf{u}$, but α_{lim} is unique. Any loading combination $\mathcal{L}_0(\mathbf{v}) + \alpha\mathcal{L}(\mathbf{v})$ with $0 \leq \alpha \leq \alpha_{lim}$ is supportable. Beyond α_{lim}, the equilibrium problem violates the strength criterion.

Remark 2.4.1:

There exist some situations where, even if $\mathcal{L}_0(\mathbf{v})$ is not supportable alone, the combination $\mathcal{L}_0(\mathbf{v}) + \alpha\mathcal{L}(\mathbf{v})$, with $\alpha_1 \leq \alpha \leq \alpha_2$, becomes supportable over a certain interval, and not only with two parallel loading.

Remark 2.4.2:

The limit load factor calculated for a two-dimensional problem, with the plane strain condition, is necessarily higher than those obtained for this problem idealized with the plane stress condition. This result gives a upper bound. If we want to treat the problem with plane stress, we have to use the kinematical approach on a three-dimensional idealization.

3 Review of numerical techniques

The implementation of the lower and upper bound methods presented above leads to difficulties. The first one requires the construction of statically admissible stress fields, which is delicate (excepted certain 2D cases), on which one must check the not exceeding of the criterion. The second one frequently provides interesting results only to the condition of choosing of discontinuous velocities fields, which are difficult to introduce into the finite elements. It however requires the minimization of a non-differentiable functional (close to that of elastoplastic damage mechanics).

One finds very few “industrial” versions of computational softwares dealing with limit analysis. This is due primarily to the low number of applications under consideration compared to the practice in calculation of the structures (in elasticity or elastoplasticity for example). However, the general balance-sheet of the methods tested by various authors makes it possible the choice of algorithms. Those presented in the literature can be classified according to three groups:

Lower bound method	Upper bound method	Mixed method
1 Criterion and nonlinear programming on discontinuous stresses 2 Criterion and nonlinear programming with a basis-reduction technique of the stress space 3 Linearization of the criterion and linear programming 4 Criterion and iterative weak admissible elastic-rigid stress fields by FEM.	1 Heuristic minimization with discontinuous velocities 2 Linearization of the criterion and linear programming with discontinuous velocities 3 Partition and partial regularization with discontinuous velocities 4 Norton-Hoff regularization, with continuous velocities.	1 Linearization of the criterion and linear programming, with continuous velocities and discontinuous stresses 2 Bingham regularization by projection with continuous velocities and collocation for the stresses 3 Norton-Hoff regularization, continuous stresses and velocities.

Table 3.1: Main algorithms characteristics.

3.1 Lower bound numerical methods of the limit load

The principal characteristics of the lower bound method are: the construction of statically admissible stress fields; the resolution of the problem of optimization with checking of the criterion everywhere. Historically, Hodge and Belytschko [13], [14] were among the first to treat the 2D plane cases and plates. The selected discretization also consists of finite elements with stresses d.o.f. (derived from an Airy’s function). The conditions of connection on the elements edges are exploited to eliminate from the d.o.f. Discontinuities can be considered only between two elements. A nonlinear programming algorithm of minimization is used.

Casciaro et al. [3], [4] underline the cost of the checking of the criterion on each element, caused by the choice of a quadratic discretization of the stress. They propose on the contrary a linear discretization, which makes it possible to limit the checking of the criterion on the nodes of the mesh. A linearization of the criterion per pieces makes it possible to use algorithms employed in linear programming, which are very effective. For the von Mises case, one would need 32 linear inequalities to approach it with less than 5%. Christiansen made this choice too to avoid very expensive problem of optimization [5].

This strategy was also used by Pastor et al. [18] in a case adapted to the axisymmetric problems. They used P1 stress finite elements, where 2 linear relations of continuity between the common edges are taken into account. In the Coulomb's case, the criterion is linearized per pieces, the cone being replaced by a polyhedron. Of course, the found limit loads will be only upper limits for the real problem with the criterion of non associated Coulomb. Once linearized, the criterion is calculated at the nodes, where the extrema are reached.

More recently, Heitzer and Staat [21], [12] have proposed to use a basis-reduction technique of the residual stress space (the elastic solution being chosen to equilibrate the external loading) so that the cost of the nonlinear programming becomes not excessive.

Another way was proposed by Ponter: the use of elastic finite elements to build by an iterative procedure a sequence of equilibrated stress fields (in a weak sense), by a progressive smoothing of zones where the criterion is reached.

3.2 Mixed approach numerical methods of the limit load

This method introduce multipliers, according to the Kuhn-Tucker's theorem. The potential risk lies in a bad conditioning: some people prefer to devote to the direct problem. The mixed methods (leading to a saddle-point problem) have the advantage of revealing at the same time the stress field and the velocities field in the collapse, and producing directly a bounding of the limit load factor.

Casciaro et al. proposed an association of linear elements for velocities as for the stresses, with discontinuities between elements, and with an *a priori* incompressibility of the velocities fields, or imposed with a dual form. Discretization of Lagrangian resulted in checking the balance and the law of flow to the weak direction only; on the other hand, it is required that the criterion be never violated, nor kinematic admissibility. Christiansen proposed a little different method, with constant stress elements. A convergence theorem was established [5].

Other works proposed not to linearize the criterion, like Zouain et al. [26], but a Newton-like algorithm, replacing the Hessian by a positive definite matrix, directly on the conditions of optimality of the Lagrangian.

3.3 Upper bound numerical methods of the limit load

Due to the difficulty lying in the not-differentiable character of the potential defining the strength criterion of material, many authors proposed either a method of regularization, to replace this potential (or its dualized form) by another which is differentiable, " adjustable "

by a parameter, of which the limiting value led to convergence towards the preceding potential, or a heuristic minimization, without the need of the Hessian.

The method of heuristic minimization of the function $\mathcal{S}_e(\mathbf{v}_h)$, (used for instance by Maghous [16], with constant or linear continuous fields $\mathbf{v}_h$) although very simple to implement and general, seems expensive and sensitive to the choice of the starting point. Its users associate it with a partitioning according to zones of the structure non concerned by the collapse flow (given roughly by some iterations of nonlinear programming).

The linearization of the criterion makes it possible to use the fast methods of linear optimization, but it can provide however results further away from the exact extreme loads (see for instance [19] with P1 elements ...).

The incompressibility is sometimes treated in a way approached by penalisation, while adding to Lagrangian term in (div $\mathbf{v}$)^2, affected of a great coefficient. If not, it is treated by Lagrange's multipliers and an Uzawa's algorithm on the dual problem.

A first regularization of the $\mathcal{S}_e(\mathbf{v}_h)$ functional, basic approach if one can say, consists in adding in the expression of the function of support of convex constant term making it derivable at 0, see for instance Clément [6], Gaudrat [10], ... Of course, the problem of minimization of the functional ${}^{\alpha}\mathcal{S}_e(\mathbf{v})$ thus obtained is very badly conditioned when α tends towards 0 (the gradient and the Hessian are difficult to calculate numerically).

One can classify the method suggested by Yan [25] in this category: he used a regularization by a fictitious perfectly plastic viscous flow potential, where the Young's modulus plays the role of parameter; the incompressibility is treated in the same manner, by penalisation.

Another approach uses laws of viscous behaviour, where the parameter of regularization is interpreted like a viscosity. A method by projection on the criterion $G_{(\mathrm{x})}$ was proposed by Mercier [17]. He chooses a law of the Bingham-Perzyna type, where the flow takes place only with the crossing of the threshold; the potential which replaces the indicator function $\Psi_G(\boldsymbol{\sigma})$ of convex having the form: $\Psi_G^{BP}(\boldsymbol{\tau}(\mathbf{x})) = \frac{1}{2\mu}||\boldsymbol{\tau}(\mathbf{x}) - \Pi_G(\boldsymbol{\tau}(\mathbf{x}))||^2$.
The Mercier's regularized functional derived from $\mathcal{S}_e(\mathbf{v})$ reads:

$$ {}^{\mu}\mathcal{S}_e(\mathbf{v}) = \mathcal{S}_e(\mathbf{v}) + \int_V \frac{\mu}{2}||\dot{\boldsymbol{\varepsilon}}(\mathbf{v})||^2 \, dV \tag{3.1} $$

Instead of regularizing the functional to be optimized, one finds also algorithms which exploit the presence of the rigid zones in the optimal solutions by a " partition ", while being reduced to the optimization of a differentiable functional. Unfortunately, these algorithms do not cross to a stage of regularization, to deal with the complete problem. One can wonder, if the use of a method of adaptive meshing, coupled with the methods above, could not be even more effective.

Finally, it seems interesting to use the method of regularization by the Norton-Hoff's viscous law (with a coefficient of " viscosity " $\mu > 0$), both on the upper bound method or

on the mixed approach. Historically, it seems that it is in the precursory work of Casciaro in 1971, that one finds a first application of this regularization. Associated with a mixed method, it led to a computational software " LIMAN ", see [3]. In 1982, these authors proposed this regularization to the mixed approach [4]. This regularization was studied in detail by Friaâ [9] in 1979. The indicator function $\Psi_G(\boldsymbol{\tau})$ is regularized in the following way, $q > 1$ (expressed with the gauge function $j(\boldsymbol{\tau})$ of the convex $G_{(\mathrm{x})}$):

$$\Psi_G^{NH}(\boldsymbol{\tau}\mathbf{x})) = \frac{\mu}{q}[j(\boldsymbol{\tau}(\mathbf{x}))]^q \tag{3.2}$$

Casciaro proposed also to choose the following expression of the regularized potential:

$$\Psi_G^{NHq}(\boldsymbol{\tau}) = \left(\frac{1}{|V|}\int_V (g(\boldsymbol{\tau}) + \sigma_y)^q \, \sigma_y^{-q} \, dV\right)^{1/q} \tag{3.3}$$

Figure 3.1 allows to compare in the one-dimensional case (the convex is represented by the segment $]-\sigma_y, \sigma_y[$) these potentials with the original non differentiable potential.

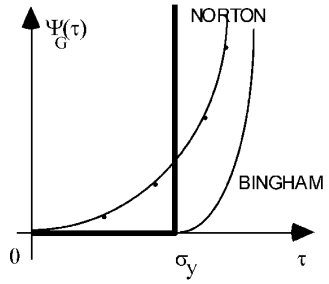

Figure 3.1: Comparison of regularized potentials in 1D case.

The form of the coercive Norton-Hoff potential leads to place itself in functional spaces in duality of the type L^p, $p > 1$, and L^q where the sum $p^{-1} + q^{-1} = 1$. We get good properties on the solutions : they become regular, and for $p = q = 2$ that leads to a problem of linear viscosity. And the solution of the initial collapse problem corresponds to the limit of the normalized sequel of the solutions $(\mathbf{u}_q, \sigma_q)$, for $q \to \infty$; by post-processing, we get decreasing values of the limit load factor. Its initialization rests on a linear calculation. A same technique was used for instance by Guennouni [11] or recently by Berak [2].

3.4 Choice of a numerical method of the limit load

One can summaries the advantages and the disadvantages of the various methods suggested in the literature as follows. The lower bound methods, in their "exact" version are limited to the 2D or plate-bending cases, and their cost is noticeable. It seems that linearizing the criterion leads to poor results. In their "weak" (in the sense of verifying the equilibrium

equations) version, with reduction technique, they appear efficient, but needs a special implementation in usual finite element codes. For the treatment of the upper bound method, it appears that the regularization is a good way, with a special mention to the Norton-Hoff one, because of its convergence properties. That is why we have decided to implement the upper bound approach, with the Norton-Hoff-Frémond-Friaâ method into a general purpose nonlinear mechanical software uses displacement formulated finite elements, namely Code_Aster: we only need to implement the Norton-Hoff constitutive relation.

4 Norton-Hoff regularization of the upper bound method

4.1 Theoretical formulation

We regularize the non-differentiable functional $\mathcal{S}_e(\mathbf{v})$ by the Norton-Hoff method. We replace the support function $\pi(\dot{\boldsymbol{\varepsilon}})$ by the regularized and differentiable support function $\pi^{NH}(\dot{\boldsymbol{\varepsilon}})$. It is adjustable by a regularization parameter $n(1 \leq n \leq +\infty)$, which limit value $n \to \infty$ gives the convergence to support function $\pi(\dot{\boldsymbol{\varepsilon}})$:

$$\pi^{NH}(\dot{\boldsymbol{\varepsilon}}) = \frac{nk^{-1/n}}{1+n} \left(\pi(\dot{\boldsymbol{\varepsilon}})\right)^m \tag{4.1}$$

In the *Code_Aster*, we choose the constant $k = \sigma_y^2/3\mu$, in order to recover the elastic incompressible problem, when $n = 1$ (2μ being the second Lamé's coefficient).

We denote the space of the admissible velocities, adapted to the viscous flow, through the Norton-Hoff constitutive relation of order m:

$$\mathcal{V}_a^{n1} = \left\{\mathbf{v} \in L^n(V), \dot{\boldsymbol{\varepsilon}}(\mathbf{v}) \in L^n(V), \mathbf{v} = \mathbf{0} \text{ on } \Gamma_u, \mathcal{L}(\mathbf{v}) = 1\right\}. \tag{4.2}$$

We define on this space the regularized functional $\mathcal{S}_e^n(\mathbf{v})$:

$$\mathcal{S}_e^n(\mathbf{v}) = \int_V \frac{nk^{-1/n}}{n+1} \pi(\dot{\boldsymbol{\varepsilon}}(\mathbf{v}))^{(1+n)/n} dV - \mathcal{L}_0(\mathbf{v}) \tag{4.3}$$

The minimization problem $\inf_{\mathrm{v} \in \mathcal{V}_a^{n1}} [\mathcal{S}_e^n(\mathbf{v})]$ is well-posed thanks to the properties of the spaces $L^n(V)$ (due to the Hölder inequality) and has a unique solution $\mathbf{u}_n$, for which the reached value of the $\inf$ is: α_n. We show that this problem can also be written as the seeking of the saddle-point $(\alpha_n, \mathbf{u}_n, p_n)$ of the following Lagrangian:

$$\max_{\alpha \in \mathbb{R}} \inf_{\mathrm{v} \in \mathcal{V}_a} \sup_{q \in L^2(V)} \int_V A(n) \left(\sqrt{\dot{\boldsymbol{\varepsilon}}(\mathbf{v}) : \dot{\boldsymbol{\varepsilon}}(\mathbf{v})}\right)^{(1+n)/n} dV + \int_V q \mathrm{div}\mathbf{v} dV - \mathcal{L}_0(\mathbf{v}) - \alpha(\mathcal{L}(\mathbf{v}) - 1) \tag{4.4}$$

with:

$$A(n) = \frac{n}{1+n}\sigma_y^{(n-1)/n}(3\mu)^{1/n}\left(\frac{2}{3}\right)^{(1+n)/2n}.$$

In practice, we take the sequence:

n	1	10	100	1000	...	∞
$A(n)$	2μ				...	$\sigma_y\sqrt{\frac{2}{3}}$

We observe that $A(n)$ is decreasing (if $E \geq \sigma_y$) from 2μ to $\sigma_y\sqrt{\frac{2}{3}}$ keeping homogeneous to a stress, and remaining bounded.

This Lagrangian (4.4) allows to force directly in the operator the isochoric condition as well the normalization to 1 of the work rate of loading. Then we build a decreasing sequence of α_n values and the limit load factor α_{lim} is the limit of this sequence when $n \to \infty$:

$$\alpha_{lim} = \lim_{n\to\infty}\left(\inf_{\mathrm{v}\in\mathcal{V}_a^{n1}}\left[\mathcal{S}_e^n(\mathbf{v})\right]\right) = \lim_{n\to\infty}\left(\mathcal{S}_e^n(\mathbf{u}_n)\right). \tag{4.5}$$

We can refer to [22] and [24] to see the proof. We show also the following property of the solutions of (4.4). If we amplify the loading $\mathcal{L} \to \beta\mathcal{L}$, when $\mathcal{L}_0 = 0$, the solutions depend on β by the following relationships:

$$\begin{aligned}
\mathbf{u}_n(\beta) &= \beta^{-1}\mathbf{u}_n(1)\\
p_n(\beta) &= \beta^{-1/n}p_n(1)\\
\boldsymbol{\sigma}^D(\mathbf{u}_n(\beta)) &= \beta^{-1/n}\boldsymbol{\sigma}^D(\mathbf{u}_n(1))\\
\mathcal{S}_e^n(\mathbf{u}_n(\beta)) &= \beta^{-(1+n)/n}\mathcal{S}_e^n(\mathbf{u}_n(1))
\end{aligned}$$

One of the advantages of this regularizing method lies in the embedding property of the spaces $L^n(V)$, that leads to an interesting property of the α_n sequence, see section 4.3. So we get the proof of the following properties [24], for a bounded body V, denoting $|V| = \int_V dV$ and $||V||_n = \int_V A(n)dV$: For any $1 \leq n$ and $1 \leq r \leq s$ and any field $\mathbf{u}$ belonging to $\mathcal{V}_a^n$, we have:

$$\begin{aligned}
\int_V A(n)\sqrt{\dot{\boldsymbol{\varepsilon}}(\mathbf{u}):\dot{\boldsymbol{\varepsilon}}(\mathbf{u})}dV &\leq ||V||_n^{\frac{r-1}{r}}\left(\int_V A(n)\sqrt{(\dot{\boldsymbol{\varepsilon}}(\mathbf{u}):\dot{\boldsymbol{\varepsilon}}(\mathbf{u}))^r}dV\right)^{\frac{1}{r}}\\
&\leq ||V||_n^{\frac{s-1}{s}}\left(\int_V A(n)\sqrt{(\dot{\boldsymbol{\varepsilon}}(\mathbf{u}):\dot{\boldsymbol{\varepsilon}}(\mathbf{u}))^s}dV\right)^{\frac{1}{s}}
\end{aligned} \tag{4.6}$$

$$\int_V \sigma_y\sqrt{\frac{2}{3}\dot{\boldsymbol{\varepsilon}}(\mathbf{u}):\dot{\boldsymbol{\varepsilon}}(\mathbf{u})}dV \leq |V|^{\frac{1}{n+1}}\left(\int_V \sigma_y^{(n+1)/n}\left(\sqrt{\frac{2}{3}\dot{\boldsymbol{\varepsilon}}(\mathbf{u}):\dot{\boldsymbol{\varepsilon}}(\mathbf{u})}\right)^{(n+1)/n}dV\right)^{\frac{n}{n+1}}, \forall\mathbf{u} \tag{4.7}$$

These properties are interesting because they remain true for heterogeneous materials, and we can consider the yield stress either as measure (as a specific mass) or as belonging to the strain energy.

4.2 Numerical aspects of the limit load calculation

To calculate with *Code_Aster* a limit load factor with the regularizing Norton-Hoff-Friaâ method, with the von Mises criterion, we need to:

- define a 2D-idealization (plane or axisymmetric) or 3D with the incompressible finite elements,
- define the material characteristics (Young's modulus $E \geq \sigma_y$, Poisson's ratio ν near to 0.5 to precise the quasi-incompressibility of the mixed finite elements in the *Code_Aster* [27], the strength parameter σ_y and Norton-Hoff coefficient n), the shear modulus being deducted: $2\mu = 2E/3$. Notice that the limit load is independent of E and ν,
- define the dead loading and the α-parametrized one,
- define the normalization of the work rate of the parametrized loading,
- make a non linear calculation with the Norton-Hoff constitutive relation with the Newton-Raphson type algorithm,
- post-process the calculation to obtain the limit load factor.

The weak form of the optimization problem reads as following:

The coefficient n given, find $(\alpha_n, \mathbf{u}_n, p_n) \in I\!R \times \mathcal{V}_a \times L^2(V)$ such that:

$$\begin{aligned} \int_V \left\{ A(n) \sqrt{\dot{\boldsymbol{\varepsilon}}(\mathbf{u}_n) : \dot{\boldsymbol{\varepsilon}}(\mathbf{u}_n)}^{\frac{1-n}{n}} \dot{\boldsymbol{\varepsilon}}(\mathbf{u}_n) : \dot{\boldsymbol{\varepsilon}}(\mathbf{v}) + p_n \text{div } \mathbf{v} \right\} dV & \\ -\alpha_n \mathcal{L}(\mathbf{v}) &= \mathcal{L}_0(\mathbf{v}) \ \ \forall \mathbf{v} \in \mathcal{V}_a \\ \int_V q \text{div } \mathbf{u}_n dV &= 0 \ \forall q \in L^2(V) \\ \mathcal{L}(\mathbf{u}_n) &= 1 \end{aligned} \tag{4.8}$$

This problem admits an unique solution for any $n \geq 1$ (see [22]). For $n = 1$ the problem is of linear incompressible elasticity type. We get an estimation of the limit load factor by an upper bound, the $\mathbf{u}_n$ field giving an idea of a collapse mode. For the incompressibility treatment, we refer to the document [27] to the weak mixed formulation:

$$\int_V q \text{div } \mathbf{u} \, dV + \int_V \frac{qp}{\xi} dV = 0 \ \ \forall q \in L^2(V),$$

the penalisation term $\int_V \frac{qp}{\xi} dV$ avoiding some difficulties with a LDLT-like linear algebra solver[1] and corresponding to a Poisson's ratio like $\nu = 0.4999\ldots$ ($\xi \to \infty$ when $\nu \to 0.5$). Then the solutions are only quasi-incompressible.

[1] Bunck-Kaufman method with LDL^T decomposition where L is a unit lower triangular matrix and D is block diagonal.

The variational formulation (4.8) is solved by the popular non linear iterative Newton-Raphson algorithm by *Code_Aster* (including other ingredients like line-search, continuation... presented in [28]), with mixed 2D and 3D finite elements (Taylor-Hood), defined by degrees of freedom vector $(\mathbf{U}, \mathbf{P})$, on the spaces $\mathcal{V}_0$ and $\mathcal{Q}$ of discretized functions.

The principle of the non linear Newton-Raphson algorithm of *Code_Aster* is presented in [28]. We get the incremental following problem:

Find $(\Delta\alpha, \Delta\mathbf{u}, \Delta p) \in I\!R \times \mathcal{V}_0 \times \mathcal{Q}$ such that:

$$\begin{aligned}\int_V \boldsymbol{\sigma}(\mathbf{u}+\Delta\mathbf{u}) : \dot{\boldsymbol{\varepsilon}}(\mathbf{v}) dV + \mathbf{B}(\mathbf{v}, p+\Delta p) & \\ -(\alpha+\Delta\alpha)\mathcal{L}_1(\mathbf{v}) &= (\mathcal{L}_0 + \Delta\mathcal{L}_0)(\mathbf{v}) \ \ \forall \mathbf{v} \in \mathcal{V}_0 \\ \mathbf{B}(\mathbf{u}+\Delta\mathbf{u}, q) &= \mathbf{D} + \Delta\mathbf{D} \ \ \forall \mathbf{q} \in \mathcal{Q} \\ \mathcal{L}_1(\mathbf{v}) &= 1\end{aligned}$$

- $\mathbf{B}$ is a linear operator containing the Dirichlet homogeneous boundary conditions, as well the incompressibility condition,
- $\mathbf{D}$ corresponds to the prescribed data (Dirichlet homogeneous boundary conditions, incompressibility),
- $\mathcal{L}_0$ is the dead load second member and $\mathcal{L}_1$ the α-parametrized load second member,
- $\mathcal{V}_0$ and $\mathcal{Q}$ are the spaces of discretized functions on the finite elements, defined by the degrees of freedoms (DOFs) vector (**U**,**P**).

The stress tensor $\boldsymbol{\sigma}(\mathbf{u})$ satisfies the Norton-Hoff constitutive relation. The deviatoric stress associated to the strain rate is:

$$\boldsymbol{\sigma}^D(\mathbf{u}) = \frac{1+n}{n} A(n) \left(\sqrt{\dot{\boldsymbol{\varepsilon}}^D(\mathbf{u}) : \dot{\boldsymbol{\varepsilon}}^D(\mathbf{u})} \right)^{(1-n)/n} \dot{\boldsymbol{\varepsilon}}^D(\mathbf{u}). \tag{4.9}$$

The nonlinear problem is solved by the Newton method, after the direct implicit discretization of the constitutive relations, see [29].

The prediction step consists to solve the following system, from the initial state $(\mathbf{u}, p)$ to obtain the first iteration solution : $(\Delta\mathbf{u}_0, \Delta p_0)$.

$$\begin{aligned}\int_V \left.\frac{d\boldsymbol{\sigma}}{d\dot{\boldsymbol{\varepsilon}}}\right|_{\varepsilon(\mathrm{u})} : \dot{\boldsymbol{\varepsilon}}(\Delta\mathbf{u}_0) : \dot{\boldsymbol{\varepsilon}}(\mathbf{v}) dV + \mathbf{B}(\mathbf{v}, \Delta p_0) - \Delta\alpha\mathcal{L}_1(\mathbf{v}) &= \Delta\mathcal{L}_0(\mathbf{v}) \ \ \forall(\mathbf{v}) \in \mathcal{V}_0 \\ \mathbf{B}(\Delta\mathbf{u}_0, q) &= \Delta\mathbf{D} \ \ \forall q \in \mathcal{Q} \\ \mathcal{L}_1(\mathbf{u}+\Delta\mathbf{u}_0) &= 1\end{aligned}$$

The tangent operator $\left.\frac{d\sigma}{d\varepsilon}\right|_{\varepsilon(\mathrm{u})}$ comes from the tangent stiffness, applied to any deviatoric tensor **e**:

$$\frac{d\boldsymbol{\sigma}^D}{d\dot{\boldsymbol{\varepsilon}}^D}\mathbf{e} = A(r) \left(\sqrt{\dot{\boldsymbol{\varepsilon}}^D(\mathbf{u}) : \dot{\boldsymbol{\varepsilon}}^D(\mathbf{u})} \right)^{(1-r)/r} \left(\mathbf{e} + \frac{1-r}{r} \frac{\dot{\boldsymbol{\varepsilon}}^D(\mathbf{u}) \otimes \dot{\boldsymbol{\varepsilon}}^D(\mathbf{u})}{\dot{\boldsymbol{\varepsilon}}^D(\mathbf{u}) \cdot \dot{\boldsymbol{\varepsilon}}^D(\mathbf{u})} : \mathbf{e} \right). \tag{4.10}$$

Then we continue with the correction step, for the i-th iteration:

$$\begin{aligned}
\int_V \left.\frac{d\boldsymbol{\sigma}}{d\dot{\boldsymbol{\varepsilon}}}\right|_{\varepsilon(\mathrm{u}+\Delta\mathrm{u}_i)} &: \dot{\boldsymbol{\varepsilon}}(\Delta\mathbf{u}_{i+1}-\Delta\mathbf{u}_i) : \dot{\boldsymbol{\varepsilon}}(\mathbf{v})dV + \mathbf{B}(\mathbf{v},\Delta p_{i+1}) - (\alpha+\Delta\alpha)\mathcal{L}_1(\mathbf{v}) \\
&= (\mathcal{L}_0+\Delta\mathcal{L}_0)(\mathbf{v}) - \left[\int_V \boldsymbol{\sigma}(\mathbf{u}+\Delta\mathbf{u}_i) : \dot{\boldsymbol{\varepsilon}}(\mathbf{v})dV + \mathbf{B}(\mathbf{v},p)\right] \ \forall \mathbf{v}\in\mathcal{V}_0 \\
\mathbf{B}(\Delta\mathbf{u}_{i+1},q) &= \mathbf{D}+\Delta\mathbf{D}-\mathbf{B}(\mathbf{u},q) \ \forall q\in\mathcal{Q} \\
\mathcal{L}_1(\mathbf{u}+\Delta\mathbf{u}_{i+1}) &= 1
\end{aligned}$$

The second member $\boldsymbol{\sigma}(\mathbf{u}+\Delta\mathbf{u}_i) : \dot{\boldsymbol{\varepsilon}}(\mathbf{v})dV$ is updated, through the computation of the stress field from the constitutive relation. The tangent operator $\left.\frac{d\sigma}{d\varepsilon}\right|_{\varepsilon(\mathrm{u}+\Delta\mathrm{u}_i)}$ is also updated on request, at certain iterations i only, to avoid an expensive assembling of the stiffness matrix.

In our case, the solution can be achieved without time-discretization, but it is interesting to update the tangent stiffness from time to time to speed-up the convergence. We use a LDLT type solver; the normalization equation, coupling a lot of DOFs being reported at the bottom of the equations system. We can prefer to make a break in the calculation, or restart from any previous solution $(\mathbf{u},p)$, even obtained from another parameter n: this enables computing time reduction. In any case, it is recommended to begin a calculation with a coarse mesh to evaluate the effect of the parameter n on the α_n values.

4.3 Post-processing and calculation of the limit load factor

The solution $(\alpha_n,\mathbf{u}_n,p_n)$ being calculated, for a given n, we have to use the α_n sequence to build the approximation of the limit load factor. We make profit of the properties (4.5), (4.6), the fact that $A(n)$ is decreasing, and the property coming from the minimization (4.4) (see [24]). From these two last properties, with $1\leq r\leq s$, we conclude that for $\mathbf{u}_r$ and $\mathbf{u}_s$ respectively solutions (satisfying also the incompressibility and normalization conditions) of (4.4) for $n=r$ and $n=s$:

$$\left(\int_V A(r)\sqrt{(\dot{\boldsymbol{\varepsilon}}(\mathbf{u}_r):\dot{\boldsymbol{\varepsilon}}(\mathbf{u}_r))^r}dV\right) \leq \left(\int_V A(s)\sqrt{(\dot{\boldsymbol{\varepsilon}}(\mathbf{u}_s):\dot{\boldsymbol{\varepsilon}}(\mathbf{u}_s))^s}\,dV\right) \tag{4.11}$$

Associated to the property (4.5), we have for $1\leq r\leq s$:

$$\begin{aligned}
\int_V A(r)\sqrt{\dot{\boldsymbol{\varepsilon}}(\mathbf{u}_r):\dot{\boldsymbol{\varepsilon}}(\mathbf{u}_r)}dV &\leq ||V||_r^{\frac{r-1}{r}}\left(\int_V A(r)\sqrt{(\dot{\boldsymbol{\varepsilon}}(\mathbf{u}_r):\dot{\boldsymbol{\varepsilon}}(\mathbf{u}_r))^r}\,dV\right)^{\frac{1}{r}} \\
&\leq ||V||_s^{\frac{s-1}{s}}\left(\int_V A(s)\sqrt{(\dot{\boldsymbol{\varepsilon}}(\mathbf{u}_s):\dot{\boldsymbol{\varepsilon}}(\mathbf{u}_s))^s}\,dV\right)^{\frac{1}{s}}
\end{aligned} \tag{4.12}$$

We denote by $\tilde{\alpha}_n$ the terms of the sequence, that we calculate in practice by post-processing from $\mathbf{u}_n$ (the loading work rate being equal to 1):

$$\tilde{\alpha}_n = ||V||_n^{\frac{1}{1+n}} \left(\int_V A(n) \sqrt{(\dot{\boldsymbol{\varepsilon}}(\mathbf{u}_n) : \dot{\boldsymbol{\varepsilon}}(\mathbf{u}_n))^{(1+n)/n}}\, dV \right)^{\frac{n}{1+n}} - \mathcal{L}_0(\mathbf{u}_n) \tag{4.13}$$

This sequence $\tilde{\alpha}_n$ is decreasing for $n \to +\infty$ and we show [24] that it converges to $\alpha_{\lim}$; that enables a good control. As we can make a minoration (knowing that $A(+\infty) = \sigma_y \sqrt{\frac{2}{3}}$) of the first term of (4.12):

$$\alpha_{lim} \leq \int_V \sigma_y \sqrt{\frac{2}{3} \dot{\boldsymbol{\varepsilon}}(\mathbf{u}_n) : \dot{\boldsymbol{\varepsilon}}(\mathbf{u}_n)}\, dV - \mathcal{L}_0(\mathbf{u}_n) \leq \tilde{\alpha}_n \tag{4.14}$$

we calculate then the decreasing sequence $\hat{\alpha}_n$ for $n \to +\infty$ converging also to α_{lim}:

$$\alpha_{lim} \leq \hat{\alpha}_n = \int_V \sigma_y \sqrt{\frac{2}{3} \dot{\boldsymbol{\varepsilon}}(\mathbf{u}_n) : \dot{\boldsymbol{\varepsilon}}(\mathbf{u}_n)}\, dV - \mathcal{L}_0(\mathbf{u}_n) \leq \tilde{\alpha}_n. \tag{4.15}$$

The precision of the approximation of the limit load factor α_{lim} is determined by comparison of the different values of $\hat{\alpha}_n$ that converge to α_{lim} from above (at $n \to +\infty$). These terms are calculated by numerical integration at the Gaussian points of the finite elements. Another interpretation of the interest of making profit of this sequence lies in the fact that it uses directly the expression of the support function of the strength convex, that is the dissipation work rate in the potential collapse modes, applied to the incompressible and normalized solutions $\mathbf{u}_n$.

If the dead loading vanishes: $\mathcal{L}_0 = 0$, we can post-process the stress field (quasi statically admissible) coming from the solution $\mathbf{u}_n$ and get an estimated value of the limit load factor, which would be a lower bound if the equilibrium equations were exactly fulfilled (see [22]). We calculate then the sequence $\underline{\alpha}_n$, which has not –unfortunately– any property of monotony:

$$\underline{\alpha}_n = \int_V A(n) \sqrt{(\dot{\boldsymbol{\varepsilon}}(\mathbf{u}_n) : \dot{\boldsymbol{\varepsilon}}(\mathbf{u}_n))}^{(1+n)/n} dV \left[\sup_{\mathrm{x} \in V} \left(\frac{\sqrt{\frac{3}{2} \boldsymbol{\sigma}^D(\mathbf{u}_n) : \boldsymbol{\sigma}^D(\mathbf{u}_n)}}{\sigma_y} \right) \right]^{-1} \leq \hat{\alpha}_n \tag{4.16}$$

This maximization (of the gauge function of the strength convex) is calculated only at the Gaussian points of the finite elements. So the obtained value, for each n, lower than $\hat{\alpha}_n$ [22], can only be considered as an indication.

5 Validation test

5.1 Reference problem

We consider a rectangular plate or a hexahedron or an axisymmetrical cylinder. The strength property of the constitutive homogeneous material satisfies the von Mises criterion (with the threshold σ_y). The body is subjected to pressures on the horizontal boundary $-\varphi f$ and on the vertical boundary $-(1-\varphi)f$ with $\varphi \geq 0.5$. With this very simple sample problem, an analytical calculation enables to get the exact limit load factor in the loading direction, as well the estimations by the regularization method. For more details we refer to [22] and [23]. That validation example corresponds to the test SSNV124 [30] of *Code_Aster*. The geometry is characterized by: inner radius $a = 1mm$, outer radius $b = 2mm$, thickness $b - a = 1mm$, height: $H = 4mm$.

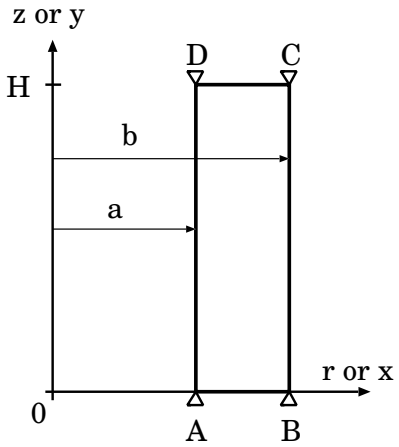

5.2 Plane case

The solid is submitted to pressures on the horizontal boundary: $-\varphi f$ and vertical one: $-(1-\varphi)f$, with: $\varphi \geq 1/2$, and the z-displacement is zero. We consider two ways to control the loading:

- case1: both pressures (horizontal and vertical) are parametrized by α,
- case2: the horizontal pressure is parametrized by α, while the vertical pressure remains constant $-(1-\varphi)f$, with $f_0 = \alpha_0 f$.

5.2.1 Limit analysis solution

The solution is homogeneous (biaxial stresses $\sigma : \sigma_{xx} = \varphi f, \sigma_{yy} = (1-\varphi)f, \sigma_{xy} = 0$, plane strain ε). We get [22] the limit load factor for these loading directions, for von Mises

criterion, in plane strain, with the threshold σ_y:

$$\text{case1: } \alpha_{lim} f = \frac{2\sqrt{3}\sigma_y}{3|2\varphi - 1|} \tag{5.1}$$

$$\text{case2: } \alpha_{lim} f = \frac{2\sqrt{3}\sigma_y}{3|\varphi|} + \frac{1-\varphi}{|\varphi|}\alpha_0 f \tag{5.2}$$

We observe that if we take $\alpha_0 = \alpha_{lim}$ in the case2, we recover the case1.

5.2.2 Regularized limit analysis solution

The solution is homogeneous. The plane strains are of the kind :

$$\dot{\boldsymbol{\varepsilon}}(\mathbf{u}) = \gamma \begin{pmatrix} 1 & 0 & 0 \\ 0 & -1 & 0 \\ 0 & 0 & 0 \end{pmatrix} \qquad \sqrt{\dot{\boldsymbol{\varepsilon}}(\mathbf{u}) : \dot{\boldsymbol{\varepsilon}}(\mathbf{u})} = |\gamma|\sqrt{2} \tag{5.3}$$

Through the Norton-Hoff constitutive relation, we get the deviatoric stresses:

$$\boldsymbol{\sigma}^D = A(n)\sqrt{2}^{(1-n)/n}|\gamma|^{(1-n)/n}\gamma \begin{pmatrix} 1 & 0 & 0 \\ 0 & -1 & 0 \\ 0 & 0 & 0 \end{pmatrix}$$
$$||\boldsymbol{\sigma}^D||_{vM} = A(n)\sqrt{2}^{(1-n)/n}|\gamma|^{1/n}\sqrt{3} \tag{5.4}$$

The loading normalization leads to:

$$\text{case1: } \gamma f = \frac{1}{H(b-a)(2\varphi - 1)} \tag{5.5}$$

$$\text{case2: } \gamma f = \frac{1}{H(b-a)\varphi} \tag{5.6}$$

The sequence terms $\hat{\alpha}_m$ of limit load factor estimation for both parametrisations of loading are:

$$\text{case1: } \hat{\alpha}_n f = \frac{2\sqrt{3}\sigma_y}{3|2\varphi - 1|} \quad \forall n \tag{5.7}$$

$$\text{case2: } \hat{\alpha}_n f = \frac{2\sqrt{3}\sigma_y}{3|\varphi|} + \frac{1-\varphi}{|\varphi|}\alpha_0 f \quad \forall n. \tag{5.8}$$

The invariance in n which can be observed here (this is a particular case) comes from the fact that the equilibrated stress field is unique. For the case1, we can also compute the sequence $\underline{\alpha}_n$:

$$\text{case1: } \underline{\alpha}_n f = \frac{2n\sqrt{3}\sigma_y}{3(1+n)|2\varphi - 1|} \tag{5.9}$$

The we get the exact limit load factor α_{lim} when $n \to \infty$.

5.3 Axisymmetrical case

For the 2D axisymmetrical case, we consider the same geometry, but the solid, the axial displacement of which vanishing, is submitted to the only pressure on the inner wall: φf parametrized by α.

5.3.1 Limit analysis solution

We get [23] the limit load factor for this loading direction, for the von Mises criterion, with axisymmetrical and zero axial strain condition, with the yield stress σ_y:

$$\alpha_{lim}\varphi f = \frac{2\sqrt{3}}{3}\sigma_y \ln\frac{b}{a} \tag{5.10}$$

5.3.2 Regularized limit analysis solution

The solution is homogeneous. The displacement being radial, the isochoric strains are, where γ is a parameter:

$$\mathrm{u}_r(r) = \frac{\gamma}{r}, \qquad \dot{\boldsymbol{\varepsilon}}(\mathbf{u}) = \frac{\gamma}{r^2}\begin{pmatrix} -1 & 0 & 0 \\ 0 & 0 & 0 \\ 0 & 0 & 1 \end{pmatrix}, \qquad \sqrt{\dot{\boldsymbol{\varepsilon}}(\mathbf{u}) : \dot{\boldsymbol{\varepsilon}}(\mathbf{u})} = \frac{|\gamma|}{r^2}\sqrt{2} \tag{5.11}$$

Through the Norton-Hoff constitutive relation, we get the deviatoric stresses:

$$\begin{aligned} \boldsymbol{\sigma}^D &= A(n)\sqrt{2}^{(1-n)/n}|\gamma|^{(1-n)/n}\gamma\, r^{-2/n}\begin{pmatrix} -1 & 0 & 0 \\ 0 & 0 & 0 \\ 0 & 0 & 1 \end{pmatrix} \\ ||\boldsymbol{\sigma}^D||_{vM} &= A(n)\sqrt{2}^{(1-n)/n}|\gamma|^{1/n} r^{-2/n}\sqrt{3} \end{aligned} \tag{5.12}$$

The axial and radial equilibrium equations give the mean stress:

$$\mathrm{tr}\,\boldsymbol{\sigma}(r) = 3A(n)\sqrt{2}^{(1-n)/n}\gamma|\gamma|^{(1-n)/n} r^{-2/n}(1-n) + 3\tau \tag{5.13}$$

where τ is a constant, calculated from the zero pressure boundary condition on the outer wall. Then we get the stresses:

$$\begin{aligned} \sigma_{rr}(r) &= \beta(b^{-2/n} - r^{-2/n}) \\ \sigma_{zz}(r) &= \beta(b^{-2/n} - (\frac{n-1}{n} r^{-2/n}) \qquad \text{with } \beta = \frac{A(n)n\sqrt{2}^{(1-n)/n}}{(\varphi f H)^{1/n}} \\ \sigma_{\theta\theta}(r) &= \beta(b^{-2/n} - \frac{n-2}{n} r^{-2/n}) \end{aligned} \tag{5.14}$$

The loading normalization gives: $\varphi f \gamma = \frac{1}{H}$.

The limit load factor sequence terms $\hat{\alpha}_n$ are :

$$\hat{\alpha}_n \varphi f = \frac{2\sqrt{3}}{3}\sigma_y H \int_a^b \frac{|\gamma|}{r^2} r dr = \frac{2\sqrt{3}}{3}\sigma_y \ln\frac{b}{a} \quad \forall n \tag{5.15}$$

Those of the sequence $\underline{\alpha}_n$ are:

$$\underline{\alpha}_n \varphi f = \frac{2\sqrt{3}n}{3(1+n)}\sigma_y \int_a^b r^{(-2n-2)/n} r dr \left(\max_{(a,b)}\left(r^{-2/n}\right)\right)^{-1} = \frac{\sigma_y\sqrt{3}n^2}{3(n+1)}\frac{b^{-2/n}-a^{-2/n}}{a^{-2/n}} \tag{5.16}$$

For $n \to \infty$, that gives:

$$\underline{\alpha}_{1^+} \varphi f = \frac{2\sqrt{3}}{3}\sigma_y \ln\frac{b}{a},$$

that is the same value $\hat{\alpha}_n$ and α_{lim}.

5.4 Three-dimensional case

In 3D we consider the same geometry, but the solid, of unit thickness, is free in the antiplane z direction. The solid is submitted to pressures applied on the horizontal boundary: $-\varphi f$ and vertical one: $-(1-\varphi)f$, with: $\varphi \geq 1/2$. Both pressures are parametrized by α.

5.4.1 Limit analysis solution

The solution is homogeneous (biaxial stresses $\boldsymbol{\sigma}$: $\sigma_{xx} = \varphi f, \sigma_{yy} = (1-\varphi)f, \sigma_{xy} = 0, \sigma_{zz} = 0$, strains ε). We get the limit load factor in this loading direction [23], for the von Mises criterion, with the yield value σ_y:

$$\alpha_{lim} f = \frac{\sigma_y}{\sqrt{3\varphi^2 - 3\varphi + 1}} \tag{5.17}$$

5.4.2 Regularized limit analysis solution

The solution is homogeneous. The isochoric strains are:

$$\dot{\boldsymbol{\varepsilon}}(\mathbf{u}) = \gamma \begin{pmatrix} 1 & 0 & 0 \\ 0 & \delta & 0 \\ 0 & 0 & -1-\delta \end{pmatrix} \qquad \sqrt{\dot{\boldsymbol{\varepsilon}}(\mathbf{u}) : \dot{\boldsymbol{\varepsilon}}(\mathbf{u})} = |\gamma|\sqrt{2(1+\delta+\delta^2)} \tag{5.18}$$

Through the Norton-Hoff constitutive relation, we get the deviatoric stresses:

$$\boldsymbol{\sigma}^D = \beta \begin{pmatrix} 1 & 0 & 0 \\ 0 & \delta & 0 \\ 0 & 0 & -1-\delta \end{pmatrix} \qquad ||\boldsymbol{\sigma}^D||_{vM} = |\beta|\sqrt{3(1+\delta+\delta^2)} \tag{5.19}$$

with $\beta = A(n)\sqrt{2(1+\delta+\delta^2)}^{(1-n)/n}|\gamma|^{(1-n)/n}\gamma$. We deduce from $\sigma_{zz} = 0$: tr$\boldsymbol{\sigma} = -3\beta(1+\delta)$. And the stresses:

$$\boldsymbol{\sigma} = \beta \begin{pmatrix} 2+\delta & 0 & 0 \\ 0 & 1+2\delta & 0 \\ 0 & 0 & 0 \end{pmatrix}.$$

The equilibrium conditions give $\sigma_{xx}(1-\varphi) = \sigma_{yy}\varphi$. We get the parameter $\delta = \dfrac{3\varphi-2}{1-3\varphi}$. The loading normalization gives:

$$\gamma f = \frac{1}{H(b-a)(\varphi+\delta(1-\varphi))} \tag{5.20}$$

The limit load factor terms $\hat{\alpha}_m$ for this loading condition are:

$$\hat{\alpha}_n f = \frac{2\sqrt{3}\sigma_y}{3}\frac{\sqrt{2(1+\delta+\delta^2)}}{\varphi+\delta(1-\varphi)} = \frac{\sigma_y}{\sqrt{3\varphi^2-3\varphi+1}} \tag{5.21}$$

Limit analysis	Regul. limit analysis solution sequence
plane case 1 $\alpha_{lim} f = \dfrac{2\sqrt{3}\sigma_y}{3\lvert 2\varphi-1\rvert}$	$\hat{\alpha}_n f = \dfrac{2\sqrt{3}\sigma_y}{3\lvert 2\varphi-1\rvert} \quad \forall n$ $\underline{\alpha}_n f = \dfrac{2n\sqrt{3}\sigma_y}{3(1+n)\lvert 2\varphi-1\rvert} \quad \forall n$
plane case 2 $\alpha_{lim} f = \dfrac{2\sqrt{3}\sigma_y}{3\lvert\varphi\rvert} + \dfrac{1-\varphi}{\lvert\varphi\rvert}\alpha_0 f$	$\hat{\alpha}_n f = \dfrac{2\sqrt{3}\sigma_y}{3\lvert\varphi\rvert} + \dfrac{1-\varphi}{\lvert\varphi\rvert}\alpha_0 f \quad \forall n.$
Axisymmetrical case	
$\alpha_{lim}\varphi f = \dfrac{2\sqrt{3}}{3}\sigma_y \ln\frac{b}{a}$	$\hat{\alpha}_n\varphi f = \dfrac{2\sqrt{3}}{3}\sigma_y \ln\frac{b}{a} \quad \forall n$ $\underline{\alpha}_n\varphi f = \dfrac{n^2\sigma_y\sqrt{3}}{3(1+n)}\dfrac{b^{-1/n}-a^{-1/n}}{a^{-1/n}} \quad \forall n$
Axisymmetrical case	
$\alpha_{lim} f = \dfrac{\sigma_y}{\sqrt{3\varphi^2-3\varphi+1}}$	$\hat{\alpha}_n f = \dfrac{\sigma_y}{\sqrt{3\varphi^2-3\varphi+1}} \quad \forall n$

Table 5.1: Direct and regularized limit analysis results

5.5 Torispherical vessel head under internal

This benchmark test concerns a vessel-head under pressure see figure 5.1.

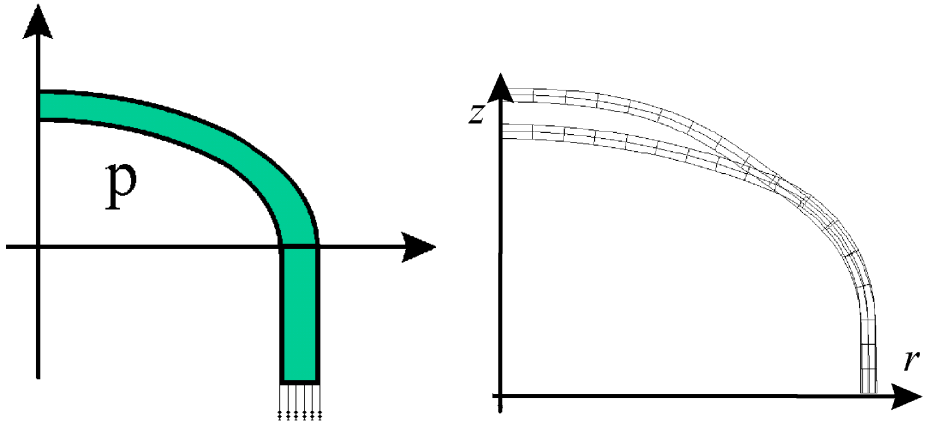

Figure 5.1: Torispherical vessel head under internal pressure ; deformed mesh (right) : 34 Q8 elements, 141 nodes.

The algorithm appears to be very efficient. We can observe on the figure 5.2 the convergence of the upper an approximated lower bound in terms of the regularization parameter. For a parameter $n = 71,0$, and 19 equivalent elastic calculations, we get the results : P_{Aster_sup}=3.9404 MPa, and P_{Aster_inf}=3.8372 MPa.

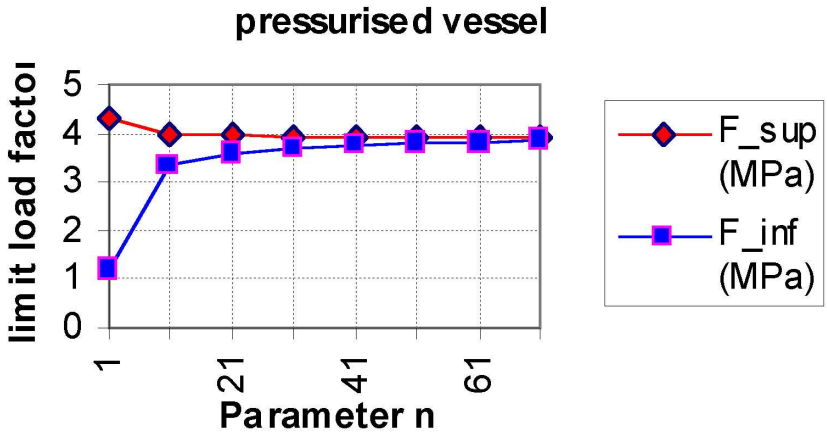

Figure 5.2: Torispherical vessel head under internal pressure: load factors vs. parameter n

5.6 Comparison with a finite strain calculation

We considered an elastoplastic pressurized structure with a flaw on the outer wall (see fig.5.3. With the *Code_Aster* regularized limit analysis algorithm, we get, after 39 equivalent elastic iterations ($n = 8,25$) the following bounding of the limit pressure : 1.353-1.916MPa, for a normalized $\sigma_y = 10.0MPa$. Moreover, we wanted to assess the predicted collapse mode by a finite strain simulation : indeed, we can suspect that a snap-through can occur, that limit analysis can not idealize. With the *Code_Aster* elastoplastic finite strain incremental simulation (using the Simo-Miehe [20] eulerian formulation, which is incrementally objective), assuming isotropic hardening from the experimental strain-stress curve, we get the maximum pressure near from 48.5 MPa, while with limit analysis, we get : 35.1 MPa (if we take the R_e-stress value on the strain-stress curve) or 93 MPa (taking the R_m stress value). The failure modes are quite similar (see fig.5.3).

We have remarked on this kind of structure (high difference of stiffness between the parts of the structure) that the computing time, for the same mesh are quite similar between limit analysis and elastoplastic finite strain incremental simulation. We can conclude that it can be safer and not too difficult to use in parallel elastoplastic calculations and limit analysis.

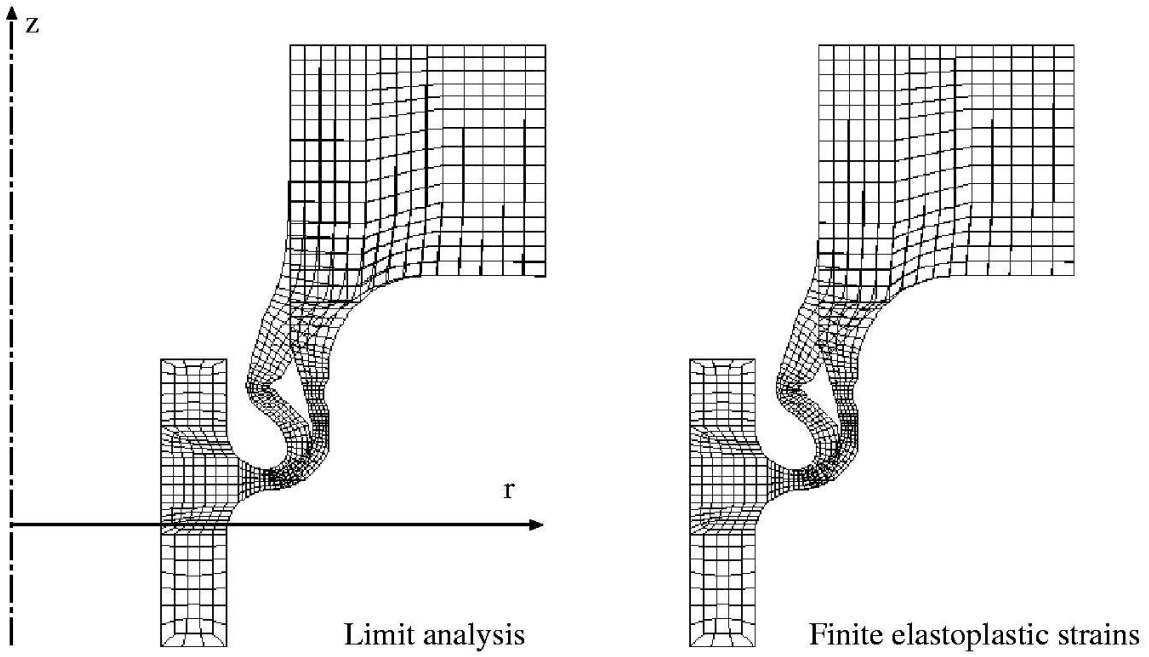

Figure 5.3: Comparison between the predicted collapses (mesh : 2D-axis, 583 Q8 elements, 1946 nodes

6 Conclusions

The limit analysis numerical method presented here has the following characteristics:

- we get an upper bound, with a monotone decreasing with respect to the regularization parameter, and convergence to the true limit load ;
- the regularized dissipation power involved in the upper bound does not include any elastic term;
- we get an estimation of the lower bound by post-processing of the obtained numerical stress field, with convergence to the limit load, in the case without dead load. The increasing of the sequence of these lower bounds can not be proved, but is observed on the benchmark tests. This estimation is of practical interest for the applications.

For the 2D-plane strain situation, we have observed that the main difficulty (of convergence) is not the heterogeneous aspect, but the localization of the collapse mode (shear bands appear). Adaptive meshing is necessary to provide better results for the bounding. For the 2D-axis and 3D cases, the convergence is good and the calculations are not expensive (especially in 2D-axis) and the results that are been obtained are very close to some available analytical simplified lower bound, and other numerical results. These tests have led to improvements of the method, as well to a better knowledge of its behaviour.

Finally, we can conclude that the proposed numerical method, easy to be implemented into any FEM nonlinear software, leads to efficient (90% time saved) and sufficient accurate bounding of limit loads with respect to incremental methods or analytical available solutions.

Acknowledgement

The research has been funded by the European Commission as part of the Brite–EuRam III project LISA: FEM–Based Limit and Shakedown Analysis for Design and Integrity Assessment in European Industry (Project N°: BE 97–4547, Contract N°: BRPR–CT97–0595).

Bibliography

[1] J. Angles, F. Voldoire: Modélisation et calcul de la charge limite d'un composant fissuré, CR-MMN 1522-07 (1996).

[2] E.G. Berak, J.C. Gerdeen: A finite element technique for limit analysis of structures. *J. Pressure Vessel Technology*, **112**, 138-144 (1990).

[3] R. Casciaro, A. Di Carlo, G. Valente: Discussion on Plane stress limit analysis by finite elements by P.G. Hodge P.G., T. Belytschko. *A.S.C.E. J. Eng. Mech. Div.*, 1560-1566 (1971).

[4] R. Casciaro, L. Cascini: A mixed formulation and mixed finite elements for limit analysis. *Int. J. Num. Meth. Eng*., **18**, 211-243, (1982).

[5] E. Christiansen: Computation of limit loads. *Int. J. Num. Meth. Eng.*, **17**, 1547-1570 (1981).

[6] D. Clément: Résolution numérique d'un problème modèle en plasticité. *Thesis*, Univ. Paris Sud (1982).

[7] E. Fisse, F. Voldoire: Eléments finis incompressibles, note EDF/DER HI-75/95/019.

[8] A. Friaâ: Loi de Norton-Hoff généralisée en plasticité et viscoplasticité, Thèse de doctorat (1979).

[9] M. Frémond, A. Friaâ: Les méthodes statique et cinématique en calcul à la rupture et en analyse limite, Journal de Mécanique théorique et appliquée, Vol. 11, No 5, 881-905 (1982).

[10] V. Gaudrat: A Newton type algorithm for plastic limit analysis. *Comp. Meth. Appl. Mech. Eng.* **88**, 207-224, (1991).

[11] T. Guennouni, P. Le Tallec: Calcul à la rupture : régularisation de Norton-Hoff et lagrangien augmenté . *J. Méca. Théo. Appl. Mech.*, **2**, 1, 75-99, (1982).

[12] M. Heitzer: Traglast- und Einspielanalyse zur Bewertung der Sicherheit passiver Komponenten. *Thesis*., RWTH Aachen (1999).

[13] P.G. Hodge, T. Belytschko: Numerical methods for the limit analysis of plates. *J. Appl. Mech.* 796-802 (1968);

[14] P.G. Hodge, T. Belytschko: Plane stress limit analysis by finite elements. *A.S.C.E. J. Eng. Mech. Div*., 931-944 (1970).

[15] J. Joch, R.A. Ainsworth, T.H. Hyde: Limit load and J-estimates for idealised problems of deeply-cracked welded joints in plane-strain bending and tension. *Fatigue Fract. Engng. Mater. Struct.*, **16**, 10, 1061-1079 (1993).

[16] S. Maghous: Détermination du critère de résistance macroscopique d'un matériau hétérogène à structure périodique. *Thesis* E.N.P.C. Paris, (1991).

[17] B. Mercier: Sur la théorie et l'analyse numérique de problèmes de plasticité. *Thesis*, Paris VI, (1977).

[18] J. Pastor, S. Turgeman: Limit Analysis in axisymmetrical problems: numerical determination of complete statical solutions. *Int. J. Mech. Sci*., **24**, 2, 95-117 (1982).

[19] J. Pastor, S. Turgeman: Limit Analysis: a linear formulation of the kinematic approach for axisymmetric mechanical problems. *Int. J. Num. Anal. Meth. Geomech*., **6**, 109-128 (1982).

[20] J.C. Simo, C. Miehe: Associative coupled thermoplasticity at finite strains: Formulation, numerical analysis and implementation, *Comp. Meth. Appl. Mech. Eng*., **98**, 41-104, North Holland, (1992).

[21] M. Staat, M. Heitzer: Limit and shakedown analysis using a general purpose finite element code in *Proceedings of the NAFEMS World Congress '97*. NAFEM Stuttgart (1997) 522-533.

[22] F. Voldoire: Calcul à la rupture et analyse limite des structures, note EDF HI-74/93/082.

[23] F. Voldoire: Analyse limite des structures fissurées et critères de résistance, note EDF/DER HI-74/95/026.

[24] F. Voldoire: Mise en œuvre de la méthode de régularisation de Norton-Hoff-Friaâ pour l'analyse limite des structures, note EDF/DER HI-74/97/026.

[25] A.M. Yan: Contributions to the direct limit state analysis of plastified and cracked structures. *Thesis*, Univ. Liège, (1999).

[26] N. Zouain, J. Herskovits, L. Borges, R. Feijoo: An alternative algorithm for limit analysis with nonlinear yield functions. *Int. J. Solids. Struct*., **30**, 10, 1397-1417 (1993).

[27] [R3.06.05] *Code_Aster* theoretical documentation : Eléments finis incompressibles.

[28] [R5.03.01] *Code_Aster* theoretical documentation : Algorithme non linéaire quasi-statique.

[29] [R5.03.02] *Code_Aster* theoretical documentation : Intégration des relations de comportement élastplastique.

[30] [V6.04.124] *Code_Aster* validation documentation : cas-test SSNV124 Analyse limite. Loi de Norton-Hoff.

Part V

Simplified shakedown analysis with the ZAC method

Valerie Cano, Said Taheri

Département Mécaniques et Modèles Numériques - Service IMA
Direction des Etudes et Recherches, Electricité de France
1 Avenue du Général de Gaulle, F-92141 Clamart Cedex, France

E-mail: said.taheri@edf.fr

1 Introduction

This present contribution concerns particularly the second subject that is the shakedown analysis through a benchmark. One of the aims of this benchmark is to find the elastic shakedown domain in a structure subjected to a cyclic thermal and mechanical loading. Two calculations have been carried out to obtain this domain. The first one uses an incremental simulation with an elastoplastic constitutive law [9] and the second one is realized with a simplified method. In this work, the question is to see if the simplified method gives the same results as the incremental calculation and then to valid this method in the elastic shakedown case. We recall that a structure is said to shake down if it behaves elastically after some initial cycles with plastic strain.

The considered structure is an axisymmetrical test-tube with variable thickness made of quenched 316L stainless steel. This tube is subjected to a thermal cyclic loading and to an internal cyclic pressure.

For the incremental elastoplastic simulations, we have used a model developed by EDF [9] and implemented in the FEM *Code_Aster* software. This model allows to describe the ratchetting in nonsymmetrical load-controlled test, the elastic and plastic shakedown in a symmetrical and nonsymmetrical loading and the cyclic hardening and softening after overloading. Its particularity is to introduce a ratchetting stress and a discrete variable.

Concerning the simplified ZAC method proposed by Zarka and Casier [10], it is based on the linear kinematic hardening and obeys the von Mises criterion. The material parameters are supposed constant with the temperature. This method can be used from a free stress or pre-stressed state and gives the limit state in a structure under cyclic thermo-mechanical loading.

In the first section, we present the ZAC method. Then, we describe the EDF model. The last section is dedicated to the presentation of the studied specimen (geometrical properties, loading and boundary conditions) and to obtained results.

All the simulations has been performed with the EDF *Code_Aster* software.

2 Description of the ZAC method

Depending on the magnitude of loading, a structure can show the structural responses symbolized in the Bree interaction diagram. In addition to the plastic collapse, the structure can fail plastically with time-variant loads through:

- incremental collapse by accumulation of plastic strains over subsequent load cycles (also termed ratchetting, progressive plasticity or cyclic creep),
- plastic fatigue by alternating plasticity in few load cycles (also termed Low Cycle Fatigue (LCF) or plastic shakedown).

The structure does not fail plastically, if finally all plastic strain rates vanish and if the dissipated energy remains finite. One says that the structure adapts to the load or it shakes down elastically. After few initially plastic cycles no difference to the purely elastic behavior can be observed in structural mechanics quantities.

First the theoretical framework of the ZAC methods has to be defined, i.e. the assumptions for its application:

- Quasi static evolution
- Linear theory (small strains)
- Temperature independent material parameters
- Periodic loading (e.g. thermal load T, body forces $\mathbf{f}_0$, surface forces $\mathbf{p}_0$ and given displacements $\mathbf{u}^0$)
- The elastic domain is defined with the von Mises yield criterion

$$F[\boldsymbol{\sigma} - \boldsymbol{\pi}] \leq \sigma_y \qquad \text{or} \qquad ||\boldsymbol{\sigma}_D - \boldsymbol{\pi}|| \leq \sigma_y \tag{2.1}$$

  with the stress tensor $\boldsymbol{\sigma}$, its deviatoric part $\boldsymbol{\sigma}_D$, the initial yield stress σ_y, the von Mises yield function F and the back-stress tensor $\boldsymbol{\pi}$ given by

$$\boldsymbol{\pi} = \mathbf{C}\boldsymbol{\varepsilon}^p, \tag{2.2}$$

  where $\boldsymbol{\varepsilon}^p$ is the plastic strain tensor and $\mathbf{C}$ the material parameter defining the kinematic function.

Within this framework and the above assumptions, Melan's shakedown theorem shows, that under periodic loading any solution of an evolution problem tends to a periodic solution in terms of stress and strain corresponding to the limit state. If the local amplitude of the plastic strain $\boldsymbol{\varepsilon}^p$ vanishes at all points of the structure the structure *shakes down elastically*, otherwise it *shakes down plastically.*

The ZAC method is based on transformed internal variables. It assumes the linear kinematic hardening and gives an approximation of the limit stress and strain. Its main advantage over the direct shakedown analysis is that is gives an estimation of plastic strain amplitudes from some elastic calculations. The quality of estimates on steady cyclic behaviour by Zarka's method is critically discussed in [6]. If all assumption given above are fulfilled for a structure V, it can be summarized as follows:

The actual tensor $\boldsymbol{\sigma}$ and its deviatoric part $\boldsymbol{\sigma}_D$ can be written as :

$$\boldsymbol{\sigma} = \boldsymbol{\sigma}^E + \boldsymbol{\rho} \qquad \text{and} \qquad \boldsymbol{\sigma}_D = \boldsymbol{\sigma}_D^E + \boldsymbol{\rho}_D \tag{2.3}$$

with the elastic stress tensor $\boldsymbol{\sigma}^E$ and the residual stress tensor $\boldsymbol{\rho}$ and its deviatoric parts $\boldsymbol{\sigma}_D^E$ and $\boldsymbol{\rho}_D$. The idea of the method is to perform uncoupled computations at each point. The

use of the modified parameter $\boldsymbol{\pi}$ allows to build an approximation of the limit state of the structure at each point, independently from the other points.

$$\mathbf{Y} = \boldsymbol{\pi} - \boldsymbol{\rho}_D \qquad \text{with the yield criteria} \qquad ||\boldsymbol{\sigma}_D^E - \mathbf{Y}|| \leq \sigma_y. \tag{2.4}$$

$\mathbf{Y}$ is the modified variable, such that in the deviatoric stress space, the yield surface represents a sphere of center $\boldsymbol{\sigma}_D^E$ and of radius σ_y.

The key point of the ZAC method [10] is the way to calculate the modified variable $\mathbf{Y}$ at the limit state at each point. The knowledge of the transformed variable $\mathbf{Y}$ at the limit state will allow to solve the elastic problem with an initial strain $\mathbf{C}^{-1}\mathbf{Y}$ verified by the residual stress $\boldsymbol{\rho}$ and then to obtain the limit stress and strain.

2.1 Condition of elastic shakedown

At each point of the structure, one defines the quantities F^E(x) on one cycle, such that

$$\mathbf{Y} = \boldsymbol{\pi} - \boldsymbol{\rho}_D \qquad \text{with the yield criteria} \qquad ||\boldsymbol{\sigma}_D^E - \mathbf{Y}|| \leq \sigma_y. \tag{2.5}$$

$$F^E(x) = \max||\boldsymbol{\sigma}^E(x,t_1) - \boldsymbol{\sigma}^E(x,t_0)|| \equiv ||\boldsymbol{\sigma}_{max}^E(x) - \boldsymbol{\sigma}_{min}^E(x)||, \tag{2.6}$$

where t_1 and t_0 correspond to the extrema of the load cycle. The global quantity F^E is the maximum $F^E(x)$ for all x.

The comparison between the quantity F^E and the initial yield stress σ_y allows to decide if there is elastic or plastic shakedown

$$\begin{cases} F^E \leq 2\sigma_y \text{ elastic shakedown} \\ F^E > 2\sigma_y \text{ plastic shakedown} \end{cases} \tag{2.7}$$

From a geometrical point of view, if the intersection C_L (see 2.1) of two spheres of center $\boldsymbol{\sigma}_{max}^E$ and $\boldsymbol{\sigma}_{min}^E$ and of radius the yield stress σ_y is not empty, there is elastic shakedown, otherwise there is plastic shakedown. One shows that at each point of a structure in an elastic shakedown situation, there is a limit factor Y_{lim} fixed in time so that this modified parameter Y_{lim} at the limit state belongs to the intersection C_L of these two spheres. In the case of elastic shakedown, the estimate of the limit variable Y_{lim} is obtained in the ZAC method, through the local projection of the initial variable Y_0 on this intersection C_L of these two spheres, according to the rules presented on figure 2.1.

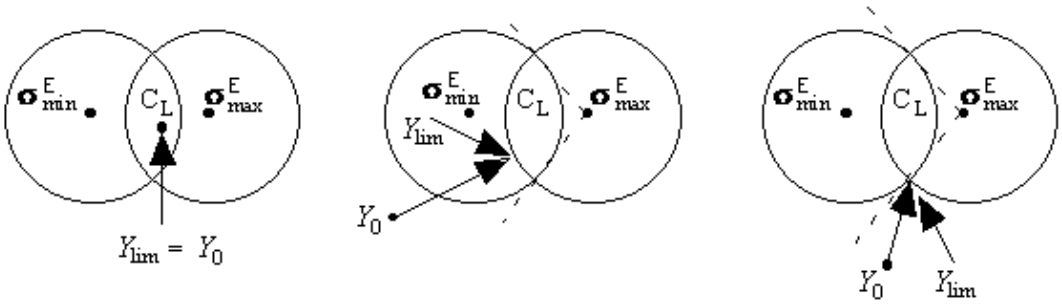

Figure 2.1: The three ways to assess Y_{lim} as a function of Y_0.

2.2 Equations verified by the actual, elastic and residual stresses

The following conditions are fulfilled for the stresses. The elastoplastic problem verifies:

$$\begin{aligned} -\text{div}\boldsymbol{\sigma} &= \mathbf{f}_0 \text{ in } V \\ \boldsymbol{\sigma}\mathbf{n} &= \mathbf{p}_0 \text{ on } \partial V_p \\ \mathbf{u} &= \mathbf{u}^0 \text{ on } \partial V_u \\ \boldsymbol{\varepsilon} &= \frac{1}{2}\left(\nabla\mathbf{u} + \nabla^T\mathbf{u}\right) \\ \boldsymbol{\sigma} &= \mathbf{E} : (\boldsymbol{\varepsilon} - \boldsymbol{\varepsilon}^p - \boldsymbol{\varepsilon}^{th}) \end{aligned} \tag{2.8}$$

The elastic problem solution is given by:

$$\begin{aligned} -\text{div}\boldsymbol{\sigma}^E &= \mathbf{f}_0 \text{ in } V \\ \boldsymbol{\sigma}^E\mathbf{n} &= \mathbf{p}_0 \text{ on } \partial V_p \\ \mathbf{u}^E &= \mathbf{u}^0 \text{ on } \partial V_u \\ \boldsymbol{\varepsilon}^E &= \frac{1}{2}\left(\nabla\mathbf{u}^E + \nabla^T\mathbf{u}^E\right) \\ \boldsymbol{\sigma}^E &= \mathbf{E} : (\boldsymbol{\varepsilon}^E - \boldsymbol{\varepsilon}^{th}) \end{aligned} \tag{2.9}$$

Calculating the difference between the sets of equations (2.8) and (2.9), one finds the self equilibrated following problem with $\boldsymbol{\rho} = \boldsymbol{\sigma} - \boldsymbol{\sigma}^E$, $\boldsymbol{\varepsilon}^R = \boldsymbol{\varepsilon} - \boldsymbol{\varepsilon}^E$ and $\mathbf{u}^R = \mathbf{u} - \mathbf{u}^E$:

$$\begin{aligned} -\text{div}\boldsymbol{\rho} &= \mathbf{0} \text{ in } V \\ \boldsymbol{\rho}\mathbf{n} &= \mathbf{0} \text{ on } \partial V_p \\ \mathbf{u}^R &= \mathbf{0} \text{ on } \partial V_u \\ \boldsymbol{\varepsilon}^R &= \frac{1}{2}\left(\nabla\mathbf{u}^R + \nabla^T\mathbf{u}^R\right) \\ \boldsymbol{\varepsilon}^R &= \mathbf{E}^{-1} : \boldsymbol{\rho} + \mathbf{C}^{-1} : (\boldsymbol{\rho}_0 + \mathbf{Y}) \end{aligned} \tag{2.10}$$

Then, the knowledge of the transformed variable at the limit state $Y_{\lim}$ will allow to solve the elastic problem (2.10) with an initial strain (Y_{lim}/C) verified by the residual stress $\boldsymbol{\rho}$ and then to obtain the limit stress and the limit plastic strain.

Remark

The initial variable Y_0 can be chosen zero or nonzero. In this last case, several loading cyclic can be performed with a linear kinematic model before applying the ZAC method.

3 Elastoplastic cyclic constitutive law

The Visc-Taheri model [9] has been developed by EDF in order to describe simultaneously the ratcheting, the elastic and plastic shakedown in symmetrical and nonsymmetrical stress-controlled tests and the cyclic hardening and softening after overloading in strain-controlled tests. More generally, this model uses a non-linear isotropic and kinematic hardening law and the evolution of internal variables is deduced from yield surfaces, from the assumption of normality and consistency conditions. Briefly, the different features of this model consists in the introduction of a ratcheting stress, of a discrete variable $\boldsymbol{\varepsilon}_n^p$ representing the plastic strain at last unloading and of a peak stress $\boldsymbol{\sigma}^P$ which, in the uni-axial case, is the maximum stress undergone during the history of loading. The introduction of a ratcheting stress is derived from some experimental tensile tests, which show that at room temperature the ratcheting phenomena occurs when the maximum stress reaches a stress threshold, independently of the amplitude of the loading.

There are four internal variables: $\boldsymbol{\varepsilon}^p$ plastic strain, peak stress $\boldsymbol{\sigma}^P$, the cumulated plastic strain $\mathbf{p}$ and the plastic strain at last unloading $\boldsymbol{\varepsilon}_n^p$. The significant variable is $\boldsymbol{\varepsilon}^p - \boldsymbol{\varepsilon}_n^p$, which measures the plastic strain amplitude. The model introduces a regularization of the temporal discontinuity of $\boldsymbol{\varepsilon}_n^p$. The law is described by three yield surfaces in the deviatoric space: a spherical loading surface F which governs the evolution of plastic strain, a spherical maximal surface G centered at the origin, containing the loading surface F and relative to the evolution of the peak stress; the third is a fixed ultimate spherical surface centered at the origin and containing the other surfaces (see [9] for the details of the model).

The constitutive law is described by the following equations:

$$F = (\tilde{\boldsymbol{\sigma}} - \boldsymbol{\pi})_{eq} - R \leq 0 \qquad \text{loading surface} \qquad (3.1)$$

$$G = \boldsymbol{\pi}_{eq} + R - \boldsymbol{\sigma}^p \leq 0 \qquad \text{maximal loading surface} \qquad (3.2)$$

$$\boldsymbol{\sigma} = 2\mu(\boldsymbol{\varepsilon} - \boldsymbol{\varepsilon}^p) + K\mathrm{tr}(\boldsymbol{\varepsilon} - \boldsymbol{\varepsilon}^{th})\mathbf{I} \qquad \boldsymbol{\varepsilon}^{th} = \alpha_t(T - T^{ref})\mathbf{I} \qquad (3.3)$$

$$R = D\left[R^0 + \left(\frac{2}{3}\right)^a A\left(\boldsymbol{\varepsilon}^p - \boldsymbol{\varepsilon}_n^p\right)_{eq}^a\right] \qquad D = 1 - me^{-bp(1-\sigma^p/S)} \qquad (3.4)$$

$$\boldsymbol{\pi} = C\left[S\boldsymbol{\varepsilon}^p - \boldsymbol{\sigma}^p\boldsymbol{\varepsilon}_n^p\right] \qquad C = C_\infty + C_1 e^{-bp(1-\sigma^p/S)} \tag{3.5}$$

$$\dot{\boldsymbol{\varepsilon}}^p = \frac{3}{2}\dot{p}\frac{\tilde{\boldsymbol{\sigma}} - \boldsymbol{\pi}}{(\tilde{\boldsymbol{\sigma}} - \boldsymbol{\pi})_{eq}} \qquad \text{plastic law (normal)} \tag{3.6}$$

$$\dot{\boldsymbol{\varepsilon}}_n^p = \dot{\zeta}(\boldsymbol{\varepsilon}^p - \boldsymbol{\varepsilon}_n^p) \qquad \text{evolution law} \tag{3.7}$$

where R is the isotropic hardening function, $\boldsymbol{\pi}$ the back-stress tensor, $\boldsymbol{\varepsilon}^{th}$ the thermal strain, K, μ the bulk and shear modulus, α_t and T^{ref} the thermal expansion coefficient and the reference temperature and R^0, a, A, b, C_∞ and C_1 the other material properties used to define the hardening functions.

The consistency conditions are given by:

$$F \leq 0 \qquad \dot{p} \geq 0 \qquad F\dot{p} = 0 \tag{3.8}$$

$$G \leq 0 \qquad \dot{\sigma}^p \geq 0 \qquad G\dot{\sigma}^p = 0 \tag{3.9}$$

$$F \leq 0 \qquad \dot{\zeta} \geq 0 \qquad F\dot{\zeta} = 0 \tag{3.10}$$

In this model, four kinds of evolutions are possible:

$$\text{real unloading} \quad \dot{\zeta} = 0,\ \dot{p} = 0 \qquad \text{pseudo unloading} \quad \dot{\zeta} > 0,\ \dot{p} = 0 \tag{3.11}$$

$$\text{real loading} \quad \dot{\zeta} = 0,\ \dot{p} > 0,\ \dot{\sigma}^p = 0 \qquad \text{pseudo loading} \quad \dot{\zeta} = 0,\ \dot{p} > 0,\ \dot{\sigma}^p > 0 \tag{3.12}$$

4 Presentation of the benchmark

4.1 Specimen test

In Fig. 4.1, the geometry and the loading of the considered specimen are represented [3]. The structure is subjected to a cyclic internal pressure P_0 and a cyclic thermal loading (heating process by Joule effect until a given temperature, then cooling). The duration of the heating is of 18s and the duration of cooling by natural convection is about 1480s to come back to the room temperature (equal to $50°C$). The advantage of the considered 316L material is that it suits with the ZAC method because the tensile curves are practically bilinear. The identification has been realized from three tensile tests at the temperatures $20°C$, $250°C$ and $450°C$ and the resulting values are given in Tab 4.1.

Remark

In a previous study about the same structure [2], [1] a first comparison was performed in the plastic shakedown case between different elastoplastic models, the ZAC method and the experiment. This study allowed to choose the most

satisfactory constitutive models for the description of ratchetting. Therefore, one considers here one of these constitutive laws and we shall suppose that the used elastoplastic model represents well the real behaviour of considered material.

Coefficient	$20°C$	$250°C$	$450°C$
Young's modulus (GPa)	192.5	168.3	160.2
Poisson's ratio	0.3	0.3	0.3
Thermal expansion coefficient (K^{-1})	16.410^{-6}	17.510^{-6}	18.210^{-6}
Yield stress (MPa)	210.9	118.4	101.2
Ultimate stress (MPa)	571	433	423
Hardening modulus (MPa)	6590	3022	2870

Table 4.1: Temperature dependent material data

4.2 Incremental calculations with the cyclic elastoplastic constitutive law

For the incremental calculation, all material parameters are chosen temperature dependent (the structure is made of 316L stainless steel). 4.2 summarizes the different simulations to evaluate the elastic shakedown domain. The maximal temperature T_{max} obtained in the structure, the minimal temperature T_{min} (at the same point where the specimen reaches T_{max}), the internal pressure , the number of simulated loading cycles, the duration of each calculation (on an ORIGIN 2000 computer) and the increment of cumulated plastic strain Δp at the last cycle at the most loaded point are presented.

To detect the elastic shakedown or plastic shakedown, we have calculated the increment of cumulated plastic strain per cycle Δp as a function of the number of the cycle, that is:

$$\Delta p = p_{n*1500} - p_{(n-1)*1500} \tag{4.1}$$

where p is the maximal cumulated plastic strain reached in the structure and n the number of the cycle. When the increment Δp vanishes, there is elastic shakedown and when the increment tends to an asymptote, there is plastic shakedown. Strictly speaking, the considered structure does not reach the stabilized state. Therefore, fixed values are chosen, which define the plastic shakedown and the elastic shakedown. These values are

$$\Delta p \cong 10^{-2}\% \qquad \text{plastic shakedown} \tag{4.2}$$

$$\Delta p \cong 10^{-4}\% \qquad \text{elastic shakedown.} \tag{4.3}$$

Between these two values, the interpretation remains delicate. The choice of these values has been suggested by the form of the curves representing the increment of Δp as a function of the number of the cycle n.

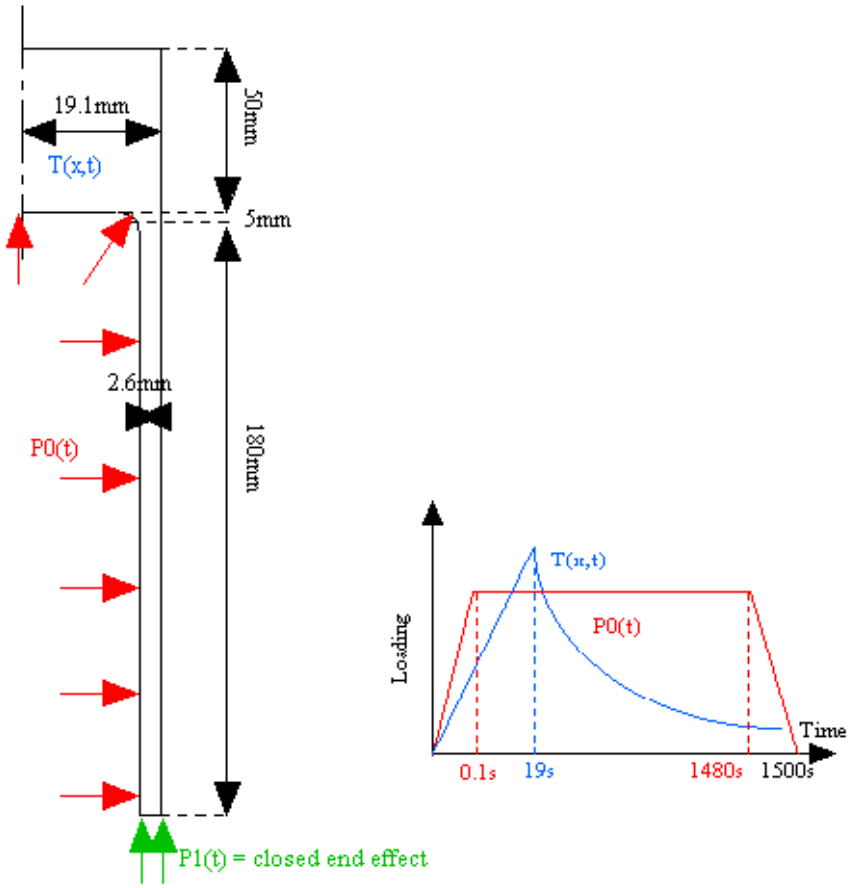

Figure 4.1: Geometry and loading

4.3 Simulation with the ZAC method

We have chosen to apply the method for the constitutive law parameters defined at the maximal temperature T_{max} reached in the structure and from a pre-stressed state. We have then carried out a first incremental elastoplastic simulation (one and half cycle) with the linear kinematic hardening model, then applied the simplified method. The two elastic problems are solved at time corresponding to maximal loading (1519s) and at time corresponding to minimal loading (1500s). In the table 4.2, we report the performed calculations and the results. Concerning the duration of one simulation, it is very short, about 300s. The used material for the specimen is considered with a good case to apply the ZAC method because the tensile curves are practically bilinear.

Remark

The used material for the specimen is considered with a good case to apply the ZAC method because the tensile curves are practically bilinear.

$T_{max}(°C)$	$T_{min}(°C)$	P_0(MPa)	Result
221	58	0	plastic shakedown
183	56	0	**elastic shakedown**
183	56	2.25	plastic shakedown
154	55	2.25	**elastic shakedown**
154	55	4.5	plastic shakedown
106	53	6.75	**elastic shakedown**
106	53	9	plastic shakedown
84	52	9	**elastic shakedown**
84	52	11.25	plastic shakedown
53	50	13.5	**elastic shakedown**
53	50	15.75	plastic shakedown

Table 4.2: Simulations with the ZAC method and results

4.4 Comparison of the two elastic shakedown domains

In the figure 4.2, we report the results of the two simulations in the diagram: variation of the temperature $\Delta T = T_{max} - T_{min}$ (at the same point) as a function of internal pressure P_0. The points represent the results obtained by the elastoplastic model (incremental simulation) and the squares are the results obtained by the ZAC method. The red color stands for the elastic shakedown case, the black color for the plastic shakedown and the blue color for a ambiguous situation in the incremental simulations case. We have reported also the lower bound of elastic shakedown domain for the ZAC method and for the elastoplastic model. One remarks on this diagram that the elastic shakedown domain found by the incremental calculation and by the simplified method are very close (the lower bound for the elastoplastic model is a little smaller than the one obtained by the ZAC method).

5 Conclusion

This study has allowed to assess the ZAC method numerically in the elastic shakedown case. If we consider that the cyclic elastoplastic model represents well the actual behaviour of the material 316L, we find with the ZAC method the same elastic shakedown domain as the one obtained by the EDF model. Despite the assumptions of the simplified method, this result is very interesting for future applications. One recalls that these assumptions are:

- linear kinematic hardening. It is true that the material 316L quenched with a bilinear curve is a good case to study the ZAC method. The choice of the hardening modulus is easier and then one eliminates the problem of constitutive law choice.
- the method applies when the material characteristics are temperature-independent.
- the method gives only an approximation of the limit state.

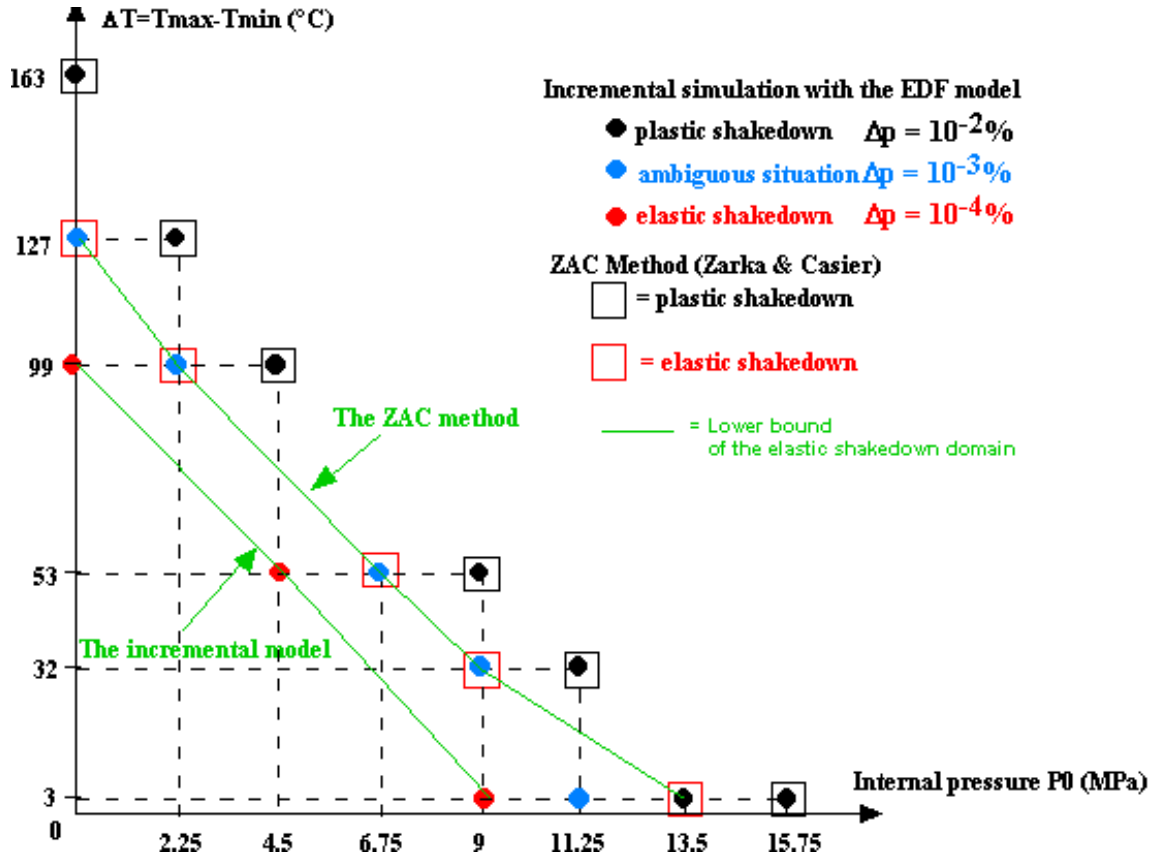

Figure 4.2: Elastic shakedown domain with the ZAC and the incremental method

Acknowledgement

The research has been funded by the European Commission as part of the Brite–EuRam III project LISA: FEM–Based Limit and Shakedown Analysis for Design and Integrity Assessment in European Industry (Project N°: BE 97–4547, Contract N°: BRPR–CT97–0595).

Bibliography

[1] J. Angles, S. Taheri: *La méthode simplifiée ZAC, appliquée au benchmark Cothaa*, 4$^{\text{ème}}$ colloque national en calcul des structures, Gien, France, May 1999.

[2] M.T. Cabrillat et. al., Benchmark on a thermal ratchetting test, comparison of different constitutive models, SMiRT 14, France, Vol. L (1997) pp.229-236.

[3] M.T. Cabrillat: *Benchmark COTHAA, spécifications*, Note technique CEA SERA/LDCS 95/6051, (1995).

[4] V. Cano, S. Taheri: Elastic shakedown domain in an axisymmetrical structure subjected to a cyclic thermal and mechanical loading – comparison between an incremental model and a simplified method. ECCOMAS 2000, CD-Rom Proceedings, Barcelona (2000).

[5] J.A. König: Shakedown of Elastic–Plastic Structures, Elsevier Amsterdam and PWN Warsaw (1987).

[6] G. Maier, C. Comi, A. Corigliano, U. Perego, H. Hübel: Bounds and Estimates on Inelastic Deformations: A Study of their Practical Usefulness. European Commission Report EUR 16555EN, Brussels (1995).

[7] A.R.S. Ponter, K.F. Carter: Shakedown state simulation techniques based on linear elastic solutions. Computer Methods in Applied Mechanics and Engineering. 140 (1997), pp.259-279.

[8] M. Save, G. de Saxcé, A. Borkowski: Computations of shakedown loads feasibility study. European Commission Report EUR 13618 EN, Brussels, Luxembourg (1991).

[9] S. Taheri, E. Lorentz: An elastic-plastic constitutive law for the description of uniaxial and multiaxial ratcheting, International Journal of Plasticity 15 (1999) pp.1159-1180.

[10] J. Zarka, C. Casier: Elastic plastic response of a structure to cyclic loading: practical rules, Mechanics today, vol.6 ed. Nemat-Nasser, Pergamon Press (1979).

Part VI

Shakedown analysis of plane stress problems via SOCP

Athanasios Makrodimopoulos, Christos Bisbos

Institute of Steel Structures, Civil Engineering Department
Aristotle University, GR-54006 Thessaloniki, Greece

E-mail: cbisbos@civil.auth.gr

Nomenclature

2D, 3D	Two-dimensional, three-dimensional
APSC	Alternating Plasticity
DOFs	Degrees of Freedom
CNLP	Convex Nonlinear Programming
CP	Conic Programming
CQO	Conic Quadratic Optimization
IPM	Interior Point Method
LISA	Limit and shakedown analysis, acronym of the project
LP	Linear Programming
MOSEK	Optimization software by MOSEK ApS, Copenhagen
MP	Mathematical Programming
QCLP	Quadratically Constrained Linear Programming
SDP	Semidefinite Programming
SIP	Semi-infinite Programming
SOCP	Second Order Cone Programming
SQP	Sequential Quadratic Programming
s.p.d.	semipositive definite (matrix)
E	modulus of elasticity
f, F, Φ	yield function
$V, \partial V$	structure and its boundary ($\partial V = \partial V_P \cup \partial V_U$)
α_t	thermal expansion coefficient
β_i	Numerical integration weight factor at i-th Gauss point
$\boldsymbol{\varepsilon}$	actual strain
$\boldsymbol{\pi}$	Back-stress
$\boldsymbol{\rho}$	residual stress
$\boldsymbol{\sigma}$	actual stress
σ_u	ultimate tensile strength
σ_y	yield stress
NF	Number of free DOFs in the structure
NE	Number of finite elements in the structure
NG	Total number of Gauss points
NV	Number of vertices of the load domain
$\mathcal{I}$	Index set: $\mathcal{I} = \{1, \ldots, NG\}$
$\mathcal{J}$	Index set: $\mathcal{J} = \{1, \ldots, NV\}$

1 Basic formulations

1.1 Introduction

All engineering structures are subjected to variable loading. In several cases the exact loading path is unknown, or it has a prominently cyclic character. Fortunately the limits of the variation of the actual loads can be usually prescribed with sufficient accuracy.

Shakedown analysis offers the possibility to estimate the load carrying capacity of an elastoplastic structure subjected to variable loads. Its basis is formed by the work of Melan ([33], [34]) and Koiter ([25]): they formulated the static and kinematic shakedown theorems by means of which, we can determine criteria as to whether a structure, subjected to loads varying inside a given load domain, will shake down or not. Based on their work, a plethora of researchers has intensively studied shakedown and formed it as a very active independent research topic. If the loading domain shrinks to a point, then the shakedown analysis problem becomes the limit analysis one. Theories, extensions and applications of limit and shakedown analysis have been extensively studied the last thirty years. Both problem types lead to extremum (optimization) problems and the presence of computers, the finite Element Method (FEM), and Mathematical Programming (MP) techniques has definitely influenced their development. (see e.g. the monographs [48]-[20], and the specialized conference proceedings [10]-[60]).

The shakedown theory has been extended to cover several aspects. Hardening and non-associative flow rules have been studied e.g. by Maier [30, 31], [45], Weichert et al. [57], Stein et al. [51], [52], Heitzer et al. [19], and Polizzotto et. al. [39]. Studies on the shakedown problem under geometric nonlinearity can be found in [31, 56, 58, 41, 53]. Shakedown has been extended also to composites [59], damaged and cracked structures [4, 14, 17, 58], and poroplasticity [9]. Another important case concerns the effects of temperature on the yield surface [6, 24, 16, 62]. The shakedown design of frames has been treated by Giambanco et al. [15] and Spiliopoulos [49].

Shakedown analysis can be cast in an abstract functional analytic setting. Its computational implementation consists in the combination of some FEM discretization and an optimization technique selected from MP. Since virtually all FEM codes are based on the displacement method, the control points are usually the Gauss points of the FEM mesh. A second crucial discretization step concerns the loading domain: it is assumed usually to be a convex polyhedron, although this assumption is not included even in the basic theorems of Melan and Koiter. Without this assumption the optimization problem renders to be a rather difficult Semi-Infinite Programming (SIP) problem (cf. e.g. [46]).

Even in the simplest case of the classical von Mises yield condition with classical boundary conditions and excluding geometric nonlinearity effects, the computational shakedown analysis is not a trivial task for engineering applications. Due to the fact that the yield condition is nonlinear, the final MP problem, resulting from e.g. the lower bound approach,

is a Convex Nonlinear Programming (CNLP) problem with a large number of variables and nonlinear constraints and consequently effective algorithms and implementations are needed. The focus of the present work essentially concerns this aspect. A discretized formulation is worked out, leading to a Second Order Cone Programming (SOCP) problem, for which efficient algorithms and implementations exist.

1.2 The computational optimization framework

1.2.1 Motivation of the present work

In the first period of the application of MP techniques to the shakedown analysis, pioneered by G. Maier and documented e.g. in [10], the involved yield surfaces have been linearized and the resulting MP formulation was a LP problem. Consequently the MP method of choice was the famous Simplex algorithm in its various forms.

If the von Mises yield surfaces are kept as nonlinear functions, the mathematical formulation of the discretized shakedown problem - using the static approach - leads to a CNLP problem. This general embedding is not in all cases computationally advantageous, since the number of unknowns is large and the specific form and the peculiar characteristics of the problem are not exploited. One effective way is to develop specifically tailored algorithms and to incorporate them in the FEM code. Stein and Zhang [51, 52] Groß-Weege [16] and Heitzer and Staat [50, 18] have developed special SQP methods based on a reduced basis technique, exploiting the inherent characteristics of the shakedown problem.

The present approach follows another way. A formulation is worked out, which allows for the application of available specific software, already developed by the MP community within the framework of Interior Point Methods (IPMs), which constitute one of the most active and fruitful research directions concerning CNLP during the last fifteen years. In this case a well-defined and clearly coded program interface between the FEM and the MP codes is needed. This approach has its own advantages and disadvantages. Depending on the availability of the MP code, communication can be achieved perhaps only through specific data files. This is not considered to be a very serious drawback for the today's computers. For the geometrically linear shakedown problems studied only one activation of the IPM software is needed. Perhaps the most important disadvantage consists in the fact that not all the peculiarities of the shakedown problem are really exploited. On the other side the number of available IPM techniques grows very rapidly. Despite their efficiency, IPMs are difficult to code and a clearly defined interface allows for independent developments on the FEM as on MP side as well. Parallelization e.g., which holds as a computationally attractive aspect, can be achieved independently on the FEM or on the MP side.

1.2.2 The IPM framework

After the publication of the Karmarkar's algorithm in 1984 a great number of IPMs have been developed for LP problems with extraordinary success. Their name reflects the fact that the points generated by the algorithms lie in the interior of the feasible region. This is in contrast to the simplex method e.g., which is an active set method, moving along the boundary of the feasible region. IPMs perform essentially Newton steps for large but sparse systems. The success of IPMs for LP problems has encouraged researchers to apply them to nonlinear problems as well (see e.g. [12]). Today the IPMs for CNLPs are considered as really competitive to other computational techniques.

A key concept within the IPMs for CNLP is the Conic Programming (CP) problem, i.e. the solution of a minimization problem with linear objective function and feasible region defined by some cone ([38, 47, 5]). CP encompasses as important special cases not only LP but the (Semi-definte Programming) SDP and the SOCP cases as well. A recent benchmarking of available SDP and SOCP software has been undertaken by Mittelmann ([35]).

In its simplest form the SDP problem consists in the minimization (maximization) of a linear function of $\mathbf{x}$ with $\mathbf{x} \in I\!R^n$ subjected to the constraint that a matrix, which is a linear function of $\mathbf{x}$, must be semipositive definite (s.p.d.). The problem data of SDP are $\mathbf{c} \in I\!R^n$ and the $n+1$ constant symmetric matrices $\mathbf{F}_0, \mathbf{F}_1, \ldots, \mathbf{F}_n$ defining the matrix function $\mathbf{F}(\mathbf{x}) = \mathbf{F}_0 + x_1\mathbf{F}_1 + x_2\mathbf{F}_2 + \ldots + x_n\mathbf{F}_n$. Then the SDP problem is formulated as:

$$\begin{array}{ll} \min & \mathbf{c}^T\mathbf{x} \\ s.t. & \mathbf{z}^T\mathbf{F}(\mathbf{x})\mathbf{z} \geq 0 \end{array}$$

There are many equivalent representations of SDP. In control theory the s.p.d. constraint is termed a Linear Matrix Inequality (LMI). Let us note that the subspace of the s.p.d. matrices form a cone. The SDP problem is a CNLP problem with a feasible region having a piecewise smooth boundary. More specifically the boundary of the feasible region consists of pieces corresponding to algebraic surfaces. Another property of SDP is that - provided that the problem is feasible - an optimal point lies always on the boundary. Although the SDP problem seems quite specialized, it has attracted much attention by the researchers, since e.g. it includes many important optimization problems as special cases (cf. e.g. the expository papers [55, 54] and the handbook [61]). Another reason, perhaps the most important one, is the fact that SDP problems can be theoretically studied and algorithmically solved efficiently. Despite its efficiency, SDP is more general than required for the LISA purposes.

1.2.3 The SOCP problem

In a SOCP problem, closely related to SDP but less general, we minimize a linear function over the intersection of an affine set (a system of linear equations) with the Cartesian prod-

uct of a finite number of second-order cones. In this section we follow the expositions of [13, 29, 7].

Recall that a set $K \subset I\!R^D$ is a cone if the following condition holds:

$$\mathbf{x} \in K \implies \lambda \mathbf{x} \in K \quad \forall\, \lambda \geq 0 \tag{1.1}$$

The cone $K^* \subset I\!R^D$, dual to K is defined by:

$$K^* \equiv \{\mathbf{s} \in I\!R^D \ : \ \mathbf{s}^T \mathbf{x} \geq 0 \quad \forall \ \mathbf{x} \in K\} \tag{1.2}$$

If $K = K^*$ the cone is self-dual. The standard or unit second-order cone of dimension d_i is defined by:

$$K_i = \{\mathbf{x}_i^T = (x_{i0}, \mathbf{x}_{i1}^T) \in I\!R \times I\!R^{d_i - 1} \ : \ x_{i0} - \|\mathbf{x}_{i1}\| \geq 0\} \quad K_i \subset I\!R^{d_i} \tag{1.3}$$

where $\|\cdot\|$ denotes the usual Euclidean norm. (1.3) can be written also in the form:

$$K_i = \{\mathbf{x}_i \in I\!R^{d_i} \ : \ x_{i,1}^2 \geq \sum_{j=2}^{d_i} x_{i,j}^2, \quad x_{i,1} \geq 0\}$$

This cone, which is self-dual, is called also the ice-cream or Lorenz cone. The general form of a second-order cone of dimension d_i for the variable $\mathbf{x} \in I\!R^n$ is defined by the inequality constraint:

$$K_i = \{\mathbf{x}_i \in I\!R^n \ : \ \|\mathbf{P}_i \mathbf{x} + \mathbf{p}_i\| \leq \mathbf{g}_i^T \mathbf{x} + r_i\} \tag{1.4}$$

with data $\mathbf{P}_i \in I\!R^{di} \times I\!R^n$, $\mathbf{p}_i \in I\!R^{di}$, $\mathbf{g}_i \in I\!R^n$, $r_i \in I\!R$. With appropriate selection of the data the standard conic constraint (1.3) is recovered. (1.4) yields a linear equation system as special case, when $\mathbf{g}_i = \mathbf{0}$ and $r_i = 0$. If further $\mathbf{p}_i = \mathbf{0}$ the condition is recovered, that $\mathbf{x}$ must lie in the null space of $\mathbf{P}_i$.

Now a representative standard second-order cone program has the following partitioned form:

$$\begin{aligned} \min \quad & \sum_{i=1}^{k} \mathbf{c}_i^T \mathbf{x}_i \\ s.t. \quad & \mathbf{x}_i \in K_i, \qquad i = 1, \ldots, k \\ & \sum_{i=1}^{k} \mathbf{A}_i \mathbf{x}_i = \mathbf{b} \end{aligned} \tag{1.5}$$

where $\mathbf{x}_i \in I\!R^{d_i}, i = 1, \ldots, k$ are the unknown variables, K_i are unit second-order cones of dimension d_i respectively and the other data are $\mathbf{b} \in I\!R^m$, $\mathbf{A}_i \in I\!R^{m \times d_i}$ and $\mathbf{c}_i \in I\!R^{d_i}$. The dual of problem (1.5) is:

$$\begin{aligned} \max \quad & \mathbf{b}^T \mathbf{y} \\ s.t. \quad & \mathbf{s}_i \in K_i^*, \qquad i = 1, \ldots, k \\ & \mathbf{A}_i^T \mathbf{y} + \mathbf{s}_i = \mathbf{c}_i, \qquad i = 1, \ldots, k \end{aligned} \tag{1.6}$$

If some unknown $\mathbf{x}_i$, present in the the linear system, is not subjected to a conic constraint, the respective dual variable $\mathbf{s}_i$ is zero, since the dual of the whole $I\!R^d$ is the singleton set, containing the origin. Defining:

$$\begin{aligned} D &\equiv d_1 + \ldots + d_k \\ K &= K_1 \times \ldots \times K_k \\ \mathbf{A} &= (\mathbf{A}_1 : \mathbf{A}_2 : \ldots : \mathbf{A}_k) \in I\!R^{m \times D} \\ \mathbf{c}^T &= (\mathbf{c}_1^T, \ldots, \mathbf{c}_k^T) \in I\!R^D \\ \mathbf{x}^T &= (\mathbf{x}_1^T, \ldots, \mathbf{x}_k^T) \in I\!R^D \\ \mathbf{s}^T &= (\mathbf{s}_1^T, \ldots, \mathbf{s}_k^T) \in I\!R^D \end{aligned}$$

the primal problem (1.5) can be compactly written as:

$$\mathbf{x}_{opt} = Arg\,[\,\min \mathbf{c}^T\mathbf{x} \mid \mathbf{A}\mathbf{x} = \mathbf{b},\ \mathbf{x} \in K\,] \tag{1.7}$$

and respectively the dual (1.6) as:

$$(\mathbf{y}, \mathbf{s})_{opt} = Arg\,[\,\max \mathbf{b}^T\mathbf{y} \mid \mathbf{A}^T\mathbf{y} + \mathbf{s} = \mathbf{c},\ \mathbf{s} \in K^*\,] \tag{1.8}$$

If we write the dual as a primal problem in the minimization form:

$$(\mathbf{y}, \mathbf{s})_{opt} = Arg\,[\,\min\ -\mathbf{b}^T\mathbf{y} \mid \mathbf{A}^T\mathbf{y} + \mathbf{I}\mathbf{s} = \mathbf{c},\ \mathbf{s} \in K^*\,]$$

its dual is simply:

$$(\mathbf{z}, \mathbf{t})_{opt} = Arg\,[\,\max \mathbf{c}^T\mathbf{z} \mid \mathbf{A}\mathbf{z} = -\mathbf{b},\ \mathbf{I}\mathbf{z} + \mathbf{t} = \mathbf{0},\ \ \mathbf{t} \in K\,]$$

Comparing (1.7) with the last problem we see:

$$\mathbf{x}_{opt} = \mathbf{t}_{opt} = -\mathbf{z}_{opt}$$

So far we have considered only unit second-order cones of the form (1.3). Considering the general second-order conic constraint form (1.4) leads to the following general SOCP problem:

$$\begin{aligned} \min \quad & \mathbf{c}^T\mathbf{x} \\ s.t. \quad & \|\mathbf{P}_i\mathbf{x} + \mathbf{p}_i\| \le \mathbf{g}_i^T\mathbf{x} + r_i,\ i = 1, \ldots, N \end{aligned} \tag{1.9}$$

Sometimes SOCP is named Conic Quadratic Optimization (CQO), if it is referred to the standard second-order conic constraint form (1.3). Although SOCP is in theory a more specialized form of CP in comparison with SDP, it has a plenty of applications in various engineering topics (cf. eg. [29]). Usually the reformulation of a problem as a SOCP one is performed by using auxiliary unknowns. Let us consider e.g. the following quadratic constraint (r_i positive) :

$$\|\mathbf{y}_i\| \le r_i, \quad \mathbf{y}_i \in I\!R^{d_i - 1}$$

This constraint is transformed to a second-order conic constraint $\mathbf{x}_i \in K_i \subset I\!R^{d_i}$ by introducing an auxilliary unknown x_{i0} with $\mathbf{x}_i^T = (x_{i0}, \mathbf{y}_i^T)$ and adding the equation $x_{i0} = r_i$ to the linear equations. This way Quadratically Constrained Linear Problem (QCLP), closely related to LISA arises naturally from SOCP with vanishing $\mathbf{g}_i$. Another problem which can be cast as SOCP, is the problem of minimizing a sum of norms, used in [8] for the limit analysis of plane stress and plate problems. Let us consider e.g. the unconstrained problem:

$$\min \qquad \sum_{i=1}^{k} \|\mathbf{P}_i\mathbf{x} + \mathbf{p}_i\| \tag{1.10}$$

It can be expressed as an SOCP problem by introducing the auxilliary unknowns $t_1, \ldots, t_k$:

$$\begin{array}{lll} \min & \displaystyle\sum_{i=1}^{k} t_i & \\ s.t. & t_i \geq 0, & i = 1, \ldots, k \\ & \|\mathbf{P}_i\mathbf{x} + \mathbf{p}_i\|^2 \leq t_i^2, & i = 1, \ldots, k \end{array} \tag{1.11}$$

Other second-order conic constraints can be easily incorporated, as e.g. linear equalities or inequalities. It is noteworthy that although the objective function of a sum-of-norms problem can be nondifferentiable (e.g. at the origin), this is not the case with (1.11), where a zero gradient condition occurs in place of the aforementioned nondifferentiability.
Now let us write (1.9) in a form similar to the partitioned one (1.5) as follows:

$$\begin{array}{lll} \min & \mathbf{c}^T\mathbf{x} & \\ s.t. & \|\mathbf{u}_i\| \ \leq \ t_i \ , & i = 1, \ldots, N \\ & \mathbf{u}_i = \mathbf{P}_i\mathbf{x} + \mathbf{p}_i \ , & i = 1, \ldots, N \\ & t_i = \mathbf{g}_i^T\mathbf{x} + r_i \ , & i = 1, \ldots, N \end{array} \tag{1.12}$$

The dual of (1.9) reads (cf. e.g. [29]):

$$\begin{array}{lll} \max & -\displaystyle\sum_{i=1}^{N} \left(\mathbf{p}_i^T\mathbf{z}_i + r_i w_i\right) & \\ s.t. & \|\mathbf{z}_i\| \ \leq \ w_i \ , & i = 1, \ldots, N \\ & \displaystyle -\sum_{i=1}^{N} \left(\mathbf{P}_i^T\mathbf{z}_i + \mathbf{g}_i w_i\right) = \mathbf{c} & \end{array} \tag{1.13}$$

with optimization variables $\mathbf{z}_i \in I\!R^{d_i - 1}$ and $\mathbf{w} \in I\!R^N$.

1.2.4 Duality in some specific forms of SOCP

Now let us consider the following problem:

$$\begin{array}{lll} \max & \mathbf{c}_0^T \mathbf{x}_0 & \\ s.t. & \|\mathbf{x}_i\| \leq 1 & i = 1, \ldots, N \\ & \mathbf{A}_0 \mathbf{x}_0 + \sum_{i=1}^{N} \mathbf{A}_i \mathbf{x}_i = \mathbf{b} & \end{array} \tag{1.14}$$

with optimization variables $\mathbf{x}_0 \in I\!R^{n_0}$, $\mathbf{x}_i \in I\!R^{n_i}$ and data $\mathbf{A}_0 \in I\!R^m \times I\!R^{n_0}$, $\mathbf{A}_i \in I\!R^m \times I\!R^{n_i}$ and $\mathbf{c}_0 \in I\!R^{n_0}, \mathbf{b} \in I\!R^m$. Its dual is the following problem with variables $\mathbf{t} \in I\!R^m$, $\mathbf{w} \in I\!R^N$:

$$\begin{array}{lll} \min & (\mathbf{b}^T \mathbf{t} + \sum_{i=1}^{N} w_i) & \\ s.t. & w_i \geq \left\| \mathbf{A}_i^T \mathbf{t} \right\| & i = 1, \ldots, N \\ & \mathbf{A}_0^T \mathbf{t} = \mathbf{c}_0 & \end{array} \tag{1.15}$$

Proof: The duality can be proven by standard enlargement. Let us set:

$$\hat{\mathbf{b}} = \begin{bmatrix} \mathbf{e} \\ \mathbf{b} \end{bmatrix}, \quad \hat{\mathbf{A}}_0 = \begin{bmatrix} \mathbf{0} \\ \mathbf{A}_0 \end{bmatrix}, \quad \hat{\mathbf{A}}_i = \begin{bmatrix} \hat{\mathbf{a}}_i & \mathbf{0} \\ \mathbf{0} & \mathbf{A}_i \end{bmatrix}$$

where $\mathbf{e}, \hat{\mathbf{a}}_i \in I\!R^N$. The vector $\mathbf{e}$ has all entries equal to one and $\hat{\mathbf{a}}_i$ has all entries equal to zero except the i-th entry which is equal to one. Setting $\hat{\mathbf{c}}_0 = -\mathbf{c}_0$, $\hat{\mathbf{x}}_0 = \mathbf{x}_0$, $\hat{\mathbf{x}}_i = (\, x_{iz}, \mathbf{x}_i) \in I\!R^{n_i+1}$ and $\hat{m} = m + N$ transforms the norm constraints of (1.14) to standard conic ones and the problem (1.14) becomes a specific case of (1.5). Let us consider its dual (1.6) with optimization variables $\hat{\mathbf{y}} \in I\!R^{\hat{m}}$. Partitioning $\hat{\mathbf{y}}$ as $\hat{\mathbf{y}} = (\mathbf{y}_e, \mathbf{y}_b)$, setting new variables $\mathbf{w} = -\mathbf{y}_e$ and $\mathbf{t} = -\mathbf{y}_b$ we transform (1.6) after some simple algebra to (1.15).

If the system of equations in (1.14) is homogeneous, i.e. if $\mathbf{b} = \mathbf{0}$, then the dual (1.15) becomes a problem of minimizing a sum of norms with additional linear equality constraints. Let us now consider further this homogeneous case with the additional assumption that a large part of the linear equation system does not contain the unknowns $\mathbf{x}_i, i = 1, \ldots, N$, i.e:

$$\mathbf{A}_0 = \begin{bmatrix} \mathbf{A}_{01} \\ \mathbf{A}_{02} \end{bmatrix}, \quad \mathbf{A}_i = \begin{bmatrix} \mathbf{A}_{i1} \\ \mathbf{0} \end{bmatrix}, \quad i = 1, \ldots, N$$

More analytically let us consider the primal problem:

$$\begin{array}{ll} \max & \mathbf{c}_0^T \mathbf{x}_0 \\ s.t. & \|\mathbf{x}_i\| \leq 1 \qquad i = 1, \ldots, N \\ & \mathbf{A}_{01}\mathbf{x}_0 \; + \; \sum_{i=1}^{N} \mathbf{A}_i \mathbf{x}_i = \mathbf{0} \\ & \mathbf{A}_{02}\mathbf{x}_0 = \mathbf{0} \end{array} \tag{1.16}$$

The dual of (1.16) is obviously:

$$\begin{array}{ll} \min & \sum_{i=1}^{N} w_i \\ s.t. & w_i \geq \left\| \mathbf{A}_{i1}^T \mathbf{t}_1 \right\| \qquad i = 1, \ldots, N \\ & \mathbf{A}_{01}^T \mathbf{t}_1 \; + \; \mathbf{A}_{02}^T \mathbf{t}_2 \; = \; \mathbf{c}_0 \end{array} \tag{1.17}$$

Finally let us consider a further specialization. Namely let us assume that only one component of $\mathbf{x}_0$ enters the linear objective function and that the respective entries of $\mathbf{A}_{02}$ are zero:

$$\mathbf{x}_0 = \begin{bmatrix} \lambda \\ \mathbf{r} \end{bmatrix}, \; \lambda \in I\!R, \quad \mathbf{c} = \begin{bmatrix} 1 \\ \mathbf{0} \end{bmatrix}, \qquad \mathbf{A}_0 = \begin{bmatrix} \mathbf{A}_{01} \\ \mathbf{A}_{02} \end{bmatrix} = \begin{bmatrix} \mathbf{a}_\lambda & \mathbf{D} \\ \mathbf{0} & -\mathbf{C} \end{bmatrix}$$

i.e. let us consider the following primal problem with variables $\lambda, \; \mathbf{r}, \; \mathbf{x}_i$:

$$\begin{array}{ll} \max & \lambda \\ s.t. & \|\mathbf{x}_i\| \leq 1 \qquad i = 1, \ldots, N \\ & \mathbf{a}_\lambda \lambda \; + \; \mathbf{D}\mathbf{r} \; + \; \sum_{i=1}^{N} \mathbf{A}_i \mathbf{x}_i = \mathbf{0} \\ & \mathbf{C}\mathbf{r} = \mathbf{0} \end{array} \tag{1.18}$$

The dual problem with variables $\mathbf{w}, \; \mathbf{z}, \; \mathbf{u}$ becomes now:

$$\begin{array}{ll} \min & \sum_{i=1}^{N} w_i \\ s.t. & w_i \geq \left\| \mathbf{A}_i^T \mathbf{z} \right\| \quad i = 1, \ldots, N \\ & \mathbf{a}_\lambda^T \mathbf{z} = 1 \\ & \mathbf{D}^T \mathbf{z} \; = \; \mathbf{C}^T \mathbf{u} \end{array} \tag{1.19}$$

where we have set $\mathbf{z} = \mathbf{t}_1$ and $\mathbf{u} = \mathbf{t}_2$. As we shall see, the static approach to the shakedown analysis problem, based on Melans theorem, leads exactly to problem (1.18), where the kinematic approach leads to its dual (1.19).

1.3 The von Mises elastoplastic continuum problem

1.3.1 Starting relations

Let us consider a continuum body V with boundary $\partial V = \partial V_U \cup \partial V_P$. On ∂V_U kinematical boundary conditions hold and on ∂V_P (with outer normal $\mathbf{n}$) surface loads $\mathbf{p}$ are applied. V is subjected also to body forces $\mathbf{f}$. In this work we restrict ourselves to geometrically linear phenomena where the small strain-displacement relation reads:

$$\varepsilon_{ij} = \frac{1}{2}(\frac{\partial u_i}{\partial x_j} + \frac{\partial u_j}{\partial x_i}) \tag{1.20}$$

The set $\mathcal{E}$ of all strain fields satisfying (1.20) and the boundary conditions imposed on ∂V_U is termed the set of kinematically admissible strain fields.
Within the framework of geometric linearity (small displacements and strains) the following additive decomposition of the strains holds:

$$\boldsymbol{\varepsilon} = \boldsymbol{\varepsilon}^0 + \boldsymbol{\varepsilon}^E + \boldsymbol{\varepsilon}^P \tag{1.21}$$

where $\boldsymbol{\varepsilon}^0, \boldsymbol{\varepsilon}^E, \boldsymbol{\varepsilon}^P$ are the initial, the elastic and plastic strains respectively.
The actual stresses satisfy the equilibrium relations:

$$\text{div}\boldsymbol{\sigma} = -\mathbf{f} \text{ in } V \quad \text{and} \quad \boldsymbol{\sigma}\mathbf{n} = \mathbf{p} \text{ on } \partial V_P \tag{1.22}$$

and the set $\mathcal{S}$ of all stress fields satisfying these equilibrium conditions for given $(\mathbf{p}, \mathbf{f})$ is termed the set of statically admissible stresses for the given loading.
The actual stresses $\boldsymbol{\sigma}$ can be considered as the sum of two components, the elastic $\boldsymbol{\sigma}^E$ and the residual stresses $\boldsymbol{\rho}$:

$$\boldsymbol{\sigma} = \boldsymbol{\sigma}^E + \boldsymbol{\rho} \tag{1.23}$$

The elastic stresses are the stresses which would have been induced in the case of infinitely linearly elastic material:

$$\sigma^E_{ij} = E_{ijkl}\varepsilon^E_{kl} \tag{1.24}$$

The residual stresses are due to the plastic strains. Since the actual and the elastic stresses satisfy the equilibrium conditions for the same loading, the residual stresses satisfy the homogeneous equilibrium conditions:

$$\text{div}\boldsymbol{\sigma} = \mathbf{0} \text{ in } V \quad \text{and} \quad \boldsymbol{\sigma}\mathbf{n} = \mathbf{0} \text{ on } \partial V_P \tag{1.25}$$

i.e. they are self-equilibrated (eigen-stresses). The set $\mathcal{S}_r$ of all stress fields satisfying the homogeneous equilibrium conditions is termed the set of statically admissible residual stresses.

Under plane stress conditions the equivalent stress σ_{equiv} and plastic strain ε^P_{equiv} are given by:

$$\begin{aligned} \sigma_{equiv} &= \sqrt{\sigma_{xx}^2 + \sigma_{yy}^2 - \sigma_{xx}\sigma_{yy} + 3\tau_{xy}^2} \;=\; \sqrt{\Phi(\boldsymbol{\sigma})} \\ \varepsilon^P_{equiv} &= \frac{2}{\sqrt{3}}\sqrt{(\varepsilon^P_{xx})^2 + (\varepsilon^P_{yy})^2 + \varepsilon^P_{xx}\varepsilon^P_{yy} + \frac{1}{4}(\varepsilon^P_{xy})^2} \end{aligned} \tag{1.26}$$

$\Phi(\boldsymbol{\sigma})$ can be written also as:

$$\Phi(\boldsymbol{\sigma}) = \boldsymbol{\sigma}^T \mathbf{M} \boldsymbol{\sigma}, \qquad \mathbf{M} = \begin{bmatrix} 1 & -0.5 & 0 \\ -0.5 & 1 & 0 \\ 0 & 0 & 3 \end{bmatrix} \tag{1.27}$$

Let us consider the classical von Mises plastic yield function:

$$F(\boldsymbol{\sigma}) = \sigma_{equiv} = \sqrt{\Phi(\boldsymbol{\sigma})} \tag{1.28}$$

and the corresponding yield criterion:

$$f(\boldsymbol{\sigma}) = \sigma_{equiv} - \sigma_y = F(\boldsymbol{\sigma}) - \sigma_y \leq 0 \tag{1.29}$$

with associative plastic flow rule, i.e. plastic deformation rate normal to the yield function:

$$\dot{\boldsymbol{\varepsilon}}^p = \frac{\partial f}{\partial \boldsymbol{\sigma}} \dot{\lambda} \tag{1.30}$$

obeying the well-known complementarity relations:

$$\dot{\lambda} \geq 0, \quad f(\boldsymbol{\sigma}) \leq 0, \quad \dot{\lambda} f(\boldsymbol{\sigma}) = 0 \tag{1.31}$$

Then the equivalent plastic strain rate is equal to:

$$\dot{\varepsilon}^P_{equiv} = \dot{\lambda} \tag{1.32}$$

and the plastic dissipation function is given by:

$$d_p[\dot{\boldsymbol{\varepsilon}}^p(x,t)] = \max_{f(\boldsymbol{\sigma})\leq 0} \boldsymbol{\sigma} : \dot{\boldsymbol{\varepsilon}}^p(x,t) = \sigma_y(x)\, \dot{\varepsilon}^P_{equiv} = \sigma_y(x)\, \dot{\lambda}(x,t) \tag{1.33}$$

1.3.2 The shakedown theorems

Consider now that V is subjected to variable loads which may assume any value inside a bounded load domain $\mathcal{L}$. Let $P(t) \in \mathcal{L}$ be some load path, where the parameter t expresses the evolution of the phenomenon and is not the natural time (inertia terms neglected).

According to Melan's static theorem the maximum factor for which the structure shakes down elastically in the load domain $\mathcal{L}_{\mathcal{SD}} = \alpha_{\mathcal{SD}}\mathcal{L}$, i.e. the shakedown factor, can be calculated as the solution of the optimization problem:

$$\begin{aligned} \max \quad & \alpha \\ s.t. \quad & f[\alpha \boldsymbol{\sigma}^E(x,t) + \boldsymbol{\rho}(x)] \leq 0 \quad \forall\, x \in V,\ \forall\, P(t) \in \mathcal{L} \\ & \boldsymbol{\rho} \in S_r \end{aligned} \tag{1.34}$$

with optimization variables a and the time-independent residual stress field $\boldsymbol{\rho}$.
Let us now assume that the load domain is a convex hyperpolyhedron with NV vertices and let us define the index set $\mathcal{J} = \{1, \ldots, NV\}$. If the load-domain is also box-shaped, i.e. if the loading has NL independently varying components:

$$P(t) = \sum_{k=1}^{NL} \mu_k(t) P_k, \quad \mu_k^- \leq \mu_k(t) \leq \mu_k^+ \tag{1.35}$$

then the number of load domain vertices is $NV = 2^{NL}$. This quite specialized form is the most commonly used in the design of structures.
Under the assumption that $\mathcal{L}$ is a convex hyperpolyhedron, the time variable can be eliminated (see e.g. [24]) and (1.34) is reduced to the form:

$$\begin{aligned} \max \quad & \alpha \\ s.t. \quad & f[\alpha \boldsymbol{\sigma}^E(x,j) + \boldsymbol{\rho}(x)] \leq 0 \quad \forall\, x \in V,\ \forall\, j \in \mathcal{J} \\ & \boldsymbol{\rho} \in S_r \end{aligned} \tag{1.36}$$

where $\boldsymbol{\sigma}^E(x,j)$ is the elastic stress at point x due to the j-th vertex of the load domain. In other words, the yield condition is checked only for the vertices of $\mathcal{L}$.

According Koiter's kinematic theorem an elastic perfectly plastic structure *does not shakedown* if and only if there exists a history of plastic strain rate field and a time moment t_o such that

$$\begin{aligned} & \int_0^{t_o} \int_V \boldsymbol{\sigma}^E(x,t) : \dot{\boldsymbol{\varepsilon}}^p(x,t) dV dt > \int_0^{t_o} \int_V d_p[\dot{\boldsymbol{\varepsilon}}^p(x,t)] dV dt \\ & \text{with} \quad \boldsymbol{\varepsilon}^p(x,t_o) = \int_0^{t_o} \dot{\boldsymbol{\varepsilon}}^p(x,t) dt, \qquad \boldsymbol{\varepsilon}^p(x,t_o) \in \mathcal{E} \end{aligned} \tag{1.37}$$

under the assumption that the initial velocities defined on ∂V_U are zero. If $\mathcal{L}$ is a convex hyperpolyhedron (see [23, 21, 22, 6]) the time variable can be eliminated again. In this case shakedown does not occur, if there exists a plastic strain field $\boldsymbol{\varepsilon}^p(x,j)$ for every j-th

vertex of $\mathcal{L}$ such that:

$$\sum_{j=1}^{NV}\int_V \boldsymbol{\sigma}^E(x,j):\boldsymbol{\varepsilon}^p(x,j)dV > \sum_{j=1}^{NV}\int_V d_p[\boldsymbol{\varepsilon}^p(x,j)]dV$$
$$\text{with} \quad \sum_{j=1}^{NV}\boldsymbol{\varepsilon}^p(x,j)\in\mathcal{E} \tag{1.38}$$

Then for all α exceeding α_{SD} there exist the aforementioned plastic strain fields $\boldsymbol{\varepsilon}^p(x,j)$ with:

$$\sum_{j=1}^{NV}\boldsymbol{\varepsilon}^p(x,j)\in\mathcal{E} \tag{1.39}$$

such that the following condition is satisfied:

$$\alpha\sum_{j=1}^{NV}\int_V \boldsymbol{\sigma}^E(x,j):\boldsymbol{\varepsilon}^p(x,j)dV > \sum_{j=1}^{NV}\int_V d_p[\boldsymbol{\varepsilon}^p(x,j)]dV \tag{1.40}$$

or:

$$\alpha > \frac{\displaystyle\sum_{j=1}^{NV}\int_V d_p[\boldsymbol{\varepsilon}^p(x,j)]dV}{\displaystyle\sum_{j=1}^{NV}\int_V \boldsymbol{\sigma}^E(x,j):\boldsymbol{\varepsilon}^p(x,j)dV} \tag{1.41}$$

Normalizing:

$$\sum_{j=1}^{NV}\int_V \boldsymbol{\sigma}^E(x,j):\boldsymbol{\varepsilon}^p(x,j)dV = 1 \tag{1.42}$$

yields α_{SD} as the solution of the following optimization problem:

$$\begin{aligned}\min \quad & \alpha = \sum_{j=1}^{NV}\int_V d_p[\boldsymbol{\varepsilon}^p(x,j)]dV\\ s.t. \quad & \sum_{j=1}^{NV}\int_V \boldsymbol{\sigma}^E(x,j):\boldsymbol{\varepsilon}^p(x,j)dV = 1\\ & \sum_{j=1}^{NV}\boldsymbol{\varepsilon}^p(j)\in\mathcal{E}\end{aligned} \tag{1.43}$$

1.3.3 A vectorial representation of stresses and strains

Considering the cartesian component representation of stresses $\boldsymbol{\sigma}$ in vector form $\boldsymbol{\sigma} \in I\!R^3$ we can use another (skew) basis to represent it:

$$\mathbf{y} = \mathbf{Q}\boldsymbol{\sigma}, \qquad \boldsymbol{\sigma} = \mathbf{Q}^{-1}\mathbf{y} \tag{1.44}$$

with $\mathbf{y} \in I\!R^3$ and $\mathbf{Q} \in I\!R^3 \times I\!R^3$ an invertible matrix. For the plane stress case considered, we select as matrix $\mathbf{Q}$ the Cholecky factor of the matrix $\mathbf{M}$, appearing in (1.27):

$$\mathbf{M} = \mathbf{Q}^T\mathbf{Q}, \qquad \mathbf{Q} = \begin{bmatrix} 1 & -0.5 & 0 \\ 0 & 0.5\sqrt{3} & 0 \\ 0 & 0 & \sqrt{3} \end{bmatrix} \tag{1.45}$$

Setting:

$$\mathbf{q} = \mathbf{Q}\boldsymbol{\sigma}^E, \quad \boldsymbol{r} = \mathbf{Q}\boldsymbol{\rho} \tag{1.46}$$

the static theorem (1.36) can be written obviously as:

$$\begin{array}{lcll} \max & \alpha & & \\ s.t. & \|\mathbf{y}(x,j)\| \le \sigma_y(x) & \forall\, x \in V,\ \forall\, j \in \mathcal{J} \\ & \alpha\mathbf{q}(x,j) + \boldsymbol{r}(x) - \mathbf{y}(x,j) = \mathbf{0} & \forall\, x \in V,\ \forall\, j \in \mathcal{J} \\ & \boldsymbol{r}(x) - \mathbf{Q}\boldsymbol{\rho}(x) = \mathbf{0} & \forall\, x \in V \\ & \boldsymbol{\rho} \in S_r \end{array} \tag{1.47}$$

We can use a similar vectorial representation of the plastic strain and of the plastic strain rate.We select the following one:

$$\dot{\boldsymbol{\varepsilon}}^P(x,t) = \mathbf{Q}^T\mathbf{z}(x,t), \quad \mathbf{z}(x,t) \in I\!R^3 \tag{1.48}$$

which yields the following relation for the equivalent plastic strain rate:

$$\dot{\varepsilon}^P_{equiv} = \|\mathbf{z}\| \tag{1.49}$$

as can be immediately verified. The plastic dissipation power now becomes:

$$d_p[\dot{\boldsymbol{\varepsilon}}^P(x,t)] = \sigma_y(x)\,\|\mathbf{z}(x,t)\| \tag{1.50}$$

Using this representation and (1.46) yields the following form of the kinematic theorem (1.43):

$$\begin{aligned} \min \quad & \alpha = \sum_{j=1}^{NV} \int_V \sigma_y(x) \, \|\mathbf{z}(x,t)\| \, dV \\ s.t. \quad & \sum_{j=1}^{NV} \int_V \left[\mathbf{q}^T(x,j) \, \mathbf{z}(x,j)\right] \, dV = 1 \\ & \boldsymbol{\varepsilon}^P(x,j) = \mathbf{Q}^T \mathbf{z}(x,j) \qquad \forall \, x \in V, \;\; j = 1, \ldots, NV \\ & \sum_{j=1}^{NV} \boldsymbol{\varepsilon}^P(j) \in \mathcal{E} \end{aligned} \tag{1.51}$$

The yield stress can be incorporated locally in the stress and strain transformations. This will be down in the next section.

1.4 The discretized problems

1.4.1 FEM discretization

Let us assume that the structure V is discretized through a displacement FEM method. Let be :

NF	Number of free DOFs in the structure	(restrained ones omitted)
d	Dimension of local stress vector	$(d = 3)$
NE	Number of finite elements	
NEG	Number of element Gauss points	
NG	Number of total Gauss points	$(NG = NE \times NEG)$

with the assumption that all elements have the same number of Gauss points. We define the index set $\mathcal{I} = \{1, 2, \ldots, NG\}$.
The local strain vector is obtained from the nodal displacement vector $\mathbf{u}$ through :

$$\boldsymbol{\varepsilon}(x) = \mathbf{B}_k(x)\mathbf{u} \quad x \in V_k, \; k \in \{1, \ldots, NE\} \tag{1.52}$$

The principle of virtual work yields the following relation for some loading $\mathbf{p}$ and stresses $\boldsymbol{\sigma}$ statically compatible with it:

$$\mathbf{p}^T \mathbf{u} = \sum_{k=1}^{NE} \int_{V_k} \boldsymbol{\varepsilon}^T \boldsymbol{\sigma} dV_k \tag{1.53}$$

Combining the last two relations:

$$\mathbf{p} = \sum_{k=1}^{NE} \int_{V_k} \mathbf{B}^T \boldsymbol{\sigma} dV_k \tag{1.54}$$

Performing the numerical integration yields the discretized equivalent to (1.22):

$$\mathbf{p} \;=\; \sum_{i=1}^{NG} \beta_i \mathbf{B}_i^T \boldsymbol{\sigma}_i \;=\; \sum_{i=1}^{NG} \mathbf{C}_i \boldsymbol{\sigma}_i \quad \text{with} \quad \mathbf{C}_i = \beta_i \mathbf{B}_i^T, \quad i \in \mathcal{I} \tag{1.55}$$

Collecting:

$$\begin{aligned} \boldsymbol{\sigma}^T &= [\boldsymbol{\sigma}_1^T, \ldots, \boldsymbol{\sigma}_{NG}^T] \\ \mathbf{C} &= [\mathbf{C}_1, \ldots, \mathbf{C}_{NG}] \end{aligned}$$

we write (1.55) finally as:

$$\mathbf{p} \;=\; \mathbf{C}\boldsymbol{\sigma} \tag{1.56}$$

and the FEM approximation of a residual stress field satisfies the homogeneous equation system:

$$\mathbf{0} \;=\; \mathbf{C}\boldsymbol{\rho} \;=\; \sum_{i=1}^{NG} \mathbf{C}_i \boldsymbol{\rho}_i \tag{1.57}$$

i.e. the set S_r is the null space of the matrix $\mathbf{C}$.

1.4.2 The static approach

Let us now introduce local transformation matrices $\mathbf{Q}_i$ defined by:

$$\sigma_{y,i} \mathbf{Q}_i = \mathbf{Q} \qquad i \in \mathcal{I} \tag{1.58}$$

and let us apply at each i-th Gauss point and for each j-th load domain vertex the transformations (1.44) and (1.46):

$$\hat{\mathbf{q}}_i^j = \mathbf{Q}_i \, (\boldsymbol{\sigma}^E)_i^j, \quad \hat{\mathbf{y}}_i^j = \mathbf{Q}_i \, \boldsymbol{\sigma}_i^j \quad \forall \, (i,j) \in \mathcal{I} \times \mathcal{J} \tag{1.59}$$

and corresponding:

$$\hat{\boldsymbol{r}}_i = \mathbf{Q}_i \, \boldsymbol{\rho}_i \quad i \in \mathcal{I} \tag{1.60}$$

Then the static theorem (1.47) has the discretized form:

$$\begin{aligned} \max \quad & \alpha \\ s.t. \quad & \left\| \hat{\mathbf{y}}_i^j \right\| \leq 1 && \forall \, (i,j) \in \mathcal{I} \times \mathcal{J} \\ & \alpha \hat{\mathbf{q}}_i^j + \hat{\boldsymbol{r}}_i - \hat{\mathbf{y}}_i^j = \mathbf{0} && \forall \, (i,j) \in \mathcal{I} \times \mathcal{J} \\ & \hat{\boldsymbol{r}}_i - \mathbf{Q}_i \boldsymbol{\rho}_i = \mathbf{0} && \forall \, i \in \mathcal{I} \\ & \sum_{i=1}^{NG} \mathbf{C}_i \boldsymbol{\rho}_i \;=\; \mathbf{0} \end{aligned} \tag{1.61}$$

Since the matrix $\mathbf{Q}$ is invertible under plane stress conditions, setting:

$$\hat{\mathbf{C}}_i = \sigma_{y,i}\mathbf{C}_i\mathbf{Q}^{-1} \qquad i \in \mathcal{I} \tag{1.62}$$

and eliminating $\boldsymbol{\rho}$ by use of (1.60) leads to the problem:

$$\begin{aligned} \max \quad & \alpha \\ s.t. \quad & \left\|\hat{\mathbf{y}}_i^j\right\| \leq 1 \qquad \forall\,(i,j) \in \mathcal{I}\times\mathcal{J} \\ & \alpha\hat{\mathbf{q}}_i^j + \hat{\boldsymbol{r}}_i - \hat{\mathbf{y}}_i^j = \mathbf{0} \quad \forall\,(i,j) \in \mathcal{I}\times\mathcal{J} \\ & \sum_{i=1}^{NG} \hat{\mathbf{C}}_i\hat{\boldsymbol{r}}_i \;=\; \mathbf{0} \end{aligned} \tag{1.63}$$

Problems (1.61) and (1.63) have exactly the SOCP form (1.18) and their duals could be obtained directly in the form (1.19). In the next section we follow a more traditional mechanical approach.

1.4.3 The kinematic approach

Let us now consider the discretized form of problem (1.51) with:

$$(\boldsymbol{\varepsilon}^P)_i^j = \mathbf{Q}^T\mathbf{z}_i^j \qquad \forall\,(i,j) \in \mathcal{I}\times\mathcal{J} \tag{1.64}$$

The plastic dissipation, i.e. the objective function now takes the form:

$$\alpha = \sum_{i=1}^{NG}\sum_{j=1}^{NV} \beta_i\sigma_{y.i}\left\|\mathbf{z}_i^j\right\| \tag{1.65}$$

and the plastic work normalization condition reads:

$$\sum_{i=1}^{NG}\sum_{j=1}^{NV} \beta_i\sigma_{y.i}\,(\hat{\mathbf{q}}^T)_i^j\mathbf{z}_i^j = 1 \tag{1.66}$$

Finally the condition of kinematic admissibility can be expressed in terms of the variables $\mathbf{z}_i$ as follows:

$$\sum_{j=1}^{NV}(\boldsymbol{\varepsilon}^P)_i^j = \sum_{j=1}^{NV}\mathbf{Q}^T\mathbf{z}_i^j = \mathbf{B}_i\mathbf{u} \qquad \forall\, i \in \mathcal{I} \tag{1.67}$$

Consequently (1.51) leads to the following discretized form:

$$\begin{aligned} \min \qquad & \alpha = \sum_{i=1}^{NG}\sum_{j=1}^{NV} \beta_i \sigma_{y.i} \left\| \mathbf{z}_i^j \right\| && \forall (i,j) \in \mathcal{I} \times \mathcal{J} \\ s.t. \qquad & \sum_{i=1}^{NG}\sum_{j=1}^{NV} \beta_i \sigma_{y.i} \left(\hat{\mathbf{q}}^T\right)_i^j \mathbf{z}_i^j = 1 \\ & \sum_{j=1}^{NV} \mathbf{Q}^T \mathbf{z}_i^j = \mathbf{B}_i \mathbf{u} && \forall\, i \in \mathcal{I} \end{aligned} \tag{1.68}$$

Let us introduce the scaled variables:

$$\hat{\mathbf{z}}_i^j = \beta_i \sigma_{y.i} \mathbf{z}_i^j \tag{1.69}$$

and use (1.62) to transform the kinematic problem (1.68) for the plane stress case to the following form:

$$\begin{aligned} \min \qquad & \alpha = \sum_{i=1}^{NG}\sum_{j=1}^{NV} \left\| \hat{\mathbf{z}}_i^j \right\| && \forall (i,j) \in \mathcal{I} \times \mathcal{J} \\ s.t. \qquad & \sum_{i=1}^{NG}\sum_{j=1}^{NV} \left(\hat{\mathbf{q}}^T\right)_i^j \hat{\mathbf{z}}_i^j = 1 \\ & \sum_{j=1}^{NV} \hat{\mathbf{z}}_i^j = \hat{\mathbf{C}}_i^T \mathbf{u} && \forall\, i \in \mathcal{I} \end{aligned} \tag{1.70}$$

which is a sum-of-norms problem with additional equality constraints.

2 Extensions, implementation and examples

2.1 Extension to limited kinematic hardening

Let us consider the two-surface model of [51, 52] describing the limited kinematic hardening behaviour of the structure. Then the following conditions replace the yield criterion constraints:

$$\Phi(\boldsymbol{\sigma}-\boldsymbol{\pi}) \le \sigma_y^2, \qquad \Phi(\boldsymbol{\pi}) \le (\sigma_u-\sigma_y)^2 \tag{2.1}$$

where $\boldsymbol{\pi}$ is a back-stress field. The shakedown factor can be calculated via the static approach by the solution of the following optimization problem:

$$\begin{array}{lcll} \max & \alpha & & \\ s.t. & \Phi[\alpha\boldsymbol{\sigma}^E(x,t)+\boldsymbol{\rho}(x)-\boldsymbol{\pi}(x)] \le \sigma_y^2 & \forall x\in V, & \forall P(t)\in\mathcal{L} \\ & \Phi[\boldsymbol{\pi}(x)] \le (\sigma_u-\sigma_y)^2 & \forall x\in V & \\ & \boldsymbol{\rho}\in S_r & & \end{array} \tag{2.2}$$

Considering again a convex polyhedral load domain and the FEM discretized structure, the static problem (2.2) takes the form:

$$\begin{array}{lcl} \max & \alpha & \\ s.t. & \Phi[\alpha\boldsymbol{\sigma}_i^E(j)+\boldsymbol{\rho}_i-\boldsymbol{\pi}_i] \le \sigma_{y.i}^2 & \forall (i,j)\in\mathcal{I}\times\mathcal{J} \\ & \Phi[\boldsymbol{\pi}_i] \le (\sigma_{u.i}-\sigma_{y.i})^2 & \forall i\in\mathcal{I} \\ & \mathbf{C}\boldsymbol{\rho}=\mathbf{0} & \end{array} \tag{2.3}$$

Setting:

$$\mathbf{q}_i^j=\mathbf{Q}\boldsymbol{\sigma}_i^E(j), \quad \mathbf{z}_i=\mathbf{Q}\boldsymbol{\pi}_i, \quad \mathbf{y}_i^j=\alpha\mathbf{q}_i^j+\mathbf{Q}\boldsymbol{\rho}_i-\mathbf{z}_i \tag{2.4}$$

yields the following QCLP problem:

$$\begin{array}{lcl} \max & \alpha & \\ s.t. & \|\mathbf{y}_i^j\|^2 \le \sigma_{y,i}^2 & \forall (i,j)\in\mathcal{I}\times\mathcal{J} \\ & \|\mathbf{z}_i^j\|^2 \le (\sigma_{u,i}-\sigma_{y,i})^2 & \forall i\in\mathcal{I} \\ & \alpha\mathbf{q}_i^j+\mathbf{Q}\boldsymbol{\rho}_i-\mathbf{z}_i-\mathbf{y}_i^j=\mathbf{0} & \forall (i,j)\in\mathcal{I}\times\mathcal{J} \\ & \mathbf{Q}\boldsymbol{\pi}_i-\mathbf{z}_i=\mathbf{0} & \forall i\in\mathcal{I} \\ & \mathbf{C}\boldsymbol{\rho}=\mathbf{0} & \end{array} \tag{2.5}$$

which can be easily transformed to an equivalent SOCP by the standard enlargement techniques discussed previously in Section 1.2. This way its formal dual can be also obtained. A mechanical interpretation can be given to this dual, leading to a kinematic theorem for the FEM discretized problem. This topic will be discussed elsewhere.

2.2 Alternating plasticity

The plastic strains can result to a zero sum over a load cycle due to the fact that the sign of plastic strains increment changes. This phenomenon is called plastic shakedown and is related with the local failure due to *alternating plasticity* (APSC).
The safety factor in APSC, α_{AP}, according to Polizzotto's theorem in [40], (see also [64]) can be calculated as follows:

$$\alpha_{AP} = Arg\ \left[\quad \max \alpha \quad | \quad f[\alpha \boldsymbol{\sigma}^E(x,t) + \boldsymbol{\sigma}^*(x)] \leq 0 \quad \forall x \in V,\, \forall t \quad \right] \tag{2.6}$$

Let us consider the corresponding local problem:

$$\alpha_{AP}^{loc}(x) = Arg\ \left[\quad \max \alpha \quad | \quad f[\alpha \boldsymbol{\sigma}^E(x,t) + \boldsymbol{\sigma}^*(x)] \leq 0 \quad \forall t \quad \right] \tag{2.7}$$

Since there is no other requirement for the stress field $\boldsymbol{\sigma}^*(x)$, the local problems are decoupled and consequently:

$$\alpha_{AP} = Arg\,[\quad \min \quad \alpha_{AP}^{loc}(x) \quad | \quad x \in V \quad] \tag{2.8}$$

i.e. a minimax problem with obvious discretized counterpart.

Let us consider a box-shaped load domain with NL independently varying components and $NV = 2^{NL}$ vertices. Then the loading has the form (1.35):

$$P(t) = \sum_{k=1}^{NL} \mu_k(t) P_k, \quad \mu_k^- \leq \mu_k(t) \leq \mu_k^+$$

Pycko and Mróz [44] proved that the safety factor can be calculated as

$$\alpha_{AP} = \min_{j \in \mathcal{J},\, x \in V} \frac{\sigma_y}{\sqrt{\Phi[\boldsymbol{\tau}^E(x,j)]}} \tag{2.9}$$

where $\boldsymbol{\tau}^E$ are the elastic stresses induced in the symmetric load domain $\mathcal{L}'$, defined as

$$P(t) = \sum_{k=1}^{NL} \nu_k(t) P_k, \quad |\nu_k(t)| \leq \frac{\mu_k^+ - \mu_k^-}{2} \tag{2.10}$$

In fact α_{AP} is the elastic factor corresponding to the $\mathcal{L}'$ load domain. By elastic factor α_E of a load domain $\mathcal{L}$ we mean

$$\begin{aligned} &\alpha_E = \max\{\alpha \ \mid f(\alpha \boldsymbol{\sigma}^E(x,t)) \leq 0, \ \ \forall x \in V, \ \ \forall P \in \mathcal{L}\} \\ \text{or} \qquad &\alpha_E = \min_{x \in V,\, j \in \mathcal{J}} \frac{\sigma_y}{\sqrt{\Phi[\boldsymbol{\sigma}^E(x,j)]}} \end{aligned} \tag{2.11}$$

Since there is no global requirement for the stress field $\boldsymbol{\sigma}^*(x)$, the safety factor in APSC is an upper bound for the (elastic) shakedown factor and obviously:

$$\alpha_E \leq \alpha_{SD} \leq \alpha_{AP} \tag{2.12}$$

2.3 The 3D case

So far all derivations concern primal the 2D plane stress case, i.e. a case with bounded yield surface. The main idea was to use a variable transformation as (1.44) in order to make the ellipsoidal yield surface a spheric one, most appropriate for the SOCP algorithms.
The same basic idea can be used also in cases with cylindrical yield surfaces as under axisymmetric or 3D conditions. Then the von Mises yield surface is a bounded ellipsoid in the deviatoric space and an appropriate transformation can make the ellipsoid again a sphere.
Let us consider the 3D case and the following vector form of $\boldsymbol{\sigma} \in I\!R^6$ (in a skew basis):

$$\hat{\boldsymbol{\sigma}}^T = (h, \mathbf{y}^T)^T, \quad h \in I\!R,\ \mathbf{y} \in I\!R^5 \tag{2.13}$$

given by the linear transformation:

$$\left[\begin{array}{c} h \\ \hline \mathbf{y} \end{array}\right] = \begin{bmatrix} h \\ \hline y_1 \\ y_2 \\ y_3 \\ y_4 \\ y_5 \end{bmatrix} = \left[\begin{array}{cccccc} 1/\sqrt{3} & 1/\sqrt{3} & 1/\sqrt{3} & 0 & 0 & 0 \\ \hline 0.5 & -1 & 0.5 & 0 & 0 & 0 \\ -0.5\sqrt{3} & 0 & 0.5\sqrt{3} & 0 & 0 & 0 \\ 0 & 0 & 0 & \sqrt{3} & 0 & 0 \\ 0 & 0 & 0 & 0 & \sqrt{3} & 0 \\ 0 & 0 & 0 & 0 & 0 & \sqrt{3} \end{array}\right] \begin{bmatrix} \sigma_x \\ \sigma_y \\ \sigma_z \\ \tau_{xy} \\ \tau_{yz} \\ \tau_{zx} \end{bmatrix} \tag{2.14}$$

or:

$$h = \mathbf{P}\boldsymbol{\sigma}, \quad \mathbf{y} = \mathbf{Q}\boldsymbol{\sigma} \tag{2.15}$$

with obvious entries of the transformation matrices $\mathbf{P} \in I\!R \times I\!R^6$, $\mathbf{Q} \in I\!R^5 \times I\!R^6$. Note that the columns of the matrix $\left[\mathbf{P}^T | \mathbf{Q}^T\right]$ form a vector basis for $I\!R^6$. Note that $\mathbf{P}^T\mathbf{P} = 1$ and $\mathbf{P}^T\mathbf{Q} = \mathbf{0}$, i.e. this transformation induces a direct decomposition of the stress vector in the volumetric and deviatoric part. In fact $\mathbf{y}$ can be considered as a representation of the five independent components of the deviator $\boldsymbol{\sigma}_D$. The yield function and the yield criterion can be written as:

$$\Phi(\boldsymbol{\sigma}) = \mathbf{y}^T\mathbf{y} \tag{2.16}$$

$$f(\boldsymbol{\sigma}) = ||\,\mathbf{y}|| \leq \sigma_y \tag{2.17}$$

Then the formulation of the static theorem (1.61) remains valid as it stays and (1.61) is slightly changed, since the volumetric parts of the residual stresses appear also in the null space condition (and only in it).
A kinematic interpretation can be given to the respective formal duals, which are obtained as described in Section 1.2. Alternatively, a direct formulation - at least for the discretized problem - can be elaborated through a respective decomposition of the strains in volumetric and deviatoric parts.

2.4 Implementation issues

It is noteworthy that the arising SOCP problems are all large but sparse i.e. most of the matrices elements are zero and exactly the exploitation of this aspect is the basis of the success of all the IPM algorithms. As we have explained in Section 1.2, we have decided to use already available specific SOCP software developed by the MP community. An effective algorithm for SOCP problems is e.g. described in [1]. We have finally decided to use the package MOSEK [13]), which implements the algorithm presented in [2]. This package contains also a general IPM solver for CNLP problems, described in [3]. Our decision has been influenced also by the benchmark tests for SDP and SOCP solvers presented in [35], where MOSEK outperforms its competitors. We have used the serial version of MOSEK and not the parallelized one.
The input to MOSEK consists in ASCII files in the MPS format, well-known in the MP community. Consequently we have implemented the solution of the arising SOCP problems in the following way:

1) The FEM code writes on binary disk files all necessary information, i.e.
   - the restraint codes of the DOFs of the structure (in order to ignore the restrained DOFs during the assembly of the structural equilibrium matrix $\mathbf{C}$).
   - element connectivity information and the element equilibrium matrices.
   - the elastic solution stresses.
2) A preprocessor
   - reads a directives file, prepared by the user, containing additional information as σ_y, σ_u etc.
   - reads the binary files generated by the FEM code, performs the necessary matrix operations in order to make the yield surfaces spheric and prepares the ASCII input files in MPS format needed by MOSEK.
   - prepares a directives file for the postprocessor
3) A run of MOSEK is made.
4) A postprocessor reads and evaluates the ASCII output file yielding the final results as $\alpha, \boldsymbol{\rho}$ etc.

At this development stage the scheme is operational for plane stress and axisymmetric conditions. An exploitation of the characteristics of the full 3D case is under development.
The sparsity effect has been clearly demonstrated. In the numerical examples the problem resulting from the static formulation has been solved faster, although in the kinematic formulation there exist fewer constraints. The problems based on the static formulation have been also successfully solved (but not with the same speed) by the more general IPM optimizer, incorporated in MOSEK. This fact was to be expected since a general IPM optimizer does not exploit the specific characteristics of the SOCP problems.

2.5 Examples

2.5.1 Square disk with a central hole

The first example concerns a disk with a central circular hole with constant modulus of elasticity and thickness under independently varying pressure loads p_1 and p_2 as in Fig. 2.1(a). The relationship between the hole diameter D and the disk side length L is $D = 0.2L$. The yield criterion is the classical von Mises one. This example has been solved in many papers both for the nonlinear von Mises criterion [50],[18], [16], [43], [7], [52] and for the linearized one [11]. The disk is discretized in 600 4-node isoparametric plane stress elements with 2×2 Gauss integration, resulting in 7200 residual stress unknowns. The shakedown analysis has been performed for the following cases of box-shaped load domains:

1) Biaxial tension:

$$\begin{aligned} 0 \leq p_1 \leq \mu_1^+ \sigma_y, \qquad & 0 \leq \mu_1^+ \leq 1 \\ 0 \leq p_2 \leq \mu_2^+ \sigma_y, \qquad & 0 \leq \mu_2^+ \leq 1 \end{aligned}$$

2) Tension and compression:

$$\begin{aligned} 0 \leq p_1 \leq \mu_1^+ \sigma_y, \qquad & 0 \leq \mu_1^+ \leq 1 \\ 0 \leq -p_2 \leq \mu_2^+ \sigma_y, \qquad & 0 \leq \mu_2^+ \leq 1 \end{aligned}$$

The number of conic constraints is 9600 for each case. The results are shown in Fig. 2.1(c). The curve 1 and the two axis is the domain where the loads can vary in any way so that no yielding will occur. Every point of curve 2 represents the upper right corner of the shakedown domain. It is not necessary that the whole elastic region will be included in a shakedown domain. In all cases the shakedown factor is the same as the safety factor in alternating plasticity (APSC). This means that APSC is the critical failure mode.
It is noteworthy that although in the second case the elastic region is reduced, the shakedown results are the same. We also notice that in the first case (biaxial tension) the limit analysis results differ a lot from the shakedown curve.

2.5.2 Restrained block under thermomechanical loading

In this example the two dimensional plane stress structure shown in Fig. 2.2(a) is considered. We examine the load domains consisted of two independently varying load cases:

- pressure $0 \leq p \leq \mu_1^+ \sigma_y, \quad 0 \leq \mu_1^+ \leq 1$
- temperature variation $0 \leq \Delta T \leq \mu_2^+ T_o, \quad 0 \leq \mu_2^+ \leq 1$ where $T_o = \dfrac{\sigma_y}{E\alpha_t}$ (E is Young's modulus, α_t the thermal expansion coefficient)

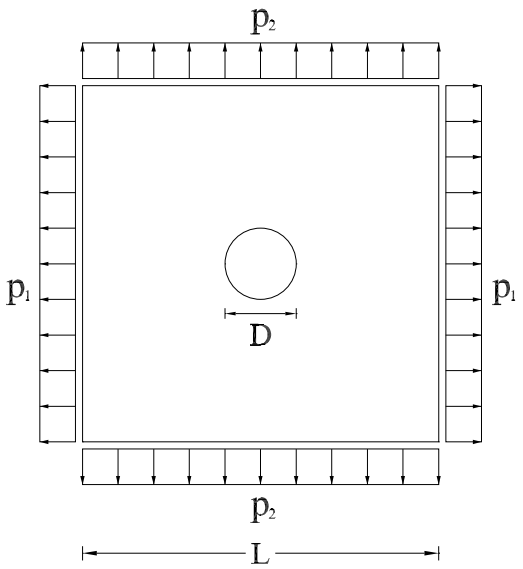

(a) Notation

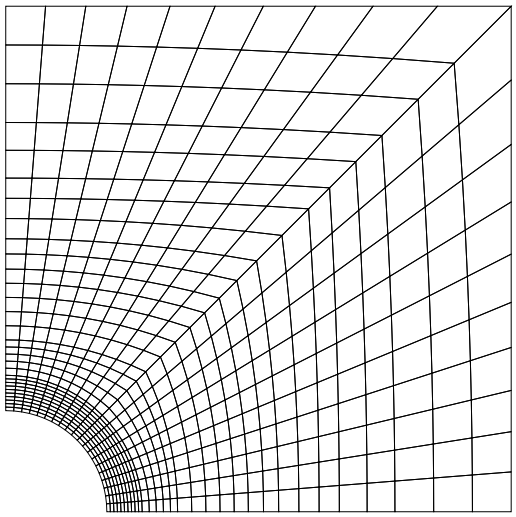

(b) Discretization

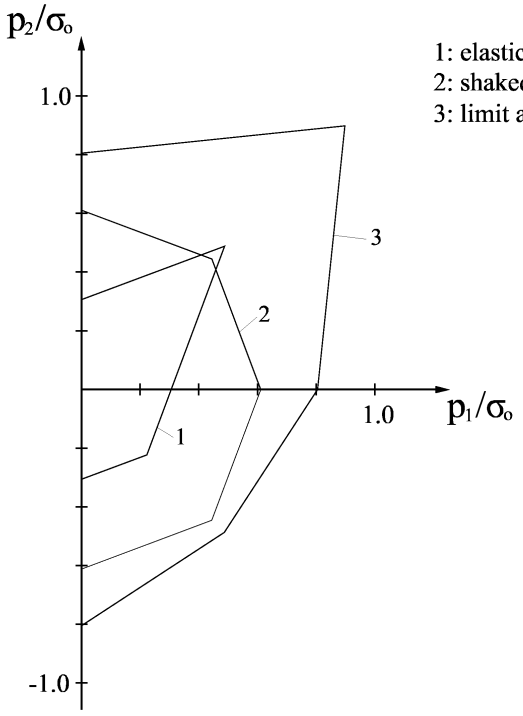

(c) Results

Figure 2.1: Square disk with a central hole under biaxial pressure

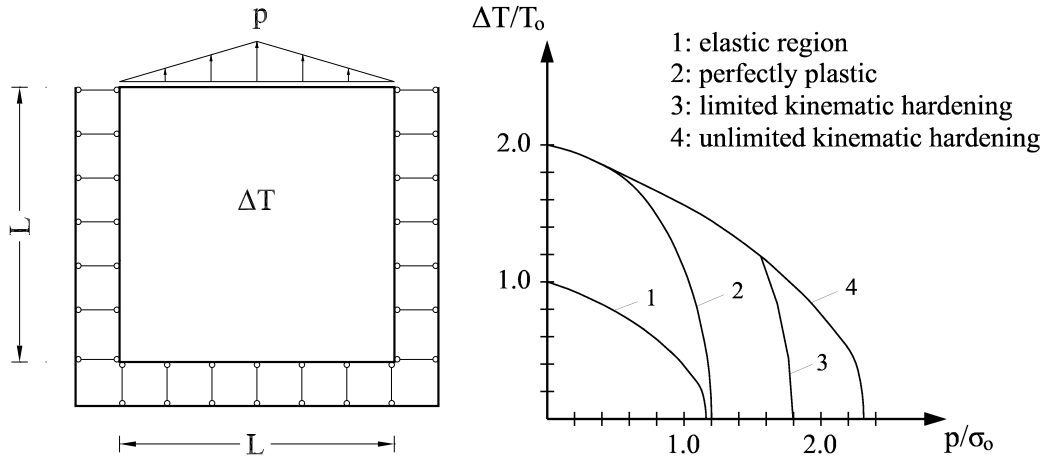

(a) Notation (b) Results

Figure 2.2: Laterally restrained disk

The cases of material considered are

- $\sigma_u = \sigma_y$ (perfectly plastic material).
- $\sigma_u = 1.5\sigma_y$
- $\sigma_u = \infty$ (unlimited kinematic hardening).

The structure has been discretized (using the vertical symmetry) in 5000 4-node isoparametric plane stress elements, integrated in 2×2 Gauss points each of them. We used this relatively large number of finite elements in order to show the efficiency of the algorithm. In case that $\mu_1^+, \mu_2^+ \neq 0$ i.e. $NV = 4$ we have to solve an optimization problem containing 80000 cone constraints. In the case of static formulation the SOCP problems were solved (in average) in less 170-180 seconds. The solution of the problems obtained by the kinematic formulation took 750-1000 seconds. The problems were solved in a PC system containing CPU Pentium III 733Mhz, RAM 512 Mb, in Windows 98 environment. Note that in the cases that the load domain contains only pressure or temperature changes then $NV = 2$ and the optimization problem contains 40000 less conic constraints.

The results for the various load domains are shown in Fig. 2.2(b). We notice that:

- in the absence of temperature loading, in the case of perfectly plastic material, we do not gain any advantage of the plastic material since the shakedown curve is very close to the elastic region. The presence of hardening helps in the safety of the structure.
- reducing the range of the applied pressure, the margins between the elastic region and the shakedown curve become all the more distant. We also notice that APSC tends to become the critical failure mode thus the hardening effects tend to be eliminated.

A case of MOSEK optimization progress is also shown in Fig. 2.3.

The next table contains numerical results obtained for various load domain conditions.

μ_1^+	μ_2^+	α_E	$\alpha_{SD}(\sigma_u = \sigma_y)$	$\alpha_{SD}(\sigma_u = 1.5\sigma_y)$	$\alpha_{SD}(\sigma_y = \infty)$
1.00	0.00	1.156	1.197	1.796	2.312
1.00	0.25	1.087	1.180	1.763	2.174
1.00	0.50	0.926	1.142	1.681	1.852
1.00	0.75	0.785	1.088	1.565	1.570
1.00	1.00	0.673	1.023	1.345	1.345
0.75	1.00	0.746	1.243	1.493	1.493
0.50	1.00	0.828	1.531	1.657	1.657
0.25	1.00	0.915	1.825	1.829	1.829
0.00	1.00	1.000	2.000	2.000	2.000

Table 2.1: Results for various load domains

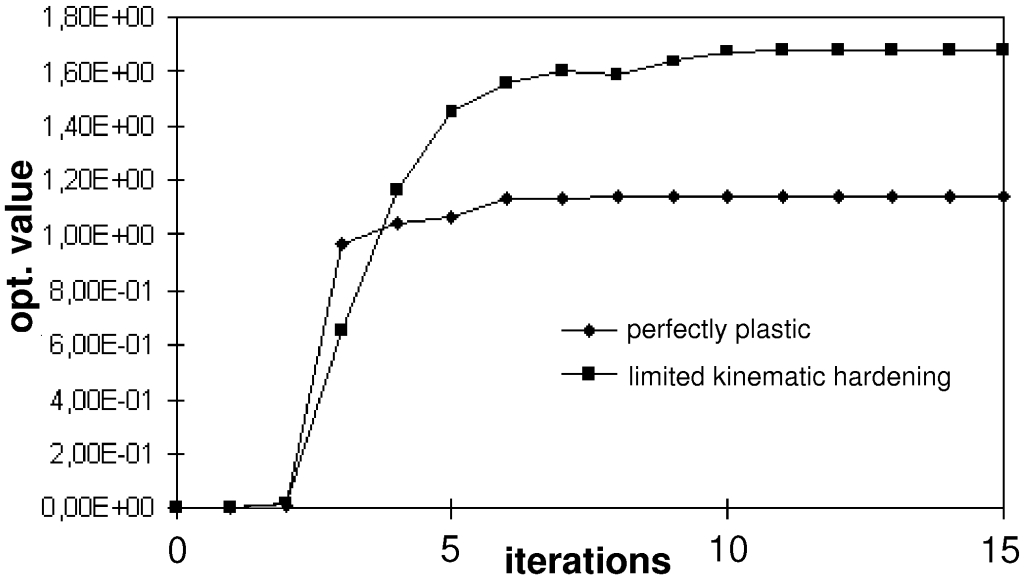

Figure 2.3: Optimization progress for $\mu_1^+ = 1,\ \mu_2^+ = 0.5$, (static formulation)

Acknowledgments

The authors would like to express their gratitude to Dr. Erling D. Andersen from EKA Consulting for making available to them the MOSEK package for use within the frame of preparation of the Doctoral Thesis of the first author ([32]). In 1998 the research has been funded by the European Commission as part of the Brite–EuRam III project LISA: FEM–Based Limit and Shakedown Analysis for Design and Integrity Assessment in European Industry (Project N°: BE 97–4547, Contract N°: BRPR–CT97–0595).

Bibliography

[1] K. Andersen, E. Christiansen, A. Conn and M. Overton: An Efficient Primal-Dual Interior Point Method for Minimizing a Sum of Eucledian Norms. Siam J. Sci. Comp. 22 (2000) 243-262.

[2] E. D. Andersen, C. Roos and T. Terlaky: On implementing a primal-dual interior point method for conic quadratic optimization. Helsinski School of Economics and Business Administration, WORKING PAPERS, W-274, December 2000.

[3] E. D. Andersen and Y. Ye: On new homogenous algorithm for the monotone complementarity problem. Math. Progr. 84 (1999) 375-399.

[4] M. A. Belouchrani and D. Weichert: An extension of the static shakedown theorem to inelastic cracked structures. Int. J. Mech. Sci. 41 (1999) 163-177.

[5] A. Ben-Tal and A. Nemirovski: Lectures on modern convex optimization: Analysis, algorithms and engineering applications SIAM, Philadelphia (2001).

[6] G. Borino: Consistent shakedown theorems for materials with temperature dependent yield functions. Int. J. Solids Struct. 37 (2000) 3121-3147.

[7] V. Carveli, Z. Cen, Y. Liu and G. Maier: Shakedown analysis of defective pressure vessels by a kinematic approach. Arch. Appl. Mech. 69 (1999) 751-763.

[8] E. Christiansen and K. D. Andersen: Computation of collapse states with Von Mises type yield condition. Int. J. Numer. Meth. Engrg 46 (1999) 1185-1202.

[9] G. Cocchetti and G. Maier: Static shakedown theorems in piecewise linearized poroplasticity. Arch. Appl. Mech. 68 (1998) 651-661.

[10] M.Z. Cohn and G. Maier, eds.: Engineering Plasticity by Mathematical Programming. Proceedings of the NATO advanced study. Institute University of Waterloo Waterloo (1977).

[11] L. Corradi, Shakedown Analysis, in: M.Z. Cohn and G. Maier, eds., Engineering Plasticity by Mathematical Programming , (Proceedings of the NATO advanced study, Institute University of Waterloo, Waterloo 1977) 269-276.

[12] D. Den Hertog: Interior Point Approach to Linear, Quadratic and Convex Programming. Kluwer Academic Publishers, Dordrecht (1993).

[13] EKA Consulting, The MOSEK optimization tools version 2.0 (Build 6). User's Manual and reference. Available from http://www.mosek.com

[14] Xi-Qiao Feng and D. Gross: A global/local shakedown analysis method of elasto-plastic cracked structures. Engrg. Fracture Mech. 63 (1999) 179-192.

[15] F. Giambanco, L. Palizzolo and C. Polizzotto: Optimal shakedown design of beam structures. Structural Optimization 8 (1994) 156-167.

[16] J. Groß-Weege: On the numerical assesment of the safety factor of elastic plastic structures under variable loading. Int. J. Mech. Sci. 39 (1997) 417-433.

[17] A. Hachemi and D. Weichert: Numerical shakedown analysis of damaged structures. Comput. Methods Appl. Mech. Engrg. 160 (1998) 57-70.

[18] M. Heitzer and M. Staat: FEM-computation of highly loaded passive components by direct methods. Nuclear Engrg. and Design 193(1999) 349-358.

[19] M. Heitzer, G. Pop, M. Staat: Basis reduction for the shakedown problem for bounded kinematic hardening material, Journal of Global Optimization 17 (2000) 185-200.

[20] J. Kamenjarzh: Limit analysis of solids and structures. CRC Press, Boca Raton (1996).

[21] J. Kamenjarzh and A. Merzljakov: On kinematic method in shakedown theory: I. Duality of extremum problems. Int. J. Plasticity 10 (1994) 363-380.

[22] J. Kamenjarzh and A. Merzljakov: On kinematic method in shakedown theory: II. Modified kinematic method Int. J. Plasticity 10 (1994) 381-392.

[23] J. Kamenjarzh and D. Weichert: On kinematic upper bound for the safety factor in shakedown theory. Int. J. Plasticity 8 (1992) 827-836.

[24] M. Kleiber and J.A. König: Incremental shakedown analysis in the case of thermal effects, Int. J. Numer. Meth. Engrg. 20 (1984) 1567-1573.

[25] W.T. Koiter: General Theorems for elastic-plastic solids, in Progress in Solid Mechanics Vol. 1 North-Holland Publishing Company, Amsterdam (1960).

[26] J.A. König: Shakedown of Elastic-Plastic Structures. Elsevier and PWN, Amsterdam and Warschau (1987).

[27] J.A. König and G. Maier: Shakedown analysis of elastoplastic structures: A review of recent developments. Nuclear Engrg and Design 66 (1981) 81-95.

[28] Y.H. Liu, V. Carveli and G. Maier: integrity assesment of defective pressurized pipelines by direct simplified methods. Int. J. Pres. Ves. & Piping 74 (1997) 49-57.

[29] M.S. Lobo, L. Vandenberghe, S. Boyd and H. Lebret: Applications of Second-Order Cone Programming, Linear Algebra and its Applications 284 (1998) 193-228.

[30] G. Maier: Shakedown theory in perfect elastoplasticity with associated and non-associated flow-laws: a finite element linear programming approach. Meccanica 4 (1969) 1-11.

[31] G. Maier, Shakedown Analysis, in: M.Z. Cohn and G. Maier, eds., Engineering Plasticity by Mathematical Programming (Proceedings of the NATO advanced study, Institute University of Waterloo, Waterloo 1977) 107-134.

[32] A. Makrodimopoulos: Computational approaches to the shakedown phenomena of metal structures under plane and axisymmetric stress state. (in Greek) Doctoral Dissertation, Aristotle University of Thessaloniki (2001).

[33] E. Melan: Theorie statisch unbestimmter Systeme aus ideal-plastischem Werkstoff, Sitzungsbericht der Österreichischen Akademie der Wissenschaften der Mathematisch-Naturwissenschaftlichen Klasse IIa 145 (1936) 195-218.

[34] E. Melan: Zur Plastizität des räumlichen Kontinuums, Ingenieur-Archiv 8 (1938) 116-126.

[35] H. Mittelmann: An Independent Benchmarking of SDP and SOCP Solvers. Technical Report, Dept. of Mathematics, Arizona State University, July 2001.

[36] R.D.C. Monteiro and T. Tsuchiya: Polynomial convergence of primal-dual algorithms for the second-order cone program based on the MZ-family of directions. Math. Program. Ser. A 88 (2000) 61-83.

[37] M.Z. Mroz, D. Weichert and S. Dorosz, eds.: Inelastic behaviour of structures under variable loads. Kluwer Academic Press, Dordrecht (1995).

[38] Y. Nesterov and A. Nemirovskii: Interior-Point Polynomial Algorithms in Convex Programming. SIAM, Philadelphia (1994).

[39] C. Polizzotto , G. Borino, S. Caddemi and P. Fuschi: Shakedown problems for material models with internal variables. Eur. J. Mech., A/Solids 10 (1991) 621-639.

[40] C. Polizzotto: On the conditions to prevent plastic shakedown of structures: Part I&II Transactions of the ASME, Journal of Applied Mechanics, 60 15-19, 20-25, 1993.

[41] C. Polizzotto and G. Borino: Shakedown and steady state responses of elastic plastic solids in large displacements Int. J. Solids Struct. 33 (1996) 3415-3437.

[42] A.R.S. Ponter and K.F. Carter: Shakedown state simulation techniques based on linear elastic solution. Comput. Methods Appl. Mech. Engrg. 140 (1997) 259-279.

[43] A.R.S. Ponter and M. Engelhardt: Shakedown for a general yield condition: implementation and application for a Von Mises yield criterion yield condition. Eur. J. Mech A/Solids 19 (2000) 423-445.

[44] S. Pycko and Z. Mróz: Alternative approach to shakedown as a solution of a min-max problem. Acta Mechanica 93 (1992) 205-222.

[45] S. Pycko and G. Maier: Shakedown theorems for some classes of nonassociative hardening elastic-plastic material models. Int. J. Plasticity 11 (1995) 367-395.

[46] R. Reemtsen and J. Rückmann (eds): Semi-infinite Programming. Kluwer Academic Publishers, Boston (1998).

[47] J. Renegar: A Mathematical View of Interior-Point Methods in Convex Optimization. SIAM, Philadelphia (2001).

[48] M. A. Save, C. E. Massonet and G. De SAXCE: Plastic limit analysis of plates, shells and disks. Elsevier, Amsterdam (1997).

[49] K.V. Spiliopoulos: A fully automatic force method for the optimal shakedown design of frames, Computational Mechanics 23 (1999) 299-307.

[50] M. Staat and M. Heitzer: Limit and shakedown analysis using a general purpose finite element code, in: Procceding of NAFEMS WORLD CONGRESS '97 on DESIGN, SIMULATION OPTIMIZATION Stuttgart, Germany 9-11 April 1997, Vol.1, 522-533.

[51] E. Stein , G. Zhang and J.A. König: Shakedown with nonlinear strain-hardening including structural computation using finite element method. Int. J. Plasticity 8 (1992) 1-31.

[52] E. Stein, R. Zhang and R. Mahnken: Shakedown analysis for perfectly plastic and kinematic hardening materials, in: E. Stein, ed., Progress in Computational Analysis of Inelastic Structures. CISM Courses 321, (Springer Verlag 1993) 175-244.

[53] H. Stumpf: Theoretical and computational aspects in the shakedown analysis of finite elastoplasticity. Int. J. Plasticity 9 (1993) 583-602.

[54] M. Todd: Semidefinite Optimization: Acta Numerica 10 (2001), 515-560.

[55] L. Vandenberghe and S. Boyd: Semidefinite Programming, SIAM Review, 38, (1996), 49-95.

[56] D. Weichert: On the influence of geometrical nonlinearities on the shakedown of elastic-plastic structures. Int. J. Plasticity 2 (1986) 135-148.

[57] Weichert, D.; Gross-Weege, J.: The numerical assessment of elastic-plastic sheets under variable mechanical and thermal loads using a simplified two-surface yield condition. Int. J. Mech. Sci. 30, (1988) 757-767.

[58] D. Weichert and A. Hachemi: Influence of geometrical nonlinearities on the shakedown of damaged structures. Int. J. Plasticity 14 (1998) 891-907.

[59] D. Weichert, A. Hachemi and F. Schwabe: Shakedown analysis of composites, Mech. Res. Comm. 26 (1999) 309-318.

[60] D. Weichert and G. Maier, eds.: Inelastic analysis of structures under variable loads: Theory and engineering applications. Kluwer Academic Press, Dordrecht (2000).

[61] H. Wolkowicz, R. Saigal and L. Vandenberghe (eds): Handbook of Semidefinite Programming. Kluwer Academic Publishers, Dordrecht (1993).

[62] M.D. Xue , X.F. Wang , F.W. Williams and B.Y. Xu: Lower-bound shakedown analysis of axisymmetric structures subjected to variable mechanical and thermal loads. Int. J. Mech. Sci. 39 (1997) 965-976.

[63] Y.-G. Zhang: An iteration algorithm for kinematic shakedown analysis. Comput. Methods Appl. Mech. Engrg. 127 (1995) 217-226.

[64] N. Zouain and J.L.L. Silveira: Extremum principles for bounds to shakedown loads. Eur. J. Mech. A/Solids 18 (1999) 879-901.

Part VII

Probabilistic limit and shakedown problems

Manfred Staat

Department of Physical Engineering
Fachhochschule Aachen Div. Jülich
Ginsterweg 1, D-52428 Jülich, Germany

E-mail: m.staat@fh-aachen.de

Michael Heitzer

Central Institute for Applied Mathematics (ZAM)
Forschungszentrum Jülich, D-52425 Jülich, Germany

E-mail: m.heitzer@fz-juelich.de

Nomenclature

$\mathbf{a}$	normal to limit state function
$\mathbf{C}$	system dependent matrix
E	expectation
F	yield function
f, F	distribution function, CFD
$\mathbf{f}, \mathbf{f}_0$	body force
$\mathcal{F}, \mathcal{F}_a$	failure region
$\partial\mathcal{F}, \partial\mathcal{F}_a$	limit state hyper-surface
g, G	limit state function
$\mathcal{L}$	load domain
L	Lagrangian function
M	strength mismatch ratio
$\mathbf{n}, n_i$	outer normal vector
$\mathcal{P}$	probability measure
P_f	failure probability
$\mathbf{p}, \mathbf{p}_0$	surface tractions
R, r	resistance
$\mathbf{R}$	correlation matrix
S, s	loading
S_m	allowable design stress
S_r	limit load parameter for F_f
U	standard normal basic variable
$\mathbf{u}^*$	design point
$\dot{\mathbf{u}}, \dot{\mathbf{u}}^0$	velocity, given velocity
$\dot{U}_{pl}$	dissipated plastic strain power
$V, \partial V$	structure and its boundary
$\dot{W}_{ex}$	external power of loading
$\dot{W}_{in}$	internally dissipated energy
X	basic variable
α	limit load factor
$\boldsymbol{\alpha}$	normal vector to g, G
β	reliability index
$\boldsymbol{\varepsilon}, \varepsilon_{ij}$	actual strain
$\boldsymbol{\lambda}, \lambda_i$	Lagrangian multipliers
$\mu, \mu_i, \boldsymbol{\mu}$	mean value, expectation
ρ, ρ_{ij}	correlation, coefficient
$\boldsymbol{\rho}$	residual stress
σ, σ_i	standard deviation
$\Sigma_{ij}, \boldsymbol{\Sigma}$	covariance, matrix
$\boldsymbol{\sigma}, \sigma_{ij}$	actual stress, stress tensor
$\boldsymbol{\sigma}^E$	fictitious elastic stress
σ_f	flow stress
σ_y	yield strength, R_{eL} or R_{p02}
Φ	Gaussian distribution function
ω	random event
Ω, Σ	space of random events
∇	gradient-operator

2D, 3D	two-dimensional, three-dimensional
ASME	American Society of Mechanical Engineers
CDF	Cumulative Distribution Function
DOFs	Degrees of Freedoms
FEM	Finite Element Method
FORM	First Order Reliability Method
LCF	Low Cycle Fatigue
LISA	Limit and Shakedown Analysis, acronym of the project and its software
MCS	Monte-Carlo Simulation
PDF	Probability Density Function
PERMAS	FEM software by INTES, Stuttgart, Germany
RSM	Response Surface Method
SORM	Second Order Reliability Method

1 Introduction

Design and assessment of engineering structures imply decision making under uncertainty of the actual load carrying capacity of a structure. Uncertainty may originate from random fluctuations of significant physical properties, from limited information and from model idealizations of unknown credibility. Structural reliability analysis deals with all these uncertainties in a rational way. Reliability assessment of structures requires on the one hand mechanical models and analysis procedures that are capable of modeling limit states accurately. On the other hand, full coverage of the present random variables is also necessary for a meaningful reliability assessment. The mechanical and stochastic model depends on the definition of the limit state. For instance, if the limit state of the structure is defined with respect to plastic collapse, then Young's modulus, hardening modulus and secondary stress need not be modeled as random variables, because they all do not influence the limit load. Conversely, elastic buckling is governed by Young's modulus, secondary stress, and geometry imperfections.

In the most general case the structural response, i.e. its statistical properties results from both the statistical properties of the loading as well as the statistical information on the structural geometry and material. The processing of this statistical information requires considerably more computational efforts than traditional, deterministic structural analysis. Hence high computational efficiency is within the focus of interest in Stochastic Structural Mechanics and Reliability.

Present structural reliability analysis is typically based on the limit state of initial or local failure. This may be defined by first yield or by some member failure if the structure can be designed on an element basis. However, this gives quite pessimistic reliability estimates, because virtually all structures are redundant or statically undetermined. Progressive member failures of such systems reduce redundancy until finally the statically determined system fails. This system approach is not defined in an obvious way for a finite element (FE) representation of a structure.

Low cycle fatigue (LCF), ratchetting and collapse as different possible failure modes are difficult to use in a mathematical expression of the limit state function separating failure from safe structure. Until today First and Second Order Reliability Methods (FORM/SORM) could not be used with standard incremental plastic analysis because non-linear sensitivity analysis would be necessary for computing the gradient of the limit state function. Therefore, one was restricted to simple but ineffective Monte-Carlo Simulation (MCS) and mostly local failure definitions.

All these problems are overcome by direct limit and shakedown analyses, because they compute directly the load carrying capacity or the safety margin. Therefore, they may be used to combine finite element methods (FEM) with FORM for defining the failure. Moreover, the solution of the resulting optimization problem provides the sensitivities with no extra costs. In comparison with MCS a typical speed up of some 100 and 1000 is

achieved with limit and shakedown analysis, respectively. The direct approach computes safety without going through the different evolution of local failures for all possible load histories. Therefore, limit and shakedown analysis is an obvious choice for reliability analysis of structural problems with uncertain data.

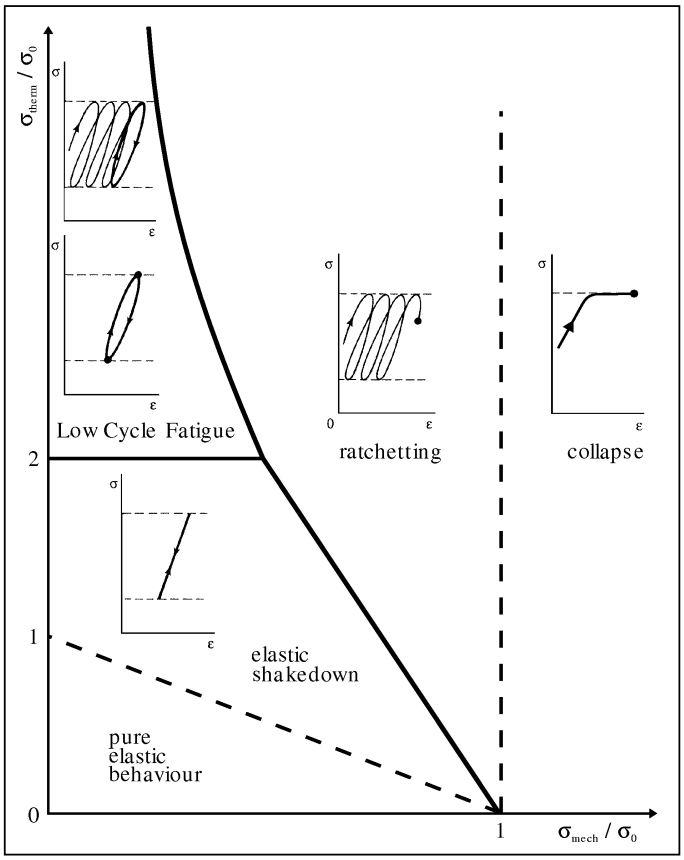

Figure 1.1: Bree-Diagram of pressurized thin wall tube under thermal loading [43][45]

Damage accumulation in LCF or plastic strain accumulation in ratchetting are evolution problems which can be modeled as stochastic process. Shakedown theorems yield much simpler time independent problems. In principle the possible structural responses, which are presented as icons in the Bree-Diagram (see Figure 1.1 and [5]) may be reproduced in a detailed incremental plastic analysis. However, this assumes that the details of the load history (including any residual stress) and of the constitutive equations are known.

It is most important for the analysis under uncertainty that limit and shakedown analyses are based on a minimum of information concerning the constitutive equations and the load history. This reduces the costs of the collection of statistical data and the need to introduce stochastic models to compensate the lack of data. Due to the so-called tail sensitivity problem there is generally insufficient data to analyze structures of high reliability which are

e.g. employed in nuclear reactor technology. Probabilistic limit and shakedown analyses were pioneered in Italy [1]. Further work seemed to remain restricted to stochastic limit analysis of frames based on linear programming [25], [51], [2], [27]. The present contribution extends plastic reliability analysis towards nonlinear programming, shakedown, and a general purpose large-scale FEM approach using lower bound theorems of limit and shakedown load to define a limit state function for reliability analysis by FORM. The resulting large-scale optimization problem is transferred to a relatively small one by the basis reduction method.

2 Introduction to probability theory

2.1 Random variables

A function $\mathrm{X} : \Omega \rightarrow \Sigma$ of a space Ω into the space Σ is called *variable*. A real variable $\mathrm{X} = x(\omega)$, which is a mapping of a space Ω of random events ω of an experiment onto $\mathbb{R}$, is called *random variable* [1].

$$x : \Omega \longrightarrow \mathbb{R}. \tag{2.1}$$

Generally, every random procedure is denoted as an experiment, like manufacturing process of material or structures. Therefore, the yield stress of a material or e.g. the diameter of a pipe are random variables. The elements of the image of $\mathrm{X} = x(\omega)$ are called *realizations* of X and denoted by x. The space of events Ω is characterized by a *probability measure*

$$P : \mathcal{P}(\Omega) \longrightarrow [0, 1], \tag{2.2}$$

of the power set $\mathcal{P}(\Omega)$ of all subsets of Ω, which satisfies the properties of a normed, non-negative, σ-additive measure

1) $0 \leq P(A) \leq 1$,
2) $P(\Omega) = 1, \;\; P(\emptyset) = 0$,
3) $P(A \cup B) = P(A) + P(B)$ if $A \cap B = \emptyset$.

A family $\{\mathrm{X}_i\}_i$ of random variables with $\mathrm{X}_i : \Omega \rightarrow \Sigma$ is called *stochastically independent* or *independent* for short, if for every choice of a subset $A_i \subset \Sigma$ the events $\{\mathrm{X}_i \in A_i\}_i$ are independent of each other.

$F(X)$ denotes the *cumulative distribution function* (CDF) of the random variable X. With the probability measure P it holds:

$$F(x) = P(X < x). \tag{2.3}$$

[1] Stochastic variables are generally denoted by capital letters and their realizations by small letters. This is often confusing in applied texts, because e.g. σ and Σ have distinct, different meanings. Therefore, we will also denote stochastic variables by $x(\omega)$ where ω represents the random event.

This means, that the value of F at x is the probability of the event, that the random variable X has a realization lower than x. A random variable is characterized by its CDF. We summarize the most important characteristics of distribution functions:

1) $F(x)$ is non-decreasing and continuous on the left,
2) $\lim_{x\to\infty} F(x) = 1, \quad \lim_{x\to-\infty} F(x) = 0, \quad P(a \leq \mathrm{X} < b) = F(b) - F(a).$

These characteristics hold for discrete and continuous random variables. A random variable X is called *continuous*, if the distribution function F has the form

$$F(x) = \int_{-\infty}^{x} f(t)dt. \tag{2.4}$$

The function f is called *probability density function* (PDF) of the distribution or *density* for short. From the properties of F one derives for f:

1) $P(a \leq \mathrm{X} < b) = \int_a^b f(t)dt,$
2) $P(\mathrm{X} = a) = 0,$
3) $\int_{-\infty}^{\infty} f(t)dt = 1.$

The appendix summarizes the most important distribution functions, densities and further details. The following distributions play a special role in structural reliability analysis:

Normal distribution and **standard normal distribution** ($\sigma = 1, \mu = 0$) with densities

$$f(x) = \frac{1}{\sqrt{2\pi\sigma^2}}\, e^{-(x-\mu)^2/2\sigma^2} \qquad \text{and} \qquad f(x) = \frac{1}{\sqrt{2\pi}}\, e^{-0.5x^2}. \tag{2.5}$$

The *expected value* $E(\mathrm{X})$ of the random variable X with the density f is defined by

$$E(\mathrm{X}) = \int_{-\infty}^{\infty} x f(x)dx, \tag{2.6}$$

if the integral converges. The following simple rules for the expectation hold:

1) $E(a) = a, \ a \in I\!R.$
2) $E(\mathrm{X} + \mathrm{Y}) = E(\mathrm{X}) + E(\mathrm{Y}), \quad E(\lambda \mathrm{X}) = \lambda E(\mathrm{X}), \ \lambda \in I\!R.$
3) $E(\mathrm{X} \cdot \mathrm{Y}) = E(\mathrm{X}) \cdot E(\mathrm{Y})$, if and only if X and Y are independent.

Let X be a random variable with continuous density f and let g be a continuous function, then the expectation $E(g(\mathrm{X}))$ exists if and only if $\int |g(x)| f(x)dx$ is bounded, with

$$E(g(\mathrm{X})) = \int_{-\infty}^{\infty} g(x)\ f(x)dx. \tag{2.7}$$

The *variance* Var(X) of a random variable X is defined by

$$\mathrm{Var}(\mathrm{X}) = E((\mathrm{X} - E(\mathrm{X}))^2) = E(\mathrm{X}^2) - (E(\mathrm{X}))^2. \tag{2.8}$$

The variance reflects the expected deviation of a realization x from the expected value $E(\mathrm{X})$. The *standard deviation* is defined by $\sigma(\mathrm{X}) = \sqrt{\mathrm{Var}(\mathrm{X})}$.

A set of n random variables may be collected in a random vector $\mathrm{x}(\omega)$ which has a joint probability density function

$$f_X : I\!R^n \longrightarrow I\!R, \tag{2.9}$$

that must satisfy certain conditions similar to those given for the above one-dimensional PDF. The multi-dimensional CDF $F(\mathbf{x})$ is defined as

$$F(\mathbf{x}) = P(X_1 < x_1, \ldots, X_n < x_n) = \int_{-\infty}^{x_1} \cdots \int_{-\infty}^{x_n} f_X(t_1, \ldots, t_n) dt_1 \ldots dt_n. \tag{2.10}$$

Two variables x_i, x_j ($i \neq j$) are independent if and only if

$$f_{x_i x_j} = f_{x_i} f_{x_j}. \tag{2.11}$$

Additionally to the concept of independence of random variable, the *covariance* $\mathrm{Cov}(\mathrm{X_i}, \mathrm{X_j})$ of random variables (written as random vector components) X_i and X_j is defined by

$$\mathrm{Cov}(\mathrm{X_i}, \mathrm{X_j}) = \Sigma_{ij} = E((\mathrm{X_i} - E(\mathrm{X_i}))(\mathrm{X_j} - E(\mathrm{X_j}))) = E(\mathrm{X_i X_j}) - E(\mathrm{X_i})E(\mathrm{X_j}). \tag{2.12}$$

The *correlation coefficient* ρ_{ij} is defined as

$$\rho_{ij} := \frac{\Sigma_{ij}}{\sqrt{\Sigma_{ii}\Sigma_{jj}}} = \frac{\Sigma_{ij}}{\sigma_i \sigma_j}, \tag{2.13}$$

where the standard deviation $\sigma_i = \sqrt{\Sigma_{ii}}$ is the ith diagonal element of the *covariance matrix* $\Sigma_X = (\Sigma_{ii})$. It is symmetric semi-definite and it holds $-1 \leq \rho_{ij} \leq +1$.

The random variables X_i and X_j are *uncorrelated*, if $\mathrm{Cov}(\mathrm{X_i}, \mathrm{X_j}) = 0$ (or $\rho_{ij} = 0$) holds. Therefore, independent random variables are uncorrelated but not vice versa. In the appendix the expectations and variances of the most important distribution functions for structural reliability analysis are listed.

2.2 Random fields

The notion of a random variable may be extended to that of a random process in time or of a *random field* in space. By use of limit and shakedown analysis a time independent

reliability problem is obtained. Therefore, no random process has to be considered and the reliability problem is considerably simplified. It remains to consider random fields which are derived in replacing the image space $I\!R$ by a real function space over a n-dimensional subspace V (the volume occupied by the considered structure) of $I\!R^n, n = 1, 2, 3$. We consider *homogeneous random fields* that are characterized by a generic PDF f and by a spatial correlation function ρ meeting the properties

1) $f(\mathrm{x}_1) = f(\mathrm{x}_2) \quad \forall \mathrm{x}_1, \mathrm{x}_2 \in V$,
2) $\rho(\mathrm{x}_1, \mathrm{x}_2) = \rho(\mathrm{x}_1 - \mathrm{x}_2) \quad \forall \mathrm{x}_1, \mathrm{x}_2 \in V$.

Random fields may be collected in a random vector field like random variables can be collected in a random vector. The correlation function measures the spatial variability of a random field. The *correlation length* $\boldsymbol{l_c} = (l_{cx}, l_{cy}, l_{cz})$ is used as normalizing parameter in the quantification of material imperfections. An *isotropic stochastic field* is obtained for $l_{cx} = l_{cy} = l_{cz} =: l_c$. The following isotropic correlation functions are commonly used in structural mechanics:

1) Triangular correlation:

$$\rho(\mathrm{x}_1, \mathrm{x}_2) = \max\left\{0, 1 - \frac{\|\boldsymbol{x}_1 - \boldsymbol{x}_2\|}{l_c}\right\}, \tag{2.14}$$

2) Exponential correlation;

$$\rho(\mathrm{x}_1, \mathrm{x}_2) = \exp\left(-\frac{\|\boldsymbol{x}_1 - \boldsymbol{x}_2\|}{l_c}\right), \tag{2.15}$$

3) Gaussian correlation:

$$\rho(\mathrm{x}_1, \mathrm{x}_2) = \exp\left(-\frac{\|\boldsymbol{x}_1 - \boldsymbol{x}_2\|^2}{l_c^2}\right), \tag{2.16}$$

For these *ergodic random fields* the correlation functions decay from one (complete correlation) to zero (uncorrelated) as the distance $\|\boldsymbol{x}_1 - \boldsymbol{x}_2\|$ between two points increases. The triangular correlation is zero for $\|\boldsymbol{x}_1 - \boldsymbol{x}_2\| \geq \mathrm{l_c}$.

The correlations of the ergodic random fields show that a complete correlation ($\rho(\mathrm{x}_1, \mathrm{x}_2) = 1$) is obtained if all components of the correlation length $\boldsymbol{l_c}$ go to infinity. In this case the stochastic field can be represented by single stochastic variable. Otherwise the random field can be discretized in two ways:

1) The random field is transformed into a finite number of stochastic variables by a finite series expansion into linearly independent, deterministic functions with stochastic coefficients. This method is not considered here, because it is restricted to Gaussian random fields.

2) The random field is discretized by stochastic elements which must contain at least one finite element. They may contain several finite elements, because they need to represent the fluctuations of material data instead of e.g. stress singularities. Inside a random element i the field is assumed constant so that it is represented by a single stochastic variable B_i. If the field is discretized with N_{se} elements it may be represented by the collection $\boldsymbol{B} = (B_1, \ldots, B_{se})^T$ of stochastic variables.

Usually the representative stochastic variable is chosen in one of the two ways:

1) Point methods:
Either the geometric center of the stochastic element (center point method) or the arithmetic mean of all of its nodal points (nodal point method) is chosen as the representative point. Then the representative stochastic variable is identified by the distribution of the stochastic field at this point. This method is preferred, because it is simple and it overestimates the spatial variance of the random field.

2) Volumetric average methods:
The volumetric mean value of the random field over a stochastic element is used as representative stochastic variable. Similarly the correlation coefficient is obtained also as a volume integral over a stochastic element. This method is not recommended, because it is more difficult to use and it underestimates the spatial variance of the random field.

A comparison of these two and other discretization methods is presented in [26]

3 Reliability analysis

The behavior of a structure is influenced by various typically uncertain parameters (loading type, loading magnitude, dimensions, or material data, ...). Data with random fluctuations in time and space is adequately described by stochastic processes and fields. Typical examples of engineering interest are earthquake ground motion, sea waves, wind turbulence, imperfections. The probabilistic characteristics of the processes are known from various available measurements and investigation in the past. In engineering mechanics, the available probabilistic characteristics of random quantities affecting the loading of the mechanical system often cannot be utilized directly to account for the randomness of the structural response due to its complexity. In structural response calculations a distinction is made between the involved structural model properties which are either considered as being deterministic or stochastic.

The numerical effort of stochastic analysis becomes large, if FEM discretization leads to high dimensional problems and if a high reliability of the structure is required. In both cases it is a necessary requirement of application in the engineering practice to achieve very effective analysis methods.

All probabilistic characteristics in this setup are described by random variables collected in the vector of basic-variables $\mathbf{X} = (X_1, X_2, ...)$. We will restrict ourselves to those basic variables X_j for which the joint density $f_X(x_1, \ldots, x_n)$ exists and the joint distribution function $F(\mathbf{x})$ is given by equation (2.10). The deterministic safety margin $R - S$ is based on the comparison of a structural resistance (threshold) R and loading S (which is usually an invariant measure of local stress at a hot spot or in a representative cross-section). With $R,\ S$ function of $\mathbf{X}$ the structure fails for any realization with non-positive limit state function $g(\mathbf{X}) = R(\mathbf{X}) - S(\mathbf{X})$, i.e.

$$g(\mathbf{X}) = R(\mathbf{X}) - S(\mathbf{X}) \begin{cases} < 0 & \text{for failure} \\ = 0 & \text{for limit state} \\ > 0 & \text{for safe structure} \end{cases} \tag{3.1}$$

Different definitions of limit state functions for various failure modes are suggested in Table 3.1. The limit state $g(\mathbf{x}) = 0$ defines the limit state hyper-surface $\partial\mathcal{F}$ which separates the failure region $\mathcal{F} = \{\mathbf{x}|g(\mathbf{x}) < 0\}$ from safe region. Figure 3.1 shows the densities of two random variables R, S, which are generally unknown or difficult to establish. The failure probability $P_f = P(g(\mathbf{X}) \leq 0)$ is the probability that $g(\mathbf{X})$ is non-positive, i.e.

$$P_f = P(g(\mathbf{X}) \leq 0) = \int_{\mathcal{F}} f_X(\mathbf{x}) d\mathbf{x}. \tag{3.2}$$

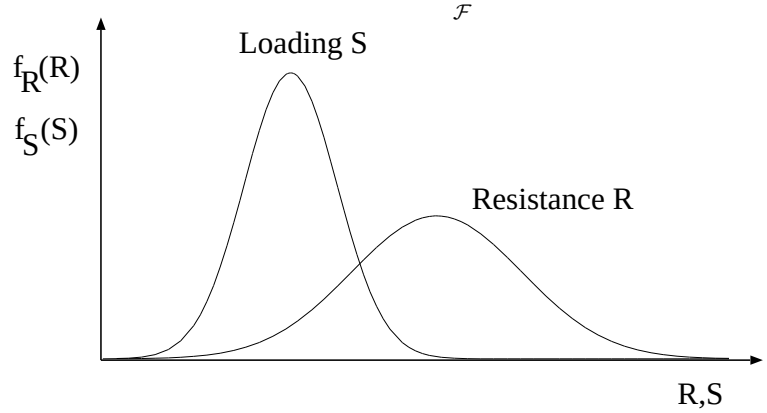

Figure 3.1: Basic $R - S$ problem in f_R, f_S presentation on one axis

Usually, it is not possible to calculate P_f analytically. Direct Monte Carlo Simulation becomes increasingly expensive with the increase of the structural reliability. Acceptable failure probabilities might be in the range of 10^{-4} to 10^{-6}. They are even lower in nuclear reactor technology. For a validation that the failure probability P_f is less than an accepted limit P_c, the sample size required for direct MCS must be at least $P_c/10$ leading to a minimum sample size in the range of 10^5 to 10^7. Such a large number exceeds particularly for complex FE-models, available resources by far. The numerical effort can be reduced by variance reduction methods like Importance Sampling and by Response Surface Methods (RSM) considerably. However, the most effective analysis is based on First and Second Order Reliability Methods (FORM/SORM) if gradient information is available [13].

Table 3.1: Different limit state functions [10]

Analysis	Resistance R	Loading S	Limit state function
Elastic strength	yield stress σ_y	equivalent stress $\hat{\sigma}$	$g = \sigma_y - \hat{\sigma}$
Serviceability	displ. threshold u_0	displacement u	$g = u_0 - u$
Fatigue	critical damage D_{cr}	accum. damage D	$g = D_{cr} - D$
Elastic stability	buckling load P_{cr}	applied load P	$g = P_{cr} - P$
Elastic vibration	eigen frequency ω_0	harm. excitation Ω	$g = \omega_0 - \Omega$
Brittle fracture	fract. toughness K_{IC}	stress intesity factor K_I	$g = K_{IC} - K_I$
Limit load	limit load	applied load	
	$P_y = \alpha_y P_0$	$P = \alpha_0 P_0$	$g = \alpha_y - \alpha_0$
Shakedown	shakedown domain	applied domain	
	$\mathcal{L}_{SD} = \alpha_{SD}\mathcal{L}_0$	$\mathcal{L}_a = \alpha_a \mathcal{L}_0$	$g = \alpha_{SD} - \alpha_a$

3.1 Monte-Carlo-Simulation

Monte Carlo Simulation (MCS) is a well known method for the evaluation of the failure probability P_f. For use with the simulation methods there are less strict requirements on the analytical properties of the limit state function and functions of the algorithmic type (like ”black box”) can be used. The straight forward (or crude) MCS become generally costly for small probabilities. The computational effort of crude MCS increases quickly with reliability [2] but not with the number of basic variables (contrary to FORM/SORM). Importance Sampling or other variance reduction techniques should be used to reduce the computational effort [3]. MSC is an approximate solution of the exact stochastic problem.

3.2 First/Second Order Reliability Method

First and Second Order Reliability Methods (FORM/SORM) are analytical probability integration methods. Therefore, the defined problem has to fulfill the necessary analytical requirements (e.g. FORM/SORM apply to problems, where the set of basic variables are continuous). Because of the large computational effort of MCS due to small failure probabilities (10^{-4} to 10^{-8}), any effective analysis is based on FORM/SORM [23]. The failure probability is computed in three steps.

- Transformation of basic variable $\mathbf{X}$ into the standard normal vector $\mathbf{U}$,
- Approximation $\mathcal{F}_a$ of the failure region $\mathcal{F}$ in the $\mathbf{U}$–space,
- Computation of the failure probability due to the approximation $\mathcal{F}_a$

3.2.1 Transformation

The basic variables $\mathbf{X}$ are transformed into standard normal variables $\mathbf{U}$ ($\mu = 0, \sigma = 1$). Such a transformation is always possible for continuous random variables. If the variables X_i are mutually independent, with distribution functions F_{X_i}, each variable can be transformed separately by the Gaussian normal distribution Φ into $\mathbf{U}_i = \Phi^{-1}[F_{X_i}(\mathbf{x}_i)]$. For dependent random variables analogous transformations can be used [23]. The function $G(\mathbf{u}) = g(\mathbf{x})$ is the corresponding limit state function in $\mathbf{U}$–space. The dimension of the $\mathbf{U}$–space depends on the dependencies of the random variables $\mathbf{X}_i$ and is not necessarily equal to the dimension of the $\mathbf{X}$–space. However, the transformation to $\mathbf{U}$–space is exact and not an approximation [3].

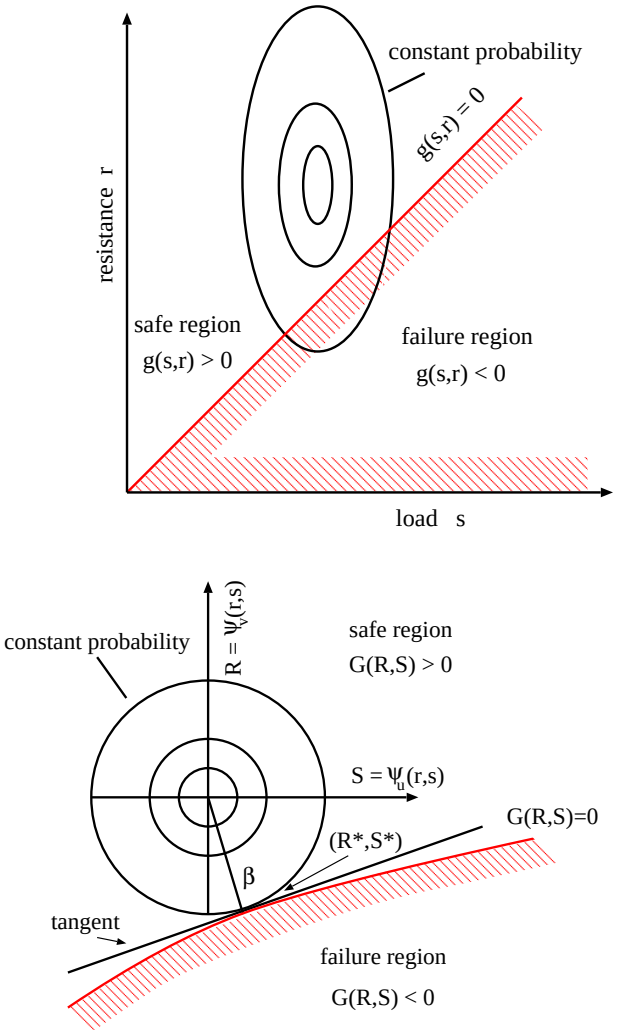

Figure 3.2: Transformation into normally distributed random variables

3.2.2 Approximation

In FORM a linear approximation $\mathcal{F}_a$ of the failure region $\mathcal{F}$ is generated. The failure region $\mathcal{F}$ is approximated at a point $\mathbf{u}_0 \in \partial\mathcal{F}$ with the normal $\boldsymbol{a} = \nabla_u G(\mathbf{u}_0)$

$$\mathcal{F}_a = \{\mathbf{u} | \nabla_u^T G(\mathbf{u}_0)\mathbf{u} + a_0 \leq 0\} = \{\mathbf{u} | \boldsymbol{a}^T\mathbf{u} + a_0 \leq 0\} \tag{3.3}$$

The limit state hyper-surface $\partial\mathcal{F}_a$ is represented in the normal form

$$\partial\mathcal{F}_a = \left\{\mathbf{u} \;\middle|\; \boldsymbol{a}^T\mathbf{u} + a_0 = 0\right\} = \left\{\mathbf{u} \;\middle|\; \boldsymbol{\alpha}^T\mathbf{u} + \beta = 0\right\}, \tag{3.4}$$

with $\boldsymbol{\alpha} = \boldsymbol{a}/|\boldsymbol{a}|$ and $\beta = a_0/|\boldsymbol{a}|$, such that $|\boldsymbol{\alpha}| = 1$. The vector $\boldsymbol{\alpha}$ is proportional to the sensitivities $\nabla_u G(\mathbf{u}_0)$. The failure event $\{\mathbf{u} \in \mathcal{F}_a\}$ is equivalent to the event $\{\boldsymbol{\alpha}^T\mathbf{u} \leq -\beta\}$, such that an approximation of the failure probability P_f is given by

$$\mathrm{P}_f = \mathrm{P}(\boldsymbol{\alpha}^T\mathbf{U} \leq -\beta) = \Phi(-\beta) = \frac{1}{\sqrt{2\pi}} \int_{-\infty}^{-\beta} e^{-0.5z^2} dz, \tag{3.5}$$

because the random variable $\boldsymbol{\alpha}^T\mathbf{U}$ is normally distributed. The failure probability depends only on β, such that it is called *reliability index*. If it is possible to derive β analytically from the input data, the probability P_f is calculated directly from the function Φ.

If the limit state function is nonlinear in U-space a quadratic approximation of the failure region $\mathcal{F}$ gives closer predictions of P_f. These second order methods (SORM) may be based on a correction of a FORM analysis. FORM/SORM give the exact solution to an approximate problem. The numerical effort depends on the number of stochastic variables but not on P_f (contrary to MCS).

3.2.3 Computation

To apply FORM/SORM one or several likely failure points on the limit state surface in **U**–space must be identified. These points are defined by having a locally minimum distance to the origin. Therefore, a nonlinear constrained optimization problem must be solved [2]

$$\beta = \min \mathbf{u}^T\mathbf{u} \;\text{ such that }\; \{\mathbf{u} \mid G(\mathbf{u}) \leq 0\}, \tag{3.6}$$

which usually needs the gradient of $G(\mathbf{u})$.

The design point $\mathbf{u}^* \in \partial\mathcal{F}_a$ is the point, which is the solution of problem (3.6), i. e. which is closest to the origin. The limit state function $G(\mathbf{U})$ is approximated by its linear Taylor series in point $\mathbf{u}_0 \in \partial\mathcal{F}$

$$G(\mathbf{u}) \approx G(\mathbf{u}_0) + \nabla_u G(\mathbf{u}_0)(\mathbf{u} - \mathbf{u}_0) \tag{3.7}$$

in order to generate the tangent hyper-plane in point $\mathbf{u}_0$. Let $\mathbf{u}_k$ be an approximation of the design point $\mathbf{u}^*$. If $\nabla_u G(\mathbf{u}_k) \neq 0$ holds, the following iterative procedure is defined

$$\mathbf{u}_{k+1} = \frac{\nabla_u G(\mathbf{u}_k)}{|\nabla_u G(\mathbf{u}_k)|^2} \left[\mathbf{u}_k^T \nabla_u G(\mathbf{u}_k) - G(\mathbf{u}_k)\right] \tag{3.8}$$

as a simple search algorithm for the design point $\mathbf{u}^*$.

The derivatives are determined by

$$\nabla_u G(\mathbf{u}) = \nabla_u g(\mathbf{x}) = \nabla_x g(\mathbf{x}) \nabla_u \mathbf{x}. \tag{3.9}$$

If the deterministic structural problem is solved by a step-by-step iterative FEM analysis this gradient information is obtained from a sensitivity analysis, which consumes much computing time. Extension of this type of reliability analysis to plastic structural failure faces several problems which are not present in linear elastic analysis: Local stress has no direct relevance to plastic failure and structural behavior becomes load-path dependent. Therefore, no straight-forward $g(\mathbf{X})$ is obtained from standard incremental analysis if failure is assumed by plastic collapse, by ratchetting or by alternating plasticity (LCF). It is even more difficult to obtain the gradient of $g(\mathbf{X})$. Therefore, as an additional draw-back MCS (improved by importance sampling or by some other means of variance reduction) is used in connection with incremental nonlinear reliability analyses with very few exceptions.

3.3 Response Surface Methods

Repeated FEM analyses are the most time consuming part in both, MCS and FORM/SORM. Therefore, the limit state function is replaced by a simple function, which is obtained as the approximation to the function values resulting from only few FEM analyses. Usually a linear or quadratic polynomial of the basic variables is employed. Starting from some values of the limit state function a fit is generated. Adopting the simpler response functions allows more efficient simulation or parameter studies. For classical, statistical methods Response Surface Methods (RSM) are well-known techniques [4].

3.4 Systems reliability

Linear elastic material models do not allow to define a limit state function such that it can describe e.g. collapse or buckling, because the yield stress σ_y or the ultimate stress σ_u is a fictitious parameter in these models. Exceeding σ_y or σ_u at any location can be associated with collapse only for statically determinate structures. Most real structures are statically indeterminate. They are thus safer, because redundancy allows some load

carrying capacity beyond partial collapse of a structural member (or section). A local threshold concept would have to define a composite limit state function in terms of stresses at different locations such as the plastic hinges in a frame structure. If these locations are known a-priori, the definition of the limit state function of a series system would be possible. Failure occurs if a sufficient number of hinges 1 AND 2 AND ... have developed.

Different sequences of hinge development may lead to different collapse mechanisms. For example a plane portal frame may fail in beam OR in sway OR in combined mode. These modes establish a parallel system in fault-tree representation. Reliability analysis of such parallel series systems may be based on the failure modes approach (event-tree representation) or on the survival modes approach (failure-graph representation). Analysis is possible with MCS and with FORM/SORM but it causes additional complications. The analyst is required to identify the complete system representation. Algorithms for automatic generation of the significant failure modes work properly for truss structures [34]. However, more complex structures may not be considered as consisting of a finite number of members with lumped parameters (e.g. beams). In a FEM discretization a series of finite elements may be formed which must all fail in order to define a possible collapse mechanism. The definition of such series systems is neither straight forward nor unique. Moreover, the resulting system may be large and complex.

These difficulties are avoided by the direct limit and shakedown approach, which formulates the limit state function as the solution of an mathematical optimization problem. It remains to define a parallel system in the typical situation that more than one failure mode is possible. According to the Bree-diagram Fig. 1.1 the thin tube may fail locally by LCF at low mechanical stress when crossing the shakedown limit. At higher mechanical stress it may fail globally by ratchetting. Using different starting points in a FORM/SORM analysis n different design points u_i^* may be obtained and collected in the vector $\mathbf{u}^*$, leading to different β_i-factors and failure probabilities $P_{fi} = \Phi(-\beta_i)$ for the respective failure modes. For linearized limit state functions a matrix $\mathbf{R} = (\rho_{ij})$ of correlations coefficients for $\mathbf{u}^*$ and $\boldsymbol{\beta}$, may be obtained. Then P_f may be estimated from the n-dimensional standard multi-normal distribution $\Phi_n(-\boldsymbol{\beta}; \mathbf{R})$. With little numerical effort also first-order series bounds for the cases of fully dependent and fully independent failure modes may be used

$$\max_{i=1..n}\{P_{fi}\} \leq P_f \leq 1 - \prod_{i=1}^{n}(1 - P_{fi}). \tag{3.10}$$

Different methods have been proposed to find all significant failure modes or at least the most dominant ones [32].

4 Limit and shakedown analysis

An objective measure of the loss of stability may be based on the loss of stable equilibrium [6]. A system is said to be in a critical state of neutral equilibrium or collapse if the second-

order energy dissipation vanishes,

$$\int_V \dot{\boldsymbol{\varepsilon}} : \dot{\boldsymbol{\sigma}} dV = 0, \tag{4.1}$$

for at least one kinematically admissible strain-rate field $\dot{\boldsymbol{\varepsilon}}$.

In a FEM discretization using a varying (symmetric part of the) stiffness matrix $\mathbf{K}$ or an appropriate update of it for nonlinear analysis this occurs, if

$$\dot{\mathbf{u}}\mathbf{K}\dot{\mathbf{u}} = 0 \tag{4.2}$$

holds, for at least one admissible nodal velocity vector $\dot{\mathbf{u}}$. This is equivalent with the limit state function $g(\mathbf{X}) =$det$\mathbf{K} = 0$. A sufficient condition is, that the smallest eigenvalue of $\mathbf{K}$ vanishes. Both limit state functions are numerically expensive and suffer from hard numerical problems (round-off and truncation error, non-uniform dependence on basic variables and possibly non-smoothness). A limiting structural stiffness may be used (e.g. half the elastic stiffness matrix $\mathbf{K}_0$ in the sense of the Double Elastic Slope Method of ASME Code, Sect. III, NB-3213.25)) on the basis of an appropriate matrix norm

$$g(\mathbf{X}) = \|\mathbf{K}(\mathbf{X})\| - 0.5\|\mathbf{K}_0(\mathbf{X})\|. \tag{4.3}$$

Such complications do not occur if plastic collapse modes are identified by limit analysis. Moreover, the Double Elastic Slope Method ntroduces the elastic properties into the plastic collapse problem, which is mechanically questionable. However, the stiffness approach may be employed for failure modes like buckling, which in turn fall outside of limit analysis.

Static limit load theorems are formulated in terms of stress and define safe structural states giving an optimization problem for safe loads. The maximum safe load is the limit load avoiding collapse. Alternatively, kinematic theorems are formulated in terms of kinematic quantities and define unsafe structural states yielding a dual optimization problem for the minimum of limit loads. Any admissible solution to the static or kinematic theorem is a true lower or upper bound to the safe load, respectively. Both can be made as close as desired to the exact solution. If upper and lower bound coincide, the true solution has been found. The limit load factor is defined in (4.4) by $\mathbf{P}_L = \alpha_L \mathbf{P}_0$, where $\mathbf{P}_L = (\mathbf{f}_L, \mathbf{p}_L)$ and $\mathbf{P}_0 = (\mathbf{f}_0, \mathbf{p}_0)$ are the plastic limit load and the chosen reference load, respectively. Here we have supposed that all loads (**f** body forces and **p** surface loads) are applied in a monotone and proportional way. The theorems are stated below.

4.1 Static or lower bound limit load analysis

Find the maximum load factor α_L for which the structure is safe. The structure is safe against plastic collapse if there exists a stress field $\boldsymbol{\sigma}$ such that the equilibrium equations

are satisfied and the yield condition is nowhere violated. The maximum problem is given by:

$$\begin{aligned} \max \quad & \alpha \\ \text{s. t.} \quad & F(\boldsymbol{\sigma}) \leq \sigma_y^2 \ \text{ in } \Omega \\ & \operatorname{div}\boldsymbol{\sigma} = -\alpha \mathbf{f}_0 \ \text{ in } V \\ & \boldsymbol{\sigma}\,\mathbf{n} = \alpha \mathbf{p}_0 \ \text{ on } \partial V_p \end{aligned} \tag{4.4}$$

for the structure V, traction boundary ∂V_p (with outer normal $\mathbf{n}$), yield function F, body forces $\alpha\mathbf{f}_0$ and surface tractions $\alpha\mathbf{p}_0$.

The FEM discretization of the lower bound problem reads (see [45])

$$\begin{aligned} \text{Maximize} \quad & \alpha_s \\ \text{s. t.} \quad & \boldsymbol{f}(\boldsymbol{s}) - \boldsymbol{r} \leq \mathbf{0}, \\ & \boldsymbol{C}\boldsymbol{s} - \alpha_s \boldsymbol{p} = \mathbf{0}. \end{aligned} \tag{4.5}$$

The inequality constraints of the NG Gaussian points were collected to the vectors $\boldsymbol{f}, \boldsymbol{s}$ and $\boldsymbol{r}$. The unknowns are the limit load factor α_s and the stresses $\boldsymbol{s}$.

4.2 Static or lower bound shakedown analysis

The shakedown analysis starts from Melan's lower bound theorem [31]. In the shakedown analysis the equilibrium conditions and the yield criterion of the actual stresses have to be fulfilled at every instant of the load history.

Find the maximum load factor α_{SD} for which the structure is safe. The structure is safe against LCF or ratchetting if there exists a stress field $\boldsymbol{\sigma}(t)$ such that the equilibrium equations are satisfied and the yield condition is nowhere and at no instant t violated. The maximum problem is given by:

$$\begin{aligned} \max \quad & \alpha_s \\ \text{s. t.} \quad & F(\boldsymbol{\sigma}(t)) \leq \sigma_y^2 \ \text{ in } V \\ & \operatorname{div}\boldsymbol{\sigma}(t) = -\alpha_s \mathbf{f}_0(t) \ \text{ in } V \\ & \boldsymbol{\sigma}(t)\,\mathbf{n} = \alpha_s \mathbf{p}_0(t) \ \text{ on } \partial V_p \end{aligned} \tag{4.6}$$

for the structure V, traction boundary ∂V_p (with outer normal $\mathbf{n}$), yield function F, body forces $\alpha_s\mathbf{f}_0(t)$ and surface loads $\alpha_s\mathbf{p}_0(t)$ for all $\mathbf{f}_0(t)$,$\mathbf{p}_0(t)$ in a given initial load domain $\mathcal{L}_0$.

The maximum problems (4.4) and (4.6) are solved by splitting the stresses $\boldsymbol{\sigma}$ and $\boldsymbol{\sigma}(t)$ into fictitious elastic stresses $\boldsymbol{\sigma}^E$, $\boldsymbol{\sigma}^E(t)$ and time invariant residual stresses $\boldsymbol{\rho}$ which fulfill the

homogeneous equilibrium conditions. This leads in the case of shakedown analysis to the mathematical optimization problem

$$\begin{array}{lrll} \max & \alpha & & \\ \text{s. t.} & F[\alpha \boldsymbol{\sigma}^E(t) + \bar{\boldsymbol{\rho}}] & \leq \sigma_y^2 & \text{in } V \\ & \text{div } \bar{\boldsymbol{\rho}} & = \mathbf{0} & \text{in } V \\ & \bar{\boldsymbol{\rho}}\, \mathbf{n} & = \mathbf{0} & \text{on } \partial V_p \end{array} \tag{4.7}$$

The resulting problem is transferred to a relatively small one by the basis reduction method and it is solved by means of Sequential Quadratic Programming techniques [14].

4.3 Kinematic or upper bound analysis

Find the minimum load factor α_{SD} for which the structure fails. The structure fails by plastic collapse if there exists a (kinematically admissible) velocity $\dot{\mathbf{u}}$ field such that the power $\dot{W}_{ex}$ of the external loads is higher than the power $\dot{W}_{in}$ which can be dissipated within the structure:

$$\begin{array}{ll} \min & \alpha_k \\ \text{with} & \alpha_k = \dot{W}_{in} = \displaystyle\int_V \dot{\varepsilon_{eq}}^P \sigma_y dV \\ \text{s. t.} & 1 = \dot{W}_{ex} = \displaystyle\int_V \mathbf{b}_0^T \dot{\mathbf{u}} dV + \int_{\partial V_p} \mathbf{p}_0^T \dot{\mathbf{u}} dS \geq 0, \\ & \dot{\boldsymbol{\varepsilon}} = \dfrac{1}{2}(\nabla \dot{\mathbf{u}} + (\nabla \dot{\mathbf{u}})^T) \quad \text{in } V\,, \\ & \dot{\mathbf{u}}(t) = \dot{\mathbf{u}}^0(t) \qquad \text{on} \quad \partial V_u, \end{array} \tag{4.8}$$

for the structure V, boundary $\partial V = \partial V_p \cup \partial V_u$ (with outer normal $\mathbf{n}$).

The FEM discretization of the upper bound limit load problem reads (see [45])

$$\begin{array}{rll} \text{Minimize} & \dot{\boldsymbol{e}}_{eq}^T \boldsymbol{r} & (= \quad \alpha_k) \\ \text{s. t.} & \dot{\boldsymbol{u}}^T \boldsymbol{p} = 1. & \end{array} \tag{4.9}$$

The objective function α_k is non-smooth at the boundary of the plastic region. Then the optimization problem resulting from a FEM discretization is also non-smooth. It may be solved with a bundle method [52]. As a practical alternative, different regularization methods are used as smoothing tools in the LISA project [48], [53]. The regularized minimization problem is solved in [53] by a reduced-gradient algorithm in conjunction with a quasi-Newton algorithm [35].

5 Plastic failure and reliability analysis

Following table 3.1 resistance R and loading S can be defined by the limit or shakedown load factor α_y and the applied load factor α_0, respectively to obtain the limit state function $g(\mathbf{X}) = \alpha_y - \alpha_0$.

The limit or shakedown ranges obtained from problems (4.4), (4.7) are linear functions of the failure stress σ_y if a homogeneous material distribution is assumed. Otherwise the random field concept has to be employed. If the structure has a heterogeneous material distribution we obtain in different Gaussian points i eventually different failure stresses $\sigma_{y,i}$. Then the limit load is no more a linear function of the failure stresses. It also ceases to be a linear function if the loading is non-proportional, e.g. in the presence of dead loads. In this case the derivatives of the limit state function may not be computed directly from the linear function of the failure stresses. The Lagrange multipliers of the optimization problem (4.4) yield the gradient information of $g(\mathbf{X})$ without any extra computation. This is derived from a variation of $\sigma_{y,i}$ as the right hand side of problem (4.4) (see [11]).

5.1 Sensitivity and mathematical programming

A constraint maximization problem **P** in the most general case is defined as

$$\begin{aligned} \max \quad & f(\mathbf{x}) \\ \text{s.t.} \quad & g_i(\mathbf{x}) \leq 0, \forall i \in \mathcal{I}. \end{aligned} \tag{5.1}$$

Suppose that $f, g_i : I\!R^n \rightarrow I\!R$ are twice continuously differentiable and let $\mathcal{I}$ be some index set. In many applications (e.g. shakedown analysis), the objective function f as well as the constraint functions g_i may depend also on other parameters. Consider the following perturbation **P**($\boldsymbol{\varepsilon}$) of the original problem **P**(**0**)

$$\begin{aligned} \max \quad & f(\mathbf{x}, \boldsymbol{\varepsilon}) \\ \text{s.t.} \quad & g_i(\mathbf{x}, \boldsymbol{\varepsilon}) \leq 0, \forall i \in \mathcal{I}, \boldsymbol{\varepsilon} \in I\!R^q, q \in I\!N \end{aligned} \tag{5.2}$$

A perturbation $\boldsymbol{\varepsilon}$ can be interpreted in two ways: as a *random* error, or as a *specific* change in the parameters defining the problem functions. The optimal solution $\mathbf{x}^*(\boldsymbol{\varepsilon})$ of problem **P**($\boldsymbol{\varepsilon}$) with the Lagrangian multipliers $\boldsymbol{\lambda}^*$ fulfills the following first order Karush-Kuhn-Tucker conditions:

$$\begin{aligned} \lambda_i^* g_i(\mathbf{x}^*, \boldsymbol{\varepsilon}) &= 0, \forall i \in \mathcal{I} \\ \lambda_i^* &\geq 0, \forall i \in \mathcal{I} \\ \nabla_x L(\mathbf{x}^*, \boldsymbol{\lambda}^*, \boldsymbol{\varepsilon}) &= \mathbf{0} \end{aligned} \tag{5.3}$$

with the Lagrangian function

$$L(\mathbf{x}, \boldsymbol{\lambda}, \boldsymbol{\varepsilon}) = f(\mathbf{x}, \boldsymbol{\varepsilon}) - \sum_{i \in \mathcal{I}} \lambda_i g_i(\mathbf{x}, \boldsymbol{\varepsilon}). \tag{5.4}$$

If the system of equations is nonsingular, the implicit function theorem implies the existence of a unique differentiable local solution $(\mathbf{x}^*(\boldsymbol{\varepsilon}),\ \boldsymbol{\lambda}^*(\boldsymbol{\varepsilon}))$ of **P($\boldsymbol{\varepsilon}$)**. The restricted Lagrangian is defined with only the active constraints $g_i = 0, i \in \mathcal{I}_0$ for second order Karush-Kuhn-Tucker conditions. The second order sufficient conditions state that a point $(\mathbf{x}^*, \boldsymbol{\varepsilon}^*)$ is a strict local maximum of $\mathbf{P}(\boldsymbol{\varepsilon})$ if (5.3) is satisfied at $(\mathbf{x}^*, \boldsymbol{\varepsilon})$ and if the Hessian $\nabla_x^2 L(\mathbf{x}^*, \boldsymbol{\lambda}^*, \boldsymbol{\varepsilon})$ of the restricted Lagrangian is negative definite on the tangent space $\{\boldsymbol{\xi} \mid \boldsymbol{\xi}^T \nabla_x g_i(\mathbf{x}^*) = 0,\ i \in \mathcal{I}_0 : \lambda_i^* > 0\}$. Let $\boldsymbol{\varepsilon} = \mathbf{0}$, then the conditions are fulfilled in a local solution $\mathbf{x}^*$ of **P(0)**. The associated theorem is given in [8], [9].

Corollary [8]:

At a local solution $\mathbf{x}^*$ of problem **P(0)**, assume that the linear independence condition, the second order sufficiency condition and the strict complementarity condition $\lambda_i^* g_i(\mathbf{x}^*, \boldsymbol{\varepsilon}) = 0$ are satisfied for all $i \in \mathcal{I}$, and that the functions defining $\mathbf{P}(\boldsymbol{\varepsilon})$ are twice continuously differentiable with respect to $(\mathbf{x}, \boldsymbol{\varepsilon})$ in a neighbourhood of $(\mathbf{x}^*, \mathbf{0})$. It follows that at, $\boldsymbol{\varepsilon}_0 = \mathbf{0}$

$$\frac{d}{d\boldsymbol{\varepsilon}} \begin{pmatrix} \mathbf{x}(\mathbf{0}) \\ \boldsymbol{\lambda}(\mathbf{0}) \end{pmatrix} = -Q_0^{-1} V_0, \tag{5.5}$$

and

$$\frac{d}{d\boldsymbol{\varepsilon}} f(\mathbf{x}(\mathbf{0}), \mathbf{0}) = \frac{\partial f(\mathbf{x}(\mathbf{0}), \mathbf{0})}{\partial \boldsymbol{\varepsilon}} - \sum_{i \in \mathcal{I}} \lambda_i^* \frac{\partial g_i(\mathbf{x}(\mathbf{0}), \mathbf{0})}{\partial \boldsymbol{\varepsilon}} \tag{5.6}$$

where

$$Q_0 = \begin{pmatrix} \nabla_x^2 L & -\nabla_x g_1 & \cdots & -\nabla_x g_m \\ \lambda_1 \nabla_x^T g_1 & g_1 & & 0 \\ \vdots & & \ddots & \\ \lambda_m \nabla_x^T g_m & 0 & & g_m \end{pmatrix} \tag{5.7}$$

and

$$V_0 = \begin{pmatrix} \frac{\partial}{\partial \boldsymbol{\varepsilon}} \left[\nabla_x L^T\right] \\ \lambda_1 \frac{\partial}{\partial \boldsymbol{\varepsilon}} \left[\nabla_x g_1\right] \\ \vdots \\ \lambda_m \frac{\partial}{\partial \boldsymbol{\varepsilon}} \left[\nabla_x g_m\right] \end{pmatrix}. \tag{5.8}$$

All quantities are evaluated at $\mathbf{x}^*(\mathbf{0})$, $\boldsymbol{\lambda}^*(\mathbf{0})$, $\boldsymbol{\varepsilon}_0$ with $m = |\mathcal{I}|$.

5.2 Sensitivity in limit and shakedown analysis

We restrict ourselves to the following perturbation **P**($\boldsymbol{\varepsilon}$) of the original static shakedown problem (4.7) with the unknowns $\mathbf{x} = (\alpha, \boldsymbol{\rho}_1, \ldots \boldsymbol{\rho}_{NG})$ and $g_i = F[\alpha \boldsymbol{\sigma}^E_{i,j}(\boldsymbol{\varepsilon}) + \boldsymbol{\rho}_i] - \sigma_y^2$:

$$\begin{aligned} \max \quad & \alpha \\ \text{s.t.} \quad & F[\alpha \boldsymbol{\sigma}^E_{i,j}(\boldsymbol{\varepsilon}) + \boldsymbol{\rho}_i] - \sigma_y^2 \leq 0, \;\; i = 1, \ldots, NG, j = 1, \ldots, NV. \end{aligned} \tag{5.9}$$

The problem fulfills the assumptions of the corollary, such that we obtain the derivatives at the solution α^* of the original problem **P(0)** with the original fictitious elastic stresses $\boldsymbol{\sigma}^E(\mathbf{0})$ by:

$$\begin{aligned} \frac{d}{d\boldsymbol{\varepsilon}} f(\mathbf{x}(\mathbf{0}), \mathbf{0}) &= \frac{d\alpha^*}{d\boldsymbol{\varepsilon}} - \sum_{i \text{ active}} \lambda_i^* \frac{\partial g_i(\mathbf{x}(\mathbf{0}), \mathbf{0})}{\partial \boldsymbol{\varepsilon}} \Bigg|_{\varepsilon=0} \\ &= -\alpha^* \sum_{i \text{ active}} \lambda_i^* \frac{\partial}{\partial \boldsymbol{\sigma}_i^E} \left[F(\alpha \boldsymbol{\sigma}_i^E(\boldsymbol{\varepsilon}) + \boldsymbol{\rho}_i) \right] \frac{\partial \boldsymbol{\sigma}_i^E(\boldsymbol{\varepsilon})}{\partial \boldsymbol{\varepsilon}} \Bigg|_{\varepsilon=0} \end{aligned} \tag{5.10}$$

This problem is solved by the basis reduction method in a recursive manner by means of Sequential Quadratic Programming techniques. The shakedown factor α_k as well as the Lagrange multipliers λ_k^* obtained during the optimization step k converge to the true solution α^* and $\boldsymbol{\lambda}^*$ [14]. Therefore, in equation (5.10) all values except

$$\frac{\partial \boldsymbol{\sigma}_i^E(\boldsymbol{\varepsilon})}{\partial \boldsymbol{\varepsilon}} \Bigg|_{\varepsilon=0} \tag{5.11}$$

are given by the limit and shakedown analysis. This means, that in the case of limit and shakedown analysis the sensitivity analysis of the plastic structural behaviour is reducible to the sensitivity analysis of the elastic structural response, which is a significant reduction of computational effort. Similar techniques can be used for structural optimization with respect to limit and shakedown constraints [15], [16]. The sensitivity analysis of the elastic response is performed by a finite-difference method for a small number of parameters, see [24] for alternative techniques.

5.2.1 Sensitivity of yield stress

In the FORM optimization problem described above the partial derivatives of the limit state function g are needed. In principle the limit load and shakedown analysis have the following form with $\boldsymbol{G}$ as vector of all inequality restrictions ϕ, the failure stresses $\boldsymbol{r} = (\sigma^2_{y,1}, \ldots, \sigma^2_{y,NG})$ and the variables $\boldsymbol{\xi} = (\alpha, \boldsymbol{\rho}_1, \ldots, \boldsymbol{\rho}_{NG})$

$$\begin{aligned} \max \quad & f(\boldsymbol{\xi}) \\ \text{s. t.} \quad & \boldsymbol{G}(\boldsymbol{\xi}) \leq \boldsymbol{r} \end{aligned} \tag{5.12}$$

The influence of the failure stresses $\sigma_{y,i}$ on the load factor α is dominated by the derivatives $\partial\alpha/\partial\sigma_{y,i}$ or by $\partial f(\boldsymbol{\xi})/\partial\boldsymbol{\delta}$. These derivatives could be generated by the corollary shown above. For the limit and shakedown analysis it follows

$$\frac{\partial\alpha}{\partial\sigma_{y,1}} = -\lambda_1^*, \ldots, \frac{\partial\alpha}{\partial\sigma_{y,NG}} = -\lambda_{NG}^*, \tag{5.13}$$

such that the influences of the failure stresses on the limit and shakedown load factor α could be obtained by the solution of the problems (4.4), (4.7). The FORM-Algorithm developed in [41] has been adapted to plastic reliability analysis.

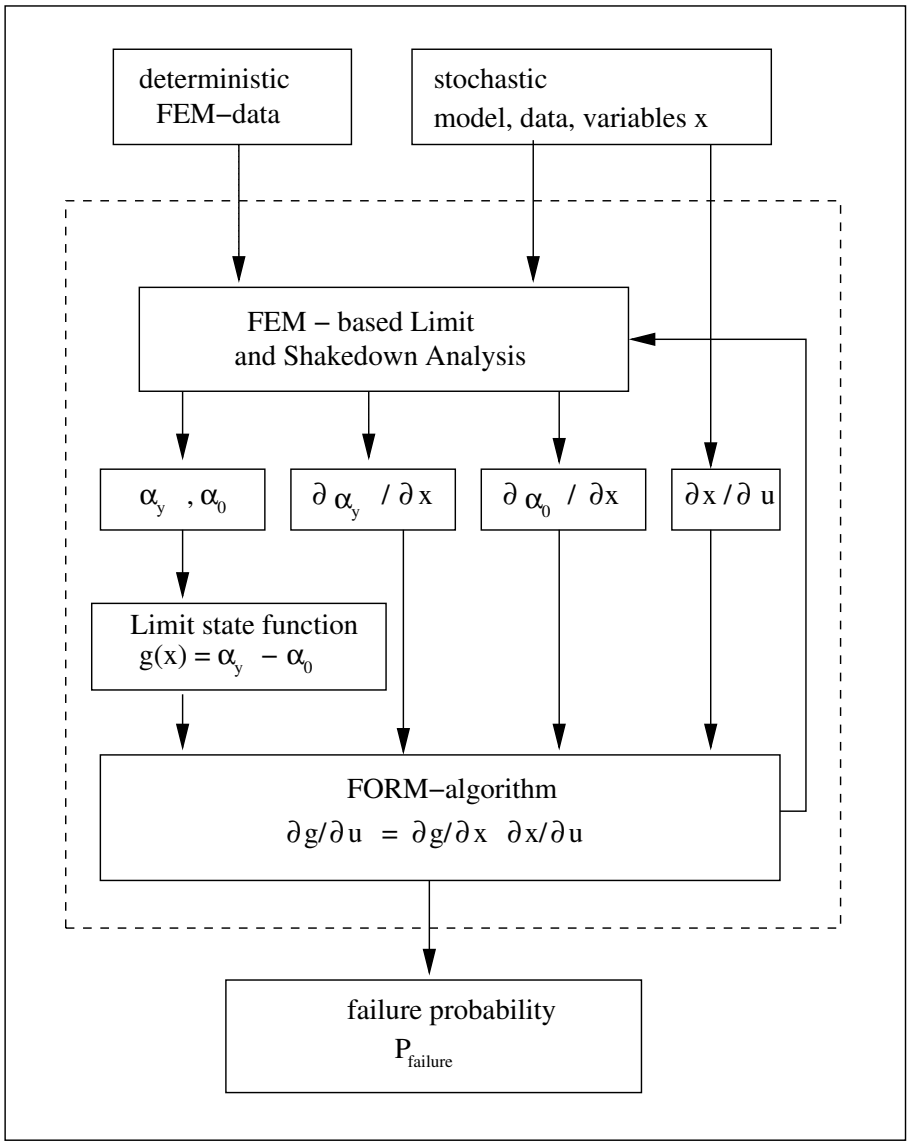

Figure 5.1: Flowchart of the probabilistic limit load analysis

The flowchart in Figure 5.1 contains the logical connections of the main analysis steps as they have been implemented in the Finite Element Software PERMAS Version 4 [36] in the LISA project.

6 Stochastic programming

In Operations Research two main approaches to optimization (programming) under uncertainty have been developed. The most important ones for decision making under uncertainty are the two-stage and multistage stochastic programs with recourse problems. Structural reliability problems in plasticity context lead more naturally to the so-called *chance constrained stochastic programming*.

Stochastic programming is not used in this sense in reliability literature such as [25], [30], [51] and has not been planned in the LISA project. Chance constrained stochastic programming will be described here as an alternative design approach following [42]. The limit load is computed for a fixed reliability instead for a fixed safety margin as in deterministic design. This is easily extended to stochastic structural optimization. A similar exposition was given for limit analysis with linear programming (for Tresca material) without duality in [40]. The application of a two-stage stochastic linear program with complete fixed recourse is described in [29].

6.1 Static approach to chance constrained programming

Starting from the static theorem of limit analysis the deterministic program (4.5 becomes

$$\max_{\alpha_s}\{\alpha_s | \boldsymbol{f}(\boldsymbol{s}) - \boldsymbol{r} \leq \boldsymbol{0}, \boldsymbol{C}\boldsymbol{s} - \alpha_s \boldsymbol{p} = \boldsymbol{0}\}. \tag{6.1}$$

For stochastic strength $\boldsymbol{r}(\omega)$ a stochastic formulation is obtained by assuming that the inequality constraints are satisfied at least by a chance $\boldsymbol{\gamma}$

$$\max_{\alpha_s}\{\alpha_s | P(\boldsymbol{f}(\boldsymbol{s}) - \boldsymbol{r}(\omega) \leq \boldsymbol{0}) \geq \boldsymbol{\gamma}, \boldsymbol{C}\boldsymbol{s} - \alpha_s \boldsymbol{p} = \boldsymbol{0}\}. \tag{6.2}$$

For continuous distributions no probability can be assigned to an equality. Therefore, the problem must be reformulated in case of stochastic loads $\boldsymbol{p}$. With $\boldsymbol{\gamma} = (\gamma_1, \ldots, \gamma_{NG})$ this is an individual chance constrained program. Alternatively a joint chance constrained program can be formulated [42].

It is assumed that $\boldsymbol{r}(\omega) = (r_1(\omega), \ldots, r_2(\omega))$ follows a multivariate Gaussian (normal) distribution with mean vector $\boldsymbol{\mu}_r$ and covariance matrix $\boldsymbol{\Sigma}_r$. Otherwise is may be transformed to such a distribution. A standard normally distributed vector $\tilde{\boldsymbol{r}}(\omega)$ is obtained by

$$\tilde{r}_i = (r_i - \mu_i)/\sigma_i. \tag{6.3}$$

Then the inequality $\boldsymbol{f}(\boldsymbol{s}) - \boldsymbol{r}(\omega) \leq \mathbf{0}$ is element-wise

$$f_i(\boldsymbol{s}) \leq r_i = \tilde{r}_i \sigma_i + \mu_i, \tag{6.4}$$

so that

$$\tilde{f}_i(\boldsymbol{s}) := (f_i(\boldsymbol{s}) - \mu_i)/\sigma_i \leq \tilde{r}_i \tag{6.5}$$

and the probabilistic inequality becomes

$$P(f_i(\boldsymbol{s}) \leq r_i(\omega)) = P(\tilde{f}_i(\boldsymbol{s}) \leq \tilde{r}_i(\omega)) \geq \gamma_i. \tag{6.6}$$

If the CDF of the standard normal distribution is denoted Φ we may use $\Phi(-x) = 1 - \Phi(x)$ to write

$$P(\tilde{r}(\omega) \geq \tilde{f}_i(\boldsymbol{s})) = 1 - P(\tilde{r}(\omega) \leq \tilde{f}_i(\boldsymbol{s})) = 1 - \Phi(\tilde{f}_i(\boldsymbol{s})) = \Phi(-\tilde{f}_i(\boldsymbol{s})) \geq \gamma_i. \tag{6.7}$$

Introducing the abbreviation $\kappa_i := \Phi^{-1}(\gamma_i)$ so that $\gamma_i = \Phi(\kappa_i)$ yields

$$\Phi(-\tilde{f}_i(\boldsymbol{s})) \geq \Phi(\kappa_i). \tag{6.8}$$

Φ is monotonic or order preserving. Therefore,

$$\kappa_i \leq -\tilde{f}_i(\boldsymbol{s}) = (\mu_i - f_i(\boldsymbol{s}))/\sigma_i \tag{6.9}$$

or rearranging

$$\mu_i - \kappa_i \sigma_i \geq f_i(\boldsymbol{s}). \tag{6.10}$$

Introducing $\boldsymbol{\sigma}_r = diag\Sigma_r = (\sigma_1, \ldots, \sigma_{NG})$ this may be written in matrix form

$$\boldsymbol{\mu}_r - \boldsymbol{\kappa}^T \boldsymbol{\sigma}_r \geq \boldsymbol{f}(\boldsymbol{s}) \tag{6.11}$$

to obtain the *deterministic equivalent* of the stochastic program (6.2)

$$\max_{\alpha_s} \{\alpha_s | \boldsymbol{f}(\boldsymbol{s}) - (\boldsymbol{\mu}_r - \boldsymbol{\kappa}^T \boldsymbol{\sigma}_r) \leq \mathbf{0}, \boldsymbol{C}\boldsymbol{s} - \alpha_s \boldsymbol{p} = \mathbf{0}\}. \tag{6.12}$$

This nonlinear program shows that the optimum limit load factor α_s decreases if the standard deviation σ_i or the required reliability γ_i and thus $\kappa_i = \Phi^{-1}(\gamma_i)$ increase for the ith strength variable r_i.

6.2 Kinematic approach to chance constrained programming

Starting from the kinematic theorem of limit analysis the deterministic program (4.9) becomes

$$\min_{\boldsymbol{\lambda}} \{\boldsymbol{\lambda}^T \boldsymbol{r} | \dot{\boldsymbol{u}}^T \boldsymbol{p} = 1\}. \tag{6.13}$$

with $\boldsymbol{\lambda} = \dot{\boldsymbol{\varepsilon}}_{eq} \geq \mathbf{0}$.

For uncertain strength $\boldsymbol{r}(\omega)$ the objective function $\boldsymbol{\lambda}^T \boldsymbol{r}(\omega)$ becomes also a stochastic variable. First the minimum of an stochastic objective function must be explained. In decision theory it is common to minimize the expectation $E(\boldsymbol{\lambda}^T \boldsymbol{r}) = \mu_{\lambda^T r} = \boldsymbol{\lambda}^T \boldsymbol{\mu}_r$ of the cost function (e.g. minimizing a possible loss). If the risk has to be minimized simultaneously,

$$\boldsymbol{\lambda}^T \boldsymbol{\mu}_r - k\sigma_{\lambda^T r} \tag{6.14}$$

may be used as objective function with some arbitrary weight $k, k > 0$. If a normal distribution is assumed again for $\boldsymbol{r}(\omega)$, the objective function can be written as

$$\boldsymbol{\lambda}^T \boldsymbol{\mu}_r - k\sqrt{\boldsymbol{\lambda}^T \boldsymbol{\Sigma}_r \boldsymbol{\lambda}}. \tag{6.15}$$

This objective function may be obtained from a chance constrained stochastic program. Consider the probability that the minimum of (6.13) is not assumed

$$P(\boldsymbol{\lambda}^T \boldsymbol{\mu}_r \geq z) = 1 - P(\boldsymbol{\lambda}^T \boldsymbol{\mu}_r \leq z) \leq \gamma. \tag{6.16}$$

Here $\gamma \in [0, 1]$ is the maximum risk that the yet undetermined level z is not achieved. This can be written as

$$1 - P\left(\frac{\boldsymbol{\lambda}^T \boldsymbol{\mu}_r - \mu_{\lambda^T r}}{\sigma_{\lambda^T r}} \leq \frac{z - \mu_{\lambda^T r}}{\sigma_{\lambda^T r}}\right) \leq \gamma. \tag{6.17}$$

where

$$\frac{\boldsymbol{\lambda}^T \boldsymbol{\mu}_r - \mu_{\lambda^T r}}{\sigma_{\lambda^T r}} \tag{6.18}$$

is a standardized stochastic variable. For the normal distribution

$$P(\boldsymbol{\lambda}^T \boldsymbol{\mu}_r \geq z) = 1 - \Phi\left(\frac{z - \mu_{\lambda^T r}}{\sigma_{\lambda^T r}}\right) \leq \gamma \tag{6.19}$$

so that

$$-\kappa := \Phi^{-1}(1 - \gamma) \leq \frac{z - \mu_{\lambda^T r}}{\sigma_{\lambda^T r}} \tag{6.20}$$

or

$$\mu_{\lambda^T r} - \kappa\sigma_{\lambda^T r} \leq z. \tag{6.21}$$

The joint chance constrained stochastic program

$$\min_{\boldsymbol{\lambda}} \{\boldsymbol{\lambda}^T \boldsymbol{r} | P(\boldsymbol{\lambda}^T \boldsymbol{\mu}_r \geq z) \leq \gamma, \dot{\boldsymbol{u}}^T \boldsymbol{p} = 1\}, \tag{6.22}$$

has the deterministic equivalent

$$\begin{aligned} &\min_z \{z | \mu_{\lambda^T r} - \kappa\sigma_{\lambda^T r} \leq z, \dot{\boldsymbol{u}}^T \boldsymbol{p} = 1\} \\ &\quad = \min_{\boldsymbol{\lambda}} \{\boldsymbol{\lambda}^T \boldsymbol{\mu}_r - \kappa\sigma_{\lambda^T r} | \dot{\boldsymbol{u}}^T \boldsymbol{p} = 1\}. \end{aligned} \tag{6.23}$$

For normally distributed $\boldsymbol{r}(\omega)$ this assumes the form

$$\min_{\boldsymbol{\lambda}}\{\boldsymbol{\lambda}^T\boldsymbol{\mu}_r - \kappa\sqrt{\boldsymbol{\lambda}^T\boldsymbol{\Sigma}_r\boldsymbol{\lambda}}|\dot{\boldsymbol{u}}^T\boldsymbol{p} = 1\}. \tag{6.24}$$

The Chebychev inequality

$$P\left(\boldsymbol{\lambda}^T\boldsymbol{r} \leq \boldsymbol{\lambda}^T\boldsymbol{\mu}_r - \kappa\sigma_{\lambda^T r}\right) \leq P\left(\frac{\boldsymbol{\lambda}^T\boldsymbol{r} - \mu_{\lambda^T r}}{\sigma_{\lambda^T r}} \geq -\kappa\right) \leq \frac{1}{\kappa^2} \tag{6.25}$$

says that the true value $\boldsymbol{\lambda}^T\boldsymbol{r}$ is less than $\boldsymbol{\lambda}^T\boldsymbol{\mu}_r - \kappa\sigma_{\lambda^T r}$ with probability $(1 - 1/\kappa^2)\cdot 100\%$ for $\kappa > 1$. The value of $\kappa = -\Phi^{-1}(1-\gamma)$ has to be determined from the risk γ in eqn. (6.16).

The model may be critizised, because it measures risk symmetrically i.e. over- and underestimations of the optimum are assessed in the same way. An asymmetric risk measure may be more plausible.

6.3 Duality in chance constrained programming

The deterministic minimum and maximum problems resulting from the static and kinematic theorems for the discretized structures are Lagrange duals [28]. We will show that the same holds true for the deterministic equivalents of the chance constraint stochastic programs for normally distributed $\boldsymbol{r}(\omega)$.

Let the deterministic equivalent of the joint chance constrained lower bound problem be the *primal program*

$$\begin{aligned} \text{Maximize} \quad & \alpha_s \\ \text{s. t.} \quad & \boldsymbol{f}(\boldsymbol{s}) - \boldsymbol{\mu}_r + \kappa\boldsymbol{\sigma}_r \leq \boldsymbol{0}, \\ & \boldsymbol{C}\boldsymbol{s} - \alpha_s\boldsymbol{p} = \boldsymbol{0}. \end{aligned} \tag{6.26}$$

The inequality constraints of the NG Gaussian points were collected to the vectors $\boldsymbol{f}, \boldsymbol{s}, \boldsymbol{\mu}_r$, and $\boldsymbol{r}$. The unknowns are the limit load factor α_s and the stresses $\boldsymbol{s}$. The minimum problem with restrictions is transformed into an unrestricted problem by the *Lagrangian* $L(\alpha_s, \boldsymbol{s}, \dot{\boldsymbol{u}}, \boldsymbol{\lambda})$, such that the optimality conditions for unrestricted problems hold (see [11], [28]). With the Lagrange factors $\boldsymbol{\lambda} \geq \boldsymbol{0}$ and $\dot{\boldsymbol{u}}$ it holds

$$L(\alpha_s, \boldsymbol{s}, \dot{\boldsymbol{u}}, \boldsymbol{\lambda}) \;=\; \alpha_s + \dot{\boldsymbol{u}}^T(\boldsymbol{C}\boldsymbol{s} - \alpha_s\boldsymbol{p}) - \boldsymbol{\lambda}^T(\boldsymbol{f}(\boldsymbol{s}) - \boldsymbol{\mu}_r + \kappa\boldsymbol{\sigma}_r). \tag{6.27}$$

In the minimum the Lagrangian $L(\alpha_s, \boldsymbol{s}, \dot{\boldsymbol{u}}, \boldsymbol{\lambda})$ has a *saddle point,* such that the optimal value is the solution of

$$\min_{\dot{\boldsymbol{u}},\boldsymbol{\lambda}} \max_{\alpha_s,\,\boldsymbol{s}} L(\alpha_s, \boldsymbol{s}, \dot{\boldsymbol{u}}, \boldsymbol{\lambda}). \tag{6.28}$$

The necessary optimality conditions of the maximum are

$$\frac{\partial L}{\partial \alpha_s} = 1 - \dot{\boldsymbol{u}}^T \boldsymbol{p} = 0, \tag{6.29}$$

$$\frac{\partial L}{\partial \boldsymbol{s}} = \dot{\boldsymbol{u}}^T \boldsymbol{C} - \boldsymbol{\lambda}^T \frac{\partial \boldsymbol{f}}{\partial \boldsymbol{s}} = \boldsymbol{0}. \tag{6.30}$$

Equation (6.29) means a normalization of the external power of loading $\dot{W}_{ex} = \dot{\boldsymbol{u}}^T \boldsymbol{p} = 1$ of the discretized structure. By substituting this in the dual objective function $l(\dot{\boldsymbol{u}}, \boldsymbol{\lambda}) = \max_{\alpha_s,\, \boldsymbol{s}} L(\alpha_s, \boldsymbol{s}, \dot{\boldsymbol{u}}, \boldsymbol{\lambda})$ we derive the Euler differential equation

$$\boldsymbol{s}^T \frac{\partial \boldsymbol{f}(\boldsymbol{s})}{\partial \boldsymbol{s}} = \boldsymbol{f}(\boldsymbol{s}). \tag{6.31}$$

With eq. (6.29) it follows with $\boldsymbol{\lambda} \geq \boldsymbol{0}$

$$\begin{aligned} l(\dot{\boldsymbol{u}}, \boldsymbol{\lambda}) &= \max_{\alpha_s,\, \boldsymbol{s}} L(\alpha_s, \boldsymbol{s}, \dot{\boldsymbol{u}}, \boldsymbol{\lambda}) \\ &= \alpha_s + \dot{\boldsymbol{u}}^T \boldsymbol{C} \boldsymbol{s} - \alpha_s - \boldsymbol{\lambda}^T (\boldsymbol{f}(\boldsymbol{s}) - \boldsymbol{\mu}_r + \kappa \boldsymbol{\sigma}_r) \\ &= \boldsymbol{\lambda}^T \frac{\partial \boldsymbol{f}(\boldsymbol{s})}{\partial \boldsymbol{s}} \boldsymbol{s} - \boldsymbol{\lambda}^T (\boldsymbol{f}(\boldsymbol{s}) - \boldsymbol{\mu}_r + \kappa \boldsymbol{\sigma}_r) \\ &= \boldsymbol{\lambda}^T (\boldsymbol{\mu}_r - \kappa \boldsymbol{\sigma}_r). \end{aligned} \tag{6.32}$$

Equation (6.28) is derived by eq. (6.29), (6.30) and (6.32), such that the *dual program* is defined by

$$\begin{aligned} \text{Minimize} \quad & \boldsymbol{\lambda}^T (\boldsymbol{\mu}_r - \kappa \boldsymbol{\sigma}_r) \\ \text{s. t.} \quad & \boldsymbol{\lambda} \geq \boldsymbol{0}, \\ & \dot{\boldsymbol{u}}^T \boldsymbol{p} = 1, \\ & \boldsymbol{C}^T \dot{\boldsymbol{u}} - \boldsymbol{\lambda}^T \frac{\partial \boldsymbol{f}}{\partial \boldsymbol{s}} = \boldsymbol{0}. \end{aligned} \tag{6.33}$$

Because of the normalization $\dot{W}_{ex} = \dot{\boldsymbol{u}}^T \boldsymbol{p} = 1$ it holds $\alpha_k = l(\boldsymbol{\lambda}) = \dot{W}_{in}(\dot{\varepsilon}_{eq})$.

The Lagrange factors of the primal problem are the unknowns of the dual problem. The dual problem is formulated in the kinematic terms $\dot{\boldsymbol{u}}$ and $\boldsymbol{\lambda}$. With

$$\dot{\boldsymbol{e}}^p = \boldsymbol{\lambda}^T \frac{\partial \boldsymbol{f}(\boldsymbol{s})}{\partial \boldsymbol{s}} \tag{6.34}$$

eq. (6.30) could be reformulated for the associated flow rule and $\dot{\boldsymbol{e}}^p = \dot{\boldsymbol{e}}$ in the collapse state

$$\boldsymbol{C}^T \dot{\boldsymbol{u}} - \dot{\boldsymbol{e}} = \boldsymbol{0}, \tag{6.35}$$

which is automatically satisfied in a displacement FEM discretization. $\boldsymbol{\lambda}$ may be replaced by the collection of effective strain rates $\dot{\boldsymbol{\varepsilon}}_{eq}$ and always $\boldsymbol{\lambda} = \dot{\boldsymbol{\varepsilon}}_{eq} \geq \mathbf{0}$. Then the dual problem reduces to

$$\begin{aligned} \text{Minimize} \quad & \alpha_k \\ \text{with.} \quad & \alpha_k = \dot{\boldsymbol{\varepsilon}}_{eq}^T(\boldsymbol{\mu}_r - \kappa\boldsymbol{\sigma}_r) \\ \text{s. t.} \quad & \dot{\boldsymbol{u}}^T\boldsymbol{p} = 1. \end{aligned} \tag{6.36}$$

This is the deterministic equivalent (6.23) of (6.22).

The saddle point properties of the Lagrangian shows, that the maximum problem is concave and the minimum problem in convex such that both problem have the same optimal value

$$\max\alpha_s = \alpha = \min\alpha_k. \tag{6.37}$$

Because of the convexity of the problem, the obtained local optimum is a global one (see [11]) such that the limit load factor is unique.

7 Examples

The plastic reliability problem can be solved analytically if the limit load is known and R and S are both normally or log-normally distributed. Simple models are used to test correctness and numerical error.

7.1 Limit load analysis

In case of a square plate of length L with a hole of diameter D (see Figure 7.1) and $D/L = 0.2$ subjected to uniaxial tension the exact limit load is given by $P_y = (1 - D/L)\sigma_y$ with the yield stress σ_y (see [12], [44]).

Thus the resistance $R = P_y$ depends linearly of the realization σ_y of the yield stress basic variable X. The load $S = P$ is a homogeneous uniaxial tension on one side of the plate. The magnitude of the tension is the second basic variable X. The limit load P_L of each realization x of X is

$$P_y(y) = (1 - D/L)\ x. \tag{7.1}$$

The limit state function is defined by

$$g(x, y) = R - S = P_y - P = (1 - D/L)\, x - y. \tag{7.2}$$

The normally distributed random variables X and Y with means μ_r, μ_s and standard deviations σ_r^2, σ_s^2 respectively, yield with

$$x = \sigma_r\ u_r + \mu_r \qquad \text{and} \qquad y = \sigma_s\ u_s + \mu_s \tag{7.3}$$

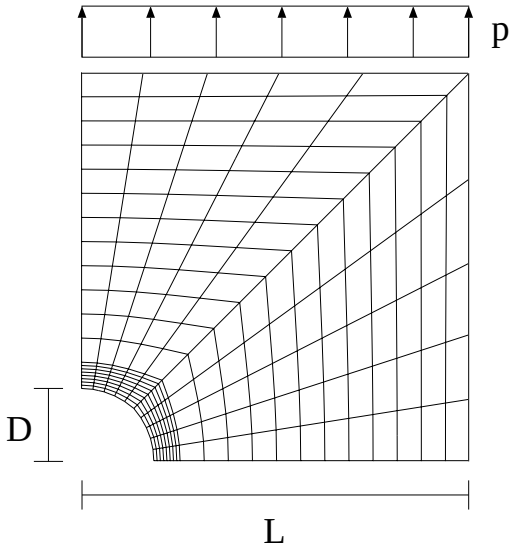

Figure 7.1: Finite element mesh of plate with a hole

the transformed limit state function

$$G(u_r, u_s) = ((1 - D/L)\mu_r - \mu_s) + (1 - D/L)\sigma_r u_r - \sigma_s u_s. \tag{7.4}$$

With realizations $\boldsymbol{u} = (u_r, u_s)^T$ of the new random variable $\mathbf{U}$ it may be written

$$G(\boldsymbol{u}) = \frac{((1 - D/L)\sigma_r, -\sigma_s)}{\sqrt{(1 - D/L)^2\sigma_r^2 + \sigma_s^2}}\,\boldsymbol{u} + \frac{(1 - D/L)\mu_r - \mu_s}{\sqrt{(1 - D/L)^2\sigma_r^2 + \sigma_s^2}}, \tag{7.5}$$

such that the reliability index β (with $D/L = 0.2$) is

$$\beta = \frac{(1 - D/L)\mu_r - \mu_s}{\sqrt{(1 - D/L)^2\sigma_r^2 + \sigma_s^2}} = \frac{0.8\mu_r - \mu_s}{\sqrt{0.64\sigma_r^2 + \sigma_s^2}}. \tag{7.6}$$

Remark

For normally distributed variables X and Y one can calculate the failure probability directly from the joint distribution. Let Z be the random variable defined by

$$\mathrm{Z} = (1 - D/L)\mathrm{X} - \mathrm{Y} = 0.8\mathrm{X} - \mathrm{Y} \tag{7.7}$$

then $\mathrm{Z} \sim N(0.8\mu_x - \mu_y, 0.64\sigma_x^2 + \sigma_y^2)$ holds with the density

$$f_z = \frac{1}{\sqrt{2\pi(\sigma_y^2 + 0.64\sigma_x^2)}}\, e^{-\frac{(z-(0.8\mu_x-\mu_y))^2}{2(\sigma_y^2+0.64\sigma_x^2)}}. \tag{7.8}$$

The failure probability is given by

$$P(g \le 0) = \int_{-\infty}^{0} f_z(z)dz = \int_{-\infty}^{0} \frac{1}{\sqrt{2\pi(0.64\sigma_x^2+\sigma_y^2)}}\, e^{-\frac{(z-(0.8\mu_x-\mu_y))^2}{2(0.64\sigma_x^2+\sigma_y^2)}}\, dz$$

$$= \frac{1}{\sqrt{2\pi}} \int_{-\infty}^{-\beta} e^{-0.5z^2} dz = \Phi(-\beta). \qquad (7.9)$$

In Figure 7.4 the failure probabilities $\mathrm{P}_f = \Phi(-\beta)$ are shown versus μ_s/μ_r. The numerical P_f of the limit analyses are compared with the analytic values resulting from the exact solution. Both variables are normally distributed with standard deviations $\sigma_r = 0.1\mu_r$ and $\sigma_s = 0.1\mu_s$.

Similar simple models are used to test correctness and numerical error (see the Fig. A1 and Tab. A1 in the appendix). The lower bound theorem generates collapse loads which are safe. But they are 1 to 2 % below the analytical limit loads by the termination error of the iteration. This error is amplified in the probabilistic analysis. The errors of the FORM calculations and of the numerical limit analyses are included in the results (see Figure 7.4 and Table 7.3). The errors are acceptable for highly reliable components, because the tail sensitivity problem is much more severe. The calculated failure probabilities correspond very well with the analytical probabilities if the analytical limit loads are reduced by 2% to obtain P_f (anal.-2%). This shows that the main part of the observed errors results from the deterministic limit analyses. SORM would give no improved results with a linear limit state function $G(\boldsymbol{u})$. Linearity may be lost, if X or Y are not normally distributed.

Much more severe deviations of the computed failure probabilities have to be expected if other limit state functions were used such as the extension of plastic zone or of the half the elastic stiffness approach (4.3). Moreover, such limit states give the wrong impression that the stochastic plastic collapse load is sensitive to the basic variable Young's modulus. Therefore some non-linear distributions are tested. First, calculations with log-normally distributed loads X and failure stresses Y are made [20]. The density of non-negative, log-normally distributed random variables x with the parameters m and δ is given by [7]

$$f(x) = \frac{1}{x\sqrt{2\pi\delta^2}}\, e^{-[\log(x/m)]^2/2\delta^2} \text{ , with } m > 0, x \ge 0. \qquad (7.10)$$

The log-normal distribution has the expectation μ and the variance σ^2

$$\mu = E(\mathrm{X}) = m\, e^{\delta^2/2}, \qquad \sigma^2 = \mathrm{Var}(\mathrm{X}) = m^2\, e^{\delta^2}(e^{\delta^2} - 1). \qquad (7.11)$$

For the comparison of the different random distributions the same expectation $\mu_{x,y}$ and variance $\sigma_{x,y}^2$ must be chosen, such that the values of $\mu_{x,y}$ and $\sigma_{x,y}$ have to be transformed

to the parameters $m_{x,y}$ and $\delta_{x,y}$:

$$m_{x,y} = \mu_{x,y}\, e^{-\delta_{x,y}^2/2} = \frac{\mu_{x,y}}{\sqrt{\left(\frac{\sigma_{x,y}^2}{\mu_{x,y}^2}+1\right)}} \qquad \text{and} \qquad \delta_{x,y} = \sqrt{\log\left(\frac{\sigma_{x,y}^2}{\mu_{x,y}^2}+1\right)}. \tag{7.12}$$

If X and Y are log-normally distributed the random variables $\bar{\mathrm{X}}$ = log (X) and $\bar{\mathrm{Y}}$ = log (Y) are normally distributed with means $\bar{\mu}_{x,y} = \log(m_{x,y})$ and deviations $\bar{\sigma}_{x,y} = \delta_{x,y}$, such that the following transformations hold

$$\log(x) = u_x\bar{\sigma}_x + \bar{\mu}_x = u_x\delta_x + \log(m_x), \tag{7.13}$$

$$\log(y) = u_y\bar{\sigma}_y + \bar{\mu}_y = u_y\delta_y + \log(m_y). \tag{7.14}$$

The transformation from X-space to U-space is nonlinear. The failure domain $\mathcal{F}$ is given by

$$\mathcal{F} = \left\{(X,Y)\,\middle|\,\frac{(1-D/L)\mathrm{X}}{\mathrm{Y}} \le 1\right\} = \{(X,Y) \mid \log(1-D/L) + \log\,(\mathrm{X}) - \log\,(\mathrm{Y}) \le 0\} \tag{7.15}$$

with the limit state function

$$g(\mathrm{X},\mathrm{Y}) = \log(1-D/L) + \log\,(\mathrm{X}) - \log\,(\mathrm{Y}). \tag{7.16}$$

With the transformation we derive

$$g(\mathrm{X},\mathrm{Y}) = u_x\delta_x - u_y\delta_y + \log(1-D/L) + \log(m_x) - \log(m_y), \tag{7.17}$$

such that β is given by

$$\beta = \frac{\log\left((1-D/L)m_x\right) - \log(m_y)}{\sqrt{\delta_x^2+\delta_y^2}}. \tag{7.18}$$

7.2 Shakedown analysis

In the shakedown analysis a convex load domain $\mathcal{L}$ is analyzed [19], [18]. The tension p cycles between zero and a maximal magnitude of $\hat{p}$. Only the amplitudes but not the uncertain full load history enters the solution

$$0 \le \quad p \le \quad \alpha\lambda\hat{p}, \qquad 0 \le \lambda \le 1. \tag{7.19}$$

In the first simple reliability analysis the maximal magnitude $\hat{p}$ is a random variable, but the minimum magnitude zero is held constant. The results of the FORM calculation are compared with an analytical approximation of the shakedown load in Table 7.3.

Table 7.1: Numerical and analytical results for $\sigma_{r,s} = 0.2\mu_{r,s}$ (Log-normal distributions)

Limit load analysis $\sigma_r = 0.2\mu_r$, $\sigma_s = 0.2\mu_s$			
μ_s/μ_r	P_f (num.)	P_f (anal.)	P_f (anal.-3%)
0.1	1.337E-13	5.655E-14	1.278E-13
0.2	6.786E-07	3.715E-07	6.459E-07
0.3	4.601E-03	2.308E-04	3.453E-04
0.4	9.443E-03	6.664E-03	8.987E-03
0.5	5.864E-02	4.665E-02	5.827E-02
0.6	1.816E-01	1.521E-01	1.792E-01
0.7	3.601E-01	3.167E-01	3.564E-01
0.8	5.458E-01	5.000E-01	5.433E-01
0.9	7.046E-01	6.629E-01	7.017E-01
1.0	8.213E-01	7.871E-01	8.173E-01
1.1	8.959E-01	8.722E-01	8.935E-01
1.2	9.414E-01	9.261E-01	9.402E-01
1.3	9.674E-01	9.584E-01	9.672E-01
1.4	9.828E-01	9.771E-01	9.824E-01
1.5	9.907E-01	9.875E-01	9.906E-01

Limit load analysis $\sigma_r = 0.1\mu_r$, $\sigma_s = 0.1\mu_s$			
μ_s/μ_r	P_f (num.)	P_f (anal.)	P_f (anal.-3%)
0.3	9.593E-12	1.790E-12	8.091E-12
0.4	1.409E-06	4.473E-07	1.316E-06
0.5	1.009E-03	4.315E-04	9.172E-04
0.6	3.485E-02	2.071E-02	3.412E-02
0.7	2.409E-01	1.719E-01	2.324E-01
0.8	5.936E-01	5.000E-01	5.854E-01
0.9	8.575E-01	7.981E-01	8.533E-01
1.0	9.648E-01	9.431E-01	9.638E-01
1.1	9.935E-01	9.880E-01	9.933E-01
1.2	9.990E-01	9.979E-01	9.989E-01
1.3	9.998E-01	9.997E-01	9.998E-01
1.4	9.999E-01	9.999E-01	9.999E-01
1.5	9.999E-01	9.999E-01	9.999E-01

Table 7.2: Numerical and analytical results for different $\sigma_{r,s}$ (Log-normal distributions)

Limit load analysis $\sigma_r = 0.2\mu_r$, $\sigma_s = 0.1\mu_s$			
μ_s/μ_r	P_f (num.)	P_f (anal.)	P_f (anal.-3%)
0.1	2.403E-20	1.800E-21	6.621E-21
0.2	8.296E-10	1.327E-10	3.197E-10
0.3	1.303E-05	3.574E-06	6.749E-06
0.4	1.807E-03	7.067E-04	1.127E-03
0.5	2.848E-02	1.442E-02	2.027E-02
0.6	1.407E-01	8.638E-02	1.101E-01
0.7	3.518E-01	2.520E-01	2.977E-01
0.8	5.860E-01	4.736E-01	5.284E-01
0.9	7.744E-01	6.790E-01	7.265E-01
1.0	8.884E-01	8.264E-01	8.594E-01
1.1	9.509E-01	9.146E-01	9.341E-01
1.2	9.796E-01	9.610E-01	9.712E-01
1.3	9.918E-01	9.831E-01	9.881E-01
1.4	9.969E-01	9.930E-01	9.952E-01
1.5	9.988E-01	9.971E-01	9.981E-01

Limit load analysis $\sigma_r = 0.1\mu_r$, $\sigma_s = 0.2\mu_s$			
μ_s/μ_r	P_f (num.)	P_f (anal.)	P_f (anal.-3%)
0.1	4.802E-15	6.295E-21	2.273E-20
0.2	3.566E-10	3.090E-10	7.315E-10
0.3	6.861E-06	6.586E-06	1.222E-05
0.4	1.168E-03	1.107E-03	1.736E-03
0.5	2.114E-02	2.000E-02	2.766E-02
0.6	1.115E-01	1.090E-01	1.369E-01
0.7	2.981E-01	2.959E-01	3.450E-01
0.8	5.338E-01	5.263E-01	5.805E-01
0.9	7.337E-01	7.248E-01	7.686E-01
1.0	8.635E-01	8.582E-01	8.867E-01
1.1	9.353E-01	9.334E-01	9.494E-01
1.2	9.715E-01	9.709E-01	9.789E-01
1.3	9.884E-01	9.879E-01	9.916E-01
1.4	9.954E-01	9.951E-01	9.968E-01
1.5	9.982E-01	9.981E-01	9.988E-01

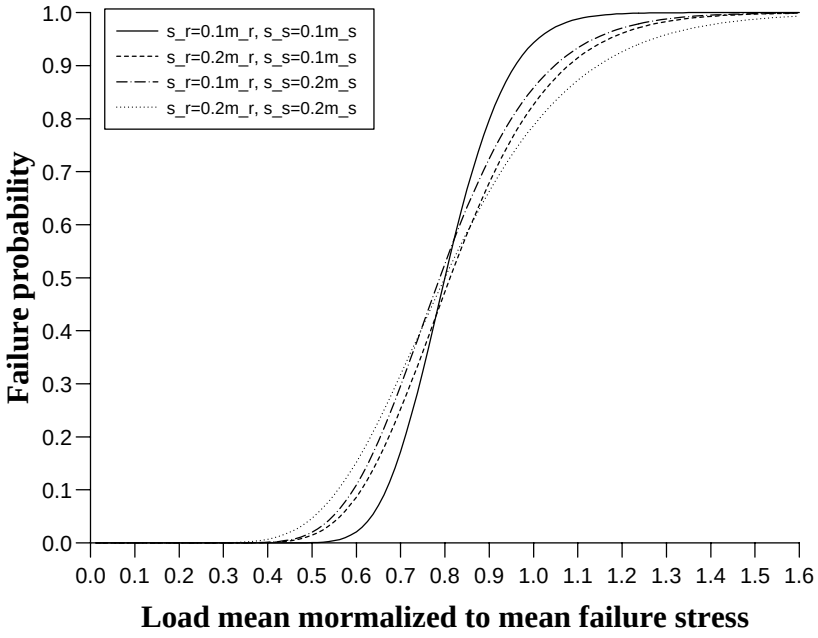

Figure 7.2: Distribution functions of log-normal variables with different σ, μ

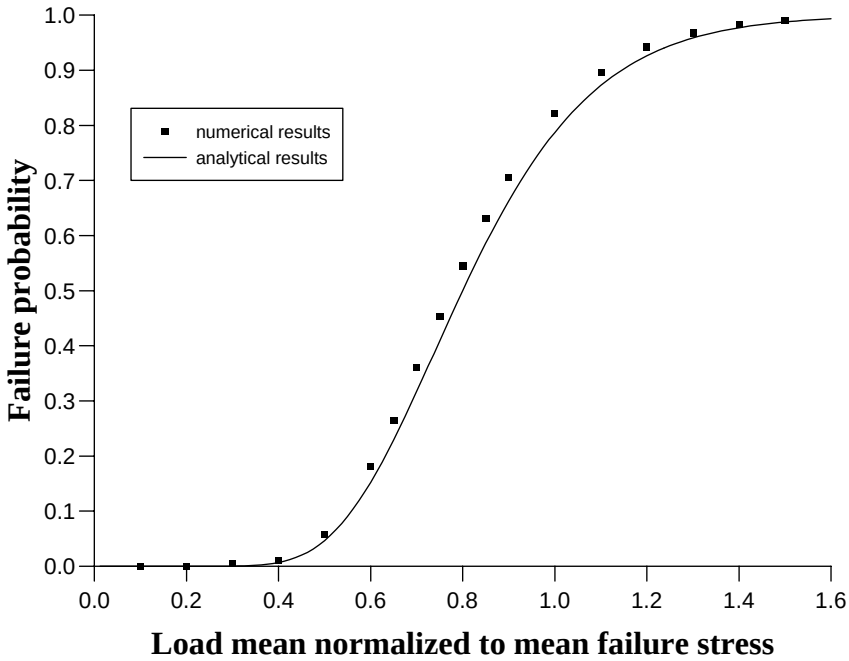

Figure 7.3: Comparison of numerical with analytical results for log-normally distributed variables with $\sigma_r = 0.2\mu_r$, $\sigma_s = 0.2\mu_s$

Table 7.3: Comparison of numerical and analytical results for $\sigma_r = 0.1\mu_r$, $\sigma_s = 0.1\mu_s$ (Normal distributions)

Limit load analysis				Shakedown analysis		
μ_s/μ_r	P_f (num.)	P_f (anal.)	P_f (anal.-2%)	μ_s/μ_r	P_f (num.)	P_f (anal.)
0.2	2.643E-13	1.718E-13	2.640E-13	0.2	1.943E-10	1.943E-10
0.3	3.843E-09	2.426E-09	4.063E-09	0.3	5.964E-06	5.963E-06
0.4	6.112E-06	3.872E-06	6.416E-06	0.4	3.877E-03	3.877E-03
0.5	1.093E-03	7.364E-04	1.128E-03	0.5	1.227E-01	1.229E-01
0.6	3.049E-02	2.275E-02	3.118E-02	0.55	3.108E-01	3.111E-01
0.7	2.067E-01	1.734E-01	2.112E-01	0.59	5.000E-01	5.000E-01
0.8	5.550E-01	5.000E-01	5.567E-01	0.6	5.485E-01	5.485E-01
0.9	8.305E-01	7.969E-01	8.344E-01	0.65	7.538E-01	7.538E-01
1.0	9.544E-01	9.408E-01	9.554E-01	0.7	8.858E-01	8.858E-01
1.1	9.900E-01	9.863E-01	9.903E-01	0.8	9.828E-01	9.828E-01
1.2	9.981E-01	9.972E-01	9.981E-01	0.9	9.980E-01	9.980E-01
1.3	9.996E-01	9.995E-01	9.996E-01	1.0	9.997E-01	9.997E-01
1.4	9.999E-01	9.999E-01	9.999E-01	1.1	9.999E-01	9.999E-01

Because of the local failure of the plate in the ligament points of the hole, the shakedown factor α_{SD} corresponding to the initial yield load p_y is equal to 2 (see [14], [50]). Therefore, from the yield load $p_y = 0.2949\sigma_y$ resulting from the deterministic FEM-computation follows that the FEM–approximation of the shakedown load is $0.5897\sigma_y$. The implemented shakedown analysis with the basis reduction technique gives very good results for the reliability analysis of the plate (listed in Table 7.3), because the deterministic shakedown factor 2 is reached in 3 to 5 steps nearly identically.

Additionally, the shakedown reliability analysis needs less computing time than the limit load reliability analysis. The results of the shakedown reliability analysis show a decrease in reliability in comparison with the limit load reliability results. For a load level of $\mu_s = 0.4\mu_r$ the reliability decrease by 3 orders of magnitude. This means that the reliability of the structure depends very strongly on the loading conditions, such that the assessment of the load carrying capacity has to be done very carefully.

7.3 Pipe-junction subjected to internal pressure

The pipe-junction [43] under internal pressure p is taken from the collection of PERMAS test examples. It is discretized with 125 solid 27-node hexahedron elements (HEXEC27). The FE-mesh and the essential dimensions of the pipe-junction are represented in Fig. 7.5. The internal pressure at first yield in the symmetry plane at the inner nozzle corner

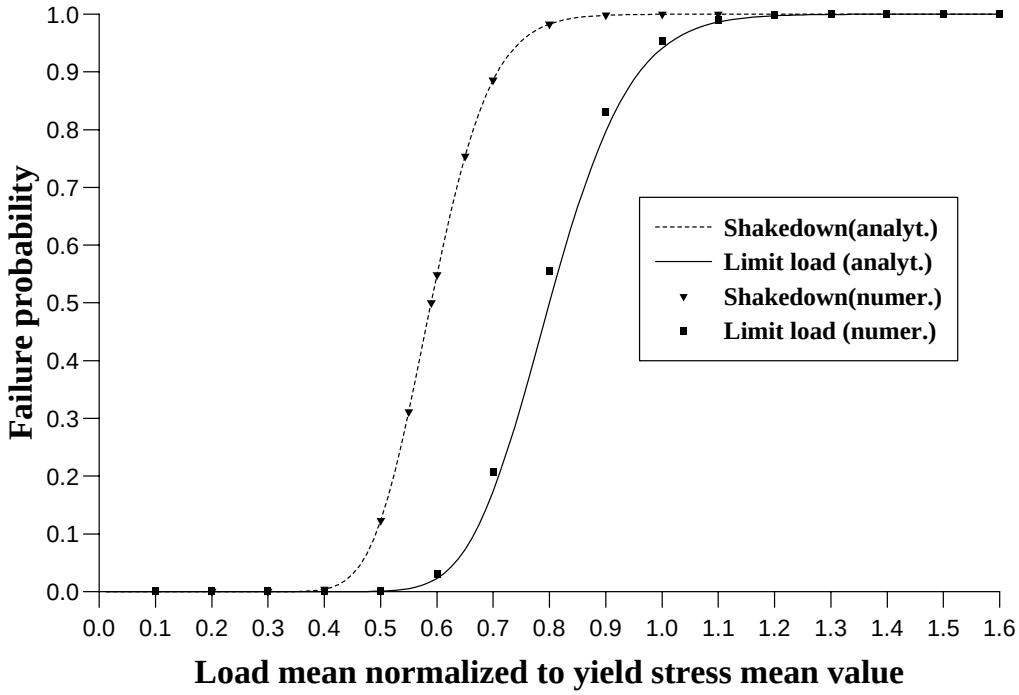

Figure 7.4: Comparison of numerical with analytical results for $\sigma_r = 0.1\mu_r$, $\sigma_s = 0.1\mu_s$

is calculated to $p_{elastic} \approx 0.0476\sigma_y$. For comparison [43] the limit pressure resulting from the German design rules AD-Merkblatt B9 is calculated to $p_{limit} = 2.85p_{elastic}$. With the safety factor 1.5 the design pressure is $p_{design} = 1.9p_{elastic} = 0.0904\sigma_y$.

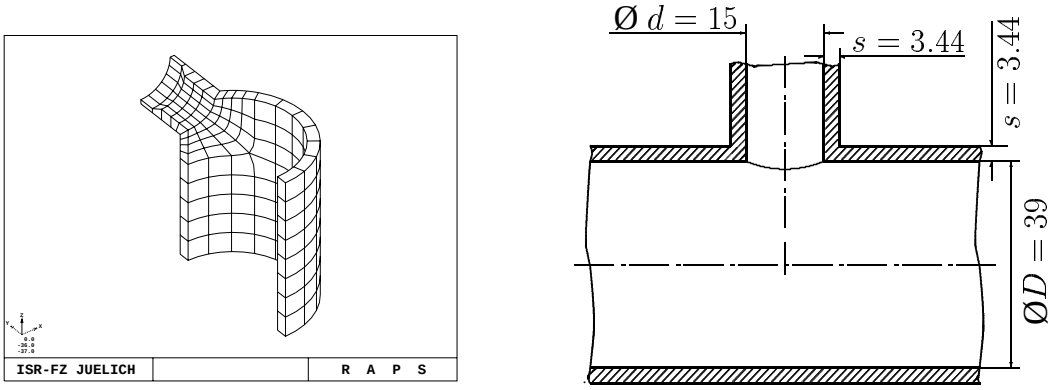

Figure 7.5: FE-mesh and dimension of a pipe-junction

Numerical limit analysis leads to a collapse pressure of $0.134\sigma_y$. In shakedown analysis the system is subjected to an internal pressure which may vary between zero and a maximum magnitude. The analysis becomes stationary after only 2 iteration steps with the shakedown pressure $p_{SD} = 0.0952\sigma_y$. The shakedown pressure is twice the elastic pressure in good

correspondence with an analytic solution [14], [21].

Thus the limit and the shakedown load are linearly dependent of the realization σ_y of the yield stress, which is the basis variable X. The second basis variable Y is the increasing inner pressure P. The limit load P_y of every realization x of X is

$$P_y(y) = 0.134x. \tag{7.20}$$

Obviously, P_y takes the role of a resistance R and P is the loading variable S. The limit state function is defined by

$$g(x, y) = P_y - P = 0.134x - y. \tag{7.21}$$

The normally distributed random variables X and Y with means μ_x, μ_x and standard deviations σ_x, σ_y, respectively, yield with $x = \sigma_x\, u_x + \mu_x$ and $y = \sigma_y\, u_y + \mu_y$ the transformation

$$G(x, y) = (0.134\mu_x - \mu_y) + 0.134\sigma_x u_x - \sigma_y u_y. \tag{7.22}$$

With the new random variable $\mathbf{U}$ with realizations $\boldsymbol{u} = (u_x, u_y)^T$, it holds:

$$G(\boldsymbol{u}) = \frac{(0.134\sigma_x, -\sigma_y)}{\sqrt{0.134^2\sigma_x^2 + \sigma_y^2}}\, \boldsymbol{u} + \frac{0.134\mu_x - \mu_y}{\sqrt{0.134^2\sigma_x^2 + \sigma_y^2}},$$

such that the reliability index β of the random variable $\mathbf{U}$ is

$$\beta = \frac{0.134\mu_x - \mu_y}{\sqrt{0.134^2\sigma_x^2 + \sigma_y^2}} = \frac{0.134\mu_x - \mu_y}{\sqrt{0.018\sigma_x^2 + \sigma_y^2}} \tag{7.24}$$

In Figure 7.6 the numerical results of the shakedown analysis are compared with the analytic values resulting from the exact solution. The results are normalized to the mean values μ_x and μ_y of the corresponding distributions. Both variables are normally distributed with standard deviations $\sigma_x = 0.1\mu_x$ and $\sigma_y = 0.1\mu_y$.

The results correspond well with the analytic results and demonstrate that reliability analysis can be performed for realistic model sizes at very low computing times compared to incremental analyses. Note, that the latter cannot be used in a quantitative comparison because incremental nonlinear analysis fails to give a sharp evidence for plastic failure.

7.4 Plate with mismatched weld and a crack

A plate with a strength mismatched weld and a centered crack under tension is investigated. One half of the plate with strength mis-matched weld has the length $L = 40mm$, the width

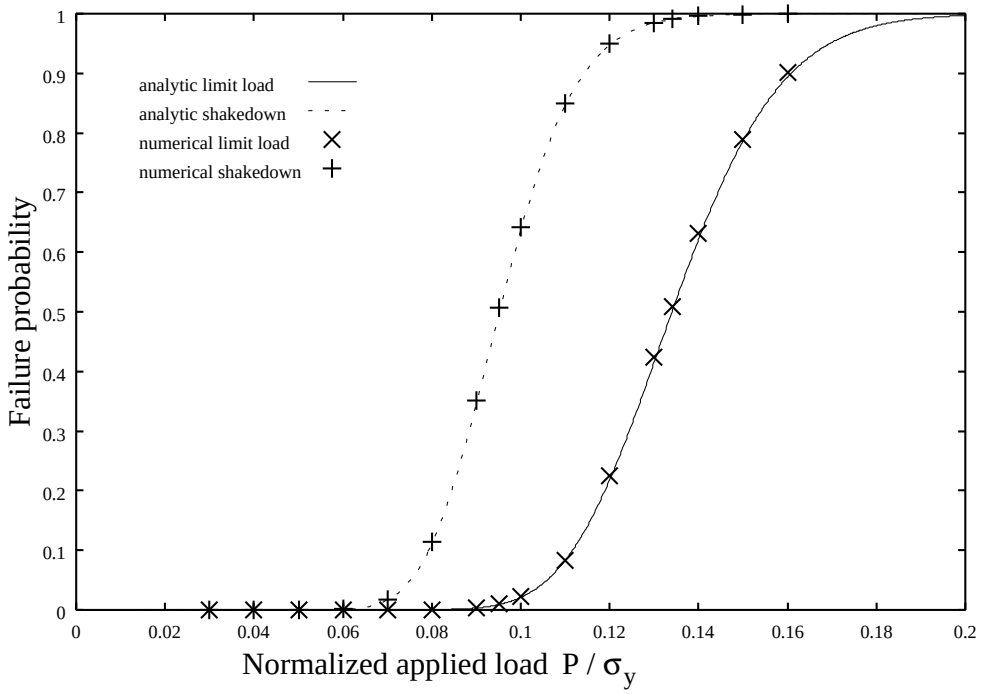

Figure 7.6: Comparison of numerical with analytical results for $\sigma_x = 0.1\mu_x$, $\sigma_y = 0.1\mu_y$

	Limit analysis		Shakedown analysis	
P/σ_y	P_f (numer.)	P_f (anal.)	P_f (numer.)	P_f (anal.)
0.03	1.8653E-14	1.8135E-14	3.4294E-11	3.2430E-11
0.04	1.1458E-11	8.9725E-12	4.7844E-08	4.5052E-08
0.05	2.2948E-09	2.1383E-09	1.3919E-05	1.3145E-05
0.06	2.5188E-07	2.3252E-07	9.2428E-04	8.7985E-04
0.07	1.2282E-05	1.1513E-05	1.7126E-02	1.6478E-02
0.08	2.7486E-04	2.6997E-04	1.1388E-01	1.1078E-01
0.09	3.3817E-03	3.2069E-03	3.5179E-01	3.4571E-01
0.0952	9.6429E-03	9.1261E-03	5.0654E-01	5.0000E-01
0.1	2.2190E-02	2.1001E-02	6.4212E-01	6.3594E-01
0.11	8.3328E-02	8.3125E-02	8.4933E-01	8.4550E-01
0.12	2.2510E-01	2.1819E-01	9.4897E-01	9.4728E-01
0.13	4.2411E-01	4.1517E-01	9.8519E-01	9.8460E-01
0.134	5.0892E-01	5.0000E-01	9.9113E-01	9.9087E-01
0.14	6.3079E-01	6.2157E-01	9.9610E-01	9.9592E-01
0.15	7.8917E-01	7.8683E-01	9.9902E-01	9.9898E-01
0.16	9.0053E-01	8.9358E-01	9.9976E-01	9.9974E-01

Table 7.4: Comparison of numerical and analytical results for $\sigma_x = 0.1\mu_x$, $\sigma_y = 0.1\mu_y$

$W = 4mm$, the crack length $2a = 4mm$, the thickness B and the weld height $h = 1.2mm$, so that $a/W = 0.5$, $h/W = 0.3$ holds (see Fig. 7.7). The different material data of the base material and the weld material are idealized by perfect plasticity with different yield stresses σ_y^B and σ_y^W, respectively. The main parameter here is the strength mismatch ratio $M = \sigma_y^W/\sigma_y^B$ of yield stress values of base and weld material. A reference value of the yield stress is $\sigma_y^B = 100$MPa. The example was proposed by the EU-project SINTAP [49] as a benchmark, see [46] for a detailed description.

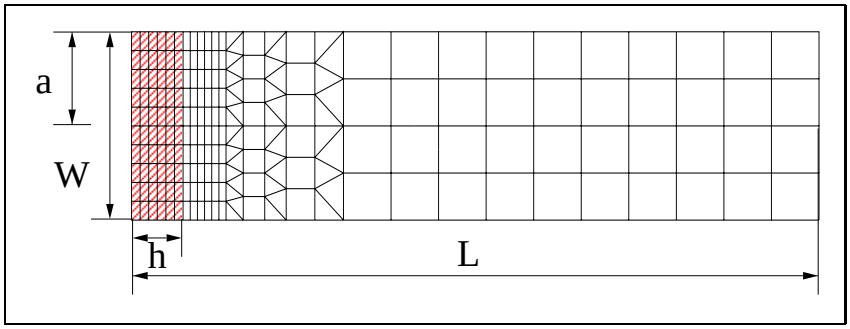

Figure 7.7: FE mesh of a plate with cracked mis-matched weld

There is a well known exact plane stress limit load F_{yb} for the situation $M = \sigma_y^W/\sigma_y^B = 1$. Estimation of the corresponding plane strain limit load yields the values

$$\underline{\text{plain stress}}: \; F_{yb} = 2B(W-a)\sigma_y^B \qquad \underline{\text{plain strain}}: \; F_{yb} = \frac{4}{\sqrt{3}} B(W-a)\sigma_y^B \quad (7.25)$$

Approximations for limit load F_{ym} are known [38] for plain stress and strain state. The plane strain results of the direct lower bound FEM approach (using triangular elements) are given in table 7.5.

Plate with a centered crack in a mismatched weld under tension					
$M = \sigma_y^W/\sigma_y^B$	0.50	0.75	1.00	1.25	1.50
analytic solution [38]	32.33	47.92	57.74	65.82	73.33
lower bound FEM	33.16	49.74	60.38	68.21	75.55

Table 7.5: Comparison of plane strain limit analysis results

There is an exact plane stress solution for the collapse load $2BWF_{yb}$ for the matched situation ($M = \sigma_y^W/\sigma_y^B = 1$):

$$F_{yb} = \left(1 - \frac{a}{W}\right)\sigma_y^B, \quad (7.26)$$

so that for the given data $F_{yb} = 50$MPa. For the mis-matched situation plane stress and plane strain approximations for limit load F_{ym} are given in [38]. With the abbreviation $\psi = (W-a)/h$ it holds for plane stress:

Undermatched $(M < 1)$**:**

$$\begin{aligned} \frac{F_{ym}}{F_{yb}} &= \begin{cases} M & \text{for } 0 \le \psi \le 1.43 \\ \min\left\{F^{(1)}, 1-(1-M)\dfrac{1.43}{\psi}\right\} & \text{for } \psi \ge 1.43 \end{cases} \\ F^{(1)} &= M\left[\frac{2}{\sqrt{3}} - \left(\frac{2-\sqrt{3}}{\sqrt{3}}\right)\frac{1.43}{\psi}\right] \end{aligned} \tag{7.27}$$

Overmatched $(M > 1)$**:**

$$\begin{aligned} \frac{F_{ym}}{F_{yb}} &= \min\left\{F^{(2)}, \frac{W}{W-a}\right\} \\ F^{(2)} &= \begin{cases} M & \text{for } \psi \le \psi_l \\ \dfrac{24(M-1)}{25}\dfrac{\psi_l}{\psi} + \dfrac{M+24}{25} & \text{for } \psi \ge \psi_l \end{cases} \end{aligned} \tag{7.28}$$

with $\psi_l = \left[1 + 0.43e^{-5(M-1)}\right] e^{-(M-1)/5}$. With the dimensions of the model (i.e. $\psi = (W-a)/h = 5/3$) and some numerical calculus the piecewise linear relations are obtained:

Undermatched $(M < 1)$**:**

$$\frac{F_{ym}}{F_{yb}} = \begin{cases} 1.022M & \text{if} \quad 0 \le M < 0.866 \\ 0.142 + 0.858M & \text{if} \quad 0.866 \le M < 1 \end{cases} \tag{7.29}$$

Overmatched $(M > 1)$**:**

$$\frac{F_{ym}}{F_{yb}} = \begin{cases} M(0.04 + 0.576\psi_l) + 0.04 - 0.576\psi_l & \text{if} \quad 1 < M < 3.628 \\ 2 & \text{if} \quad 3.628 \le M. \end{cases} \tag{7.30}$$

The resistance R and the load S are respectively given by the limit load F_y and by the increasing uniaxial tension F. We define the normally distributed basis variables X as variable for the tension F, M as variable of the mismatch ratio and the variable for the yield stress of the base material. Their realizations are denoted $x = F, m = \sigma_y^W/\sigma_y^B, r = \sigma_y^B$ such that the limit load $F_y(m, r)$ is a function of m and r.

The limit state function g is defined by

$$g(m, x, r) = F_y(m, r) - F = F_y(m, r) - x. \tag{7.31}$$

The numerical results are normalized to the mean values μ_x and μ_m/μ_r of the corresponding distributions. All variables are normally distributed with standard deviations $\sigma = 0.1\mu$.

In addition a comparison of the failure probabilities for one and two material variables in the matched case ($M = 1$) is performed (see Fig. 7.9). Case 1 (one variable) represents a homogeneous material distribution. Case 2 (two parameters) is represented by two independent identically distributed variables for the weld and the base material. The analytical limit load is given for this example by $F/F_y = 1$, such that the analytical failure probability is $P_f = 0.5$ for any two symmetric distributions, which fits very well with the numerical results.

For case 1 the limit load $F_y(r) = F_{yb}(r)$ of every realization r of the yield stress of the base material is

$$F_{yb}(r) = 0.5r. \tag{7.32}$$

The limit state function is defined by

$$g(x, r) = F_{yb}(r) - F = F_{yb}(r) - x. \tag{7.33}$$

The normally distributed random variables X and R with means μ_x, μ_r and standard deviations σ_x, σ_r, respectively, yield with $x = \sigma_x\, u_x + \mu_x$ and $r = \sigma_r\, u_r + \mu_r$ the transformation

$$G(u_x, u_r) = (0.5\mu_r - \mu_x) + 0.5\sigma_r u_r - \sigma_x u_x. \tag{7.34}$$

With the new random variable $\mathbf{U}$ with realizations $\boldsymbol{u} = (u_r, u_x)^T$, and $G_u(\boldsymbol{u}) = \boldsymbol{\alpha}^T \mathbf{u} + \beta$ with $|\boldsymbol{\alpha}| = 1$, it holds:

$$G(\boldsymbol{u}) = \frac{(0.5\sigma_r, -\sigma_x)}{\sqrt{0.25\sigma_r^2 + \sigma_x^2}}\, \boldsymbol{u} + \frac{0.5\mu_r - \mu_x}{\sqrt{0.25\sigma_r^2 + \sigma_x^2}},$$

such that the reliability index β of the random variable $\mathbf{U}$ is

$$\beta = \frac{0.5\mu_r - \mu_x}{\sqrt{0.25\sigma_r^2 + \sigma_x^2}} \;\text{ with }\; \mathrm{P}_f = \Phi(-\beta) \tag{7.36}$$

The design point is calculated with standard deviations $\sigma = 0.1\mu$ by:

$$\mathbf{u}^* = -\beta\boldsymbol{\alpha} = -\frac{0.5\mu_r - \mu_x}{\sqrt{0.25\sigma_r^2 + \sigma_x^2}}\, \frac{(0.5\sigma_r, -\sigma_x)}{\sqrt{0.25\sigma_r^2 + \sigma_x^2}} \tag{7.37}$$

$$= 10\, \frac{0.5\mu_r - \mu_x}{(0.5\mu_r)^2 + \mu_x^2}\, (\mu_x, -0.5\mu_s). \tag{7.38}$$

In the X-space the equivalent value is $\boldsymbol{x}^* = (r^*, x^*)$ with $x^* = \sigma_x\, u_x^* + \mu_x$ and $r^* = \sigma_r\, u_r^* + \mu_r$. For example the means μ_r= 100 MPa and $\mu_x = 25$MPa (i.e. $F/F_{yb} = 0.5$) yields

$$\beta = \frac{25}{\sqrt{31.25}},\;\; \boldsymbol{\alpha} = \frac{(5, -2.5)}{\sqrt{31.25}},\;\; \mathbf{u}^* = (-4, 2) \;\text{ and }\; \boldsymbol{x}^* = (60, 30)MPa. \tag{7.39}$$

F/F_{yb}	P_f Case 1	P_f Case 2	analytical
0.5	2.8817E-05	7.5016E-06	3.8721E-06
0.6	4.5558E-04	5.7639E-04	3.0182E-04
0.7	1.9351E-02	1.0271E-02	6.9915E-03
0.8	5.0113E-02	6.2066E-02	5.9174E-02
0.9	0.1678	0.2826	0.2286
1.0	0.5184	0.5076	0.5000
1.1	0.8058	0.8286	0.7494
1.2	0.9489	0.9726	0.8997
1.3	0.9872	0.9957	0.9663
1.4	0.9973	0.9993	0.9899
1.5	0.9995	0.9999	0.9972

Table 7.6: Comparison of case 1, case 2 and the analytical solution

Therefore, collapse will occur most probably with a realization around $F = 30$MPa and $\sigma_y^B = 60$MPa leading to a failure probability of $P_f = 3.8721 \cdot 10^{-6}$. The numerical results converge to these values depending on the starting values.

Typical structural components demonstrate that reliability analysis can be performed for realistic model sizes at very low computing times compared to incremental analyses. Note, that the latter cannot be used in a quantitative comparison because incremental nonlinear analysis fails to give a sharp evidence for plastic failure.

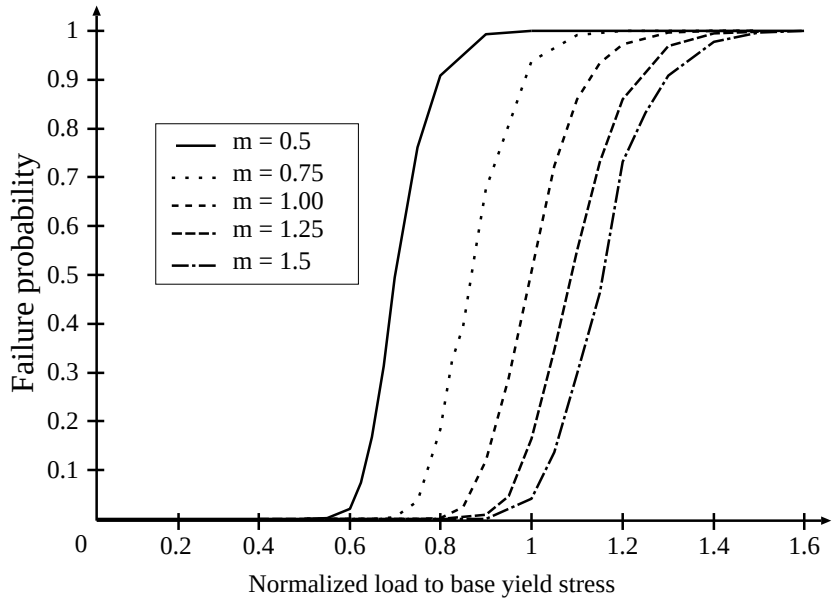

Figure 7.8: Reliability analysis for different values of $m = \sigma_y^W / \sigma_y^B$

The static theorem generates bounds for collapse loads which are safe. But they are 1 to 2 % below the analytical limit loads by the termination error of the iteration. This error

is amplified in the probabilistic analysis. The errors of the FORM calculations and of the numerical limit analyses are included in the results. The calculated failure probabilities correspond very well with the analytical probabilities.

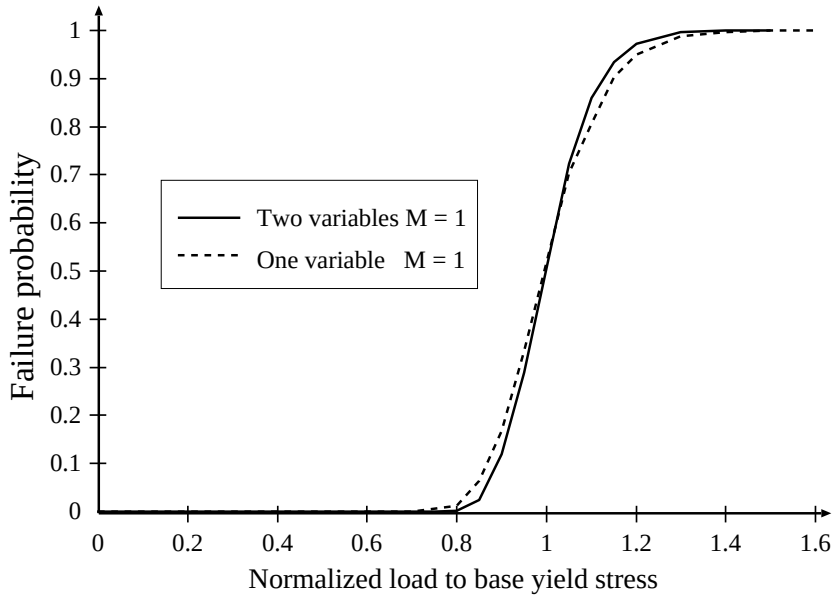

Figure 7.9: Comparison between results for one and two material variables for the same value of the means of σ_y^W and σ_y^B, $M = 1$

8 Conclusions

Traditional structural analysis treats the inherent uncertainties intuitively and subjectively. The current status of computational facilities, however, allows a more rational treatment of these uncertainties by stochastic procedures. Limit and shakedown theorems of plastic structural failure provide unique definitions of limit state functions. In combination with FEM and with FORM, failure probabilities of passive components are obtained with sufficient precision at very low computational efforts compared to incremental analyses with MCS. The advantage of the approach suggested here is the fact that the discretization procedures can be directly utilized. In this approach sensitivities need no extra FEM analysis. The remaining numerical error may be estimated or reduced by the additional use of upper bound theorems. It is most important for the analysis under uncertainty that limit and shakedown analyses are based on a minimum of information concerning the constitutive equations and the load history. In fact the shakedown problem is made time invariant. This reduces the costs of the collection of statistical data and the need to introduce stochastic models to compensate the lack of data. Further research is also addressed to more realistic material modeling including non-linear kinematic hardening and continuum damage.

Acknowledgement
The research has been funded by the European Commission as part of the Brite–EuRam III project LISA: FEM–Based Limit and Shakedown Analysis for Design and Integrity Assessment in European Industry (Project N°: BE 97–4547, Contract N°: BRPR–CT97–0595).

Bibliography

[1] G. Augusti, A. Baratta, F. Casciati: *Probabilistic Methods in Structural Engineering*. Chapman and Hall, London (1984).

[2] P. Bjerager: Plastic systems reliability by LP and FORM. *Computers & Structures* **31** (1989) 187–196.

[3] P. Bjerager: Methods for structural reliability computations in *Course on Reliability Problems: General Principles and Applications of Solids and Structures, International Center for Mechanical Sciences, Udine, Italy, 1990*. CISM lecture notes, Springer, Wien, 1991 (1991).

[4] C.G. Bucher, U. Bourgund: *Efficient Use of Response Surface Methods*. Universität Innsbruck, Inst. für Mechanik, Report No. 9 – 87, Innsbruck, 1987.

[5] J. Bree: Elastic–plastic behaviour of thin tubes subjected to internal pressure and intermittent high–heat fluxes with applications to fast–nuclear–reactor fuel elements. *Journal of Strain Analysis* **2** (1967) 226–238.

[6] J. Carmeliet, R. de Borst: Gradient damage and reliability: instability as limit state function. In F. Wittmann (ed.): *Fracture mechanics of concrete structures. Vol.2*. Aedificatio, Freiburg (1995).

[7] M. Evans, N. Hastings, B. Peacock: *Statistical Distributions*. John Wiley & Sons New York (1993).

[8] A. Fiacco: Sensitivity analysis for nonlinear programming using penalty methods. *Mathematical Programming* **10** (1976) 287–311.

[9] A. Fiacco: *Introduction to Sensitivity and Stability Analysis in Nonlinear Programming*. Academic Press New York (1983).

[10] G.-L. Fiorini, M. Staat, W. von Lensa, L. Burgazzi: *Reliability Methods for Passive Safety Function*. Proceedings of Post SMiRT 14, Seminar 18 Passive Safety Features in Nuclear Installations, Pisa, August 25-27, 1997.

[11] R. Fletcher: *Practical Methods of Optimization*. John Wiley & Sons New York (1987).

[12] F. A. Gaydon, A. W. McCrum: A theoretical investigation of the yield– point loading of a square plate with a central circular hole. *Journal of the Mechanics and Physics of Solids* **2** (1954) 156–169.

[13] S. Gollwitzer, T. Abdo, R. Rackwitz: *FORM (First Order Reliability Method) Manual* 1988. RCP GmbH, München.

[14] M. Heitzer: Traglast– und Einspielanalyse zur Bewertung der Sicherheit passiver Komponenten. *Berichte des Forschungszentrums Jülich* **3704** (1999).

[15] M. Heitzer: FEM-based Structural Optimization with Respect to Shakedown Constraints. In: P.M.A. Sloot et al. (eds.): *ICCS 2002*, Lecture Notes in Computer Sciences (Vol. 2329), Springer. Heidelberg (2002) 833-842.

[16] M. Heitzer: Structural Optimization with FEM-based Shakedown Analyses, *Journal of Global Optimization* **24** (2002) 371–384.

[17] M. Heitzer, G. Pop, M. Staat: Basis reduction for the shakedown problem for bounded kinematic hardening material, *Journal of Global Optimization* **17** (2000) 185–200.

[18] M. Heitzer, M. Staat: Structural reliability analysis of elasto-plastic structures. In G. Schuëller, P. Kafka (eds.): *Safety and Reliability*. A.A.Balkema, Rotterdam, Brookfield (1999) 513–518.

[19] M. Heitzer, M. Staat: Reliability Analysis of Elasto-Plastic Structures under Variable Loads. In G. Maier, D. Weichert (Eds.): *Inelastic Analysis of Structures under Variable Loads: Theory and Engineering Applications*. Kluwer, Dordrecht, 269-288 (2000).

[20] M. Heitzer, M. Staat: Direct static FEM approach to limit and shakedown analysis. In M. Papadrakakis, A. Samartin, E. Onate: *CD-ROM Proceedings of the Fourth International Colloquium on Computation of Shell & Spatial Structures*, Chania-Crete, Greece, 2000, paper 058, 14 pages.

[21] M. Heitzer, M. Staat: Direct FEM limit and shakedown analysis with uncertain data. In E. Onate, G. Bugeda, B. Suarez *CD-ROM Proceedings of the European Congress on Computational Methods in Applied Sciences and Engineering, ECCOMAS 2000*, Barcelona, Spain, paper 483, 13 pages.

[22] M. Heitzer, M. Staat: Limit and Shakedown Analysis with Uncertain Data, in K. Marti (Ed.): *Stochastic Optimization Techniques, Numerical Methods and Technical Applications*. Lecture Notes in Economics and Mathematical Systems **513**, Springer, Heidelberg, 253-267 (2002).

[23] M. Hohenbichler, S. Gollwitzer, W. Kruse, R. Rackwitz: New light on first– and second–order reliability methods. *Structural Safety* **4** (1987) 267–284.

[24] M. Kleiber, H. Antúnez, T.D. Hien, P. Kowalczyk: *Parameter Sensitivity in Nonlinear Mechanics: Theory and Finite Element Computations*. J. Wiley & Sons New York (1997).

[25] O. Klingmüller: *Anwendung der Traglastberechnung für die Beurteilung der Sicherheit von Konstruktionen*. Thesis Forschungsberichte aus dem Fachbereich Bauwesen **9**, Universität Essen Gesamthochschule (1979).

[26] C.-C. Li, A. D. Kiureghian: *An Optimal Discretization of Random Fields.* Report No. UCV/SEMM-92/04, Dept. of Civil Engineering, Univ. of California, Berkeley, CA 1992.

[27] J. M. Locci: Automatization of limit analysis calculations, application to structural reliability problems in M. Lemaire, J.-L. Favre, A. Mébarki (eds.): *Proceedings of the ICASP7 Conference, Paris, 10–13.7.1995, Vol. 2: Applications of Statistics and Probability.* A. A. Balkema Rotterdam, Brookfield (1995) 1095–1110.

[28] D. G. Luenberger: *Linear and Nonlinear Programming*. Addison–Wesley Publishing Company, Reading (1984).

[29] K. Marti: Optimal structural design under stochastic uncertainty by stochastic linear programming. In G. Schuëller, P. Kafka (eds.): *Safety and Reliability*. A.A. Balkema, Rotterdam, Brookfield (1999) 9–15.

[30] K. Marti: Plastic structural analysis under stochastic uncertainty. *CD-ROM Proccedings of European Conference on Computational Mechanics*, Cracow, Poland 26-29.6.2001, paper 617, 19 pages.

[31] E. Melan: Theorie statisch unbestimmter Systeme aus ideal–plastischem Baustoff. *Sitzungsbericht der Österreichischen Akademie der Wissenschaften der Mathematisch–Naturwissenschaftlichen Klasse IIa* **145** (1936) 195–218.

[32] R. Melchers: *Structural Reliability - Analysis and Prediction*. Ellis Horwood, Chichester (1987).

[33] D. Morgenstern: *Einführung in die Wahrscheinlichkeitsrechnung und mathematische Statistik.* Springer–Verlag, Berlin, Heidelberg, New York (1968).

[34] Y. Murotsu, S. Shao, S. Quek: Some studies on automatic generation of structural failure modes in A. der Kiureghian, P. Thoft-Christensen (eds.): *Reliability and optimization of structural systems '90, Proceedings of the 3rd IFIP WG 7.5 Conference*. Springer, Berlin (1991).

[35] B. A. Murtagh, M. A. Saunders:. *MINOS 5.1 - User's Guide.* Stanford University 1987. Technical Report SOL 83-20R.

[36] PERMAS: *User's Reference Manuals*. INTES Publications No. 202, 207, 208, 302, UM 404, UM 405 Stuttgart (1988).

[37] K. Schittkowski: The nonlinear programming method of Wilson, Han and Powell with augmented Lagrangian type line search function. *Numerische Mathematik* **38** (1981) 83–114.

[38] K.-H. Schwalbe, U. Zerbst, Y.-J. Kim, W. Brocks, A. Cornec, J. Heerens, H. Amstutz: *EFAM ETM97 – the ETM method for assessing the significance of crack-like defects in engineering structures, comprising the versions ETM97/1 and ETM97/2.* Report GKSS 98/E/6, GKSS-Forschungszentrum Geesthacht 1998.

[39] W. Shen: *Traglast– und Anpassungsanalyse von Konstruktionen aus elastisch, ideal plastischem Material*. Thesis Universität Stuttgart (1986).

[40] K. Sikorski, A. Borkowski: Ultimate load analysis by stochastic programming. In D. Lloyd Smith (ed.): *Mathematical Programming Methods in Structural Plasticity*. Springer, Wien (1990) 403–424.

[41] M. Staat: *Problems and Chances for Probabilistic Fracture Mechanics in the Analysis of Steel Pressure Boundary Reliability*. In: Technical feasibility and reliability of passive safety systems for nuclear power plants. Proceedings of an Advisory Group Meeting held in Jülich 21-24 November 1994, IAEA-TECDOC-920, Vienna, December 1996, pp.43–55.

[42] M. Staat: *Chance Constrained Limit Analysis*. Fachhochschule Aachen, Div. Jülich, Labor Biomechanik, Internal Report, Oct. 2001.

[43] M. Staat, M. Heitzer: Limit and shakedown analysis for plastic safety of complex structures. *Transactions of SMiRT* **14** (1997) B02/2.

[44] M. Staat, M. Heitzer: Limit and shakedown analysis using a general purpose finite element code. In *Proceedings of the NAFEMS World Congress '97*. NAFEM Stuttgart (1997) 522–533.

[45] M. Staat, M. Heitzer: LISA a European Project for FEM-based Limit and Shakedown Analysis. *Nuclear Engineering and Design* (2001) 151–166.

[46] M. Staat, M. Heitzer, A.M. Yan, V.D. Khoi, Nguyen Dang Hung, F. Voldoire, A. Lahousse: *Limit Analysis of Defects*, Berichte des Forschungszentrums Jülich, 3746, (2000).

[47] E. Stein, G. Zhang, R. Mahnken: Shakedown analysis for perfectly plastic and kinematic hardening materials in E. Stein (ed.): *Progress in computational analysis of inelastic structures.* Springer, Wien (1993) 175–244.

[48] F. Voldoire: Regularised limit analysis and applications to the load carrying capacities of mechanical components. In E. Onate, G. Bugeda, B. Suarez: *CD-ROM Proceedings of the European Congress on Computational Methods in Applied Sciences and Engineering, ECCOMAS 2000*, Barcelona, Spain (2000), paper 643, 20 pages.

[49] U. Zerbst, C. Wiesner, M. Koçak, L. Hodulak: SINTAP: Entwurf einer vereinheitlichten europäischen Fehlerbewertungsprozedur – eine Einführung, Report GKSS 99/E/65, GKSS-Forschungszentrum Geesthacht (1999).

[50] G. Zhang: *Einspielen und dessen numerische Behandlung von Flächentragwerken aus ideal plastischem bzw. kinematisch verfestigendem Material*. Thesis Universität Hannover (1991).

[51] J. J. Zimmermann: *Analysis of structural system reliability with stochastic programming*. Thesis John Hopkins University, Baltimore, Maryland (1991).

[52] J. Zowe: Nondifferentiable optimization in K. Schittkowski (ed.): *Computational Mathematical Programming*. Springer Berlin (1985) 323–356.

[53] A.M. Yan, H. Nguyen-Dang: Direct finite element kinematical approaches in limit and shakedown analysis of shells and elbows. In D. Weichert, G. Maier (eds): *Inelastic analysis of structures under variable loads*. Kluwer Academic Publishers, Dordrecht (2000), 233–254.

Appendix

A1 Distribution functions and densities

Normal distribution

$$\begin{aligned} f(x) &= \frac{1}{\sqrt{2\pi\sigma^2}}\, e^{-(x-\mu)^2/2\sigma^2}, \\ E(\mathrm{X}) &= \mu, \;\; \mathrm{Var}(\mathrm{X}) = \sigma^2 \end{aligned}$$

Standard normal distribution ($\sigma = 1, \mu = 0$)

$$\begin{aligned} f(x) &= \frac{1}{\sqrt{2\pi}}\, e^{-0.5x^2}, \\ E(\mathrm{X}) &= 0, \;\; \mathrm{Var}(\mathrm{X}) = 1 \end{aligned}$$

Exponential distribution

$$\begin{aligned} f(x) &= \begin{cases} \lambda\, e^{-\lambda x} & \text{for} \quad x \geq 0 \\ 0 & \text{for} \quad x < 0 \end{cases} \text{, with } \lambda > 0, \\ E(\mathrm{X}) &= 1/\lambda, \;\; \mathrm{Var}(\mathrm{X}) = 1/\lambda^2 \end{aligned}$$

Weibull distribution

$$\begin{aligned} f(x) &= \begin{cases} \dfrac{p\, x^p - 1}{b^p}\, e^{-(x/b)^p} & \text{for} \quad x \geq 0 \\ 0 & \text{for} \quad x < 0 \end{cases} \text{, with } b, p > 0, \\ E(\mathrm{X}) &= b\, \Gamma\left(\frac{p+1}{p}\right) \;\; , \mathrm{Var}(\mathrm{X}) = b^2 \left[\Gamma\left(\frac{p+2}{p}\right) - \Gamma^2\left(\frac{p+1}{p}\right)\right] \end{aligned}$$

Log-normal distribution

$$\begin{aligned} f(x) &= \frac{1}{\sqrt{2\pi x^2 \delta^2}}\, e^{-[\log(x/m)]^2/(2\delta^2)} \text{ , with } m > 0, x \geq 0. \\ E(\mathrm{X}) &= m\, e^{\delta^2/2}, \;\; \mathrm{Var}(\mathrm{X}) = m^2\, e^{\delta^2}(e^{\delta^2} - 1) \end{aligned}$$

In the following we summarize the characteristics of joint distributions.

1) Let X and Y be independent random variables with the densities $f_1(x)$ and $f_2(y)$, then the density $f_3(z)$ of the random variable $\mathrm{Z} = \mathrm{X} + \mathrm{Y}$ is given by convolution:

$$f_3(z) = \int_0^z f_1(z-u)\, f_2(u)\, du. \tag{A1}$$

If X and Y are independent and normally distributed, e.g. $\mathrm{X} \sim N(\mu_1, \sigma_1^2)$ and $\mathrm{Y} \sim N(\mu_2, \sigma_2^2)$, then the random variable $\mathrm{Z} = \mathrm{X} \pm \mathrm{Y}$ $N(\mu, \sigma^2)$ is normally distributed with $\mu = \mu_1 \pm \mu_2$ and $\sigma^2 = \sigma_1^2 + \sigma_2^2$. Thus it holds $E(\mathrm{Z}) = \mu_1 \pm \mu_2$ and $\mathrm{Var}(\mathrm{Z}) = \sigma_1^2 + \sigma_2^2$.

2) Let X and Y be independent random variables with $\mathrm{Y} > 0$ and the densities $f_1(x)$ and $f_2(y)$, then the density $f_3(z)$ of the random variable $\mathrm{Z} = \mathrm{X}/\mathrm{Y}$ is given by

$$f_3(z) = \int_0^\infty y \; f_2(y) \; f_1(yz) \; dz. \tag{A2}$$

The expectation $\mathrm{E}(\mathrm{Z})$ of the random variable Z is given for independent variables X and Y by (see [33]):

$$\mathrm{E}(\mathrm{Z}) = \int_{-\infty}^{\infty} \int_{-\infty}^{\infty} \frac{x}{y} \; f_1(x) \; f_2(y) \; dx \; dy. \tag{A3}$$

3) For log-normally distributed random variables X and Y with expectations μ_x and μ_y and variances σ_x^2 and σ_y^2 the random variables $\log(\mathrm{X})$ and $\log(\mathrm{Y})$ are normal distributed. The corresponding expectations $\hat{\mu}_x$ and $\hat{\mu}_y$ and variances $\hat{\sigma}_x^2$ and $\hat{\sigma}_y^2$ are

$$\begin{aligned} \hat{\mu}_x &= \log\mu_x - 0.5\sigma_x^2 \qquad & \hat{\mu}_y &= \log\mu_y - 0.5\sigma_y^2 \\ \hat{\sigma}_x^2 &= \sigma_x^2 \qquad & \hat{\sigma}_y^2 &= \sigma_y^2. \end{aligned} \tag{A4}$$

The random variable $\log(\mathrm{Z})$ with

$$\log(\mathrm{Z}) = \log(\mathrm{X}) - \log(\mathrm{Y}) = \log(\mathrm{X}/\mathrm{Y}) \tag{A5}$$

as difference of the normally distributed variables logX and logY is normally distributed with the expectation $\hat{\mu}_z$ and the variance $\hat{\sigma}_z^2$:

$$\hat{\mu}_z = \hat{\mu}_x - \hat{\mu}_y = \log\frac{\mu_x}{\mu_y} - 0.5(\sigma_x^2 + \sigma_y^2) \tag{A6}$$

$$\hat{\sigma}_z^2 = \hat{\sigma}_x^2 + \hat{\sigma}_y^2 = \sigma_x^2 + \sigma_y^2. \tag{A7}$$

Therefore, $\mathrm{Z} = \mathrm{X}/\mathrm{Y}$ is a log-normally distributed random variable with the expectation μ_z and the variance σ_z^2

$$\mu_z = \frac{\mu_x}{\mu_y} \tag{A8}$$

$$\sigma_z^2 = \sigma_x^2 + \sigma_y^2 \tag{A9}$$

A2 Reliability analyses for the plate with a hole

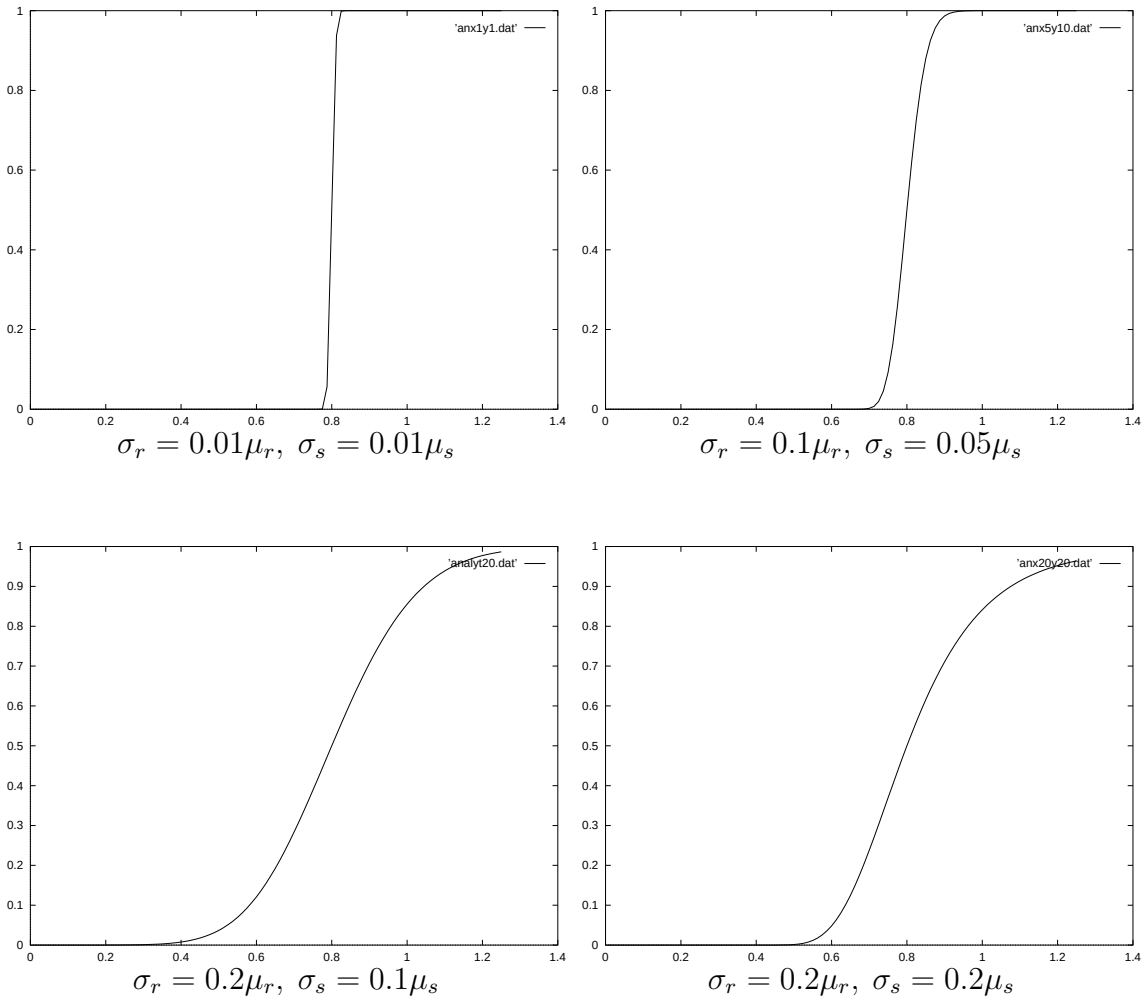

$\sigma_r = 0.01\mu_r,\ \sigma_s = 0.01\mu_s$ $\sigma_r = 0.1\mu_r,\ \sigma_s = 0.05\mu_s$

$\sigma_r = 0.2\mu_r,\ \sigma_s = 0.1\mu_s$ $\sigma_r = 0.2\mu_r,\ \sigma_s = 0.2\mu_s$

Figure A1: Distribution functions for fixed mean value and different standard deviations for normally distributed variables

μ_r/μ_s	P_f (numerical)	P_f (analytical)	abs. error	rel. error
0.1	6.455E-06	6.313E-06	1.867E-07	1.910E-07
0.2	1.085E-04	9.919E-05	9.299E-06	1.017E-05
0.3	1.205E-03	1.065E-03	1.403E-04	1.587E-04
0.4	8.763E-03	7.646E-03	1.117E-03	1.280E-03
0.5	4.163E-02	3.675E-02	4.873E-03	5.519E-03
0.6	1.361E-01	1.209E-01	1.519E-02	1.709E-02
0.7	3.103E-01	2.835E-01	2.683E-02	2.936E-02
0.8	5.319E-01	5.000E-01	3.189E-02	3.392E-02
0.9	7.397E-01	7.070E-01	3.271E-02	3.422E-02
1.0	8.765E-01	8.554E-01	2.105E-02	2.156E-02
1.1	9.499E-01	9.388E-01	1.105E-02	1.118E-02
1.2	9.821E-01	9.772E-01	4.873E-03	4.897E-03
1.3	9.943E-01	9.925E-01	1.961E-03	1.964E-03
1.4	9.983E-01	9.976E-01	6.443E-04	6.447E-04
1.5	9.995E-01	9.993E-01	2.090E-04	2.090E-04
1.6	9.999E-01	9.998E-01	6.920E-05	6.920E-05

Table A1: $\sigma_r = 0.2\mu_r$, $\sigma_s = 0.1\mu_s$

μ_r/μ_s	P_f (numerical)	P_f (analytical)	abs. error	rel. error
0.1	7.271E-06	7.085E-06	2.152E-07	2.208E-07
0.2	1.514E-04	1.374E-04	1.404E-05	1.547E-05
0.3	1.948E-03	1.717E-03	2.311E-04	2.621E-04
0.4	1.437E-02	1.267E-02	1.698E-03	1.925E-03
0.5	6.271E-02	5.590E-02	6.788E-03	7.614E-03
0.6	1.742E-01	1.587E-01	1.557E-02	1.709E-02
0.7	3.427E-01	3.190E-01	2.366E-02	2.541E-02
0.8	5.256E-01	5.000E-01	2.558E-02	2.688E-02
0.9	6.843E-01	6.610E-01	2.332E-02	2.414E-02
1.0	8.021E-01	7.826E-01	1.957E-02	2.005E-02
1.1	8.775E-01	8.649E-01	1.254E-02	1.272E-02
1.2	9.258E-01	9.172E-01	8.537E-03	8.617E-03
1.3	9.550E-01	9.493E-01	5.700E-03	5.734E-03
1.4	9.729E-01	9.686E-01	4.259E-03	4.278E-03
1.5	9.823E-01	9.802E-01	2.079E-03	2.083E-03
1.6	9.882E-01	9.873E-01	8.666E-04	8.673E-04

Table A2: $\sigma_r = 0.2\mu_r$, $\sigma_s = 0.2\mu_s$

Part VIII

Limit analysis of frames - Application to structural reliability

Philippe Rucho, Sebastién Sonnenberg

Direction Marine - Département Technologie Avancée
Bureau Veritas S.A., 17 BIS Place des Reflets, F-92077 Courbevoie, France

E-mail: philippe.rucho@bureauveritas.com

1 Introduction

The safety level of a structure is a function of the mechanical and 'strength' properties of the material and of loads depending on environmental parameters. All these data are never known exactly, inducing the random character of all the basis elements of the problem. The whole of these random variables means that the structure has never a non-zero probability of failure.

The present report describes a methodology, based on the limit analysis method, to appraise the probability of plastic failure of a frame structure subject to extreme environmental conditions.

Limit analysis yield the limit loads of the most general structures, without further approximations than these involved in the finite element modelization. Otherwise it enables to directly obtain a simple series representation of the structure, with a simply linear limit state function associated with each component of the series system. In this way it permits to reduce the whole structure to a set of hyperplanes in the space of the random force and resistance variables.

2 General formulation

We consider a frame structure loaded by actions represented by a vector $\mathbf{F}$. According to limit analysis theory, collapse is identified with the development of plastic hinge in such a number and location to allow a movement of the whole or of a part of the structure without requiring deformation of the zones with stresses below the yield limit.

The load conditions at the limit of collapse are determined on the basis of the two theorems:

Static theorem proves that collapse does not occur if there exist a stress field in equilibrium with the applied loads and not violating the strength inequality at any point of the structure.

Kinematic theorem proves that collapse occurs if there exist a displacement field, compatible with the collapse mechanism, such that the work done by the applied loads $\mathbf{F}$ is larger than the corresponding internal plastic work.

Static and kinematic theorems can be expressed as the primal and dual formulation of an optimization problem. They give respectively a lower and an upper bound of the load conditions $\mathbf{F}_R$ that correspond to the threshold of collapse.

Our approach is based on the static formulation of limit analysis, which gives a lower bound of $\mathbf{F}_R$ and consequently goes in the sense of safety.

Let $\mathbf{F}$ be the applied load vector and $\mathbf{S}$ the vector of generalized internal forces in the relevant sections of the structure. The condition of equilibrium between $\mathbf{S}$ and $\mathbf{F}$ is:

$$\mathbf{AS} = \mathbf{F} \tag{1}$$

where $\mathbf{A}$ is the rectangular force matrix.

The condition of admissibility of the internal force vector corresponding to each critical section can be expressed by simple inequalities:

$$\Phi^{(k)}(\mathbf{S},\mathbf{R}) - \mathbf{e}^{(k)} \leq \mathbf{0} \quad k = 1,\ldots,NS \tag{2}$$

With:

NS the number of critical sections.
$\Phi^{(k)}(\mathbf{S},\mathbf{R}) = \mathbf{C}^{(k)}(\mathbf{R})\mathbf{S}^{(k)}$
$\mathbf{C}^{(k)}(\mathbf{R})$ a matrix depending on the strength vector $\mathbf{R}$ and the k-th critical section
$\mathbf{S}^{(k)}$ the vector of internal forces corresponding to the k-th critical section
$\mathbf{e}^{(k)} = (1,\ldots,1)^T$

These inequalities correspond to a piecewise linear *yield condition* in each critical section, which can be written in the generalized form:

$$\Phi(\mathbf{S},\mathbf{R}) - \mathbf{e} \leq \mathbf{0}. \tag{3}$$

Example:

If we consider the axial force $N^{(k)}$ and bending moment $M^{(k)}$ we could specify the following conditions as first approximation:

$$\frac{\left|N^{(k)}\right|}{N_P} - 1 < 0 \text{ and } \frac{\left|M^{(k)}\right|}{M_P} - 1 < 0$$

with $\mathbf{R} = (N_P, M_P)$ the generalized internal yield forces.

These relations can be expressed in a matrix formulation:

$$\begin{bmatrix} 1/N_P & 0 \\ -1/N_P & 0 \\ 0 & 1/M_P \\ 0 & -1/N_P \end{bmatrix} \begin{pmatrix} N^{(k)} \\ M^{(k)} \end{pmatrix} - \begin{pmatrix} 1 \\ 1 \\ 1 \\ 1 \end{pmatrix} \leq \begin{pmatrix} 0 \\ 0 \\ 0 \\ 0 \end{pmatrix}.$$

But if we consider that the axial force reduces the yield moment we use relations combining these two internal forces, like the following one:

$$\begin{aligned} \frac{\left|N^{(k)}\right|}{N_P} + \frac{\left|M^{(k)}\right|}{1.18M_P} - 1 &\leq 0 \\ \frac{\left|M^{(k)}\right|}{M_P} - 1 &\leq 0 \end{aligned}$$

we have:

$$\begin{bmatrix} 1/N_P & 1/(1.18M_P) \\ -1/N_P & 1/(1.18M_P) \\ -1/N_P & -1/(1.18M_P) \\ 1/N_P & -1/(1.18M_P) \\ 0 & 1/M_P \\ 0 & -1/M_P \end{bmatrix} \begin{pmatrix} N^{(k)} \\ M^{(k)} \end{pmatrix} - \begin{pmatrix} 1 \\ 1 \\ 1 \\ 1 \\ 1 \\ 1 \end{pmatrix} \leq \begin{pmatrix} 0 \\ 0 \\ 0 \\ 0 \\ 0 \\ 0 \end{pmatrix}.$$

Considering a factor α applied to the load $\mathbf{F}$, and according to (1) and (3), the static approach can be formulated as a maximum problem:

$$\max\{\alpha | \mathbf{AS} = \alpha\mathbf{F}, \Phi(\mathbf{S}, \mathbf{R}) - \mathbf{e} \leq \mathbf{0}\}. \tag{4}$$

This is the expression of a linear programming problem that can be solved by the simplex method, giving the maximum load factor α_R and the internal force distribution $\mathbf{S}$ producing the collapse mechanism.

Notice that in the past decade primal-dual algorithms have emerged [8], which, in addition to a good complexity, have the advantage of solving the primal and dual forms of the problem, i.e. the static (internal force distribution) and the kinematic (displacement and plastic strains) form of the limit analysis problem.

3 Application to structural reliability

We will consider now NP nodal loads $y_n\mathbf{F}^{(n)}$ with $\mathbf{F}^{(n)}$ a vector associated with the node n and y_n the realization of a random variable Y_n.

Let

$$\mathbf{F}(y_1, \ldots, y_{NP}) = \begin{Bmatrix} y_1\mathbf{F}^{(1)} \\ \cdots \\ y_{NP}\mathbf{F}^{(NP)} \end{Bmatrix}$$

be the generalized load vector, and

$$\mathbf{R} = \begin{Bmatrix} \mathbf{R}^{(1)} \\ \cdots \\ \mathbf{R}^{(NS)} \end{Bmatrix}$$

be the generalized yield strength vector. Elements of $\mathbf{R}$ will be also considered as random variables.

According to the realization of the random variables $(\mathbf{R}, \mathbf{Y})$ the frame structure can be subject to an important number of collapse mechanisms. We will associate a limit state function with each mechanism:

3.1 Limit state function

Starting from a realization of the random variables $(\mathbf{R}, \mathbf{Y})$, the solution of the corresponding optimization problem (4) gives a realization of the internal force distribution $\mathbf{S}$ corresponding to a collapse mechanism.

Notice, that when the index k corresponds to a plastic hinge we have from the yield condition (2):

$$\mathbf{C}_{i_k\bullet}^T \mathbf{S}^{(k)} - 1 = \sum_{j=1}^{m} C_{i_k,j} S_j^{(k)} - 1 = 0 \text{ for a row } i_k \text{ of the matrix } \mathbf{C}^{(k)1} \tag{1}$$

$$\mathbf{C}_{i\bullet}^T \mathbf{S}^{(k)} - 1 < 0 \text{ for the others.} \tag{2}$$

Consequently it is possible, from the result of the static formulation, to retrieve the location of the plastic hinges constituting the collapse mechanism.

Once the mechanism is identified we can write the equality between the virtual works corresponding to the collapse mechanism:

$$\begin{aligned} \delta W &= \mathbf{S}^T \boldsymbol{\varepsilon} - \mathbf{F}^T \boldsymbol{\delta} = \sum_{k=1}^{NS} \mathbf{S}^{(k)T} \boldsymbol{\varepsilon}^{(k)} - \sum_{n=1}^{NP} y_n \mathbf{F}^{(n)T} \boldsymbol{\delta}^{(n)} \\ &= \sum_{k=1}^{NS} \sum_{j=1}^{m} S_j^{(k)} \varepsilon_j^{(k)} - \sum_{n=1}^{NP} \sum_{i=1}^{p} y_n F_i^{(n)} \delta_i^{(n)} = 0 \end{aligned} \tag{3}$$

With:

$\boldsymbol{\delta}^{(n)}$	vector of general virtual displacement of node n, compatible with mechanism
$\boldsymbol{\varepsilon}^{(k)}$	vector of virtual strains in critical section k, compatible with mechanism
$y_n \mathbf{F}^{(n)}$	forces at node n
$\mathbf{S}^{(k)}$	internal forces at section k.

As the collapse corresponds to a rigid body mechanism the virtual strain elements $\varepsilon_j^{(k)}$ are non-zero uniquely for the indices j fulfilling (1). Consequently we have:

$$\delta W = \sum_{k=k_1,\ldots,k_N} \sum_{j \in \mathcal{J}(k)} S_j^{(k)} \varepsilon_j^{(k)} - \mathbf{F}^T \boldsymbol{\delta} = 0 \tag{4}$$

where $\{k_1, \ldots, k_N\}$ are the indices of the plastic hinges and $\mathcal{J}(k)$ the family of indices j appearing in (1) for the hinge k. Notice that $\{k_1, \ldots, k_N\}$ defines the considered collapse mechanism (m).

[1] To simplify notations $C_{i_k,j}$ will be used instead of $C_{i_k,j}^{(k)}(\mathbf{R})$

3.1.1 Simple case

Firstly we will consider the following elementary conditions of admissibility:

$$\frac{S_j^{(k)}}{R_j^{(k)}} - 1 \leq 0 \quad j = 1, \ldots, m \tag{5}$$

which consist in taking:

$$\mathbf{C}^{(k)} = diag\left(\frac{1}{R_1^{(k)}}, \ldots, \frac{1}{R_m^{(k)}}\right).$$

Moreover, $\forall k \in \{k_1, \ldots, k_N\}$ we have $\mathcal{J}(k) = \{j_k\}$ and $S_{j_k}^{(k)} = R_{j_k}^{(k)}$ Consequently:

$$\delta W = \sum_{k=k_1,\ldots,k_N} R_{j_k}^{(k)} \varepsilon_{j_k}^{(k)} - \mathbf{F}^T \boldsymbol{\delta} = 0. \tag{6}$$

We can write:

$$\langle R_{j_1}, \ldots, R_{j_N} \rangle \left\{ \begin{array}{c} \varepsilon_{j_1} \\ \cdots \\ \varepsilon_{j_N} \end{array} \right\} = \mathbf{R}^T \mathbf{D}^{(m)} \boldsymbol{\varepsilon} \tag{7}$$

with $\mathbf{D}^{(m)}$ a square and diagonal matrix such that: $D_{j,j}^{(m)} = 1 \Leftrightarrow j \in \{j_{k1}, \ldots, j_{kN}\}$

In addition we have the condition of compatibility between the vectors of the generalized virtual strains and virtual displacements:

$$\boldsymbol{\varepsilon} = \mathbf{A}^T \boldsymbol{\delta}. \tag{8}$$

Finally from (7) and (8) we have:

$$\delta W = \left(\mathbf{A}\mathbf{D}^{(m)}\mathbf{R}\right)^T \boldsymbol{\delta} - \mathbf{F}^T \boldsymbol{\delta} = \left(\mathbf{A}\mathbf{D}^{(m)}\mathbf{R} - \mathbf{F}\right)^T \boldsymbol{\delta} = 0. \tag{9}$$

Notice, that for every virtual displacement $\boldsymbol{\delta}$ compatible with the collapse mechanism (m), we have: $\boldsymbol{\delta} = \mu \boldsymbol{\delta}^{(m)}$ where μ is a scalar and $\boldsymbol{\delta}^{(m)}$ is a basis vector corresponding to (m).

The j-th column of the matrix $\mathbf{A}\mathbf{D}^{(m)}$ is equal to the j-th column of $\mathbf{A}$ if $j \in \{j_{k_1}, \ldots, j_{k_N}\}$, it is equal to zero otherwise.

Consider now the following function:

$$g_{(m)}(\mathbf{R}, \mathbf{F}) = \left(\mathbf{A}\mathbf{D}^{(m)}\mathbf{R} - \mathbf{F}\right)^T \boldsymbol{\delta}^{(m)} \tag{10}$$

with $\boldsymbol{\delta}^{(m)}$ the displacement vector associated with the mechanism (m). As $\boldsymbol{\varepsilon} = \mathbf{A}^T \boldsymbol{\delta}^{(m)}$ we have:

$$g_{(m)}(\mathbf{R}, \mathbf{F}) < 0 \Leftrightarrow \mathbf{R}^T \mathbf{D}^{(m)} \mathbf{A}^T \boldsymbol{\delta}^{(m)} - \mathbf{F}^T \boldsymbol{\delta}^{(m)} < 0 \Leftrightarrow \mathbf{R}^T \mathbf{D}^{(m)} \boldsymbol{\varepsilon} - \mathbf{F}^T \boldsymbol{\delta}^{(m)} < 0. \tag{11}$$

Thus if $g_{(m)}(\mathbf{R}, \mathbf{F}) < 0$ there exist a displacement field $\boldsymbol{\delta}^{(m)}$, compatible with the collapse mechanism (m), such that the work done by the applied loads $\mathbf{F}$ is larger than the corresponding internal plastic work. We deduce from the kinematic theorem that the collapse occurs in this case. Reciprocally,if $g_{(m)}(\mathbf{R}, \mathbf{F}) > 0$ the kinematic theorem proves that the structure is safe.

We conclude that $g_{(m)}(\mathbf{R}, \mathbf{F})$ defines a limit state function associated with the collapse mechanism resulting from the solution of (4).

3.1.2 Generalization

The previous result can be extended to the general case of any linear yield condition. Let us recall the Hill principle (1950) specifying that the variation vector of plastic strains is oriented along the external normal to the boundary of the elastic domain.

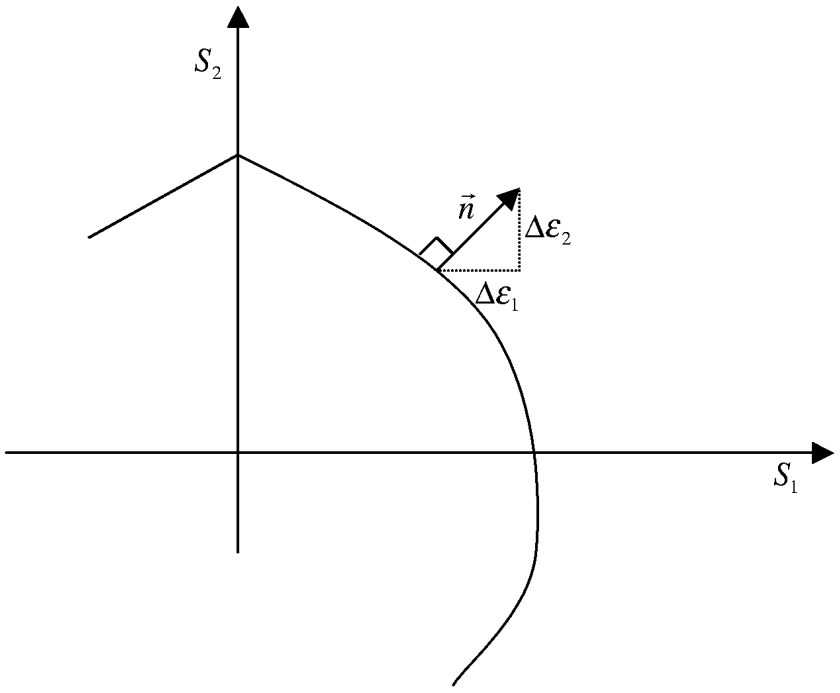

Figure 1: Normality rule

As the boundary of the elastic domain is defined by $\partial\mathcal{E} = \{S | \mathbf{C}_{i_k \bullet}^T \mathbf{S}^{(k)} - 1 = 0, k \in \{k_1, \ldots, k_N\}\}$, we have:

$$\frac{\varepsilon_j^{(k)}}{\varepsilon_{j_k^*}^{(k)}} = \frac{C_{i_k,j}}{C_{i_k,j_k^*}} \forall j \neq j_k^* \tag{12}$$

where j_k^* is some index of the family $\mathcal{J}(k)$.

Consequently:

$$\sum_{k_1,\ldots,k_N} \mathbf{S}^{(k)T}\boldsymbol{\varepsilon}^{(k)} = \sum_{k_1,\ldots,k_N} \left[S^{(k)}_{j^*_k}\varepsilon^{(k)}_{j^*_k} + \sum_{j\neq j^*_k} S^{(k)}_j \frac{C_{i_k,j}}{C_{i_k,j^*_k}}\varepsilon^{(k)}_{j^*_k} \right] \tag{13}$$

$$= \sum_{k_1,\ldots,k_N} \left[S^{(k)}_{j^*_k}\varepsilon^{(k)}_{j^*_k} + \frac{\varepsilon^{(k)}_{j^*}}{C_{i_k,j^*_k}} \sum_{j\neq j^*_k} C_{i_k,j} S^{(k)}_j \right]$$

And from the definition of $\partial\mathcal{E}$ we deduce:

$$\sum_{j\neq j^*_k} C_{i_k,j} S^{(k)}_j = 1 - C_{i_k,j^*_k} S^{(k)}_{j^*_k}. \tag{14}$$

Thus:

$$\sum_{k_1,\ldots,k_N} \mathbf{S}^{(k)T}\boldsymbol{\varepsilon}^{(k)} = \sum_{k_1,\ldots,k_N} \frac{\boldsymbol{\varepsilon}^{(k)}_{j^*_k}}{C_{i_k,j^*_k}}. \tag{15}$$

Finally we obtain:

$$\delta W = \sum_{k=k_1,\ldots,k_N} \frac{\varepsilon^{(k)}_{j^*_k}}{C_{i(k),j^*_k}} - \mathbf{F}^T\boldsymbol{\delta} = \boldsymbol{\chi}(\mathbf{R})^T\boldsymbol{\varepsilon} - \mathbf{F}^T\boldsymbol{\delta} \tag{16}$$

where:

$$\boldsymbol{\chi}^{(m)}(\mathbf{R}) = \left\{ \begin{array}{l} \chi^{(1)}(\mathbf{R}) \\ \cdots \\ \chi^{(NS)}(\mathbf{R}) \end{array} \right\} \text{ with } \left\{ \begin{array}{ll} \chi^{(k)}_{i_k} = \dfrac{1}{C_{i_k,j^*_k}} & \text{for } k \in \{k_1,\ldots,k_N\} \\ \chi^{(k)}_i = 0 & \text{otherwise.} \end{array} \right.$$

We have: $\boldsymbol{\varepsilon} = \mathbf{A}^T\boldsymbol{\delta}$ and $\boldsymbol{\delta} = \mu\boldsymbol{\delta}^{(m)}$, therefore: $\delta W = \left(\mathbf{A}\boldsymbol{\chi}^{(m)}(\mathbf{R}) - \mathbf{F}\right)^T \boldsymbol{\delta}^{(m)}$. And as previously, we prove from the kinematic theorem that:

$$g_{(m)}(\mathbf{R},\mathbf{F}) = \left(\mathbf{A}\boldsymbol{\chi}^{(m)}(\mathbf{R}) - \mathbf{F}\right)^T \boldsymbol{\delta}^{(m)}$$

defines a limit state function.

Remark: In the simple case previously treated we have $\boldsymbol{\chi}^{(m)}(\mathbf{R}) = \mathbf{D}^{(m)}\mathbf{R}$.

3.2 Failure probability of each collapse mechanism

In this way we can associate a linear limit state function with each collapse mechanism (m), dividing the probability space into a safe set $\mathcal{S}^{(m)} = \{(\mathbf{R},\mathbf{S}) | g_{(m)}(\mathbf{R},\mathbf{F}) > 0\}$ and a

failure set $\mathcal{F}^{(m)} = \{(\mathbf{R}, \mathbf{S}) | g_{(m)}(\mathbf{R}, \mathbf{F}) < 0\}$. The corresponding probability of survival is then calculated as:

$$P_s^{(m)} = P(g_{(m)}(\mathbf{R}, \mathbf{F}) > 0). \tag{17}$$

As an alternative to $P_s^{(m)}$ a reliability index $\beta^{(m)}$ is often defined as:

$$\beta^{(m)} = \Phi^{-1}(P_s^{(m)}) = -\Phi^{-1}(P_f^{(m)}) \tag{18}$$

where $P_f^{(m)} = 1 - P_s^{(m)} = P(g_{(m)}(\mathbf{R}, \mathbf{F}) < 0)$ is the failure probability, and Φ the Gaussian normal distribution function. In general the above expressions cannot be computed analytically, except when the basic variables $(\mathbf{R}, \mathbf{Y})$ are jointly normally distributed where the failure probability is:

$$P_f^{(m)} = \Phi(-\beta^{(m)}) \tag{19}$$

with $\beta^{(m)}$ the Hasofer and Lind reliability index equal to the minimum distance from the origin to a point on the failure surface.

In the general case it is always possible to transform the basic variables $\boldsymbol{X} = (\mathbf{R}, \mathbf{Y})$ into uncorrelated and standard normal variables $\boldsymbol{U} = \boldsymbol{T}(\mathbf{R}, \mathbf{Y})$.

The simplest definition of the transformation T appears when the basic variables are mutually independent. Then each variable can be transformed separately with the following transformation:

$$U_i = T(X_i) = \Phi^{-1}\left(F_{X_i}(X_i)\right)) \tag{20}$$

where F_{X_i} is the distribution function corresponding to the variable X_i.

When the basic variables are not mutually independent the *Rosenblatt* transformation [7] gives analogous results.

The function $G_{(m)}(\mathbf{U}) = g_{(m)}\left(\mathbf{T}^{-1}(\mathbf{U})\right)$ is the corresponding limit state function in the U-space. As it defines a failure surface which is not a hyperplane of the U-space the relation given by (18) provides an approximation of $P_f^{(m)}$ which correspond to a linearization of the failure surface at a design point $\mathbf{U}^*$. The design points are defined as the local solutions of the following optimization problem:

$$\beta^{(m)} = \min\{||\mathbf{U}|| \; | G_{(m)}(\mathbf{U}) \leq 0\}. \tag{21}$$

The tangent hyperplane to the failure surface at the design point has the equation:

$$\sum_i \frac{\partial G_{(m)}}{\partial U_i}\left(\mathbf{U}^*\right)\left(U_i^* - U_i\right) = 0. \tag{22}$$

This equation can also be written into the following form:

$$\frac{\nabla_U^T G_{(m)}\left(\mathbf{U}^*\right)}{\left|\nabla_U G_{(m)}\left(\mathbf{U}^*\right)\right|}\mathbf{U}^* - \frac{\nabla_U^T G_{(m)}\left(\mathbf{U}^*\right)}{\left|\nabla_U G_{(m)}\left(\mathbf{U}^*\right)\right|}\mathbf{U} = \beta^{(m)} + \boldsymbol{\alpha}^{(m)T}\mathbf{U} = 0 \tag{23}$$

where

$$\boldsymbol{\alpha}^{(m)} = -\frac{\nabla_U G_{(m)}\left(\mathbf{U}^*\right)}{\left|\nabla_U G_{(m)}\left(\mathbf{U}^*\right)\right|}$$

is the unit vector normal to the failure surface at the design point and

$$\beta^{(m)} = -\boldsymbol{\alpha}^{(m)T}\mathbf{U}^*$$

the Hasofer and Lind reliability index.

A reliability method based on this procedure is called *first order reliability method* (FORM), and $\beta^{(m)}$ is the *first order reliability index.*

Numerous general iterative algorithms are available to solve the optimization problem (20). The following iteration method is very simple and has proved to work well for practical problems:

$$\mathbf{U}^{(k+1)} = \left(\mathbf{U}^{(k)T}\boldsymbol{\alpha}^{(k)}\right)\boldsymbol{\alpha}^{(k)} + \frac{G_{(m)}\left(\mathbf{U}^{(k)}\right)}{\left|\nabla_U G_{(m)}\left(\mathbf{U}^{(k)}\right)\right|}\alpha^{(k)} \tag{24}$$

with:

$$\nabla_U G_{(m)}\left(\mathbf{U}\right) = \nabla_U g_{(m)}\left(\mathbf{X}\right) = \nabla_X g_{(m)}\left(\mathbf{X}\right)\nabla_U \mathbf{X}. \tag{25}$$

In our case:

$$\nabla_U g_{(m)}\left(\mathbf{X}\right) = \nabla_R g_{(m)}\left(\left(\mathbf{R},\mathbf{F}\right)\right)\nabla_U R + \nabla_F g_{(m)}\left(\mathbf{R},\mathbf{F}\right)\nabla_Y \mathbf{F}\nabla_U \mathbf{Y} \tag{26}$$

i.e.:

$$\frac{\partial g_{(m)}\left(\mathbf{R},\mathbf{F}\right)}{\partial U_i} = \sum_j \frac{\partial g_{(m)}\left(R,F\right)}{\partial R_j}\frac{\partial R_j}{\partial U_i} + \sum_k \frac{\partial g_{(m)}\left(\mathbf{R},\mathbf{F}\right)}{\partial F_k}\left(\sum_l \frac{\partial F_k}{\partial Y_l}\frac{\partial Y_l}{\partial U_i}\right). \tag{27}$$

We have:

$$g_{(m)}(\mathbf{R},\mathbf{F}) = \boldsymbol{\chi}^{(m)T}\mathbf{A}^T\boldsymbol{\delta}^{(m)} - \mathbf{F}^T\boldsymbol{\delta}^{(m)} = \sum_{k_1,\ldots,k_N} \chi_{i_k}^{(k)}\left(\mathbf{A}_{\bullet i_k}^T\boldsymbol{\delta}^{(m)}\right) - \sum_k F_k\delta_k^{(m)}. \tag{28}$$

Consequently:

$$\frac{\partial g_{(m)}\left(\mathbf{R},\mathbf{F}\right)}{\partial R_j} = \sum_{k_1,\ldots,k_N} \frac{\partial \boldsymbol{\chi}_{i_k}\left(\mathbf{R}\right)}{\partial R_j}\left(\mathbf{A}_{\bullet i_k}^T\boldsymbol{\delta}^{(m)}\right) = \sum_{k_1,\ldots,k_N} \frac{\partial \chi_{i_k}\left(\mathbf{R}\right)}{\partial R_j}\varepsilon_i \tag{29}$$

$$\frac{\partial g_{(m)}\left(\mathbf{R},\mathbf{F}\right)}{\partial F_k} = -\delta_k^{(m)} \tag{30}$$

And as $\mathbf{F} = \left\{\begin{array}{c} y_1\mathbf{F}^{(1)} \\ \cdots \\ y_{NP}\mathbf{F}^{(NP)} \end{array}\right\}$ we have: $\frac{\partial F_k}{\partial Y_l} = \left\{\begin{array}{ll} F_q^{(l)} & \text{when } k = (l-1)p+q \\ 0 & \text{otherwise} \end{array}\right.$

3.3 Reliability of series systems

We saw previously that a frame structure exposed to random force and resistance variables can be subject to an important number of collapse mechanisms. With each mechanism we associate a linear limit state function, dividing the probability space into a safe set and a failure set. The structure collapses if at least one limit state function is negative. Consequently it is possible to express the structure as the series system of all the different mechanisms.

Boolean state variables for each failure mode (m) are defined by:

$$\begin{aligned} A_m &= 1 \quad \text{if } g_{(m)}(\mathbf{R},\mathbf{S}) > 0 \\ A_m &= 0 \quad \text{if } g_{(m)}(\mathbf{R},\mathbf{S}) < 0 \\ B_m = 1 - A_m, &\quad m = 1,\ldots,NM \text{ with } NM \text{ the number of failure modes.} \end{aligned}$$

Denoting A_S and B_S the Boolean state variables for the system we have:

$$A_S = A_1 A_2 \ldots A_{NM}. \tag{31}$$

From this last expression we deduce [6] :

$$B_S = B_1 + A_1 B_2 + A_1 A_2 B_3 + \cdots + A_1 A_2 \cdots A_{NM-1} B_{NM}. \tag{32}$$

Since the variables A_m and B_m can only take the values 0 and 1 we deduce:

$$\max_m \{B_m\} \leq B_S \leq \sum_{m=1}^{NM} B_m. \tag{33}$$

Consequently we obtain some general bounds on the failure probability:

$$\max_m \left\{ P\left(g_{(m)}(\mathbf{R},\mathbf{F}) \leq 0\right)\right\} \leq P_f \leq \sum_{m=1}^{NM} P\left(g_{(m)}(\mathbf{R},\mathbf{F}) \leq 0\right). \tag{34}$$

Closer bounds were given by Ditlevsen:

$$P_1 + \sum_{m=1}^{NM} \max\left(P_m - \sum_{n=1}^{m-1} P_{mn}, 0\right) \leq P_f \leq \sum_{m=1}^{NM} P_m - \sum_{m=2}^{NM} \max_{n<m} P_{mn} \tag{35}$$

with:

$$P_m = P\left(g_m\left(\mathbf{R},\mathbf{F}\right) \leq 0\right)$$

and

$$P_{mn} = P\left(\left\{g_{(m)}\left(\mathbf{R},\mathbf{F}\right) \leq 0\right\} \cap \left\{g_{(n)}\left(\mathbf{R},\mathbf{F}\right) \leq 0\right\}\right) = P\left(\mathcal{S}^{(m)} \cap \mathcal{S}^{(n)}\right).$$

In a first order analysis, P_m and P_{mn} are approximated by linearization of the limit state functions expressed in the U-space. Hence P_m is calculated by the formula (19) while P_{mn} is obtained by approximating the joint failure set $\mathcal{S}^{(m)} \cap \mathcal{S}^{(n)}$ by the set bounded by the tangent hyperplanes at the design points for the two failure modes.

We saw previously that the tangent hyperplanes are characterized by the linear safety margins:

$$M^{(m)} = \beta^{(m)} + \boldsymbol{\alpha}^{(m)T}\mathbf{U} \text{ and } M^{(n)} = \beta^{(n)} + \boldsymbol{\alpha}^{(n)T}\mathbf{U}.$$

As $M^{(m)}$ and $M^{(n)}$ are standardized normally distributed, we have:

$$P_{mn} = \Phi\left(-\beta^{(m)}, -\beta^{(n)}; \rho_{mn}\right). \tag{36}$$

Where Φ is the probability density function for a bivariate normal vector with zero mean values, unit variance, and correlation coefficient $\rho_{mn} = \boldsymbol{\alpha}^{(m)T}\boldsymbol{\alpha}^{(n)}$.

3.4 Identification of the significant collapse mechanisms

In practice, even if the considered frame is small, the identification of all the possible mechanisms is cumbersome. But generally only the mechanisms of high probability (with a low value of reliability index) are sufficient to obtain a good approximation of the probability of collapse. Furthermore, it is worth mentioning that many mechanisms are mutually highly correlated (mechanisms having common bars in yielding). Consequently even a mechanism with a low value of the reliability index may not be important in the sense that it contributes significantly to the failure probability, since most of the failure set of that mechanisms already may have been accounted for by another (highly correlated) mechanism.

Locci [5] suggests a simple algorithm to compute the principal mechanisms needed to approach the structural reliability: resolution of optimization problem (4), formulated with the mean values of strengths and forces, yields the lowest load factor associated with those values. If a new solution is searched after one of the constraints of the basic solution is suppressed, a new mechanism will be found with a necessarily higher load factor. A large number of mechanisms can therefore be found with increasing load factors by suppressing in turn each rupture component of each previously computed mechanism and reordering the set of mechanism by ascending load factors at each step. Since there is an obvious correlation between ascending load factors computed on mean values and ascending reliability indices, a truncated series system will be satisfactory in practice.

4 Conclusion

The use of the limit analysis in reliability carries out some important improvements in comparison with classical methods. It allows to easily automate the failure mode determination, from components available in any finite element code. Otherwise it allows to associate a linear limit state function with each collapse mode and so easily estimate the failure probability of the considered frame.

Notice to conclude some possible improvements:

- The use of sophisticated methods to approach the failure surface.
- The study of more realistic failure criteria, leading to an improvement of the limit state functions.
- The development of efficient algorithms to select the significant failure modes.

Acknowledgement
The research has been funded by the European Commission as part of the Brite–EuRam III project LISA: FEM–Based Limit and Shakedown Analysis for Design and Integrity Assessment in European Industry (Project N°: BE 97–4547, Contract N°: BRPR–CT97–0595).

Bibliography

[1] G. Augusti, A. Baratta, F. Casciati: *Probabilistic Methods in Structural Engineering*. Chapman and Hall, London (1984)

[2] CTICM: *Méthodes de calcul aux états limites des structures à barres*. Conférences et textes présentés au séminaire organisé par le CTICM du 14 au 17 Novembre 1972.

[3] J. Goyet, B. Remy: *Fiabilité des structures. Méthodologie d'ensemble et applications aux structures à barres*. Construction Métallique, n ° 4, 1988.

[4] Y. Lescouarc'h: *Calcul en plasticité des structures*. Edit. COTECO, Paris, Octobre 1983.

[5] J.M. Locci: *Automatization of limit analysis calculations, application to structural reliability problems*. In M. Lemaire, J.-L. Favre, A. Mébarki (eds): *Proceedings of the ICASP7 Conference, Paris, 10-13.7.1995, Vol.2: Applications of Statistics and Probability.* A. A. Balkema, Rotterdam, Brookfield (1995) 1095-1110.

[6] H.O. Madsen, S. Krenk, N.C. Lind: *Methods of Structural Safety*. Prentice-Hall, Englewood Cliffs, New Jersey (1986).

[7] M. Rosenblatt: Remarks on a Multivariate Transformation. *The annals of mathematical Statistics*. **23**, (1952) 470-472.

[8] S.J. Wright: *Primal-Dual Interior-Point Methods*. Society for Industrial and Applied Mathematics, New York (1996).

Already published:

Modern Methods and Algorithms of Quantum Chemistry - Proceedings
Johannes Grotendorst (Editor)
NIC Series Volume 1
Winterschool, 21 - 25 February 2000, Forschungszentrum Jülich
ISBN 3-00-005618-1, February 2000, 562 pages
out of print

Modern Methods and Algorithms of Quantum Chemistry - Poster Presentations
Johannes Grotendorst (Editor)
NIC Series Volume 2
Winterschool, 21 - 25 February 2000, Forschungszentrum Jülich
ISBN 3-00-005746-3, February 2000, 77 pages
out of print

Modern Methods and Algorithms of Quantum Chemistry - Proceedings, Second Edition
Johannes Grotendorst (Editor)
NIC Series Volume 3
Winterschool, 21 - 25 February 2000, Forschungszentrum Jülich
ISBN 3-00-005834-6, December 2000, 638 pages

Nichtlineare Analyse raum-zeitlicher Aspekte der hirnelektrischen Aktivität von Epilepsiepatienten
Jochen Arnold
NIC Series Volume 4
ISBN 3-00-006221-1, September 2000, 120 pages

Elektron-Elektron-Wechselwirkung in Halbleitern: Von hochkorrelierten kohärenten Anfangszuständen zu inkohärentem Transport
Reinhold Lövenich
NIC Series Volume 5
ISBN 3-00-006329-3, August 2000, 145 pages

Erkennung von Nichtlinearitäten und wechselseitigen Abhängigkeiten in Zeitreihen
Andreas Schmitz
NIC Series Volume 6
ISBN 3-00-007871-1, May 2001, 142 pages

Multiparadigm Programming with Object-Oriented Languages - Proceedings
Kei Davis, Yannis Smaragdakis, Jörg Striegnitz (Editors)
NIC Series Volume 7
Workshop MPOOL, 18 May 2001, Budapest
ISBN 3-00-007968-8, June 2001, 160 pages

Europhysics Conference on Computational Physics - Book of Abstracts
Friedel Hossfeld, Kurt Binder (Editors)
NIC Series Volume 8
Conference, 5 - 8 September 2001, Aachen
ISBN 3-00-008236-0, September 2001, 500 pages

NIC Symposium 2001 - Proceedings
Horst Rollnik, Dietrich Wolf (Editors)
NIC Series Volume 9
Symposium, 5 - 6 December 2001, Forschungszentrum Jülich
ISBN 3-00-009055-X

Quantum Simulations of Complex Many-Body Systems: From Theory to Algorithms - Lecture Notes
Johannes Grotendorst, Dominik Marx, Alejandro Muramatsu (Editors)
NIC Series Volume 10
Winter School, 25 February - 1 March 2002, Rolduc Conference Centre, Kerkrade, The Netherlands
ISBN 3-00-009057-6, February 2002, 548 pages

Quantum Simulations of Complex Many-Body Systems: From Theory to Algorithms- Poster Presentations
Johannes Grotendorst, Dominik Marx, Alejandro Muramatsu (Editors)
NIC Series Volume 11
Winter School, 25 February - 1 March 2002, Rolduc Conference Centre, Kerkrade, The Netherlands
ISBN 3-00-009058-4, February 2002, 85 pages

Strongly Disordered Quantum Spin Systems in Low Dimensions: Numerical Study of Spin Chains, Spin Ladders and Two-Dimensional Systems
Yu-cheng Lin
NIC Series Volume 12
ISBN 3-00-009056-8, May 2002, 131 pages

Multiparadigm Programming with Object-Oriented Languages - Proceedings
Jörg Striegnitz, Kei Davis, Yannis Smaragdakis (Editors)
Workshop MPOOL 2002, 11 June 2002, Malaga
NIC Series Volume 13
ISBN 3-00-009099-1, June 2002, 133 pages

Quantum Simulations of Complex Many-Body Systems: From Theory to Algorithms - Audio-Visual Lecture Notes
Johannes Grotendorst, Dominik Marx, Alejandro Muramatsu (Editors)
NIC Series Volume 14
Winter School, 25 February - 1 March 2002, Rolduc Conference Centre, Kerkrade, The Netherlands
ISBN 3-00-010000-8, November 2002, DVD

All volumes are available online at http://www.fz-juelich.de/nic-series/.